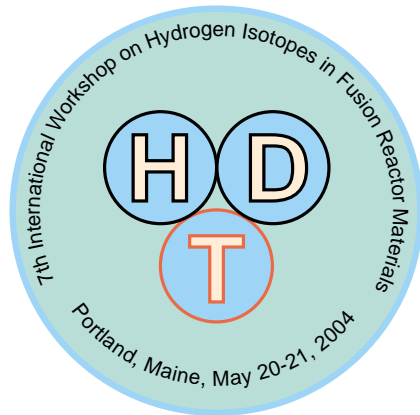


7th International Workshop on Hydrogen Isotopes in Fusion Reactor Materials

May 20–21, 2004

Sebasco Harbor Resort
Sebasco Estates, Maine 04565–0075, USA



P R O C E E D I N G S

Thursday, May 20, 2004

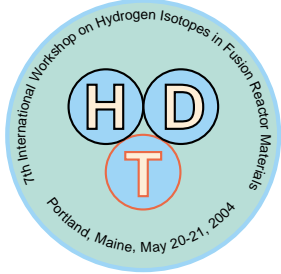
Session 1: H Isotopes in Metals

Session 2: General Topics on H Isotopes in PFCs

Friday, May 21, 2004

Session 3: The Codeposited Layer

organized by: Sandia National Laboratories, Livermore, California R. A. Causey, Workshop Chairman

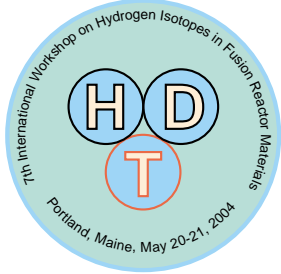


SESSION 1 – Part A

Hydrogen Isotopes in Metals

Session chair: R. P. Doerner

- 1 A 1 pp. 9-26 *Hydrogen retention and desorption behavior from type 316 stainless steel*
Y. Oya, University of Tokyo
- 1 A 2 pp. 27-37 *Deuterium permeation through multilayer sample W-Al₂O₃-Eurofer*
D. Levchuk, Max-Planck-Institut für Plasmaphysik
- 1 A 3 pp. 38-53 *Helium and hydrogen retention in polycrystalline tungsten due to sequential and simultaneous ion bombardment*
J. W. Davis, University of Toronto

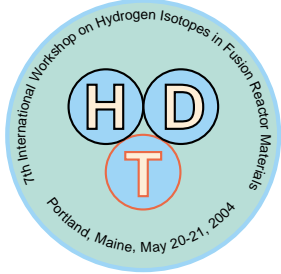


SESSION 1 – Part B

Hydrogen Isotopes in Metals

Session chair: R. P. Doerner

- 1 B 1 pp. 54-100 Influence of gas content in the near surface layers on sputtering of metals under irradiation by H^+ and He^+ with a mean energy of 10 and 20 keV*
N. V. Volkov, Moscow Engineering & Physics Institute
- 1 B 2 pp. 101-127 TMAP4 modeling of deuterium trapping in tungsten*
R. G. Macauley-Newcombe, University of Toronto
- 1 B 3 pp. 128-149 Deuterium retention in tungsten materials*
J. Roth, Max-Planck-Institut für Plasmaphysik



SESSION 1 – Part C

Hydrogen Isotopes in Metals

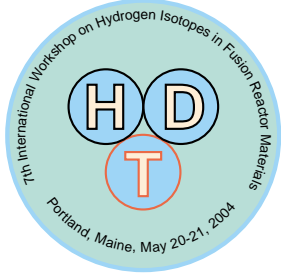
Session chair: R. P. Doerner

1 C 1 pp. 150-218 Ion driven deuterium behaviour in tungsten

O. V. Ogorodnikova,
Max-Planck-Institut für Plasmaphysik

1 C 2 pp. 219-229 Tungsten blister formation and deuterium retention measurements in PISCES-B

M. J. Baldwin, University of California, San Diego

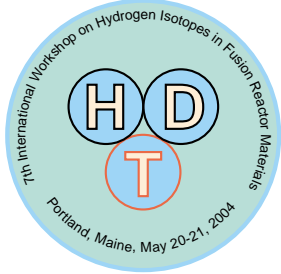


SESSION 2 – Part A

General Hydrogen in PFCs

Session chair: A. A. Haasz

- 2 A 1 pp. 230-242 *Behavior of hydrogen isotopes interacting with defects in Li_2O*
T. Oda, University of Tokyo
- 2 A 2 pp. 243-268 *Experience with deuterium retention and carbon migration in DIII-D*
D. Whyte, University of Wisconsin
- 2 A 3 pp. 269-292 *The safety and tritium applied research (STAR) facility*
J. P. Sharpe, Idaho National Laboratory

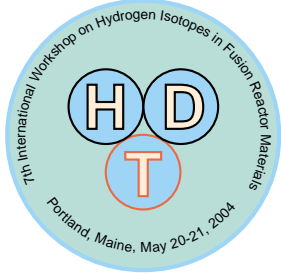


SESSION 2 – Part B

General Hydrogen in PFCs

Session chair: A. A. Haasz

- 2 B 1 pp. 293-315 *Non-statistical behavior of surface-induced dissociation of HD_2^+*
W. Schustereder, University of Innsbruck
- 2 B 2 pp. 316-333 *Mechanism of hydrogen blistering on covalent bonding materials*
T. Tanabe, Nagoya Univeristy

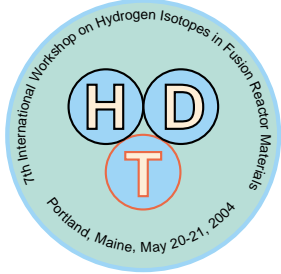


SESSION 3 – Part A

The Codeposited Layer

Session chair: J. Roth

- 3 A 1 pp. 334-352 *A quantitative model for chemical sputtering of carbon materials in thermonuclear fusion devices*
W. Jacob, Max-Planck-Institut für Plasmaphysik
- 3 A 2 pp. 353-365 *Initial results on carbon film removal by thermo-oxidation in low-pressure nitrogen oxides*
D. Tafalla, Laboratorio Nacional de Fusion
- 3 A 3 pp. 366-376 *Thermal release rate data of tritium trapped in surface and bulk specimens obtained from the JET MKIIA divertor tiles*
N. Bekris, Forschungszentrum Karlsruhe
- 3 A 4 pp. 377-392 *Property of tritium and carbon co-deposition on JET Mk-IIA divertor tiles*
K. Sugiyama, Nagoya Univeristy



SESSION 3 – Part B

The Codeposited Layer

Session chair: J. Roth

- 3 B 1 pp. 393-432 *Comments on the estimation of tritium retention in ITER*
T. Tanabe, Nagoya University
- 3 B 2 pp. 433-452 *Defects generated by H^+ impact onto graphite surfaces and their reactivity towards atomic H*
T. Angot, Université de Provence
- 3 B 3 pp. 453-464 *DIII-D/TRINITY collaboration on carbon and hydrogen codeposition*
W. P. West, General Atomics

compiled by: R. Bastasz, Sandia National Laboratories, Livermore, California



東京大学
THE UNIVERSITY OF TOKYO



静岡大学



Hydrogen retention and desorption behavior from type 316 stainless steel

Y.Oya^{a)}, Y.Onishi^{b)}, H.Kodama^{b)}, T.Kawano^{c)}, Y.Asakura^{c)},
T.Uda^{c)}, K.Okuno^{b)} and S.Tanaka^{d)}

^{a)}Radioisotope Center, The University of Tokyo

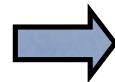
^{b)}Radiochemistry Research Laboratory, Shizuoka University

^{c)}Safety and Environmental Research Center, NIFS

^{d)}Graduate School of Engineering, The University of Tokyo

Introduction

Stainless Steel (SS)



fusion reactor for various component materials like cooling pipe



Hydrogen isotopes including tritium

one of the most important issues for assessment of fusion safety

the tritium release to the environment
the radiation exposure for workers.

Type 316 SS



Deuterium with various methods

Water adsorption

Electrolysis

Ion irradiation

Chemical states of SS component : XPS (X-ray photoelectron spectroscopy)

Deuterium(D_2 and D_2O) desorption behavior : TDS (Thermal desorption spectroscopy)

Experimental(1)

- Sample : Type 316 SS
(Size 10x10x1mm³)
- Two kinds of surface finish:
 - 1: Non pretreatment sample (**As received sample**)
 - 2: Polished and annealed at 1273K for 30 min. to remove surface oxide layer (**Pretreated sample**)



- Deuterium was charged by various adsorption / absorption methods, **water adsorption**, **electrolysis**, and **ion irradiation**

Experimental(2)

Water adsorption

- The sample was immersed in heavy water for 30 min..

Electrolysis

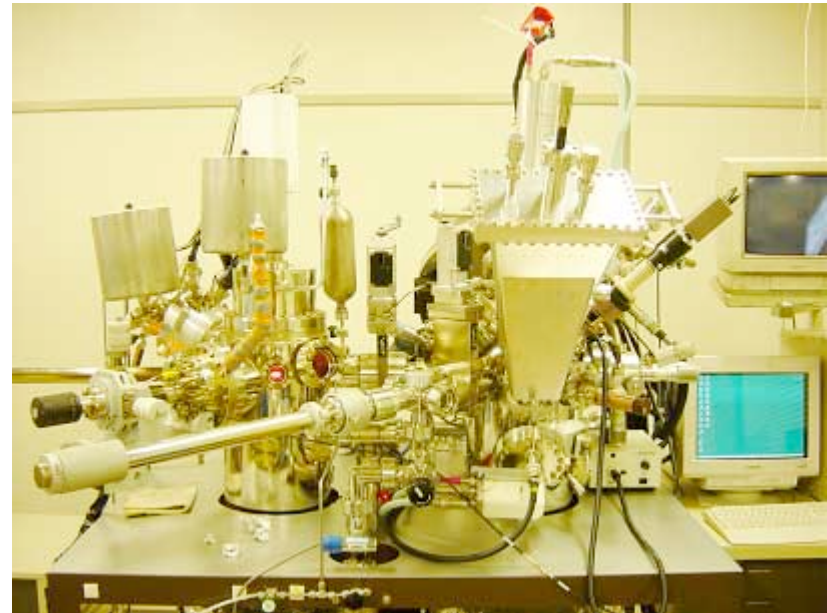
- The sample was used as a cathode. The 0.1mmol NaOD was added into the heavy water as electrolyte and electrolysis was performed for 60 min. with the current of 0.1A.

Ion irradiation

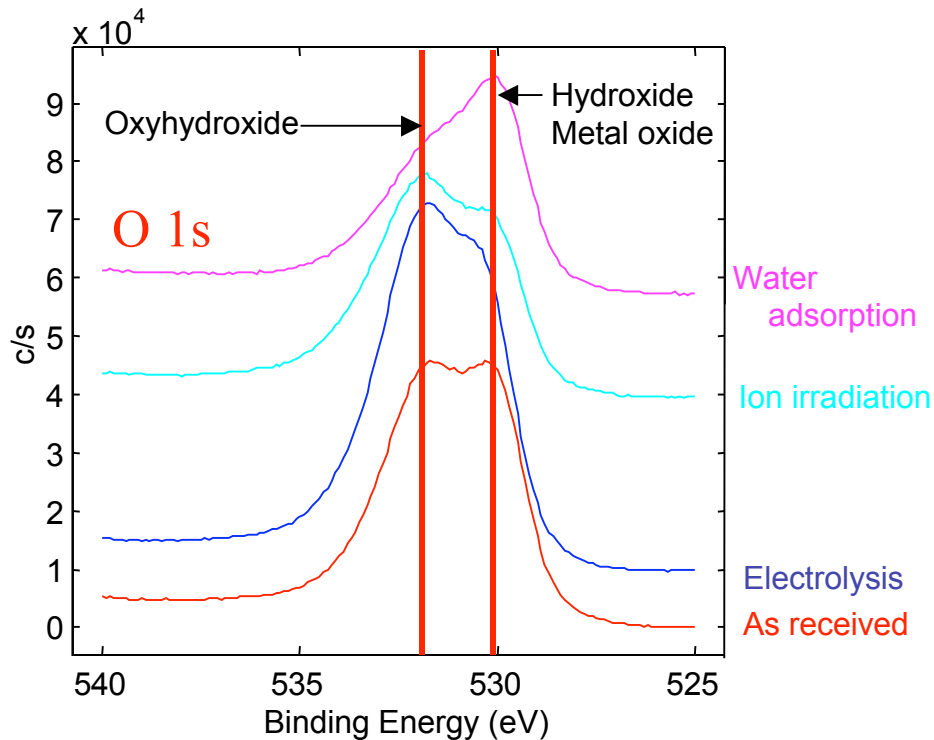
- The 4keV deuterium ion was implanted into the sample with the flux of $5.1 \times 10^{18} \text{ D}^+ \text{m}^{-2} \text{s}^{-1}$ and the fluence of $2.04 \times 10^{22} \text{ D}^+ \text{m}^{-2}$, implantation area of $3.0 \times 3.0 \text{ mm}^2$, and incident angel of 0 degree oriented from the surface normal at room temperature.

Experimental(3)

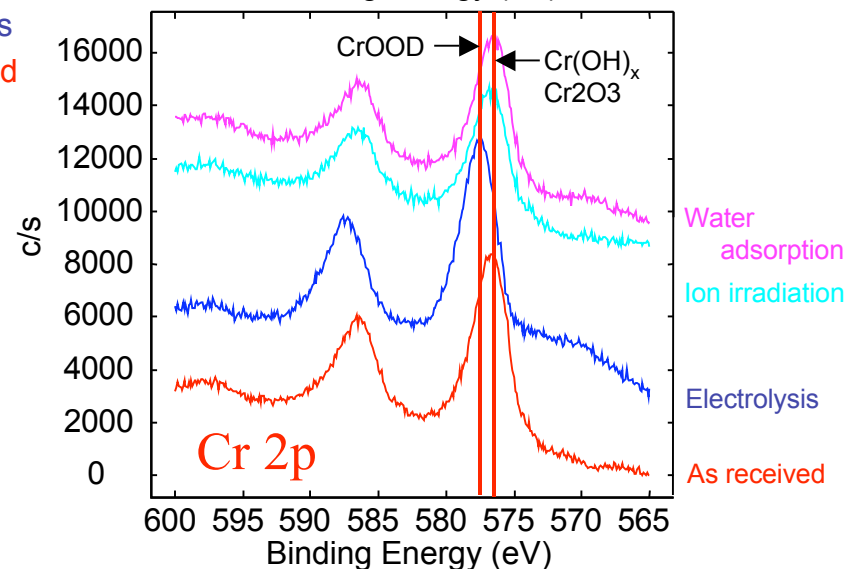
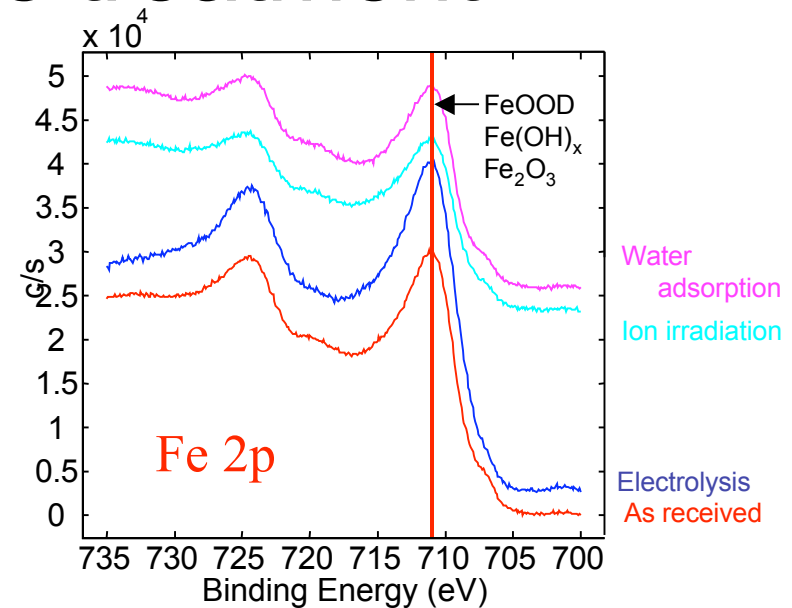
- XPS (X-ray photoelectron spectroscopy)
(ESCA 1600, ULVAC-PHI Inc.)
X-ray source : Al-K α
(1486.6eV) 400W
- TDS (Thermal desorption spectroscopy)
Heating rate : 30 K/min
Heated up to 1273K



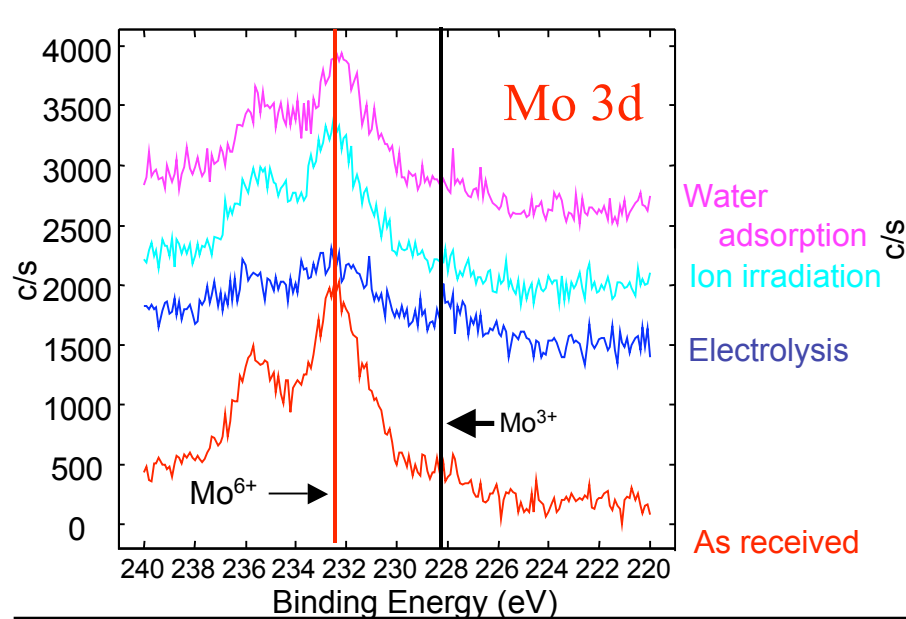
XPS spectra of **as received** 316-SS after various treatment



The oxide layer still exists even after ion irradiation. Hydrogen may be trapped in this layer.
Electrolysis : oxyhydroxide
Water adsorption : Hydroxide

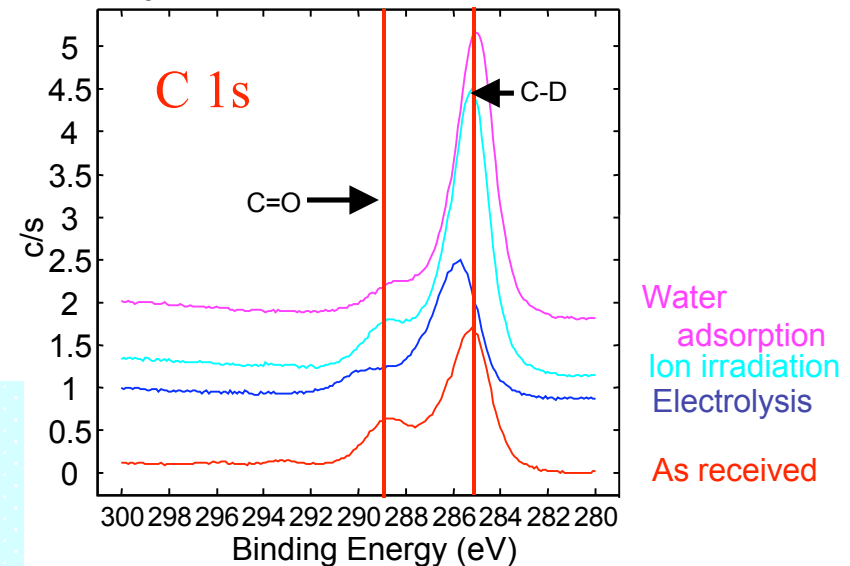
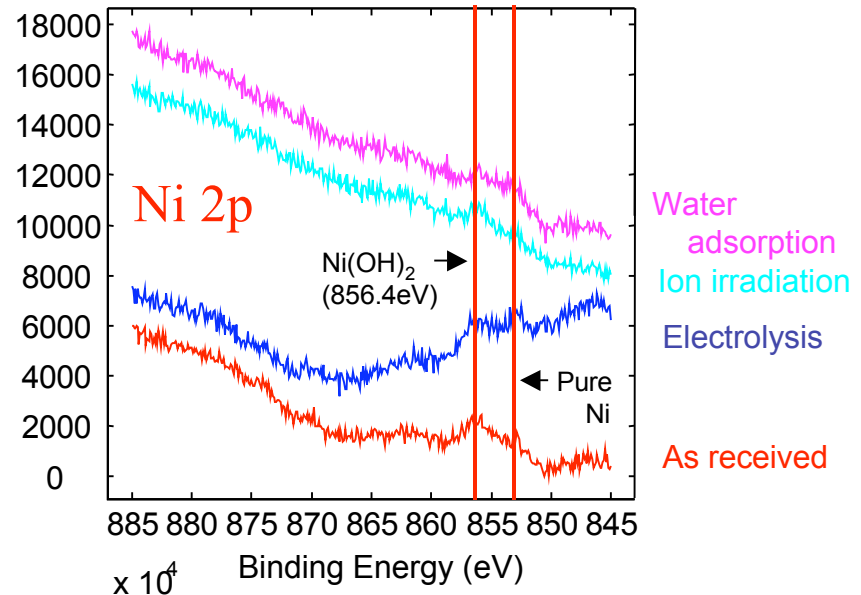


XPS spectra of as received 316-SS after various treatment



Chemical shift of Mo	
227.9eV	Mo metal
228.3eV	Mo ³⁺
229.2eV	MoO ₂
229.3eV	Mo ⁴⁺
230.7eV	Mo ⁵⁺
231.6eV	Mo ₂ O ₅
232.2eV	Mo ⁶⁺ , MoO ₃ or Mo(O ₄) ²⁻

Mo⁶⁺ is a major chemical form in 316-SS. Small amount of Ni oxide was found. C was found with forming C-D or C=O bond

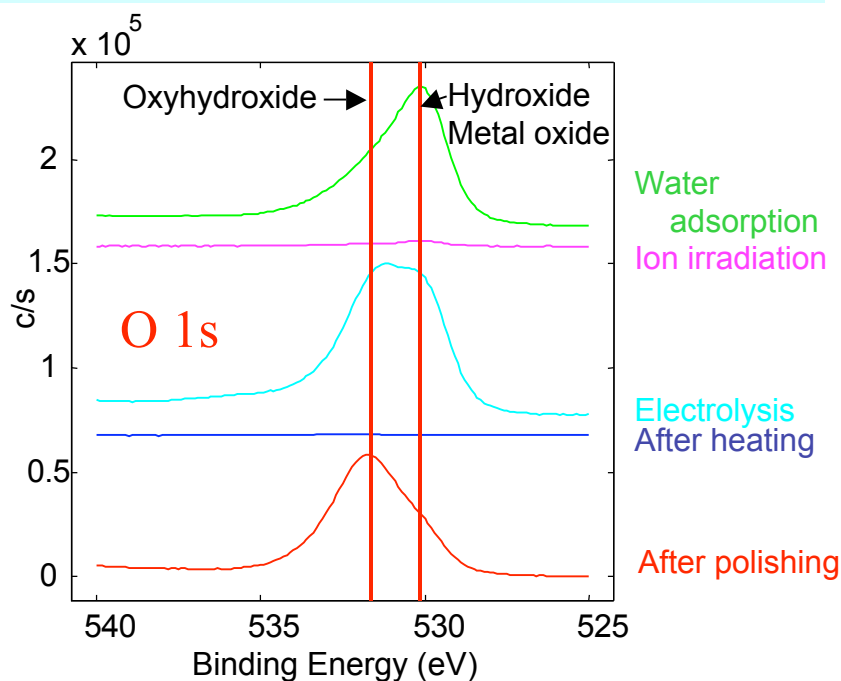


XPS spectra of pretreated 316-SS after various treatment

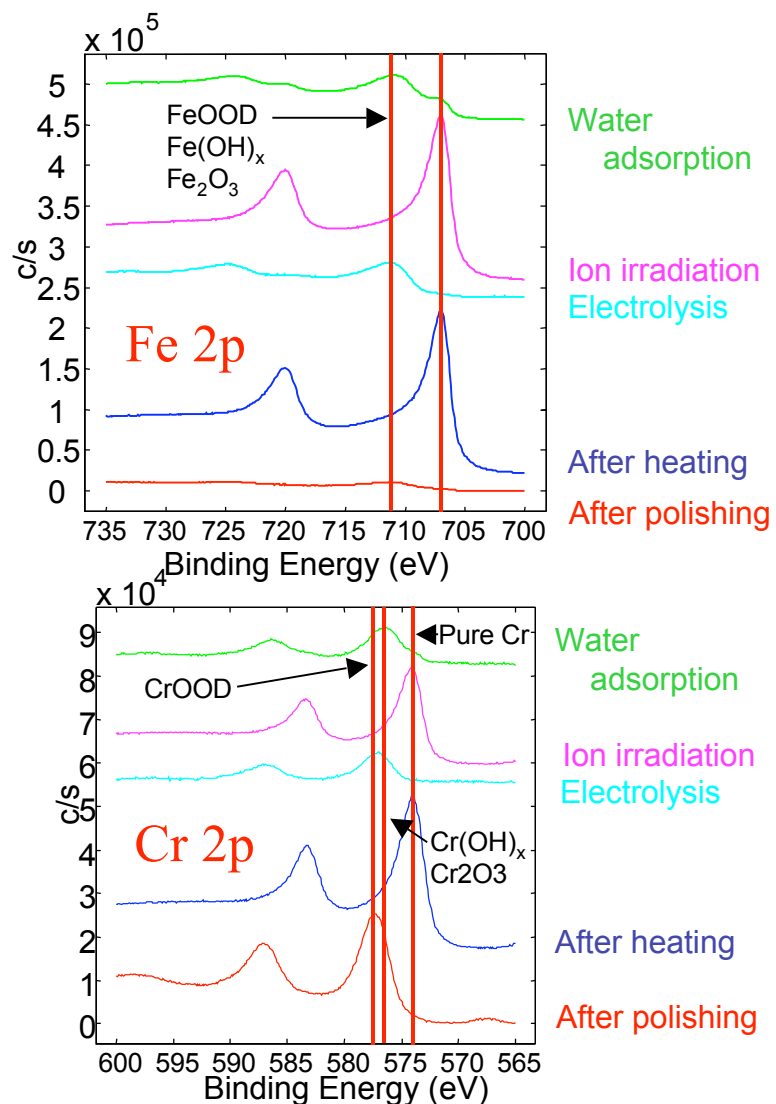
Pretreatment : polishing and heating



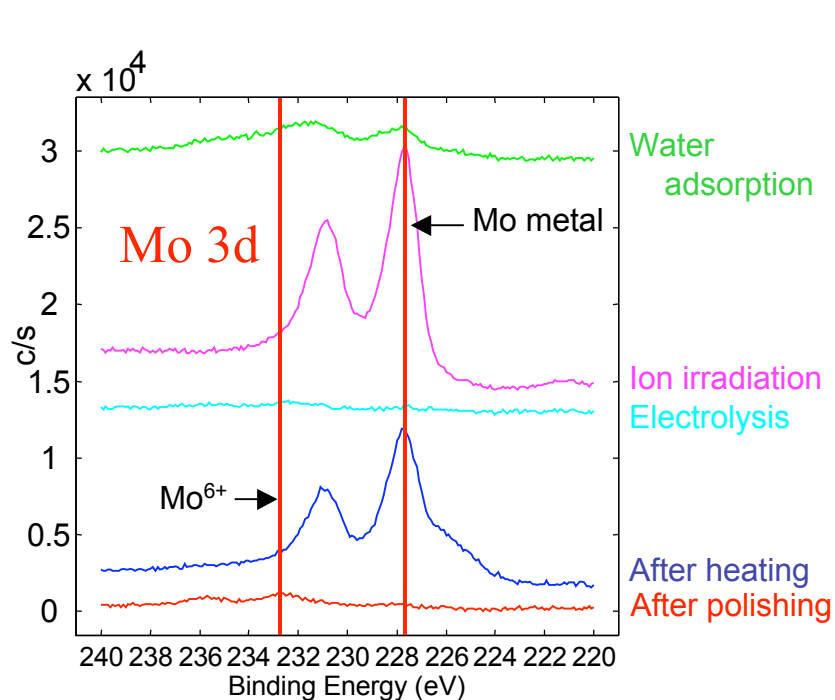
Water adsorption, Electrolysis or Ion irradiation



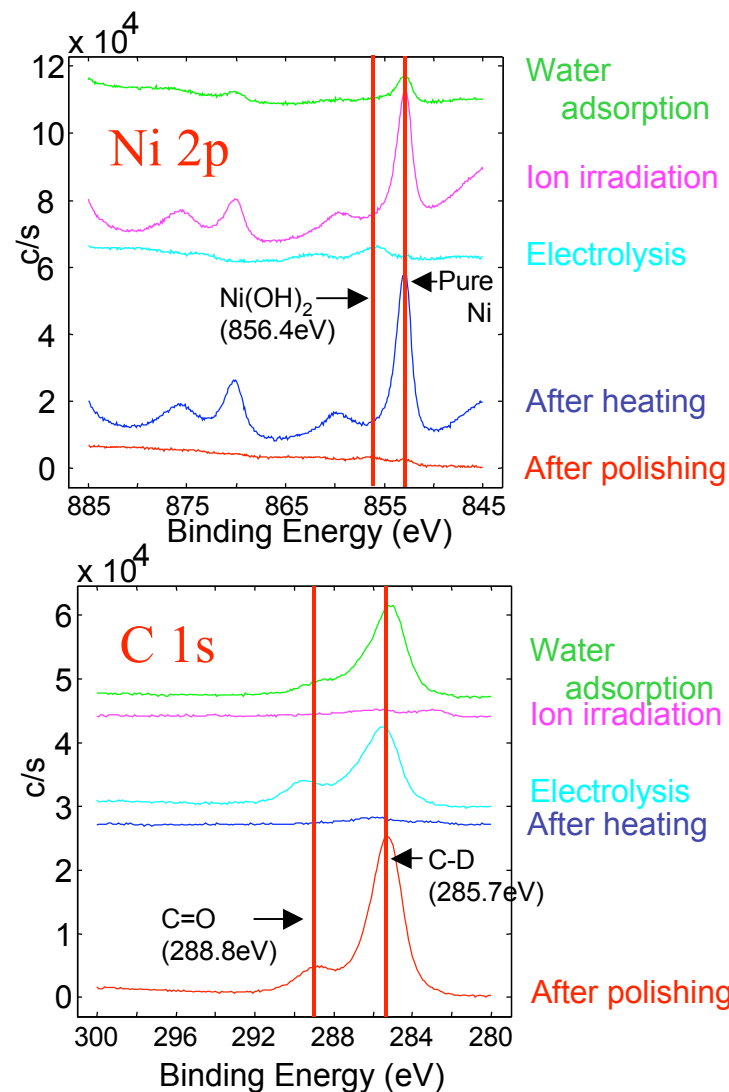
Electrolysis : oxyhydroxide
 Water adsorption : Hydroxide
 Ion irradiation : No oxide layer



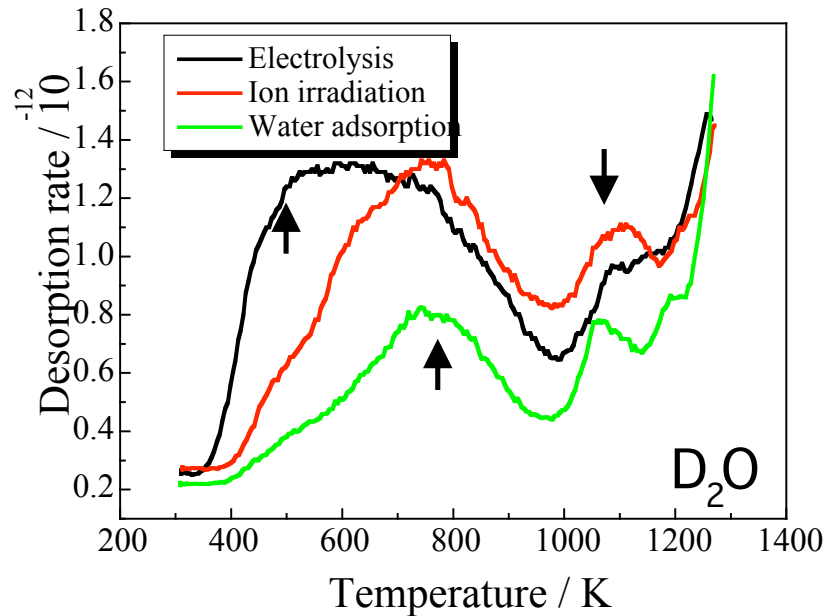
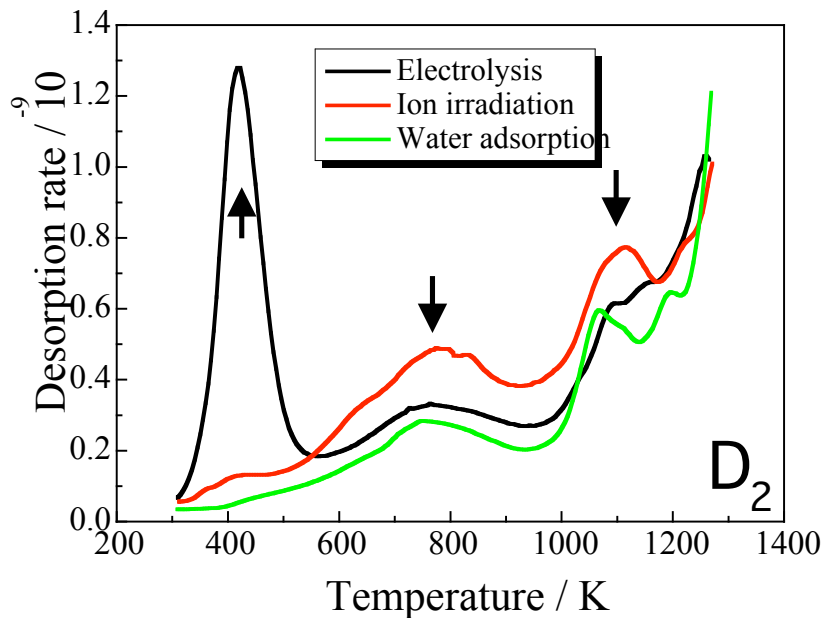
XPS spectra of pretreated 316-SS after various treatment



By the pretreatment, pure Mo was observed. It was not oxidized by the various treatment and only its amount was decreased by electrolysis and water adsorption.

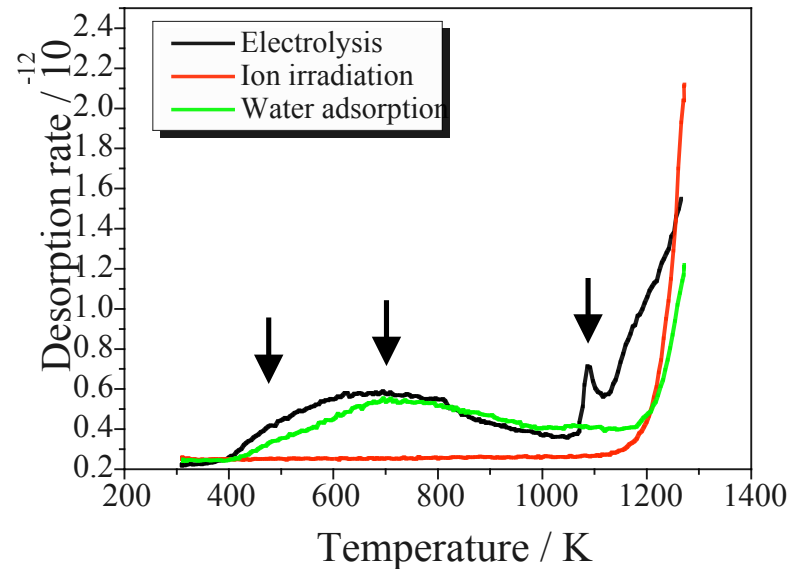
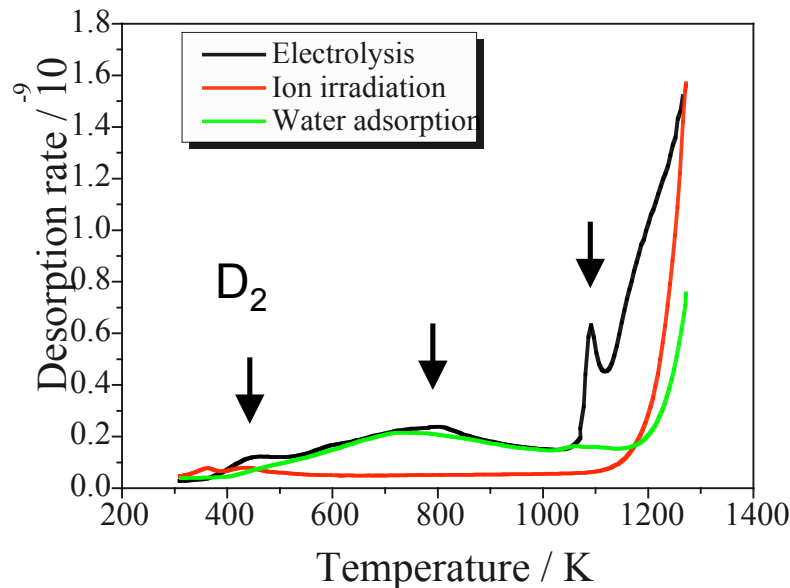


TDS spectra of D_2 and D_2O from as received 316-SS



Three desorption stages from type 316 SS were observed at around 400, 800 and 1100 K.
Large amount of D_2 was desorbed at around 400 K from the sample with electrolysis.

TDS spectra of D_2 and D_2O from pretreated 316-SS

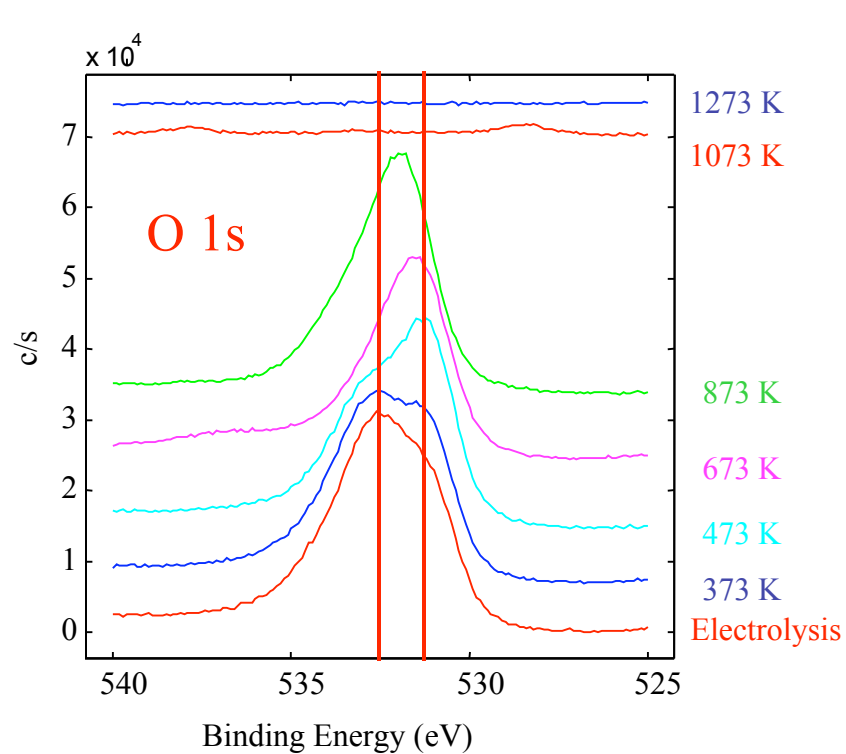


The amount of desorbed deuterium clearly decreased, especially, 1st stage compared to the as-received sample..

This fact indicates that the surface finish largely contributes to the hydrogen retention.

In the ion irradiation, the hydrogen isotopes were not retained in 316-SS because no oxide layer was formed on the surface.

XPS spectra of **as received** 316-SS after heating

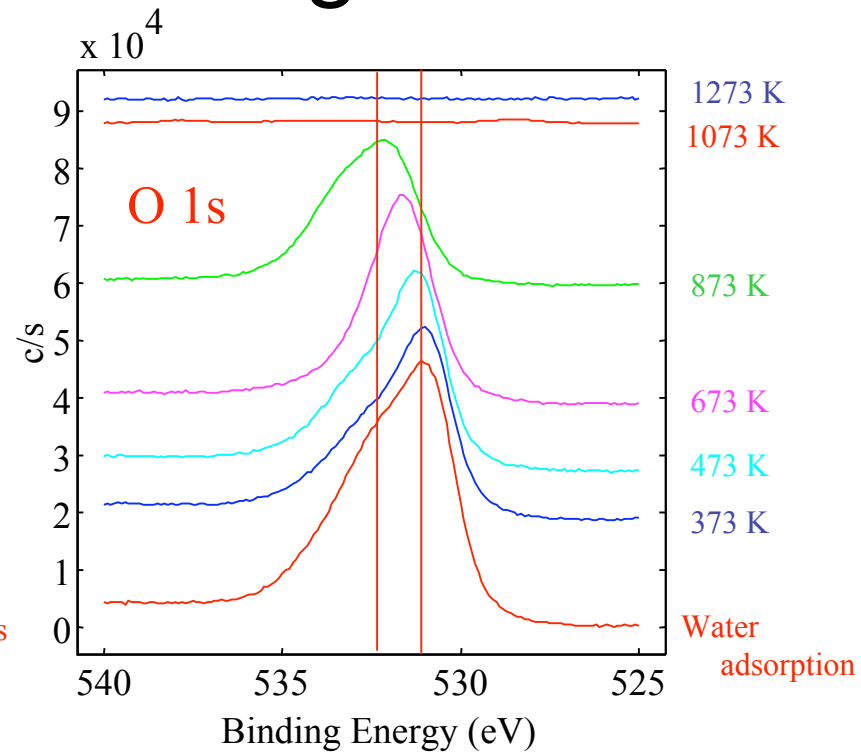


Electrolysis

After heating at 473 K, major chemical form of oxygen was changed from oxyhydroxide to hydroxide.



1st desorption peak of TDS



Water adsorption

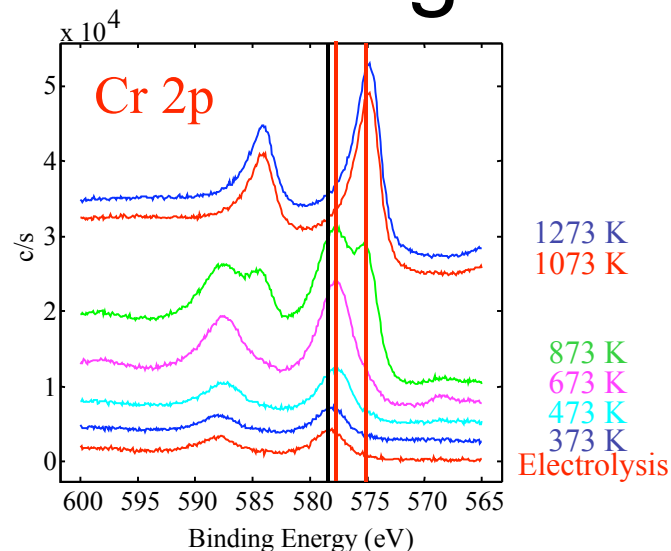
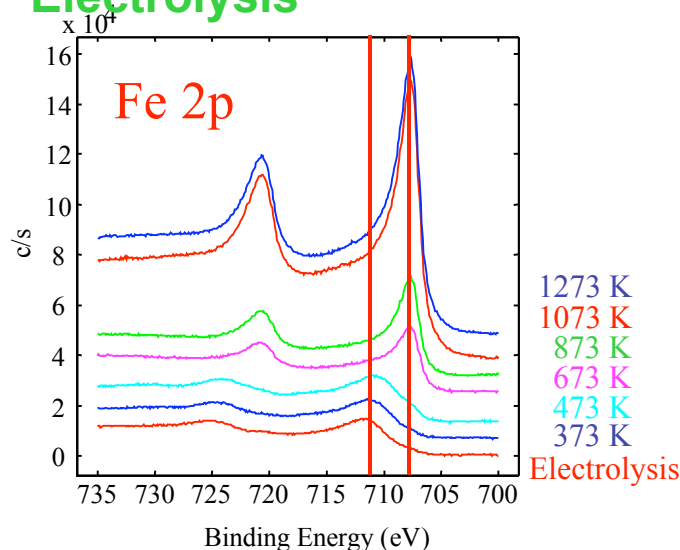
O 1s peak was broadened at 873 K. Some hydroxide may be decomposed.



2nd desorption peak of TDS

XPS spectra of as received 316-SS after heating

Electrolysis

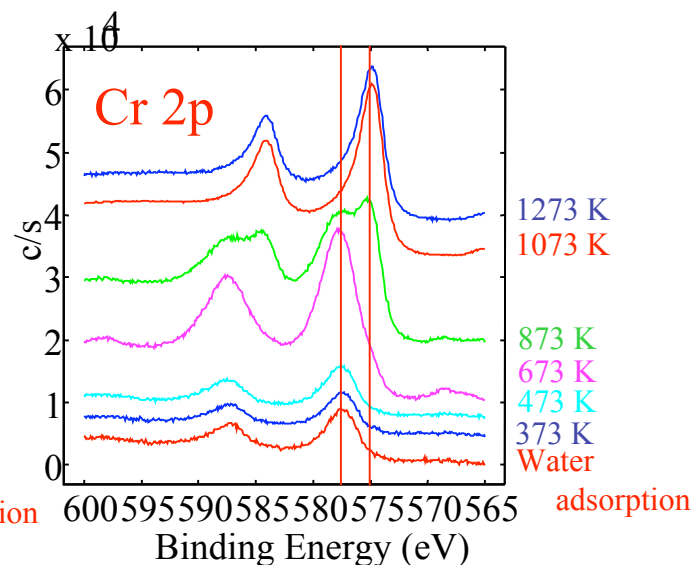
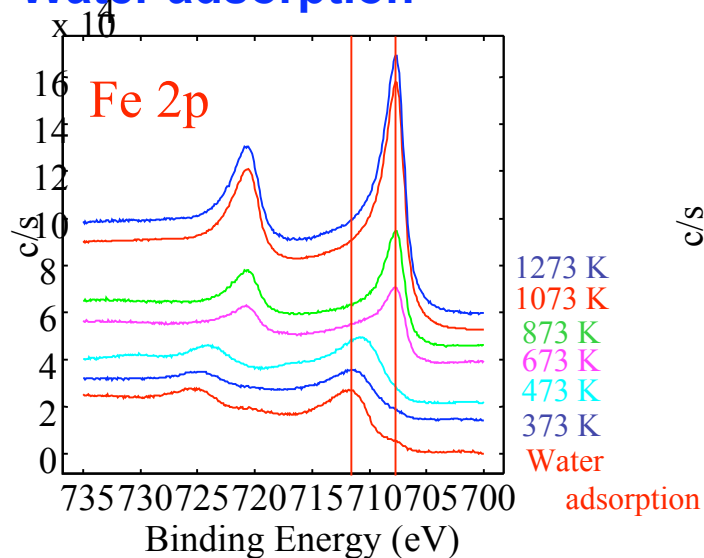


Decomposition of
iron oxide



473-673 K

Water adsorption

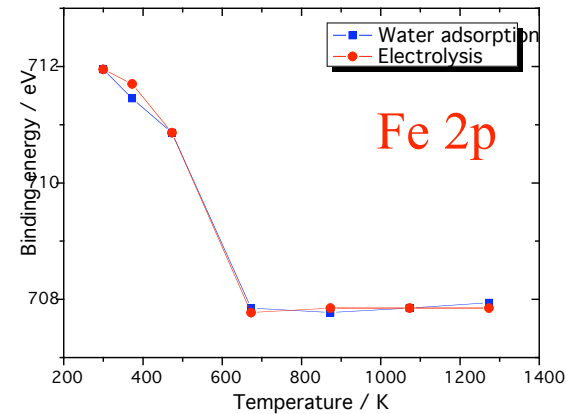
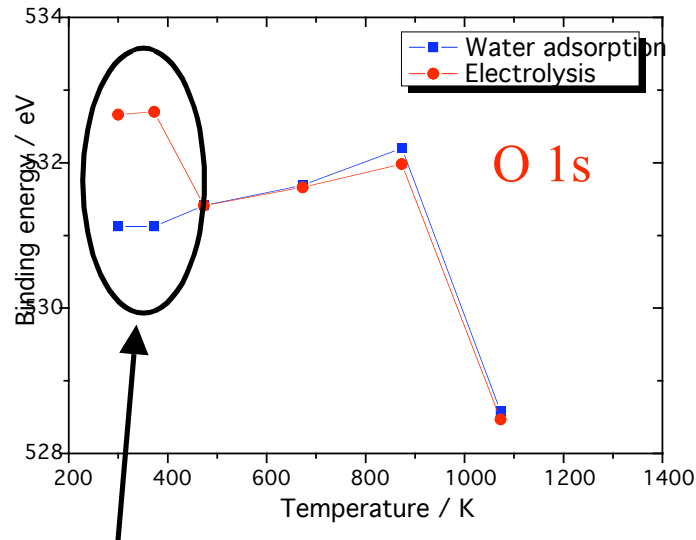


Decomposition of
chromium oxide



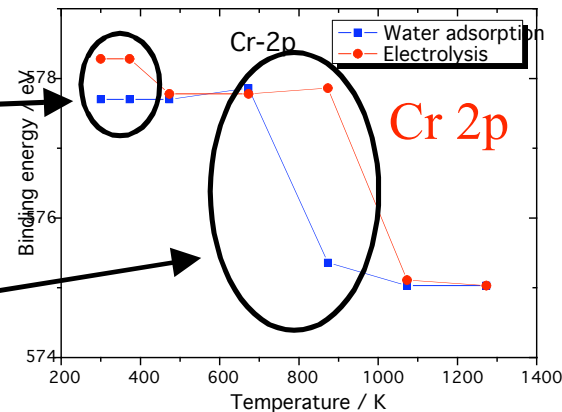
873 K

Summary of the chemical shift of as received 316-SS after heating



Initial surface chemical form was clearly different. \Rightarrow Oxyhydroxide or hydroxide

Peak recovery to the original pure Cr position for 316-SS with electrolysis was suppressed, because of the thicker oxide layer.



Depth profiles of **as received** 316-SS by Ar^+ sputtering

Depth profiles of as received 316-SS after electrolysis and water adsorption was studied by Ar^+ ion sputtering.

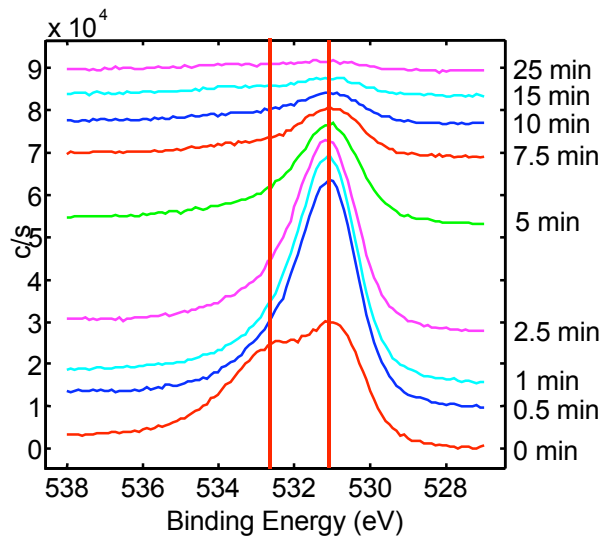
Ar^+ : 1.0 keV

Ion flux : $4.6 \times 10^{17} \text{ Ar}^+ \text{ m}^{-2} \text{ s}^{-1}$

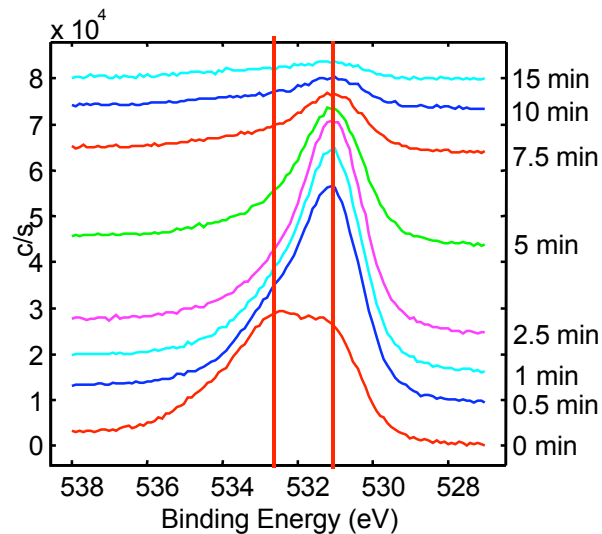
Incident angle : 30°

Sputtering rate : $2.21 \text{ nm min}^{-1} (\text{SiO}_2)$

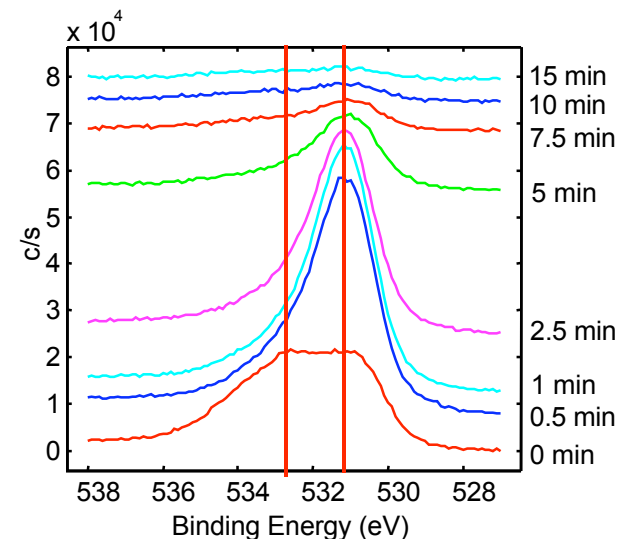
O 1s



As received sample

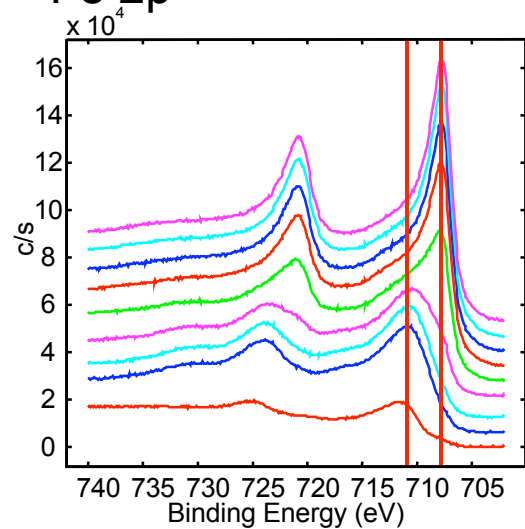


Electrolysis

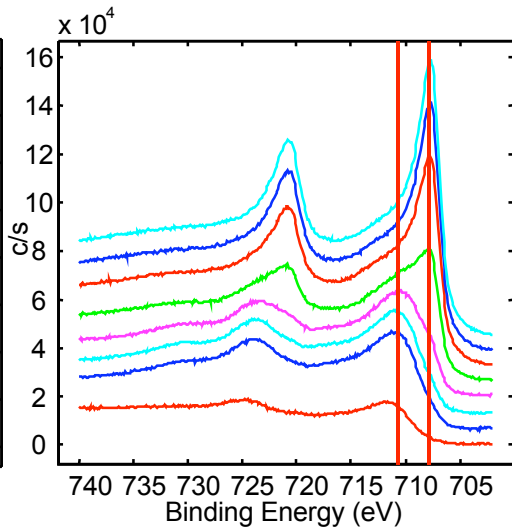


Water adsorption

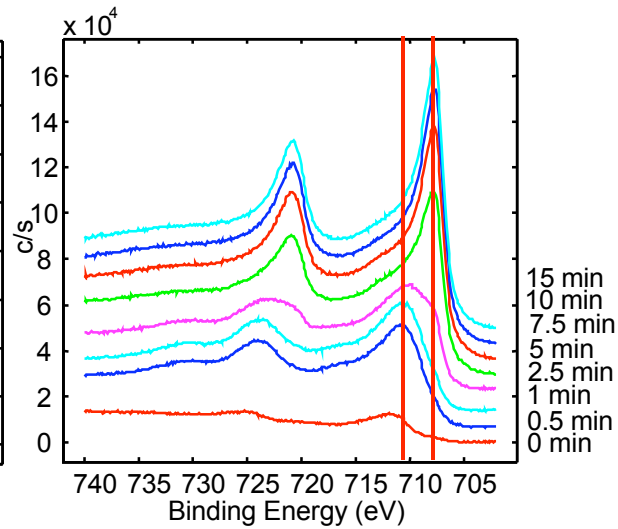
Fe 2p



As received sample

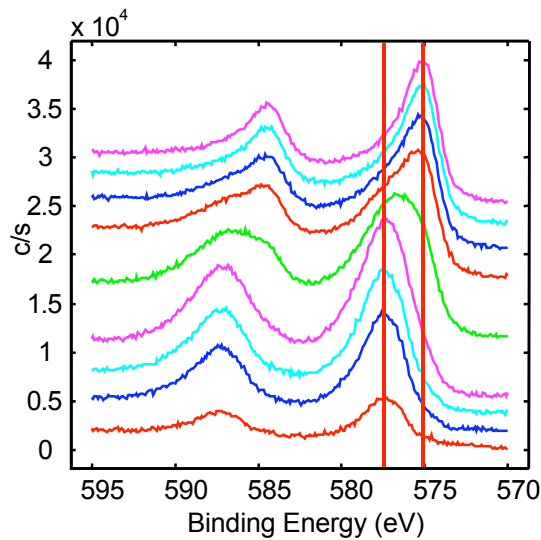


Electrolysis

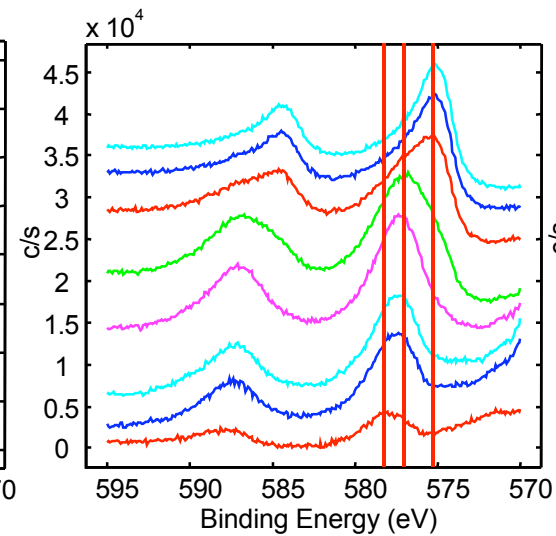


Water adsorption

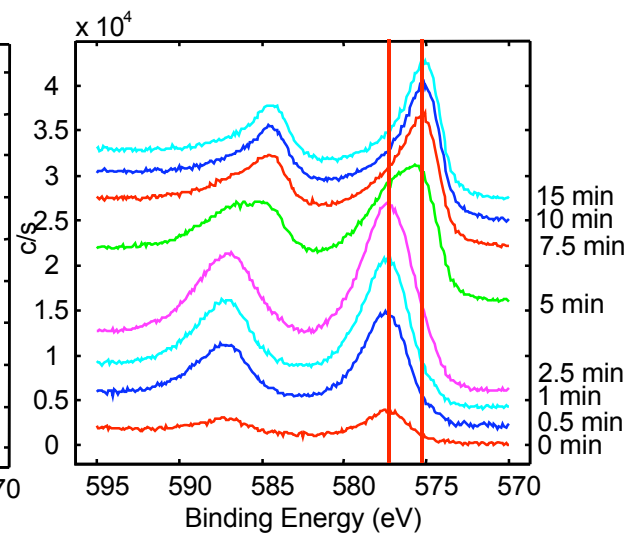
Cr 2p



As received sample

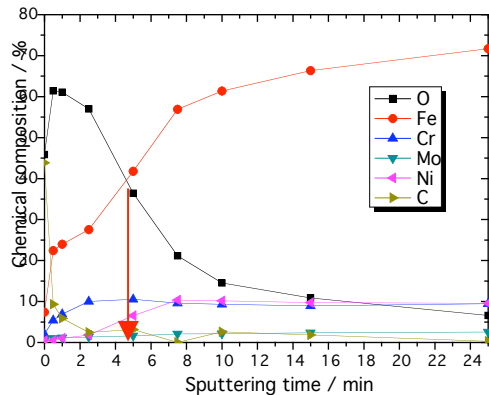


Electrolysis

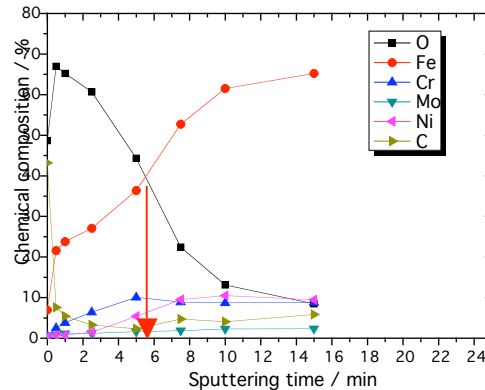


Water adsorption

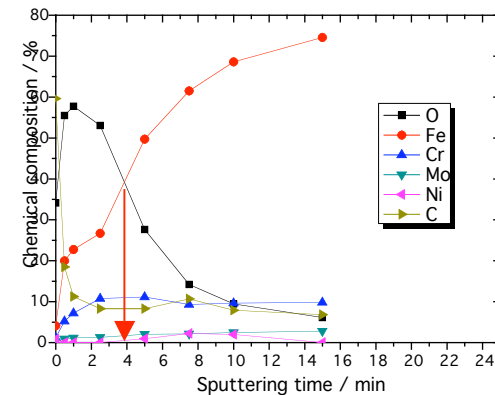
Summary of Depth profile



As received sample



Electrolysis



Water adsorption

A thick oxide layer was observed at the sample with electrolysis.



The existence of oxyhydroxide layer may contribute to the expansion of the oxide layer.

The thickness of the oxide layer of the sample with water adsorption was not so different from as-received sample.

Carbon impurity was accumulated on the surface of the sample.

Conclusions

- The oxyhydroxide was formed on the surface layer and major hydrogen isotopes were trapped by this layer. To decrease tritium retention, this oxyhydroxide layer should be removed. (Surface finish may be one of the key methods.)
- The thickness of Cr oxide layer was larger than that of Fe oxide layer.
- Small amount of dissolved hydrogen isotopes would be desorbed by dissociating the oxide layer.

Deuterium permeation through multilayer sample W-Al₂O₃-Eurofer

D. Levchuk, T. Köck, F. Koch, H. Maier, H. Bolt
Max-Planck-Institut für Plasmaphysik, D-85748 Garching, Germany

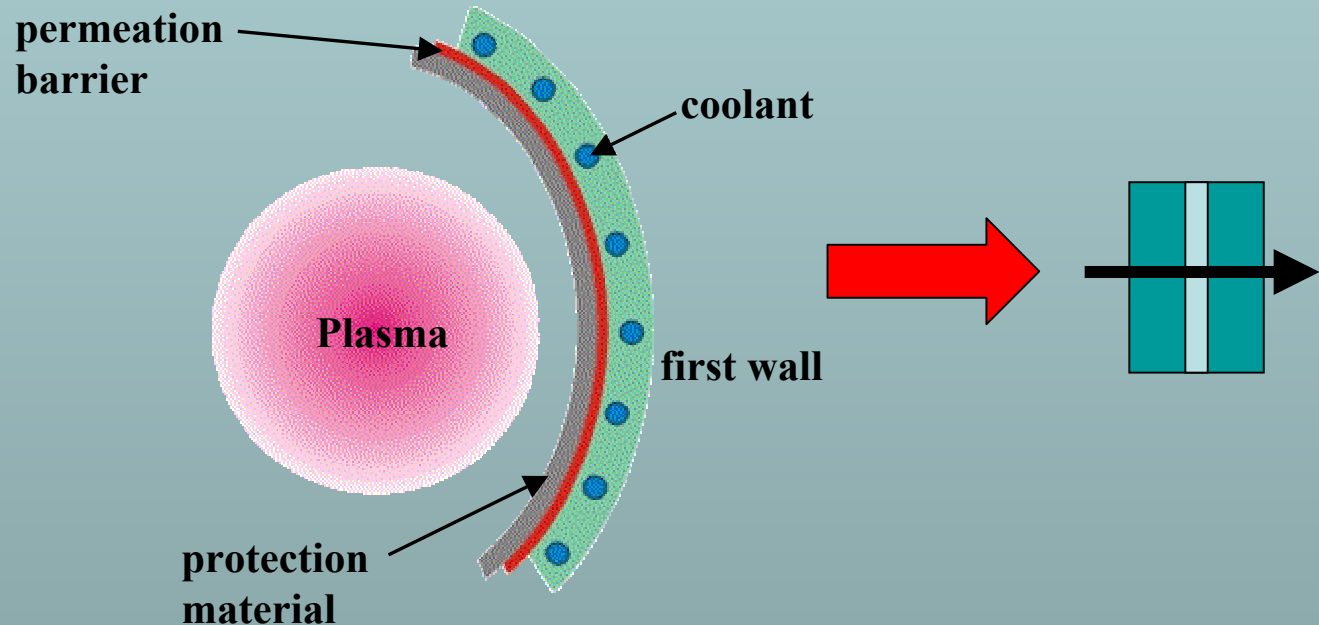
- Motivation
- Experimental details
- Results
- Questions & Future plans

Barrier coatings for reduction of permeability

Literature: Strong surface influence (for alumina)



First wall:
NO surface effects!



Fusion relevant materials testing

Eurofer, tungsten, alumina

Materials compatibility

Different expansion coefficients

Different deposition parameters

Experimental details

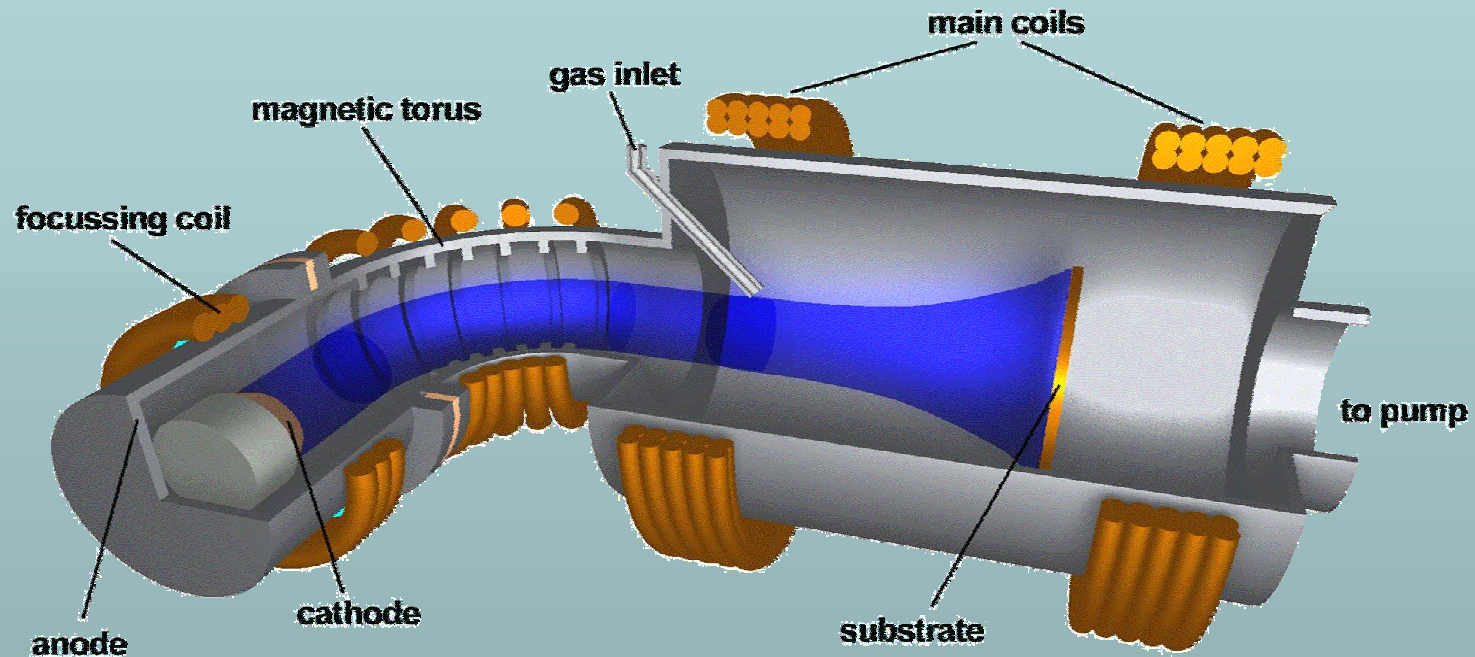
Used samples

- bare Eurofer (0.46 mm)
- α -Al₂O₃ – Eurofer (0.5 μ m / 0.23 mm)
- W – Eurofer (1 μ m / 0.24 mm)
- W – α -Al₂O₃ – Eurofer (1 μ m / 0.5 μ m / 0.27 mm)

Analysis

SEM (surface structure), XRD (crystallinity), EDX (surface contamination with impurities)

Filtered arc deposition facility



Deposition of $\alpha\text{-Al}_2\text{O}_3$: 1000 K in O_2 atmosphere, bias -200 V

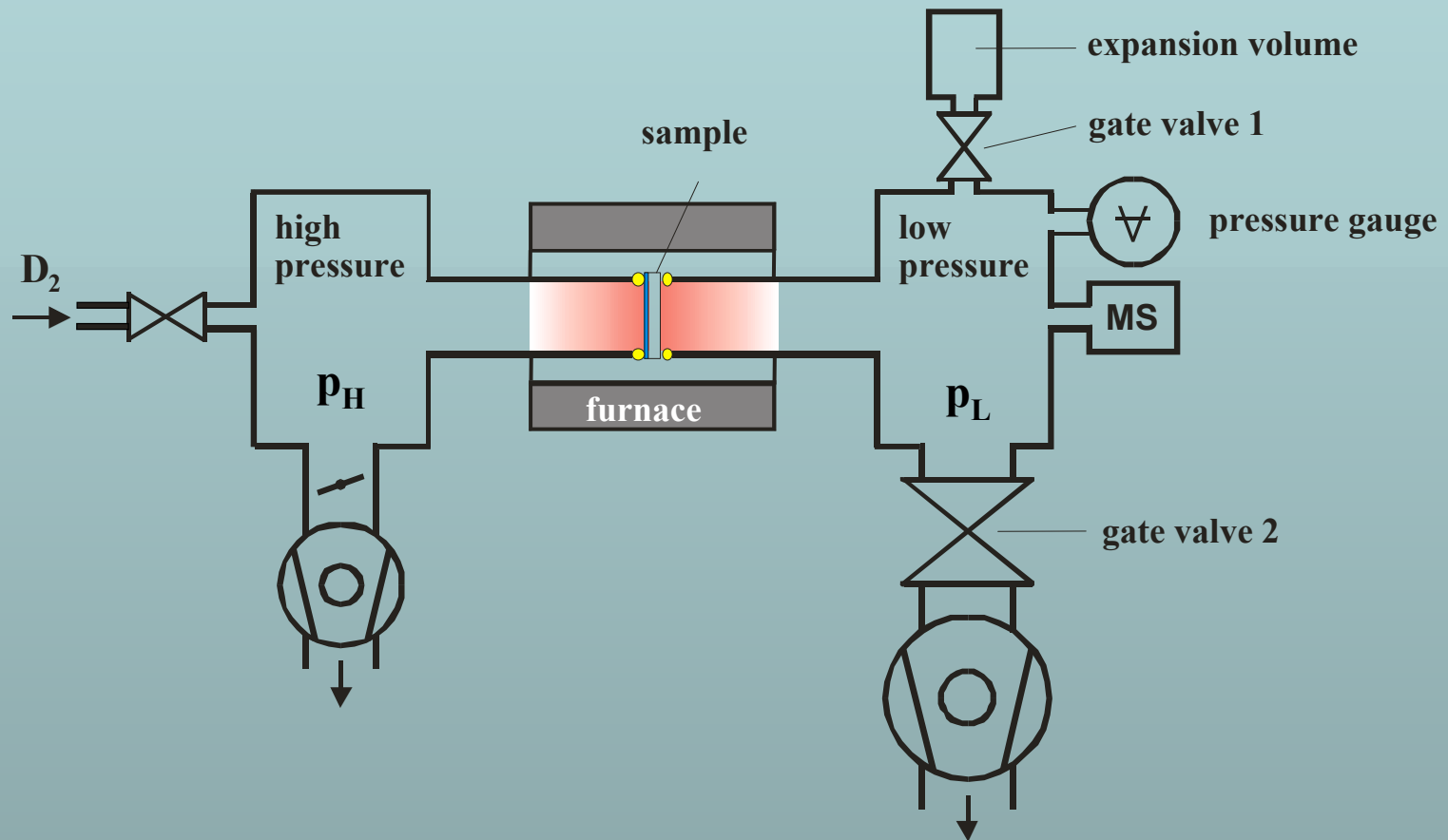
Magnetron sputtering facility



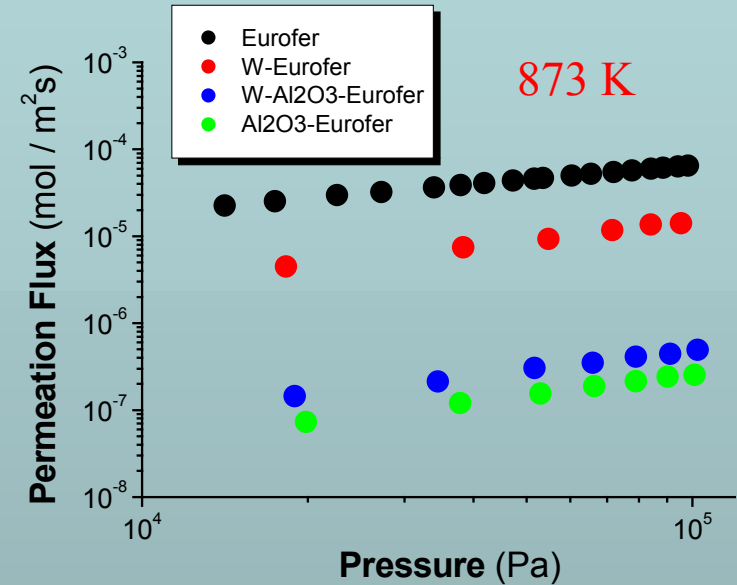
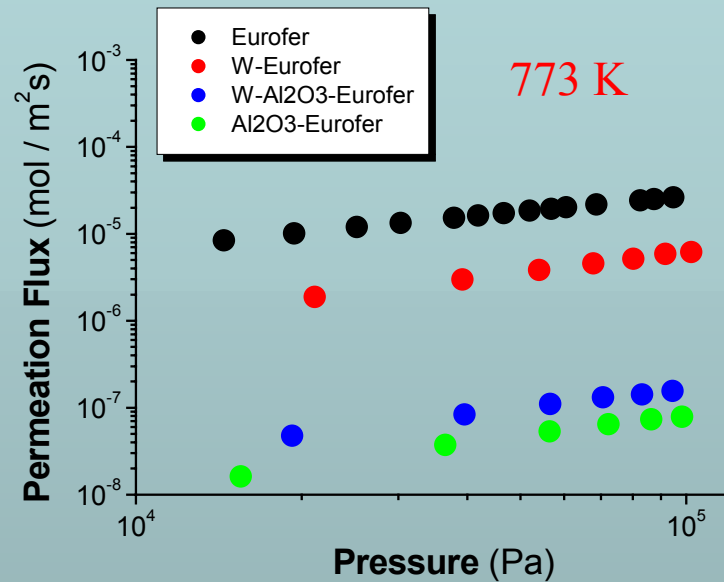
Deposition of W: 470 K

Etching of the back surface from oxide in glow discharge

Permeation facility

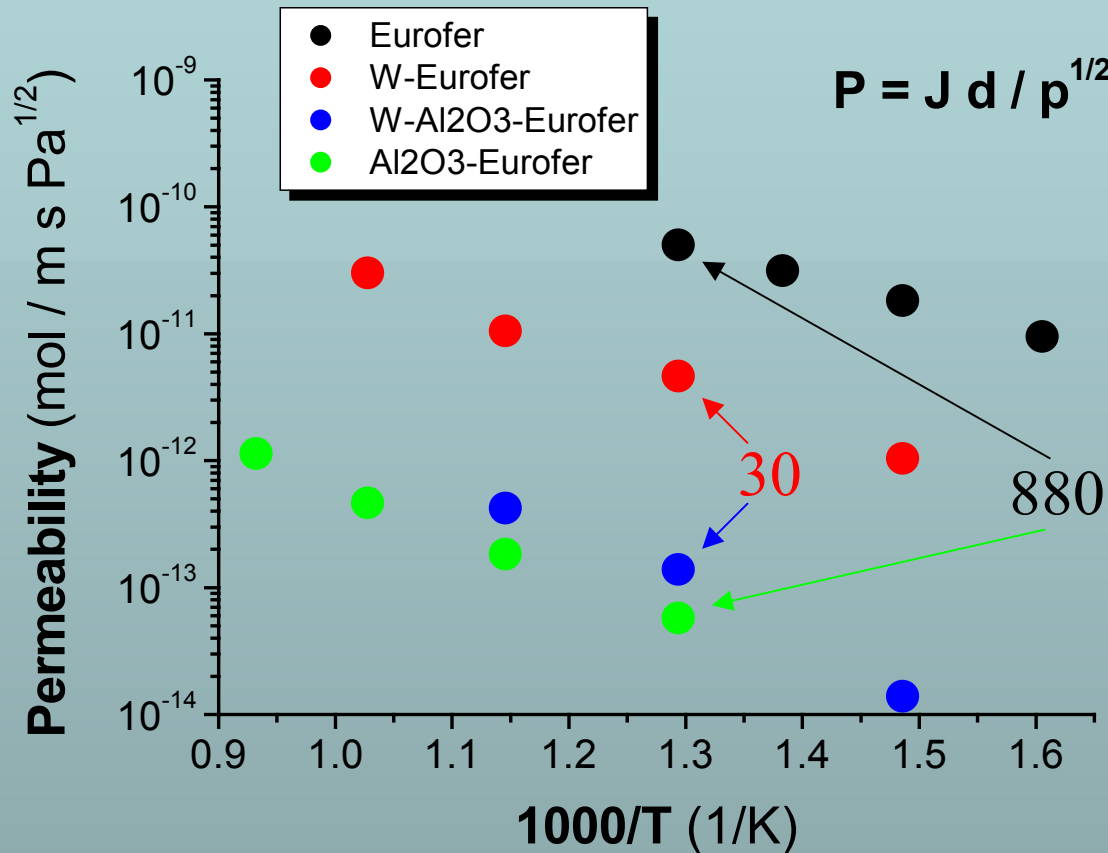


Permeation flux dependence on pressure



Mixed permeation regime for all samples

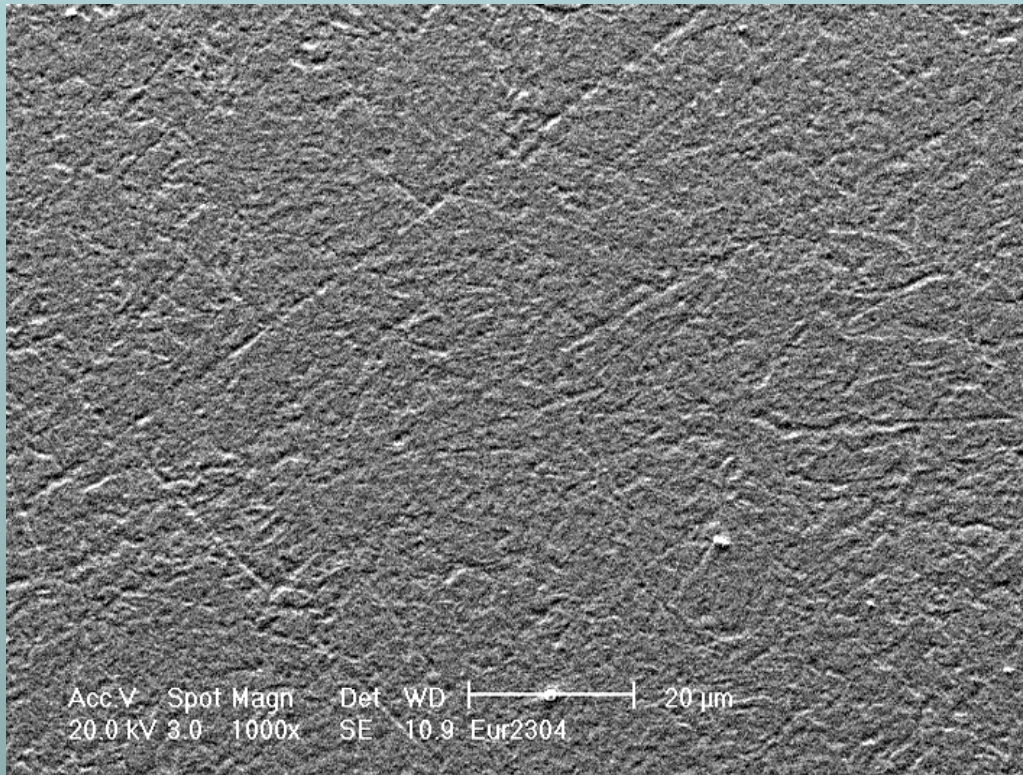
Permeability dependence on temperature



Real reduction factor is **MUCH** lower than reported in literature

Further barrier degradation is possible due to thermal cycle loads

Materials compatibility



Different expansion coefficients

W: 4.5 ppm/K

α -Al₂O₃: 6-7 ppm/K

Eurofer: 10 ppm/K

Different deposition temperatures

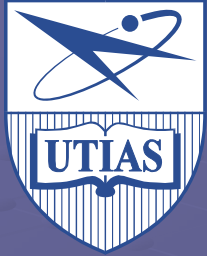
No surface damage after experiments

Open questions

- thicker alumina coating performs significantly better?
- look for another coating or PRF=30 is enough?
- thermal cycle loading influences 3-layer system?

Plans

- test thicker barrier coatings
- thermal loading tests
- irradiation experiments



Helium and Hydrogen Retention in Polycrystalline Tungsten Due to Sequential and Simultaneous Ion Bombardment

J. W. Davis, Heun Lee, R.G. Macaulay-Newcombe and A. A. Haasz

University of Toronto Institute for Aerospace Studies

Overview

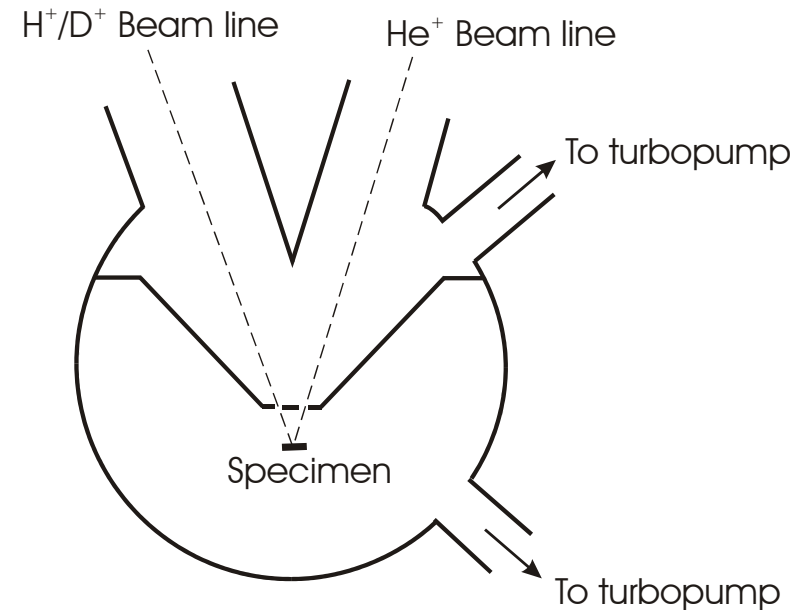
- Introduction
- Experiment
- Review: D^+ retention in PCW
- Results: He^+ retention in PCW
- Results: $He^+ + H^+$ Sequential and Simultaneous Implantation
- Results: $He^+ + D^+$ Sequential and Simultaneous Implantation
- Summary

Introduction

- Plasma-facing materials in future D/T burning fusion reactors will be subjected to large fluxes of both He^+ and D^+/T^+ ions.
- There are many measurements of low-energy D^+ retention in tungsten:
 - While there is not complete agreement amongst various researchers, the general trends are agreed upon.
- Helium is also known to trap in tungsten, although there is much less data available for low-energy implantation.
- Since it is thought that both hydrogen and helium share similar trapping mechanisms in tungsten, it might be expected that multi-species bombardment will lead to an alteration of trapping levels.

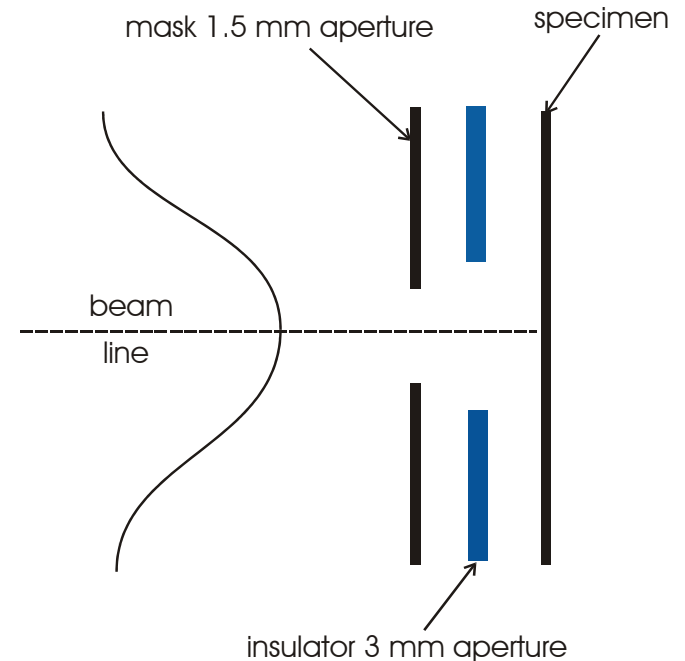
Experiment 1: Ion Implantation

- All specimens were implanted using the UTIAS dual-beam accelerator
- Specimen temperature: 300K
- Ion Energies: 500 eV/He⁺
500 eV/H⁺ or D⁺
- Fluxes: $\sim 3 \times 10^{19}$ (H⁺ or D⁺)/m²s
 $\sim 5 \times 10^{17}$ He⁺/m²s



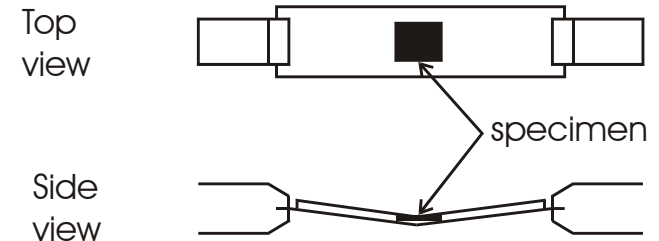
Experiment 2: Specimens

- Rembar hot-rolled, 25 μm thick polycrystalline W foil, 99.95 wt%
- Specimens $\sim 8 \times 8 \text{ mm}^2$, annealed at 1500K for 30 min.
- Specimen holder allows specimens to be implanted through a mask to define beam area

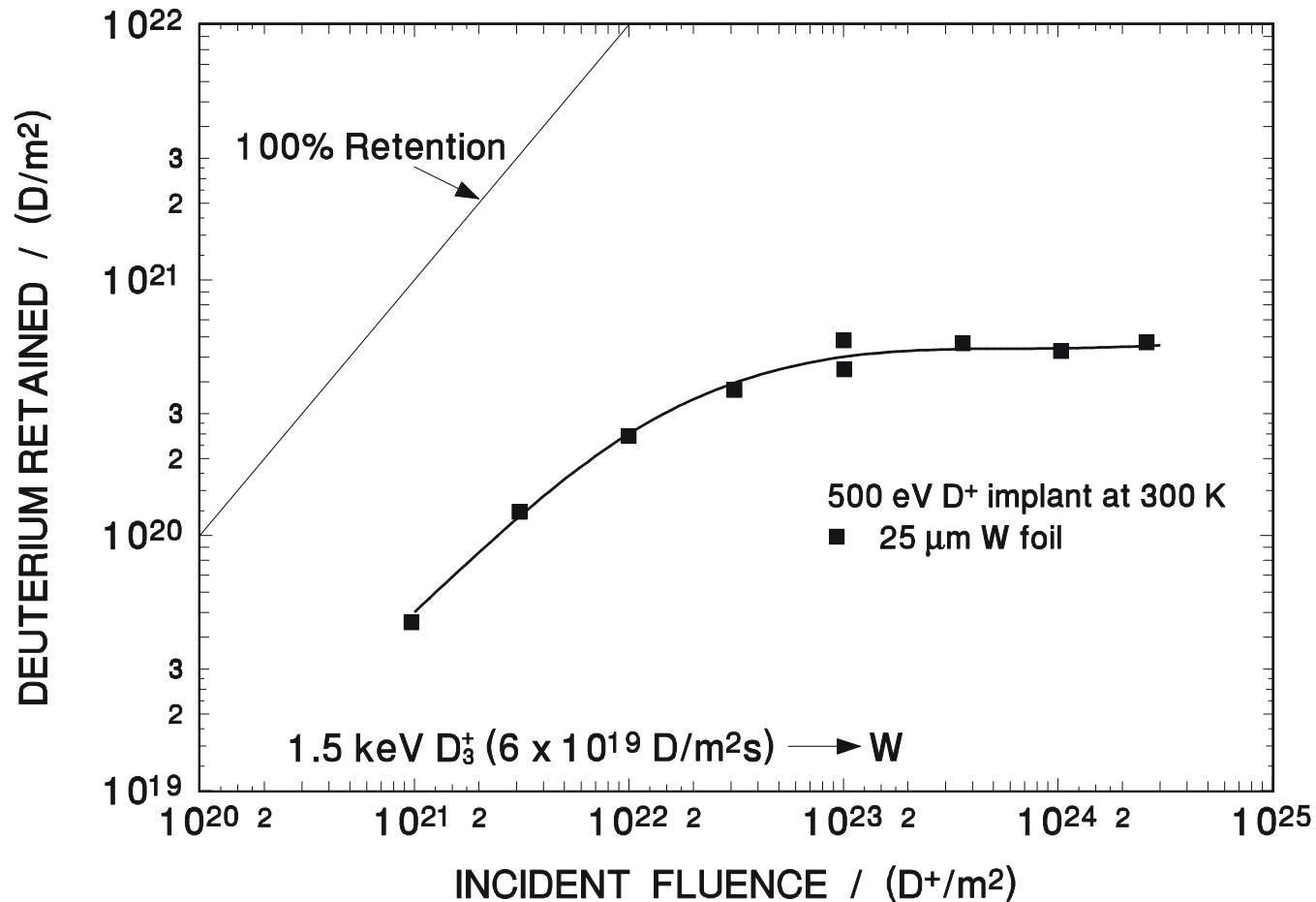


Experiment 3: Thermal Desorption

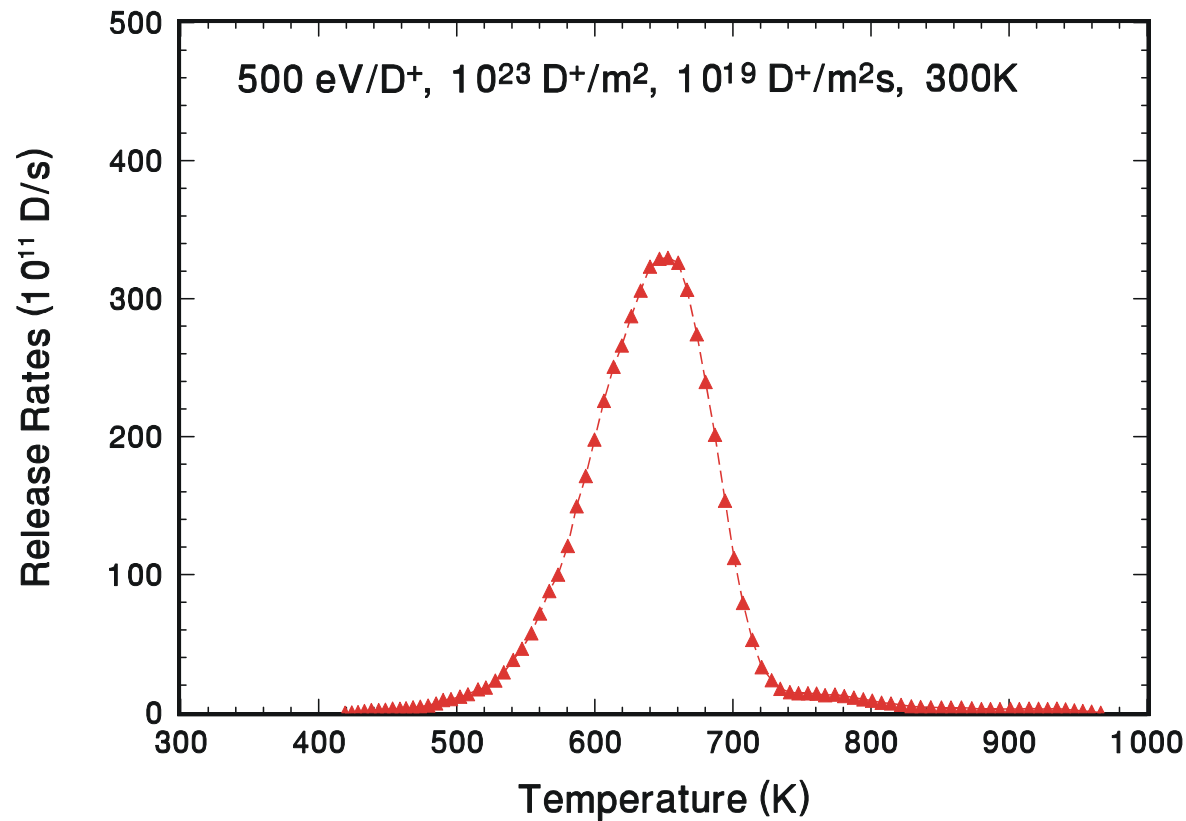
- Baked UHV system
- Hiden quadrupole mass spectrometer used to monitor M2, M3, M4 and M20 in residual gas
- Absolute calibration for D₂
- Specimens placed on a resistively heated tungsten boat
- Temperature measured by W/Re thermocouple
- Ramping rate ~ 3-4 K/s



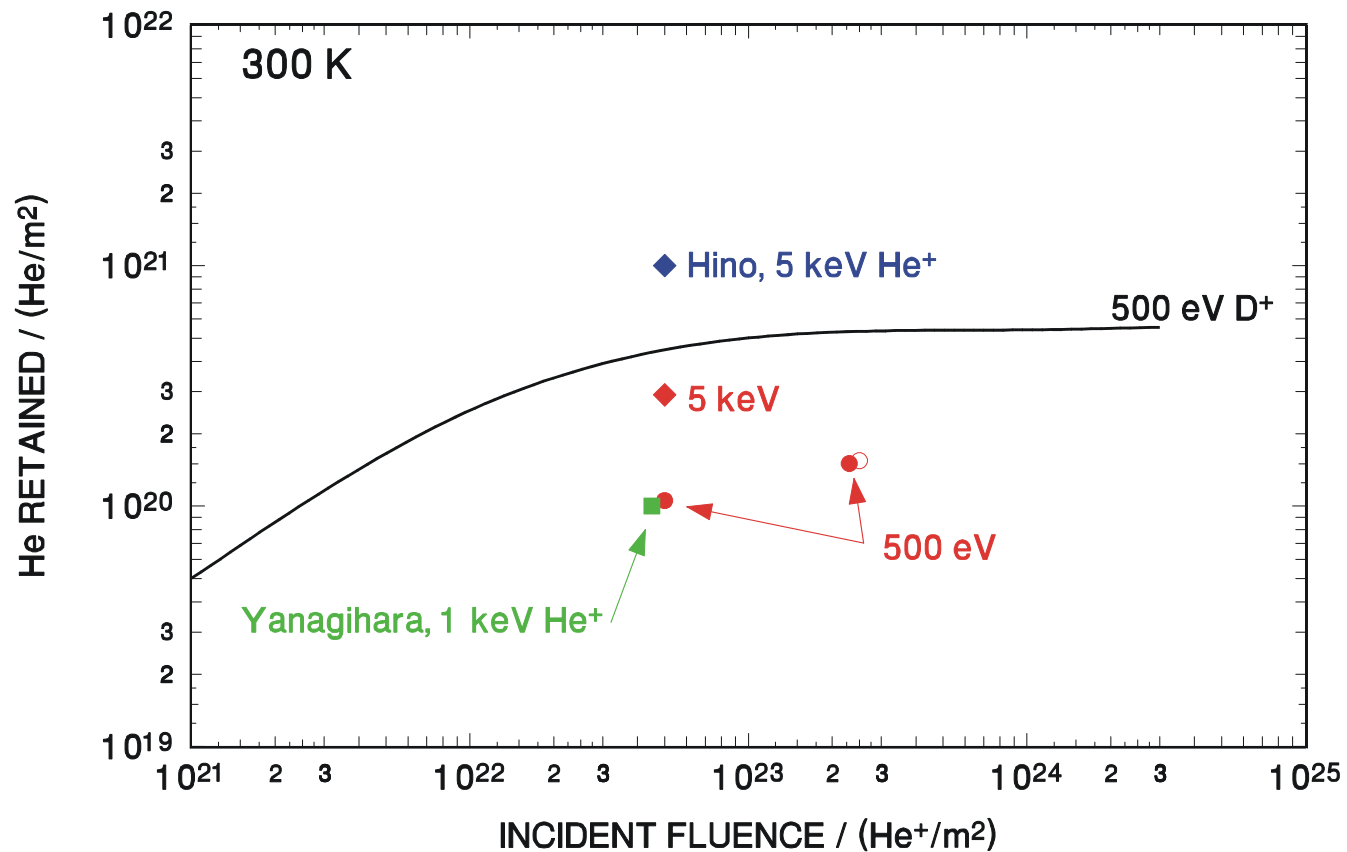
Review 1: D⁺ Retention in Polycrystalline W



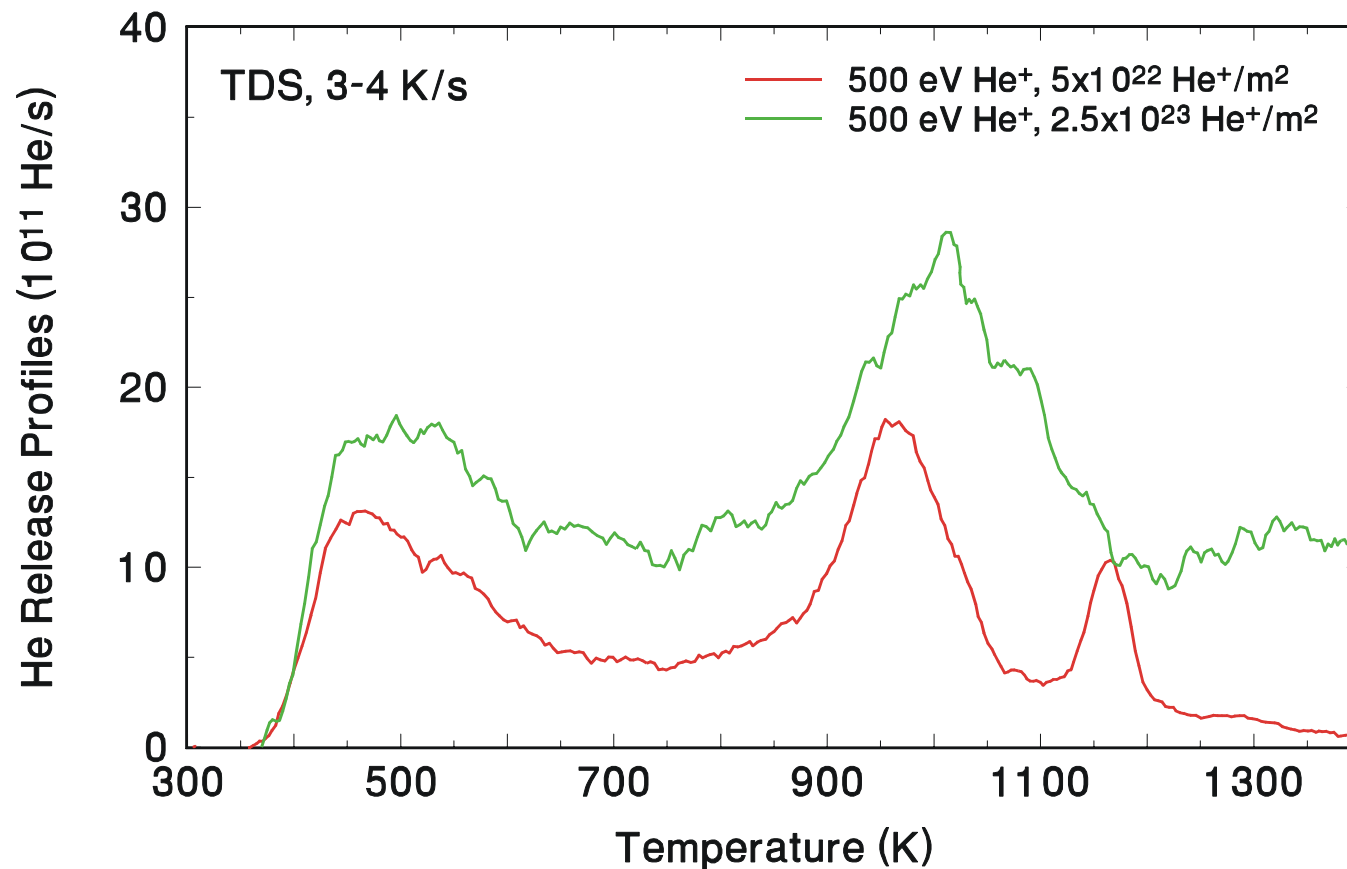
Review 2: D⁺ Retention in Polycrystalline W



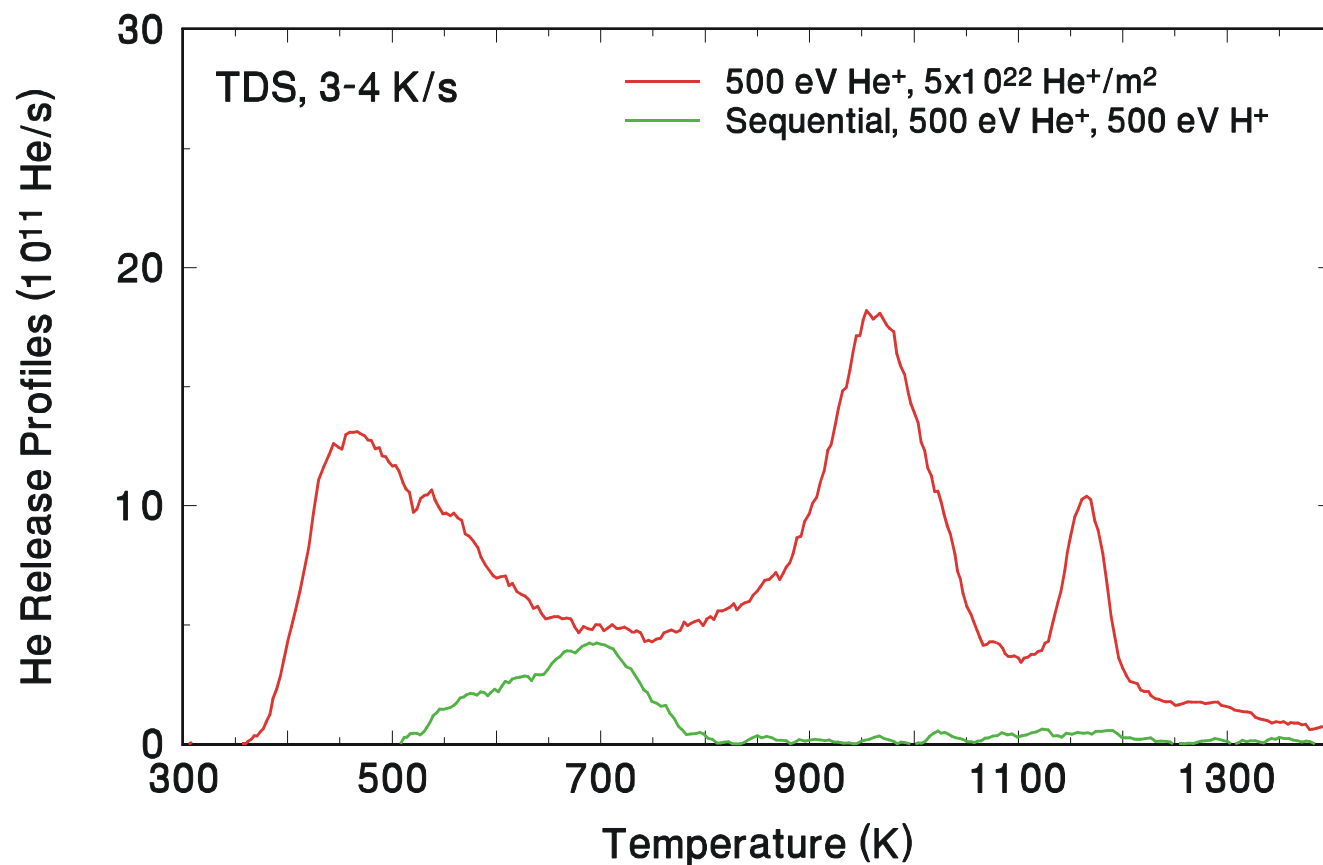
Results 1: He⁺ Retention in Polycrystalline W



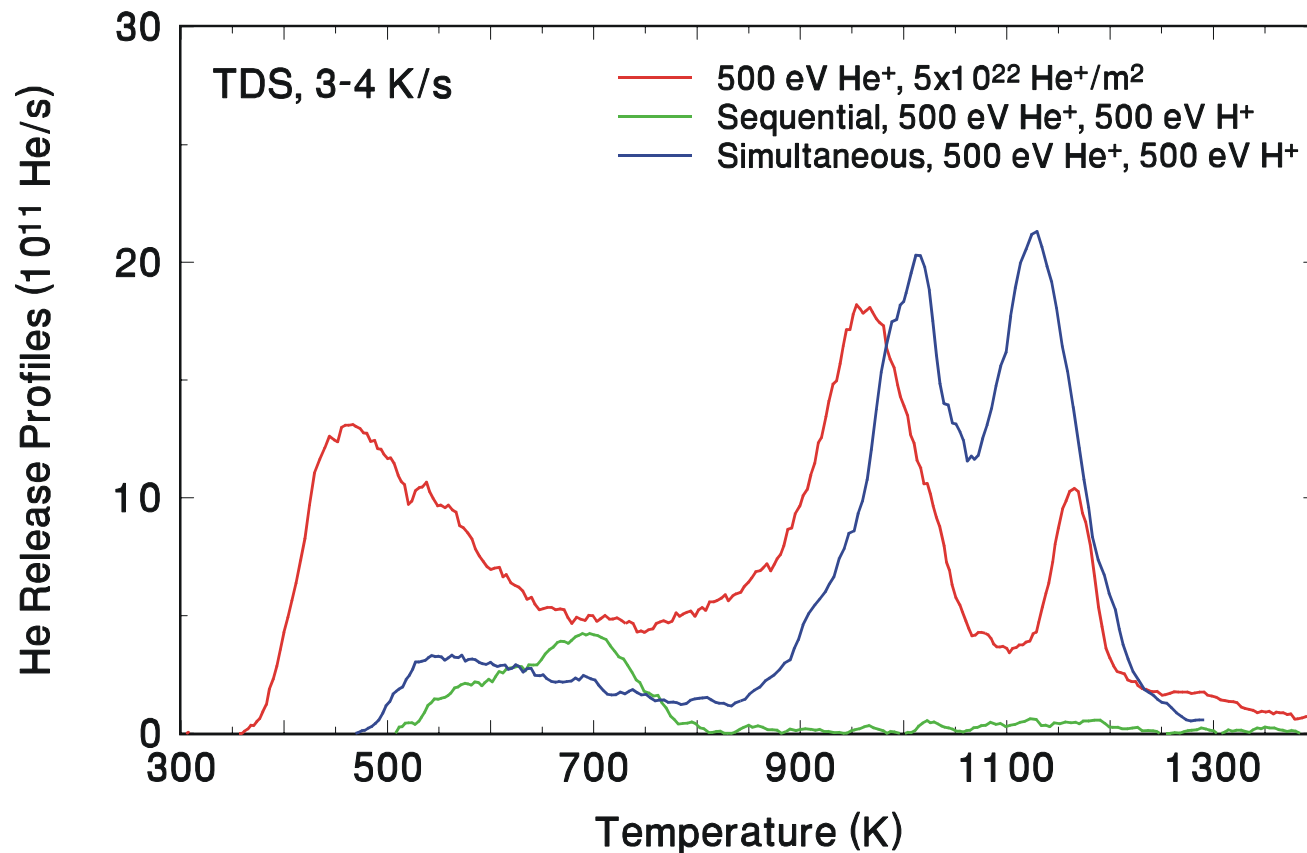
Results 2: He⁺ Retention in Polycrystalline W



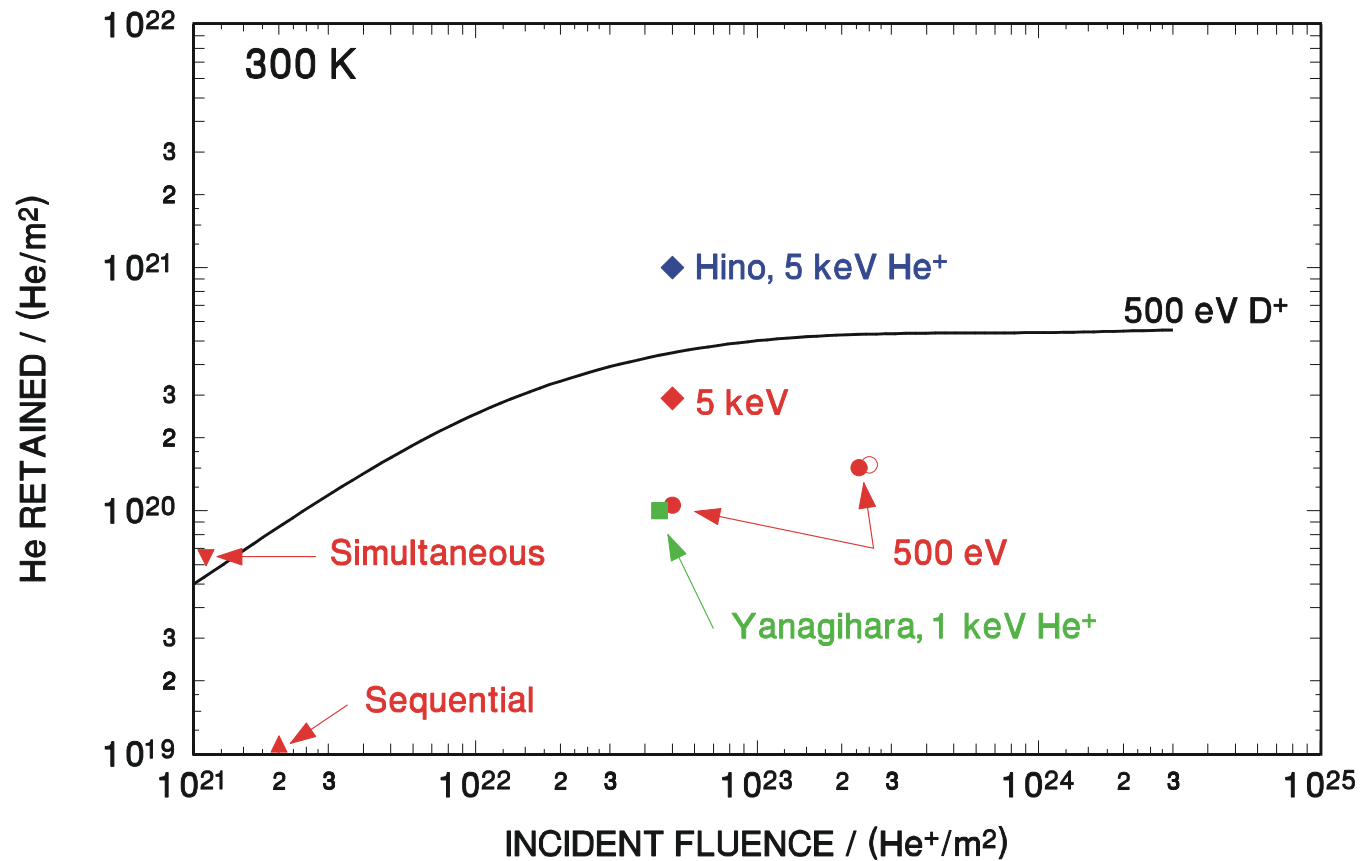
Results 3: Sequential He⁺ and H⁺ implantations



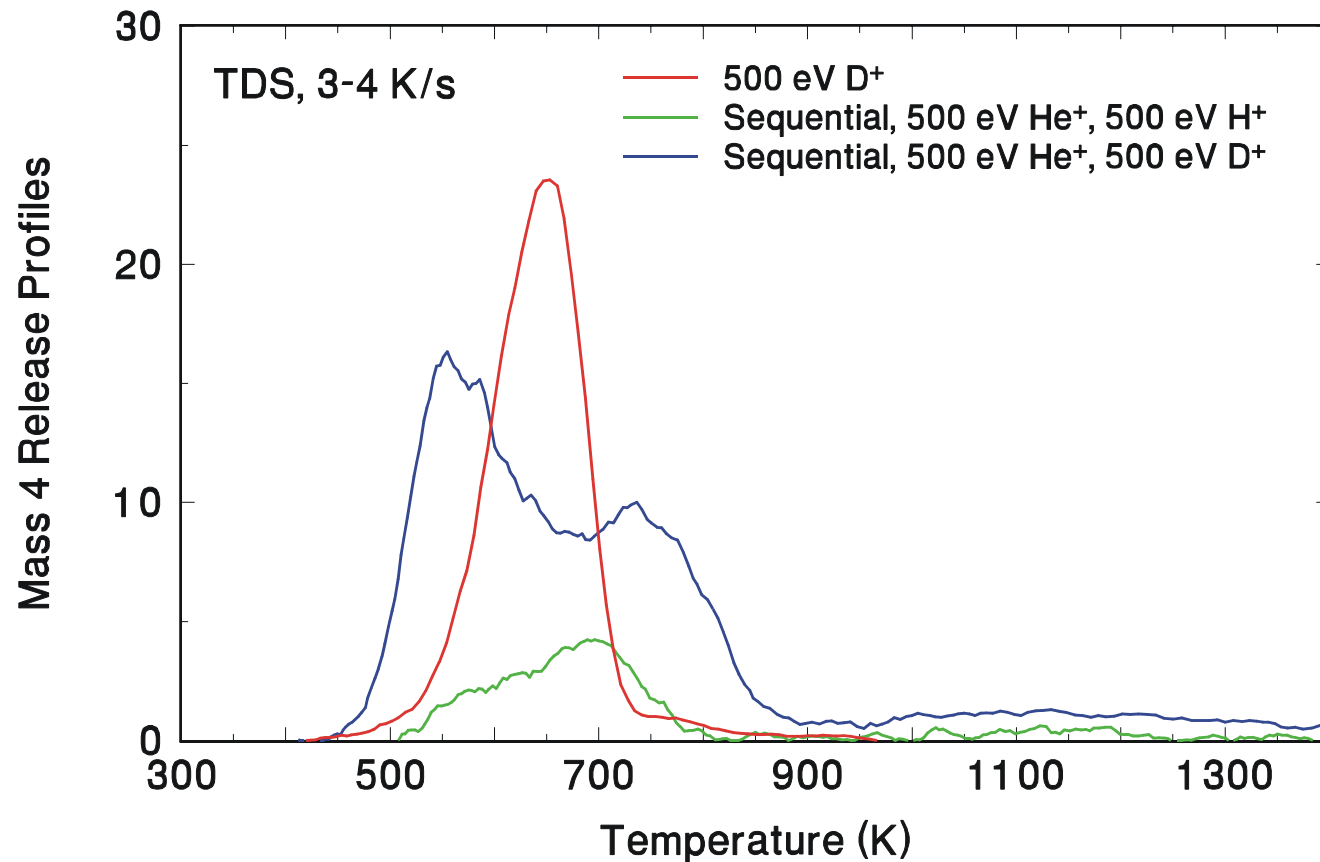
Results 4: Simultaneous He⁺ and H⁺ implantations



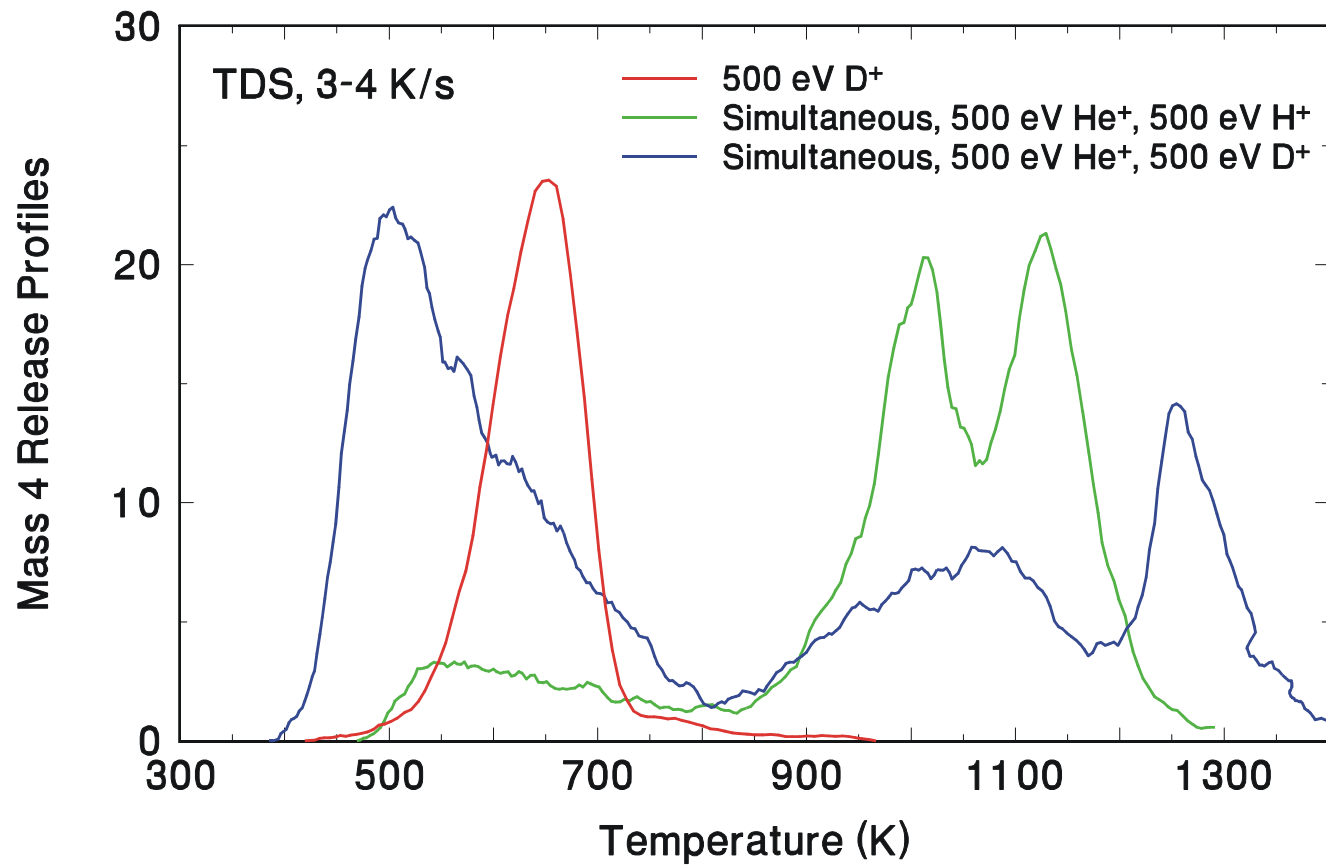
Results 5: He⁺ and H⁺ implantations



Results 6: Sequential He⁺ and D⁺ implantations



Results 7: Simultaneous He⁺ and D⁺ implantations



Summary

- Preliminary measurements have been made for the sequential and simultaneous implantation of helium and hydrogen in polycrystalline tungsten.
- In both sequential and simultaneous cases, substantial differences are observed in the desorption temperatures for both helium and hydrogen.
- Future work will involve similar measurements with different fluences and implantation temperatures.

Influence of gas content in the near surface layers on sputtering the metals under irradiation by H^+ , He ions with a mean energy of 10 and 20 keV

N.V.Volkov, B.A.Kalin

Moscow Engineering-Physics Institute
(State University)

•The plan of the report

•Introduction

Methods and equipment for implantation, parameters

Application of a polyenergy irradiation, advantage

Methods, simulating an irradiation by a polyenergy ion beam

Materials and conditions of an irradiation

•Methods of research

Sputtering of massive samples and films on them

Formation of topography of a surface

Introduction of the film atoms (mono- and multi layer films)

Distribution of the introduced atoms on depth of a massive samples

Change of the characteristics of a materials:

sputtering yield, microhardness, reflective ability,

formation an intermetallic compound in a body of a matrix,

The plan of the report

•Experimental results

Sputtering of massive samples and films on them, formation of a surface topography,

Implantation of film atoms (singl- and multi- layer films)

Distribution of the doped atoms in samples

Change of the characteristics of a material:

sputtering yield, microhardness, reflective ability,
formation an intermetallic compound in a body of a matrix,
wear resistant, corrosion resistance, structure oxide films

■Discussion of results

Sputtering of a «multilayer film - polycrystalline substrate» systems

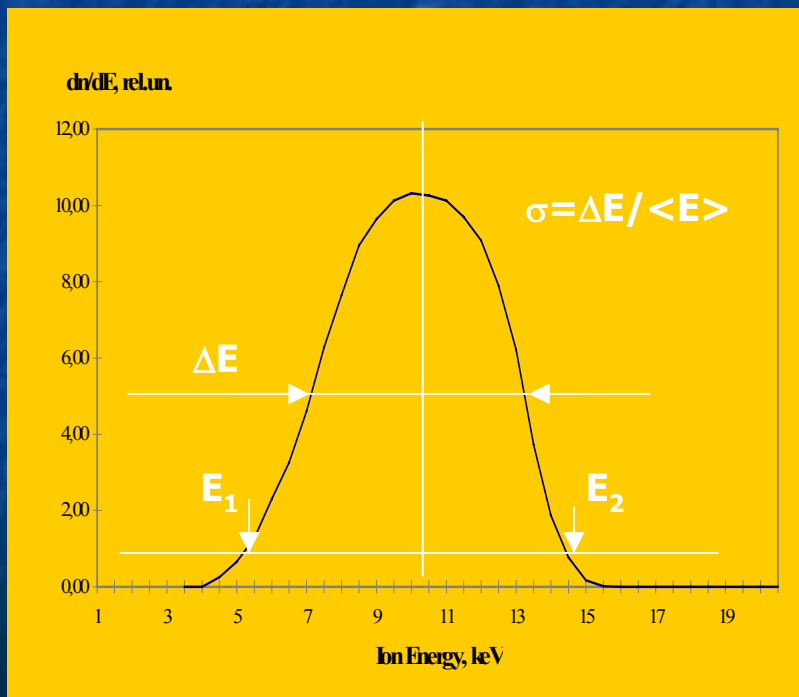
Ion mixing of a «multilayer film - polycrystalline substrate» systems

Influence of physicochemical interaction on migration of the atoms

•Conclusion

Methods and equipment for implantation, parameters

The energy distribution of the ions in a beam, parameters



The basic parameters of irradiation

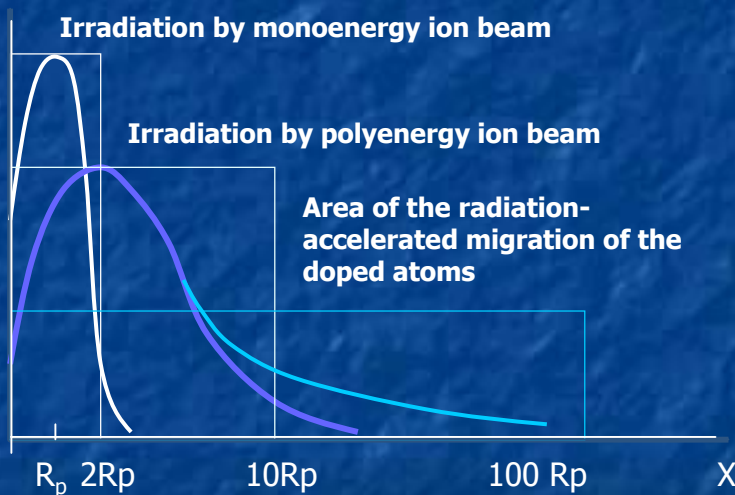
Type of ions.....	$\text{H}^+, \text{He}^+, \text{N}^+, \text{Ar}^+$
Energy.....	10... 300 keV
Ion current (flax).....	1 mkA – 1 A
Fluence.....	$10^{16} - 10^{18} \text{ ion/cm}^2$
Angle of irradiation.....	0 – 45°
Temperature of a sample.....	20 – 300 °C
Pressure of residual gases.....	$10^{-4} - 10^{-8} \text{ Pa}$
Partial pressure.....	$< 10^{-10} \text{ Pa}$

The time characteristics

pulse time.....	$\tau_{\text{pulse}} = \text{un.ms} - \text{un.mks}$
time of forward front of a pulse....	$\approx 0,1 \tau_{\text{pulse}}$
Time of back front of a pulse.....	$\approx 0,1 \tau_{\text{pulse}}$
Ratio.....	$Q = T \setminus \tau_{\text{pulse}}$
The type of an energy distribution of ions in beam	
Mean energy of ions in a beam	$\langle E \rangle$
Wide of energy distribution.....	$E_1 - E_2$
Wide on half-height of energy distribution.....	ΔE
Relative width of distribution.....	$\sigma = \Delta E / \langle E \rangle$

Application of a polyenergy irradiation, advantage

$C(x)$, rel. un.



Decrease of specific power loading
 $F_q \approx E_i/x$ [eV/nm]

More uniform distribution of the doped atoms on depth in a matrix

Decrease of internal mechanical pressure in a doped zone

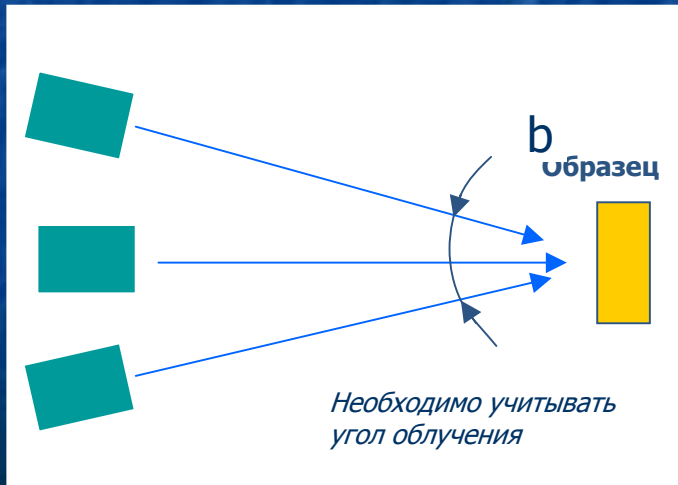
Formation of distribution of the doped atoms

$$C(x) = \frac{D}{2\pi \cdot \Delta R_p} \times \exp\left(-\frac{(x - R_p)^2}{2\Delta R_p^2}\right)$$

Simulating an irradiation by a ion polyenergy beam

$$C(x) = \frac{D}{2\pi \cdot \Delta R_p} \times \exp\left(-\frac{(x - R_p)^2}{2\Delta R_p^2}\right)$$

$$C(x) = \sum_{j=1}^n C(x)_i$$



Change of energy of ions in beam (change of accelerating potential)

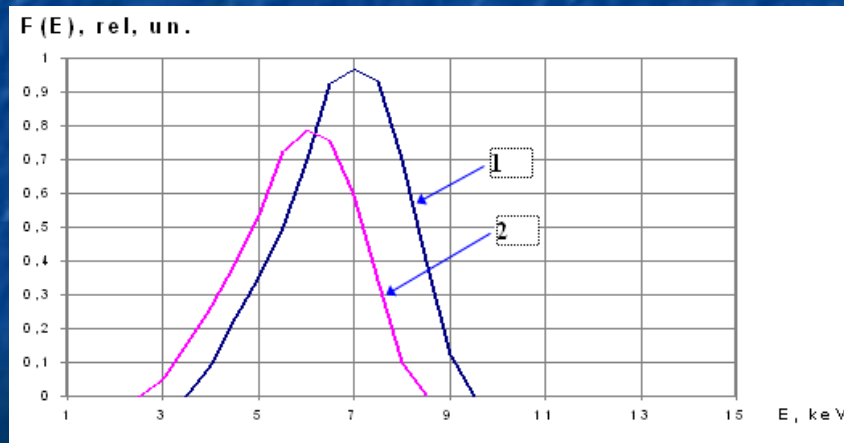
Change of a angle of an irradiation

Application of a filters (thin films)

Application of several accelerating systems (two and three пучковые accelerators of ions)

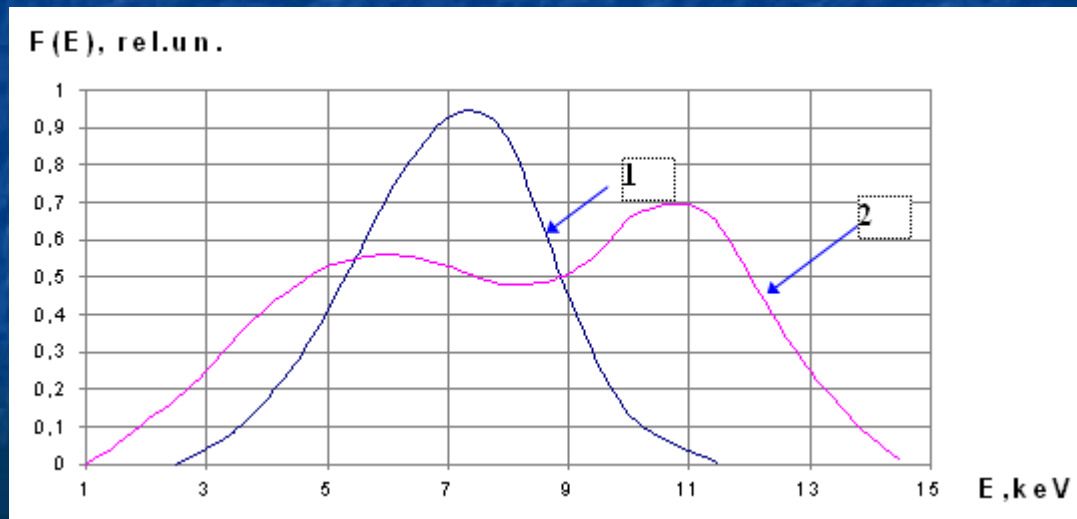
Instalation T-4

- The energy spectrum of He⁺ ions bombarding the first wall of the instalation T-4: 1- the mean energy of ions $\langle E \rangle = 7$ keV, the temperature of plasma $T_{pl} \approx 0$ eV; 2 - the mean energy of ions $\langle E \rangle = 6.3$ keV, the temperature of plasma $T_{pl} = 100$ eV



Instalation 2XIIB

The energy spectrum of He^+ ions bombarding the first wall in the instalation 2XIIB: 1- the mean energy of ions $\langle E \rangle = 8 \text{ keV}$, the temperature of $T_{\text{pl}} \approx 0 \text{ eV}$; 2 – the mean energy of ions $\langle E \rangle = 10 \text{ keV}$, the temperature of plasma $T_{\text{pl}} = 100 \text{ eV}$



Purpose of the work

To reveal laws of doped atoms from multilayer films in a polycrystalline substrate at an irradiation by a ion beams with a wide energy spectrum

Polyenergy ion beam

Type of ions.....	H ⁺ , He ⁺ and Ar ⁺
Mean energy of ion beam.....	10; 20 keV
Wide of energy distribution	1 – 17; 2 - 30 keV
Ion current.....	10 – 50 μ A
Pressure in the working chamber.....	< 1×10^{-5} Pa
Temperature of an irradiation.....	50-150 $^{\circ}$ C
Fluence.....	$(1-100) \times 10^{17}$ ion/sm ²

Materials

monocrystal: C, Si, Cu, Mo, W

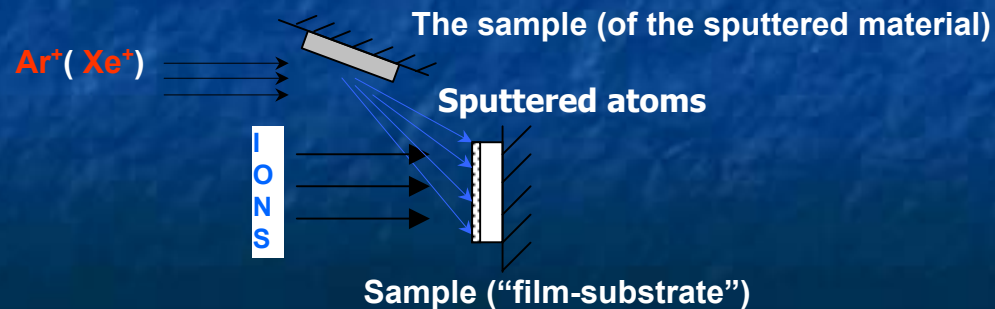
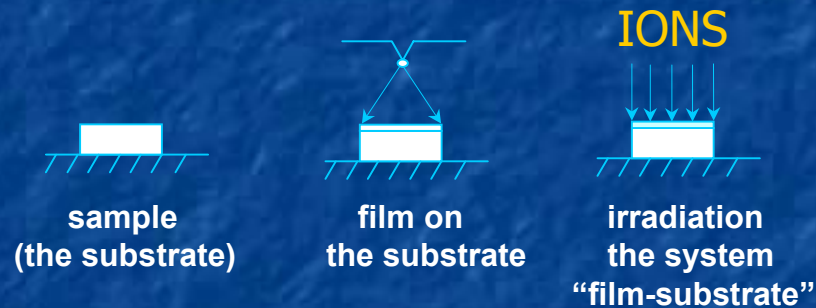
polycrystal:

Be, Al, Ti, Fe, Cu, Zr, Mo, W, Steels 12X18H10T, 0X16H15M3Б

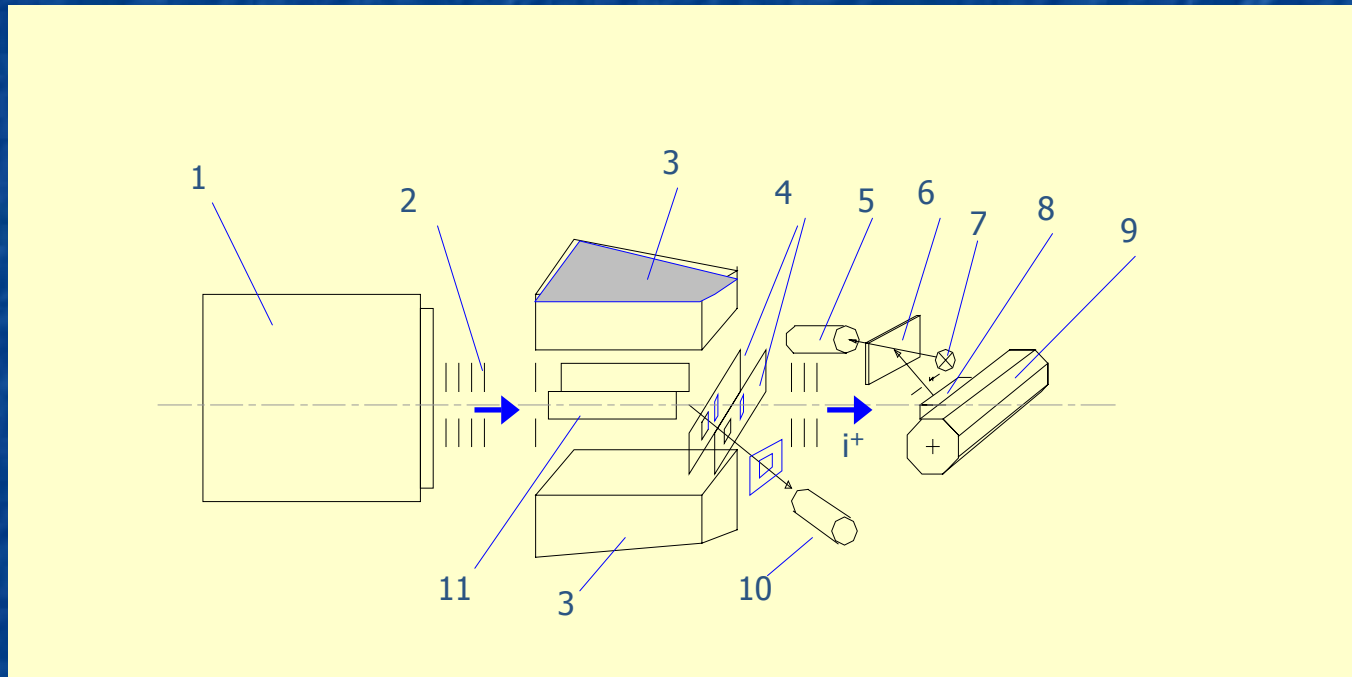
Таблица данных матриц для расчета радиационно стимулированного проникновения внедренных атомов вглубь мишени.														
		40Ar	9Be	12C	27Al	28Si	50Ti	51V	56Fe	59Ni	64Cu	91Zr	96Mo	119Sn
Решетка			Гекс	Алм	ГЦК	Алм			ОЦК	ГЦК	ГЦК	Гекс	ОЦК	#####
га, нм		0,192	0,113	0,077	0,143	0,118			0,126	0,124	0,128	0,16	0,14	0,158
Саг, нм ²		0,115753	0,040095	0,018617	0,06421	0,043721	0	0	0,049851	0,048281	0,051446	0,080384	0,061544	0,078387
V ат		0,029633	0,006041	0,001911	0,012243	0,006879	0	0	0,008375	0,007982	0,00878	0,017149	0,011488	0,016514
а, нм			0,229	0,357	0,405	0,543			0,287	0,352	0,361	0,323	0,315	
а/с														
Е, ГПа			300	1140	70	140			200	210	120	90	320	
п			0,03		0,31	0,44			0,28	0,35	0,38	0,35	0,31	
г, г/см ³			1,85	3,5	2,7	2,33	4,5	5,96	7,87	8,91	8,96	6,45	10,22	6
N x10 ²² , см ⁻³			12,3	11,3	6,03	5,19	5,7	7,2	8,49	9,13	8,47	4,25	6,4	3,7
М, аем		40	9	12	27	28	50	51	56	59	64	91	96	119
Vэл.об., нм ³			0,0081	0,0057	0,0166	0,02	0,0185	0,0141	0,0118	0,011	0,012	0,0234	0,0156	0,032
а, нм			0,201	0,179	0,255	0,272	0,265	0,242	0,228	0,223	0,229	0,286	0,25	0,318
Δα=1.41α-2ρα		1	0,05741	0,09839	0,07355	0,14752			0,06948	0,06643	0,06689	0,08326	0,0725	0,13238
Δs=a2-pra^2		1	0,000306	0,013424	0,000815	0,030263			0,002133	0,001448	0,000995	0,001412	0,000956	0,022737
ΔV=V-4/3pra^3		1	0,002059	0,003789	0,004357	0,013121			0,003425	0,003018	0,00322	0,006251	0,004112	0,015486

Materials (**films**)

Monocrystal: C, Si, Cu, Mo, W **Polycrystal:** Be, Al, Ti, Fe, Cu, Zr, Mo, W,



Installation VOKAL



A scheme of the installation VOKAL to investigate the ion beam action with a wide energy spectrum: 1- an ion source, 2- an accelerating tube, 3- poles of Vina's separator electromagnet, 4- apertures, 5- a photodiode, 6- a glass collector to accumulate sputtered atoms, 7- a photometric lamp, 8- an irradiated sample, 9- a mechanism to change samples (a massive cylinder), 10- a faraday cylinder for measuring the current of an ion beam, 11- electrodes to form an electric field in Vina's separator

Methods of research

Measurement of a sputtering yield of the samples
by step, photometry of sputter layer

Topography of surface samples

SEM, optical microscopy

Measurement of a distribution doped atoms

RBS H^+ and He^+ ions with start energy $E_0 = 1,6 \text{ MeV}$

SIMS HP-660 (USA)

Auger-spectroscopy (Oxford-Link)

Sputtering of the massive samples

Sputtering yield of the materials, at/ion

Material of samples		Be		Ti	
Ion	T, °C	20	500	20	500
H^+		$(1.0 \pm 1.0) \times 10^{-2}$	$(1.5 \pm 1.0) \times 10^{-2}$	$(8 \pm 1) \times 10^{-4}$	
He^+		$(9.0 \pm 1.0) \times 10^{-2}$	$(10.0 \pm 1.0) \times 10^{-2}$	$(1.1 \pm 0.5) \times 10^{-2}$	$(1.3 \pm 0.5) \times 10^{-2}$
$H^+ + He^+$		$(5.0 \pm 1.0) \times 10^{-2}$	$(6.0 \pm 1.0) \times 10^{-2}$	$(6.1 \pm 0.5) \times 10^{-3}$	$(6.5 \pm 0.5) \times 10^{-3}$
Ar^+		4.0 ± 1.0	4.0 ± 1.0	4.0 ± 1.0	4.0 ± 1.0
$He^+ + Ar^+$		2.0 ± 1.0	-	2.0 ± 1.0	2.0 ± 1.0

Sputtering of the massive samples, at/ion

Material of samples		Fe		Cu	
Ion	T, °C	20	500	20	500
H ⁺		$(4 \pm 1) \times 10^{-3}$	$(4.3 \pm 1) \times 10^{-3}$	$(5 \pm 1) \times 10^{-3}$	
He ⁺		$(8 \pm 0.7) \times 10^{-2}$	$(10.0 \pm 1.0) \times 10^{-2}$	0.4 ± 0.1	0.4 ± 0.1
H ⁺ +He ⁺		$(4.1 \pm 0.5) \times 10^{-2}$	$(5.5 \pm 0.5) \times 10^{-2}$	0.2 ± 0.1	
Ar ⁺		4.0 ± 1.0	4.0 ± 1.0	6.0 ± 1.0	7.0 ± 1.0
He ⁺ +Ar ⁺		2.0 ± 1.0	-	4.0 ± 1.0	4.0 ± 1.0

■ **Table 1**

- Sputtering coefficients (S_p , at./ion) of a number of materials under irradiation by a polyenergetic ion beam with a mean energy of 10 keV

	Material of samples				
Ions	Be	Fe	Cu	Mo	W
H^+	$(1.0 \pm 0.5) \times 10^{-2}$	$(4.0 \pm 1.0) \times 10^{-3}$	$(1.0 \pm 0.5) \times 10^{-2}$	$(3.7 \pm 0.5) \times 10^{-3}$	$(9.0 \pm 1.0) \times 10^{-4}$
He^+	$(9.0 \pm 1.0) \times 10^{-2}$	$(8.0 \pm 0.7) \times 10^{-2}$	$(4.0 \pm 0.5) \times 10^{-1}$	$(2.0 \pm 1.0) \times 10^{-2}$	$(3.0 \pm 0.5) \times 10^{-2}$
$H^+ + He^+$	$(5.0 \pm 1.0) \times 10^{-2}$	$(4.1 \pm 0.5) \times 10^{-2}$	$(2.1 \pm 0.5) \times 10^{-1}$	$(1.1 \pm 0.3) \times 10^{-2}$	$(1.7 \pm 0.2) \times 10^{-2}$

Sputtering of the massive samples

Maximum of the sputtering yield (Sp_{max} , at/ion) for alloys irradiation by H^+ , He^+ and Ar^+ , $\sigma = 40\%$, $T = 20^\circ C$.

Alloys	V-10%Ti	V-20%Ti	V-30%Ti	0X16H15M3B	12X18H10T
Ions					
$H^+ - He^+$	0.093^\pm	0.09^\pm	0.087^\pm	0.018^\pm	0.022^\pm
$H_{tot}=2.5$ a.u.m.	± 0.01	± 0.01	± 0.01	± 0.01	± 0.01
$\langle E \rangle$, keV	3.5	3	3	4	4
$He^+ - Ar^+$	0.55 ± 0.1	0.55 ± 0.1	0.58 ± 0.1	0.21 ± 0.1	0.24 ± 0.1
$M_{tot} = 22$ a.u.m.					
$\langle E \rangle$, keV	7	7	7	6	6
$H^+ - He^+ - Ar^+$	0.34 ± 0.1	0.40 ± 0.1	0.41 ± 0.1	0.13 ± 0.1	0.13 ± 0.1
$M_{tot} = 15$ a.u.m.					
$\langle E \rangle$, keV	4	4	4	4.5	4.5

The note:

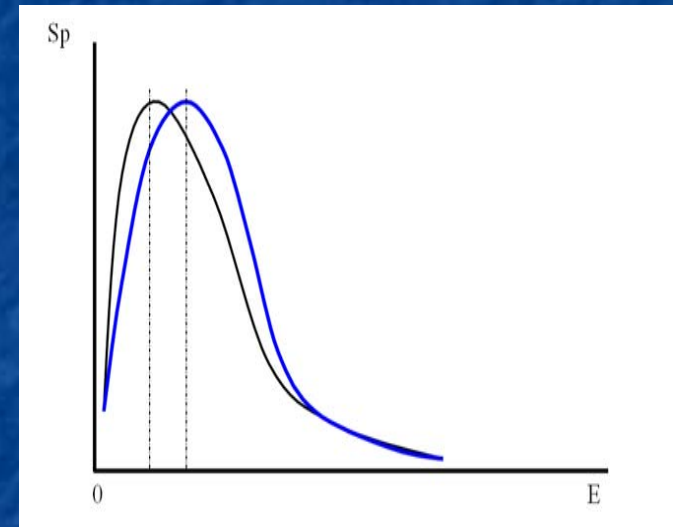
$H^+ - He^+ \quad C_H : C_{He} = 1:1:1 \quad He^+ - Ar^+ \quad C_{He} : C_{Ar} = 1:1 \quad H^+ - He^+ - Ar^+ \quad C_H : C_{He} : C_{Ar} = 1:1:1$

Sputtering of the massive samples

$$Sp(E) = \frac{\int_{E_1}^{E_2} Sp(E) (dN/dE) dE}{\int_{E_1}^{E_2} (dN/dE) dE}$$

where:

$Sp(E)$ sputtering yield for case irradiation by monoenergy ion beam with energy $E \pm dE$,
 dN/dE energy distribution of an ions in beam,
 E_1 и E_2 start and finish of the energy distribution.



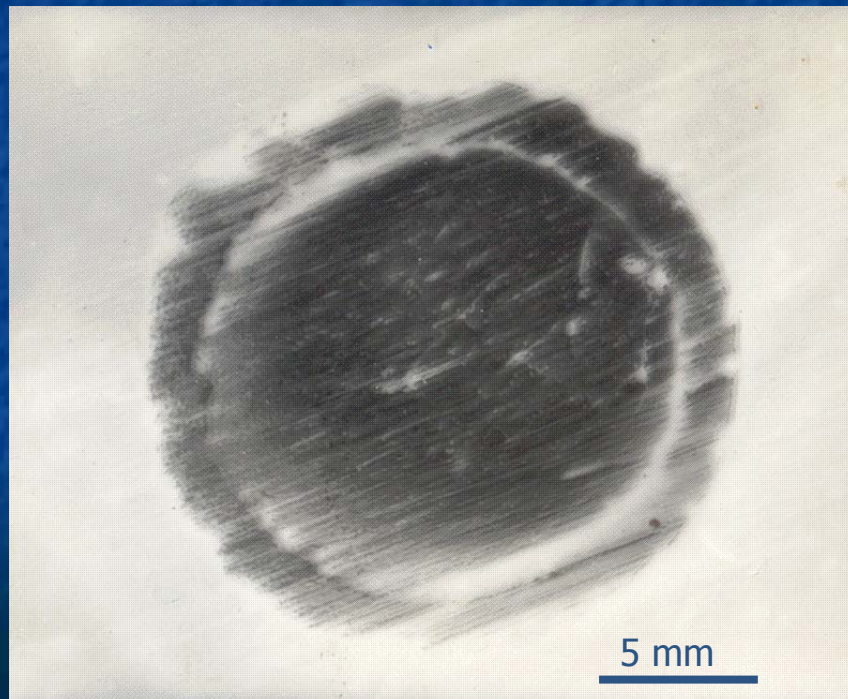
Sputtering of the films on massive substrates

Change of size S_p (at/ion) depending on reduced atomic mass of a ion beam
(mean energy 10 keV, fluence 1×10^{18} ion/cm²)

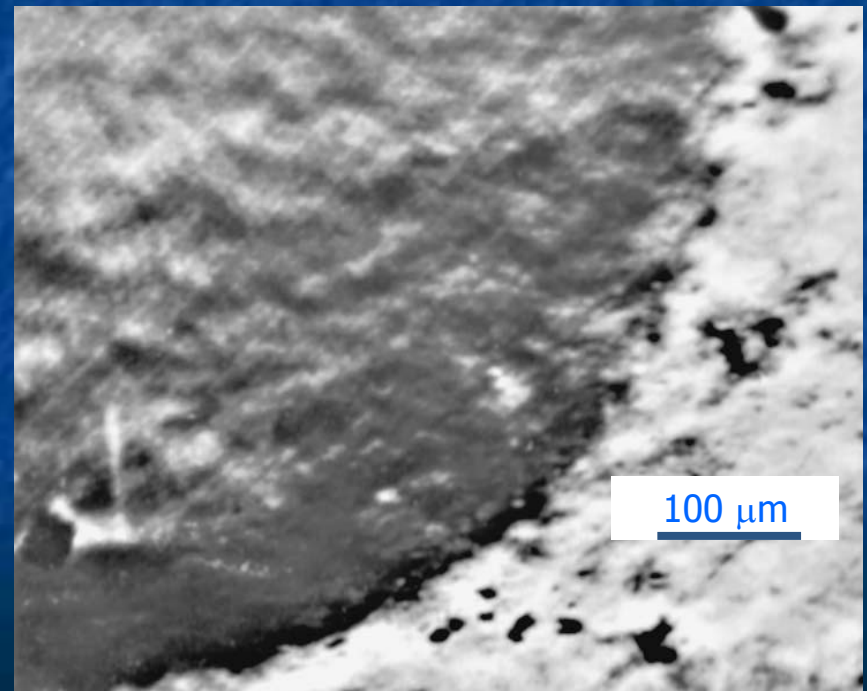
$C_{He}:C_{Ar}$	1:0	10:1	5:1	2:1	1:1	1:2	1:5	0:1
$(M_i), aum$	4	7	10	16	22	28	34	40
Be	0,10± 0,03	0,3± 0,1	0,5± 0,1	0,8± 0,1	1,3± 0,3	1,7± 0,3	2,4± 0,3	3,6± 0,3
Al on Be	0,15± 0,03	0,5± 0,1	0,9± 0,1	1,5± 0,1	2,2± 0,3	3,1± 0,3	4,1± 0,3	5,3± 0,3
Fe on Be	0,10± 0,03	0,4± 0,1	0,6± 0,1	0,8± 0,1	1,4± 0,3	1,9± 0,3	2,2± 0,3	3,2± 0,3
Mo on Be	0,03± 0,01	0,13± 0,1	0,2± 0,1	0,5± 0,1	0,9± 0,3	1,5± 0,3	1,7± 0,3	2,1± 0,3
Fe-Al on Be	0,04± 0,01	0,10± 0,03	0,2± 0,1	0,5± 0,1	1,2± 0,3	1,5± 0,3	2,2± 0,3	3,0± 0,3
Ti-Al on Be	0,03± 0,01	0,07± 0,03	0,2± 0,1	0,4± 0,1	0,9± 0,3	1,3± 0,3	2,4± 0,3	3,3± 0,3

Topograhpy of surface

Trace from influence of a polyenergy ion beam (Ar^+ , mean energy 10 keV



Trace from influence of a polyenergy ion beam ($\text{He}^+ - \text{Ar}^+$, mean energy 10 keV, fluence $3,4 \times 10^{18}$ ion/cm²)



Surface topography of materials after irradiation

Photo of a surface 12X18H10T after irradiation by monoenergy He^+ beam mean energy 20 keV, fluence $1,2 \times 10^{18}$ ion/cm²

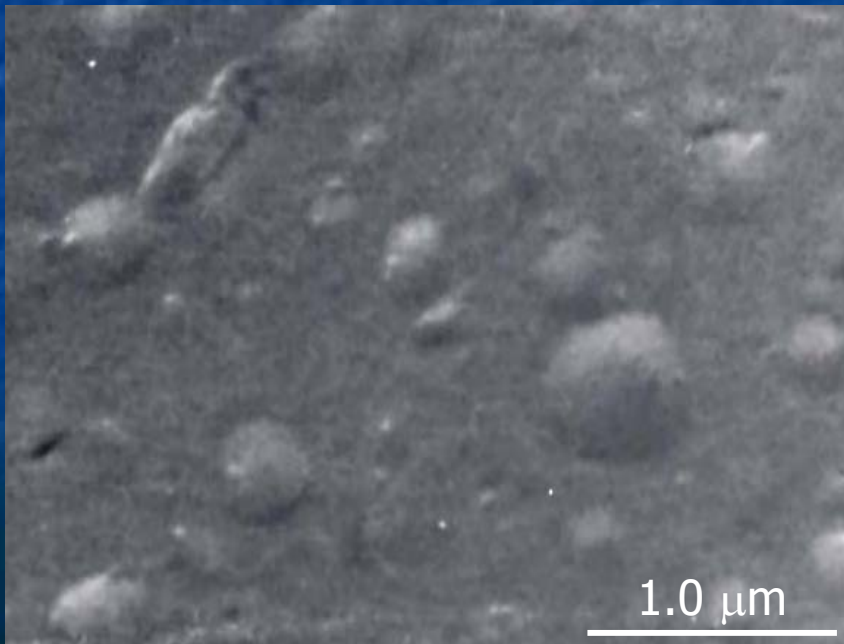
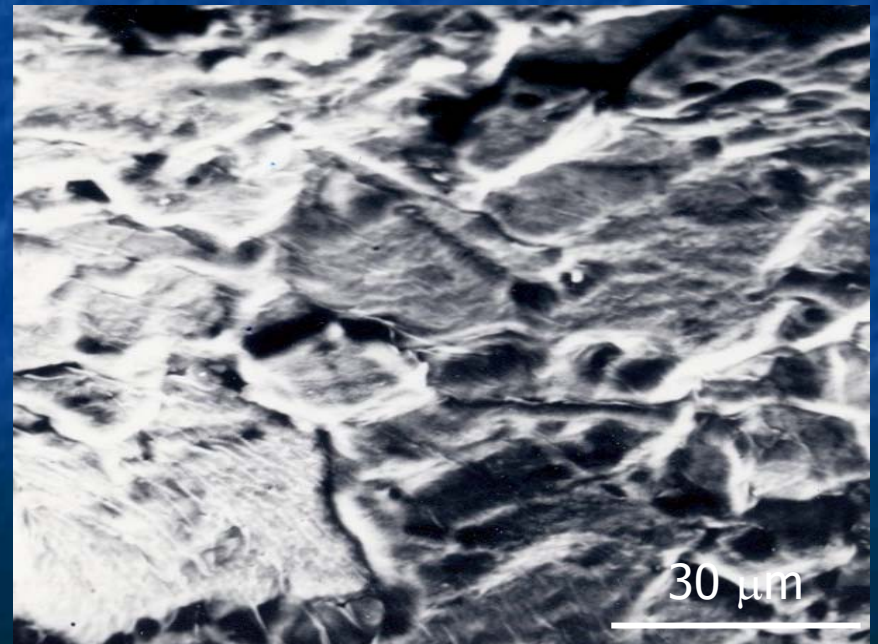


Photo of a surface 12X18H10T after irradiation by polyenergy He^+ beam mean energy 10 keV, fluence $5,7 \times 10^{18}$ ion/cm²



Surface topography of the massive samples

Photo of a W surface after irradiation by polyenergy $\text{Ar}^+ + (\text{He}^+)$ with mean energy 10 keV, fluence $2,3 \times 10^{18}$ ion/cm²

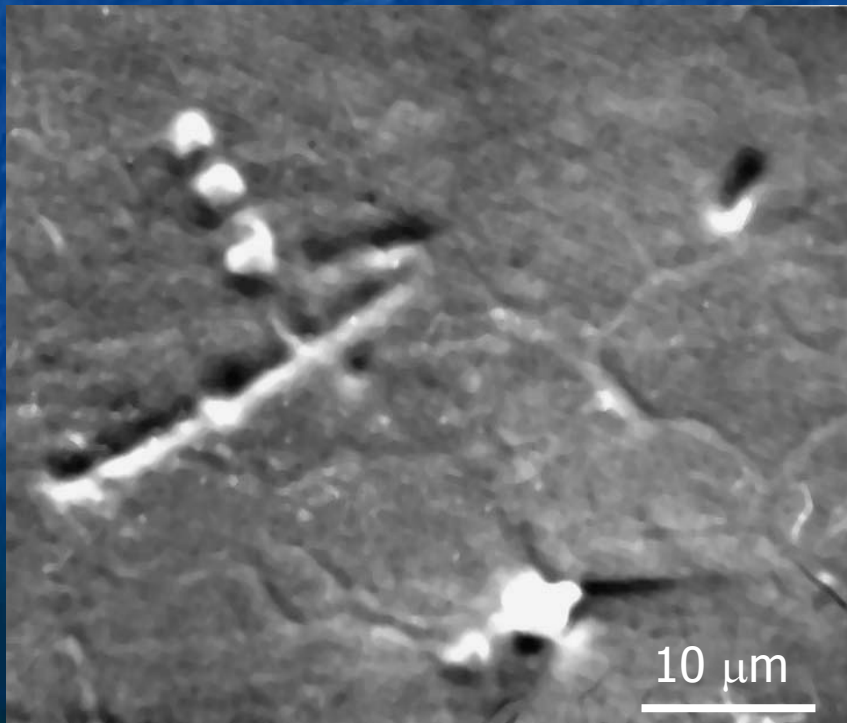
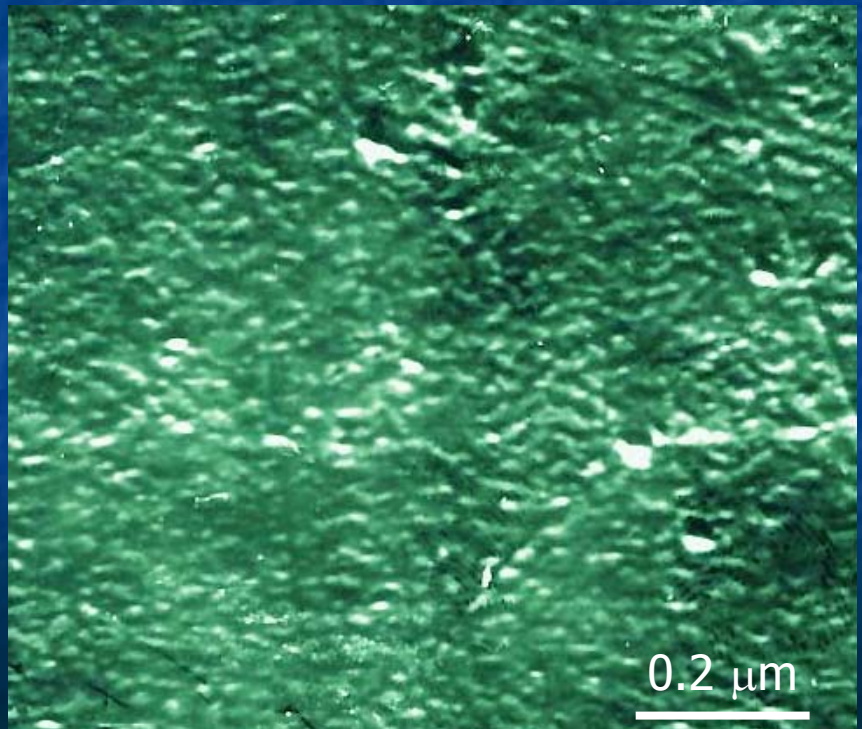
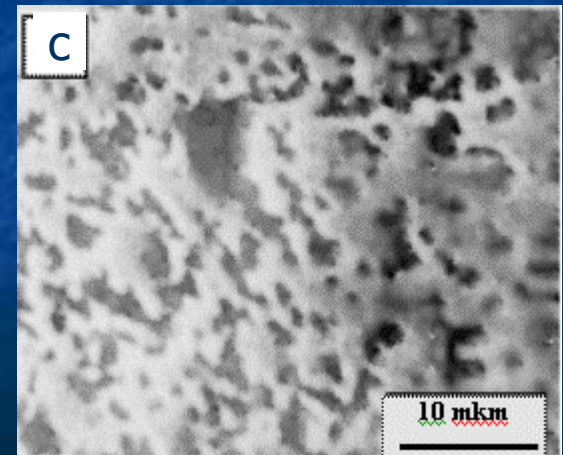
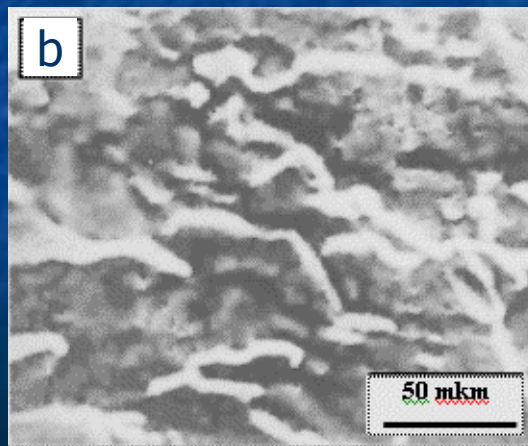
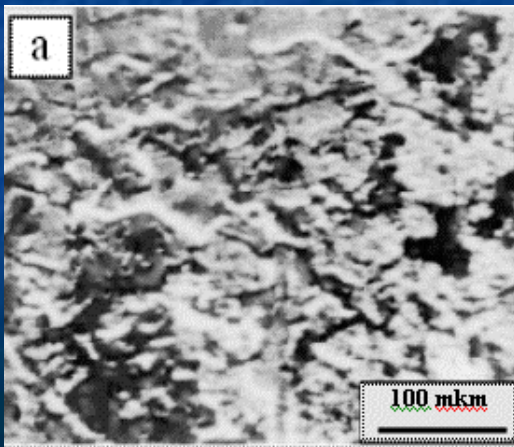


Photo of a W surface after irradiation by polyenergy $\text{Ar}^+ + (\text{He}^+)$ with mean energy 10 keV, fluence $2,3 \times 10^{18}$ ion/cm²

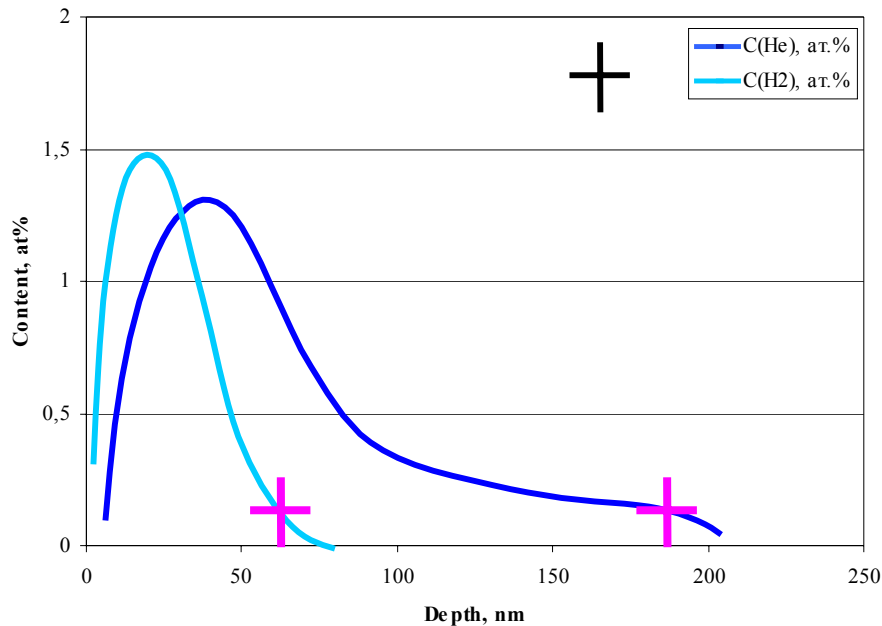


- A surface photo in secondary electrons (SEM) of Cu samples irradiated by a polyenergetic beam of ions with a mean energy of 10 keV:
- **a** - H^+ , $D=2 \times 10^{18}$ ion/cm²; **b** - He^+ , $D=1 \times 10^{18}$ ion/cm²,
- **c** - $\text{H}^+ + \text{He}^+$ ($C_{\text{H}}:C_{\text{He}} = 1:1$), $D=1 \times 10^{18}$ ion/cm²

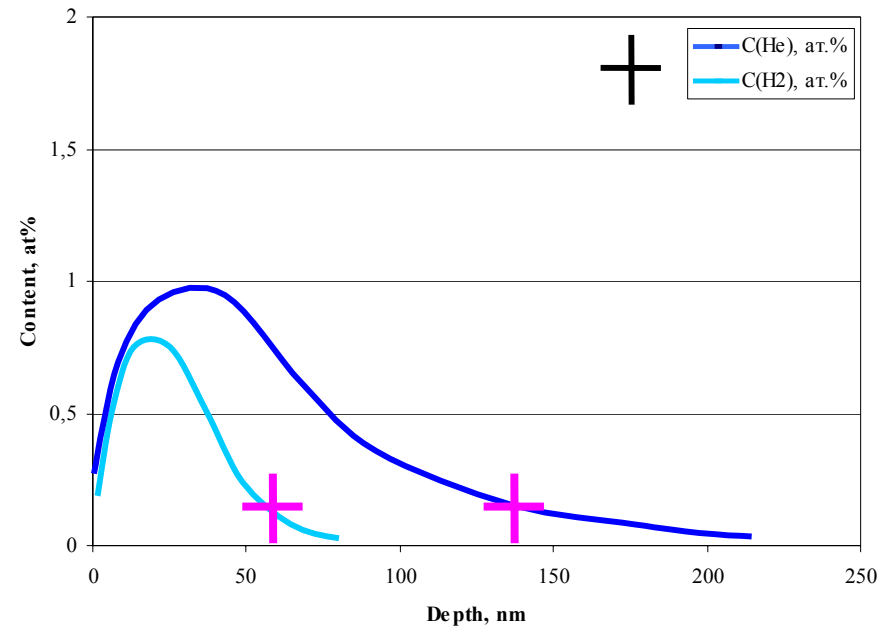


Distribution of the implanted atoms (ions)

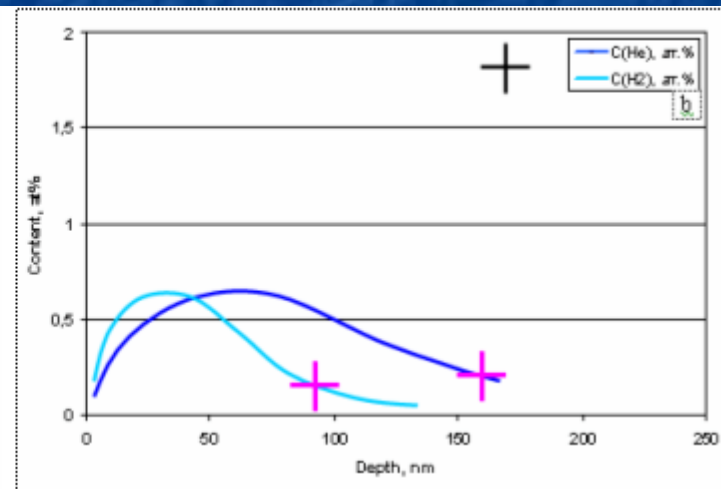
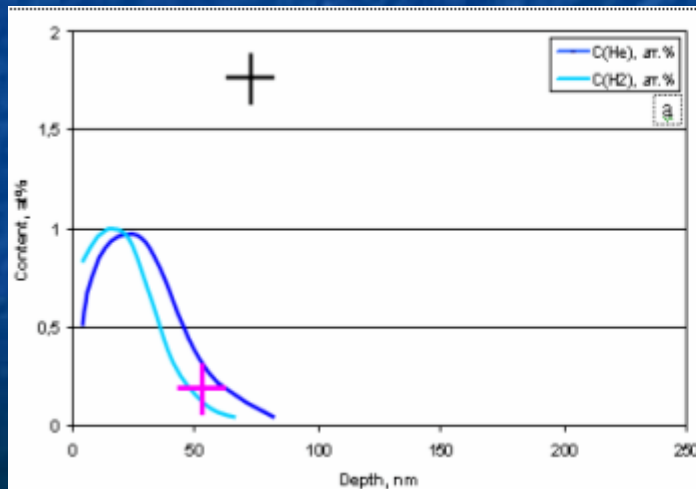
Irradiation of Be sample ion beams in series H^+ and He^+ with mean energy 10 keV, fluence 1×10^{18} ion/cm²



Irradiation of Be sample ion beam of $\text{H}^+ + \text{He}^+$ (1:1) with mean energy 10 keV, fluence 1×10^{18} ion/cm²



The distribution of implanted atoms in W under irradiation by a polyenergetic beam of $H^+ + He^+$ ($C_{H^+} : C_{He^+} = 1:1$) ions with a mean energy of 10 keV, at an irradiation dose of (a) $D(H+He) = 2.0 \times 10^{18}$ ion/cm² and (b) 20 keV, $D(H+He) = 2.2 \times 10^{18}$ ion/cm²

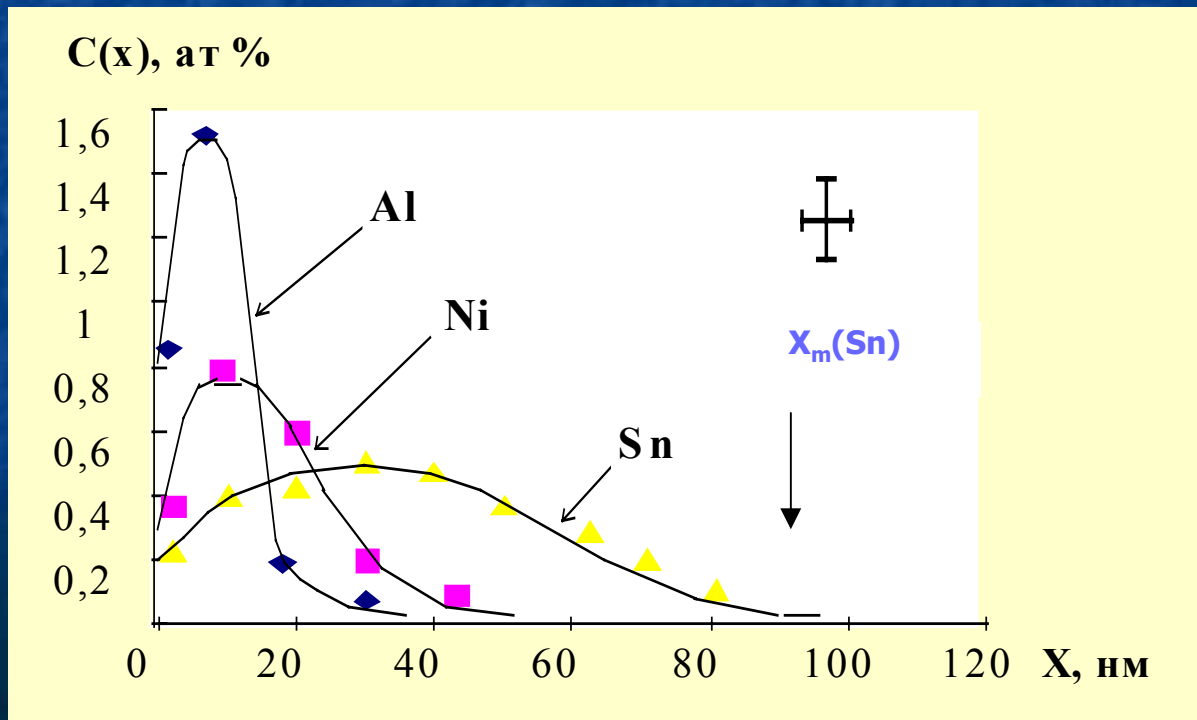


CONCLUSION

- The sputtering yields of a number of materials such as Be, Ti, Fe, Cu, Mo, and W have been measured under irradiation by one- and two-component beams of H^+ and He^+ ions with a wide energy spectrum (1...30 keV). It has been shown that the sputtering yields decrease with an increase of the mean ion energy in a beam ($\langle E \rangle = 10$ and 20 keV). In doing so, the sputtering yields of Be, Fe and W ($\langle E \rangle = 20$ keV) are close to $\approx ((1.5 \dots 2.0) \pm 0.5) \times 10^{-2}$ at./ion.
- A regularity has been found of an increase of the sputtering yield with the reduced mass of H^+ , He^+ , and $H^+ + He^+$ ions in a beam $M_{tot} = (\sum M_j)/j$ ($M_i = (M_1 + M_2)/2$) for double component).
- To calculate the total sputtering yield of materials under their irradiation by a polyenergetic multicomponent ion beams, it has been proposed to take the non- monochromatism and the atomic composition of a beam on the basis of the additivity principle into consideration (a linear approximation of the atomic cascades displacement).
- A developed surface (porous) relief is formed under irradiation of Be and W by a polyenergetic beam of H^+ and He^+ ions with a mean energy of 10 and 20 keV. It increases the sputtering of a material and is due to the presence of implanted gas atoms in the surface layer of the material.

Distribution of the doped film atoms in a substrate

Distribution $C(x)$ doped atoms Al, Ni, Sn in Cu-substrate after irradiation by a polyenergy Ar^+ beam with $\langle E \rangle = 10$ keV, fluence $D \approx 5,7 \times 10^{18}$ ion/cm²



Distribution of the doped film atoms in the substrates

	<u>R_p, nm</u>	<u>X_c, nm</u>	<u>X_m, nm</u>	<u>X_m/R_p</u>
Matrix	<u>Dopen atom Ar</u>			
9Be	10	48	82	8,2
27Al	12	22	40	3,33
64Cu	5,3	10	40	7,55
96Mo	8	11	38	4,75
	<u>Dopen atom Be</u>			
27Al	7	5	12	1,7
64Cu	5	7	18	3,6
96Mo	3	10	21	7
	<u>Dopen atom Al</u>			
9Be	20	40	50	2,5
27Al	5	9	-	-
64Cu	6	11	45	7,5
96Mo	7	5	30	4,29
	<u>Dopen atom Ni</u>			
9Be	12	33	60	5
27Al	8	25	40	5
64Cu	5	20	65	13
96Mo	6	11	40	6,67
	<u>Dopen atom Mo</u>			
9Be	11	15	30	2,73
27Al	8	10	20	2,5
64Cu	4	7	50	12,5

In the table the dependences of relative depth of penetration X_m/R_p for atoms Be, Al, Ni, Mo, Sn in various substrates (Be, Al, Cu, Mo) are submitted.

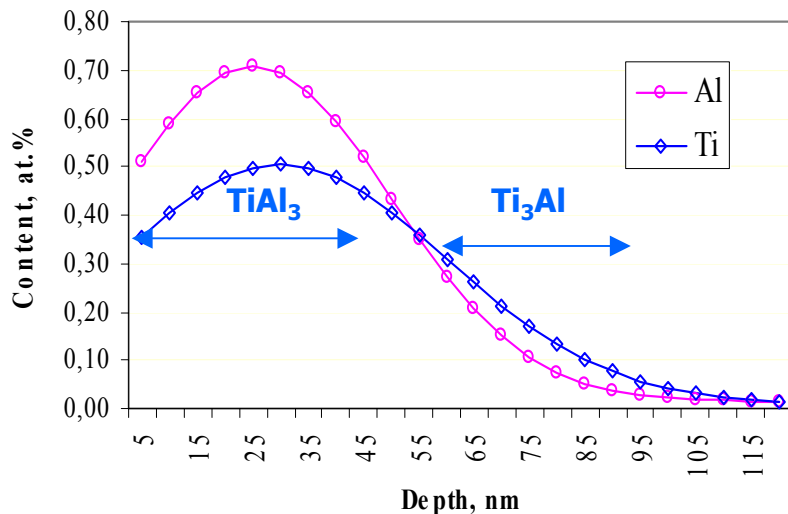
Depths of a rule of a maximum of distribution of the doped atoms X_c , maximal penetration of the introduced atoms X_m ,

And meanings projective range - R_p in the appropriate material to a matrix

Distribution of the doped film atoms in a substrates

The simultaneous implantation of Al and Ti film atoms in a polycrystalline Cu-substrate results in formation of a layer enriched with doped atoms, which can form intermetallic compound

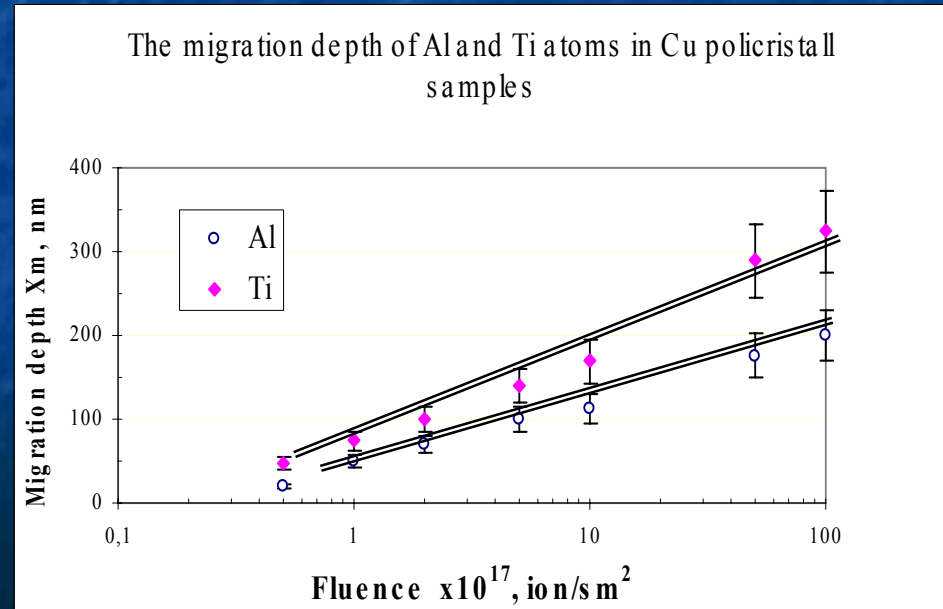
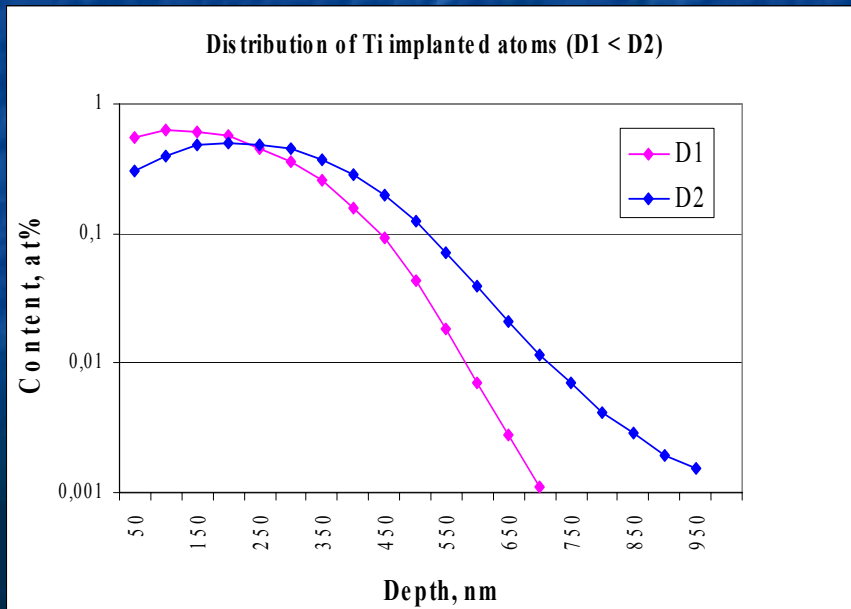
Distribution of implanted Al and Ti atoms in
Cu polycrystall substrate
[Al-Ti, $D(\text{Ar}^+) = 1,8 \times 10^{18} \text{ ion/s/m}^2$]



No of line	2 Θ , grad.	D, nm	I, rel.un.	I/I _{max}	Fasa
1	21,1	4,21	15	6	Ti ₃ Al
2	24,6	3,62	38	12	TiAl ₃
3	26,3	3,39	11	5	Ti ₃ Al
4	37,5	2,4	8	3	Ti ₃ Al
5	42,5	2,12	28	9	V
6	43,5	2,08	298	100	Cu
7	50,5	1,81	240	81	Cu
8	74,2	1,28	215	72	Cu
9	90	1,09	188	63	Cu
10	117	0,903	45	15	Cu
11	136,5	0,829	175	59	Cu

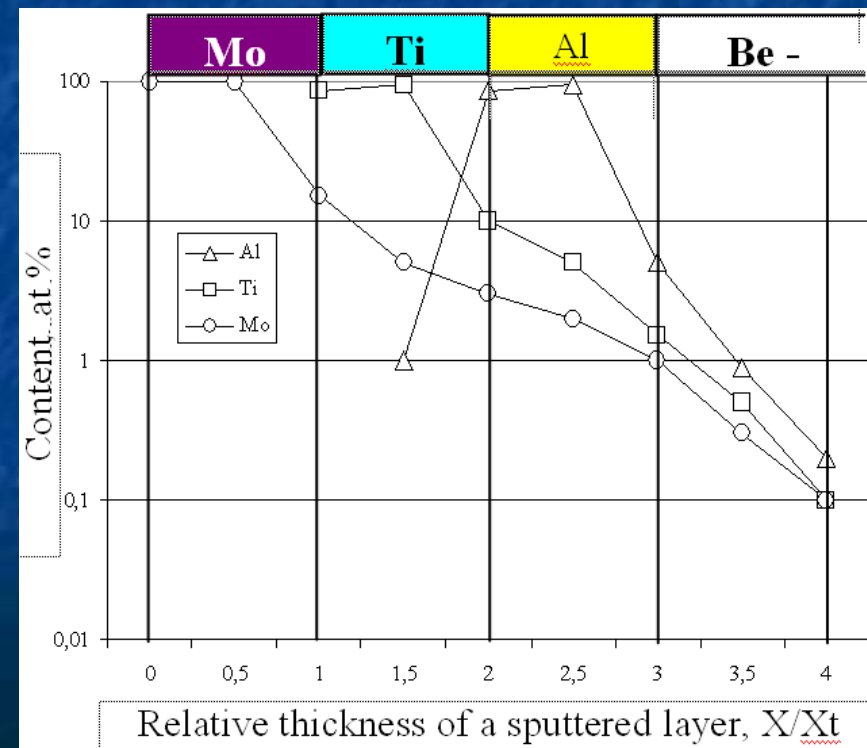
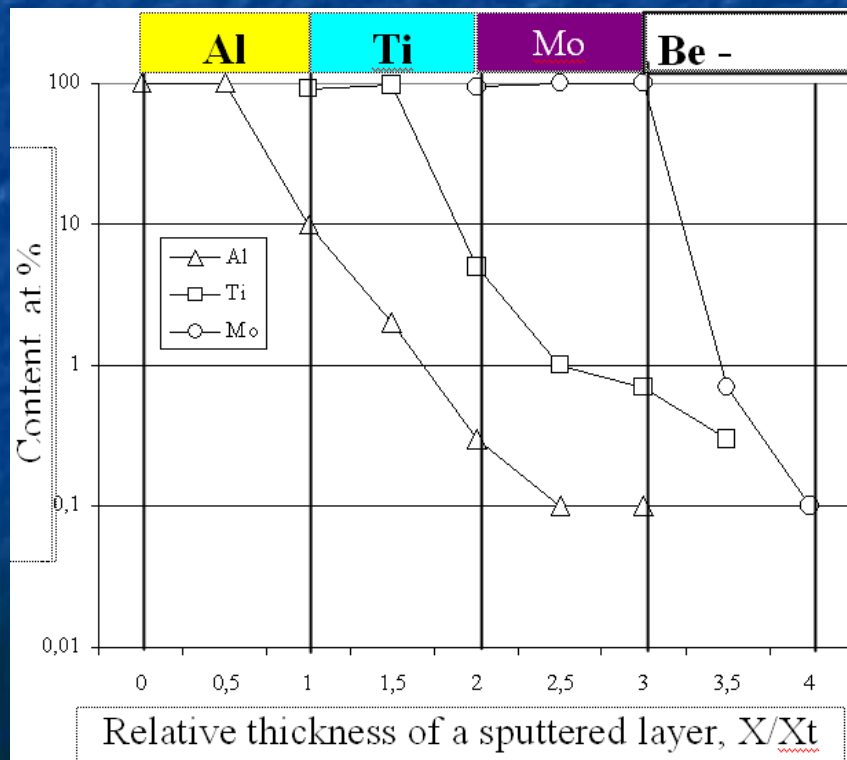
Distribution of the doped film atoms in a sabstrates

Distribution of the doped Ti-atoms in Cu-substrate after irradiation by polyenergy Ar^+ ion beam with mean energy 10 keV, fluences $D1=0,7 \times 10^{18} \text{ ion/cm}^2$ and $D2 = 1,2 \times 10^{18} \text{ ion/cm}^2$



Distribution of the doped film atoms in a polycrystal substrates

Change of content on a surface of «multilayer film - polycrystalline substrate» system under irradiation by a polyenergy Ar^+ ions beam with mean energy 10 keV



Basic data of the experiments

- At an irradiation by a polyenergy ion beams the maximum of sputtering yield is displaced in area large energy (for lighth ions)
- Sputtering yield of films on substrates essentially differs from sizes, received on massive samples
- The depth of migration of the doped film atoms linearly depends on a fluence of an irradiation
- At implantation of the atoms from a multilayer film the mixing process goes intensively in all layers, the formation an intermetallic compound of connections in a near surface layer of a matrix is possible

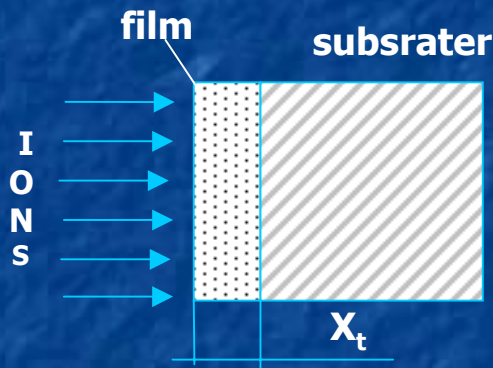
Basic data of the experiments

Increase of efficiency of ion mixing process:

- Reduction of sputtering speed of a film and doped layer of a matrix;
- Optimum thickness of a film and arrangement of layers in a multilayer film;
- Choice of ion energy and ion current of a beam;
- Choice of an irradiation dose for reception intermetallic compound in a polycrystalline matrix

Data of the experiments

The basic models of ion mixing



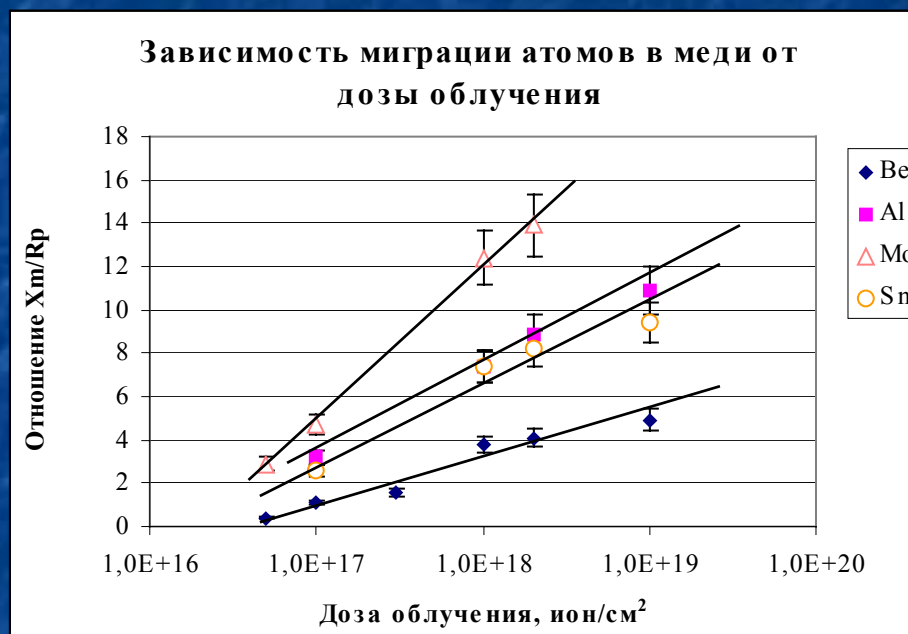
Ions	Substrate	Film
M_i	M_s	M_f
E_i		
$R_{p_{if}}$	$R_{p_{ss}}$	$R_{p_{ff}}$
$R_{p_{is}}$		$R_{p_{fs}}$

$$E_{pka} = \mu_{if} E_i$$

$$E_{ska} = \mu_{fs} E_{pka}$$

$\mu_{if} = \frac{4M_i M_f}{(M_i + M_f)^2}$	$\mu_{fs} = \frac{4M_f M_s}{(M_f + M_s)^2}$
---	---

- 1 $R_{pi} \ll X_t$ - KI-
 2. $R_{pi} \approx (0,5-1)X_t$ - KI+ Sp
 3. $R_{pi} \approx (1-2)X_t$ $X_t \approx 0,75R_p$ Ki+RSM
 4. $R_{pi} > 2X_t$ Sp+Ki+RSM (film and substrate atoms)
- projective of ballistic hashing
 - projective of interaction with defects
 - projective of migration



Doped atom in Cu	r_f nm	r_f/r_s	μ	α^0
Be	0,113	0,883	0,459	25
Al	0,143	1,127	0,862	44
Mo	0,140	1,094	0,943	54
Sn	0,158	1,234	0,806	40

Sputtering of films on a massive samples

Sputtering for P.Smitt:

$$Sp(Me_f) = (\alpha/U_0) \times (Z_i^* Z_{Mef})^2 \times (M_i/M_{Mef}) \times (E_f)/(E_f + 50 \times Z_i \times Z_{Mef})^2$$

For H.Coufal and H. Winters (Model of reflection of energy of displacement of atoms on border «film-substrater»: $E_f = E_i \times G(m_i, m_s)$

$$Sp(film) = Sp(Me, E); \dots E_f = E_i \times \left\{ A \left(\frac{M1}{M2} \right)^n + B \left(\frac{M1}{M2} \right)^m + C \left(\frac{M1}{M2} \right)^k \right\}$$

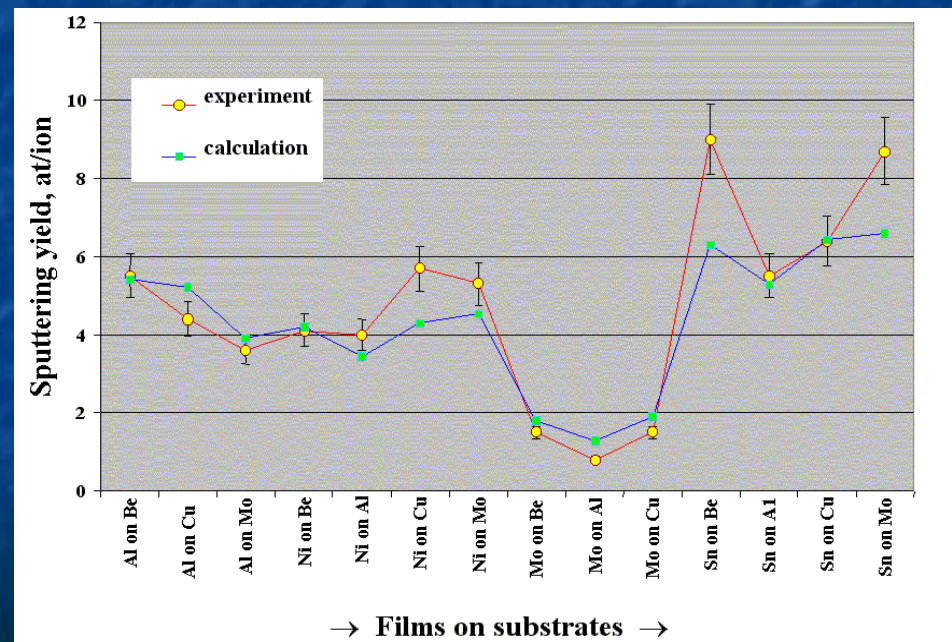
For Ar⁺ polyenergy beam:

$$E_f = \langle E_i \rangle \times A_o \left[\frac{E(Me_f)}{E(Me_s)} \right]^j \times \left[A \left(\frac{\mu_{if}}{1 - \mu_{fs}} \right)^k + B \left(\frac{\mu_{if}}{1 - \mu_{fs}} \right)^l + C \left(\frac{\mu_{if}}{1 - \mu_{fs}} \right)^m + D \left(\frac{\mu_{if}}{1 - \mu_{fs}} \right)^n \right]$$

Sputtering films on a massive samples

$$E_f = \langle E_i \rangle \times A_0 \left[\frac{E(Me_f)}{E(Me_s)} \right]^j \times \left[A \left(\frac{\mu_{if}}{1 - \mu_{fs}} \right)^k + B \left(\frac{\mu_{if}}{1 - \mu_{fs}} \right)^l + C \left(\frac{\mu_{if}}{1 - \mu_{fs}} \right)^m + D \left(\frac{\mu_{if}}{1 - \mu_{fs}} \right)^n \right]$$

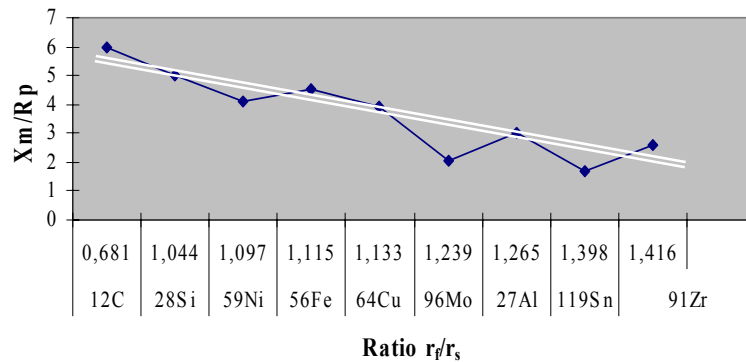
$A_0 = 0,45$	$j = -0,7$
$A = 1,5$	$k = 0,3$
$B = 0,5$	$l = 0,1$
$C = 2$	$m = 0,2$
$D = 5$	$n = 1,1$
$\mu_{fs} = 2 \times M_s \times M_f / (M_s + M_f)^2$	$\mu_{if} = 2 \times M_i \times M_f / (M_i + M_f)^2$



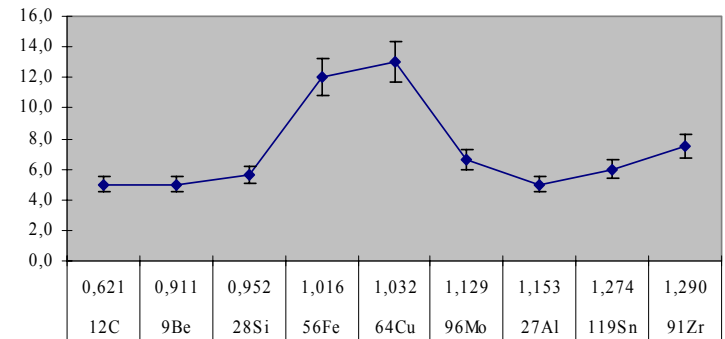
M_i, M_f, M_s - atomic weights of ions Ar, film materials and substrate materials accordingly

Implantation the film atoms in substrates

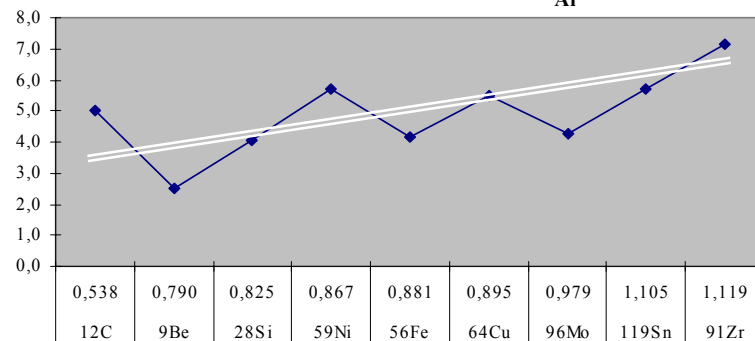
Penetration of Be-atoms in other sabstrates



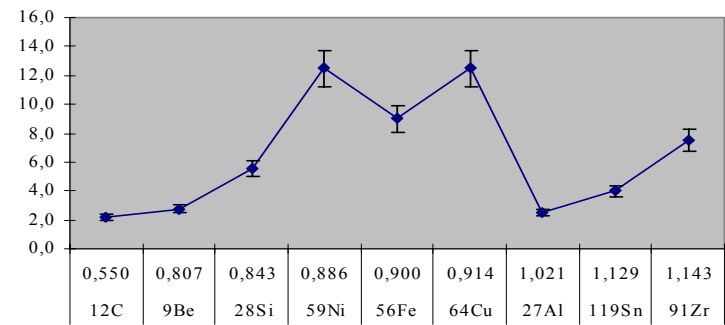
Ni



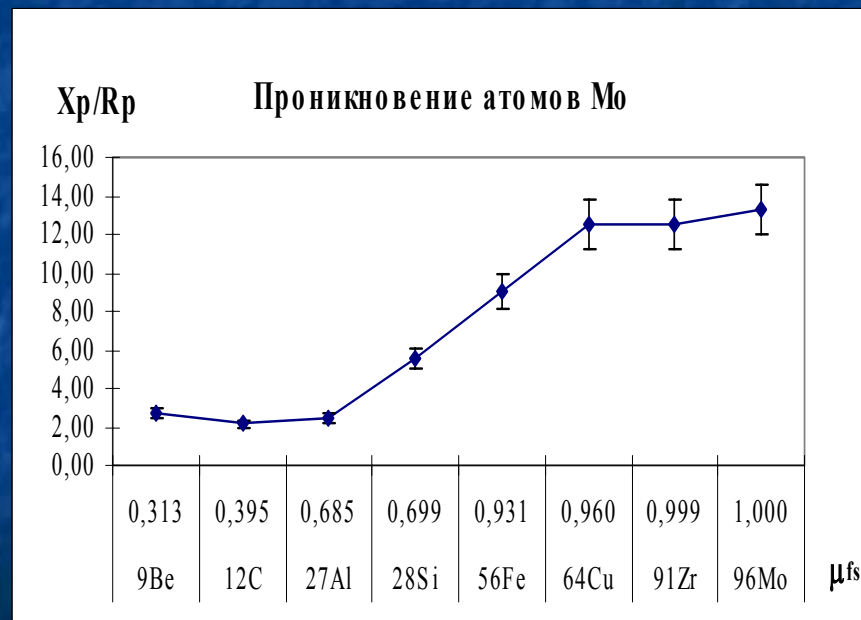
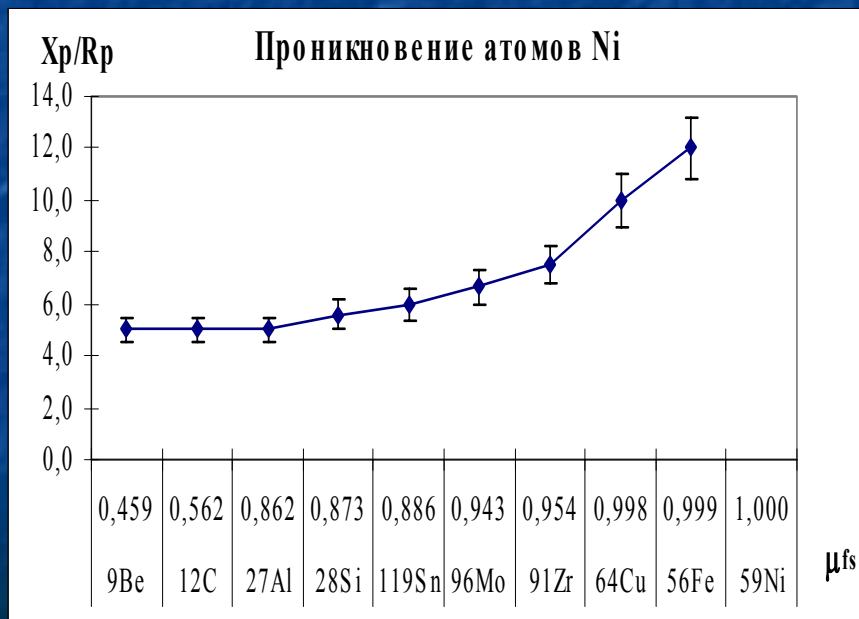
Al



Mo



Implantation the film atoms in substrates



Implantation of the film atoms in a substrates

The submitted results testify to some dependence of penetration depth of the doped atoms from kinematic parameters of a “film - substrate” systems.

For an explanation of effect of deep penetration of the introduced atoms the method PKA at an irradiation by a polyenergy Ar^+ ions beam considered the following three models:

- On classical representation about distribution of the implantation atoms $C(x)$ and basis of the equation Puassona, where the maximal projective range for irradiation by polyenergy beams equal $\approx 2R_p$;

Implantation of the film atoms in substrates

- Model of logarithmic attenuation,

$$C(X) = A \times \exp(-X/L),$$

$$A = f(D, R_p),$$

$$L = 0,375 \times \mu \times E_0, \quad E_0 - \text{ion energy},$$

Taking into account exponential the recession of concentration of the doped atoms after a maximum (gives the maximal of penetration depth up to 2-3 R_p);

- Migration of the doped atoms in fields of internal pressure

$$C(x) = N_0 (1 - kx),$$

$$k = 1/Bojt,$$

Bo - factor, taking into account strength properties of a material,

j - density of a ion current (beam) ,

t - time of an irradiation

(maximal of penetration depth can reach 5 - 10 R_p) .

Implantation of the film atoms in substrate

DISCUSSION of RESULTS on ION MIXING

Model of isotropic mixing (P.Sigmund, A.Gras-Marti):

$$\frac{\langle X \rangle}{R_p} = \left[0.202 \frac{F_q(x)D}{N_o E_d(\mu)^{0.5}} \right]^{0.5}$$

$F_q(x)$ - energy-release in a substrate at the depth, eV/nm;

D - irradiation dose, ion/cm²;

R_p - projective pass of a PKA film, nm;

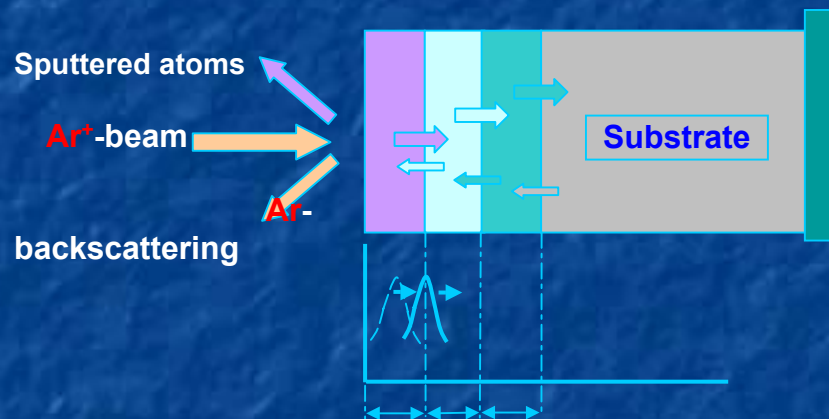
N_o - density of the substrate material, at/cm³;

E_d - energy of shifting the substrate atoms, eV;

$C_?$ = 0.001 - 0.002 – sensitivity threshold in measurements.

SPUTTERING of THREE-LAYER FILMS

Implantation of film atoms in substrate



Under irradiation of three-layer films by argon ions it has been found that sputtering is accompanied by mixing the atoms of neighboring layers and the substrate dependent on the ratio of equivalent masses in the layers ($\mu_{if}/1-\mu_{fs}$) and the electronegativity difference.

Implantation of film atoms in substrates

PENETRATION DEPTH and ELECTRONEGATIVITY

$$\chi = (E + I)/2$$

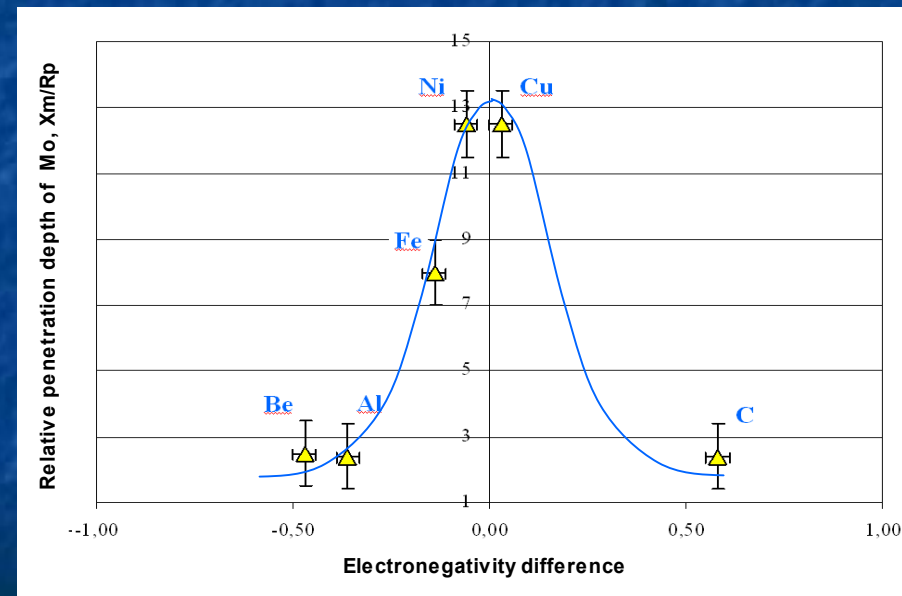
I- the potential of atom ionization;
E - the affinity energy of
an atom to an electron.

Difference between the electronegativity
of film- and substrate-atoms

$$\Delta\chi = 0.208 \times \delta^{0.5}$$

$$\delta = D_{AB} - (D_{AA} + D_{BB})/2$$

D_{ij} - corresponding dissociation energies
for molecules of the following types:
AA, BB, and AB.



Implantation of film atoms in to substrates

DISCUSSION of RESULTS on ION MIXING

Model of isotropic mixing (P.Sigmund, A.Gras-Marti):

$$\frac{X_m}{R_p} = C_o \frac{M_i M_f}{(M_i + M_f)^2} \times \left[0.202 \frac{F_q(x)D}{N_o E_d (1 - \mu_{if})} \right]^{0.3} \times \Phi \left(\left| \Delta \chi \right|^n \right)$$

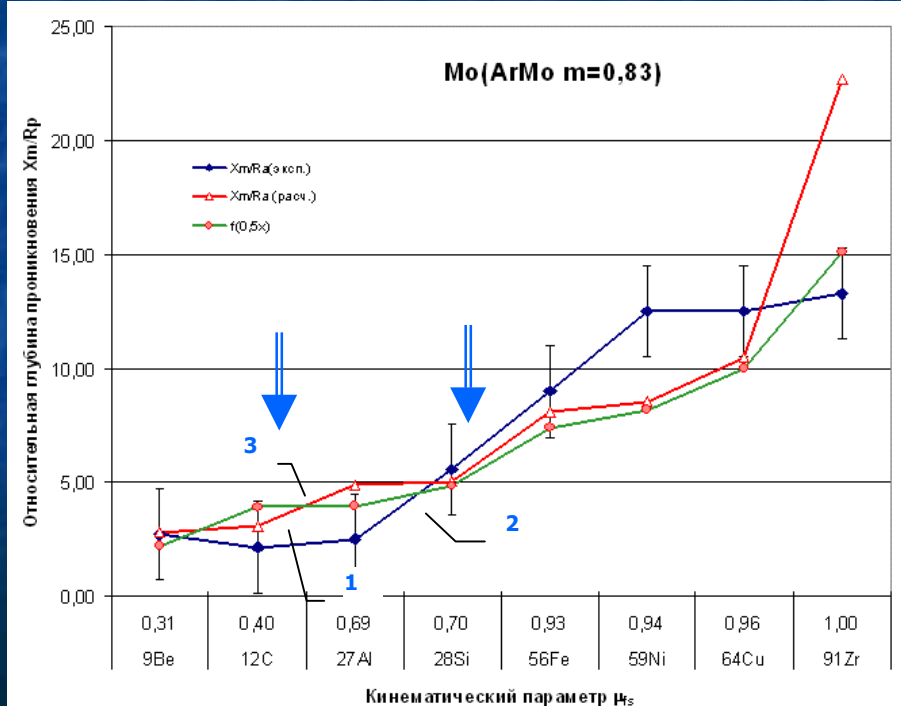
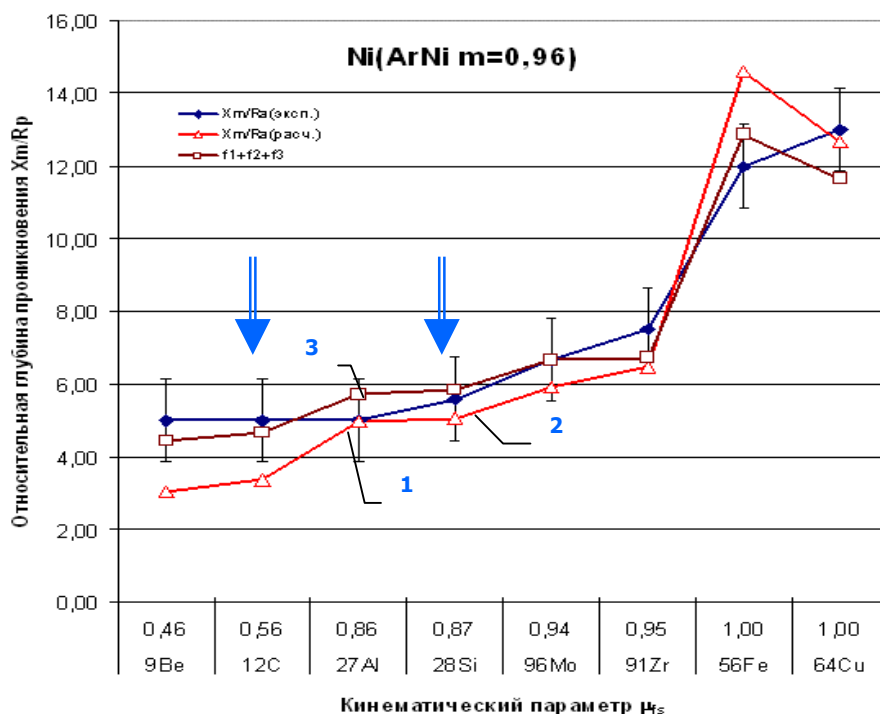
$$\Phi \left(\left| \Delta \chi \right|^n \right) = \sum_{k=0}^{k=2} A_k \chi_k^{n_k}$$

A_k – coefficient, dependent on a material of a film;

$\chi_o \chi_1$ – electronegativity of a substrate and film materials, accordingly.

Implantation of a film atoms in substrates

↓ - implantation in monocrystal



Conclusion

In case of an irradiation of various systems «film - substrate» by a polyenergy beam of ions Ar with mean energy 10 keV

The change of size of relative penetration depth of the doped atoms (X_m/R_p) is satisfactorily described within the framework of isotropic model of ion mixing in view of efficiency of preservation of own energy of the introduced atom ($1-\mu^*$) and physicochemical interaction with its environment;

At ion mixing of parameter of physicochemical interaction between introduced atom of a film and atom of a substrate there can be a size electronegativity.

TMAP4 MODELING of DEUTERIUM TRAPPING in TUNGSTEN

R.G. Macaulay-Newcombe,
M. Poon, A.A. Haasz, J.W. Davis
University of Toronto Institute for
Aerospace Studies
4925 Dufferin Street, Toronto, ON
M3H 5T6 Canada

7th IWHIFRM, May 20, 2004

Presentation Overview

- * Introduction
- * Objectives
- * Experiments (Poon et al., SCW, compared with Oliver, Causey and Maloy, PCW)
- * Results
- * TMAP Simulations
- * Conclusions

Introduction

- ✧ Tungsten armor in fusion reactors will be exposed to high fluxes of deuterium, tritium and neutrons, at temperatures from 300 K to greater than 1000 K (usually > 800 K?)
- ✧ The tungsten will trap and retain tritium in quantities which will depend upon the temperature and the amount of radiation damage (traps)

Objectives

- * Enhance our understanding of tritium trapping and transport in tungsten.
- * Formulate a qualitative mechanism governing tritium trapping in tungsten.
- * Predict the tritium inventory for tungsten and its implications for the use of tungsten in a fusion reactor device.

Experimental Methods

- * Ion / Plasma / Neutron Irradiations
- * Thermal Desorption Spectroscopy
- * Secondary Ion Mass Spectroscopy

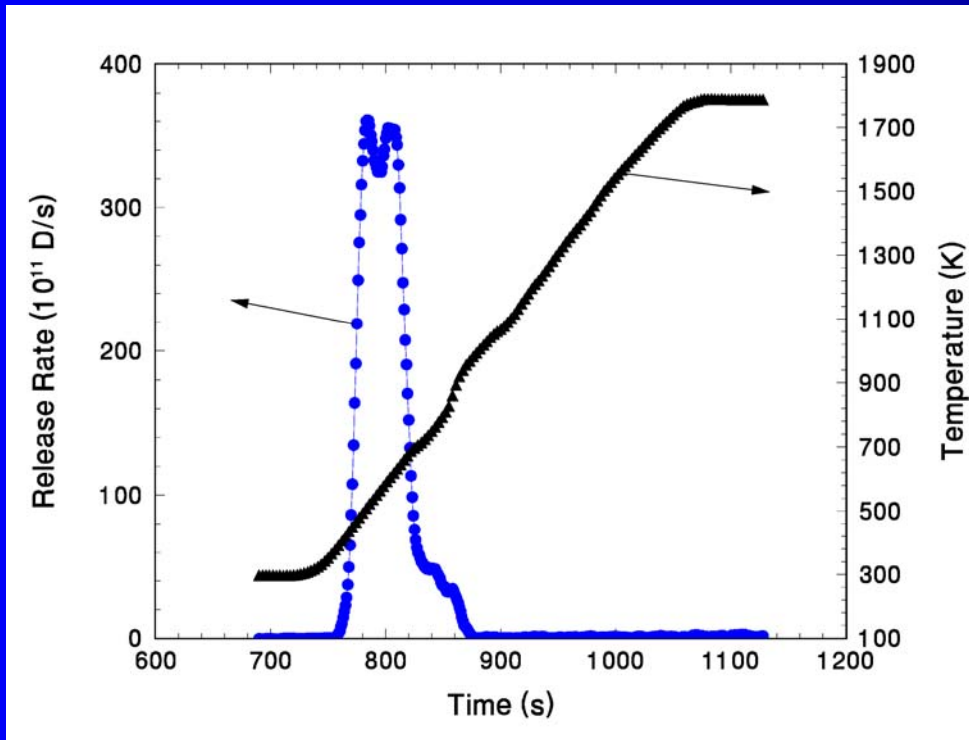
Ion Irradiation (M. Poon data)

- * Ion irradiation was used to simulate experimentally the type of ion impact that may occur at tokamak PFMs.
- * Ion Accelerator conditions:
 - 500 eV D^+ at normal incidence (no elastic collision damage)
 - Flux density: up to $2 \times 10^{20} D^+/m^2s$
 - Fluence: up to $3 \times 10^{25} D^+/m^2$
 - Specimen temperature: 300 K to 700 K

Plasma / Neutron Irradiation (Oliver, Causey, Maloy data)

- * 8 dpa at 440 K, or 0.3 dpa at 310 K, in water
- * Samples cut from 99.96% pure W rod
- * Then annealed 6 h at 1273 K in vacuum, in order to outgas H, D and T from nuclear reactions
- * Plasma discharge in 0.5-1 Torr of D₂ gas
- * Fluence = $2 \times 10^{24} \text{ D}^+/\text{m}^2$
- * Flux = $10^{20} \text{ D}^+/\text{m}^2$
- * D⁺ net energy at surface $\sim 100 \text{ eV}$
- * Sample at about 300 K

Thermal Desorption Spectroscopy



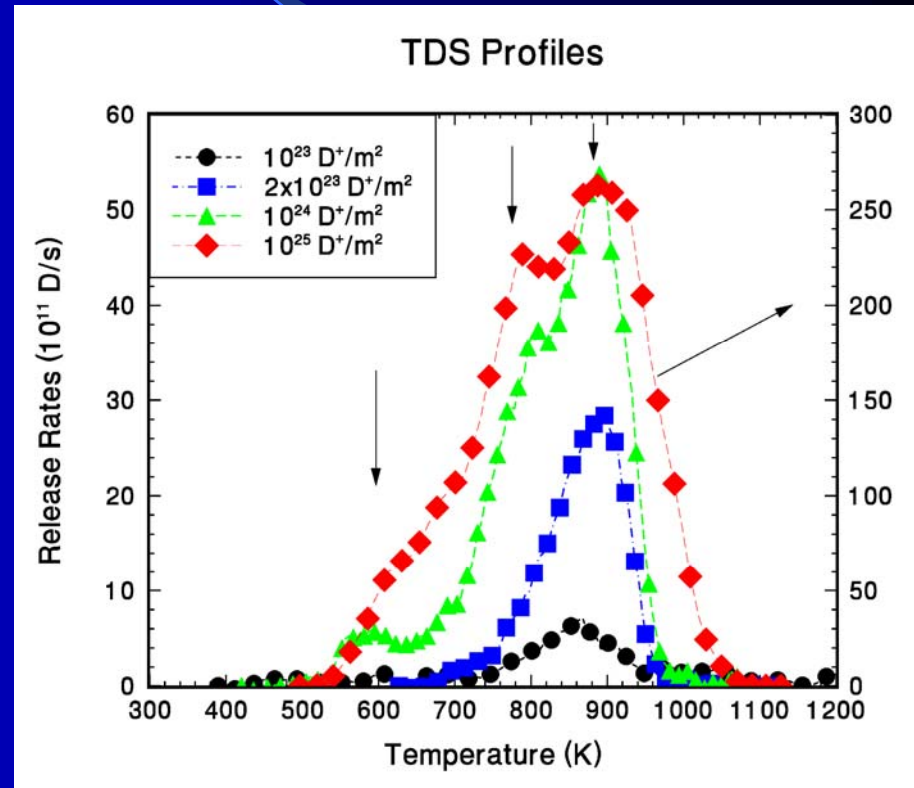
- ✧ If the temperature ramp is capable of desorbing all of the D atoms, then integration of this signal will give the total trapped inventory.

Information from TDS

- * Consider two cases:
 - lightly bound D located far into the specimen
 - highly bound D located near the surface
- * The lightly bound D may detrapp and become mobile at a lower temperature, however it may take time for the mobile D to reach the surface.
 - During this time, the temperature of the specimen may have increased significantly so the detected temperature (desorption temperature) may be much greater than the detrapping temperature (related to the binding energy).
- * Trapped D near the surface will not experience this diffusion delay.

RESULTS: M. Poon data

- * Single crystal W
- * Polished, annealed at 1773 K in vacuum
- * Implanted at 500 K
- * Removed from implanter, then heated in TDS system



Key points

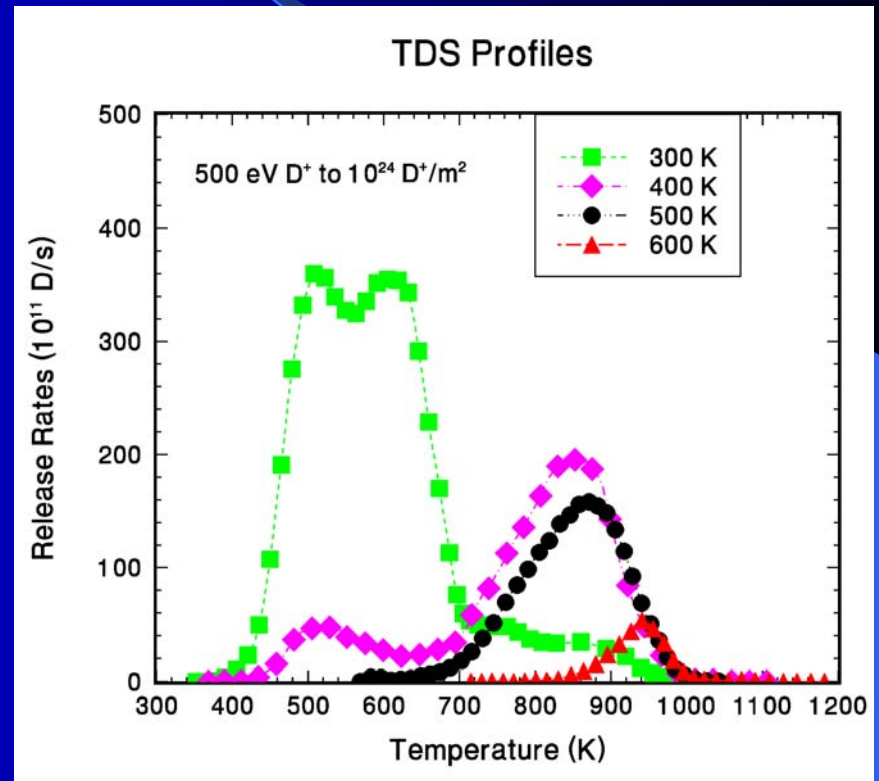
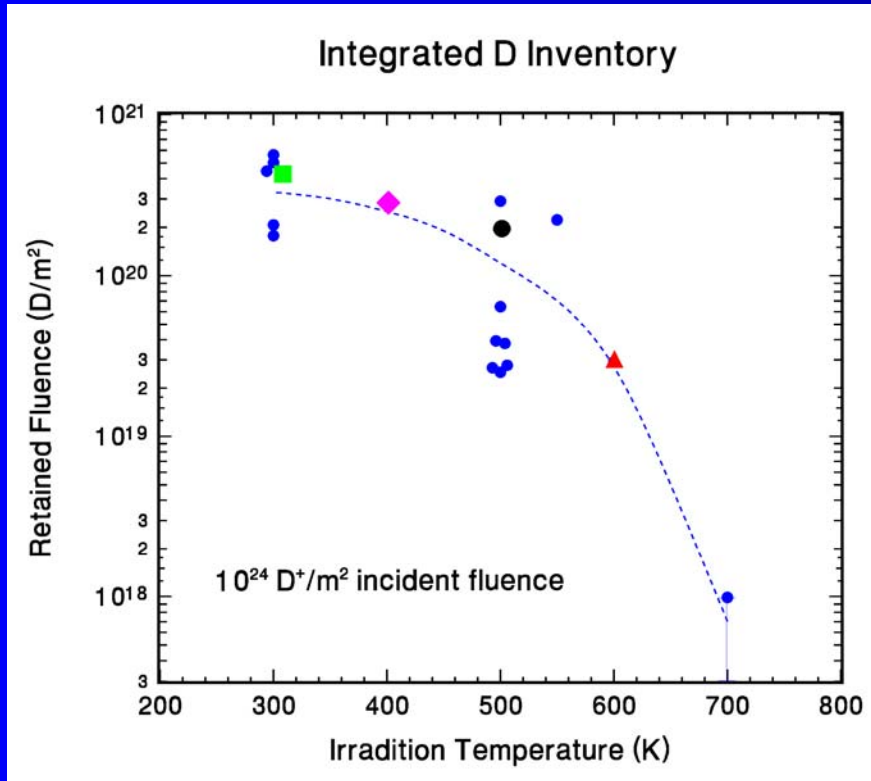
* Irradiations at 300 K:

- D trapping at room temperature is associated with desorption peaks at 520 K and 620 K.
- The trap site associated with the 880 K desorption profile is not available for RT irradiations.

* Irradiations at 500 K:

- D trapping at 500 K is primarily associated with an 880 K desorption peak.

Temperature Dependence



D Trapping at Vacancies

- ✱ It has been reported by Fransens that a single vacancy can trap two D atoms with different binding energies – *this explains the multiple desorption peaks at 300 K.*
- ✱ Vacancies are immobile at 300 K, but at elevated temperatures, vacancies become mobile and may cluster or coalesce into voids – *this explains the evolution of the desorption peaks with increasing irradiation temperature.*

D Trapping at Vacancies

- * At high D^+ flux densities, the stresses from the supersaturation concentration of D in the tungsten lattice may be sufficient to create vacancies
 - *this explains the decreased retention at low flux, and*
 - *the increased D trapping within the mean ion range where the supersaturation condition would be highest.*
- * The strongest evidence for the role of vacancies is the fact that surface blisters on tungsten have been observed after low energy D^+ irradiation.

Modelling – TMAP

- ✧ Tritium Migration Analysis Program (TMAP) [Longhurst et al.] used to obtain trapping energies, and compare them to literature values.
- ✧ TMAP is a one-dimensional finite difference solver that takes into account the movement of solute species across structure surfaces, movement by diffusion in the bulk with trapping, and thermal response of structures to applied heat or boundary temperature loading conditions.

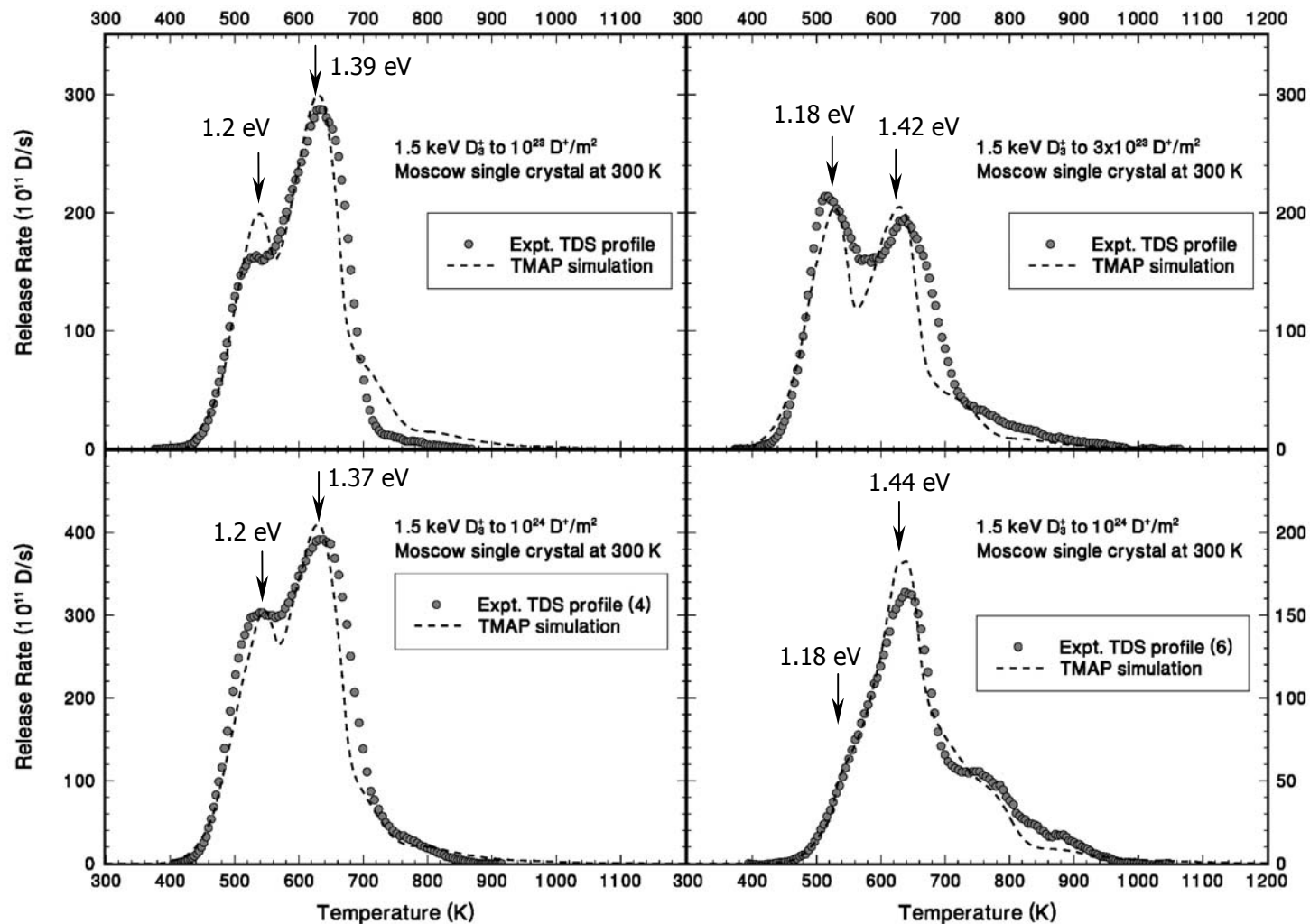
Modelling – TMAP

- ✧ To extract the trap energies from the TDS data, TMAP simulations were performed to fit the experimental profiles.
- ✧ To limit the number of free parameters, the initial distribution and concentration of trapped D was taken from the measured SIMS profiles.
- ✧ The total trapped D inventory for the simulation was set by the measured D inventory from TDS.

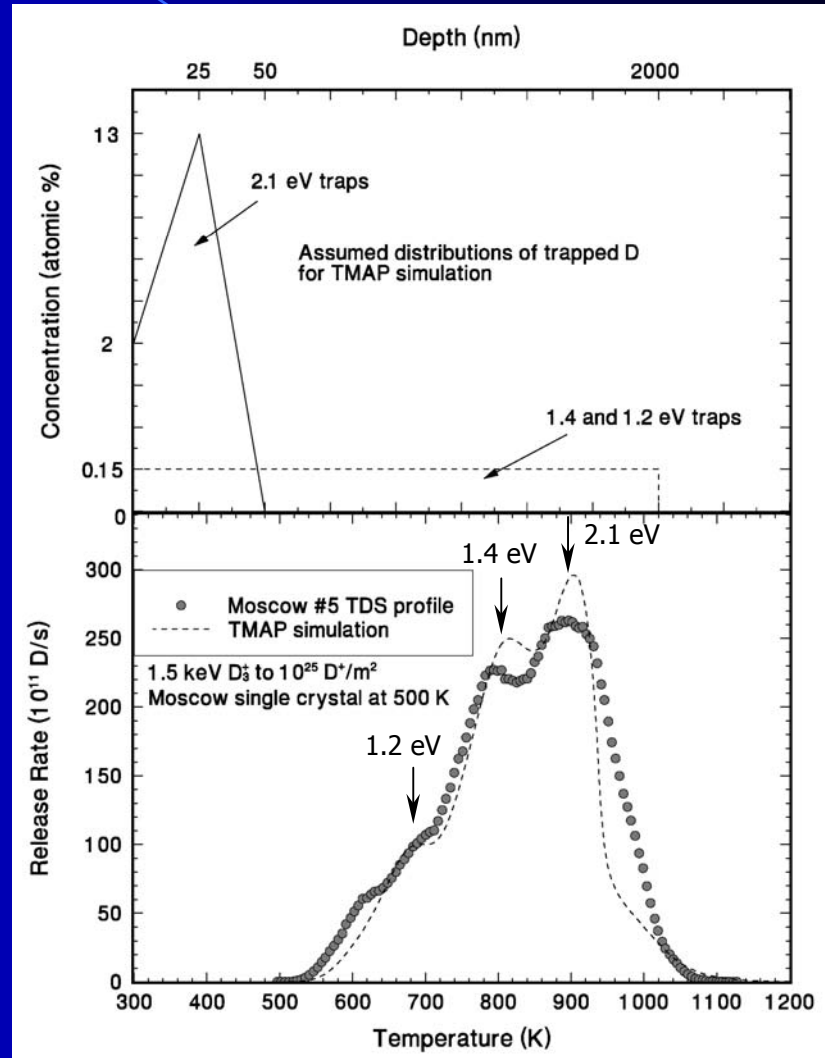
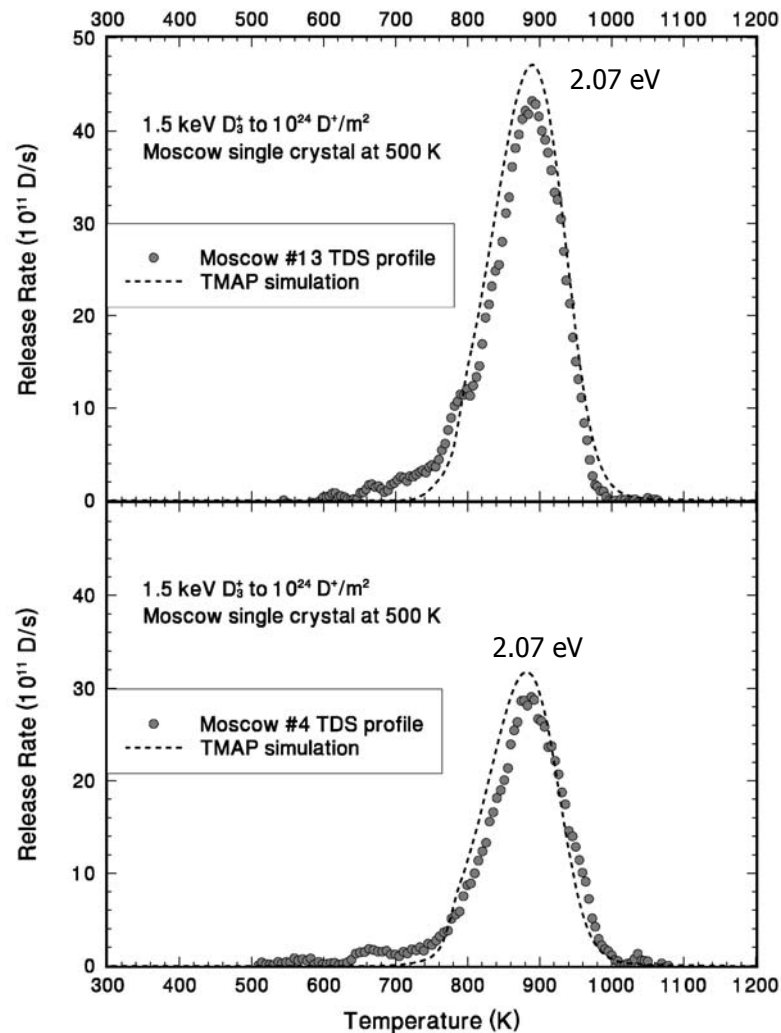
Modelling – TMAP

- ✧ Only two parameters were adjusted to perform the fits – the trap energy and the trap concentration.
- ✧ Trap distributions were assumed to be uniform and all other parameters were set using literature values.

Modelling – Results – 300 K



Modelling – Results – 500 K



Modelled Trap Energies

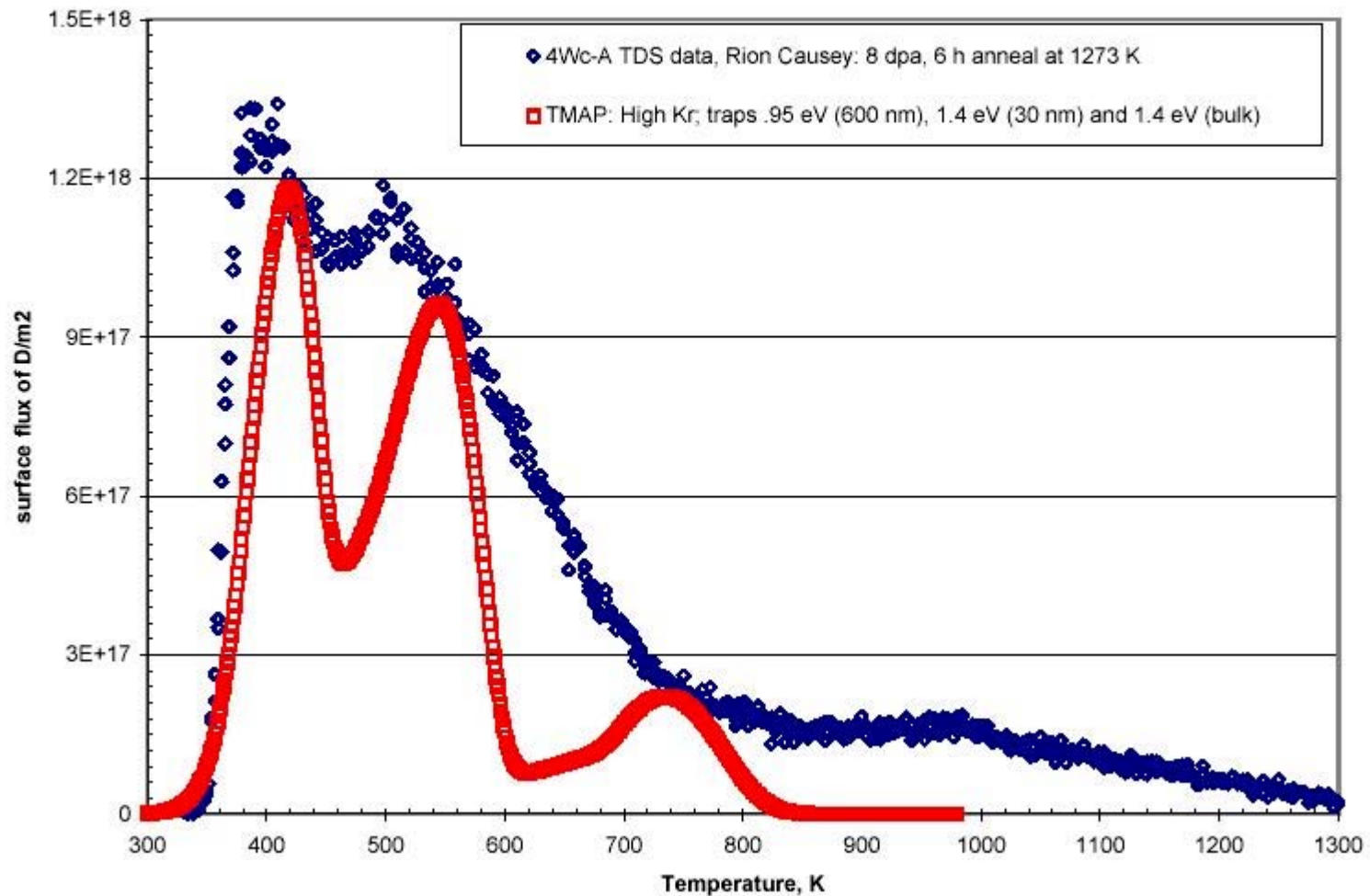
- ✧ The trap energies for the first and second D trapped at a vacancy has been reported at 1.55 eV and 1.38 eV, respectively [Fransens].
- ✧ The present research has determined 1.4 ± 0.4 eV and 1.19 ± 0.1 eV for the first and second vacancy traps, respectively.
- ✧ These results are in agreement to within 10%.

Modelled Trap Energies

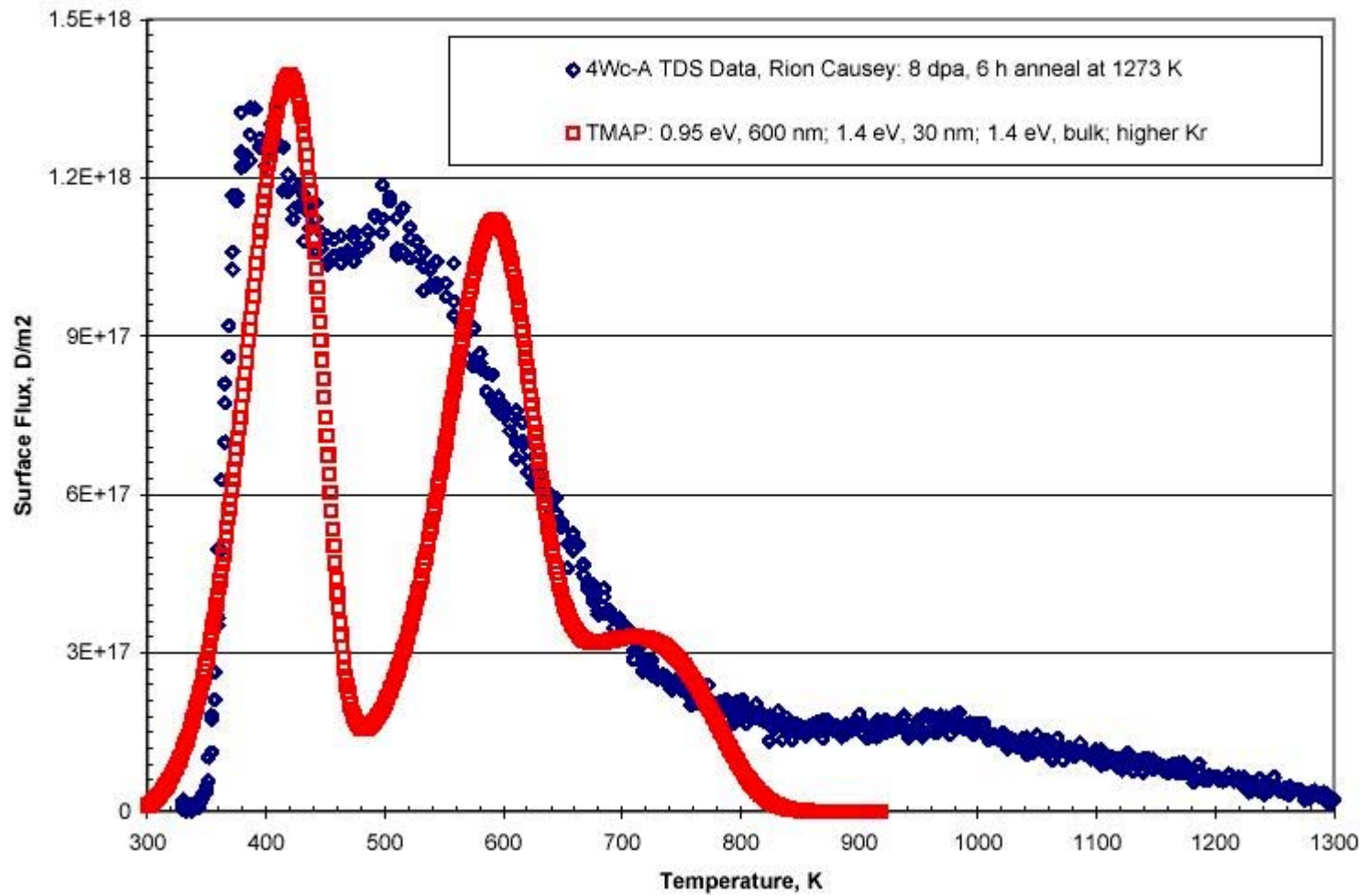
- ✧ It has been suggested that D adsorbed onto the inner surface of a void will have a trap energy of 1.8 – 2.1 eV, while D₂ from an overpressurized cavity will be released at less than 1.4 eV [van Veen et. al.].
- ✧ The present research has yielded a trap energy of 2.07 eV for adsorption of atomic D on a cavity wall, and 1.2 eV for molecular D₂ inside the cavity.
- ✧ Again, the results are in good agreement.

Oliver, Causey, Maloy (ICFRM-11)

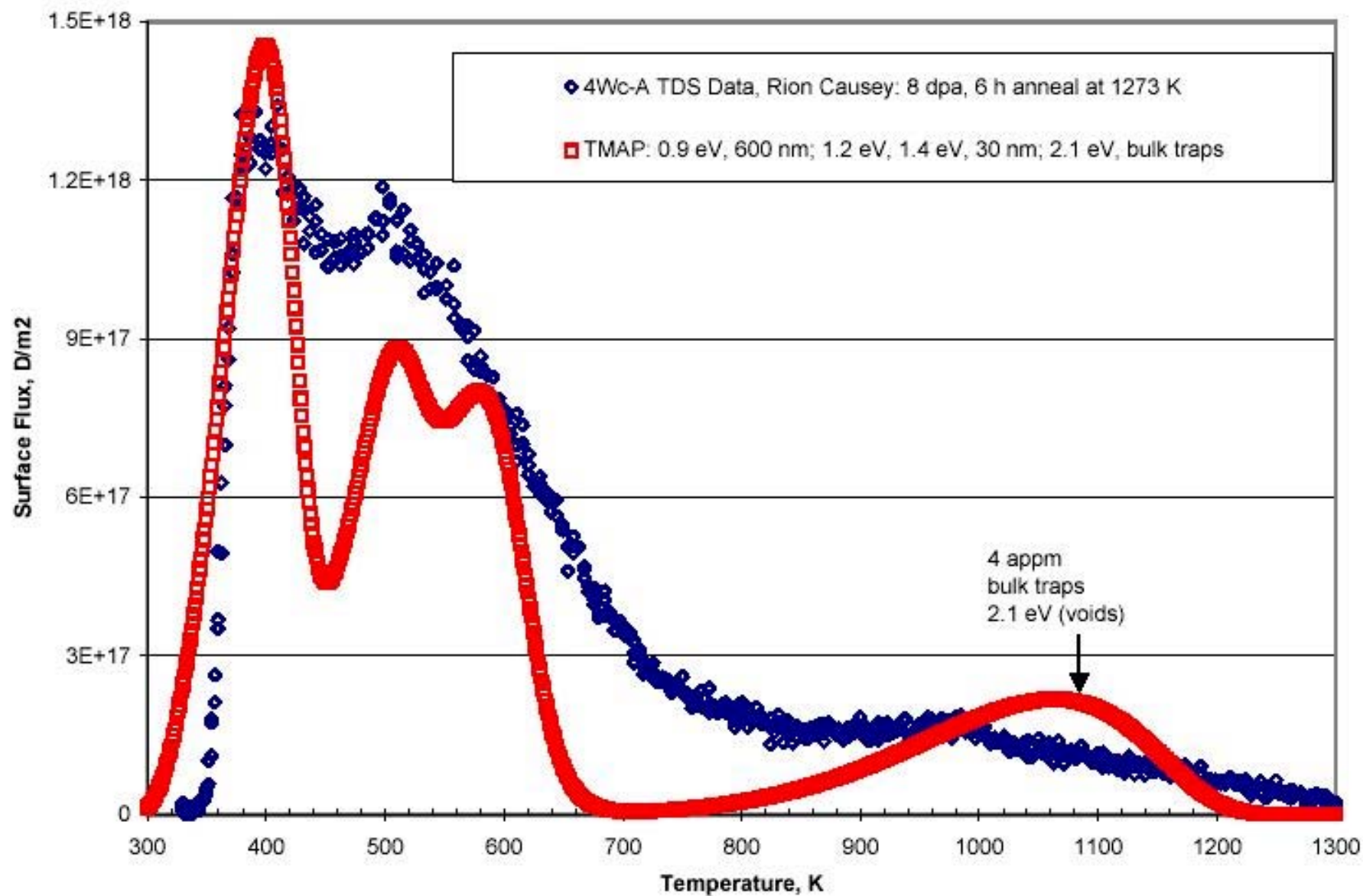
TMAP Calculation to Model Causey TDS Data 4Wc-A: Infinite Recombination Rate



TMAP Calculations to Model Causey TDS Data 4Wc-A: Anderl et al. recombination



TMAP Calculations to Model Causey TDS Data 4Wc-A (Anderl et al. recombination)



- ✱ Key Point: how much damage will survive in W irradiated by neutrons at $T > 800$ K?
- ✱ If 2 appm of 2.1 eV traps, then only 10 g of tritium trapped in W
- ✱ If 200 appm, then 1000 g!
- ✱ Sakamoto showed 8 keV H^+ ions causing bubble formation at 1000 K
- ✱ Need measurements of neutron damage in W at 800 K and higher

Conclusions

- ✧ Deuterium is trapped in tungsten at vacancies and voids.
- ✧ With room temperature irradiations, trapping at vacancies will dominate because immobile vacancies cannot coalesce.
- ✧ At elevated irradiation temperatures, vacancy mobility creates voids and D is trapped both as atoms on the inner surfaces and as molecules inside the cavity.

Conclusions (2)

- ✱ It is anticipated that the trapped tritium inventory in tungsten will not be a problem if the tungsten is kept at room temperature, or at elevated temperatures > 700 K, unless neutron damage at higher temperatures does not anneal out
 - saturation levels were observed at RT
 - retention decreased with increasing temperature.
- ✱ However, the permeation of tritium will be a problem, particularly in polycrystalline materials where grain boundaries may enhance permeation.

Deuterium Retention in W Materials

V.Kh. Alimov, J. Roth, M. Mayer

Max-Planck-Institut für Plasmaphysik, EURATOM Association, 85748 Garching, Germany

Outline:

Deuterium depth profiling using the $D(^3\text{He},p)^4\text{He}$ resonance

Deuterium depth profiles in W single crystals

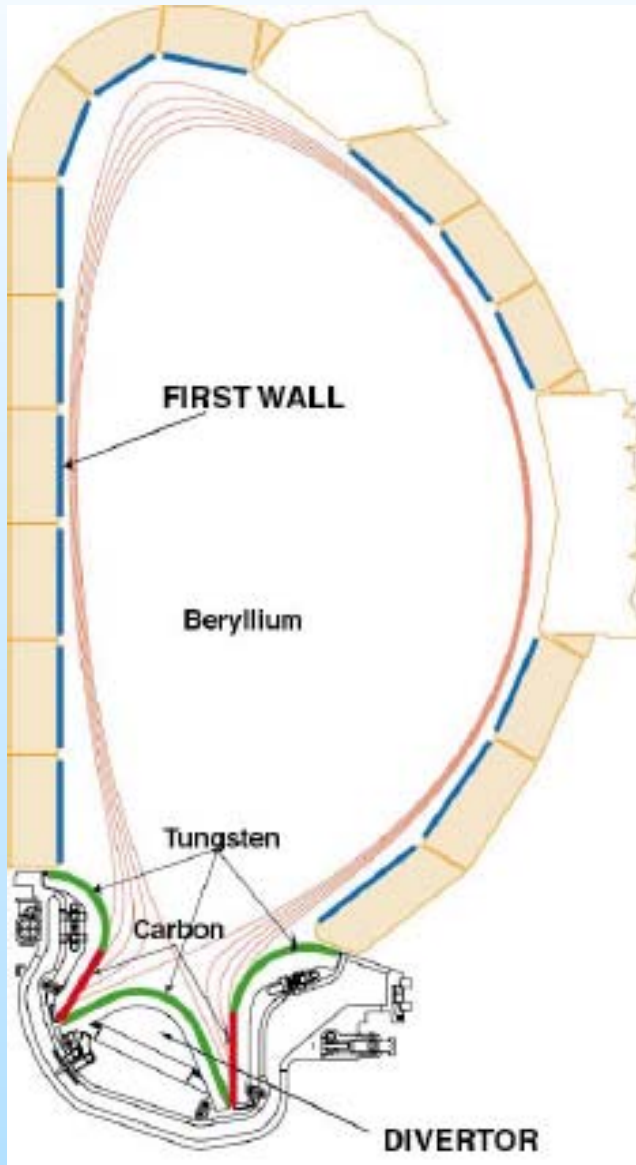
Deuterium depth profiles in polycrystalline W

Deuterium depth profiles in porous vacuum plasma sprayed W

With compliments from V. Alimov



Motivation



Tungsten is foreseen as plasma-facing material in future fusion devices, such as ITER.

Of special interest are hydrogen isotope transport and trapping properties, as they may have a significant impact on tritium inventory.

Available data indicate that hydrogen retention in tungsten depends on both the type of tungsten structure and the implantation conditions.

Information about the total amount of hydrogen retained in W materials and about hydrogen detrapping energies can be obtained from **thermal desorption measurements**.

Hydrogen depth profiles can give detailed information about the depth distribution of defects which are responsible for hydrogen trapping.

Experimental: W materials

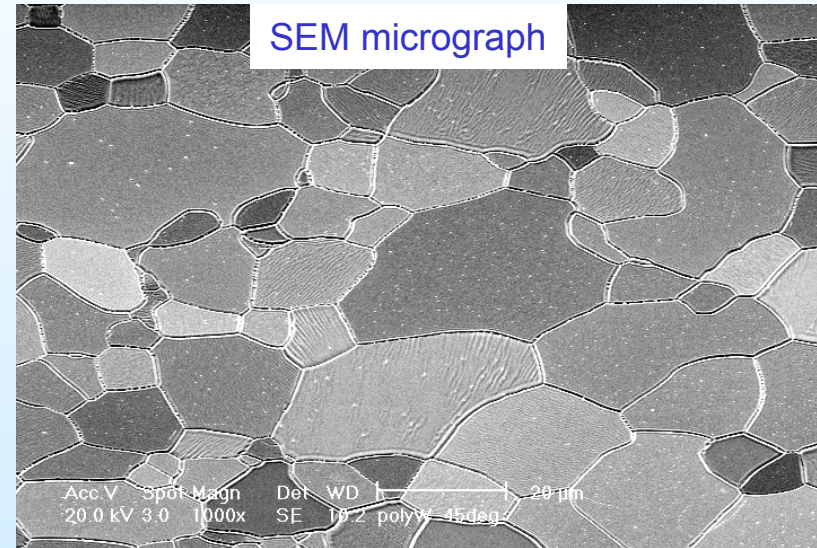
(i) W single crystals (99.9 at.% purity)

(ii) polycrystalline W specimens (99.6 at.% purity)

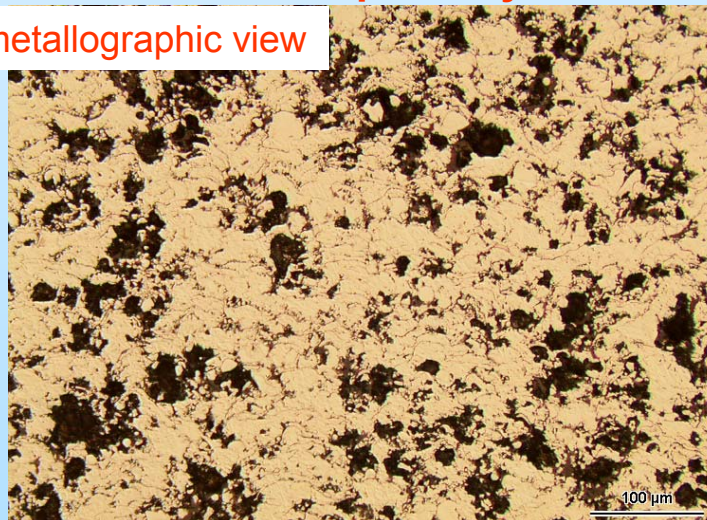
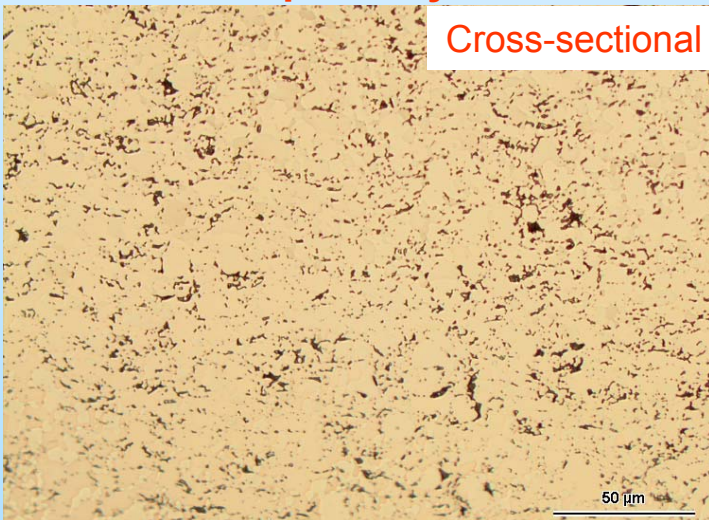
(iii) vacuum plasma sprayed W coatings
(0.5-2 mm thick)

9% porosity

30% porosity



Cross-sectional metallographic view



Experimental: D ion irradiation

The Garching high current ion source:

- mono-energetic mass-separated ion beam
- temperature controlled (300-873 K)

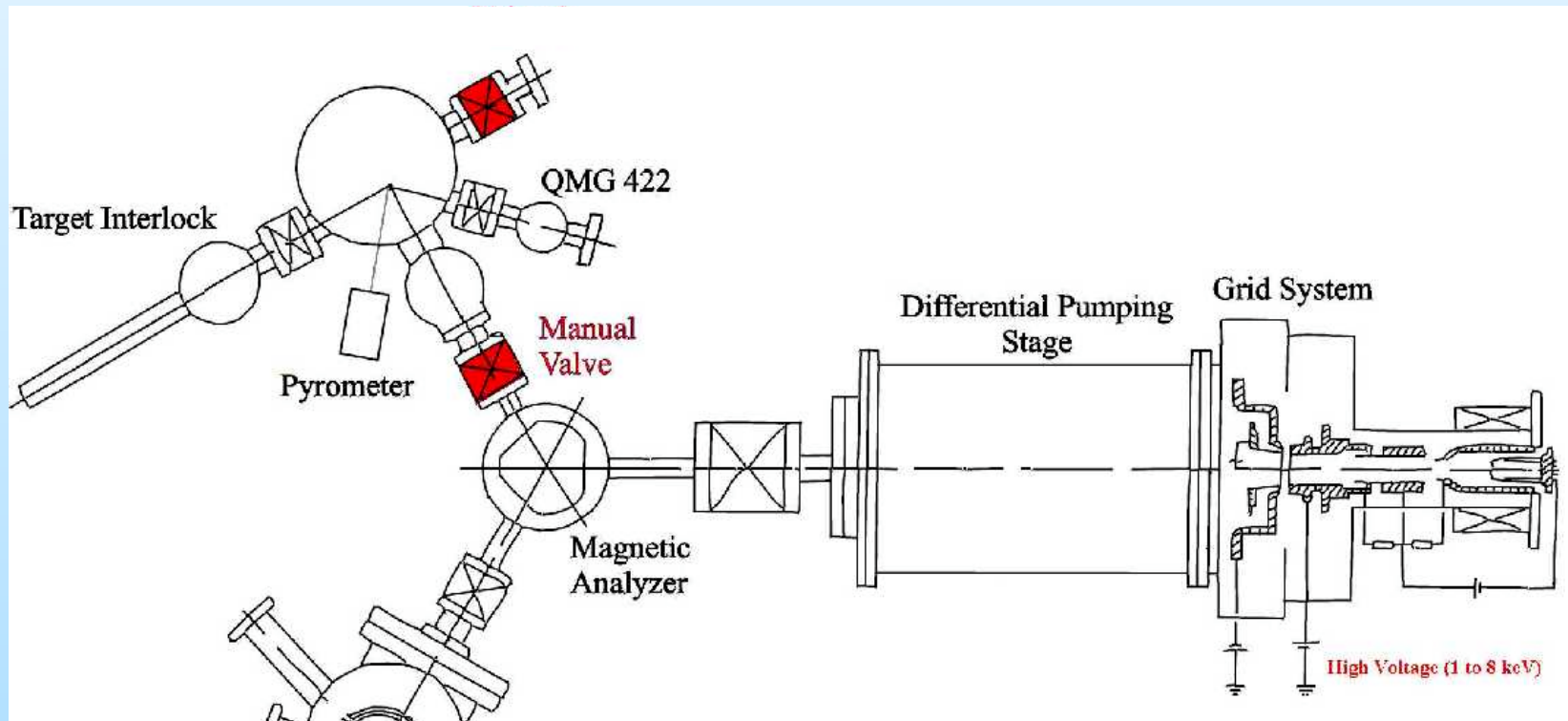
600 eV D_3^+ ions \Rightarrow **200 eV D ions**

flux = $(1.9 \pm 0.2) \times 10^{18}$ D/m²s (W single crystals)

flux = $(3.6 \pm 1.1) \times 10^{19}$ D/m²s (other W materials)

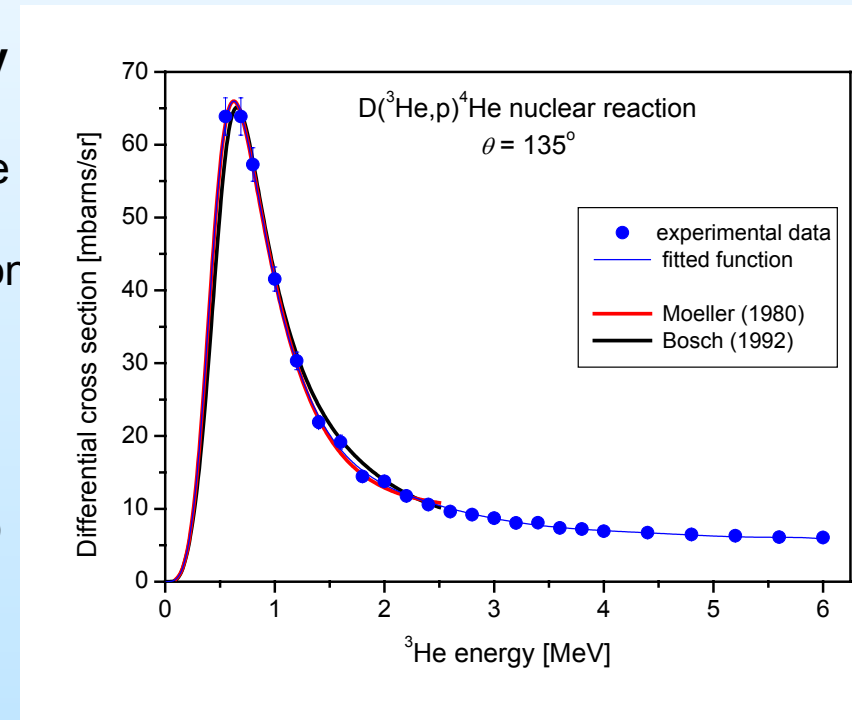
3000 eV D_2^+ ions \Rightarrow **1500 eV D ions**

flux = $(2.7 \pm 0.5) \times 10^{19}$ D/m²s



Deuterium depth profiling using the $D(^3\text{He},p)^4\text{He}$ resonance

- The $D(^3\text{He},p)^4\text{He}$ nuclear reaction is utilized. ^4He 3MeV, p 14MeV.
- Energy of analyzing ^3He beam: **0.69 to 4.0 MeV**
- Energy analysis of ^4He gives near surface profile
- The proton yields as a function of incident ^3He ion energy are measured.
- The computer program SIMNRA is used for the deconvolution of the proton yield.
A depth distribution $C_D(x)$ is assumed taking into account the near-surface depth profile obtained from the α particles spectrum, and the proton yields for different ^3He energies are calculated.
- The form of $C_D(x)$ is then varied using an iterative technique until the calculated proton yields match the proton yields measured.

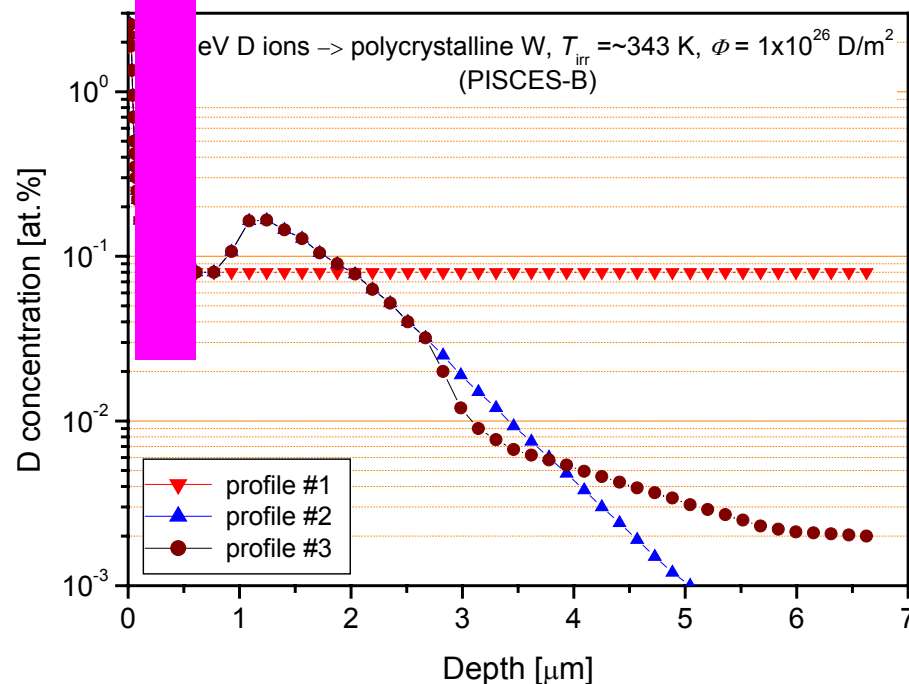
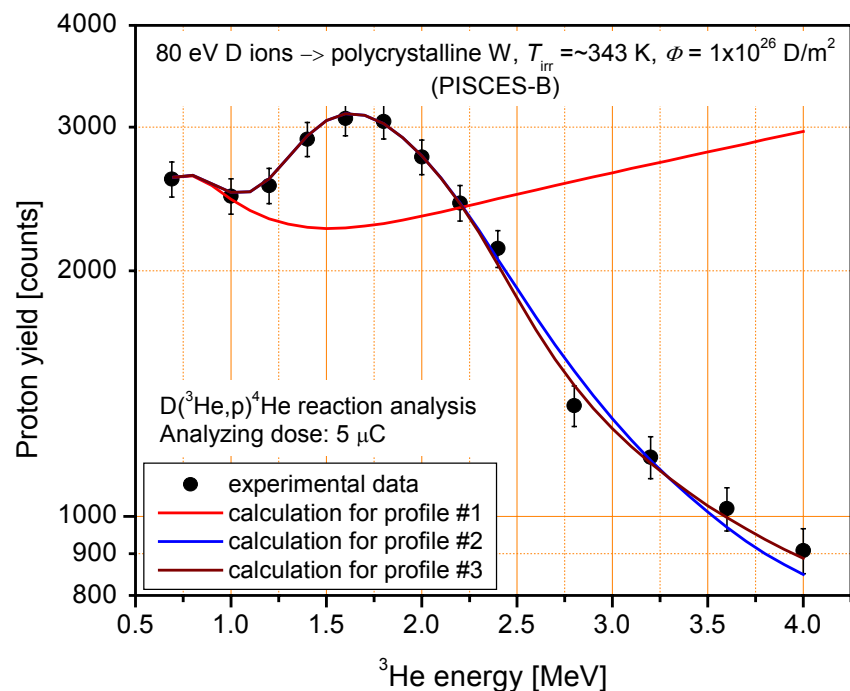


Deuterium depth profiling using the $D(^3\text{He},p)^4\text{He}$ resonance.

Representative example of depth profile determination

Specimen: polycrystalline W exposed to low energy (~ 80 eV/D) and high flux (10^{22} D/m²s) D plasma at 343 K to $\Phi = 1 \times 10^{26}$ D/m² (PISCES-B, R. Doerner, M. Baldwin, UCSD)

The D profile up to depth of 0.6 μm was determined by means of the $D(^3\text{He},\alpha)\text{H}$ reaction at a ^3He energy of 0.69 MeV

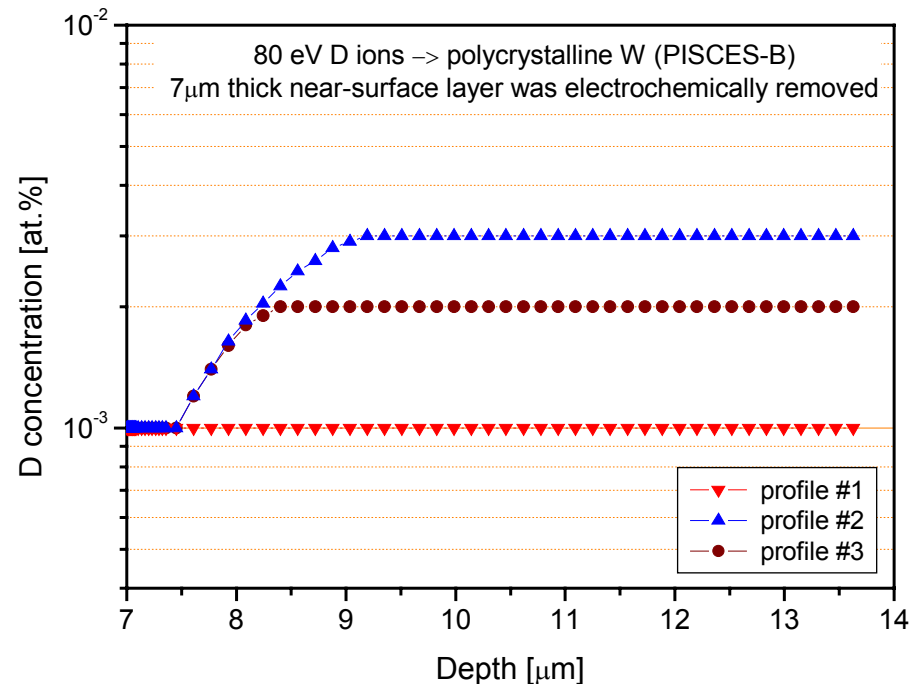
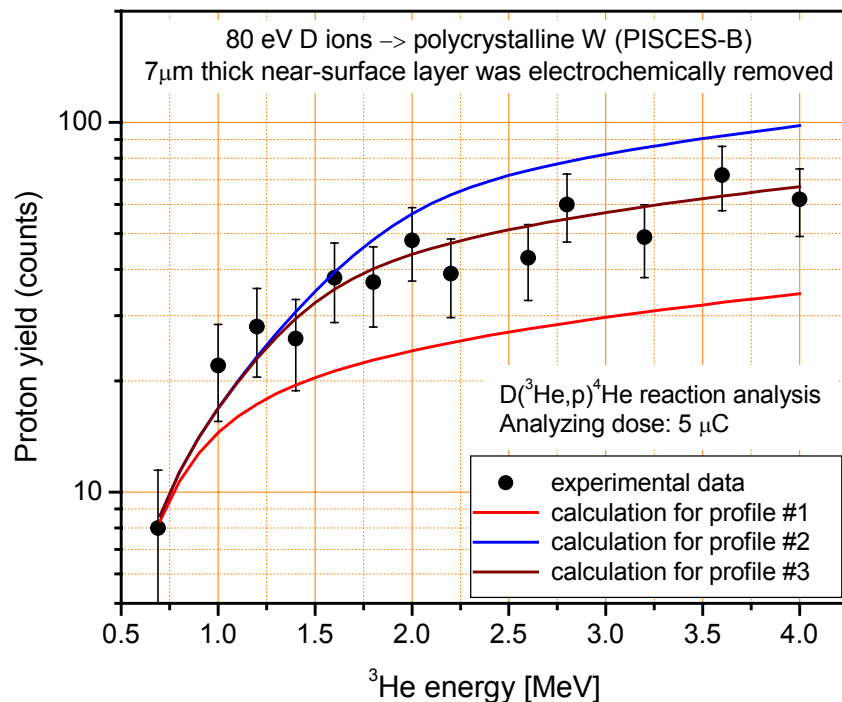


Deuterium depth profiling using the $D(^3\text{He},p)^4\text{He}$ resonance.

Representative example of depth profile determination

Specimen: polycrystalline W exposed to low energy (~ 80 eV/D) and high flux (10^{22} D/m 2 s) D plasma at 343 K to $\Phi = 1 \times 10^{26}$ D/m 2 (PISCES-B, R. Doerner, M. Baldwin, UCSD)

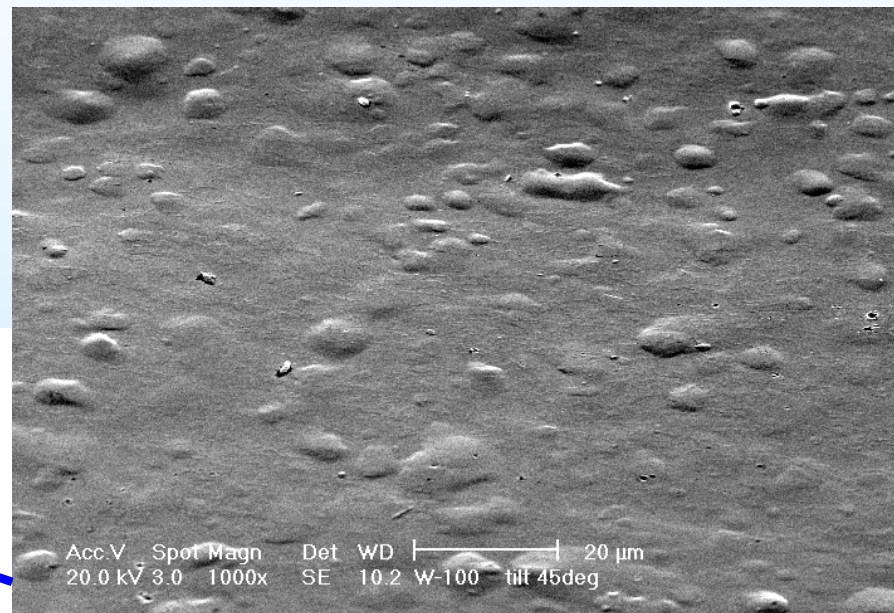
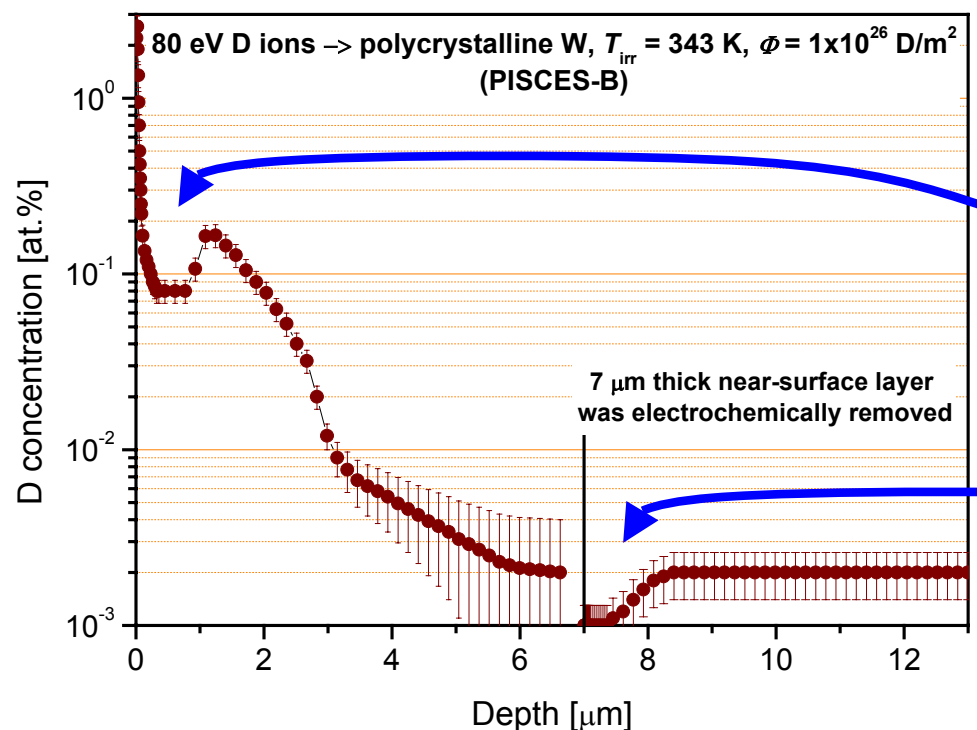
In order to estimate the D concentration in the bulk, 7 μm thick near-surface layer was electrochemically removed



Deuterium depth profiling using the $D(^3\text{He},p)^4\text{He}$ resonance.

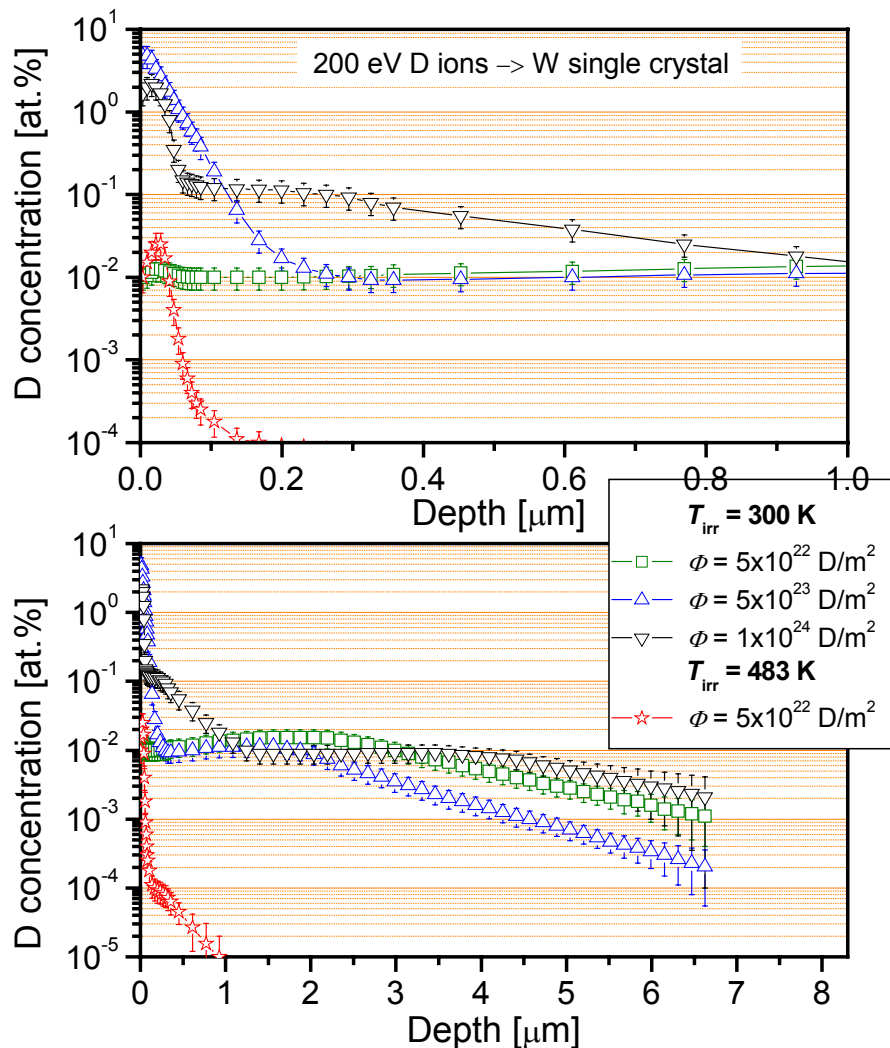
Representative example of depth profile determination

The minimum in the D concentration at depths of 0.5-1 μm is related to blister formation. Interconnected porosity is formed and molecular deuterium is released.



Due to electrochemical removal, the near-surface layer is saturated with protium, and isotopic exchange takes place.

W single crystals irradiated with 200 eV D ions

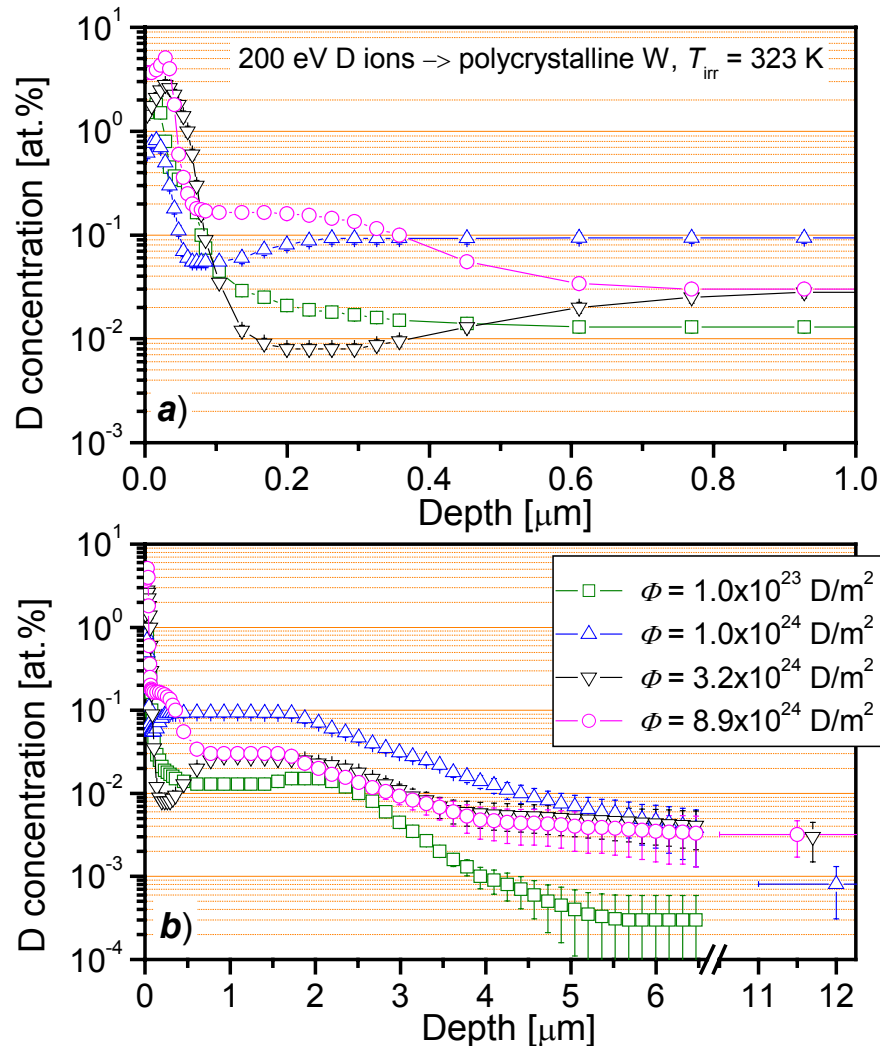


The depth at which deuterium is retained can be divided into three zones:

- (i) the near-surface layer (up to a depth of $\sim 0.2 \mu\text{m}$),
- (ii) the sub-surface layer (from ~ 0.5 to $\sim 3 \mu\text{m}$),
- (iii) the bulk ($> 4 \mu\text{m}$).

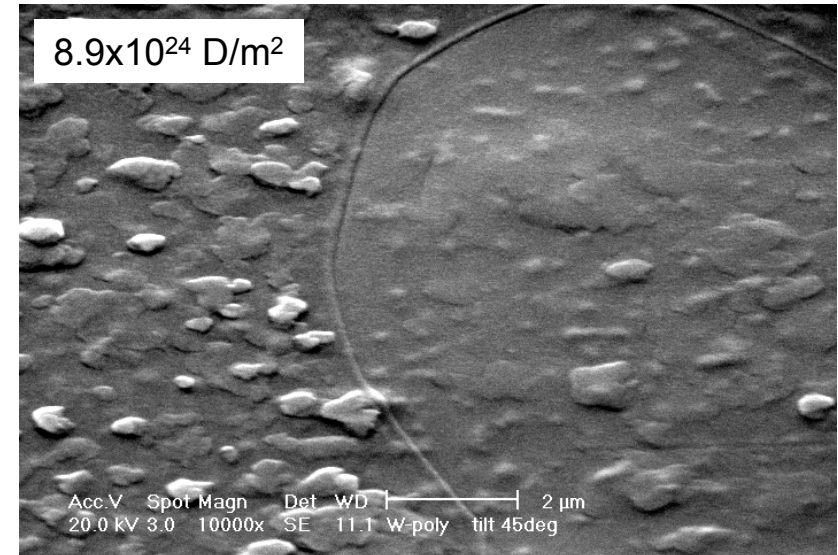
- At $T_{\text{irr}} = 300 \text{ K}$, the sub-surface structure (0.5 to $3 \mu\text{m}$) is transformed at $\Phi < 5 \times 10^{22} \text{ D/m}^2$.
- The drastic increase of the D concentration in the near-surface layer (up to $0.2 \mu\text{m}$) at $5 \times 10^{22} < \Phi < 5 \times 10^{23} \text{ D/m}^2$ can be only explained by a sudden structure change during the low-energy D ion irradiation.
- At $T_{\text{irr}} = 488 \text{ K}$, deuterium is accumulated mainly in the near-surface layer.
At the same ion fluence, the D concentration in the near-surface layer at $T_{\text{irr}} = 488 \text{ K}$ is slightly higher than that for $T_{\text{irr}} = 323 \text{ K}$.

Polycrystalline W irradiated with 200 eV D ions at 323 K



The depth at which deuterium is retained can be divided into three zones:

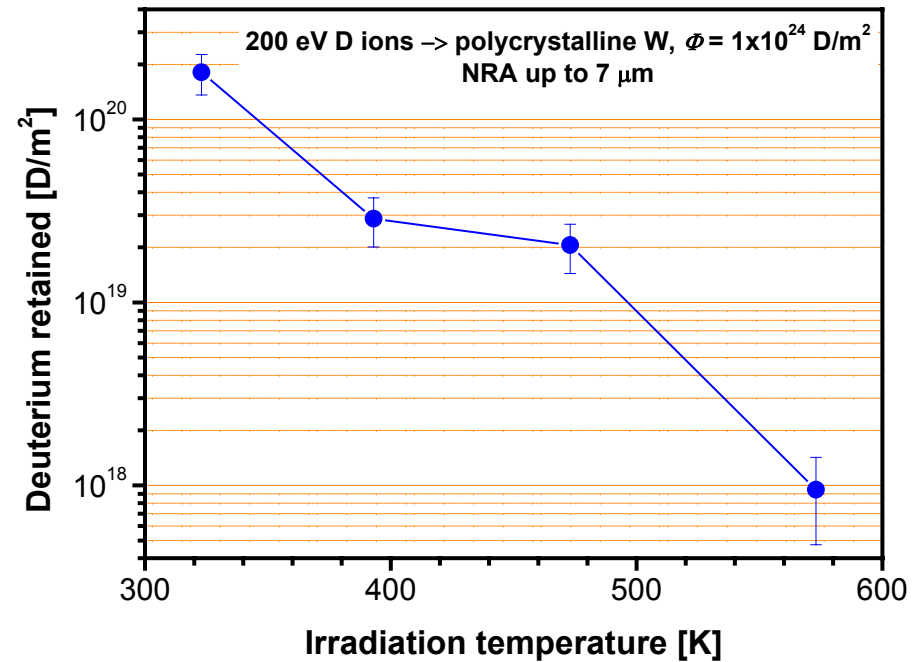
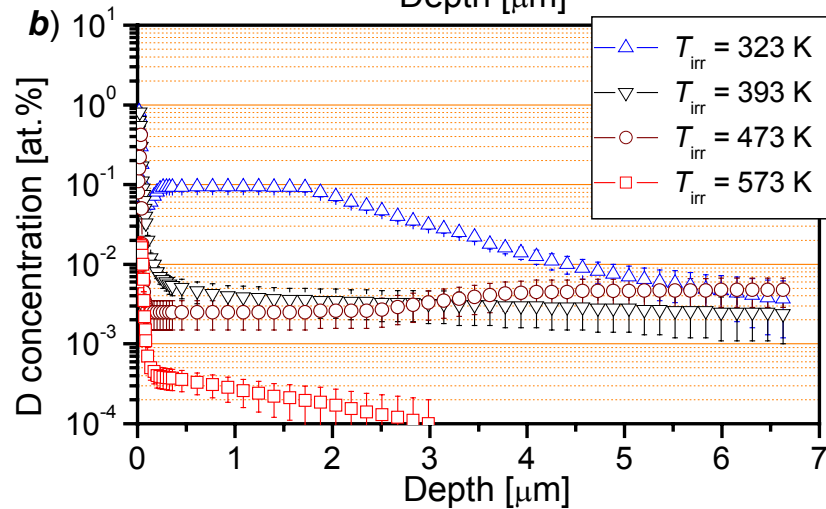
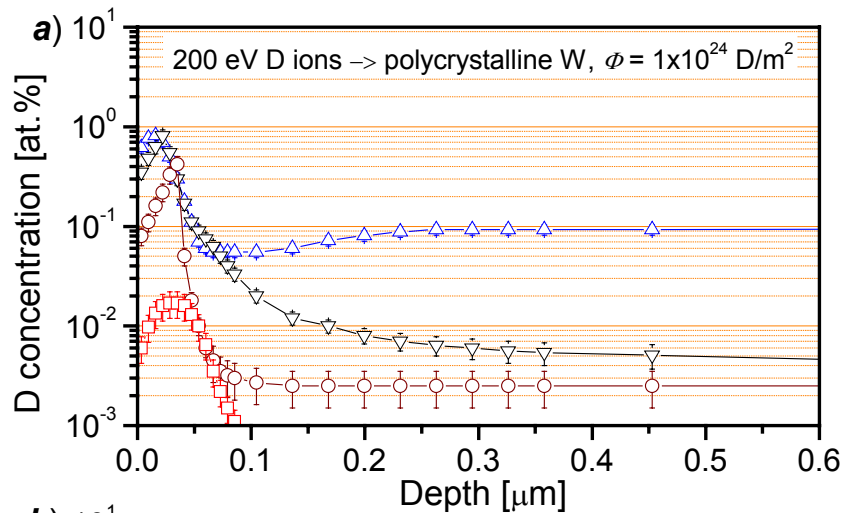
- (i) the near-surface layer (up to a depth of ~ 0.2 μm),
- (ii) the sub-surface layer (from ~ 0.5 to ~ 2 μm),
- (iii) the bulk (> 5 μm).



- D_2 - filled voids are formed in the near- and sub-surface layers.
- As Φ increases, interconnected porosity starts develop.
- A fraction of the molecular deuterium is released.
- In the bulk deuterium is trapped at intrinsic defects.

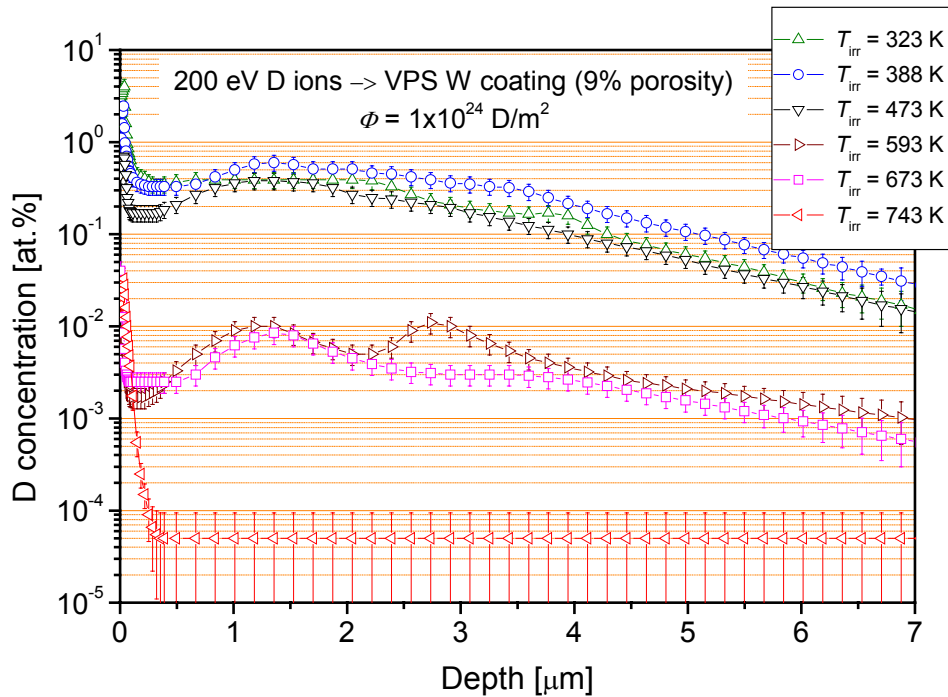
Polycrystalline W irradiated at different temperatures

with 200 eV D ions, fluence 1×10^{24} D/m²

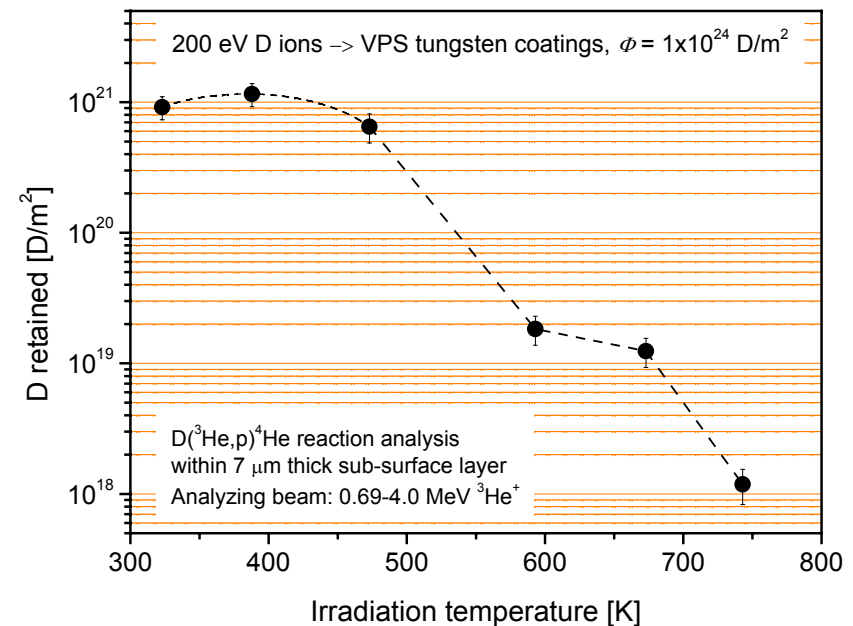
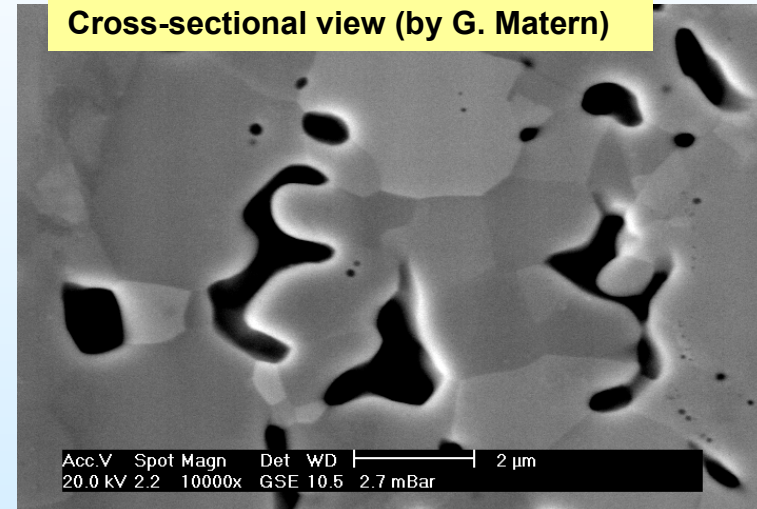


Plasma vacuum spray W coatings (9% porosity)

200 eV D ions at T_{irr} between 328 and 743 K, $\Phi = 1 \times 10^{24}$ D/m²



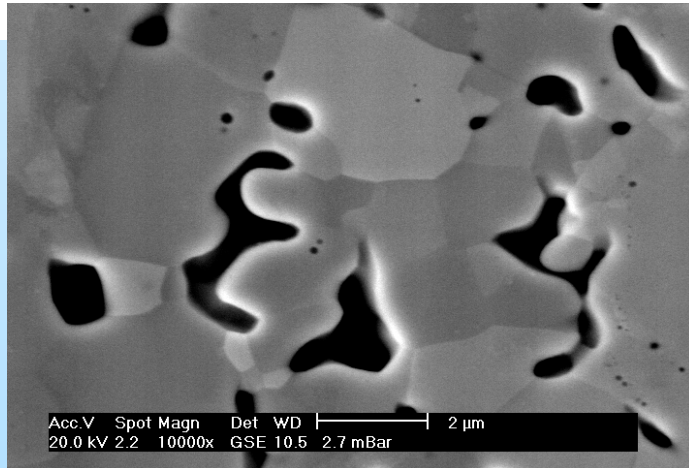
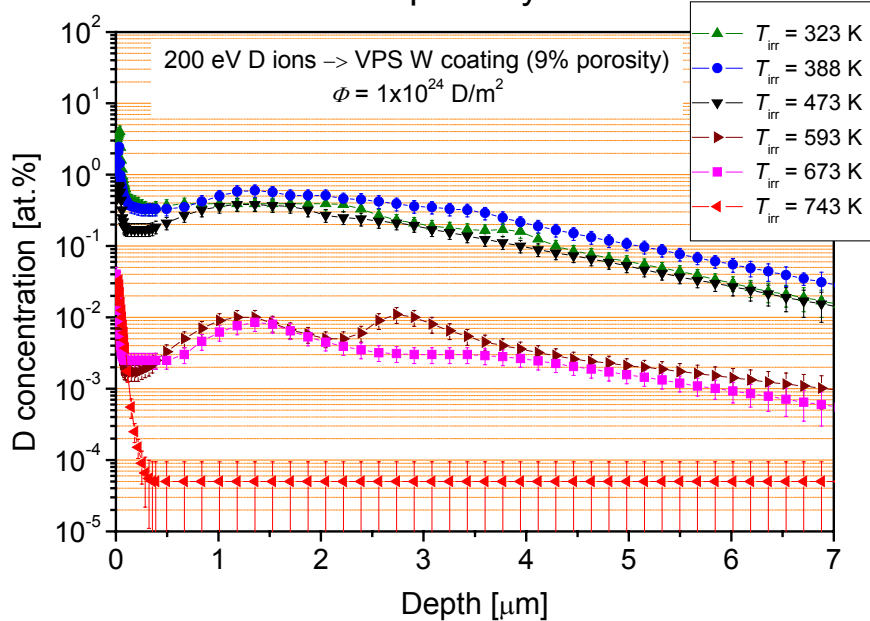
Cross-sectional view (by G. Matern)



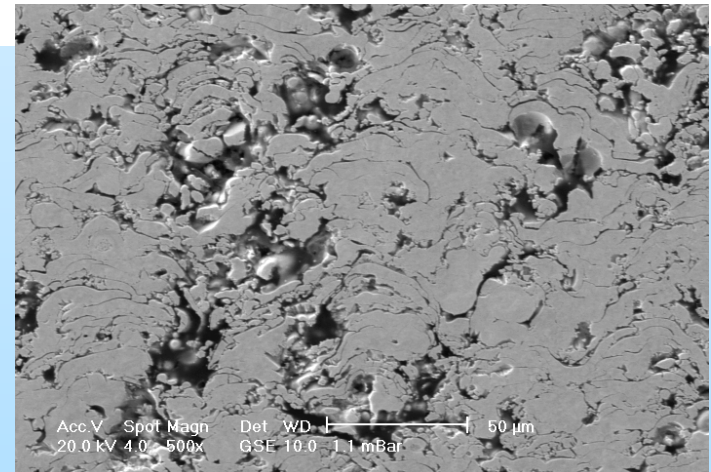
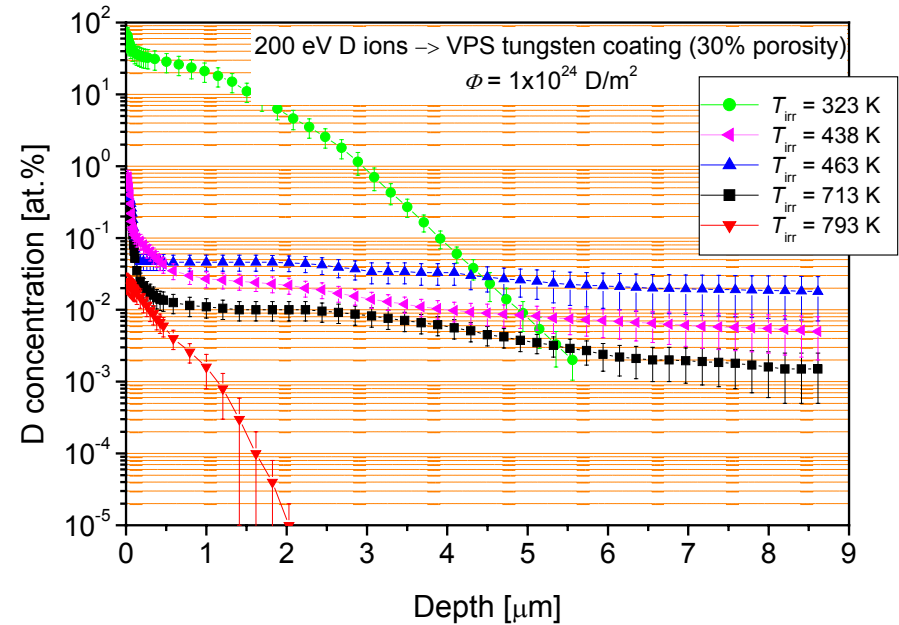
Plasma vacuum spray W coatings

200 eV D ions at T_{irr} between 328 and 743 K, $\Phi = 1 \times 10^{24}$ D/m²

9% porosity



30% porosity



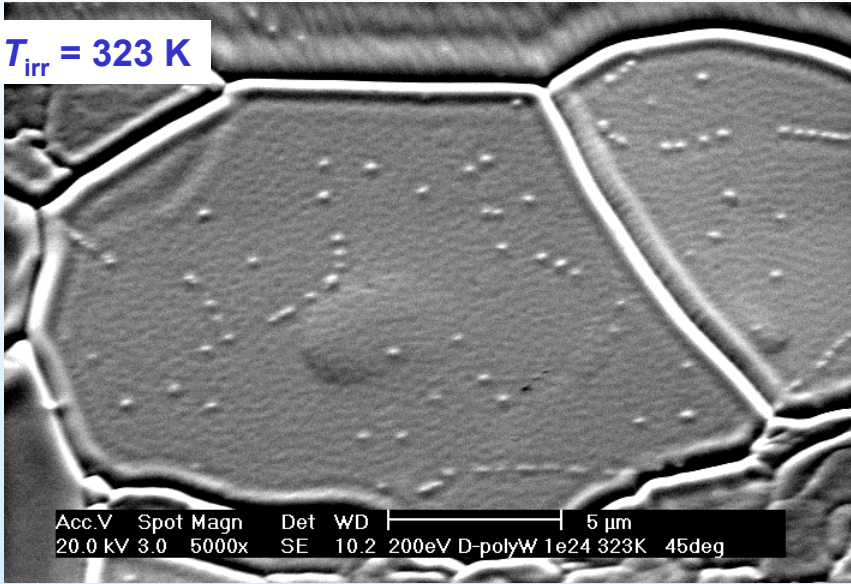
Summary

- Depth profiles of deuterium trapped in W materials have been determined up to a depth of 7 μm using the $\text{D}(^3\text{He},\text{p})^4\text{He}$ reaction in a resonance-like technique.
- The depth at which deuterium is retained in W single crystals and polycrystalline W can be tentatively divided into three zones:
 - (i) the near-surface layer (up to a depth of $\sim 0.2 \mu\text{m}$),
 - (ii) the sub-surface layer (from ~ 0.5 to $\sim 2 \mu\text{m}$),
 - (iii) the bulk ($> 5 \mu\text{m}$).
- The D concentration at high ion fluences $\geq 1 \times 10^{24} \text{ D/m}^2$ decreases from several at.% in the near-surface layer to below 10^{-4} at.% for W single crystal and 3×10^{-3} at.% for polycrystalline W in the bulk.
- Blister formation at high fluences accompanied by D release is observed for polycrystalline W, but not for W single crystals.
- D ion irradiation with ion energies well below the displacement threshold modifies the W structure to depths of up to about 5 μm , both in W single crystals and polycrystalline W.
- Plastic deformation of the W matrix caused by deuterium supersaturation within the near-surface layer is proposed as explanation of the present results.
- D retention depends strongly on the structure of W materials. The highest D concentrations were found in VPS W coatings.

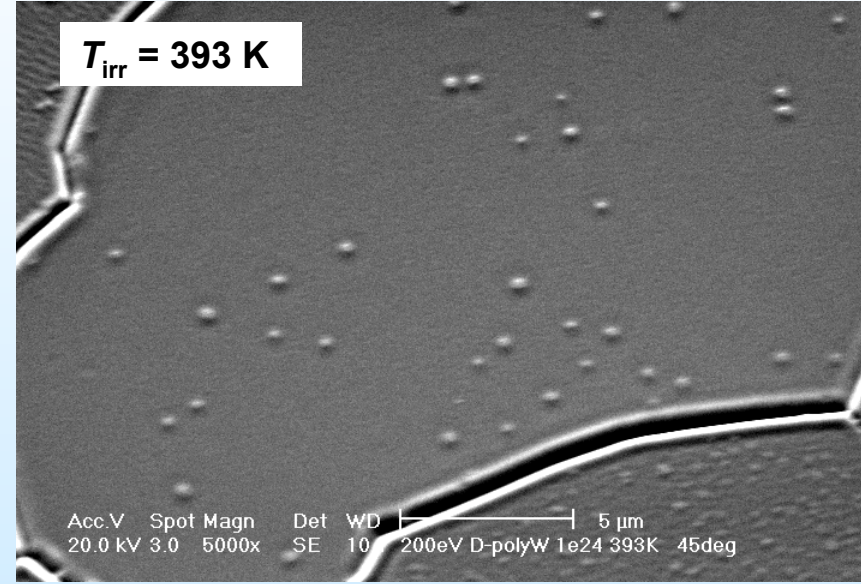
Polycrystalline W irradiated at different temperatures

with 200 eV D ions, fluence 1×10^{24} D/m²

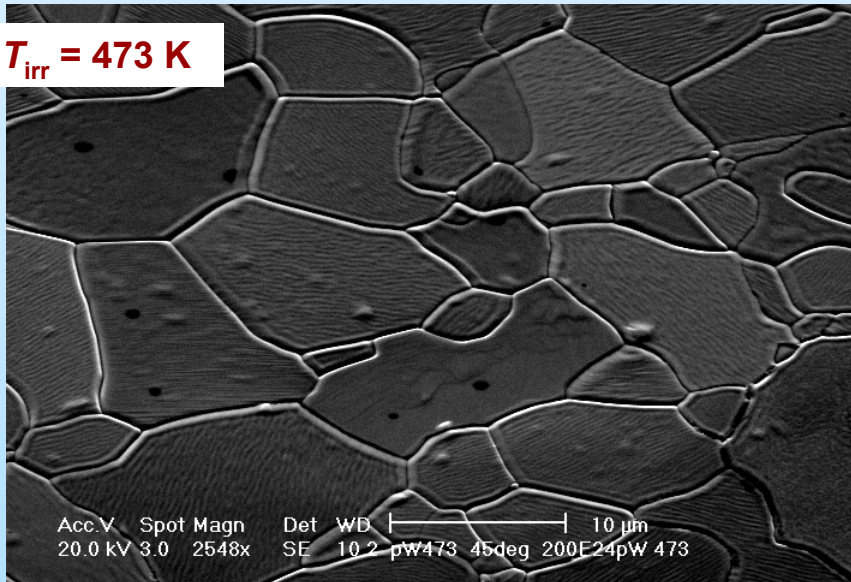
$T_{\text{irr}} = 323$ K



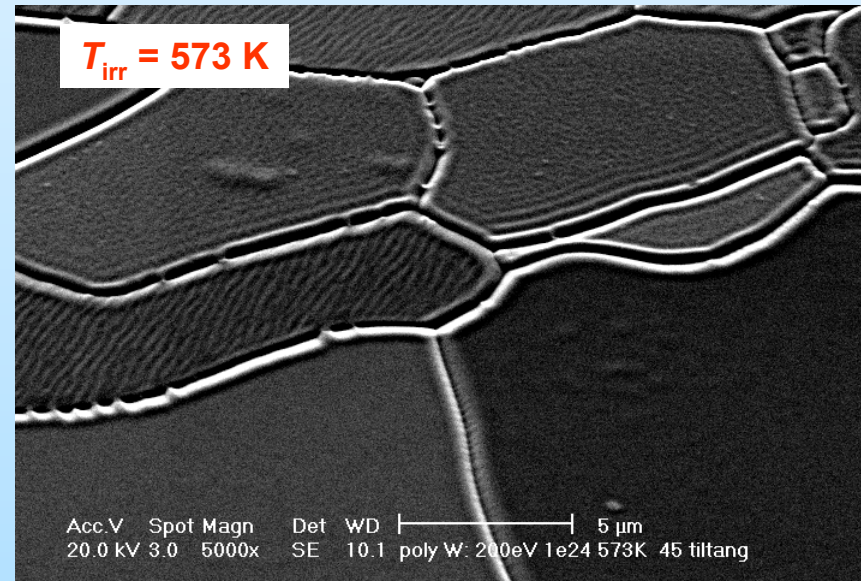
$T_{\text{irr}} = 393$ K



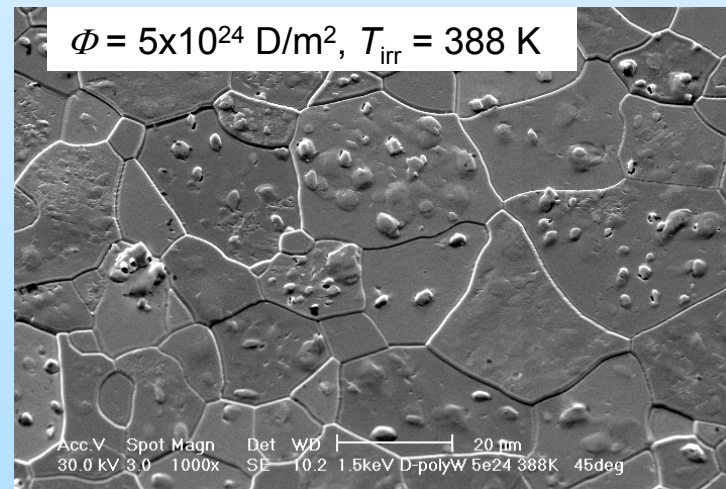
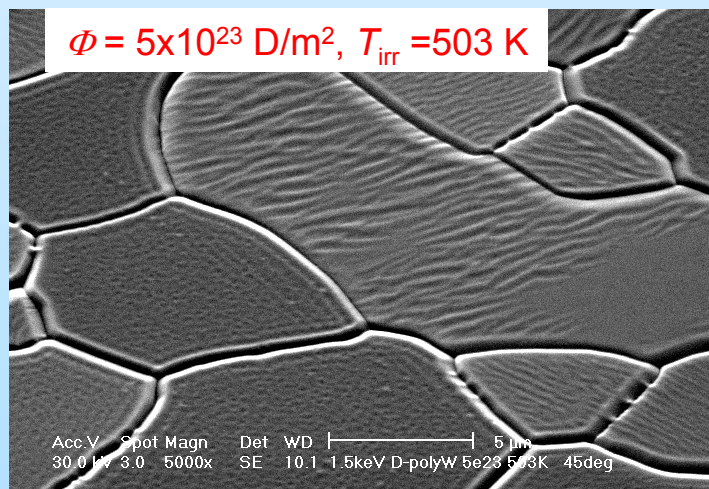
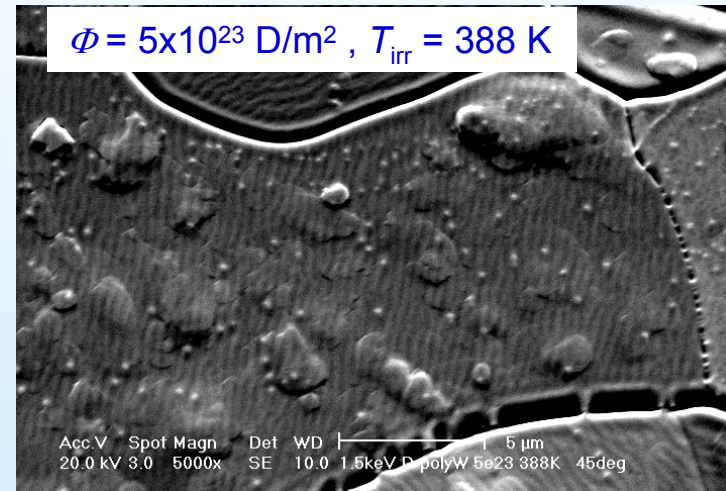
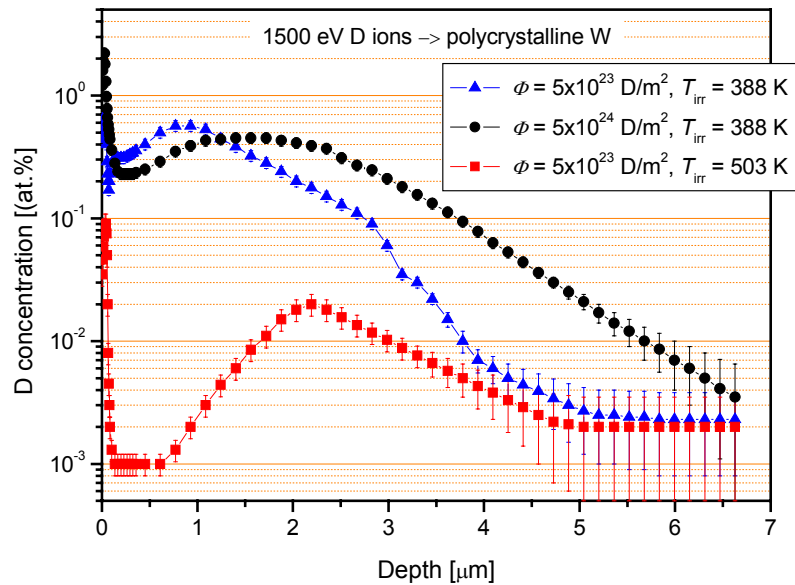
$T_{\text{irr}} = 473$ K



$T_{\text{irr}} = 573$ K

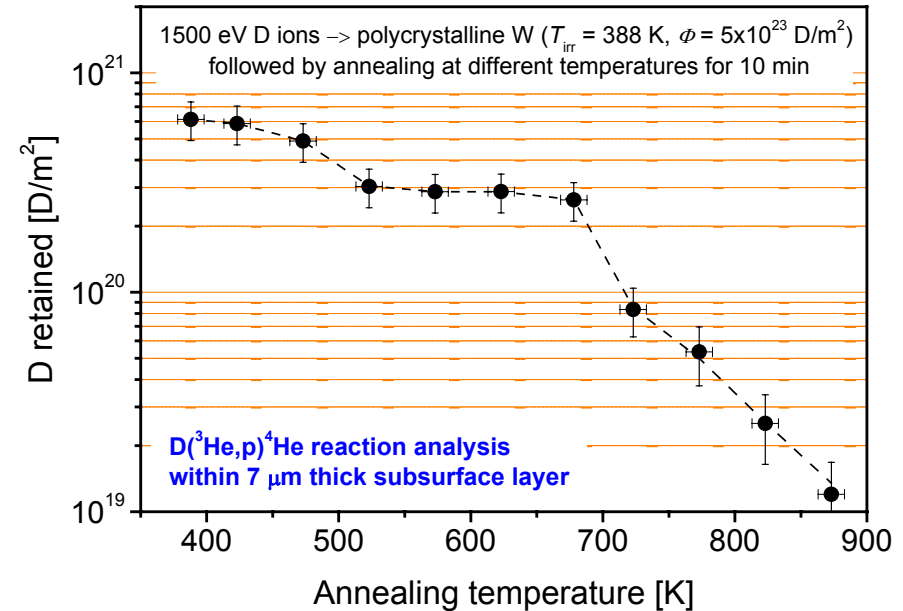
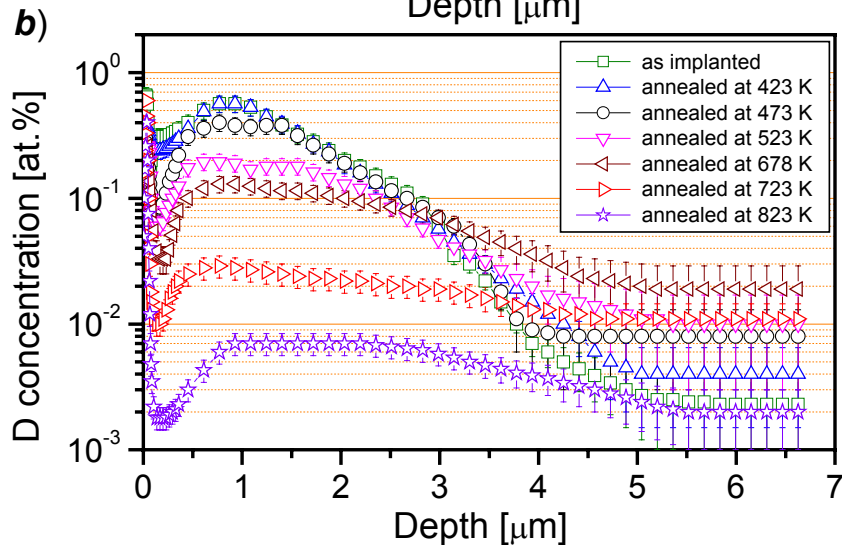
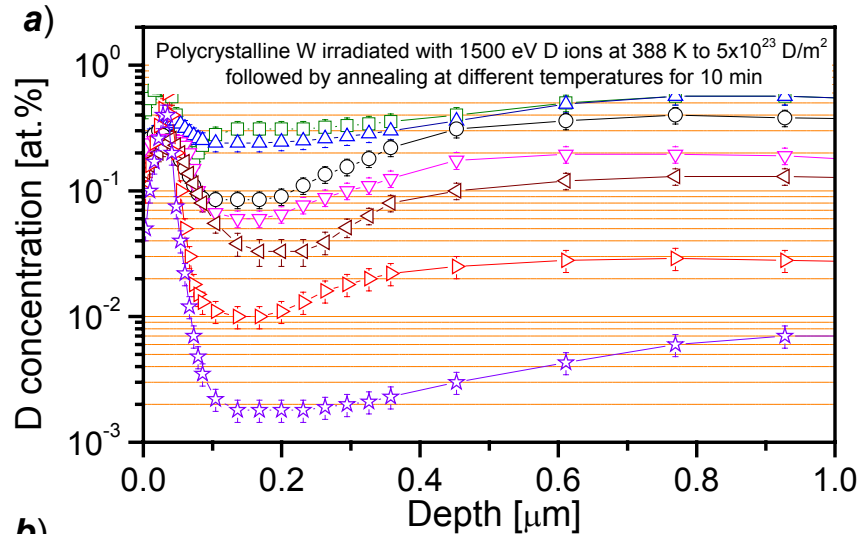


Polycrystalline W irradiated with 1500 eV D ions



Polycrystalline W irradiated with 1500 eV D ions

at 388 K to a fluence of 5×10^{23} D/m² followed by annealing at different temperatures for 10 min

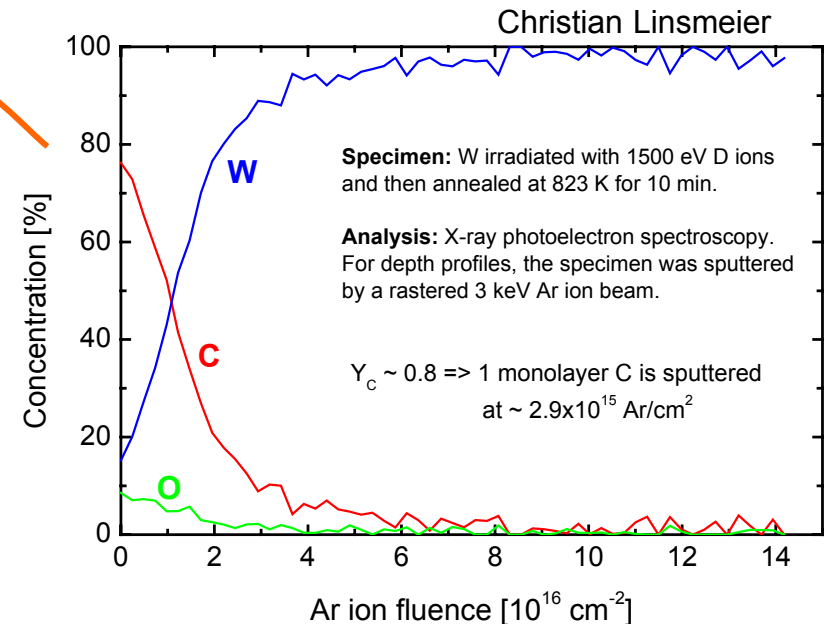
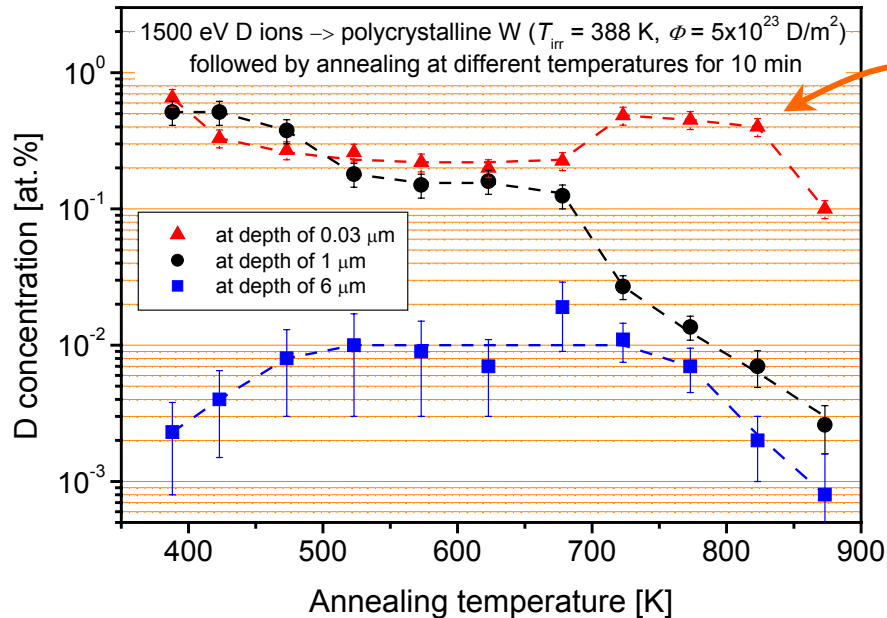


There are two temperature ranges in which the decrease of the D content is observed:

- (1) 450-520 K;
- (2) >680 K.

Polycrystalline W irradiated with 1500 eV D ions

at 388 K to a fluence of 5×10^{23} D/m² followed by annealing at different temperatures for 10 min



A. van Veen *et al.* [1985] PA study of deuterium-defects interaction in W:

D_2 gas inside the voids is expected to be released during annealing at 400-600 K (dissociation energy ~ 1.4 eV);
D atoms bound on the inner surface of voids (binding energy ~ 2.1 eV) is released at 700-900 K.

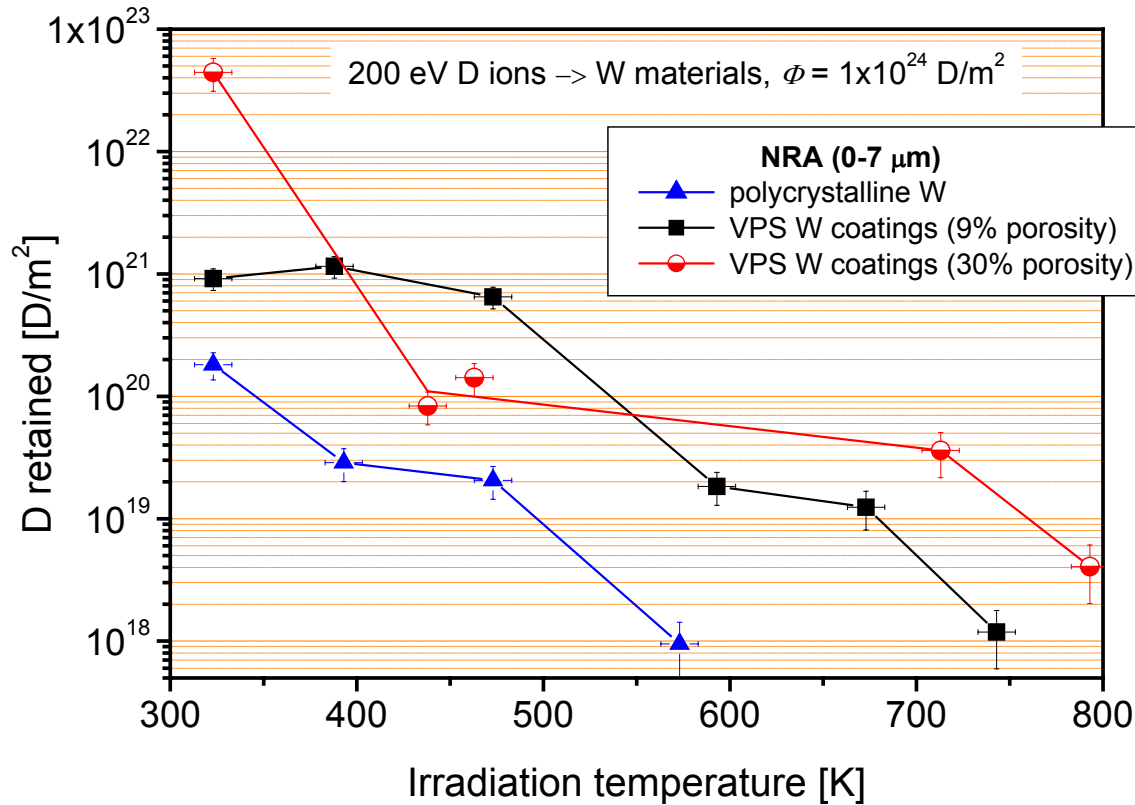
During D ion irradiation at $T_{\text{irr}} = 323$ K:

in the near- and subsurface layers - D_2 molecules are accumulated in the stress-induced voids.

in the bulk - chemisorption of D atoms on inner surfaces of microscopic-sized cavities (intrinsic defects) takes place.

Plasma vacuum spray W coatings

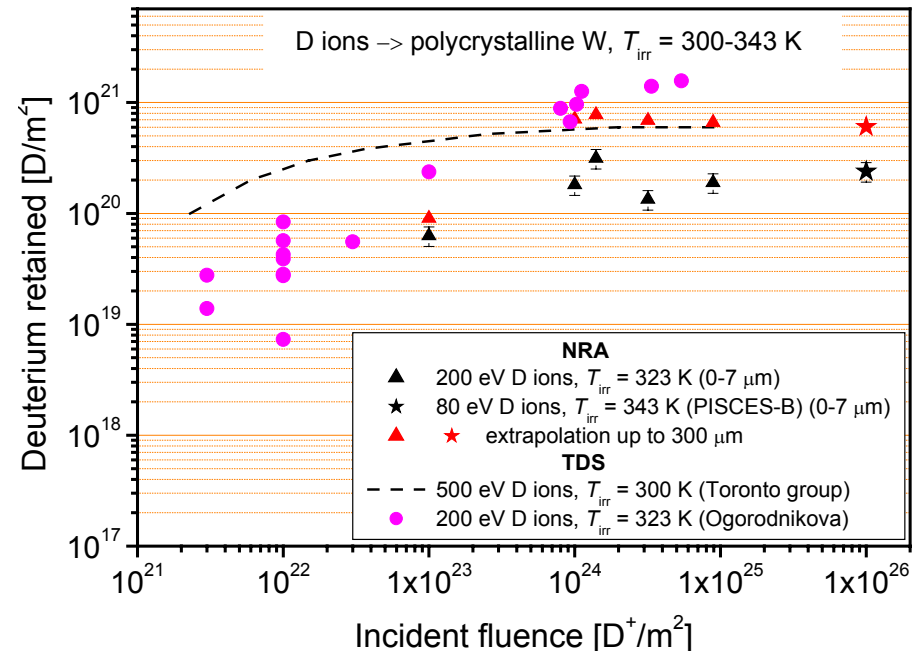
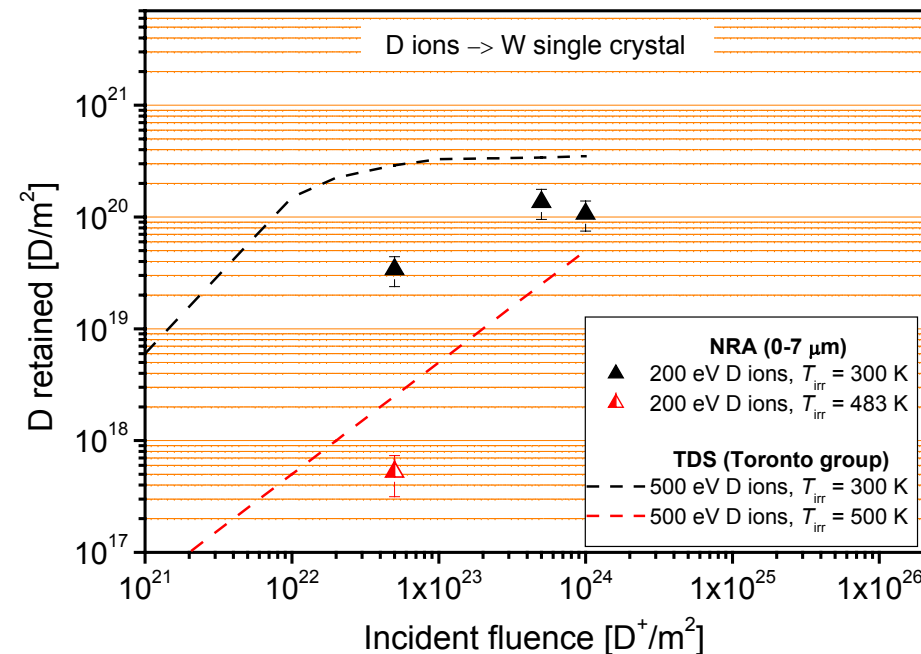
200 eV D ions at T_{irr} between 328 and 743 K, $\Phi = 1 \times 10^{24}$ D/m²



D retention in W single crystals and polycrystalline W

- During low energy D ion irradiation, the D concentration in the implantation zone greatly exceeds the solubility limit and stresses the matrix lattice.
- Plastic deformation with formation of voids and vacancy clusters occurs to alleviate these tensions.
- Concurrently the accumulation of deuterium both in the form of D_2 molecules and D atoms takes place.

The D content in W crystal and polycrystalline W (0-7 μm) agrees well with values measured by TDS.



Acknowledgments

J. Dorner

M. Fußeder

S. Lindig

Ch. Linsmeier

G. Matern

J. Perchermeier

A. Weghorn

A. Wiltner



ION-DRIVEN DEUTERIUM BEHAVIOUR IN TUNGSTEN

O.V. Ogorodnikova¹, J. Roth², M. Mayer²,

¹*IWV-2, FZ-Jülich GmbH, EURATOM ASS., D-52425 Jülich, Germany*

²*Max-Planck-Institut für Plasmaphysik, EURATOM ASS., Garching, Germany*

Inventory in polycrystalline tungsten as a function of

(i) fluence

(ii) energy

(iii) temperature

**Mechanism of D retention: ion-induced defects as a result
of the D diffusion and trapping in stress field.**

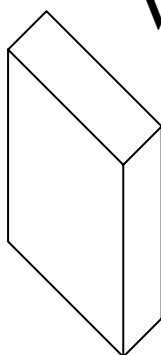


Method: Thermal desorption spectroscopy

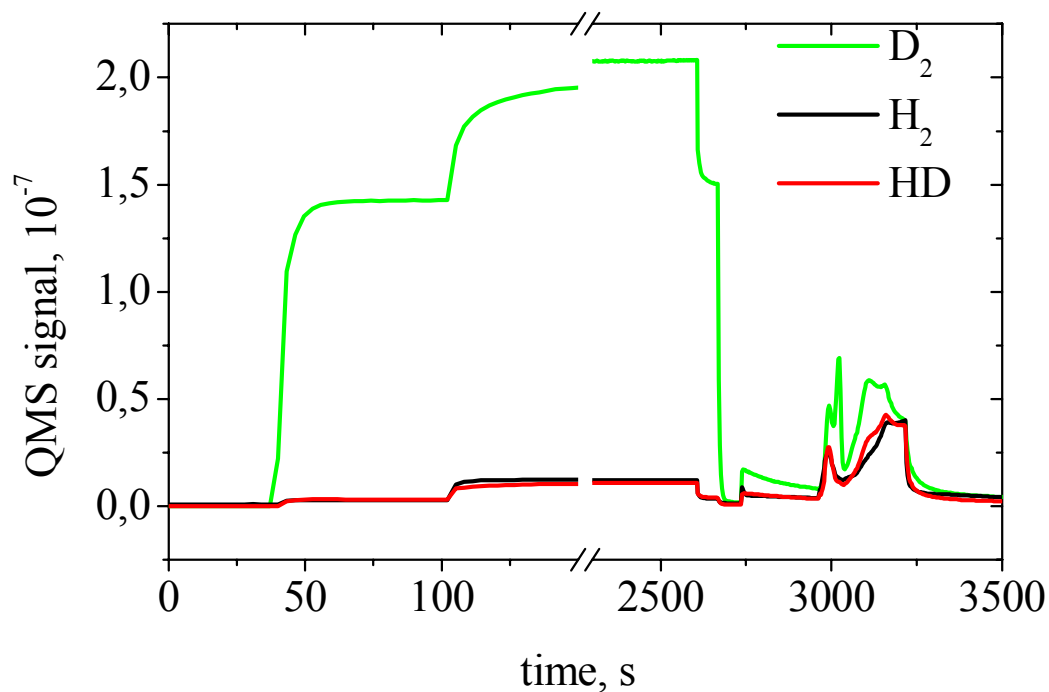


polycrystalline W (99.96%)
W (99.999%) (L=0.5 mm)

Implantation of D⁺
200 eV
3000 eV



Linear temperature ramp
-> TDS



Sample preparation:

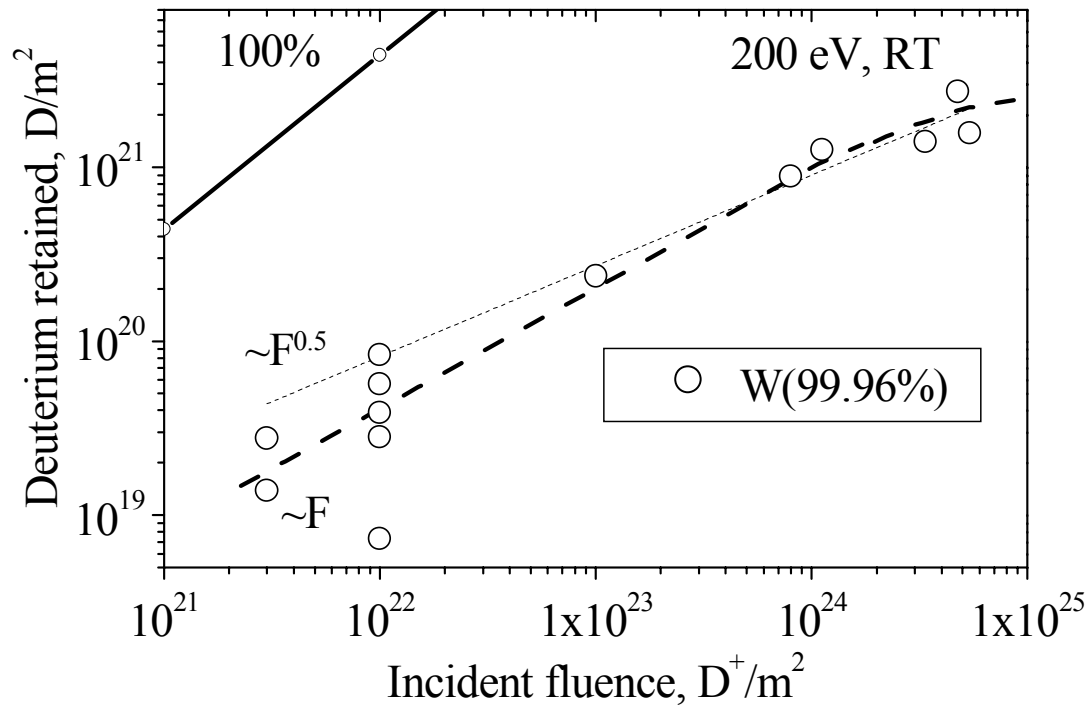
-1300°C 3 hours heating at $p=10^{-6}$ Torr

*- outgasing at 1000°C 10 min.
just before implantation*

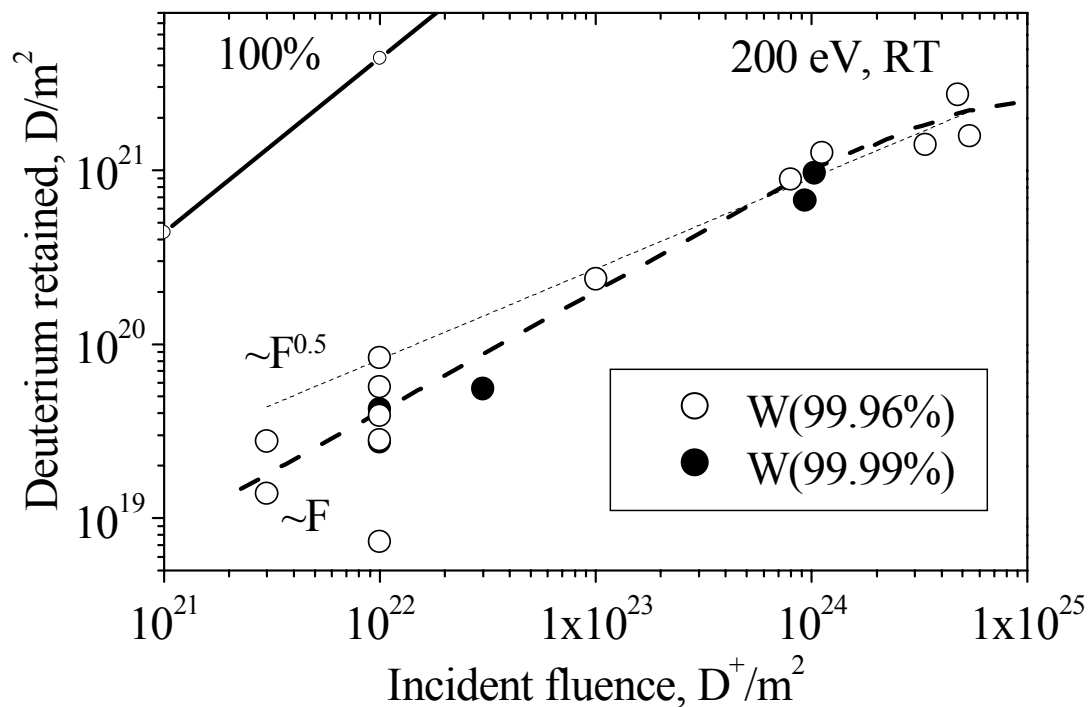


200 eV D⁺ -> PCW: Fluence dependence

IPP



1. D retention increases slightly faster than a square root of the fluence \Rightarrow diffusion-limited trapping
2. Causey et al. and Van Veen et al. demonstrated a similar fluence dependence

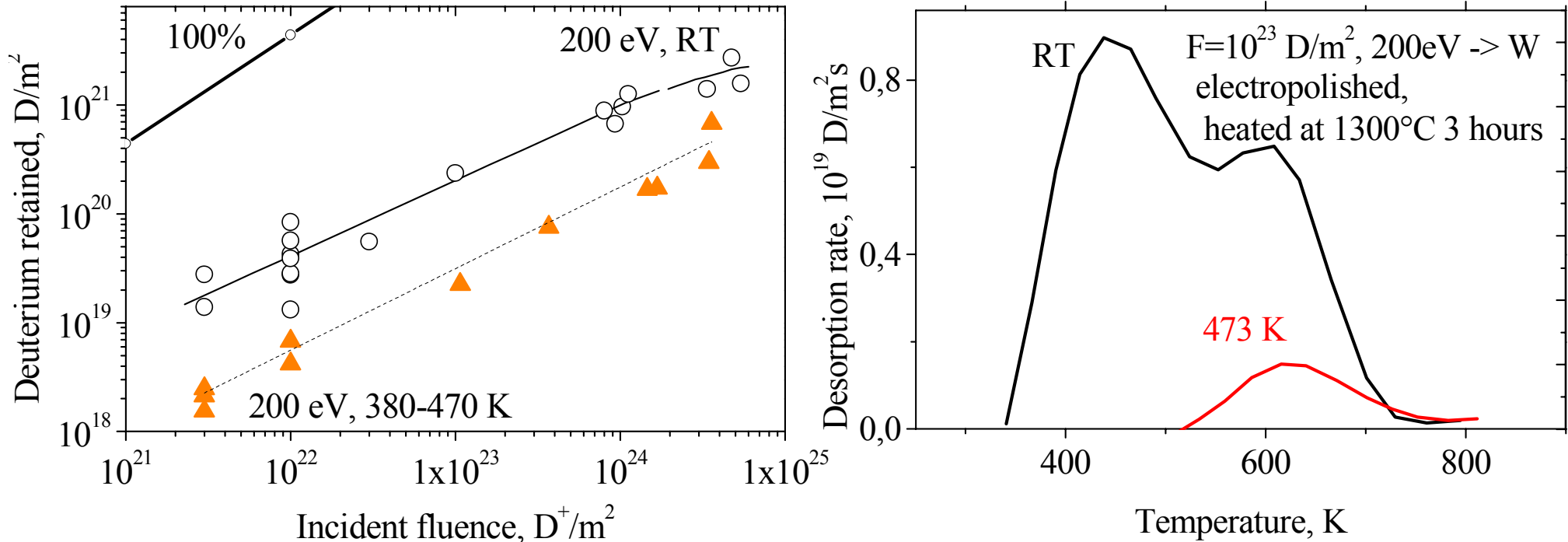


Small change in Purity of W does not influence deuterium inventory

- 1. D retention increases slightly faster than a square root of the fluence \Rightarrow diffusion-limited trapping**
- 2. Causey et al. and Van Veen et al. demonstrated a similar fluence dependence**



200 eV D⁺ -> PCW: Temperature dependences



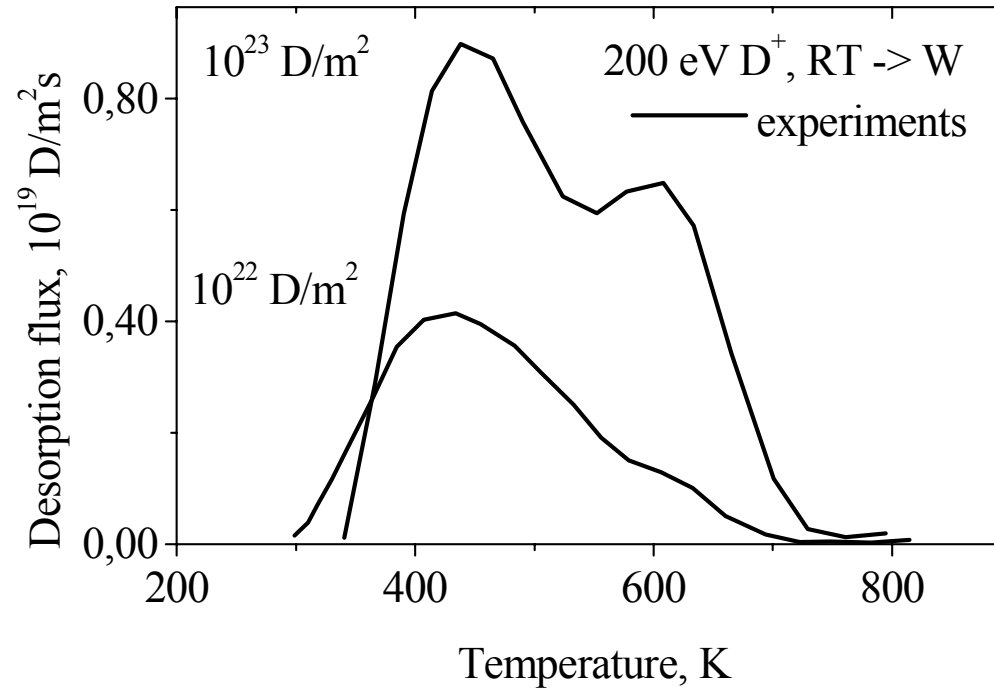
**Increase of the temperature \Rightarrow
decrease of the retention for pre-annealed W**

***However:* D retention most probably
increases with temperature for high
fluences**



TDS of 200 eV D⁺ -> PCW

IPP



D retention in both peaks increases with fluence



What is the mechanism of D trapping in Polycrystalline W?



Trapping of deuterium in Polycrystalline W

IPP

Present model

1. natural defects:

$$W_t = \text{const}$$

Dislocations,
Grain boundaries

Vacancies

2. ion-induced defects:

$$W_t = f(W_m, \eta, I_0)$$



$$dW_t/dt = (1-r)I_0\psi(x)(1-\eta W_t/W_m)$$

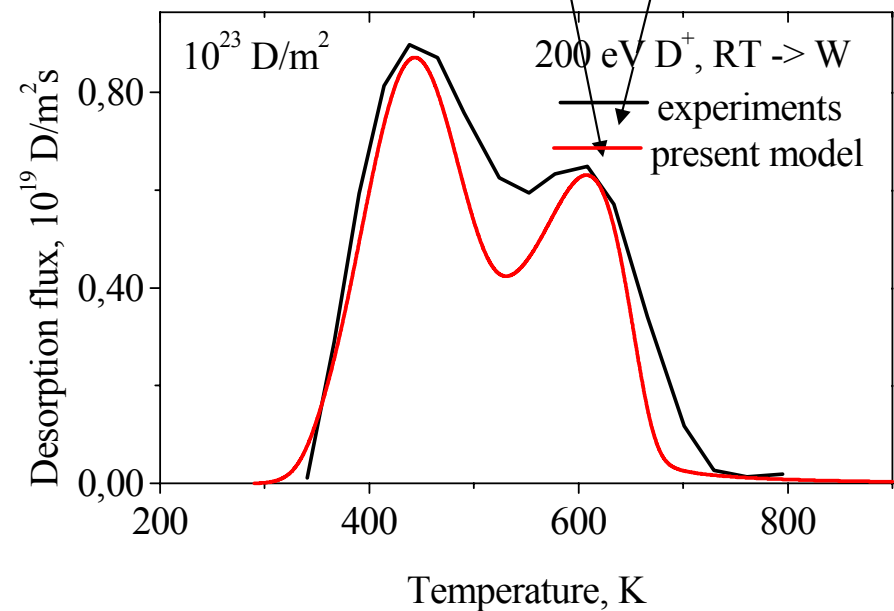
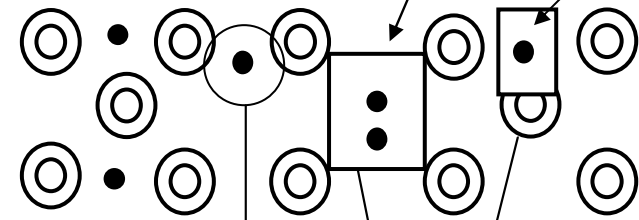
E_i

G. Duesing: Spontaneous Recombination
of Defects in Metal

$$W_t(x,t) = W_m(1 - \exp(-(1-r)I_0\psi(x)\eta t/W_m))$$

Dislocations,
Grain boundaries

Bubbles, Vacancies





Evidence of ion-induced defects: no ion-induced defects => no second peak in TDS



Present model

1. natural defects:

$$W_t = \text{const}$$

Dislocations,
Grain boundaries

Vacancies

2. ion-induced defects:

$$W_t = f(W_m, \eta, I_0)$$



$$dW_t/dt = (1-r)I_0\psi(x)(1-\eta W_t/W_m)$$

E_i

G. Duesing: Spontaneous Recombination
of Defects in Metal

$$W_t(x,t) = W_m(1 - \exp(-(1-r)I_0\psi(x)\eta t/W_m))$$

Anderl-Longhurst's model

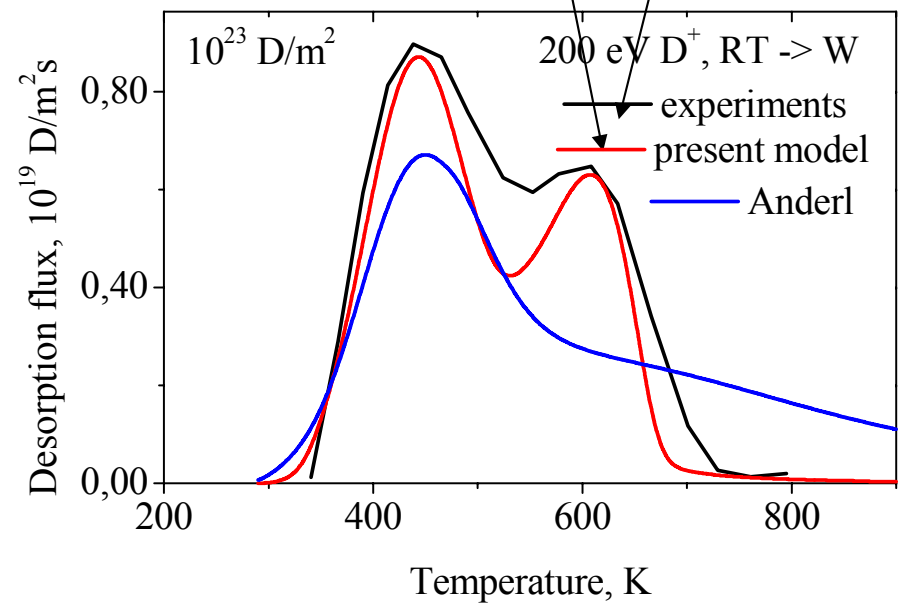
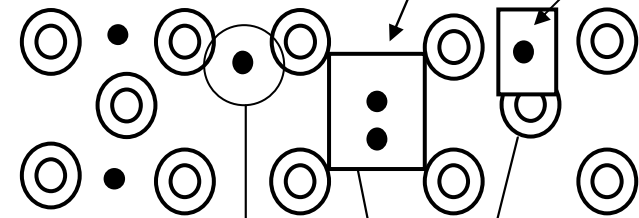
1. natural defects:

$$W_t = \text{const}$$

Vacancies

Dislocations,
Grain boundaries

Bubbles, Vacancies



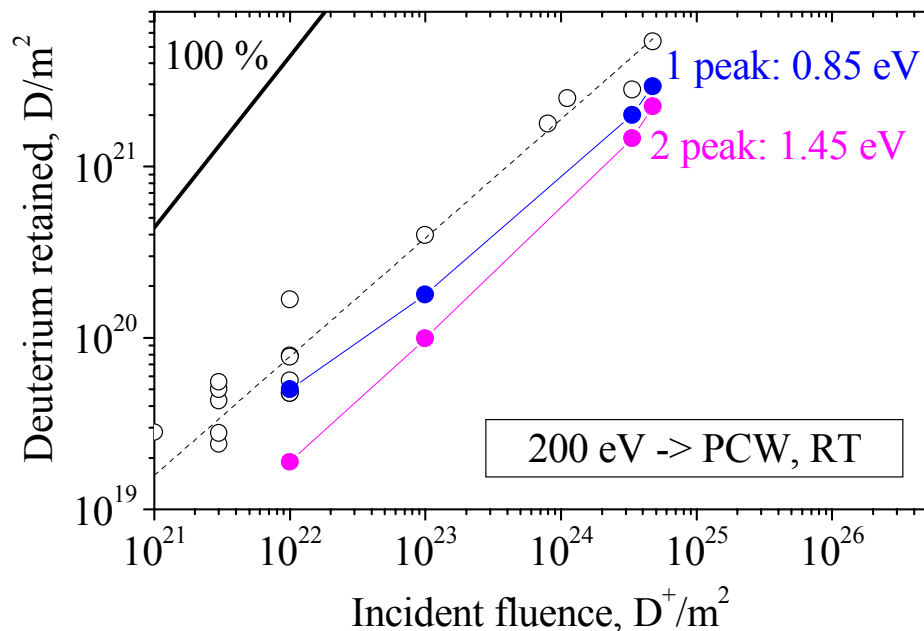


Diffusion-limited trapping of deuterium in PCW



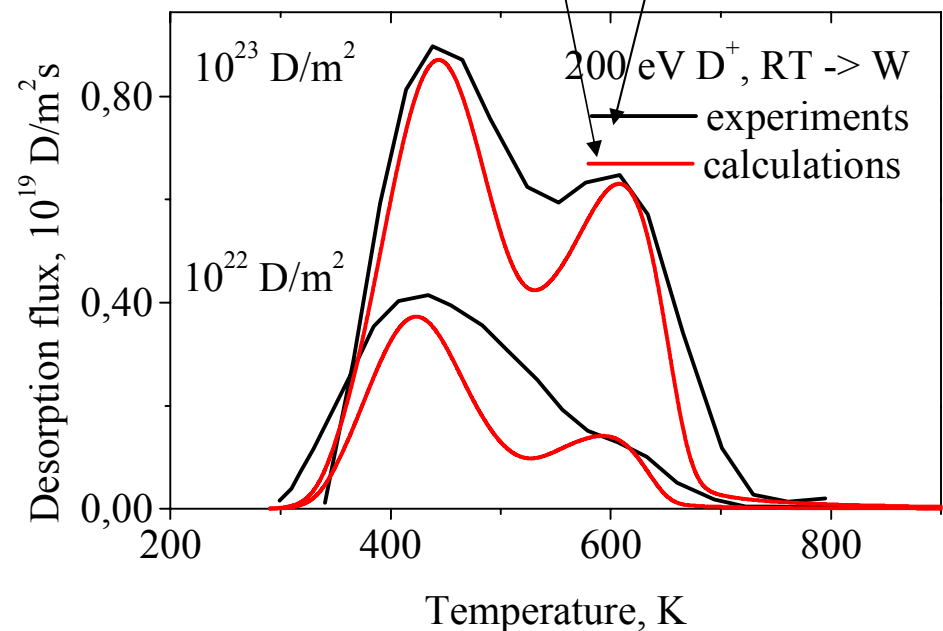
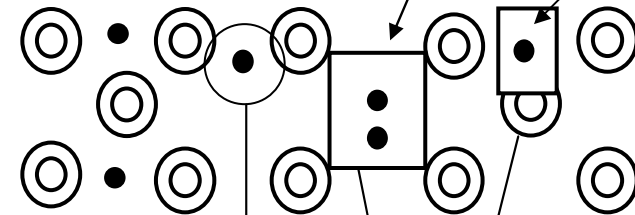
-The D retention in **0.85 eV** traps increases with fluence because of diffusion and ion-induced dislocations

- The concentration of **1.45 eV** traps increases during implantation



Dislocations,
Grain boundaries

Bubbles, Vacancies

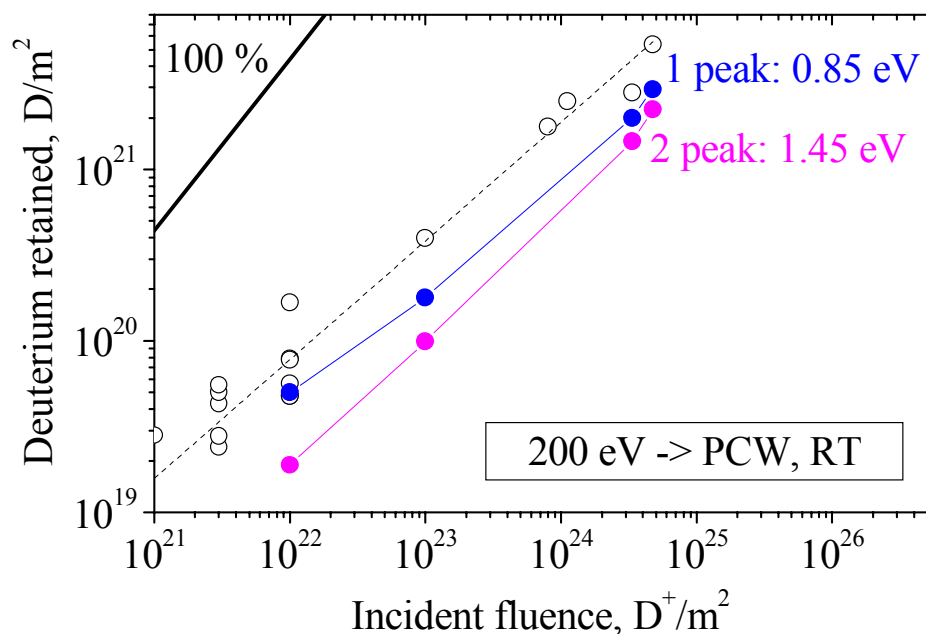




Diffusion-limited trapping of deuterium in PCW

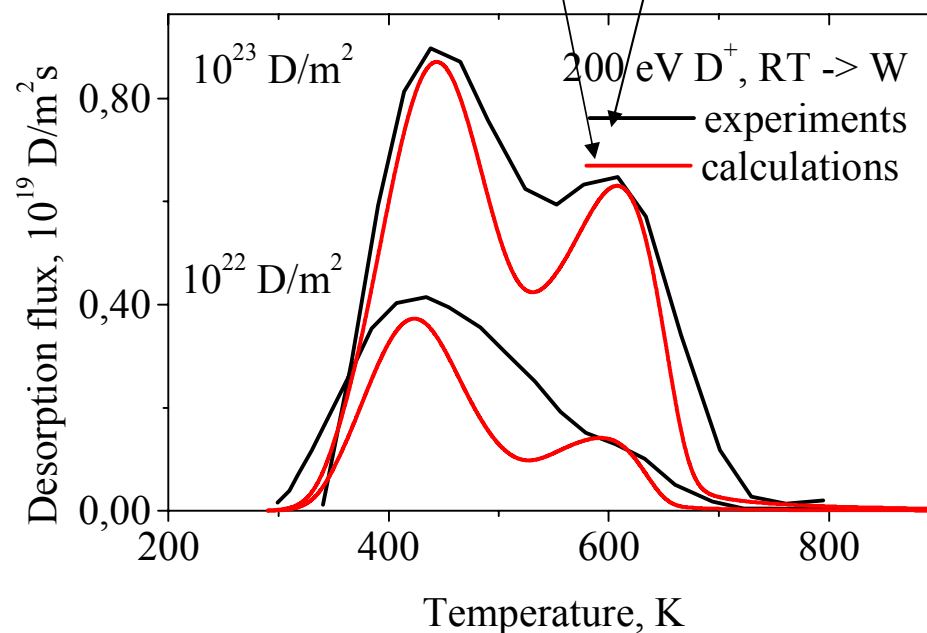
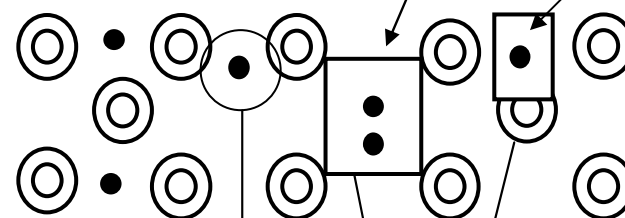


*Which kind of ion-induced defects of **1.45 eV** can be produced by 200 eV?*



Dislocations,
Grain boundaries

Bubbles, Vacancies



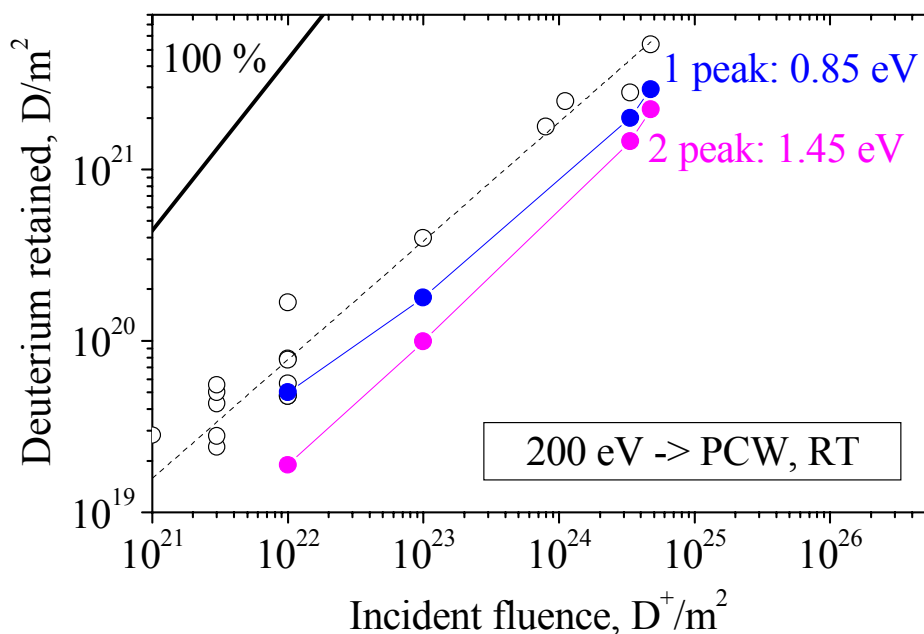


Diffusion-limited trapping of deuterium in PCW



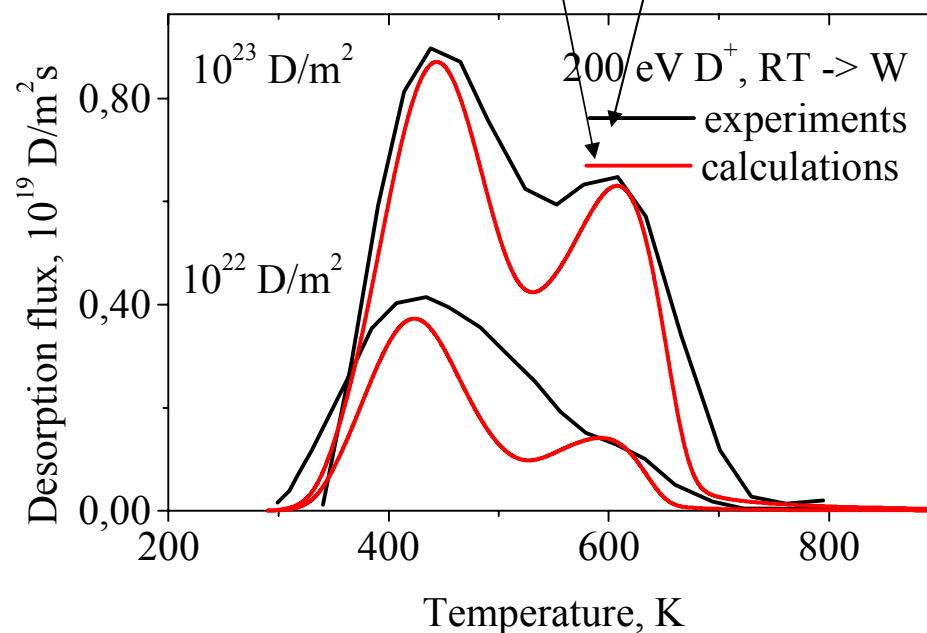
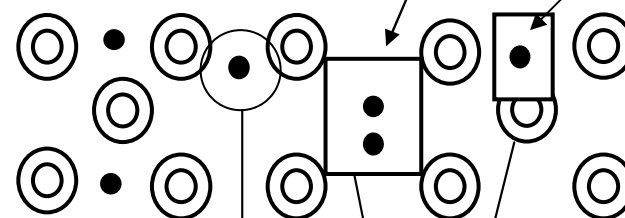
*Which kind of ion-induced defects of **1.45 eV** can be produced by 200 eV?*

- 200 eV cannot produce vacancies



Dislocations,
Grain boundaries

Bubbles, Vacancies



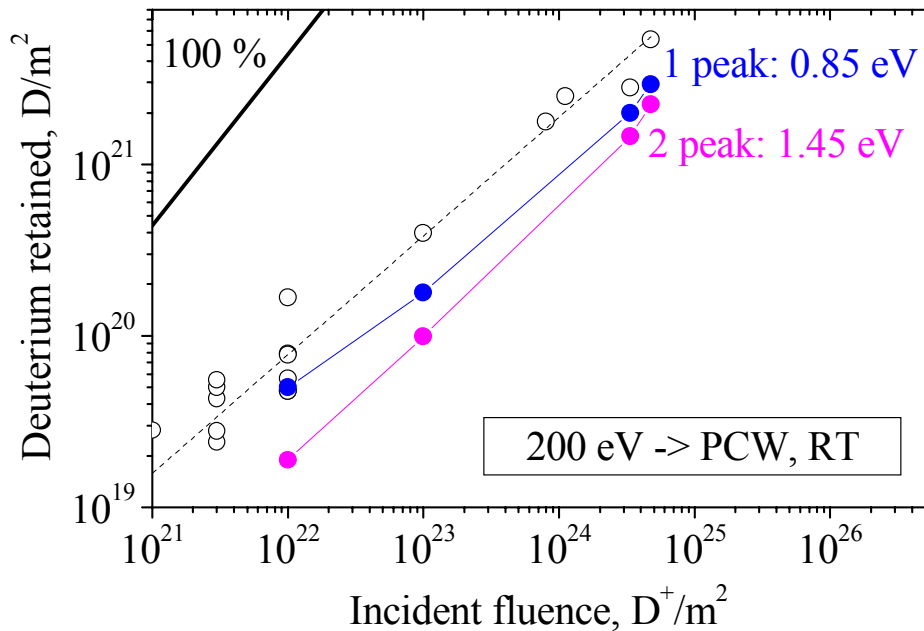


Diffusion-limited trapping of deuterium in PCW

IPP

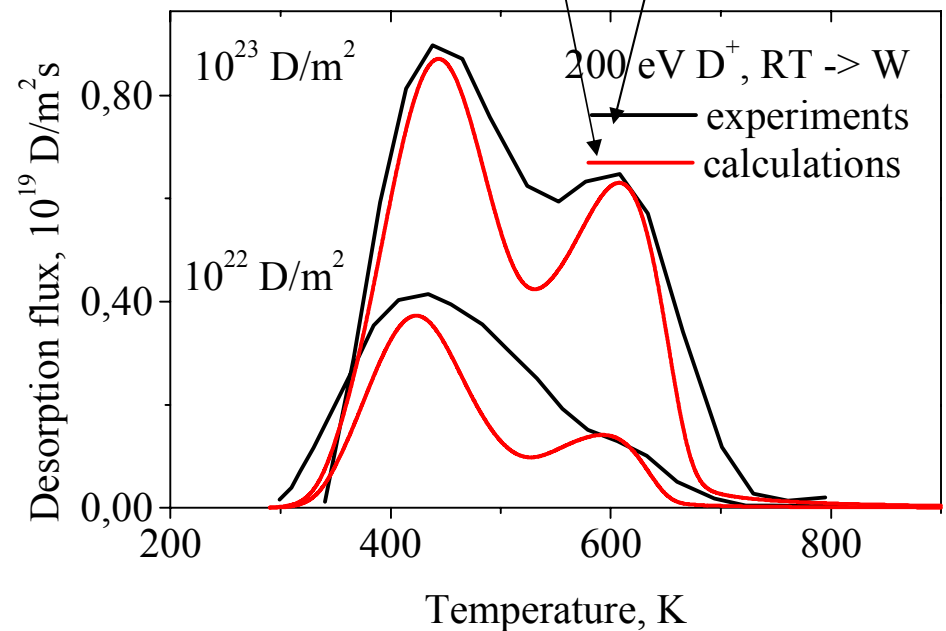
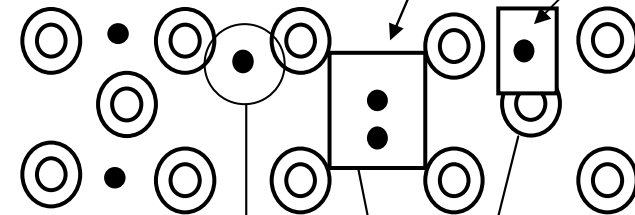
*Which kind of ion-induced defects of **1.45 eV** can be produced by 200 eV?*

- **200 eV cannot produce vacancies**
- **D association in clusters due to stress field created by implanted D**



Dislocations,
Grain boundaries

Bubbles, Vacancies





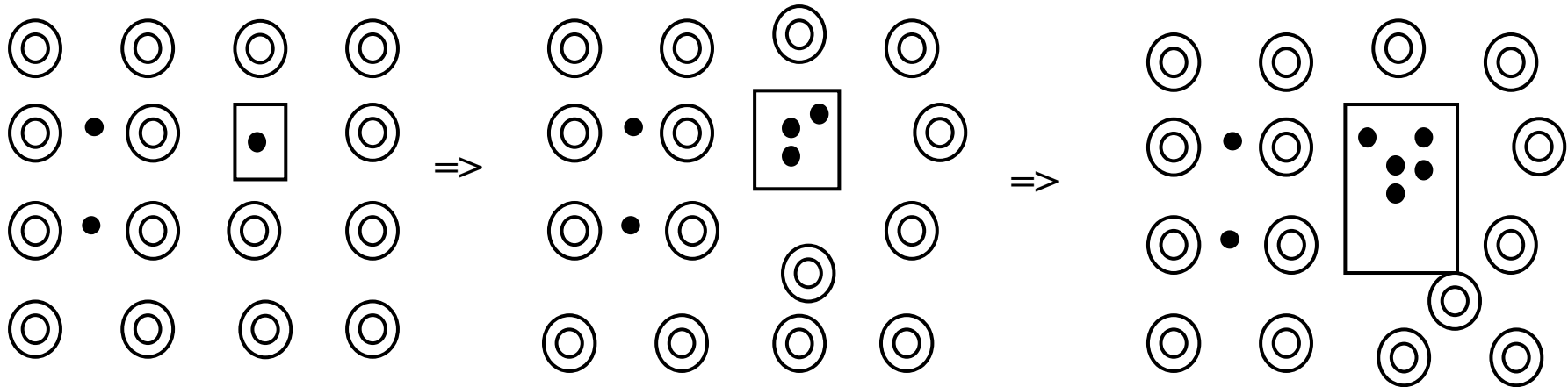
Why D agglomerates in clusters only near the implantation surface? =>

Because of stress field induced by ion implantation



D agglomeration in clusters and bubble growth

IPP

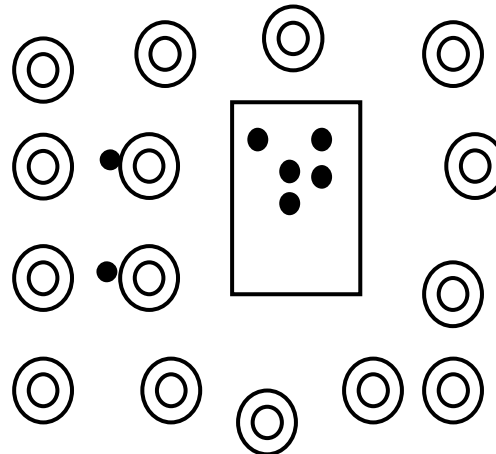


D traps by vacancy

Several D trap by vacancy

**Tension and stress=>
Displacement of W atom=>
Di-vacancy=>
Bubble growth**

**Tension and stress=>
Dislocation (loop punching?)**



- Conditions for bubble formation:**
- 1) **Saturation in D concentration**
 - 2) **Saturation in vacancies**



Conditions for cluster formation in W

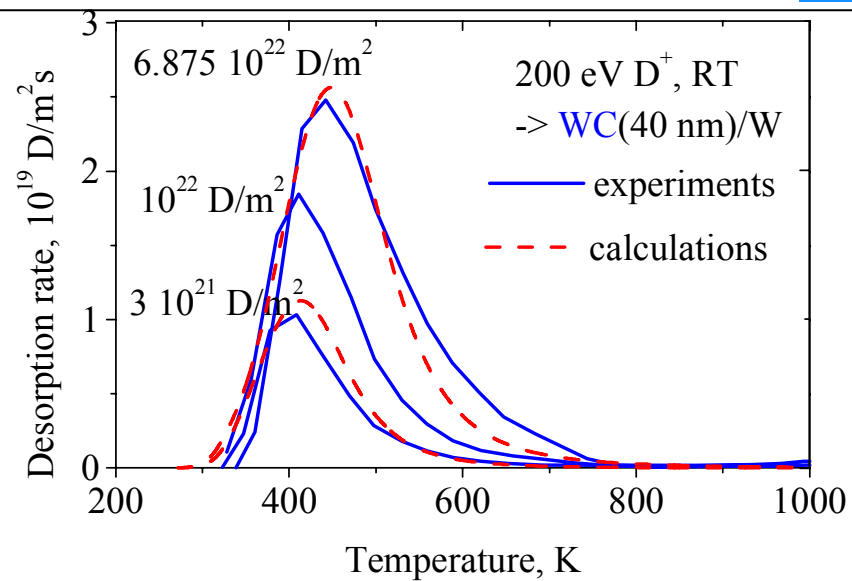
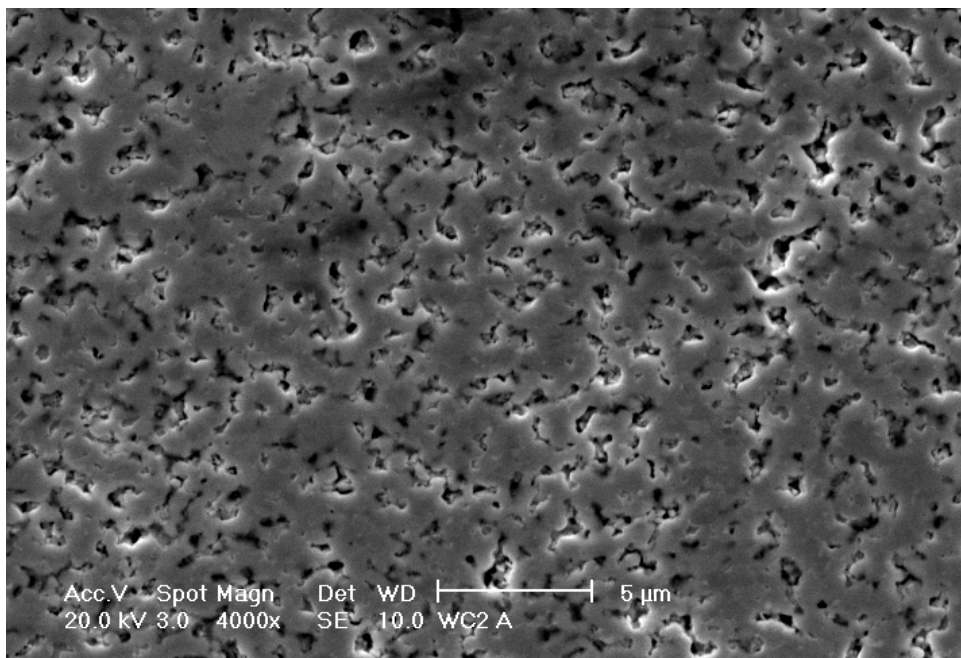
- **Initial amount of defects**
- **Low solubility and diffusivity**
- **No pores**



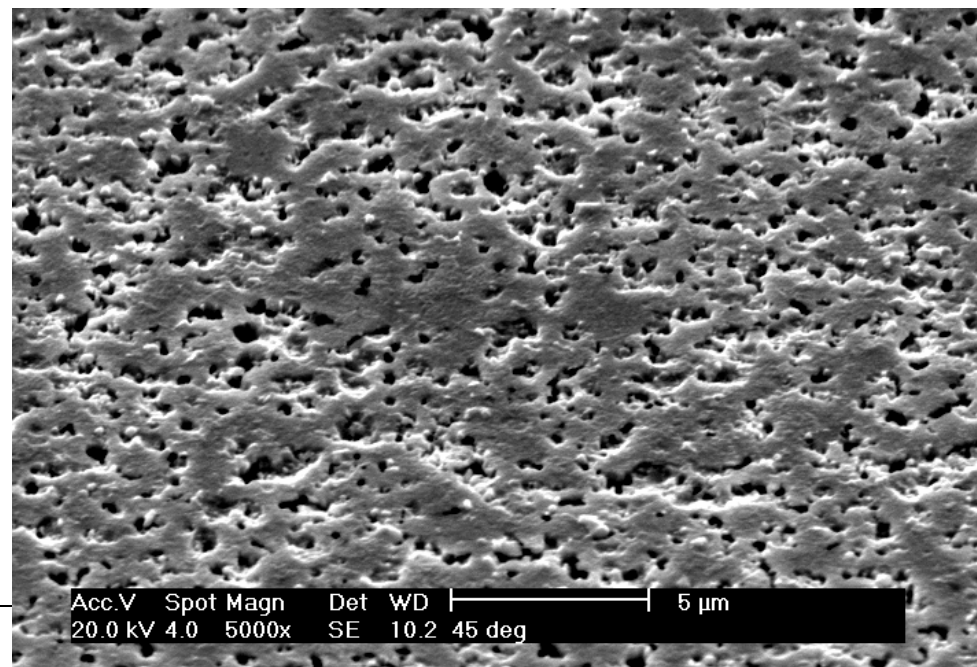
WC

IPP

Unimplanted WC



WC: 3 keV D⁺, RT

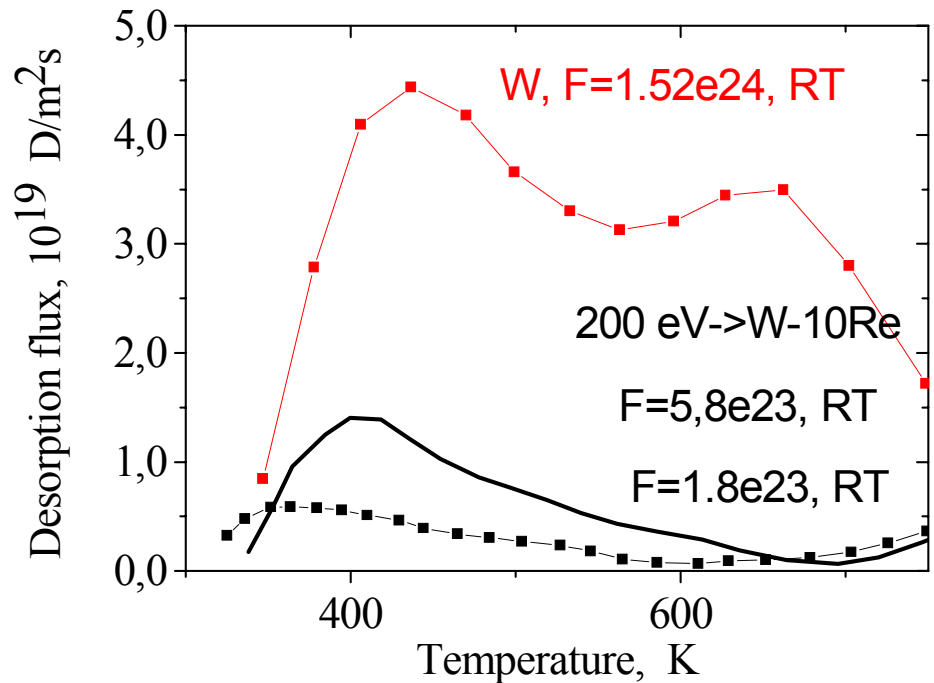
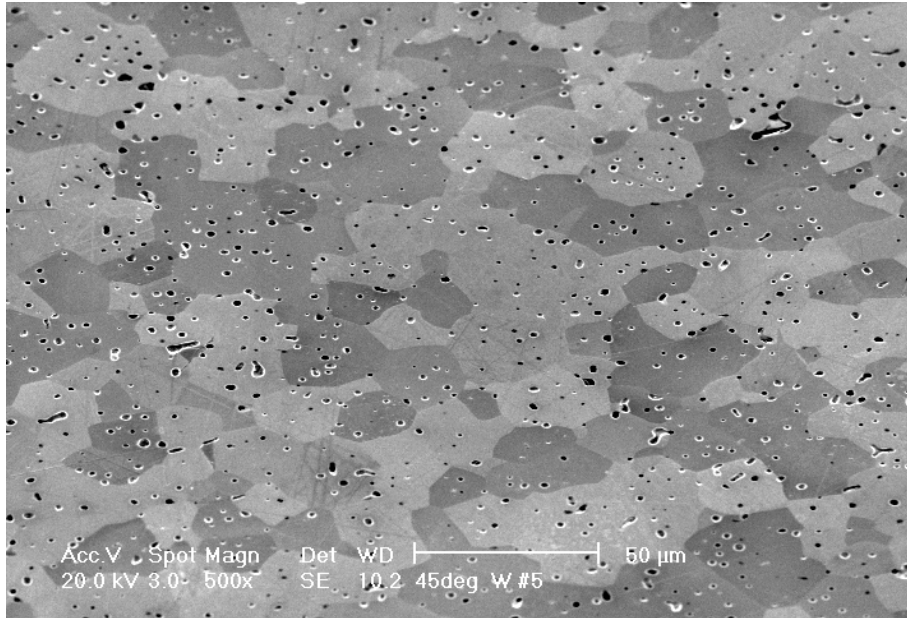




Evidence that ion-induced defects are created by stress: pores materials \Rightarrow no second peak in TDS

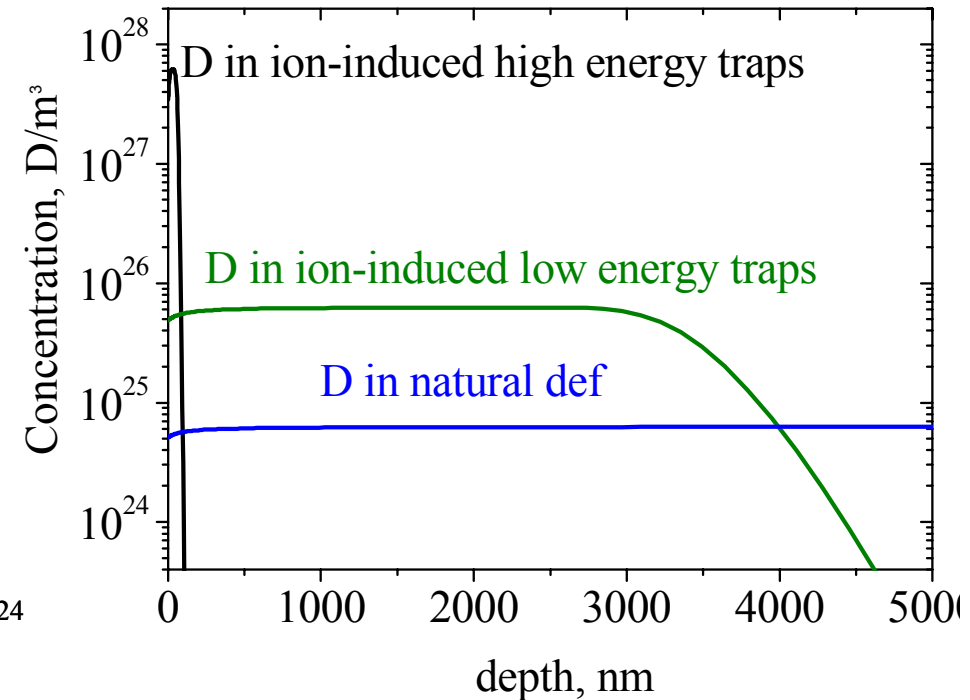
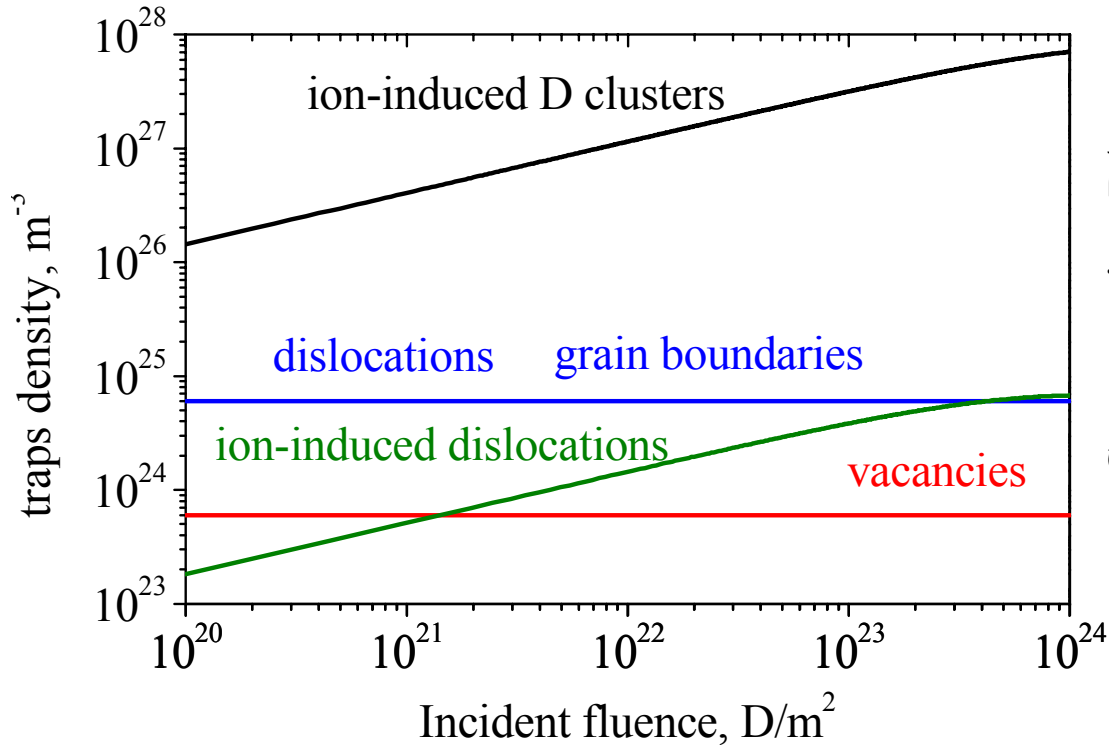


W-10%Re :Investigation together with A. Golubeva and S. Lindig





Model of low energy D behaviour in W



The density of 1.45 eV traps increases with fluence: ion-induced D clusters

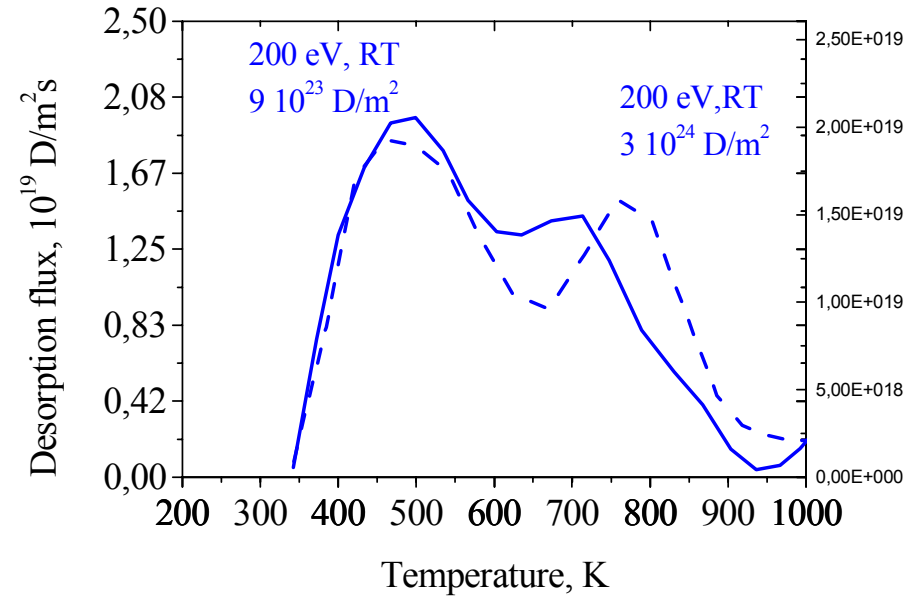
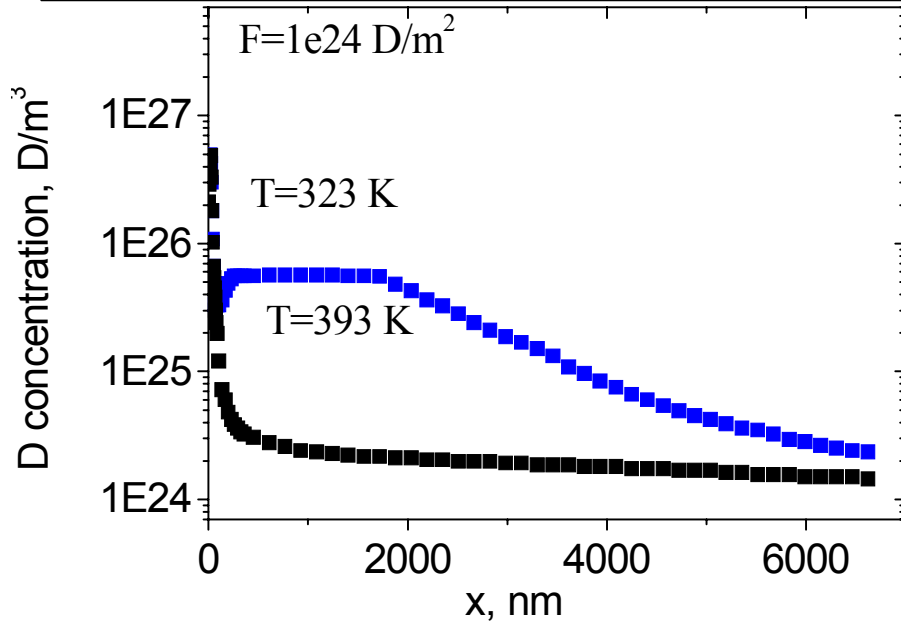
The density of 0.85 eV traps increases with fluence: ion-induced dislocations

1.45 eV traps are close to the implantation range

0.85 eV traps are distributed over whole thickness of W

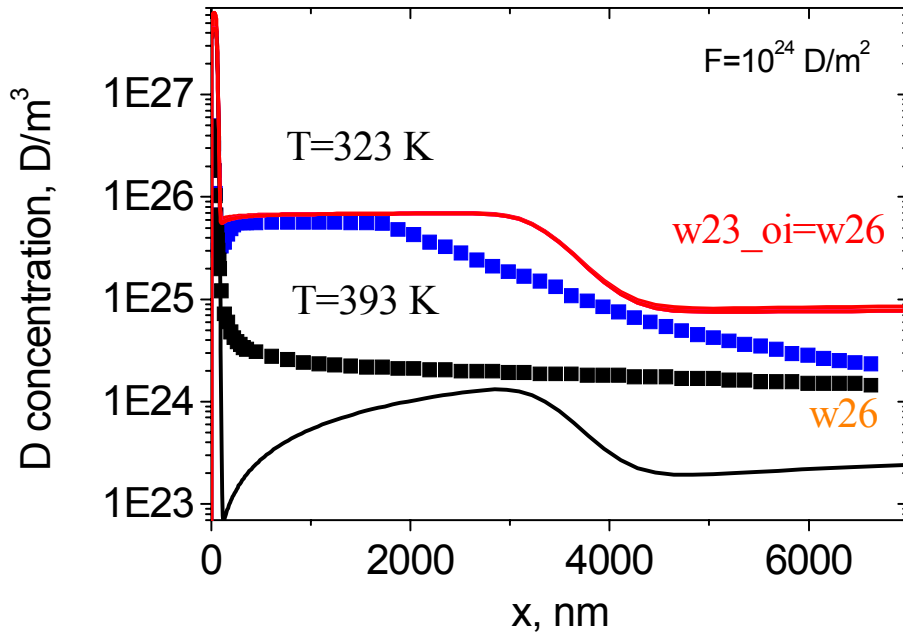


Depth profile (experimental data of V. Alimov et. al.)





Depth profile (experimental data of V. Alimov et. al.)



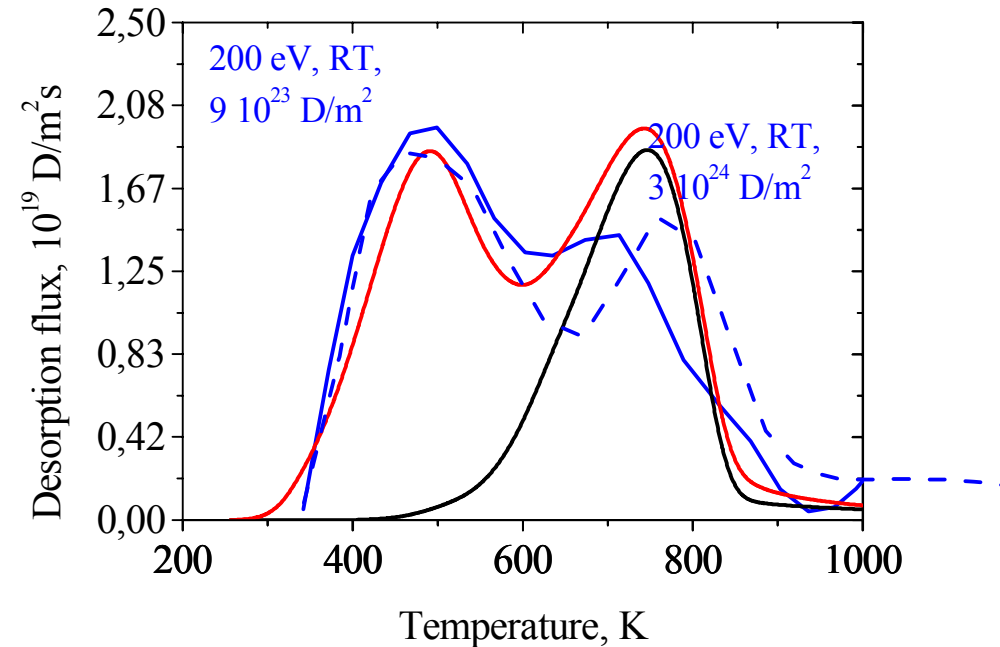
2 kinds of ion-induced defects + dislocation type defect distributed over all W thickness

W25: $E_c=0$ eV

$E_{b1}=1.05$, $W_m=1e-1$, $\epsilon_{ta}=1e-3$, $\psi=5r$

$E_{b2}=0.45$ eV, $W_m=1e-3$, $\epsilon_{ta}=2e-3$; $\psi=50r$

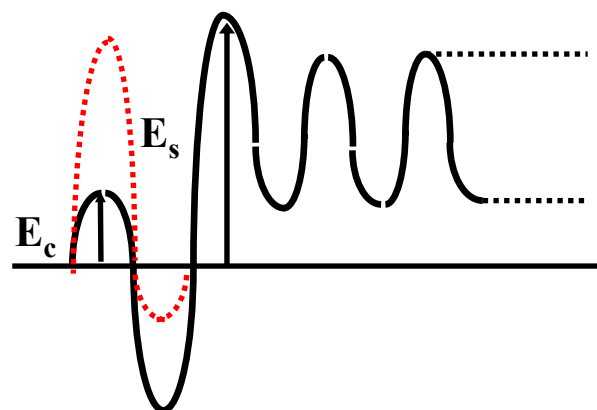
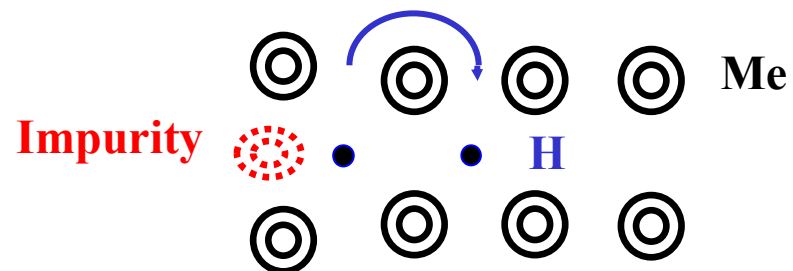
$E_{b3}=0.45$ eV, $W=1e-4=const$



- 1) Parameters describe well both depth profiles and TDS for RT. But they do not suit depth profile for high temperature
- 2) Higher D concentration should be just near the implantation side compared to that found by depth profile

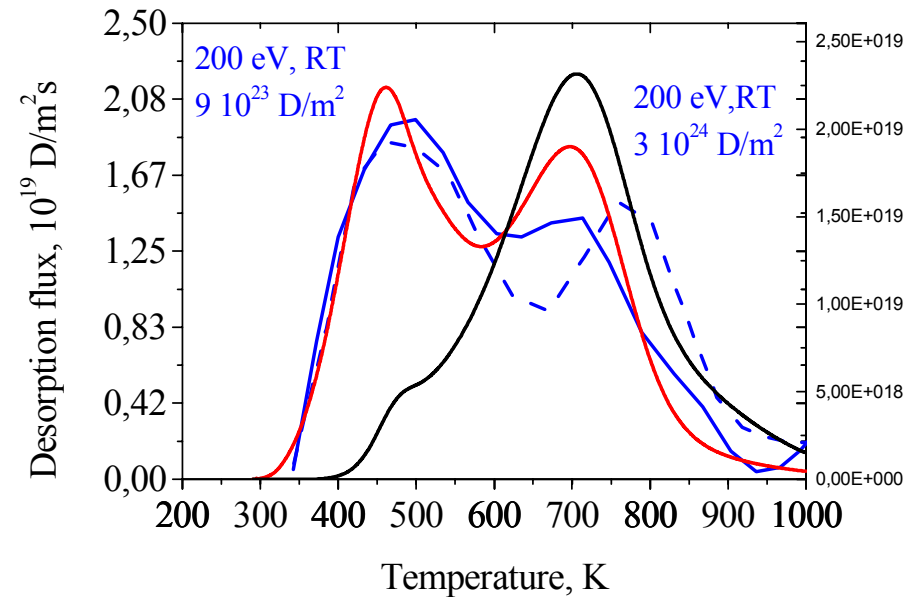
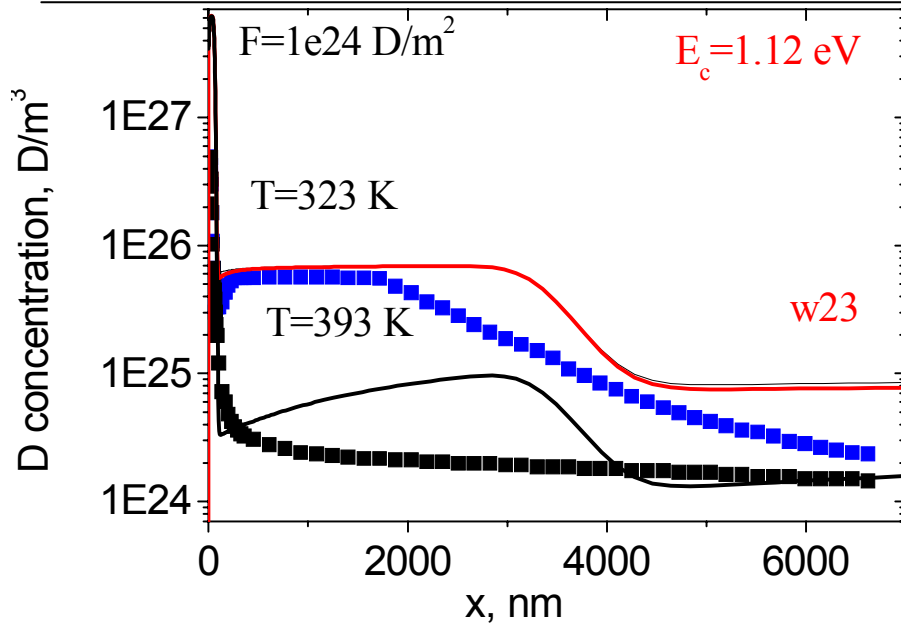


Potential diagram





Depth profile (experimental data of V. Alimov et. al.)



2 kinds of ion-induced defects + dislocation type defect distributed over all W thickness

w23: $E_c=1.12$ eV

$E_{b1}=0.9$, $W_m=1e-1$, $\epsilon_{tta}=1e-3$, $\psi=5r$

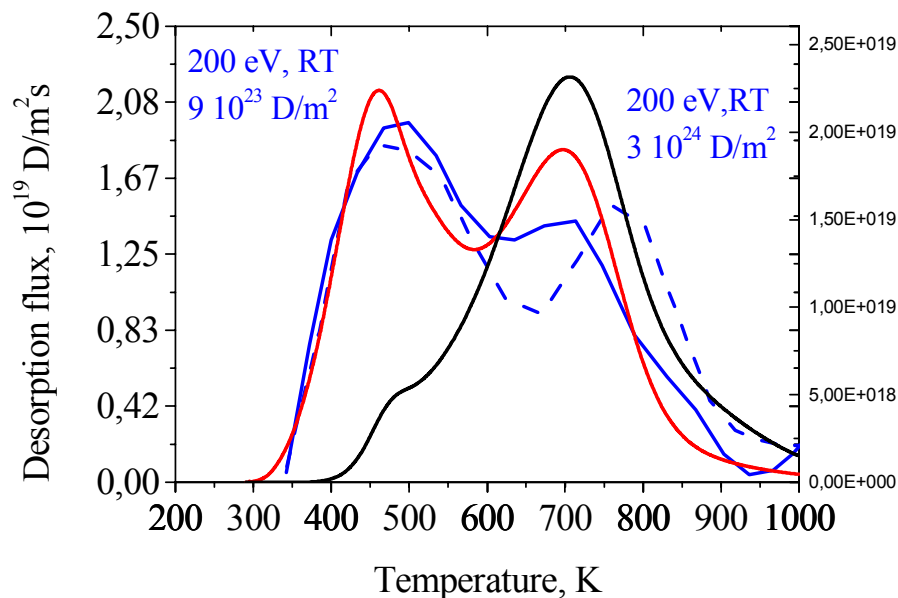
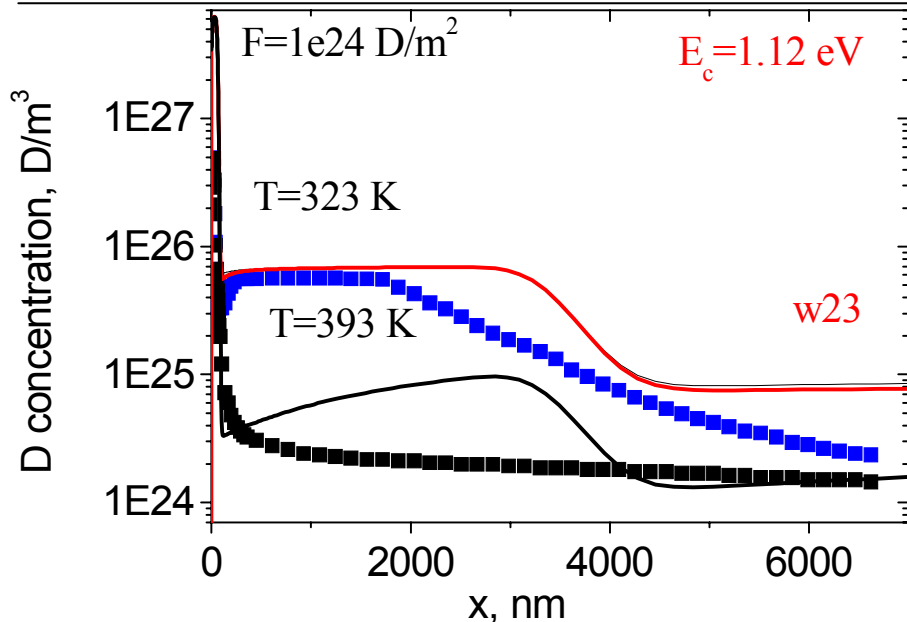
$E_{b2}=0.45$ eV, $W_m=1e-3$, $\epsilon_{tta}=2e-3$; $\psi=50r$

$E_{b3}=0.45$ eV, $W=1e-4=const$

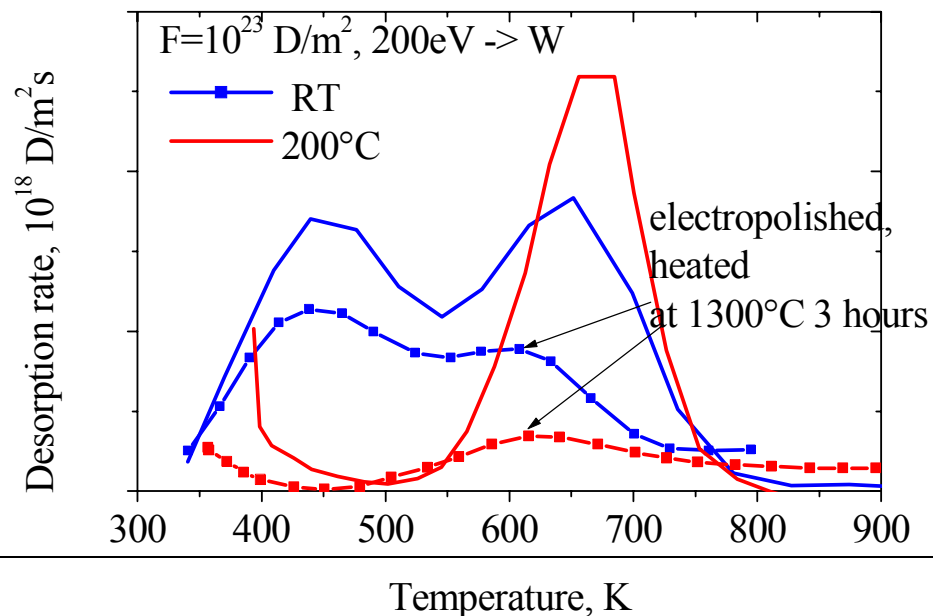
- 1) Parameters describe well both depth profiles and TDS for RT. But they do not suit D retention from TDS for high temperature
- 2) Higher D concentration should be just near the implantation side compared to that found by depth profile



Influence of sample preparation

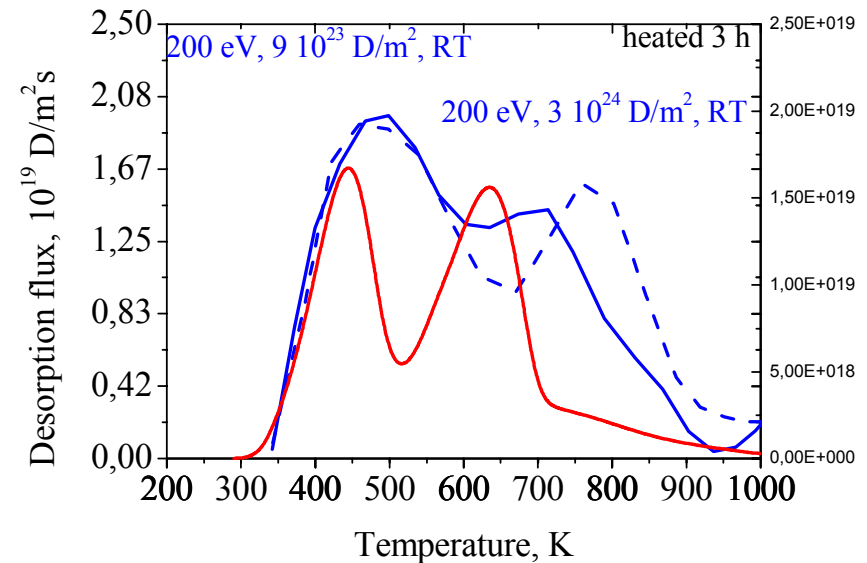
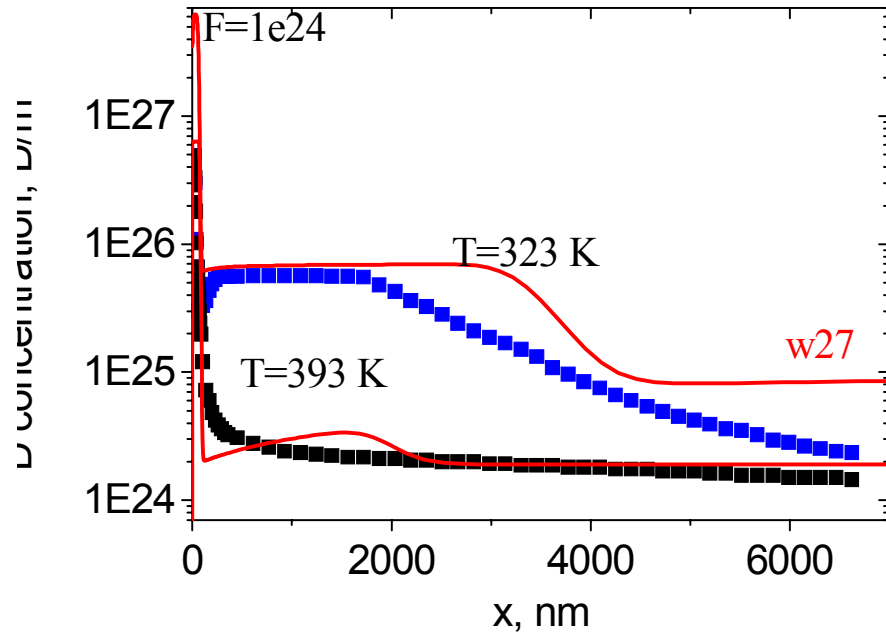


An increase of high temperature peak with temperature was observed for unannealed samples





Depth profile (experimental data of V. Alimov et. al.)



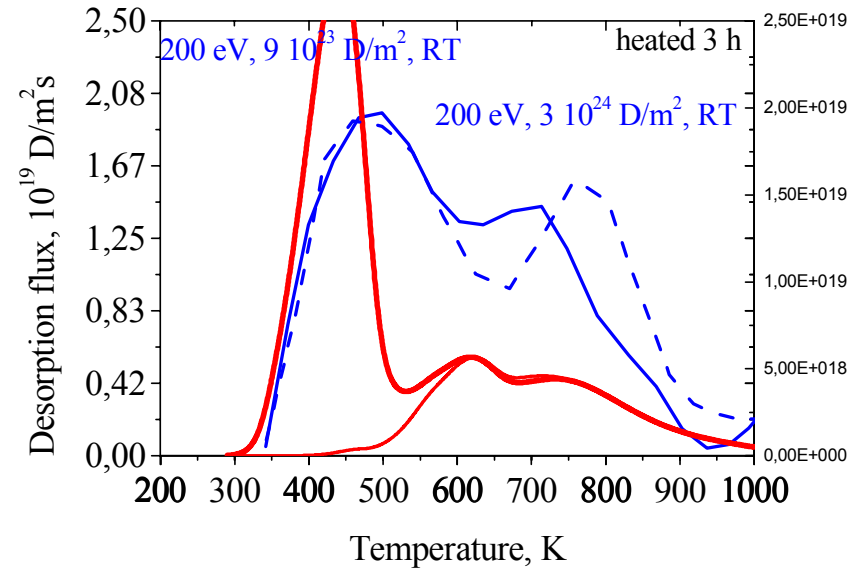
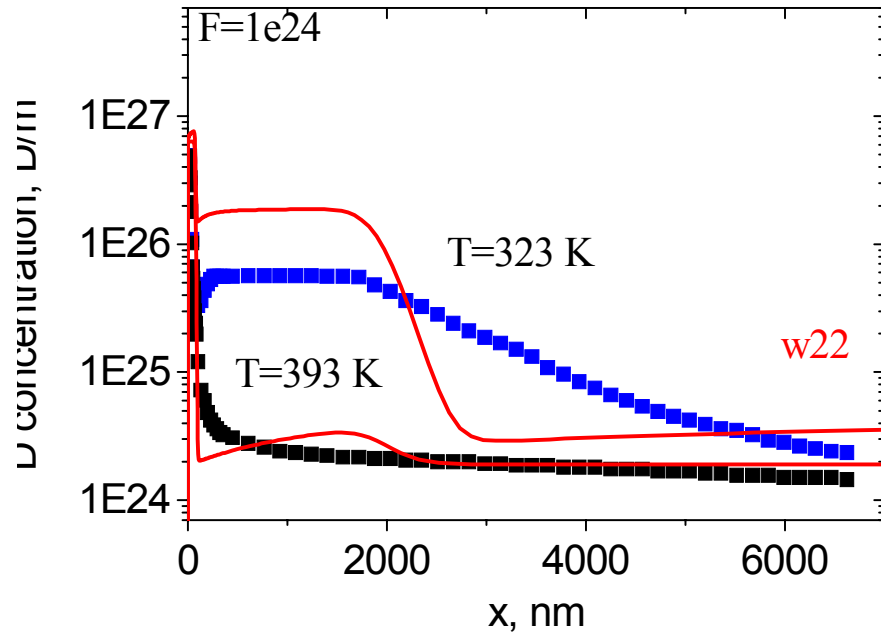
2 kinds of ion-induced defects + vacancy type defect distributed over all W thickness
 $E_{b1}=1,05$, $W_m=1e-1$, $\epsilon_{tta}=1e-3$, $\psi=5r$
 $E_{b2}=0.45$ eV, $W_m=1e-3$, $\epsilon_{tta}=2e-3$; $\psi=30r$
 $E_{b3}=0.9$ eV, $W=3e-5=const$

It is possible to describe TDS assuming natural traps to be vacancies

Better agreement of calculations with experiment is using 4 kinds of traps: 2 ion-induced and 2 natural



Depth profile (experimental data of V. Alimov et. al.)



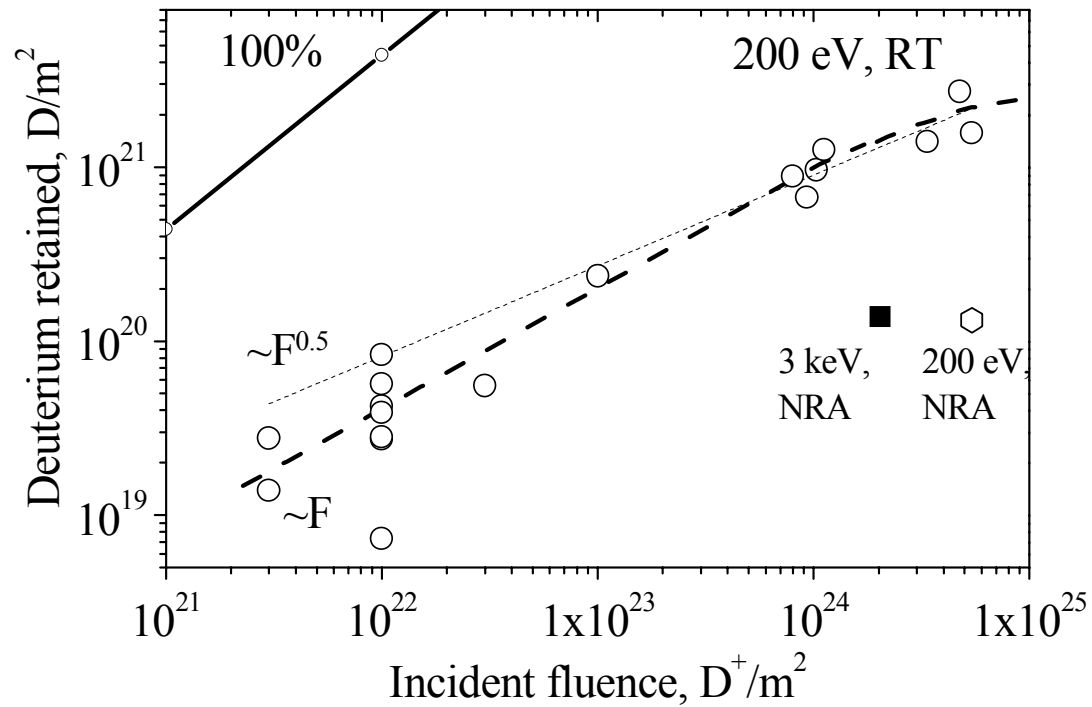
2 kinds of ion-induced defects + vacancy type defect distributed over all W thickness
Eb1=1,05, Wm=1e-2, etta=1e-3, psi=5r
Eb2=0.45 eV, Wm=3e-3, etta=2e-3; psi=30r
Eb3:=0.9 eV, W=3e-5=const

Parameters describing well depth profiles, do not suit TDS



200 eV D⁺ -> PCW: Surface and bulk retention

IPP

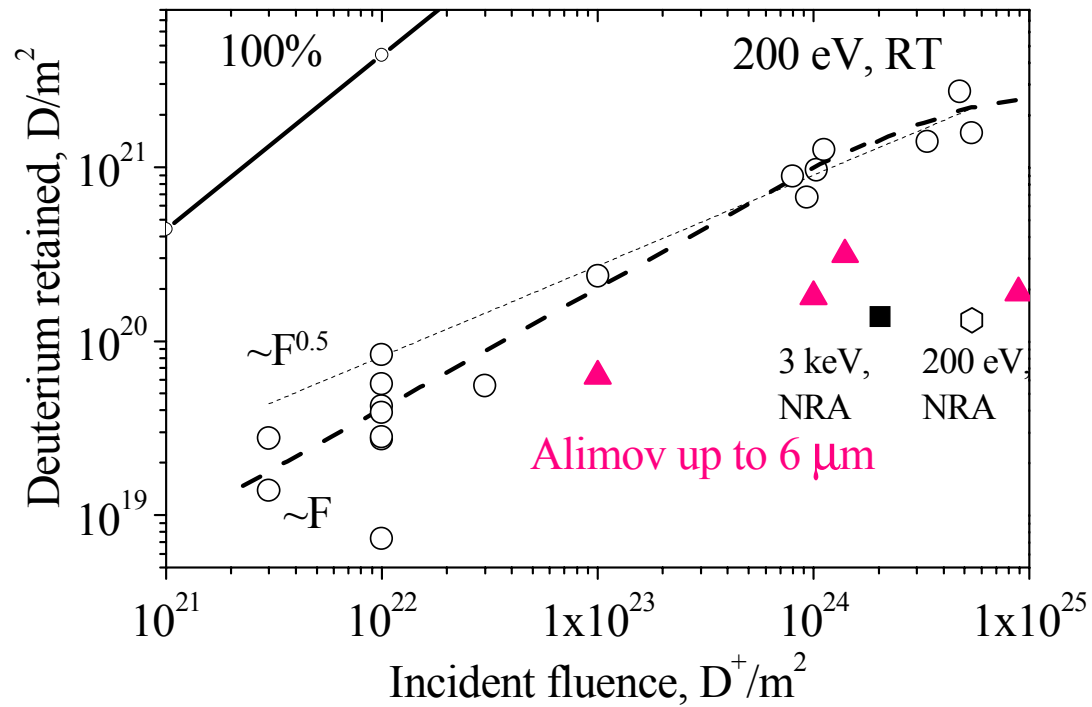


NRA up to 800 nm show lower D retention than TDS => most of D is in the bulk of PCW



200 eV D⁺ -> PCW: Surface and bulk retention

IPP

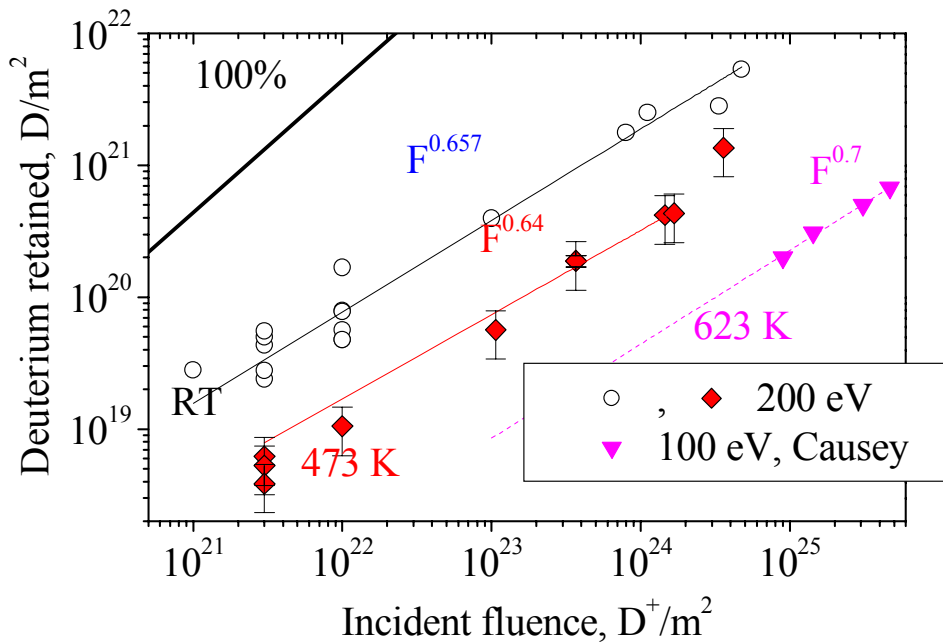


NRA up to 800 nm and **up to 6 μm** show lower D retention than TDS



200 eV D⁺ -> PCW: Temperature dependences

IPP



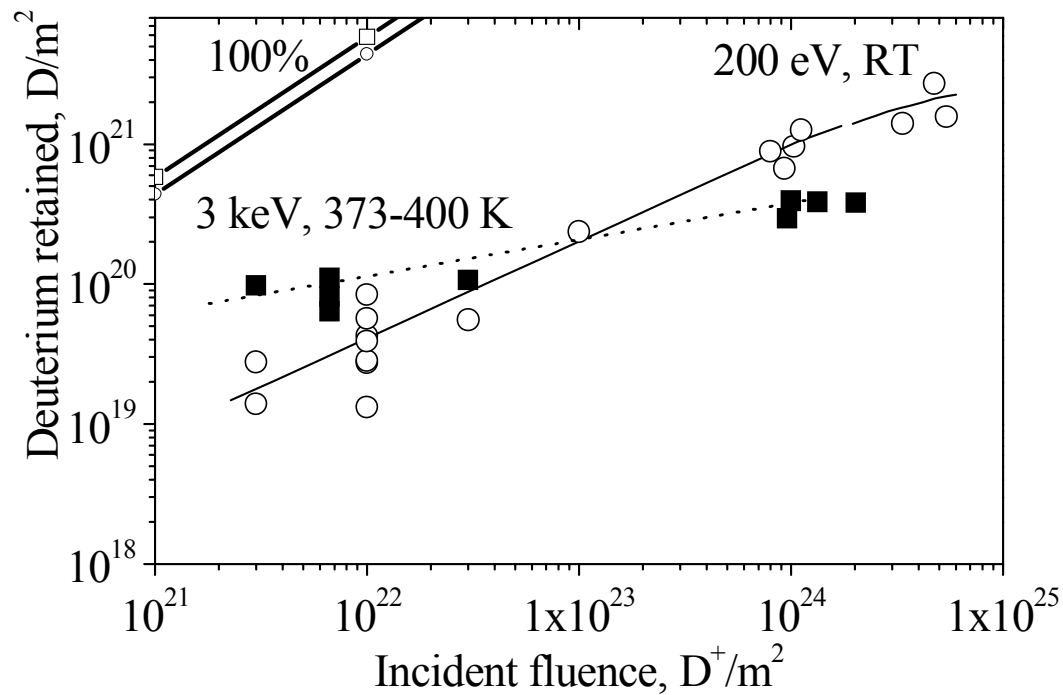
**Increase of the temperature \Rightarrow
decrease of the retention for pre-annealed W**

***However:* D retention most probably
increases with temperature for high
fluences**



Energy dependence

IPP



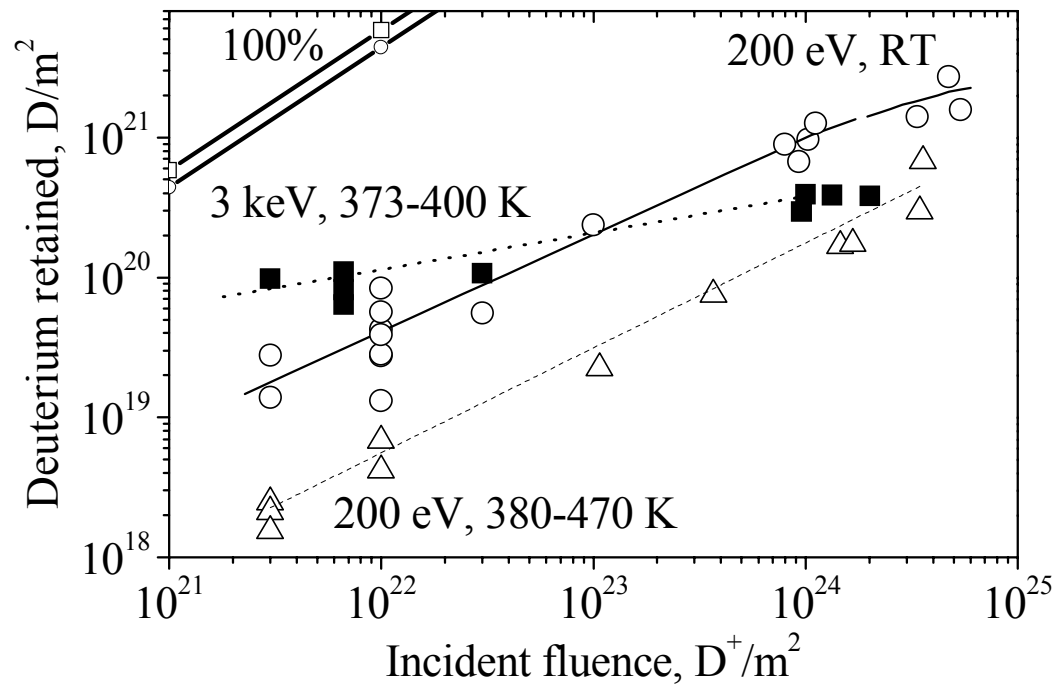
Higher D retention for 3 keV than for 200 eV for low fluences

Saturation behaviour for 3 keV D⁺ implantation for high fluences



Energy dependence

IPP

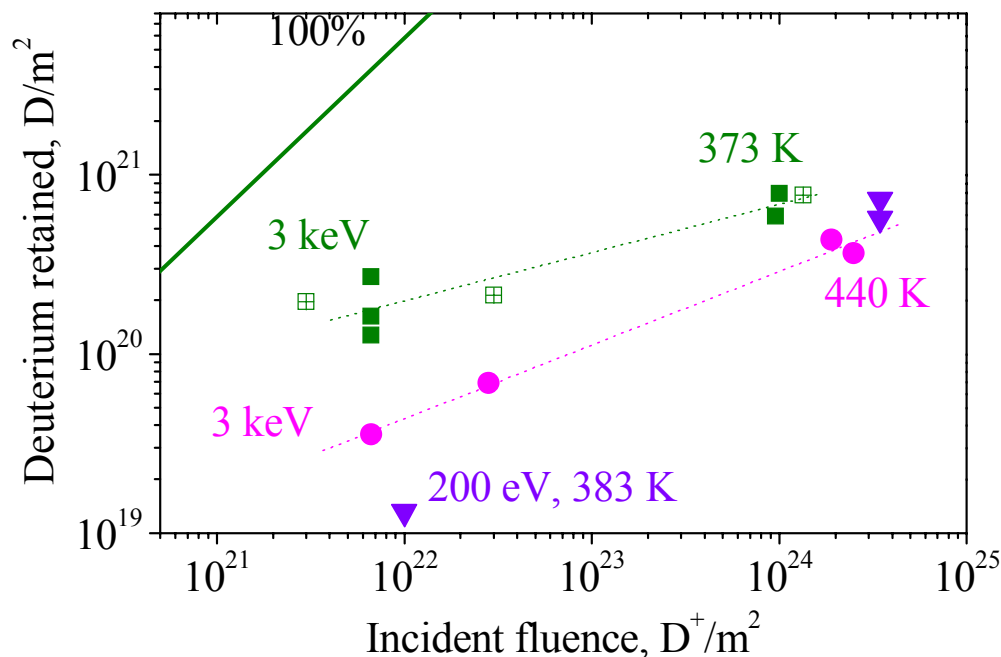


Higher D retention for 3 keV than for 200 eV for low fluences

Saturation behaviour for 3 keV D⁺ implantation for high fluences

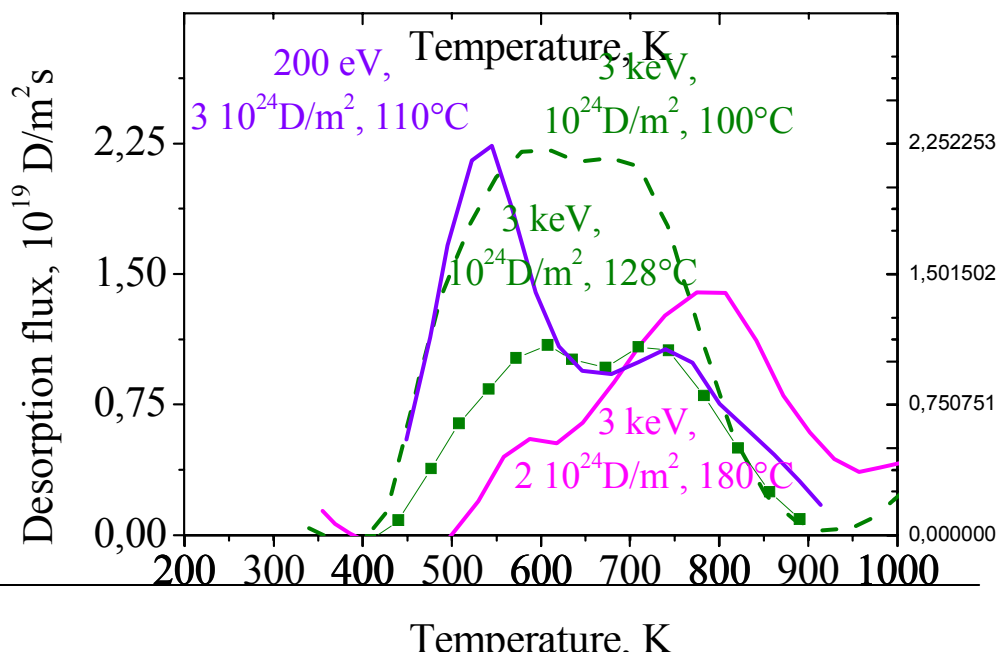
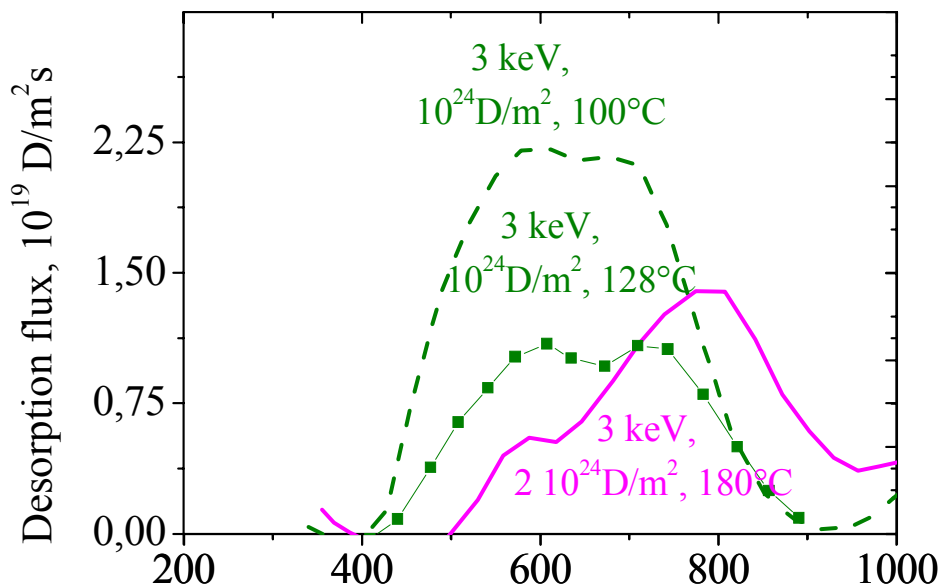


3 keV D⁺ -> PCW: Temperature dependences



**Increase of the temperature ⇒
decrease of the retention for pre-annealed W**

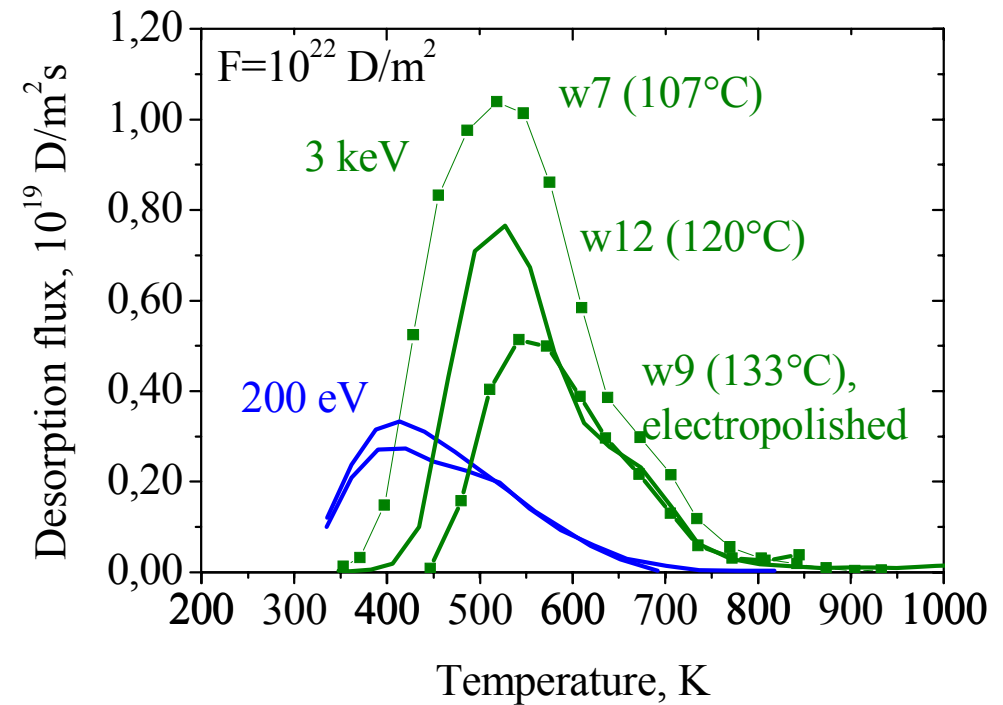
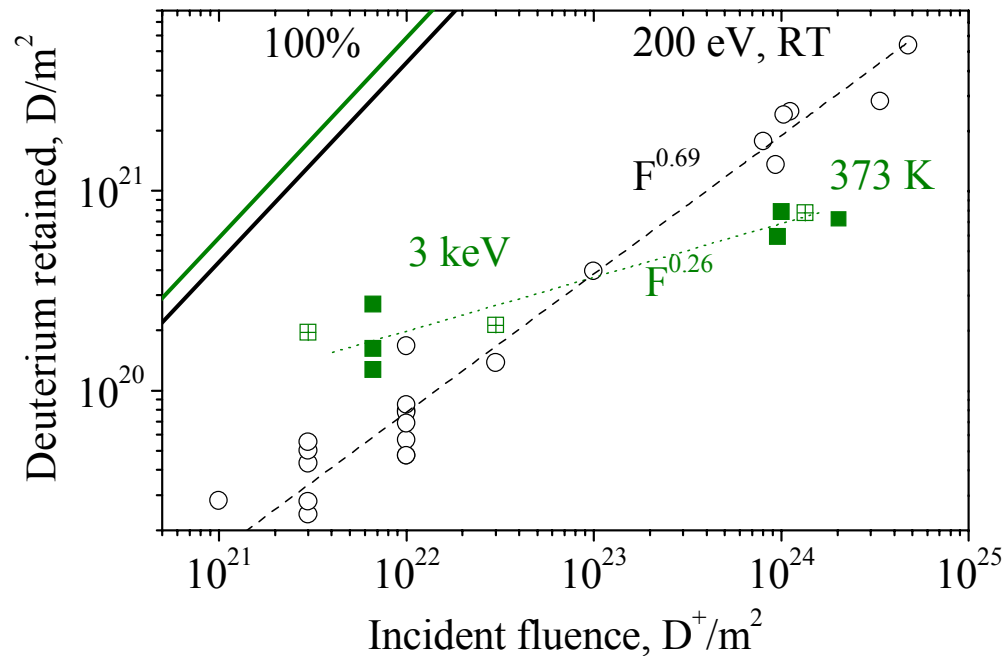
**However: D retention most probably
increases with temperature for high
fluences**





Energy dependence

IPP



Higher D retention for 3 keV than for 200 eV for low fluences

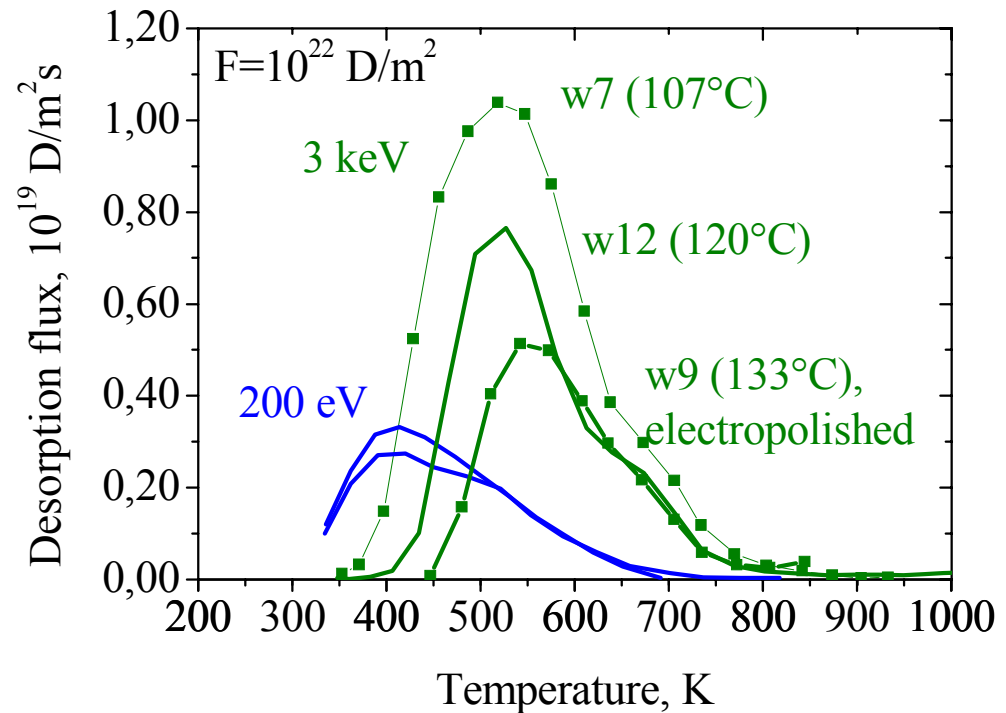
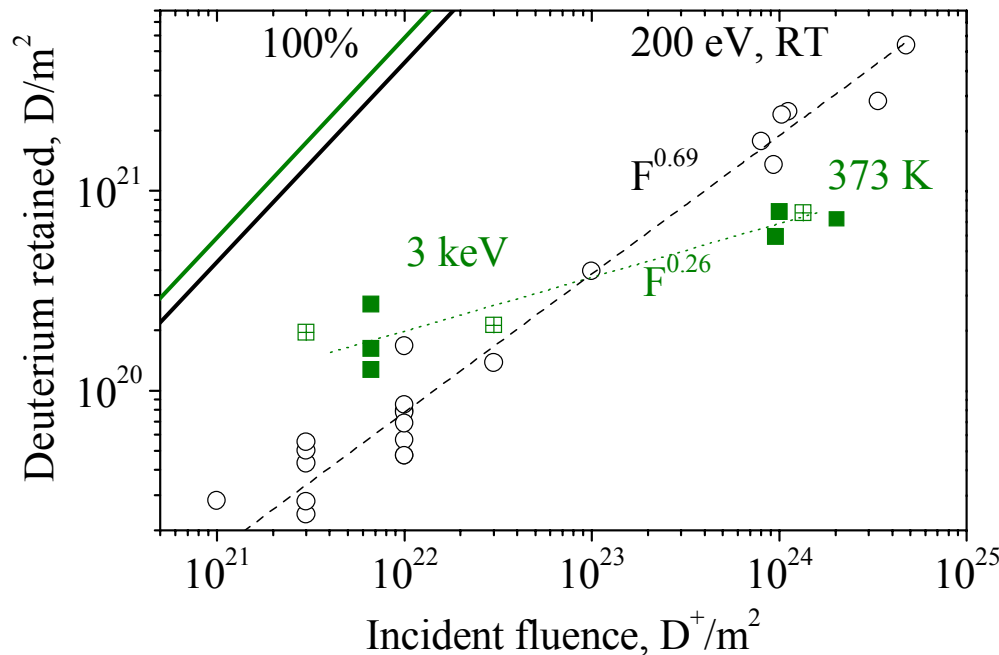
Saturation behaviour for 3 keV D^+ implantation for high fluences

-Scattering of the data is due to uncontrolled heating of W by ion beam during implantation



Energy dependence

IPP



Higher D retention for 3 keV than for 200 eV for low fluences

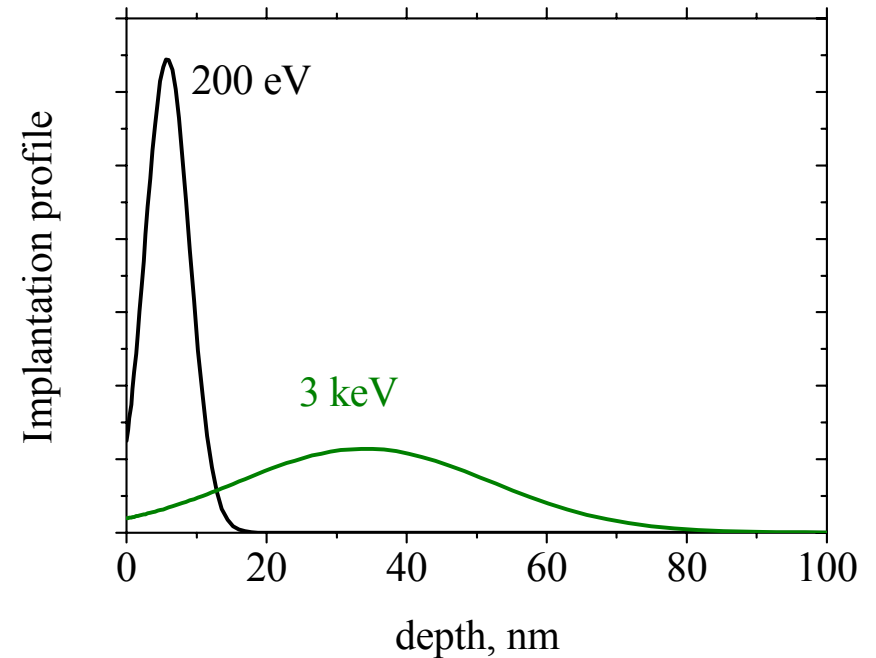
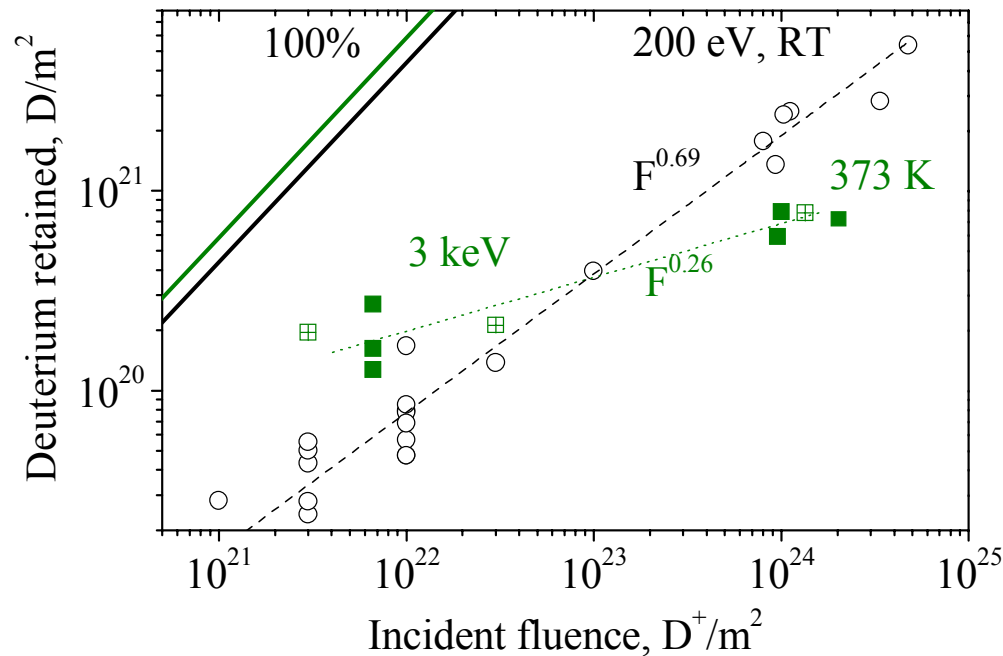
Saturation behaviour for 3 keV D^+ implantation for high fluences

- TDS for 200 eV has a max at about 400 K: most of D is trapped in defects with 0.85 eV
- Deuterium does not retained in traps with 400 K for 3 keV implantation because the temperature of W rises during implantation
- TDS for 3 keV has a max about 550 K



Energy dependence

IPP



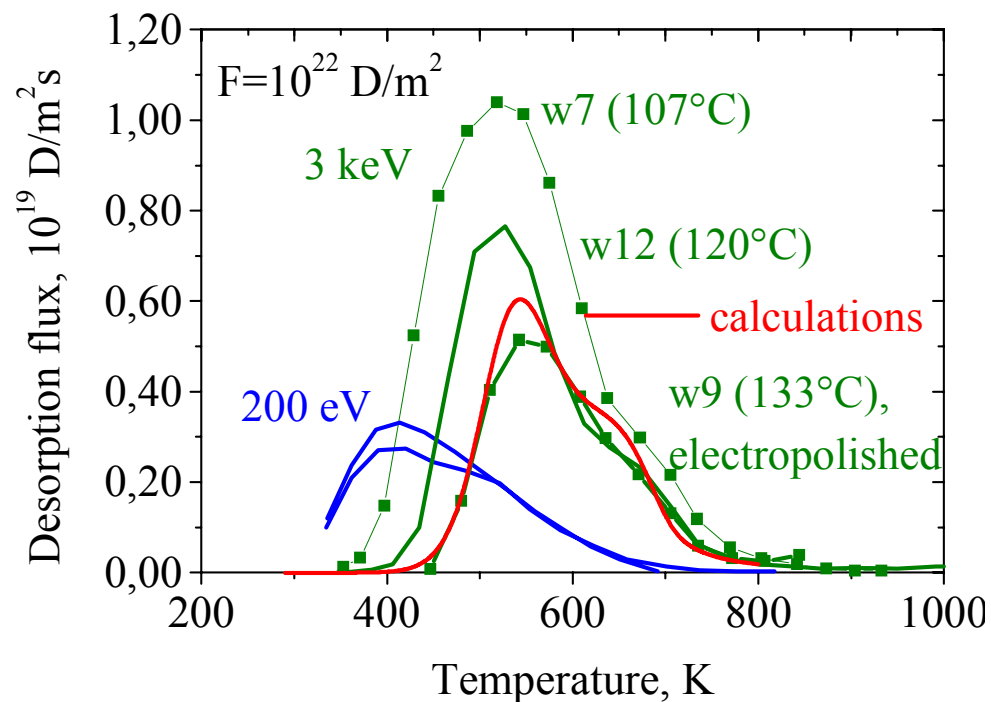
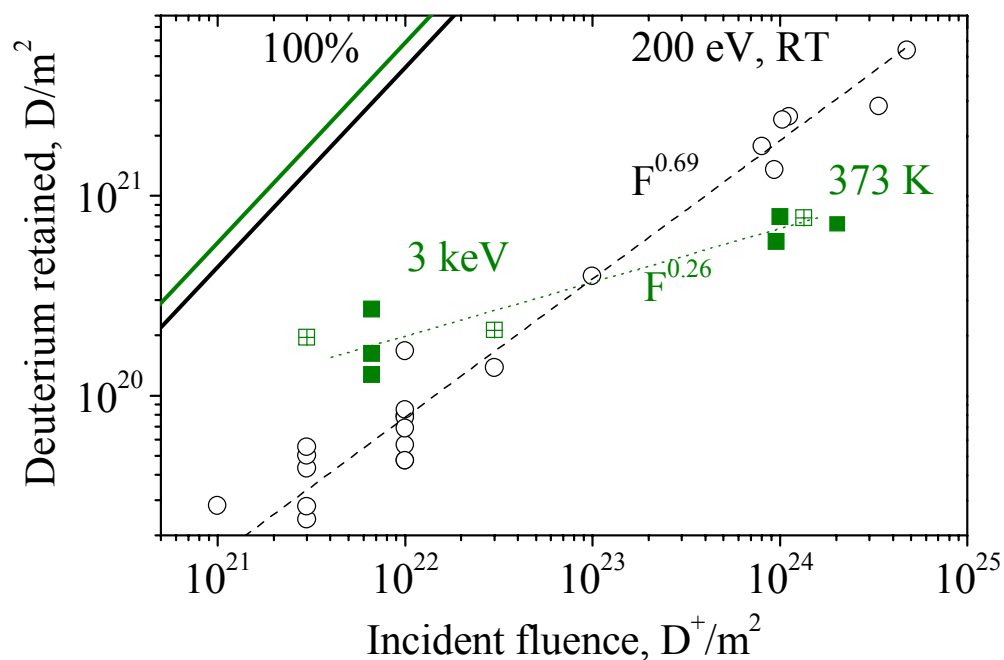
Why D retention for 3 keV higher than for 200 eV for low fluences?

Because

- 1) Higher implantation range
- 2) Vacancies generation



Energy dependence

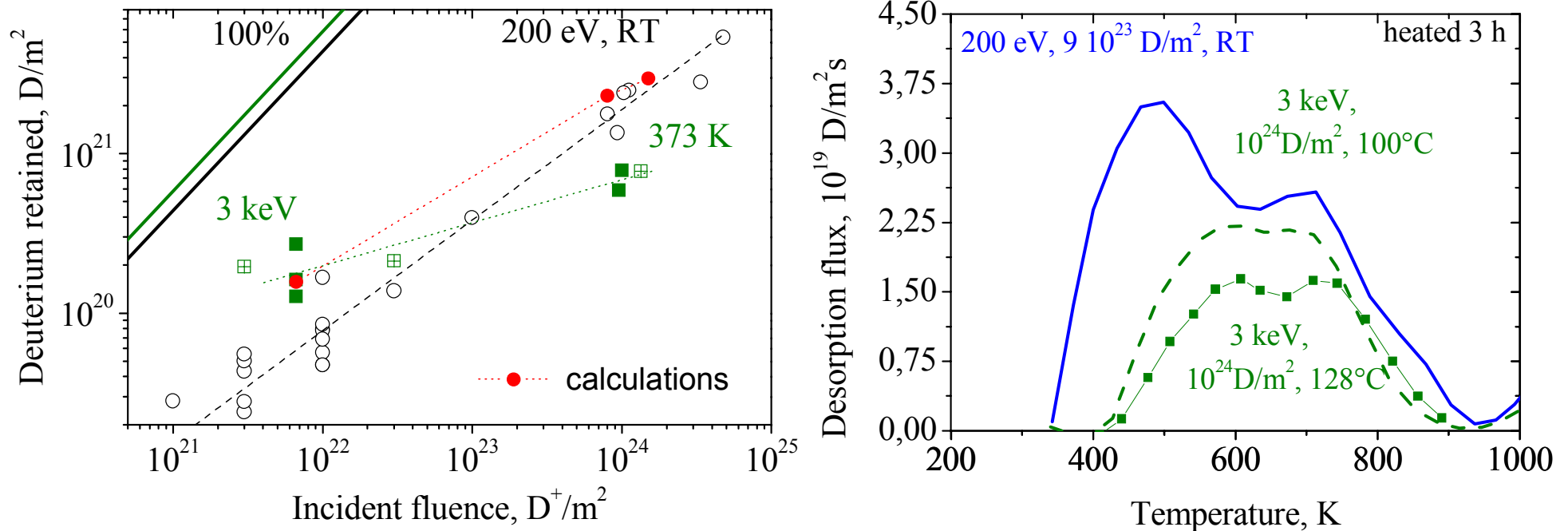


Calculations describe experiments well for low fluences



Energy dependence

IPP



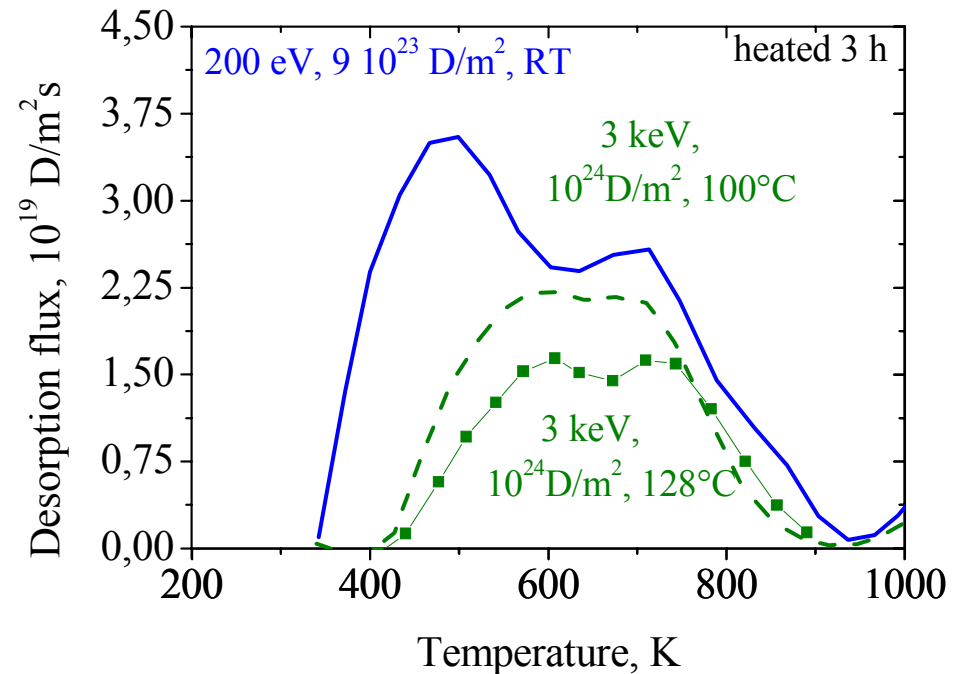
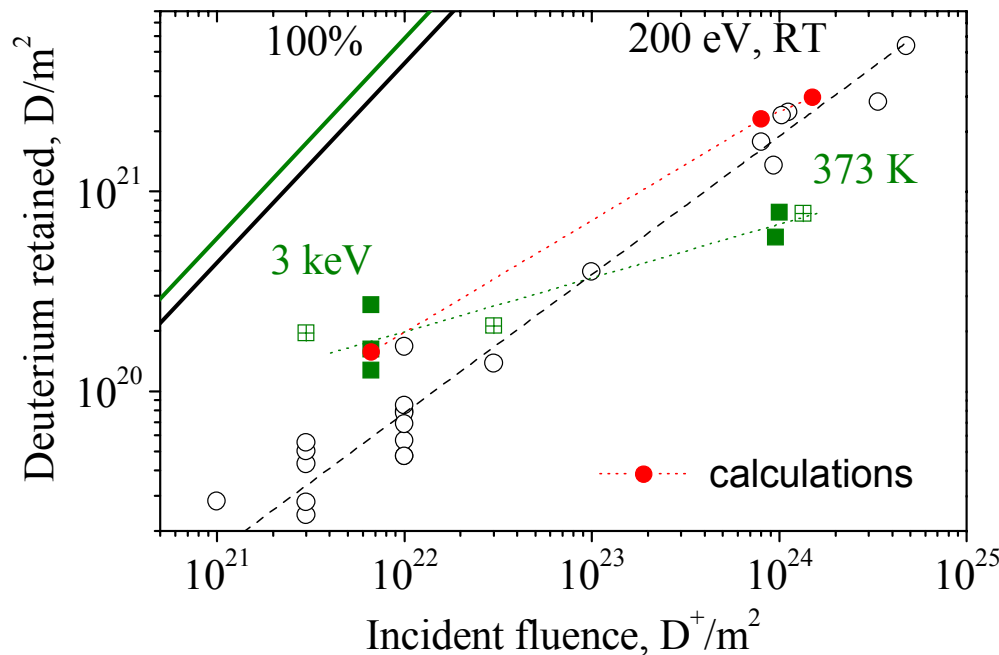
Model does not describe the saturation behaviour. Reasons:

- permeation?
- clusters formation (D is trapped with high binding energy: $T > 1000^\circ\text{C}$) ?
- increase of the diffusion coefficient near the surface with fluence?
- creation of vacancies during bombardment and trapping in these defects which prevent Deuterium to move into the bulk of W?



Energy dependence

IPP



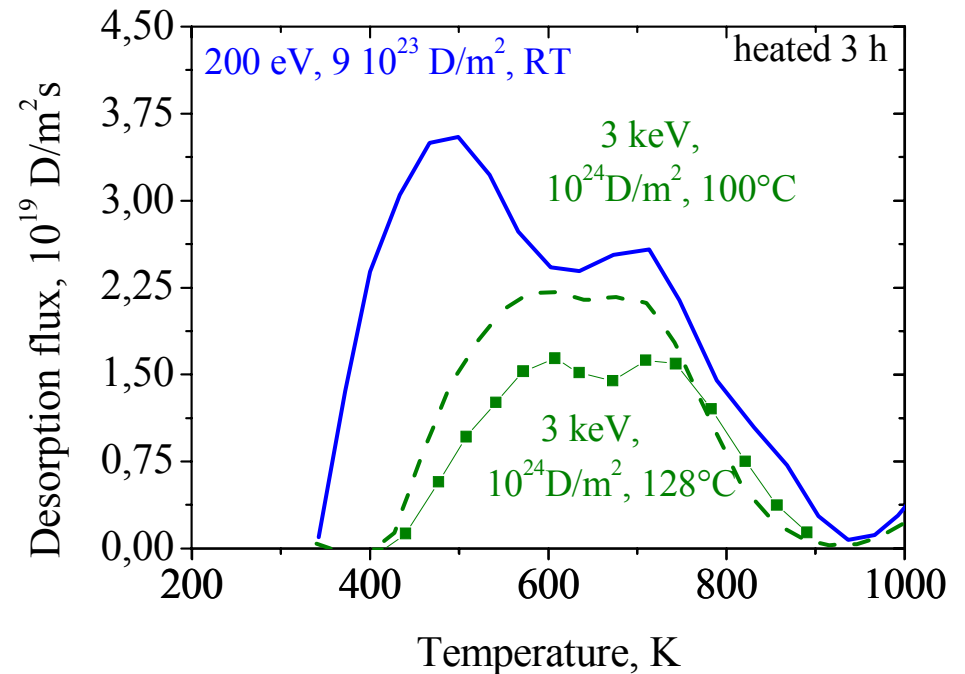
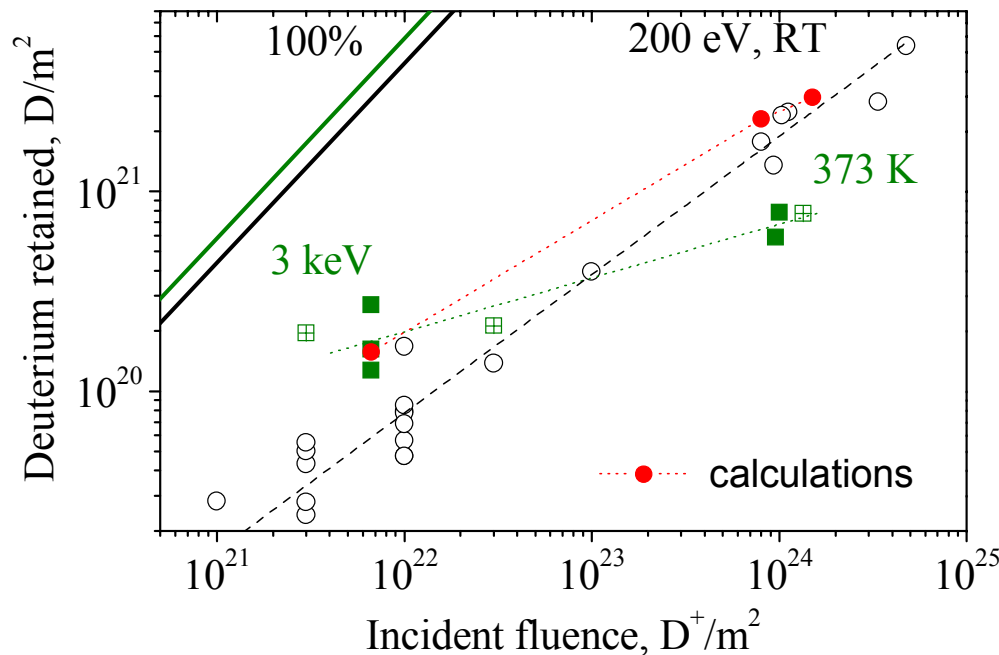
Model does not describe the saturation behaviour. Reasons:

- permeation? – **No! (NRA shows much less D on the back side than on the front side)**
- clusters formation (D is trapped with high binding energy: $T > 1000^\circ C$) ?
- increase of the diffusion coefficient near the surface with fluence?
- creation of vacancies during bombardment and trapping in these defects which prevent Deuterium to move into the bulk of W?



Energy dependence

IPP



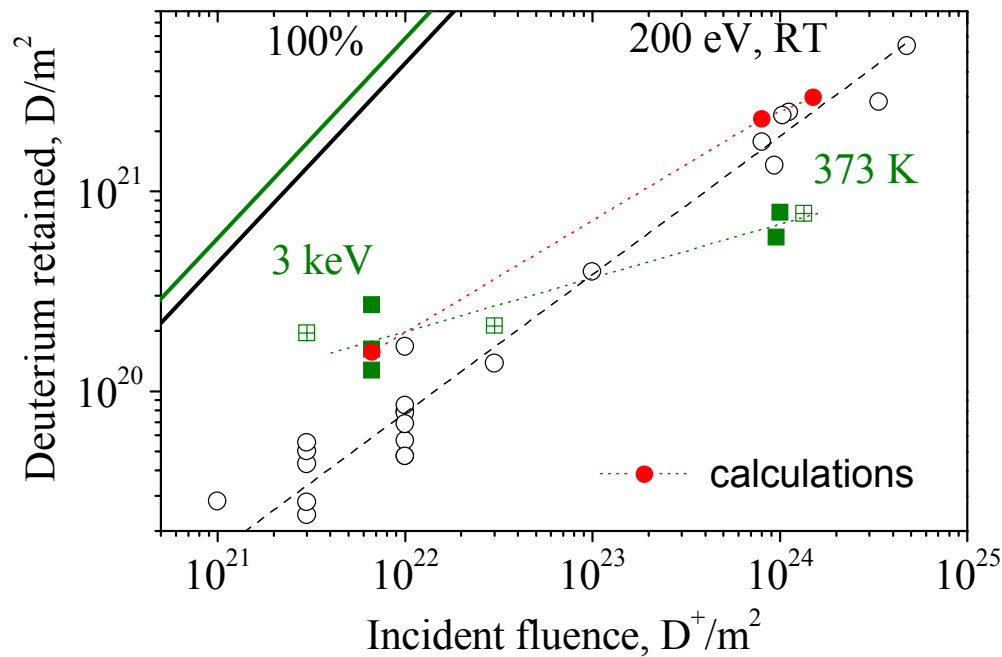
Model does not describe the saturation behaviour. Reasons:

- permeation? – **No!** (NRA shows much less D on the back side than on the front side)
- clusters formation (D is trapped with high binding energy: $T > 1000^\circ C$) ? – **No!**
- increase of the diffusion coefficient near the surface with fluence?
- creation of vacancies during bombardment and trapping in these defects which prevent Deuterium to move into the bulk of W?



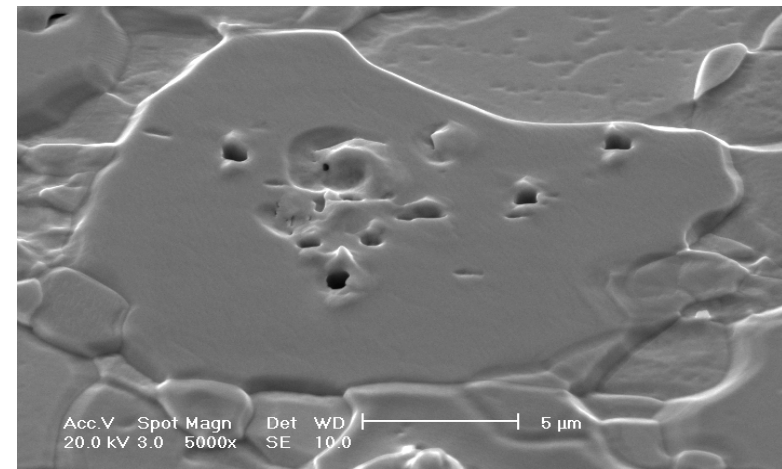
Energy dependence

IPP

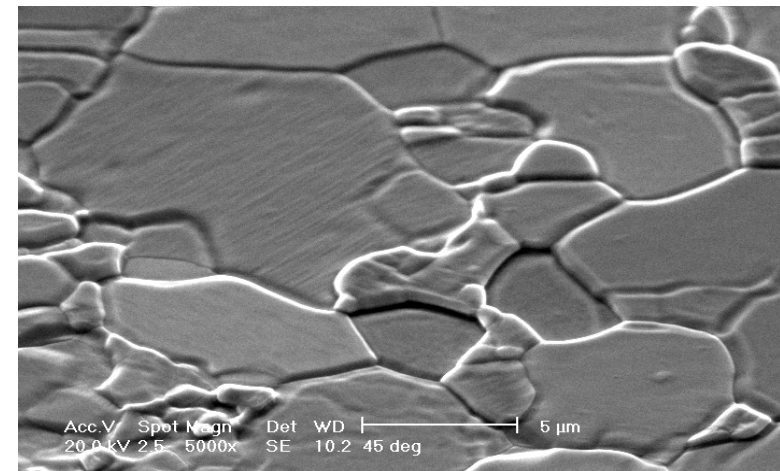


Model does not describe the saturation behaviour.
Increase of the diffusion coefficient near the surface with fluence?

W11: 3 keV D⁺, 100°C (190°C)



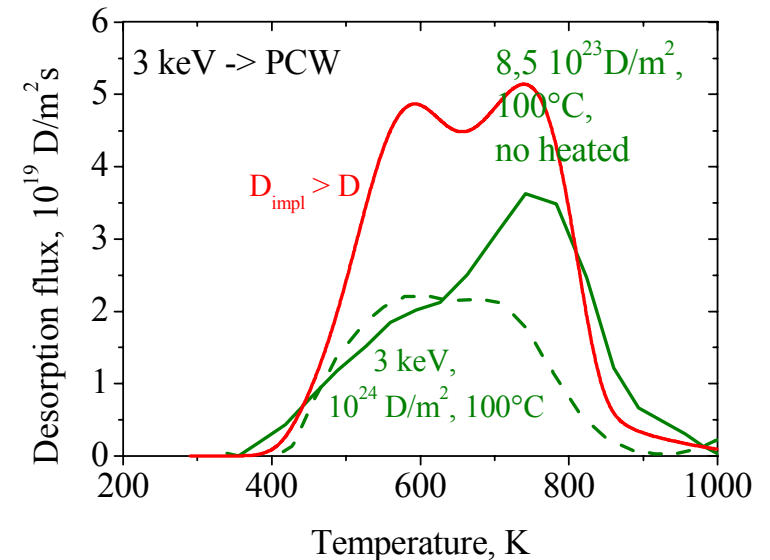
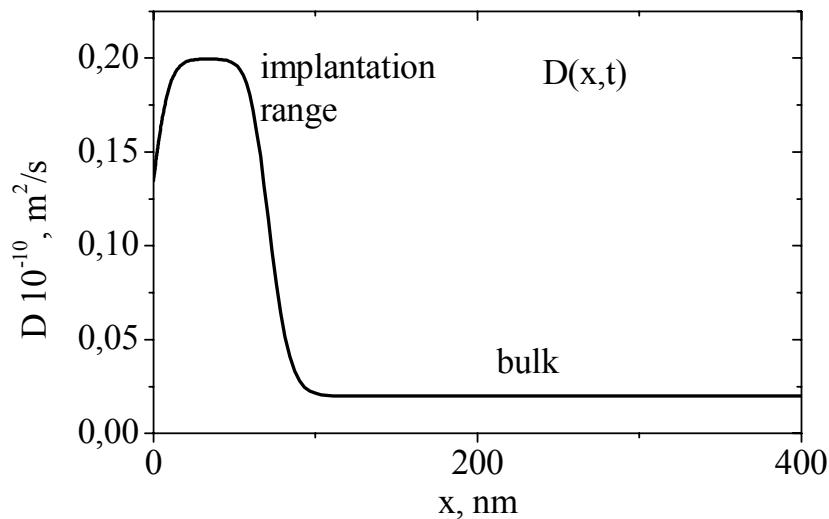
W13: 3 keV D⁺, 100°C (170°C)





Ion - induced effects in PCW: increase of diffusion coefficient

Ion induced diffusion: $D(x,t) = (1 - (1 - D/D_m) \exp(-(1-r)I_0\psi(x)t/u_m))$



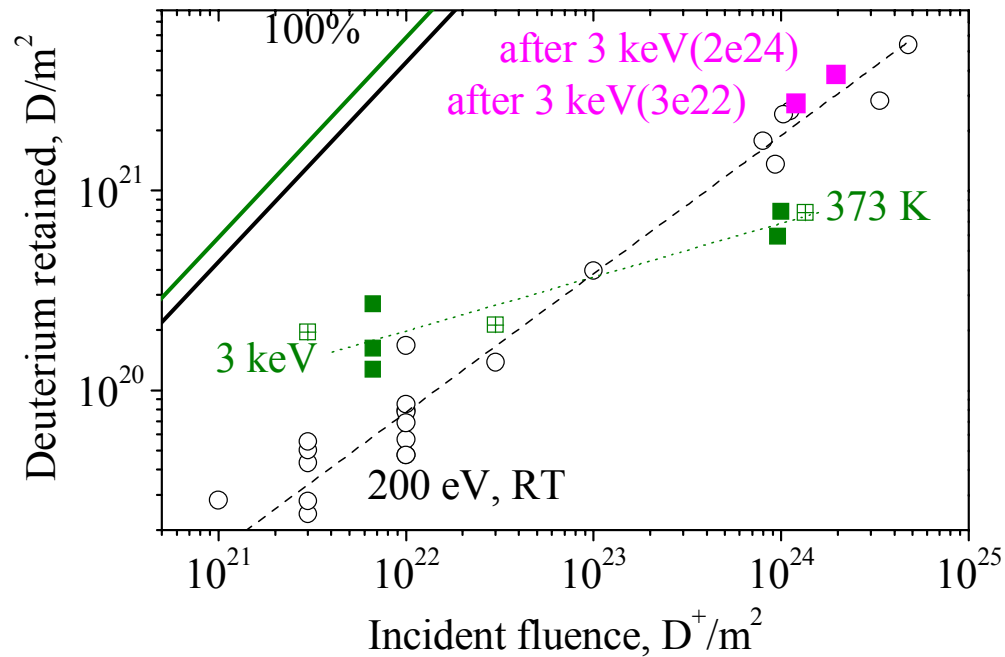
Model does not describe the saturation behaviour. Reasons:

- increase of the diffusion coefficient near the surface with fluence? – **No! The retention is still high for $D_{\text{impl}} > D$**



Ion - induced effects in PCW: pre-implantation effect

IPP



Model does not describe the saturation behaviour. Reasons:

- increase of the diffusion coefficient near the surface with fluence? – **No!**

Surface modification by 3 keV does not influence 200 eV retention at high fluences!



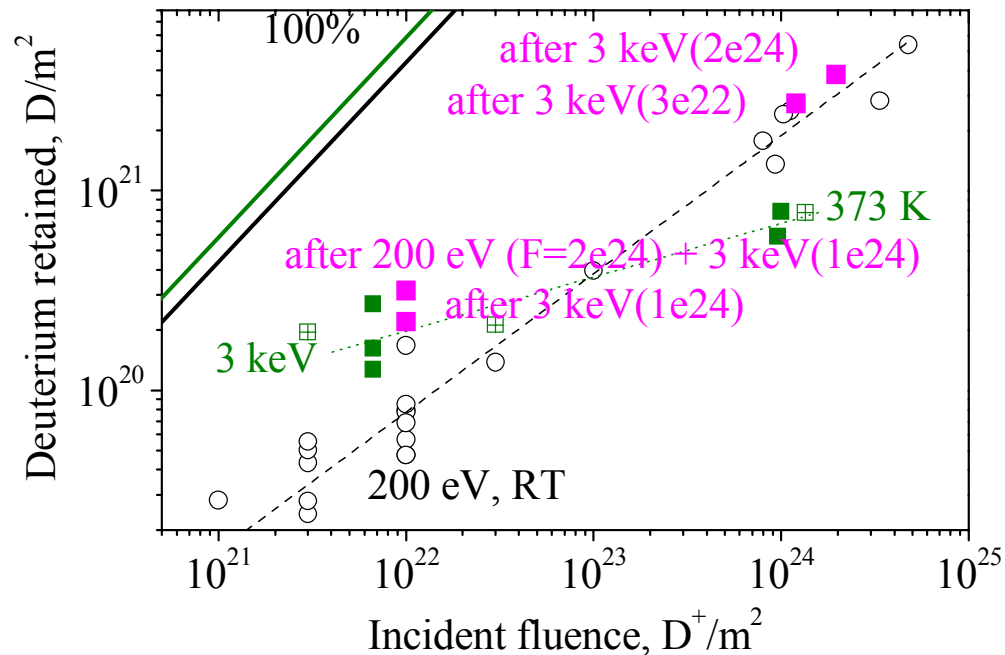
Summary of deuterium retention in W



- D retention is slightly faster than the square root of the fluence for 200 eV D^+
- D retention is saturated for 3 keV D^+
- D retention decreases with increasing temperature for low fluences but most probably increases for high fluences
- Both pre-implantation by 200 eV D^+ and by 3 keV D^+
 - a) increases D retention at low fluences
 - b) does not influence D retention at high fluences
- Model including two kinds of traps describes experiments well
- Two TDS peaks in PCW: 0.85 eV - dislocations, grain boundaries
1.45 eV - traps which grow during implantation
slowly for 200 eV and fast for 3 keV
- The speed of ion-induced defects production depends on the energy -> higher energy
higher the speed of molecule creation -> lattice stress



Ion - induced effects in PCW: pre-implantation effect



Model does not describe the saturation behaviour. Reasons:

- increase of the diffusion coefficient near the surface with fluence? – **No!**

Surface modification by 3 keV does not influence 200 eV retention at high fluences!

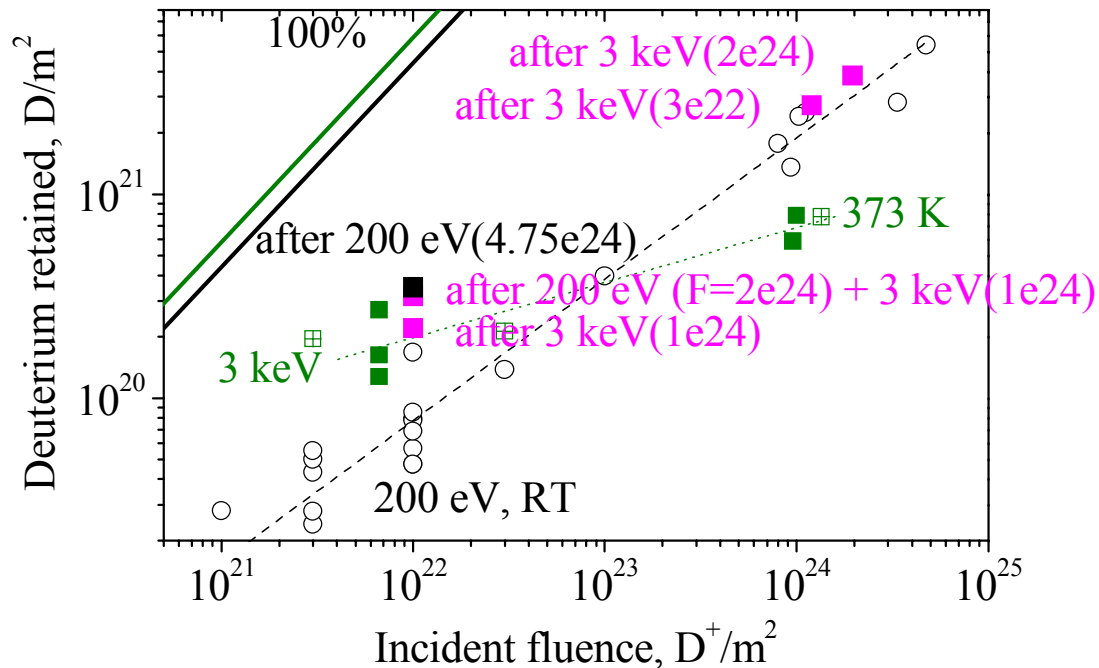
3 keV D⁺ pre-implantation results in:

- high D retention of 200 eV at low fluences**
- does not influence D retention of 200 eV at high fluences**



Ion - induced effects in PCW: pre-implantation effect

IPP



200 eV D⁺ or 3 keV D⁺ pre-implantation results in the same surface modification to create conditions for faster bubble formation

Model does not describe the saturation behaviour. Reasons:

- increase of the diffusion coefficient near the surface with fluence? – **No!**

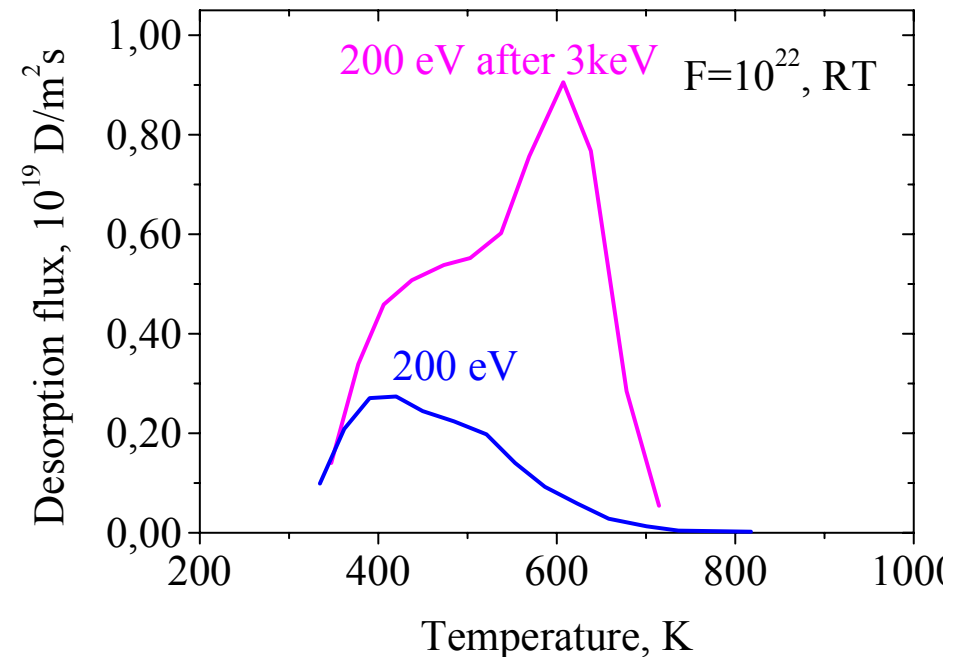
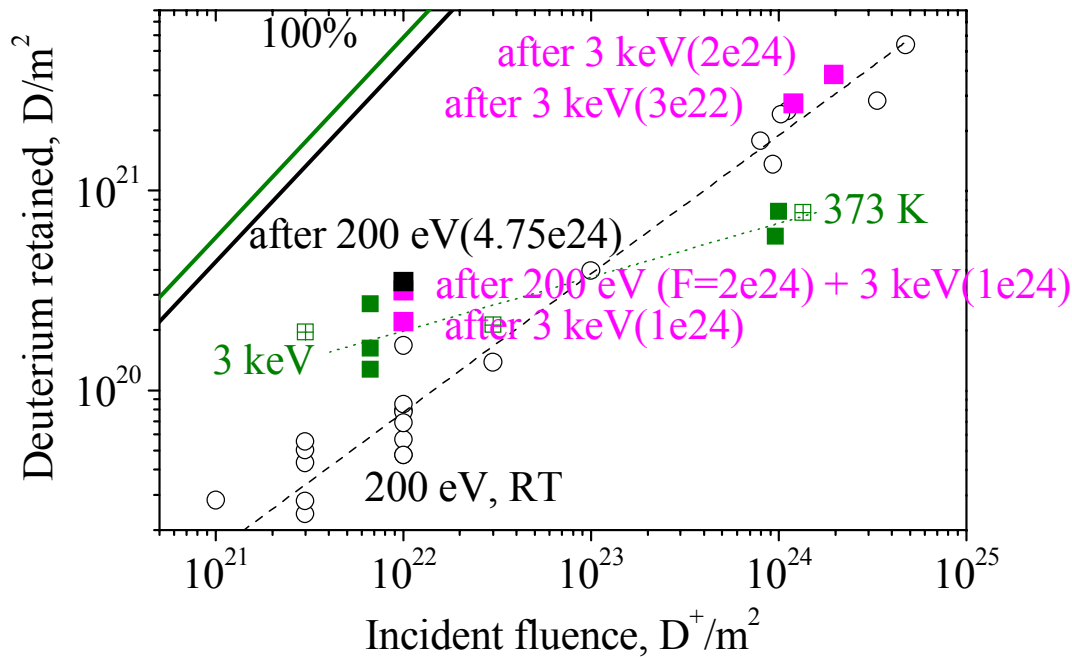
Surface modification by 3 keV does not influence 200 eV retention at high fluences!

200 eV D⁺ or 3 keV D⁺ pre-implantation results in the same effect:

- high D retention of 200 eV at low fluences**
- does not influence D retention of 200 eV at high fluences**



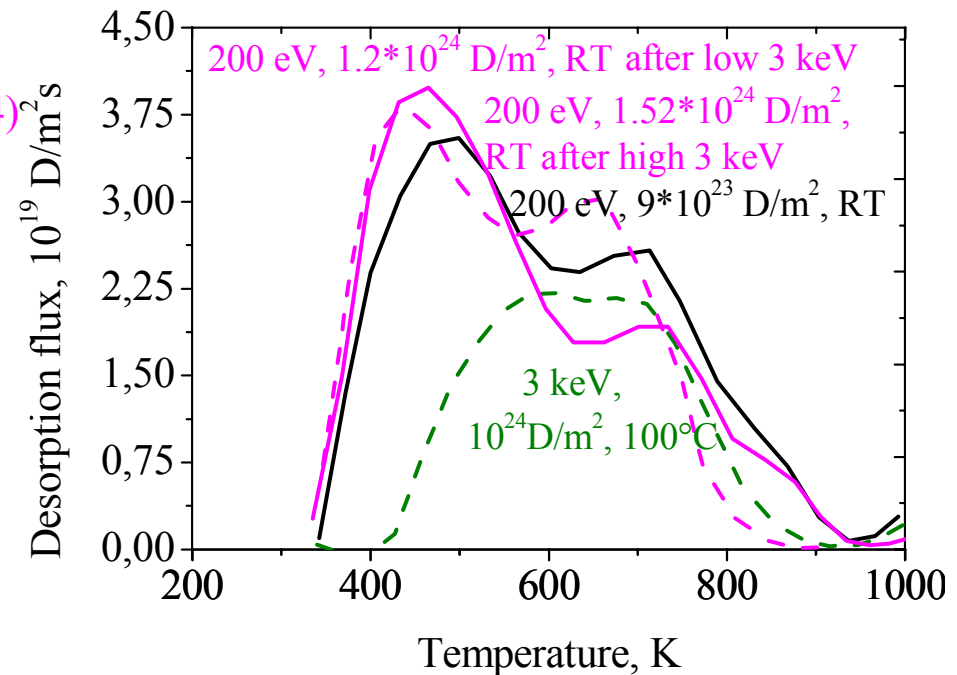
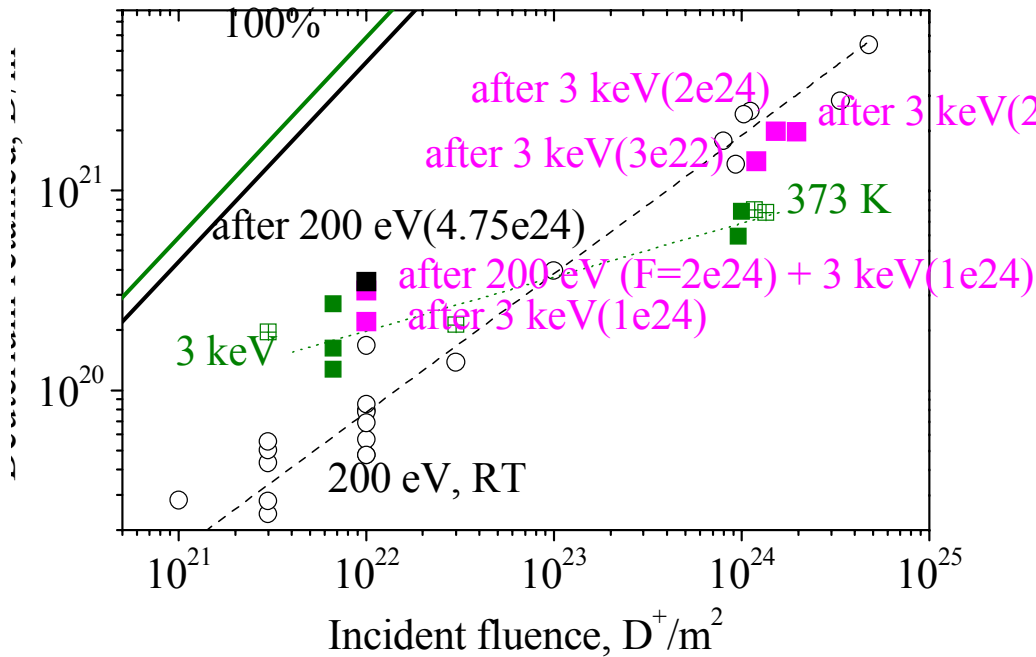
Ion - induced effects in PCW: pre-implantation effect



The concentration of ion-induced traps (1.45 eV) are strongly increased after long implantation of 3keV D^+ in W ($F=10^{24} D/m^2$)



Ion - induced effects in PCW: pre-implantation effect



The concentration of ion-induced traps (1.45 eV) are strongly increased after long implantation of 3keV D^+ in W ($F=10^{24} D/m^2$)

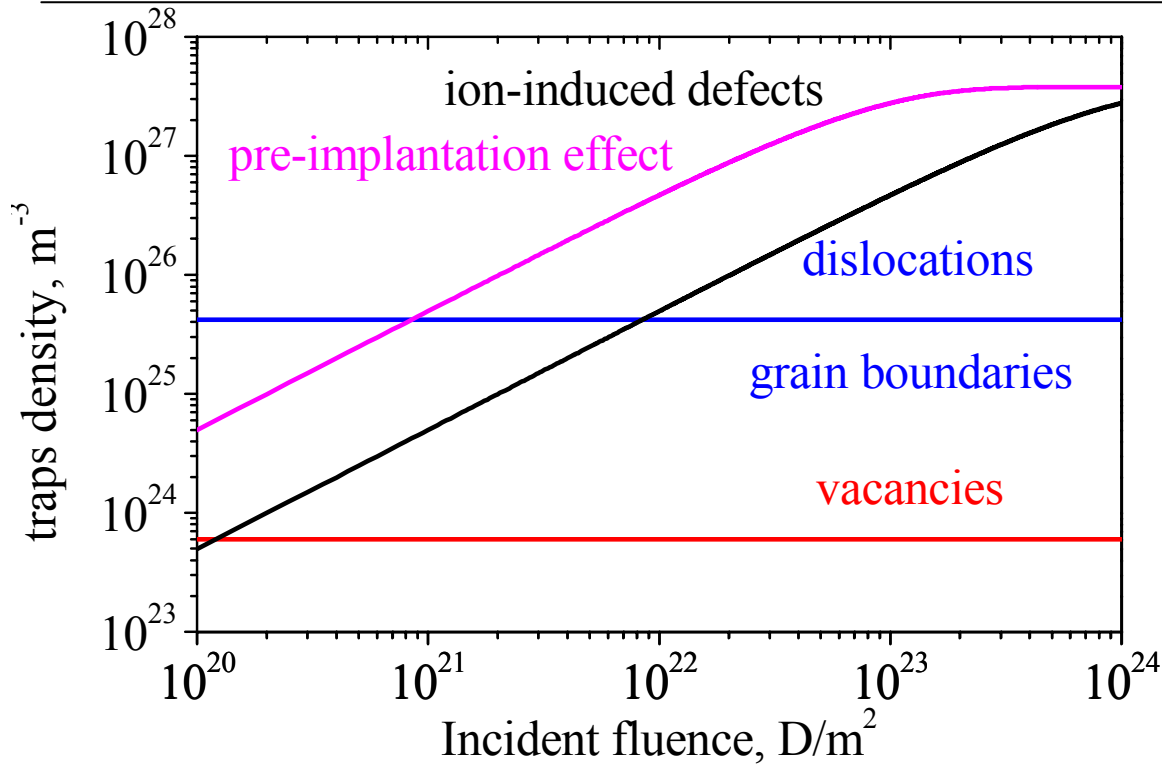
However:

No memory effect for long fluences implantation



Pre-implantation effect of D retention in W

IPP



-Pre-implantation effect results in an increase of speed of D agglomeration in bubbles

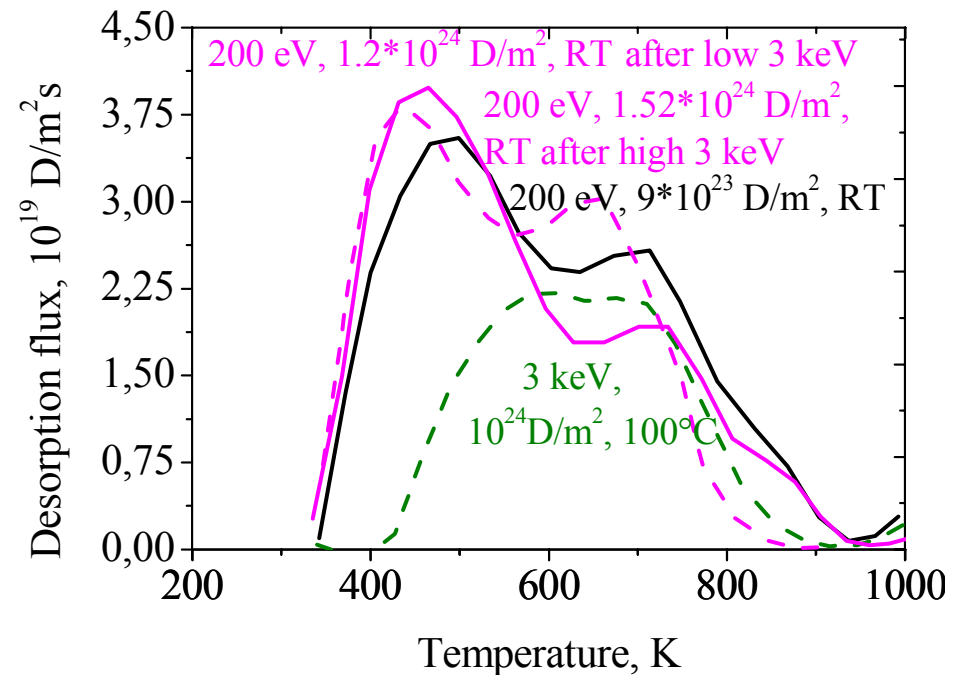
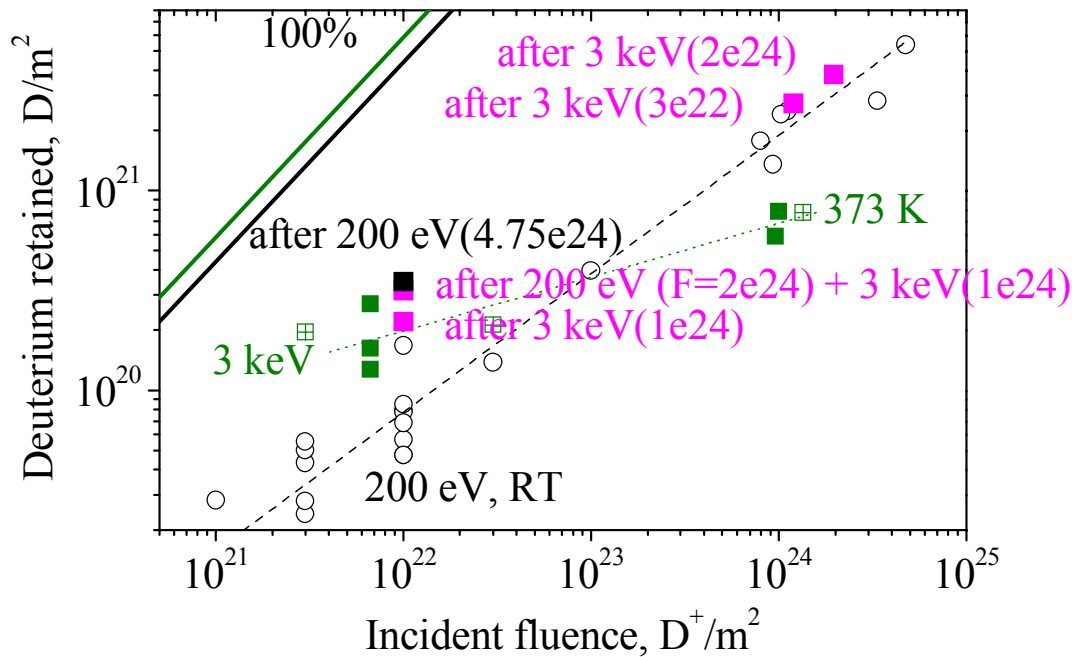
The concentration of ion-induced traps (1.45 eV) are strongly increased after long implantation of 3keV D⁺ in W (F=10²⁴ D/m²)

However:

No memory effect for long fluences implantation



Ion - induced effects in PCW: pre-implantation effect



*Which kind of ion-induced defects of **1.45 eV** can be produced by 3 keV?*

- **vacancies** -> **nucleation sites for D_2 formation**
- **agglomeration in bubbles**

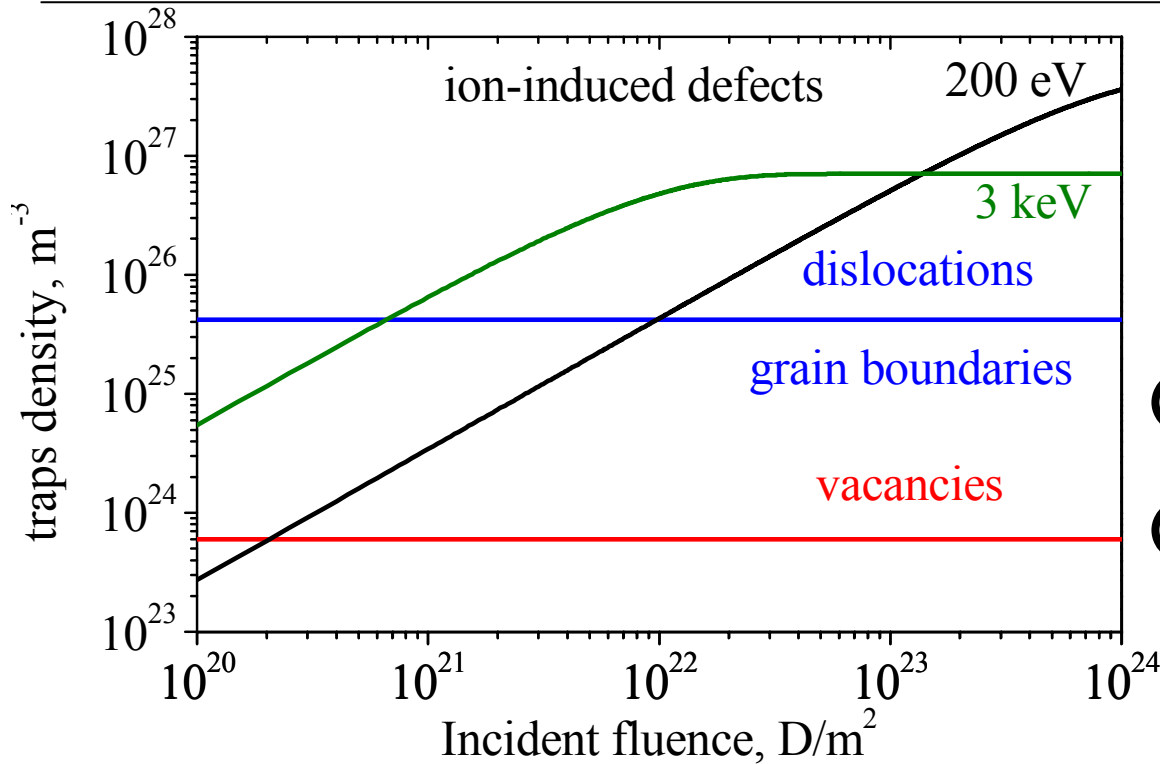
The concentration of ion-induced traps (**1.45 eV**) are strongly increased after long implantation of 3keV D^+ in W ($F=10^{24} D/m^2$)

However:

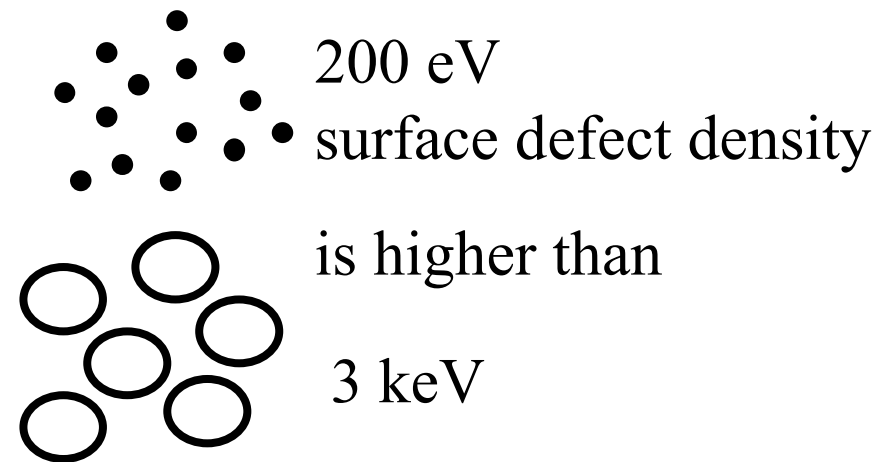
No memory effect for long fluences implantation



Model of D behaviour in W for various energies



Sakamoto:



- The speed of ion-induced defects production depends on the energy -> higher energy higher the speed of molecule creation -> lattice stress
- **Reason of saturation for 3 keV:** Creation of vacancies during bombardment which accelerate D agglomeration in bubbles and prevent Deuterium to move into the bulk of W



Summary of deuterium retention in W



- D retention is slightly faster than the square root of the fluence for 200 eV D^+
- D retention is saturated for 3 keV D^+
- D retention decreases with increasing temperature for low fluences but most probably increases for high fluences
- Both pre-implantation by 200 eV D^+ and by 3 keV D^+
 - a) increases D retention at low fluences
 - b) does not influence D retention at high fluences
- Model including two kinds of traps describes experiments well
- Two TDS peaks in PCW: 0.85 eV - dislocations, grain boundaries
1.45 eV - traps which grow during implantation
slowly for 200 eV and fast for 3 keV
- The speed of ion-induced defects production depends on the energy -> higher energy
higher the speed of molecule creation -> lattice stress



Summary of deuterium retention in W-10%Re and WC



- **W-10%Re:**
 - a) pore structure
 - b) no ion-induced defects; no pre-implantation effect
- **D retention in W-10%Re is less than in W**

- **WC and WC(40 nm)/W:**
 - a) pore structure
 - b) no ion-induced defects; no pre-implantation effect
- **D retention in WC and WC(40 nm)/W is higher than in W**

- **D retention in WC and WC(40 nm)/W is surface-limited**



Conditions for bubble formation of D in W



- Dislocations? -> atomic D implantation in SCW**
- Grain boundaries? -> atomic D implantation in SCW**
- Impurities (O)?**
- Microstructure?**

- Pre-implantation by energetic ions creates the conditions for bubble formation and increases the speed of D agglomeration in bubbles -> lattice stress**

- The speed of ion-induced defects depends on the energy -> higher energy higher the speed of ion-induced defects -> lattice stress**

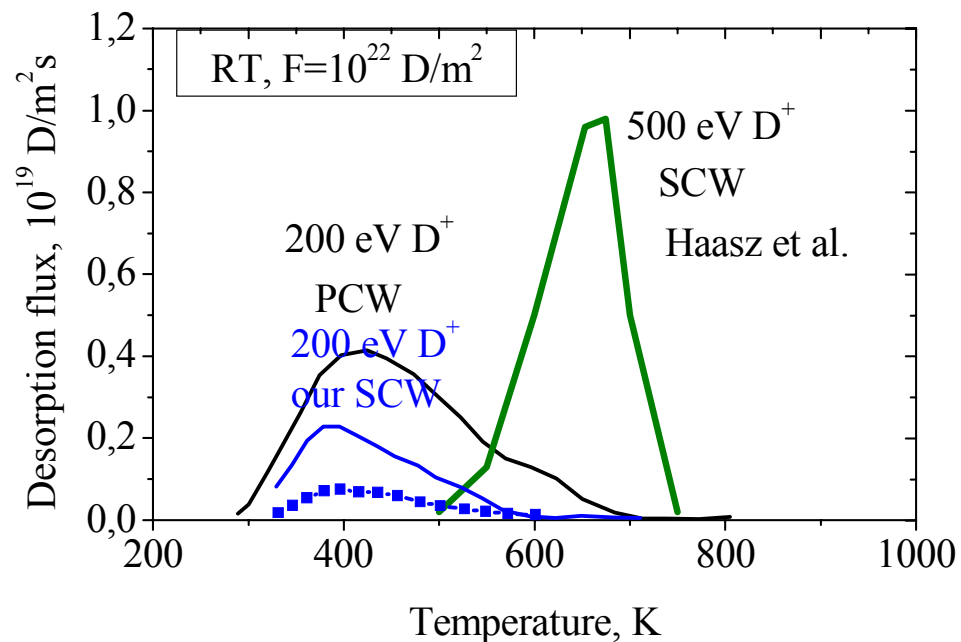
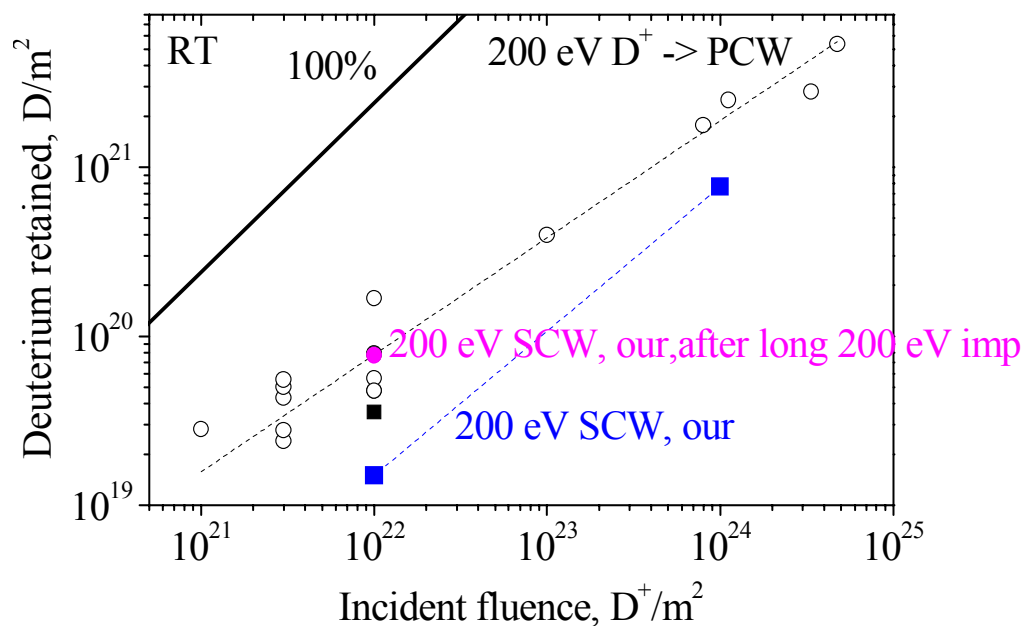
- An increase of the temperature and fluence increases bubble formation**

- Pores result in the reduction of molecular D :**
 - 1) W-10%Re: pore structure: no ion-induced defects**
 - 2) WC and WC(40 nm)/W: pore structure: no ion-induced defects**

- No ion-induced defects -> no pre-implantation effect**



D retention in SCW



- D retention in SCW is less than in PCW. Up to a fluence 10²⁴D/m² the ion-induced defects are absent.
- Disagreement with Haasz et al.



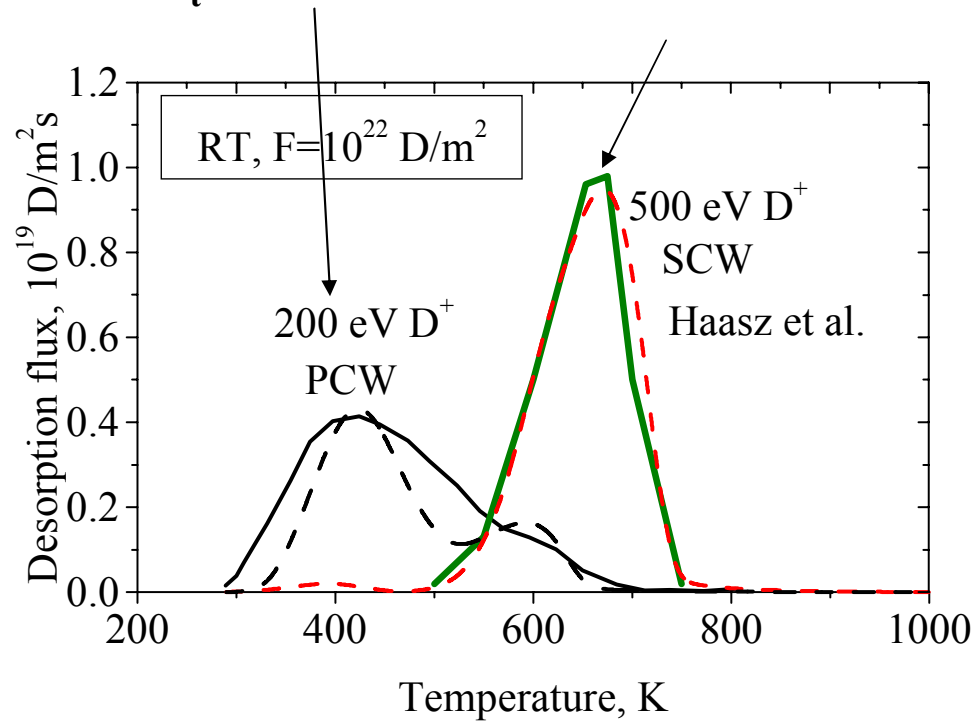
Polycrystalline W and Single crystal W



dislocations,
grain boundaries
 $E_t=0.85$ eV

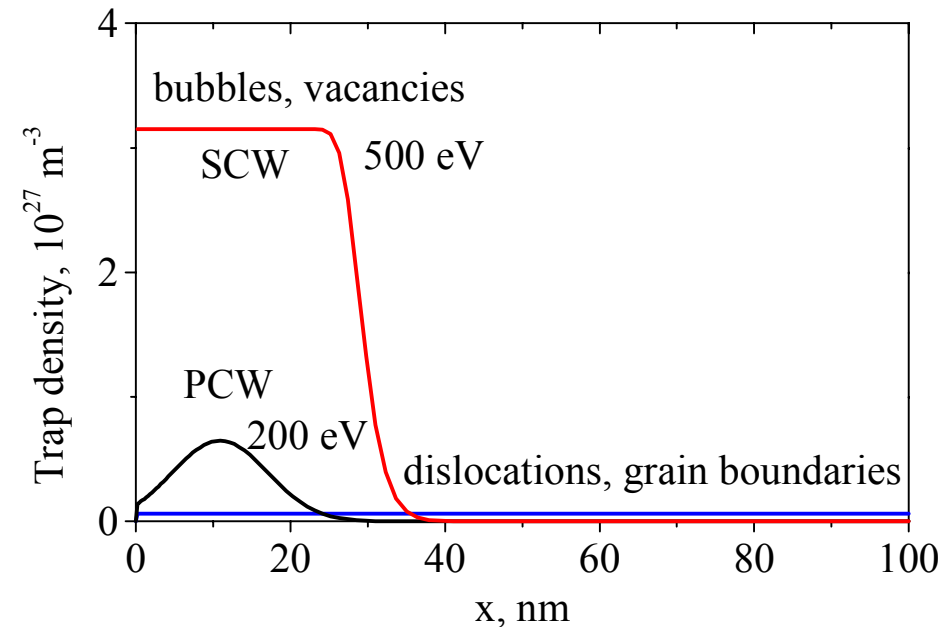
bubbles
in the near surface: 1.45 eV;
vacancies 1.45 eV

SCW: most of D is
trapped near the
surface



— experiments
..... calculations

TDS



Trap density from modeling



Future plan for TDS and depth profile

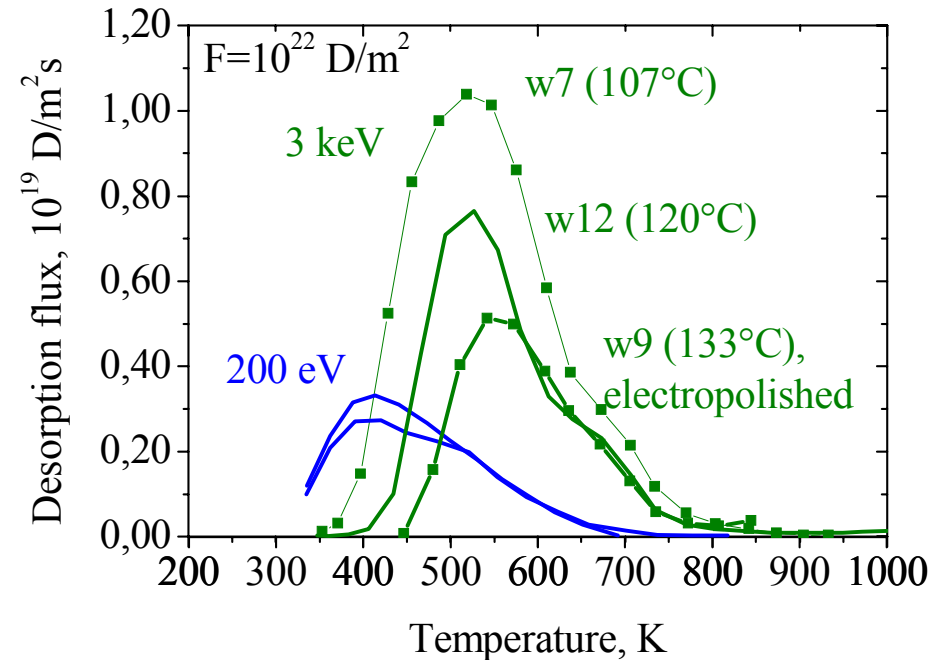
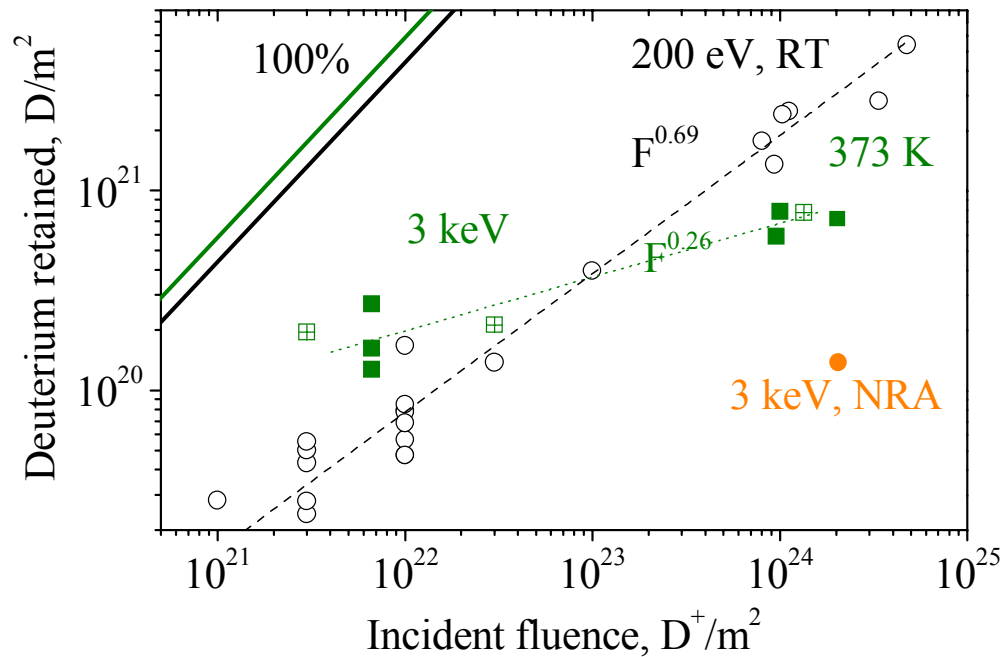


- **Less porosity W-X%Re: 200 eV D⁺ and 3 keV D⁺ implantation**
- **High fluence, high temperature implantation of 60 eV D⁺ and 3 keV D⁺ in PCW**
- **Atomic D implantation in SCW**
- **Influence of defects:**
 - He⁺ pre-implantation**
 - H⁺ pre-implantation**



Energy dependence

IPP



Higher D retention for 3 keV than for 200 eV for low fluences

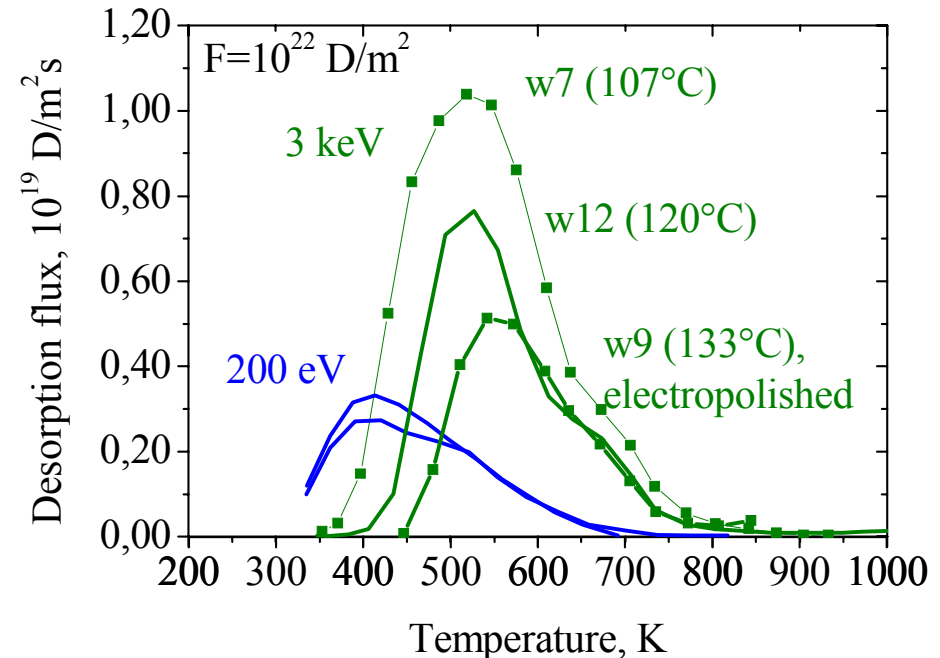
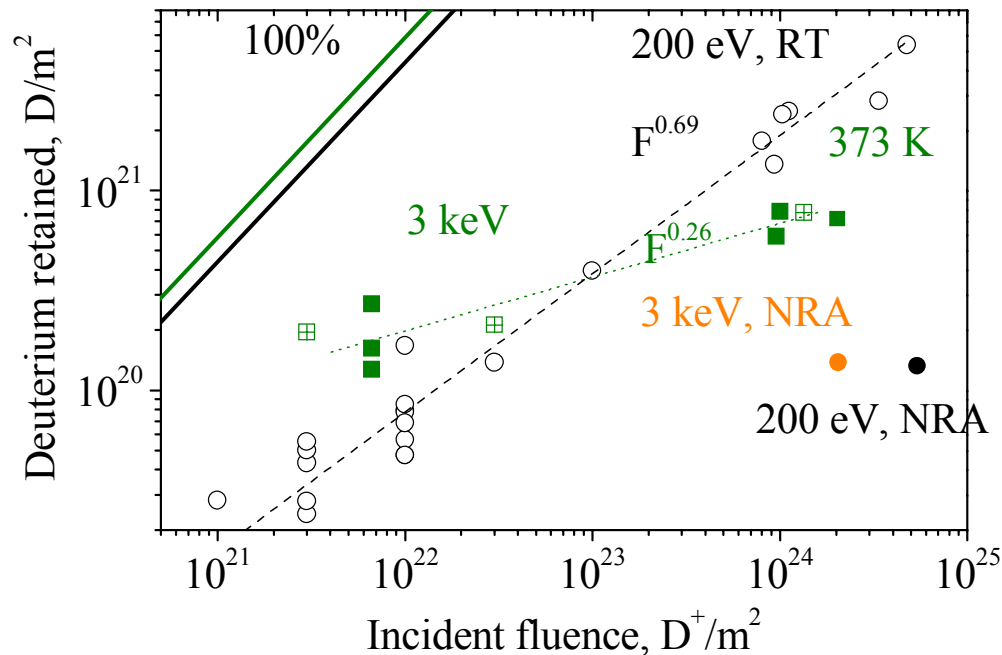
**NRA show less D retention than TDS:
Most of D is in the bulk for 3 keV
implantation**

- TDS for 200 eV has a max at about 400 K: most of D is trapped in defects with 0.85 eV
- Deuterium does not retained in traps with 400 K for 3 keV implantation because the temperature of W rises during implantation
- TDS for 3 keV has a max about 550 K



Energy dependence

IPP



Higher D retention for 3 keV than for 200 eV for low fluences

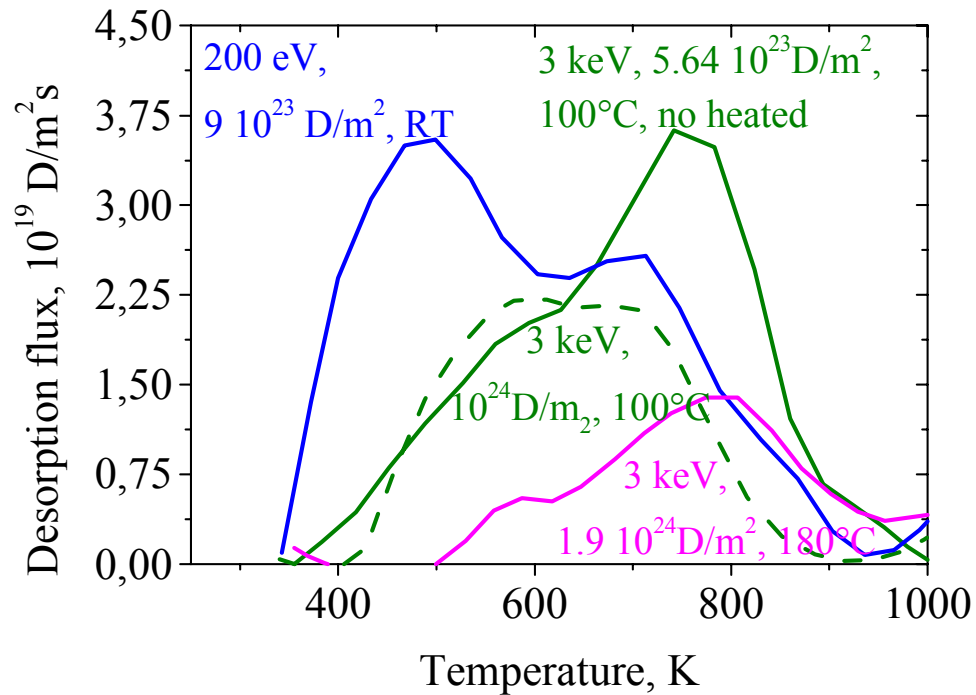
**NRA show less D retention than TDS:
Most of D is in the bulk for both 200 eV
and 3 keV implantation**

- TDS for 200 eV has a max at about 400 K: most of D is trapped in defects with 0.85 eV
- Deuterium does not retained in traps with 400 K for 3 keV implantation because the temperature of W rises during implantation
- TDS for 3 keV has a max about 550 K

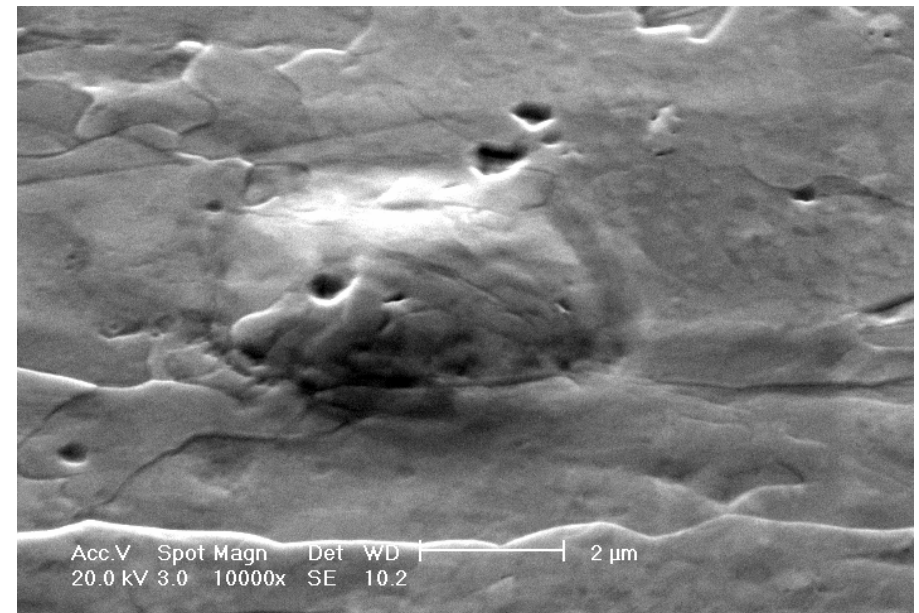


3 keV D⁺ -> PCW: TDS

IPP



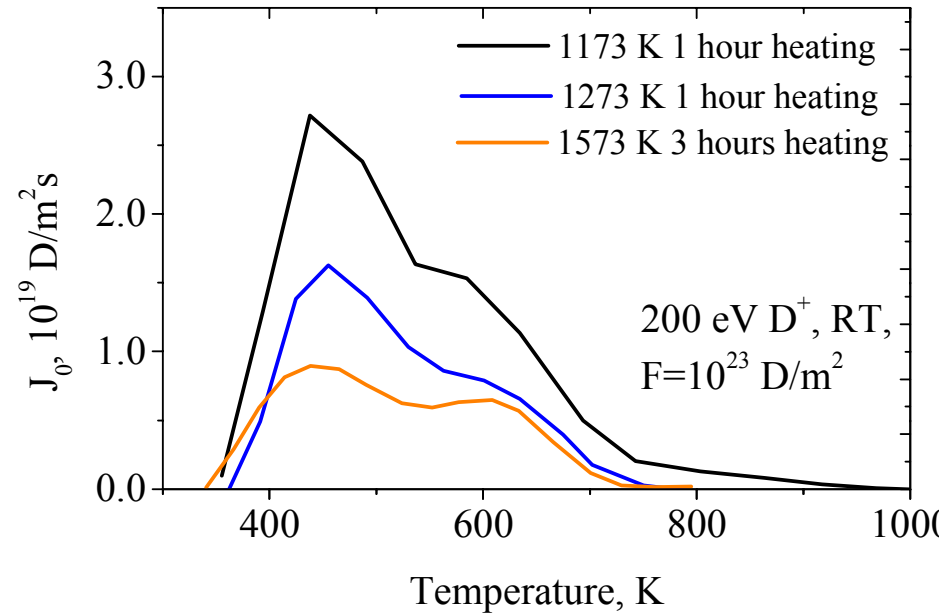
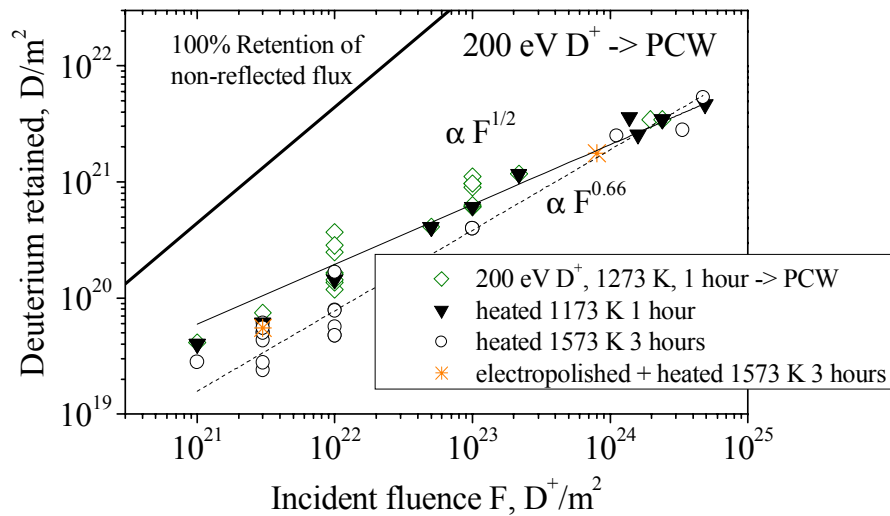
W10: 3 keV D⁺, RT, unannealed



Dislocations, or impurities, or diffusion responsible for the bubble growth?



200 eV D⁺ -> PCW: Influence of sample preparation

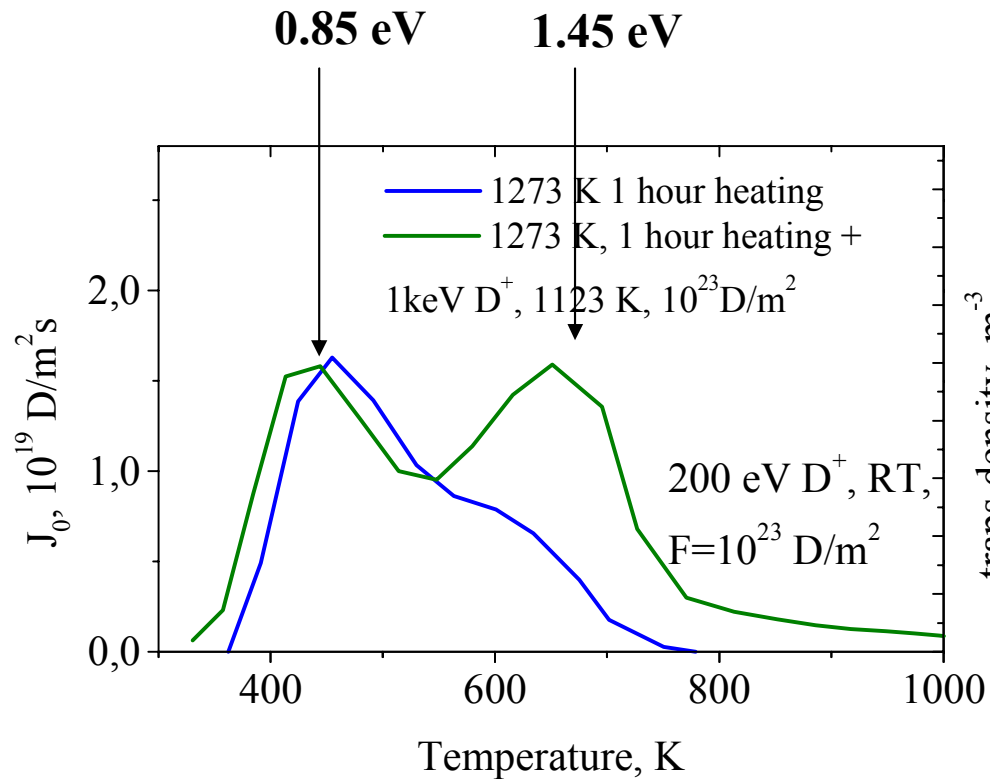


Annealing reduces the concentration of grain boundaries, dislocations and surface impurities \Rightarrow retention decreases

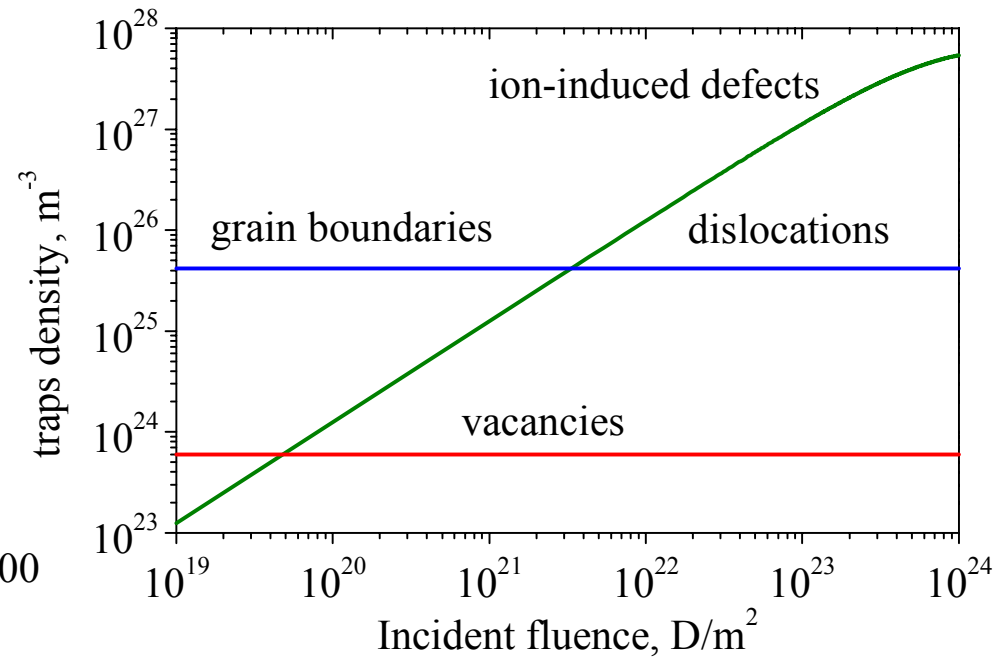
Solubility is extremely low: small change in the defect concentration results in significant change in the retention



200 eV D⁺ -> PCW: Influence of ion-produced traps



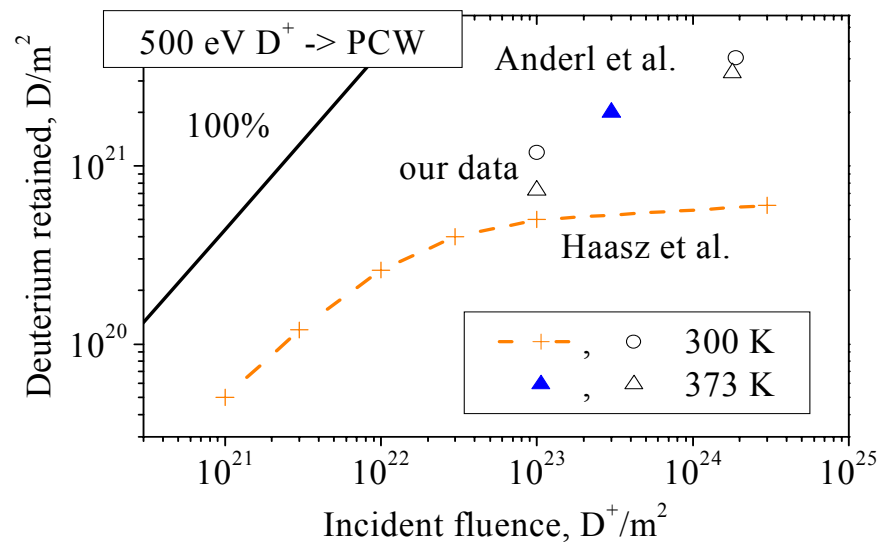
Ion-induced traps with trapping energy of 1.45 eV are created during implantation



The density of 1.45 eV traps increases with fluence



PCW: Comparison with literature

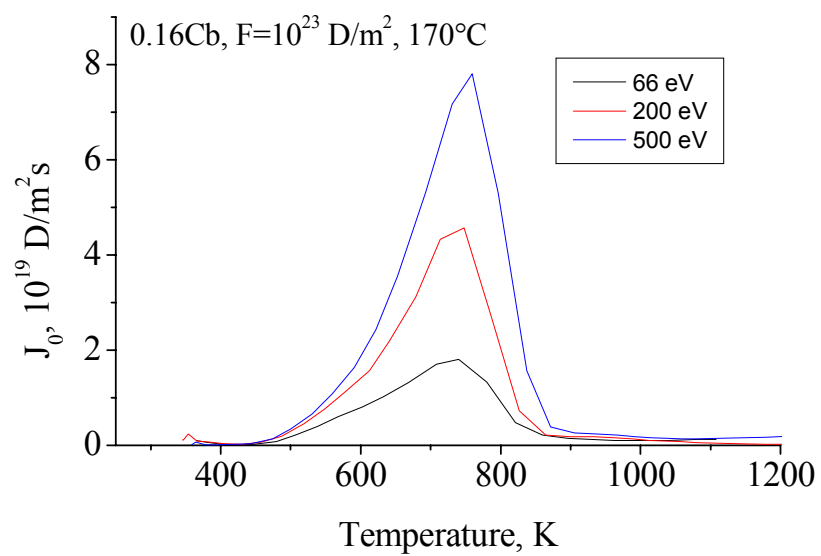


1. Agreement with Anderl et al. data

2. Disagreement with Haasz et al. data

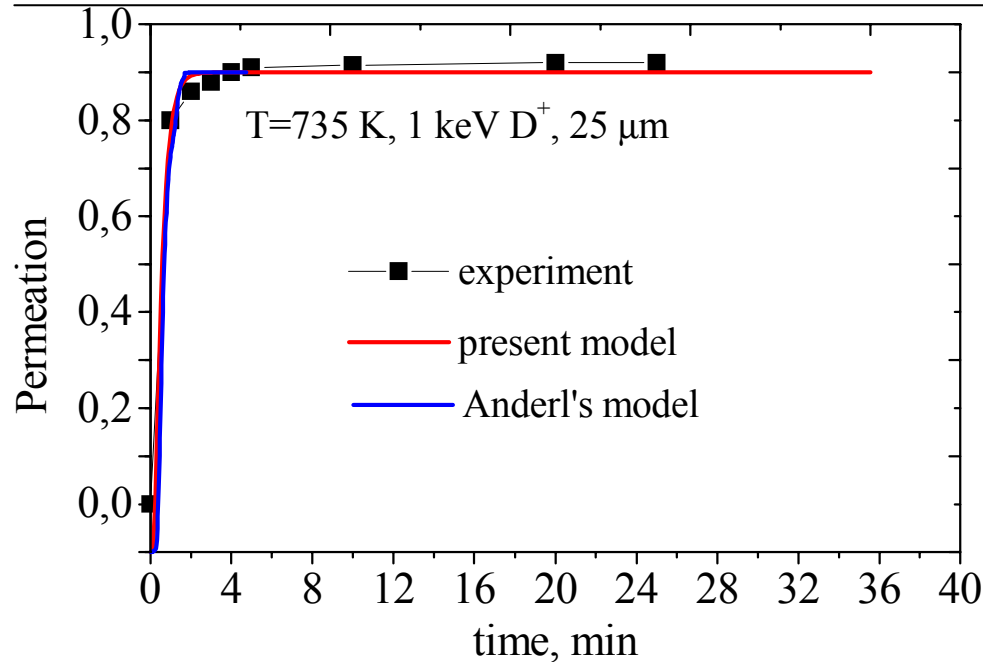


Energy dependence

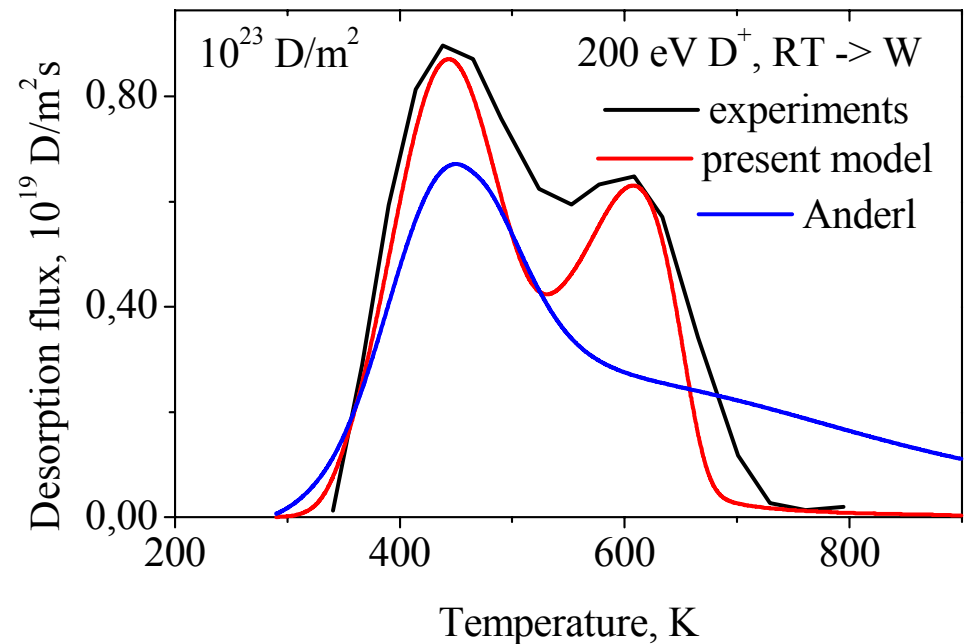




Recombination coefficient of deuterium on W



Permeation data can be described well by both Anderl's parameters and our parameters (K_r , E_t , W_t)



TDS calculated with Anderl's parameters results in a disagreement with experiment.

Present model: $K_r^{\text{clean}} = 3 \cdot 10^{-25} / T^{1/2} \exp(2/kT)$, intrinsic (dislocations) + ion-induced defects:
 $E_t = 0,85\text{ eV}$, $W_t = 8 \cdot 10^{-4}\text{ at.fr.}$ + $E_t = 1,45\text{ eV}$, $W_t^{\text{max}} = 6 \cdot 10^{-2}\text{ at.fr.}$

Anderl's model: $K_r = 1,3 \cdot 10^{-17} \exp(-0.84/kT)$, intrinsic (vacancies) defects:
 $E_t = 1,34\text{ eV}$, $W_t = 2 \cdot 10^{-5}\text{ at.fr.}$



D can re-place from one kind of traps to another during annealing:

van Veen :

vacancies becomes mobile at about 600 K and form vacancy clusters. =>

TDS does not show D distribution in trapping sites during implantation

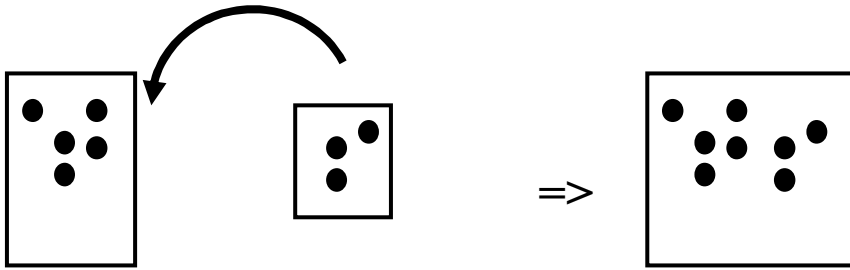
D can release from other traps created during annealing than it was initially distributed during implantation

At $T=1400$ K 40-60 vacancies clusters are formed

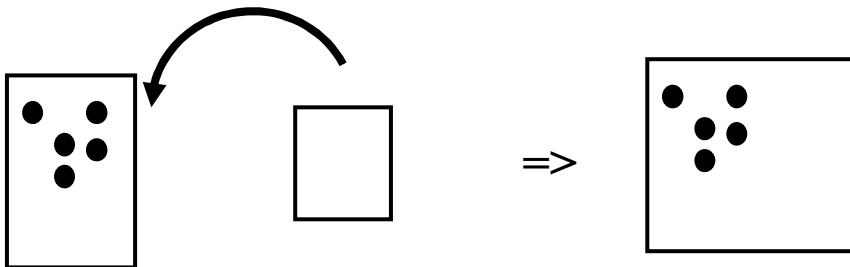
At $T>1700$ K vacancies clusters disappear



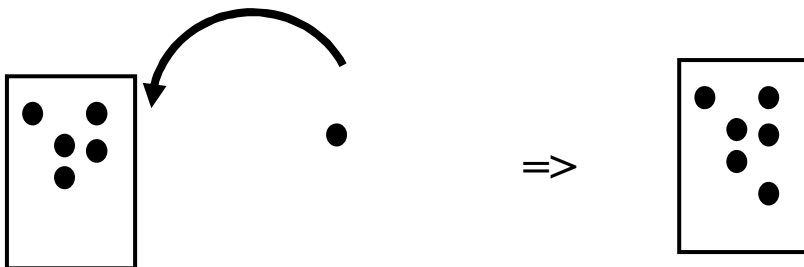
TDS and void growth during annealing



Void growth by bubbles migration



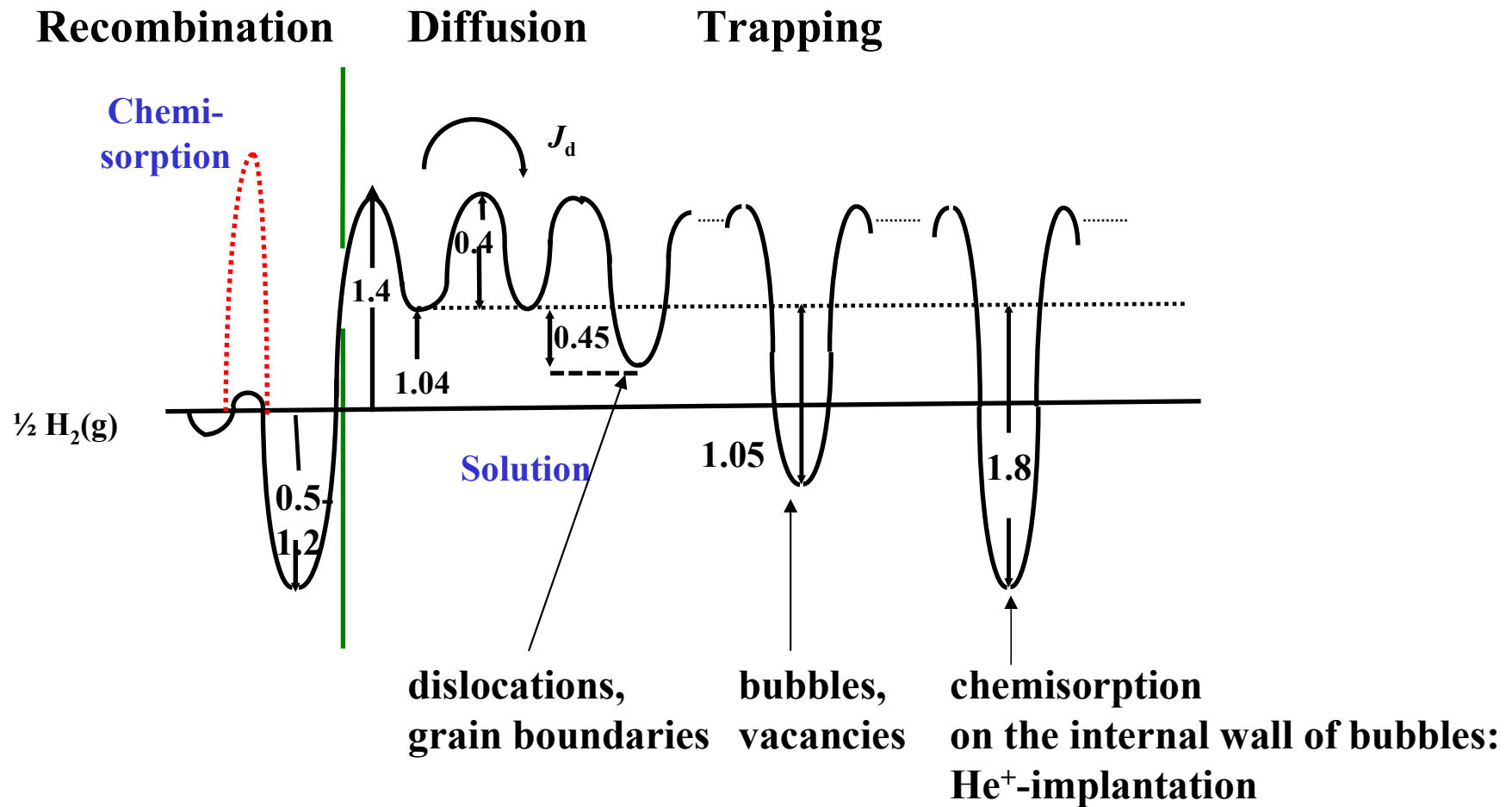
Void growth by vacancies migration



Void growth by atomic D diffusion



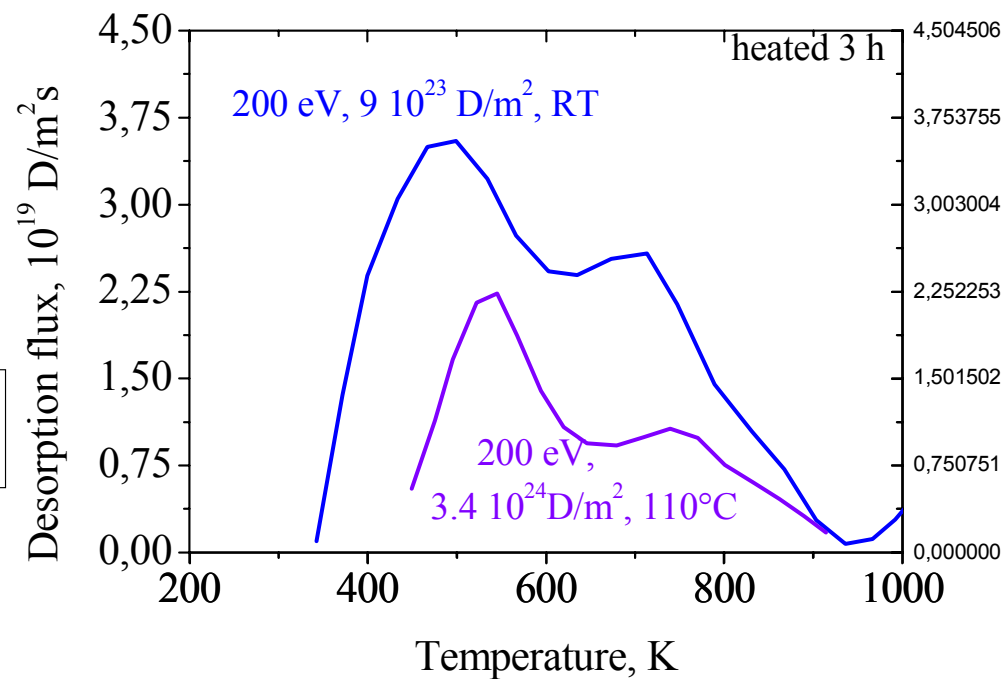
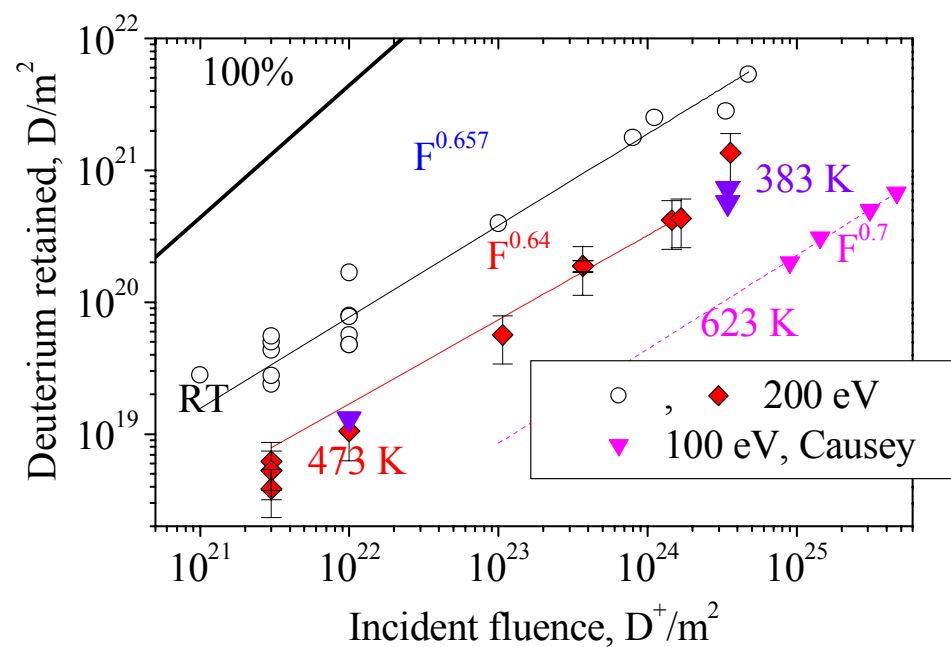
Mechanism of deuterium behaviour in W



$$E_b^{\text{vacancy}} = (Q_c + Q_s)/2$$



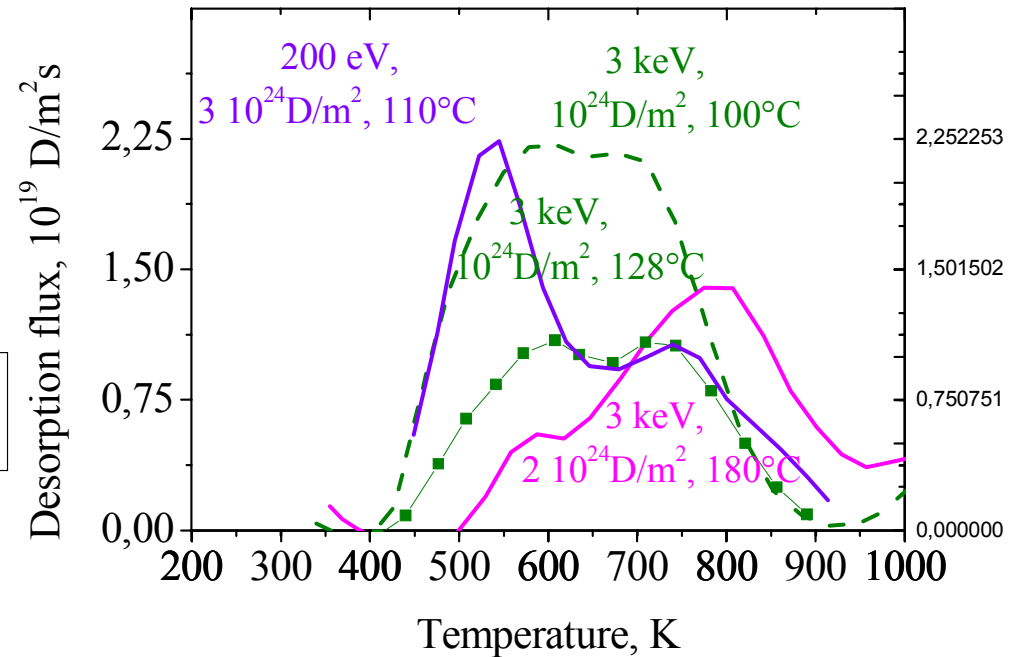
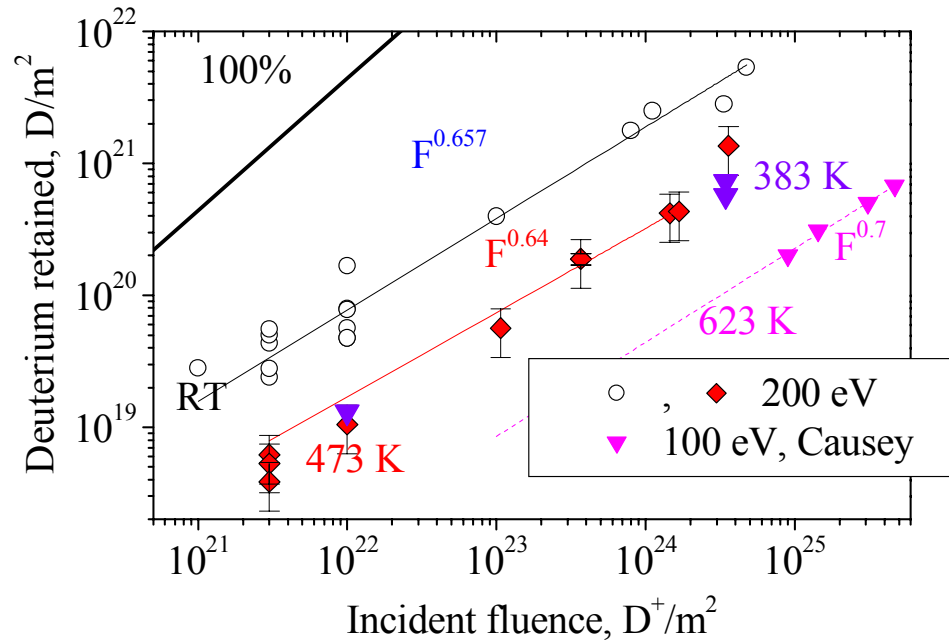
Temperature dependence





200 eV D⁺ -> PCW: Temperature dependences

IPP



**Increase of the temperature \Rightarrow
decrease of the retention for pre-annealed W**

***However:* D retention most probably
increases with temperature for high
fluences**

Tungsten Blister Formation & Deuterium Retention Measurements in PISCES-B

M. J. Baldwin & R. P. Doerner, UC San Diego USA

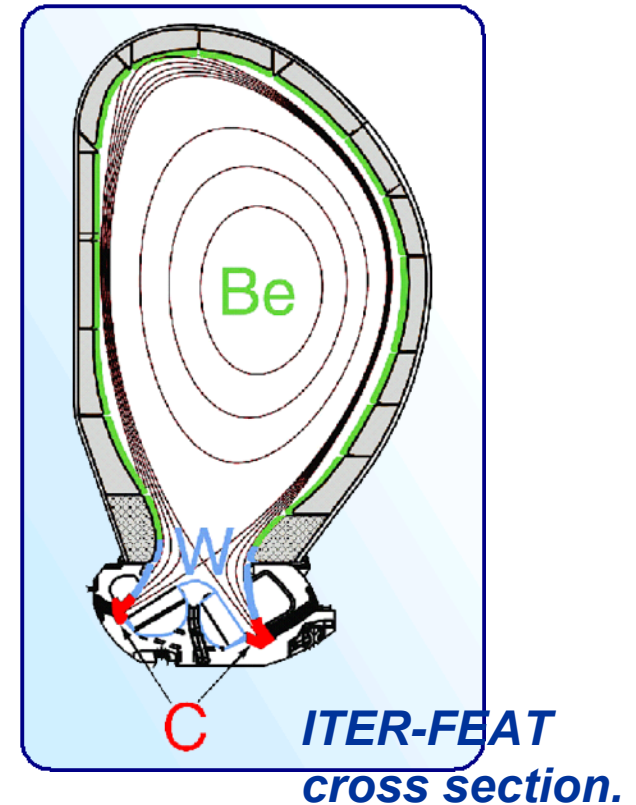
K. Tokunaga, Kyushu University, Japan

K. Schmid, Max-Planck Institut für Plasmaphysik, Germany



1. Motivation

- The UC San Diego PISCES team and the European Fusion Development Agency (EFDA) are investigating the influence of Be impurities on plasma-materials interactions relevant to the ITER project.
- In ITER, the first wall will be Be, the divertor W, and the strike points C.
- Be impurity flow in the divertor plasma is expected to be as high as 10 %.
- Recent PISCES experiments (Schmid *et al.*, Baldwin *et al.* PSI-16) have focused on Be influences on graphite target erosion and deposition /co-deposition.
- Experiments using W targets are aimed at understanding influences on W armor.



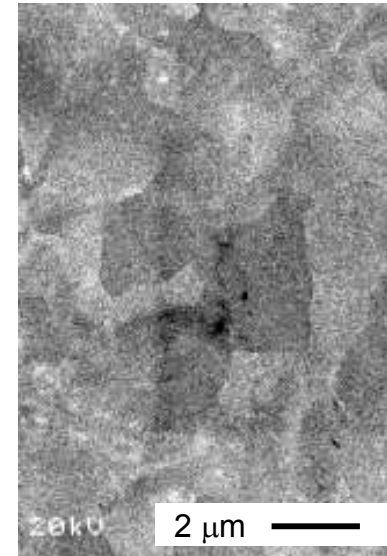
- Tungsten is a good candidate PFC material because of its low sputtering yield and good thermal properties.
- Years of research on blister formation due to ion (H, D, He) irradiation have been carried out. Typically, ion energies were high enough to cause lattice damage.
- More recently, blistering has been observed under divertor relevant parameters where incident ion energies are below that required for elastic displacement.
- Blistering may affect hydrogen isotope trapping and erosion resulting from surface flaking.
- Experiments are underway to systematically investigate and identify the mechanisms involved.



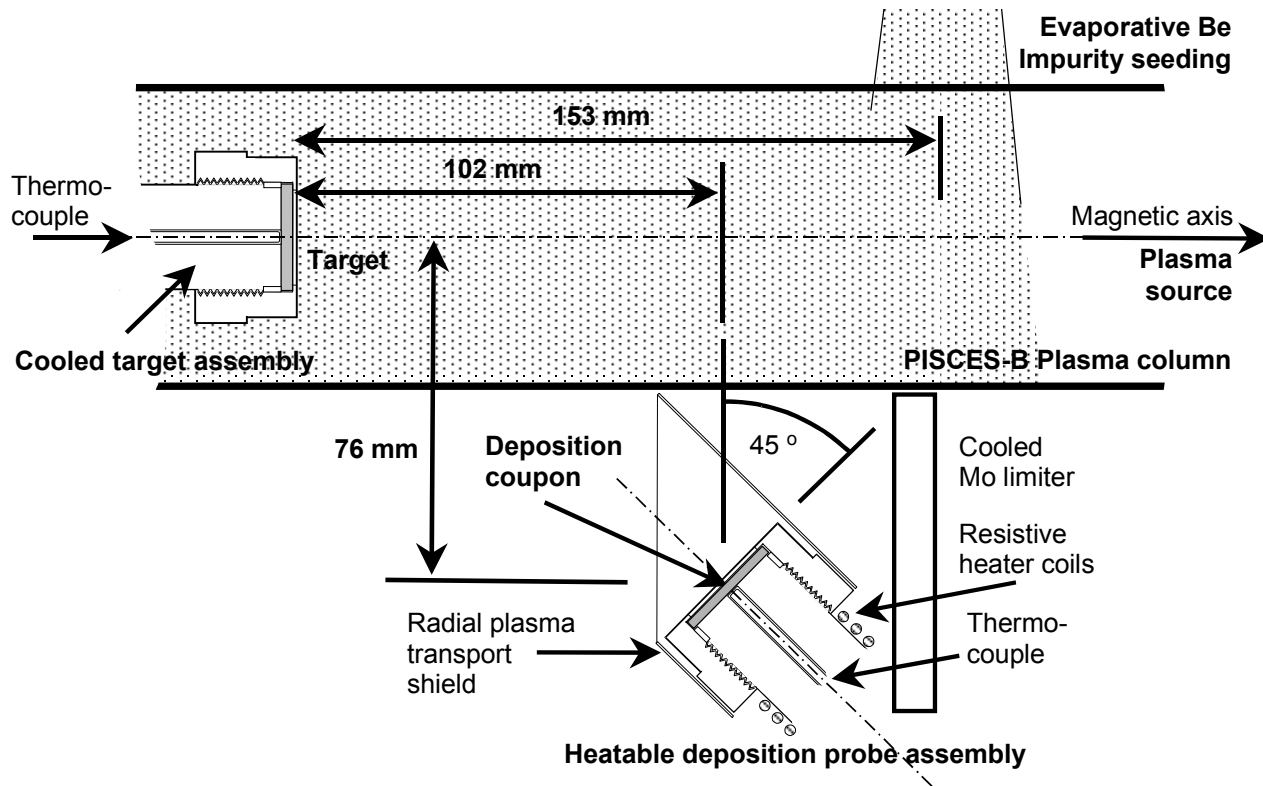
2. Samples

Rolled Powder metallurgy specimens:

- Fabricated by Allied Material Corp.
- Rolling ratio 87.4 %.
- Purity : 99.99 wt %.
- Size : 25.4 mm diameter, 2 mm thick.
- Electro-polished.
- Thermally desorbed / annealed at 1300 K for 20 mins.



3. Plasma exposure in PISCES-B



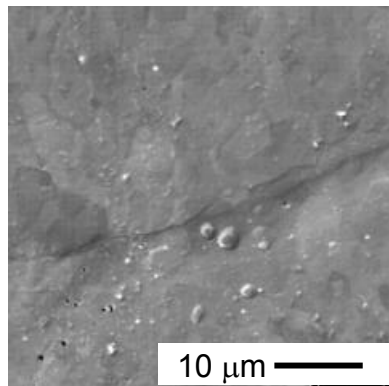
PISCES-B and confinement devices (edge) compared

	PISCES	Conf. device
Ion flux (cm^2s^{-1})	10^{19}	10^{19}
Ion energy (eV)	20–300 (bias)	10–300 (thermal)
Heat flux (MWcm^{-2})	10^{-4} – 10^{-3}	10^{-4} – 10^{-3}
T_e (eV)	2–40	1–100
n_e (cm^{-3})	10^{12}–10^{13}	10^{12}–10^{13}
Be Imp. fraction (%)	Up to a few %	1–10 (ITER)
Pulse length (s)	Steady state	10–30
Target materials	C, W, Be	C, W, Be ..
Plasma species	H, D, He	H, D, T, He

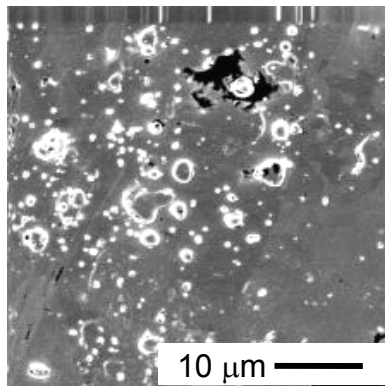


4. *Blister formation is found to be optimal ~650 K*

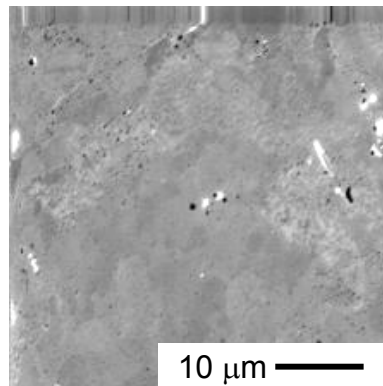
333 K \pm 20 K



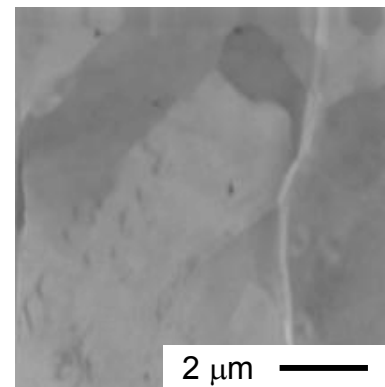
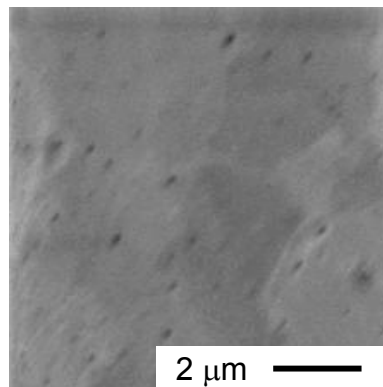
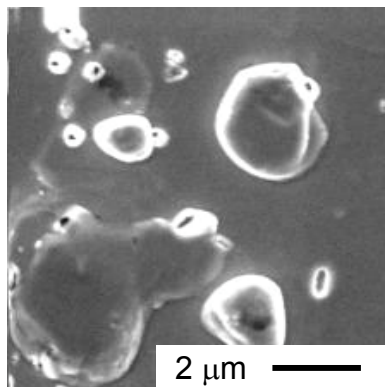
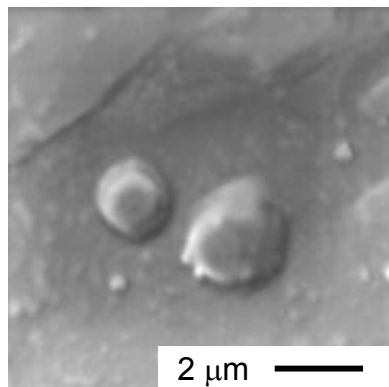
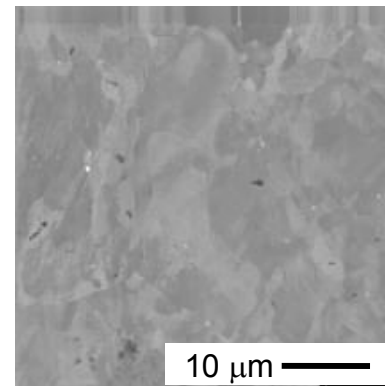
673K \pm 100 K



723 K \pm 20 K



1130K \pm 10 K



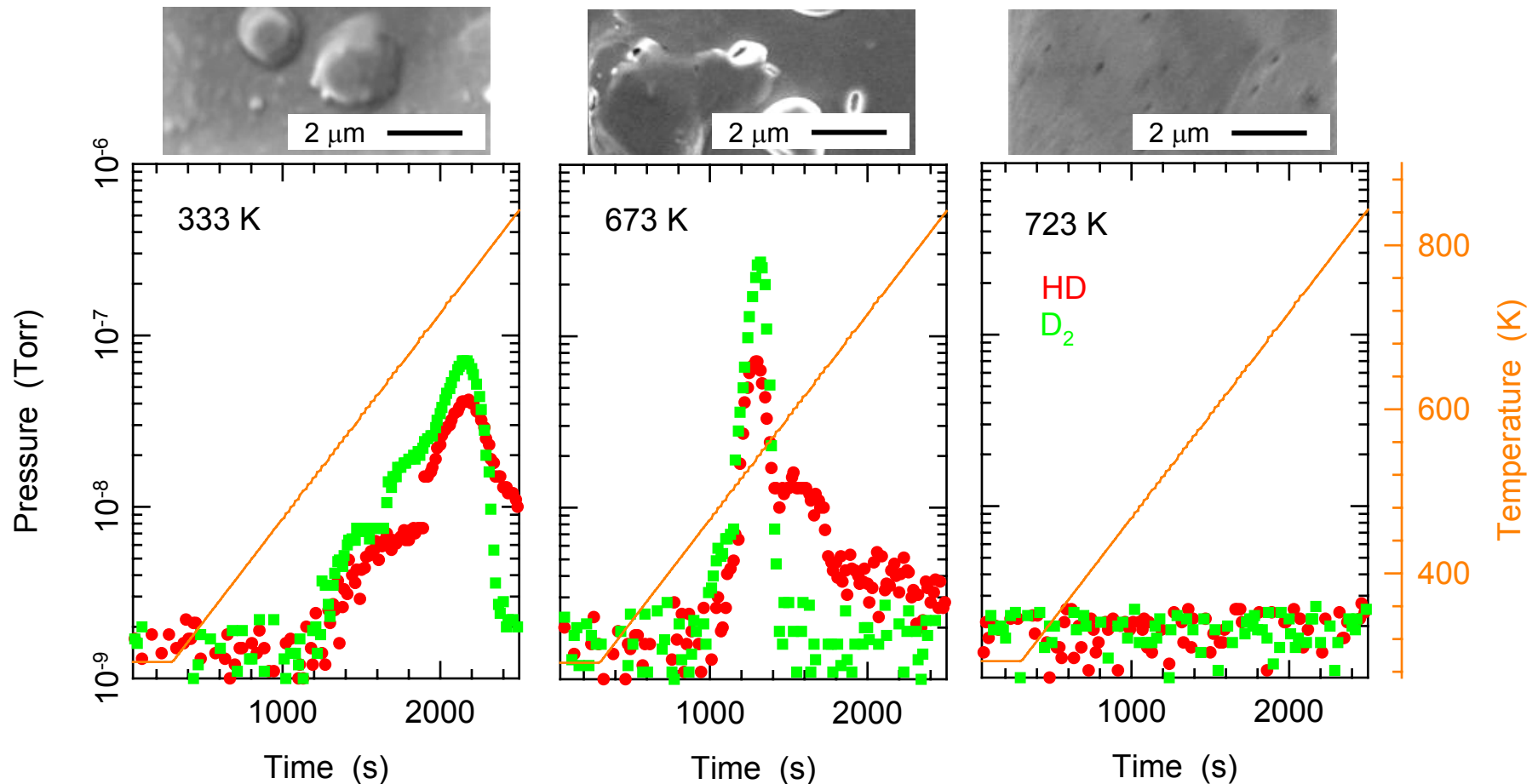
E_{ion} : 100 eV

Γ_D^+ : $1 \times 10^{22} \text{ m}^{-2} \text{ s}^{-1}$

Fluence: $1 \times 10^{26} \text{ m}^{-2}$



5. Deuterium retention correlates with blistering



6. What role will Be impurities play?

Plasma exposures
were compared:

Case 1

No Be impurities.

Case 2

~0.1 % Be impurity
seeding.

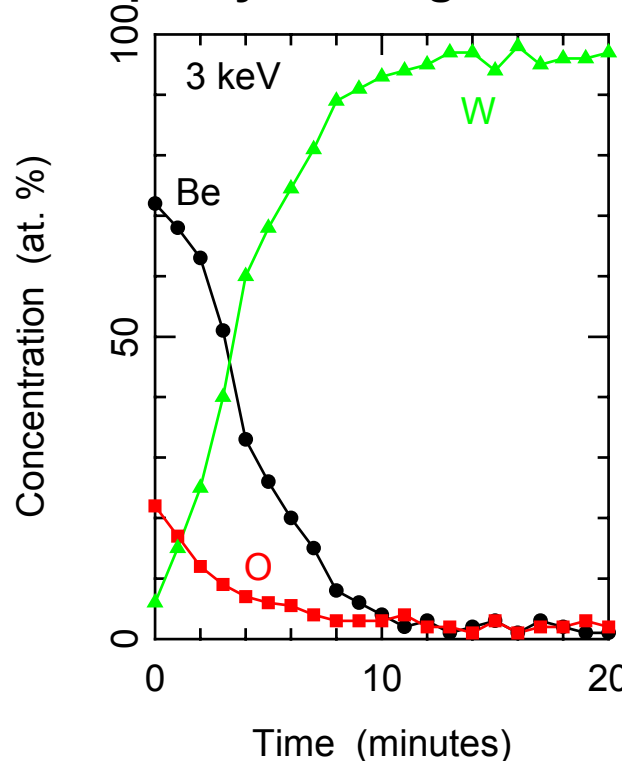
E_{ion} : 75 eV

T: ~ 550 K

Γ_D^+ : $1 \times 10^{22} \text{ m}^{-2} \text{ s}^{-1}$

Fluence: $5 \times 10^{25} \text{ m}^{-2}$

AES depth profile for W target with Be impurity seeding - Case 2.



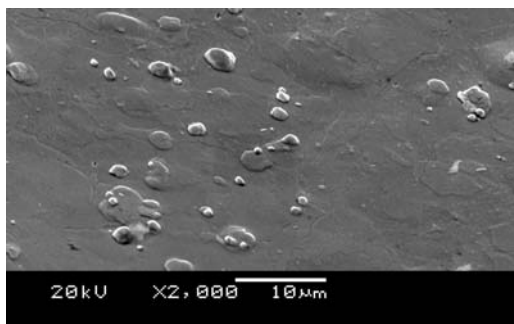
*Be impurities in
the plasma can
give rise to thin
surface films.
(~10 nm est.)*

*Mean range for D^+
in Be at 100 eV is
~ 3 nm*



Be impurities, blistering and retention (initial results).

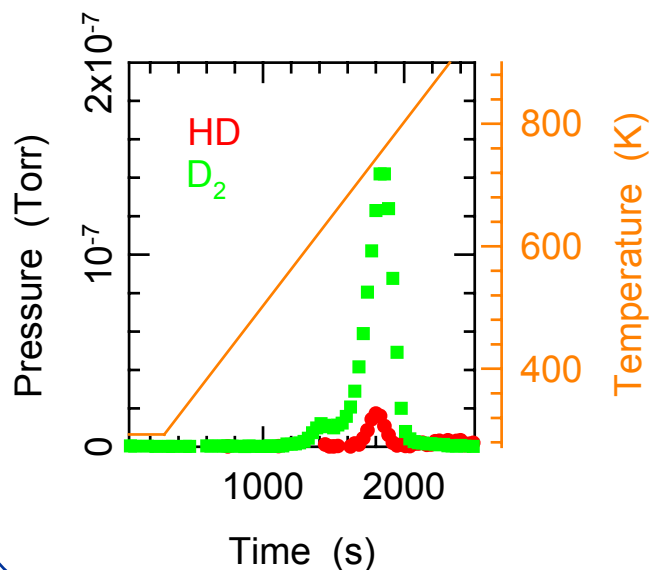
Case 1.



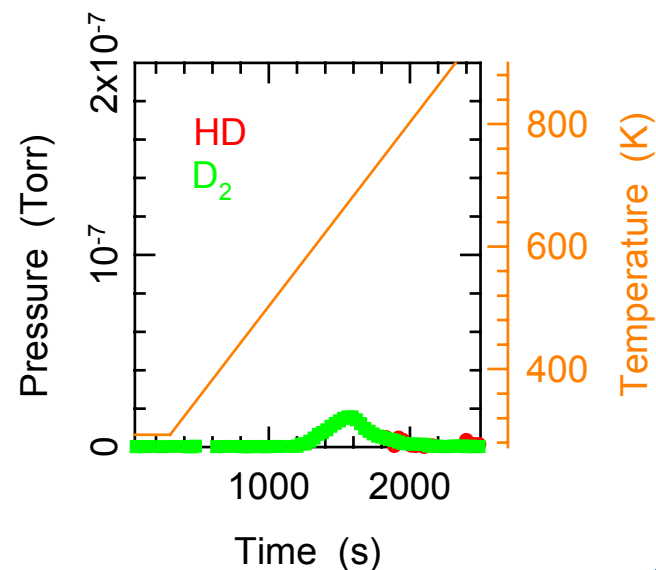
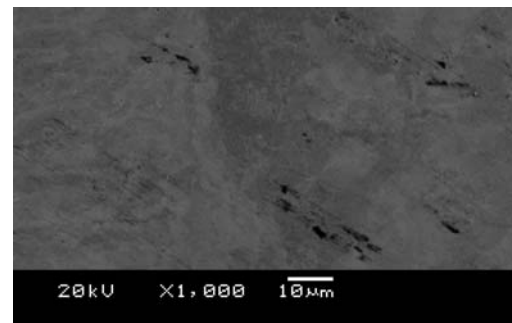
➤ Be impurity flux inhibits blistering.

➤ Be forms a thin protective layer.

➤ Retention in Be coated W is comparable to retention in unblistered W.



Case 2. (~0.1 % Be)



7. Concluding remarks

- Rolled Powder metallurgy W specimens have been exposed to low-energy high fluence plasma exposures in PISCES-B.
- Hydrogen isotope retention is found to be optimal ~650 K in agreement with literature (E.g. *Venhaus et al., J Nucl. Mater, 290-3 (2001) 505*).
- Larger retention is systematically observed with blistered targets compared to unblistered targets.
- A small Be impurity flux ~0.1 % in PISCES inhibits blistering and leads to reduced retention.
- Ongoing experiments will address the location of retained deuterium (W or Be layer), the role of temperature under Be impurities and conditions under which Be layers form.





Behavior of hydrogen isotopes interacting with defects in Li₂O

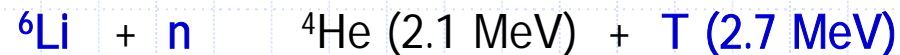
Takuji Oda, Yasuhisa Oya, Satoru Tanaka
The University of Tokyo

Contents

1. Background & purpose
2. Approaches: experiment & calculation
 - 2-1. Experiment: in-situ FT-IR during D⁺ irr.
 - 2-2. Quantum chemical calculation: DFT
3. Results & discussion
4. Summary

1. Background & purpose

To establish a secure and efficient fuel cycle in a fusion reactor, produced tritium must be recovered rapidly from breeding blanket.



In the case of a solid breeding material (Li_2O , Li_2TiO_3 etc)...., **influence of radiation defects** is one of the most important factors that determine the tritium behavior.

Behaviors of tritium and defects in Li_2O have been extensively studied. However,

- ◆ The evaluated tritium diffusivities are scattered.
- ◆ The concrete influences of defects are not understood sufficiently.



The purpose is **to understand the hydrogen isotope behavior in an atomic scale with considering concrete influence of defects.**

2. Approach

: Experiment & quantum chemical calculation

To understand the hydrogen isotope behavior **in an atomic scale**,
&

To clarify **the influence of radiation defects**,



‘Experiment’ + ‘Quantum chemical calculation’

Experiment

Directly observe the hydrogen
isotopes interacting with defects.

IR spectroscopy during D⁺ irradiation

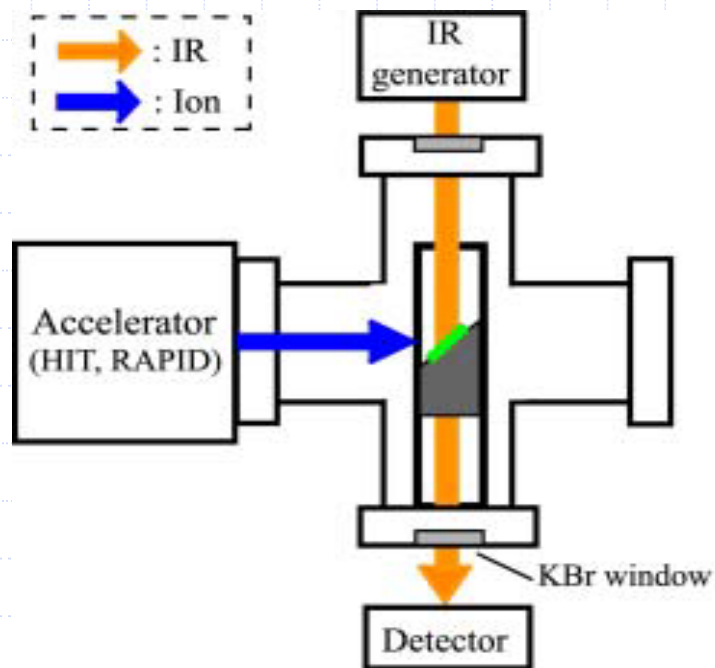
Calculation

Investigate the hydrogen isotope
behavior **in a system containing defects**.

DFT by CASTEP code

2-1. Experimental

: In-situ FT-IR during D⁺ irradiation



Sample Li_2O s.c. disk (10 x 1 mm)

Sample temp.: 373 K during irr.

2×10^{16} (300 keV D⁺) m⁻² s⁻¹



<D⁺ irradiation> : D⁺ irr. makes the situation where the hydrogen isotopes interact with radiation defects.

<FT-IR> : IR absorption of O-D shows multiple peaks by interacting with surrounding defects.

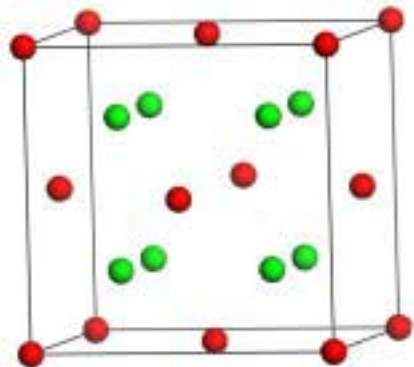
2-2. Calculation technique

: Density Functional Theory (DFT) with a supercell

Approximation: **GGA**
Functional: **PBE**
Tolerance: 2.0×10^{-5} eV/atom

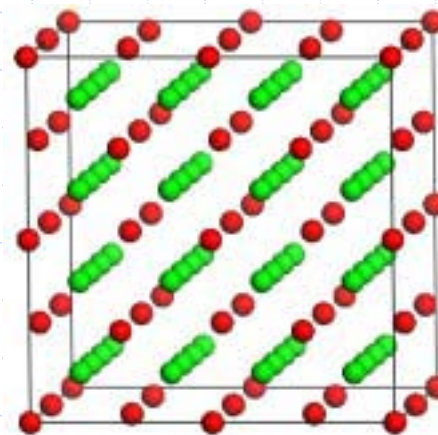
- ◆ To treat properly the relaxation induced by defects, **all atoms were permitted to move.**
- ◆ Calculation cost was reduced by use of **plane wave basis** and **pseudopotential (O 1s).**

Li : ● O : ● H : ●



Conventional cell

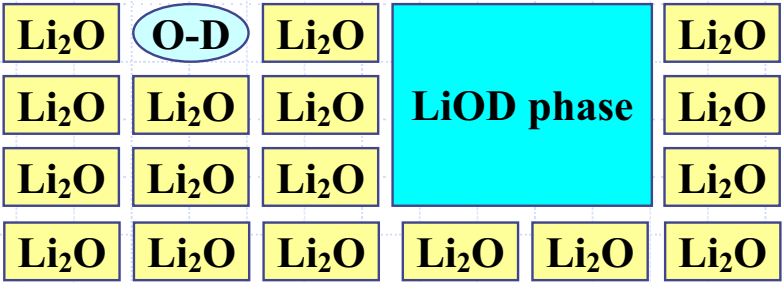
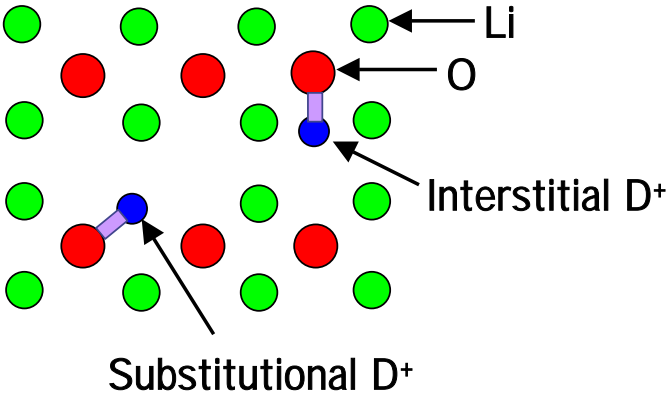
2x2x2



2x2x2 supercell

Li vac.(V center), Li colloidal metal,
O vac. (F^{2+} center), F^+ (O vac. with 1 e), F^0 (O vac. with 2 e), F_n

- ◆ LiOD phase, aggregating O-Ds, will be touched.



3. Results & discussion -1

: Multiple IR absorption peaks of O-D in Li_2O

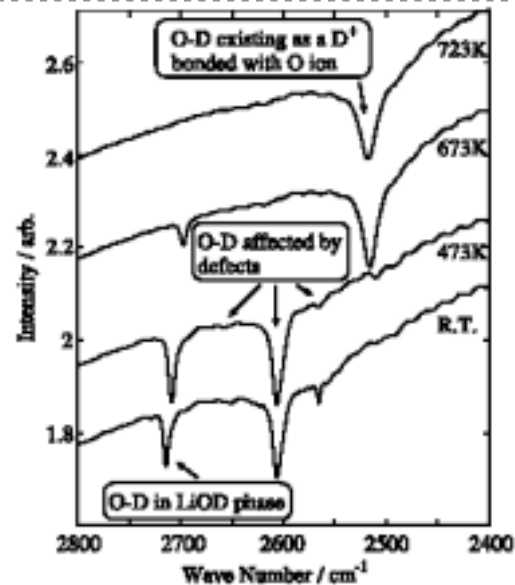


Fig.1 O-D peaks in Li_2O which absorbed D

* H. Tanigawa et al., Fusion Eng. Des. 51 (2000) 193.

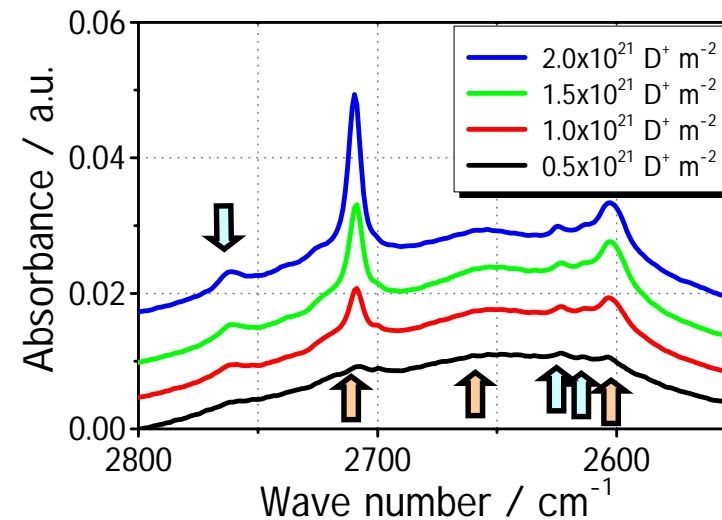


Fig. 2. During 300 keV D^+ irradiation

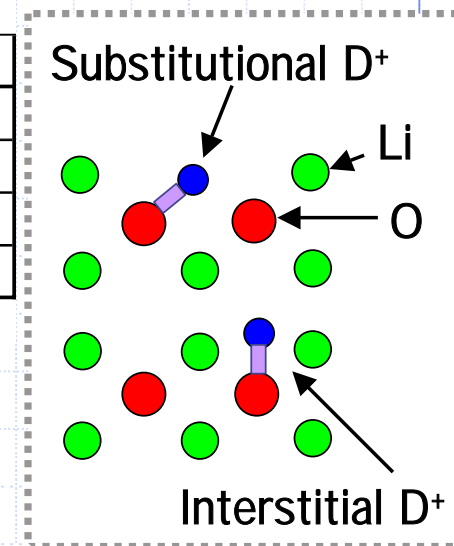
	2710 cm^{-1}	2625 cm^{-1}	2615 cm^{-1}	2605 cm^{-1}	2520 cm^{-1}
Thermal absorption	○	×	×	×	×
Thermal quenching	○	×	×	○	×
300 keV D^+ irradiation	○	○	○	○	×
Heating above 673 K	×	×	×		○

3. Results & discussion -2

: $<2710, 2625, 2615, 2605 \text{ \& } 2520 \text{ cm}^{-1}>$ O-Ds in Li_2O

In the case of Li_2O , an anti-fluorite crystal, Li vacancies are easily formed.

	2710 cm^{-1}	2625 cm^{-1}	2615 cm^{-1}	2605 cm^{-1}	2520 cm^{-1}
Thermal absorption	○	×	×	×	×
Thermal quenching	○	×	×	○	×
300 keV D^+ irradiation	○	○	○	○	×
Heating above 673 K	×	×	×		○



2710 cm^{-1} \Rightarrow LiOD phase (aggregation of D^+)

2605 cm^{-1} \Rightarrow Substitutional D^+ (D^+ with Li vac.)

◆ This O-D can be observed by the quenching method.

2520 cm^{-1} \Rightarrow Interstitial D^+

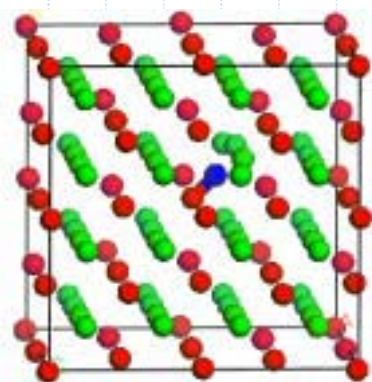
◆ The chemical state of diffusing D^+ . **The stability is lower than sub. D^+ .**

$2625 \text{ \& } 2615 \text{ cm}^{-1}$ \Rightarrow (Substitutional) D^+ interacting with O defect

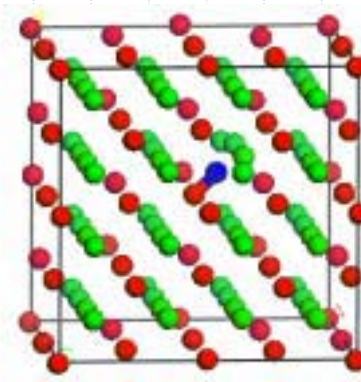
◆ The similar behavior to 2605 cm^{-1} is found during irr. or heating.

3. Results & discussion -3

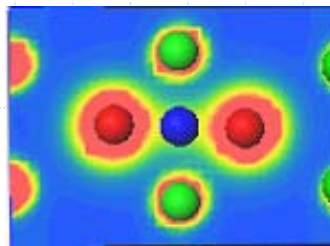
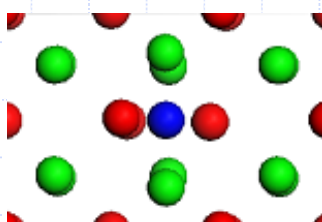
: $<2520\text{ cm}^{-1}>$ Interstitial H^+



Rotate : 0.1 eV



Migrate : 0.6 eV



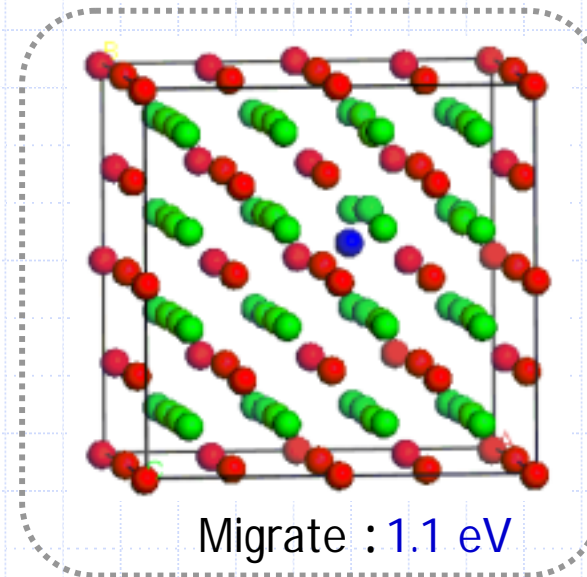
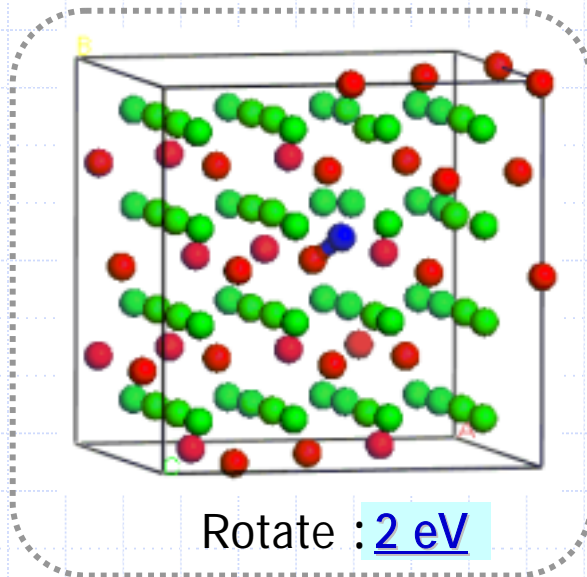
Transition state

	O-H	
	disatnce	population
stable state	0.98	0.84 e
transition state	1.28	0.44 e

Diffusion barrier of inter. H^+
is about 0.6 eV !!

3. Results & discussion -4

: $<2605\text{ cm}^{-1}>$ Substitutional H^+



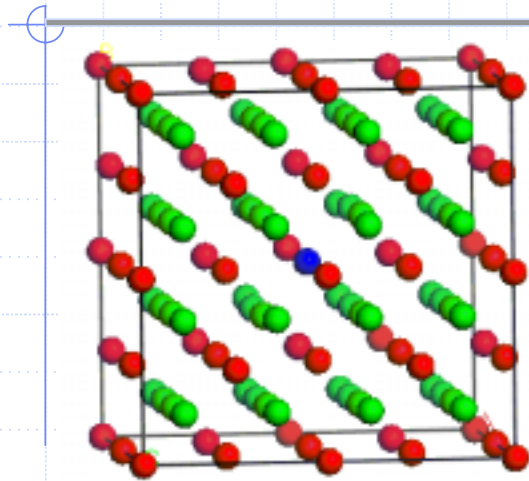
Diffusion barrier of sub. H^+ is about 2 eV.



Interstitial H^+ (0.6 eV) can diffuse more easily than substitutional H^+ (2 eV), as consistent with the experimental results.

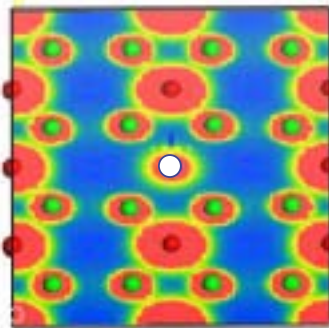
3. Results & discussion -5

: $<2625 \text{ \& 2615 cm}^{-1}>$ Stable state of H interacting with O defects

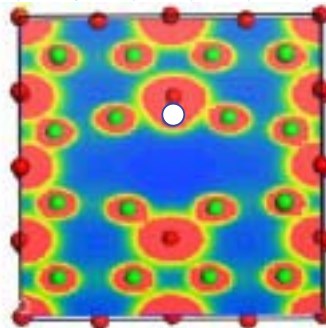


- ◆ 3 types of O point defect has been reported:
 F^{2+} (O vac.), F^+ (O vac. with 1 electron) & F^0 (with 2 electrons)
- ◆ 2 stable positions exist around an O defect:
O defect site & O-H site

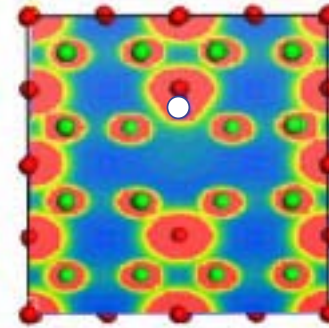
O defect site



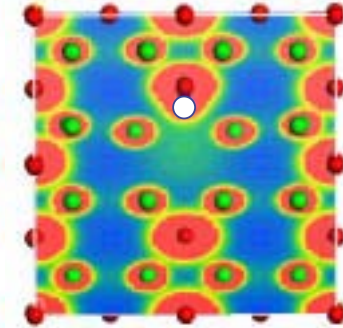
O-H site



F^{2+} (O vac.)



F^+ (with 1 e)



F^0 (with 2 e)

4. Summary

To reveal the concrete influence of various defects on the hydrogen isotopes behavior in Li_2O in an atomic scale, IR spectroscopy and DFT calculation were conducted complementarily.

		IR absorption	Diffusion barrier
Institutional		2520 cm^{-1}	0.6 eV
Substitutional (Li vac.)		2605 cm^{-1}	2 eV (overestimated)
F^{2+} (O vac.)		-	1.2 eV
	sub. O-D	2615 or 2625 cm^{-1}	(~ 2 eV)
F^+ (O vac. with 1 e)		-	1.6 eV
	sub. O-D	2615 or 2625 cm^{-1}	(~ 2 eV)
F^0 (O vac. with 2 e)		-	3.4 eV
LiOD phase (aggrigation)		2710 cm^{-1}	more than 2 eV



Li vac. (due to high concentration) & F^0 center (to strong trapping)



Experience with D retention and Carbon migration in DIII-D



D. Whyte, *U. Wisconsin-Madison*

P. Stangeby, A. Mclean, J. Davis, *U. Toronto/GA/LLNL*

S. Allen, M. Fenstermacher, *LLNL*

N. Brooks, W.P. West, G. L. Jackson, M.A. Mahdavi,

T. Taylor, P.L. Taylor, C.P.C. Wong, *General Atomics*

J. Watkins, *Sandia National Laboratories*

& the DIII-D team

7th International Workshop on Hydrogen Isotopes in Fusion Reactor Materials

**Special acknowledgement to the
Sandia research group providing ion beam analysis of DIII-D surfaces
W. Wampler, B. Doyle, D. Walsh, R. Bastasz**

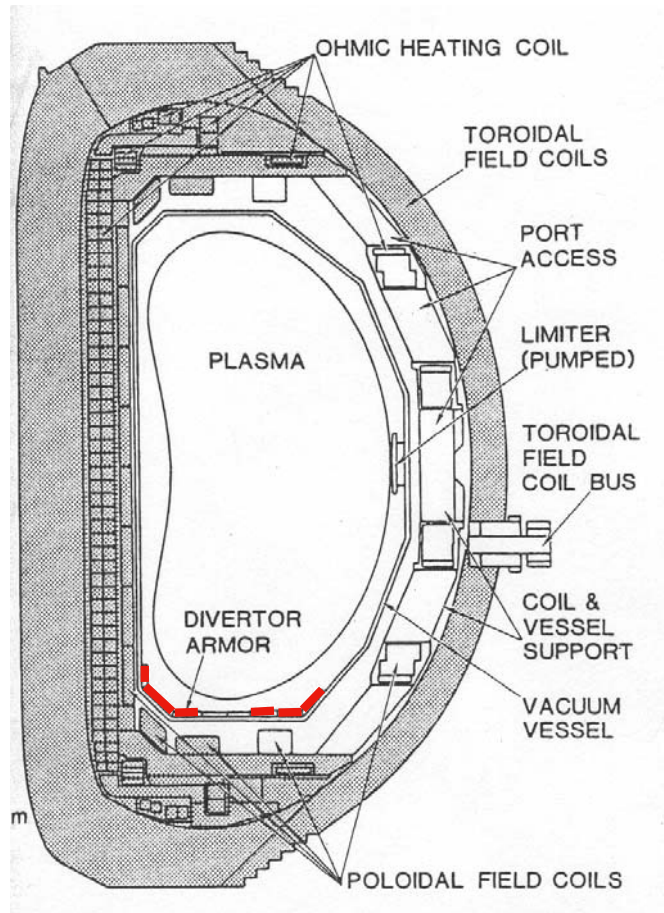


Background info on DIII-D

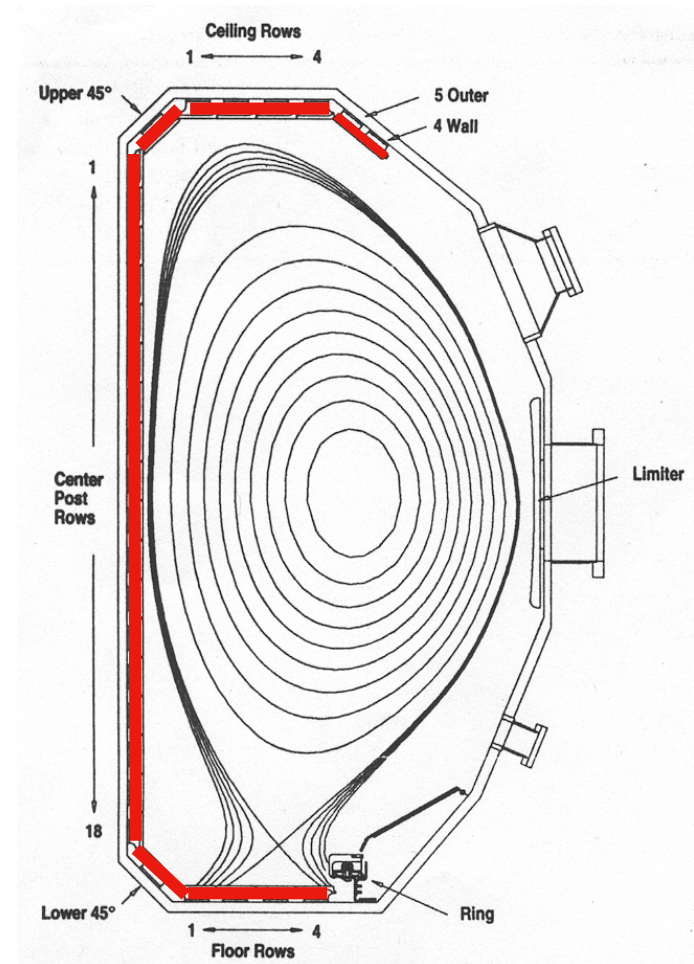


- Inconel vacuum vessel.
 - Water cooled (room temperature) for plasma operations.
 - Air heated (~350 C) for baking.
- Evenly aligned tiles for plasma operation with arbitrary helicity.
- Tiles
 - Mechanically attached to vessel wall for passive cooling.
 - Carbon: dense, fine-grain ATJ or POCO graphite.
- The vessel armor history, evolution to graphite walls:
 - start - 1987: 9% C at lower divertor strikepoints, Inconel elsewhere
 - 1988-1992: 40% C (divertors and inner wall), Inconel elsewhere
 - 1992 - present: ~ 100% C coverage.

DIID-D armor evolution



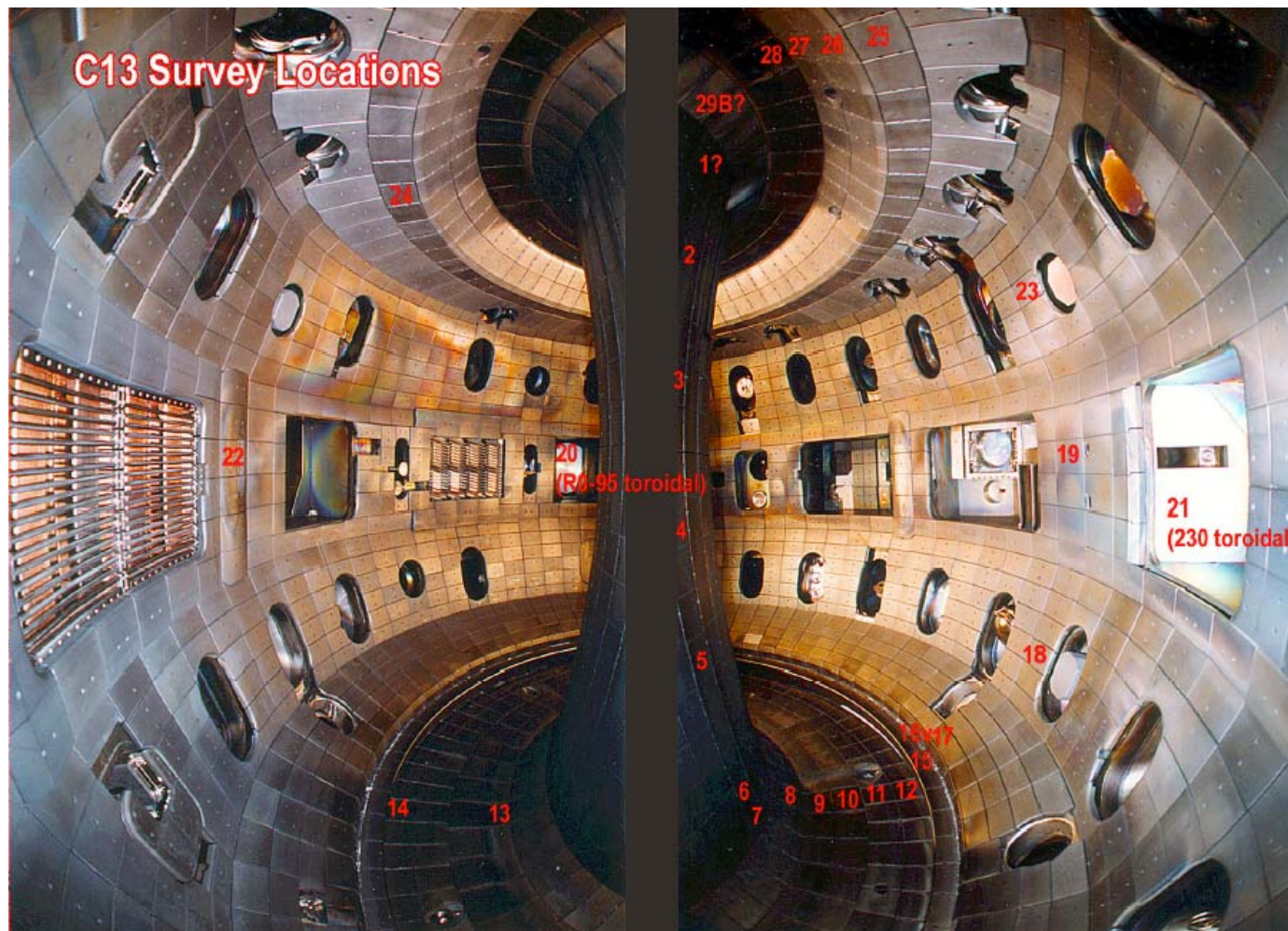
9% carbon



40% carbon + lower pumping



DIID-D armor evolution



~100% carbon + lower pumping + upper in/out pumping



Part I: Deuterium retention





Hydrogenic retention measured several different ways



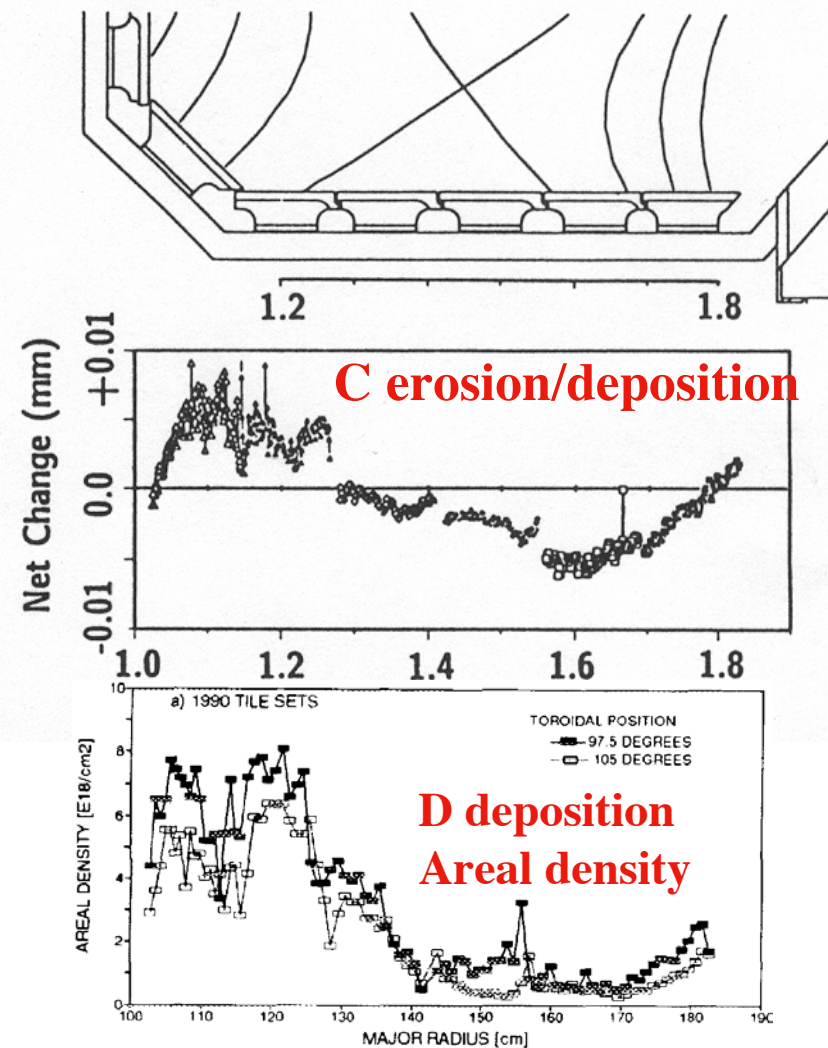
- Post run-period analysis of divertor tiles with IBA.
- Tritium accounting from removed tiles.
- DiMES exposures to single plasma conditions.
- Carbon-13 injection (*preliminary data in C erosion talk*).
- Gas balance.



Divertor Deuterium retention pattern is consistent with codeposition.



- Divertor tiles analyzed after one run-period.
- Carbon deposition pattern shows that D retained in deposit layers, I.e. codeposition.
- High degree of toroidal symmetry in D deposition results.
- Both long term exposures and DiMES have measured $D/C \sim 0.25$ in codeposits.

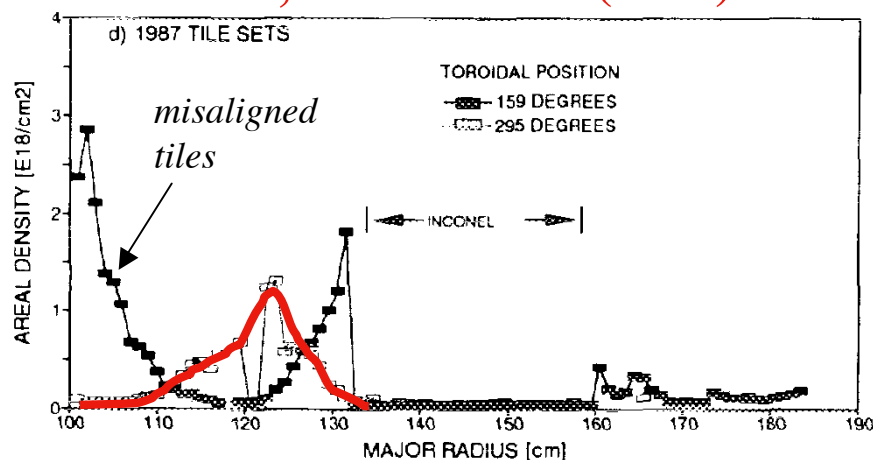




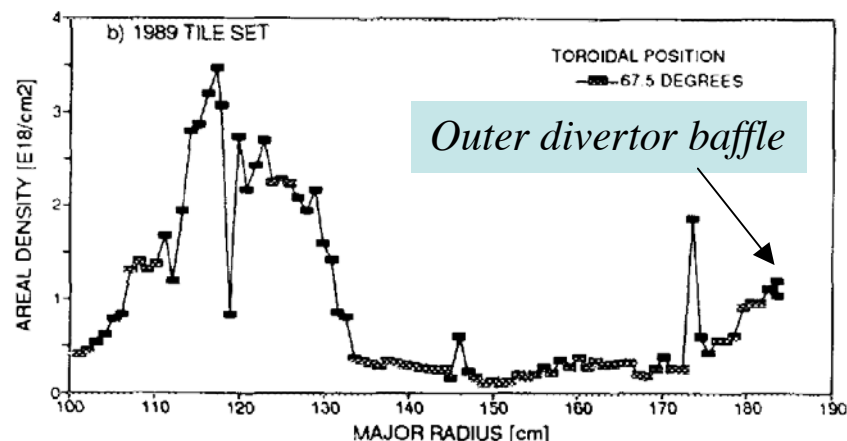
Run-period D deposition show consistent pattern now familiar: inner divertor deposition & outer divertor erosion



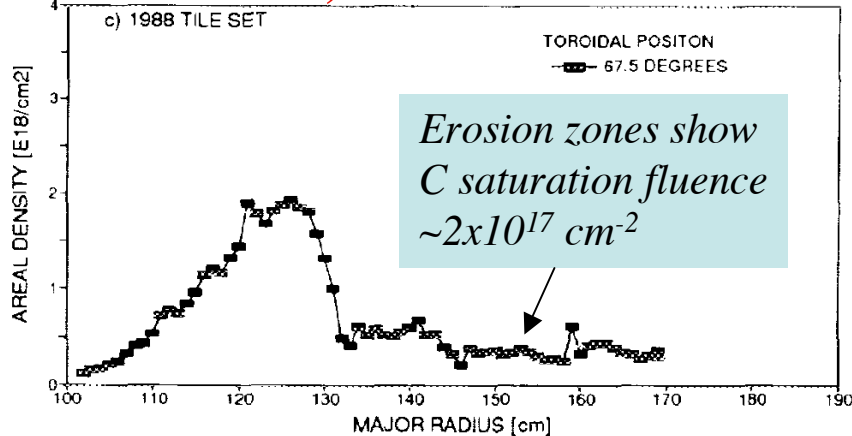
9% C, ~ 5000 shots (LSN)



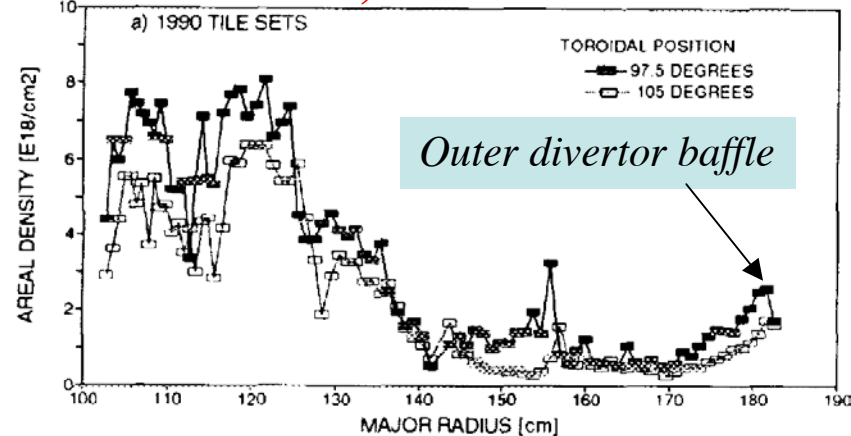
40% C, ~ 3500 shots



40% C, ~ 1000 shots



40% C, ~ 1000 shots



40% of divertor D retention is down tile gaps, but is < 1 cm from surface

ARROWS INDICATE SCAN DIRECTION

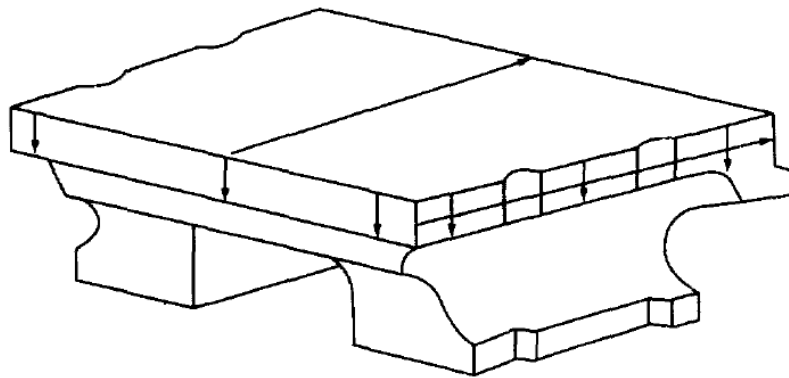
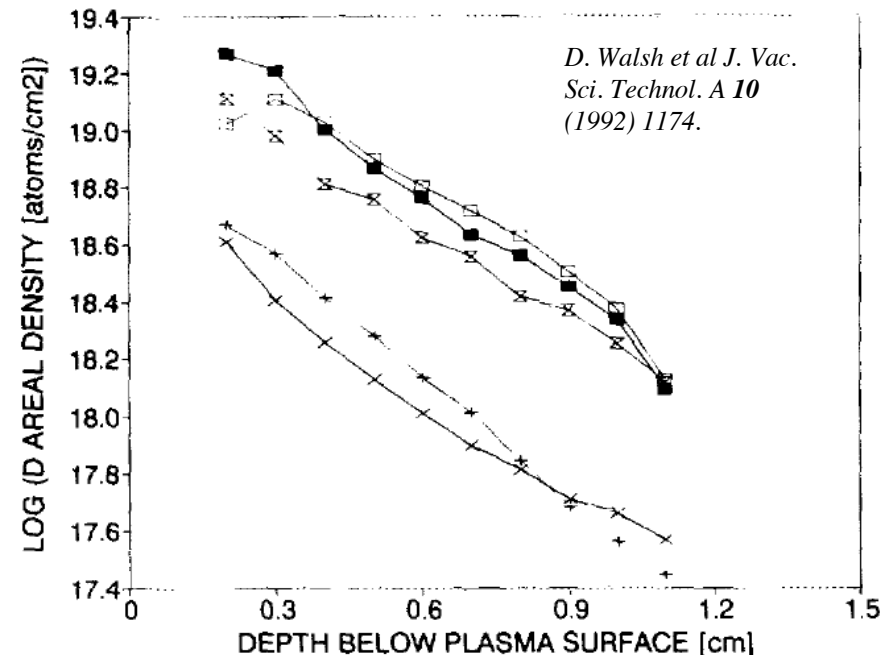


FIG. 1. Typical analysis scans performed on the divertor tiles. The tile pictured is from the third divertor row. The arrows indicate the scans.

D deposition pattern in tile gaps



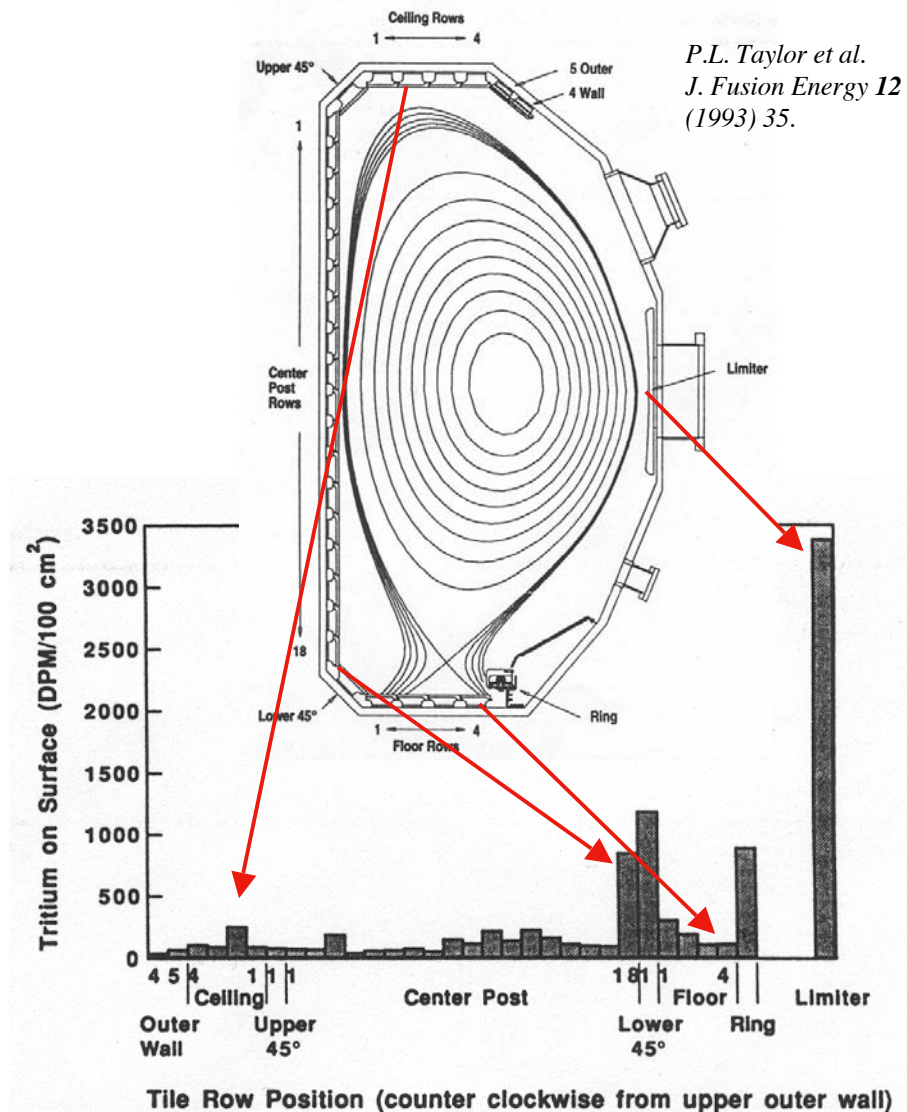
- Deposition has e-folding distance ~ 0.5 cm $\sim 2 \times$ gap width.
- Deposition near top of gap typically tracked plasma-facing surface D concentration
- DiMES experiments suggested some of this due to leading edge ablation.



Tritium trapping in graphite tiles is consistent with codeposition

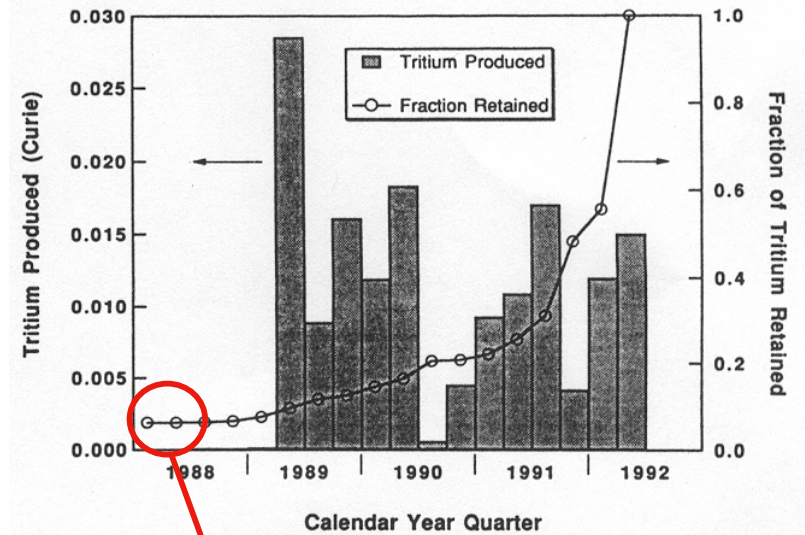
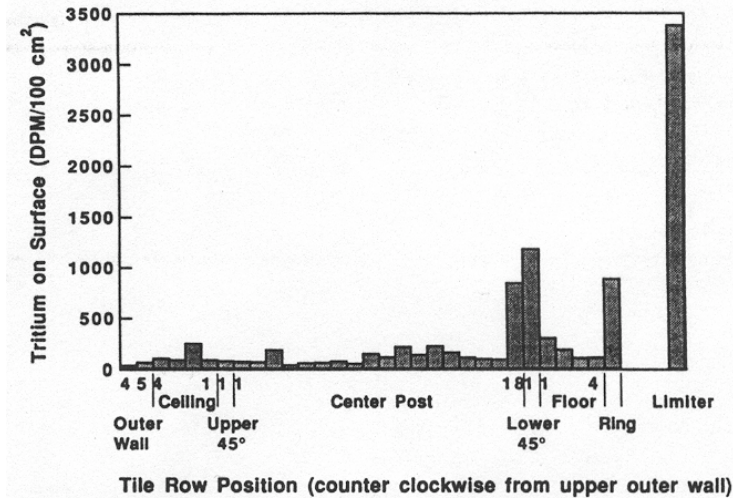


- Tritium produced by beam-plasma D-D fusion
- Tritium production well-accounted
 - Accompanying neutrons always measured for radiation safety.
- Small fraction of 1 MeV tritons on large banana orbits strike outside limiter and implant few microns, the remainder thermalize
- Surface tritium follows D retention pattern in lower divertor.
- Total tritium content measured by long 1000 C bakes of sample tiles.
- Grit blasting of ~20 microns off tile surface removed essentially all the tritium, consistent with codeposition.





Overall tritium codeposition rate ~ 5%. ~30% T recovery with vacuum 350 C bake

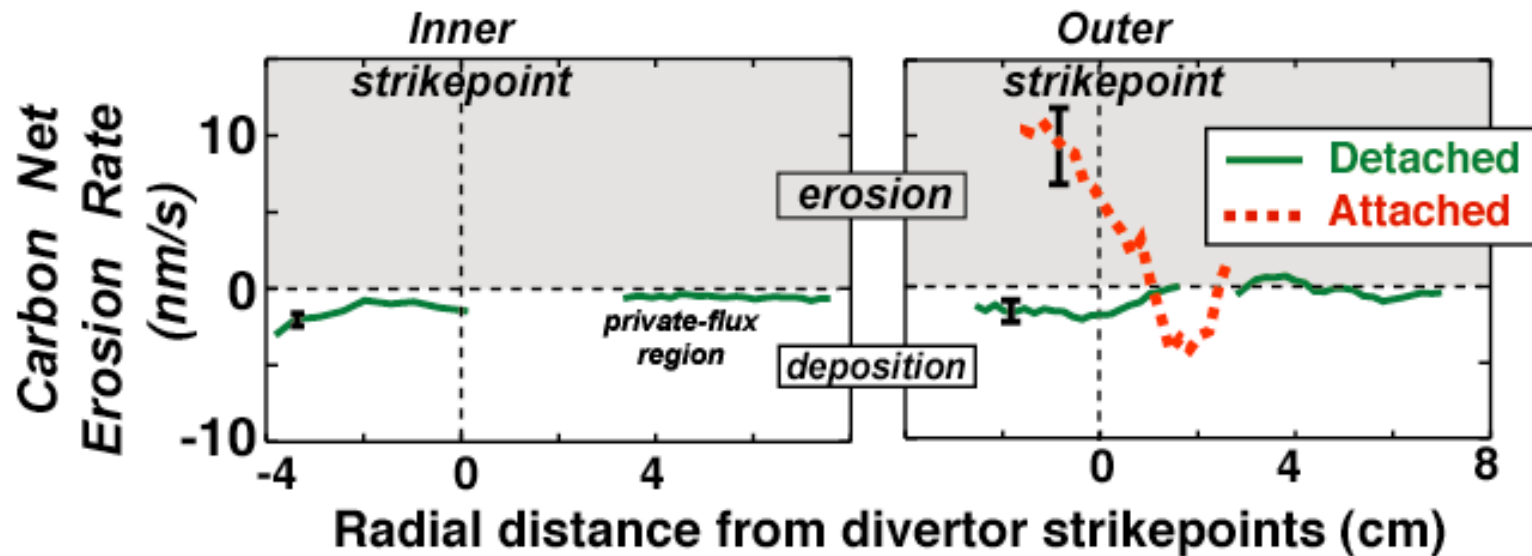


- Total tritium content in tiles did not exactly follow surface wipe concentration as shown here.
- **Some main-wall center post tiles had codeposited T concentrations as high as tiles from the inner divertor!!**

- Integrated Tritium content from sample tiles indicated ~5% retention rate in 40% graphite coverage DIII-D.
- **Relative Tritium removal from codeposited layers with 7 hr bake:**
 - 30% @ 350 C (soft films in gaps?)
 - 70% @ 1000 C (hard films on surface?)



DiMES mapped carbon erosion/deposition and D retention across lower divertor for detached H-mode plasma



- **Detached ELMy H-mode plasma:**
carbon deposition $\sim 1\text{-}2$ nm/s near strikepoints and ~ 0.2 nm/s in private flux.
- Divertor D co-deposition concurrent with C deposition; $\sim 10^{20}$ D/s.
- Total divertor retention rate / D fuelling rate: **3%.**

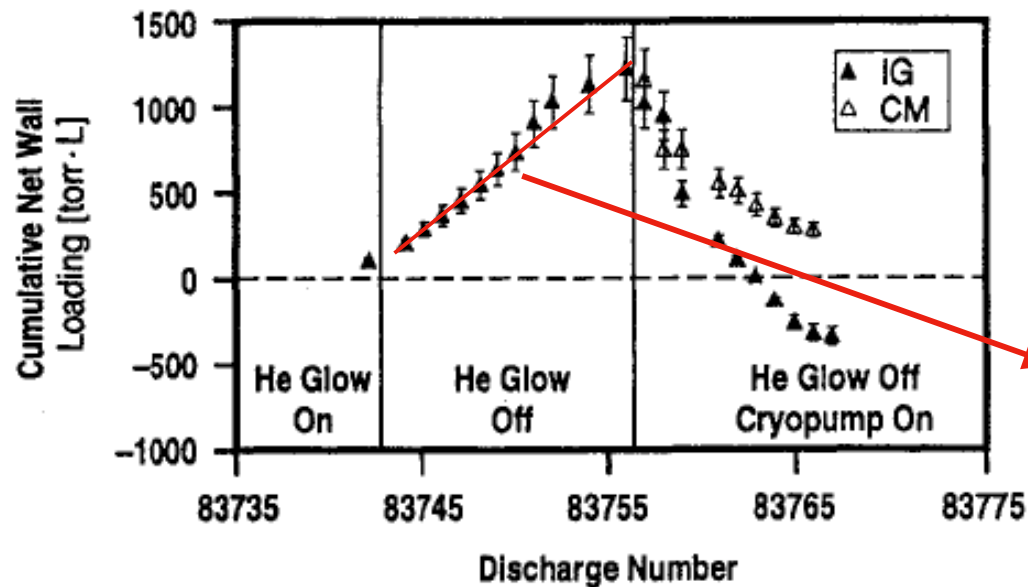




Gas balance gives global D retention rate ~10 times larger than measured divertor D retention



100% C coverage



Maingi, et al Nucl. Fusion **36** (1996) 245.

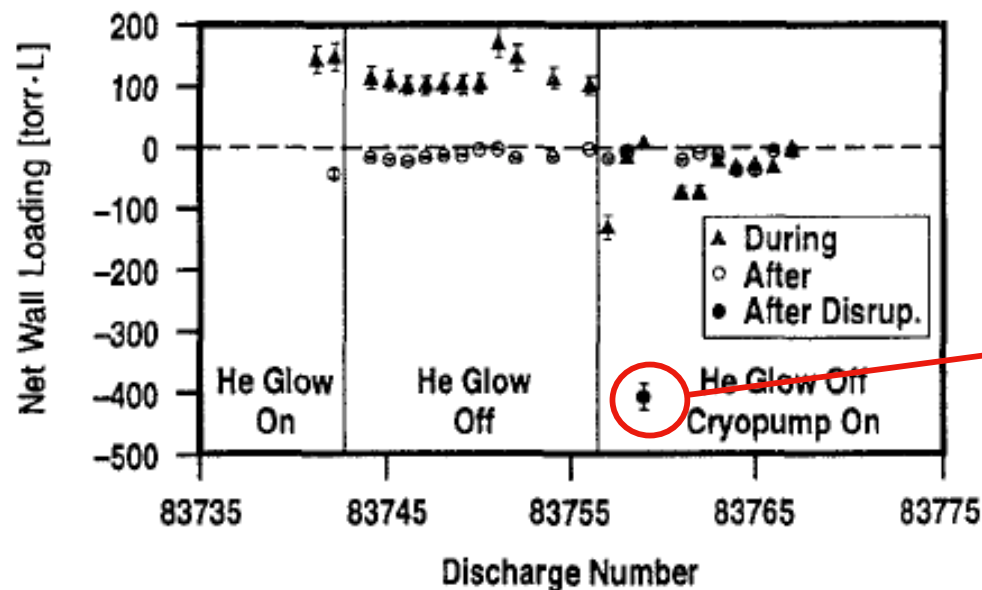
- **Plasma conditions:**
ELMy H-mode, natural H-mode density (attached) with ~7 MW neutral beam heating.
- Accurate gas balance obtained by turning off all pumping and Helium glow.
- **Unsaturable wall uptake strongly suggests codeposition as cause for D "pumping"....**
- But the total retention rate ~ 20 Torr-L/s $\sim 1.4 \times 10^{21}$ D/s is over a factor of 10 higher than measured in the divertor $\sim 10^{20}$ D/s ?!



Gas balance measurements showed that disruptions recover D from wall



100% C coverage



Maingi, et al Nucl. Fusion **36** (1996) 245.

- Major disruption ended discharge.
- Gas balance showed Deuterium recovery roughly equivalent to uptake during 4 discharges.
- Similar results recently seen on Alcator C-Mod.
- **Indicates that thermal desorption can be efficient for hydrogenic recovery even with low energy densities of present tokamaks.**



Summary: D retention & recovery



- **DIII-D history shows dramatically increasing D retention rate with evolution to graphite wall.**
- Early DIII-D configuration is “ITER-like”, 9% C coverage at lower strikepoint: **Divertor D retention rate < 0.1%.**
- 100% C divertor retention rate $\sim 5\% \ll 50\%$ from gas balance and TFTR/JET tritium experience.
 - Cause is unclear: *D deposition at main wall? Or gas balance physics not understood? Differences in details of DIII-D wall design?*
- Extremely consistent divertor patterns of C deposition and D codeposition.
- Tile gaps contributed $\sim 1/2$ of divertor D retention.
- Recovery of deuterium:
 - Disruptions seem efficient.
 - Low temperature vacuum bake 350 C removed $\sim 30\%$

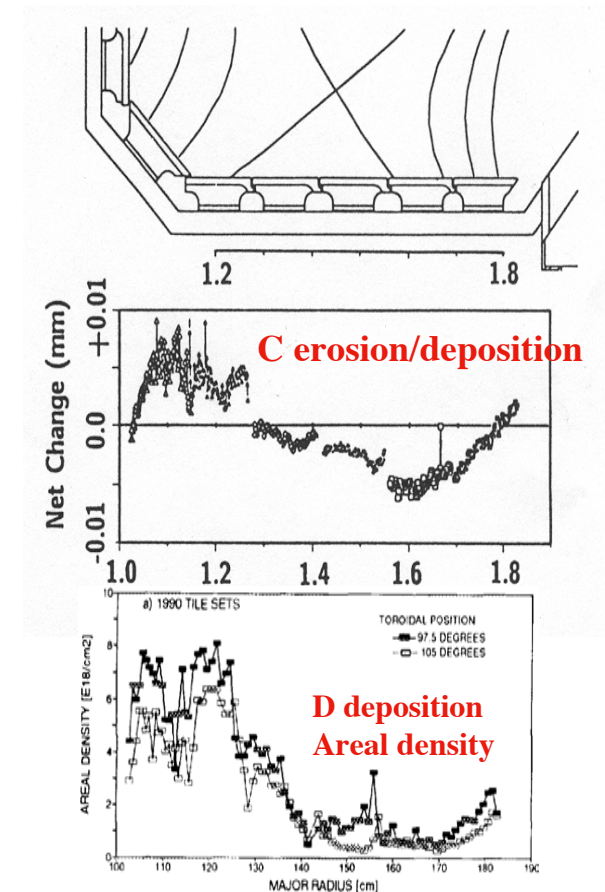
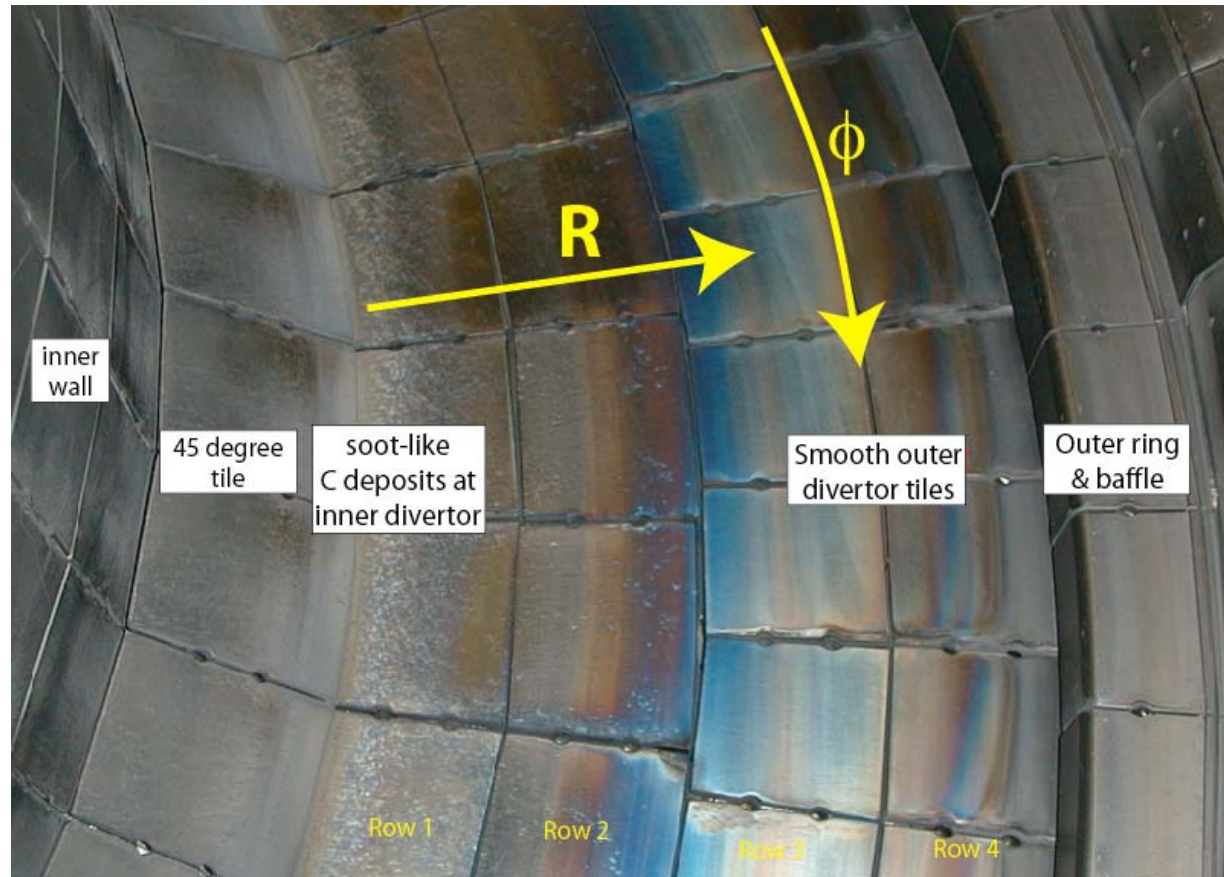


Part II: Carbon migration





Lower divertor carbon deposition pattern is readily observed

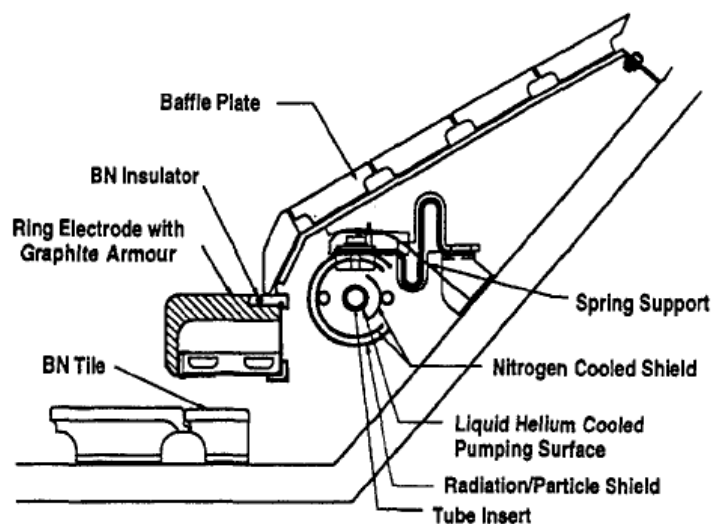




Liquid-N₂ cooled cryopump shields under baffles show no signs of carbon deposition after over 12 years of service

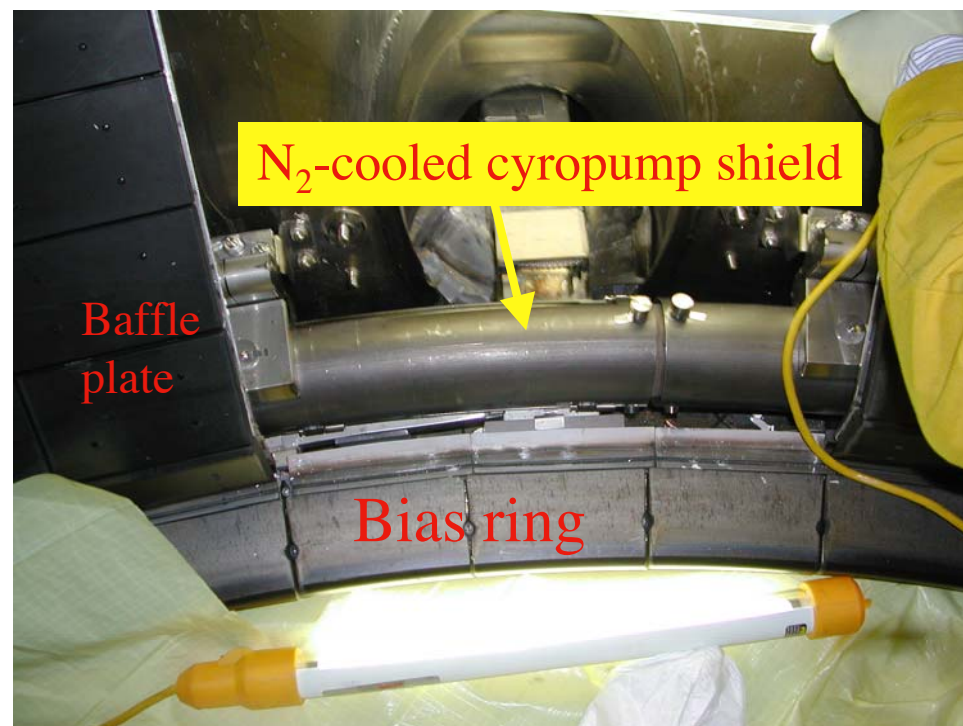


CRYOPUMP UNDER DIVERTOR BAFFLE



- **> 10⁵ s plasma in lower single null.**
- Strikepoint often placed under baffle for optimal pumping.
- **Shield and surrounding areas have bare metallic appearance.**

2002: Looking down with baffle plate removed

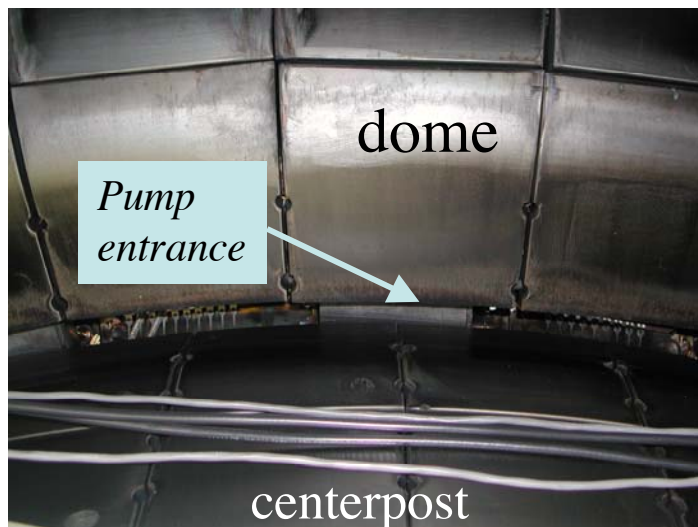




Visual inspection of DIII-D found no evidence for significant deposition under the inner divertor baffle



Looking upward at entrance to inner baffle



With baffle cover removed



- Metallic appearance and color deposition pattern indicate < 100 nm thick carbon films.
- Thin films only with line-of-sight to strikepoints...**no long-range carbon transport to hidden cold regions under baffles.**



The single occasion of thick carbon layers under divertor baffles was caused by ablation of leading-edge “bolt-holes”



Looking up at top divertor

Bolt-hole

Large erosion
“divots” from
ablation

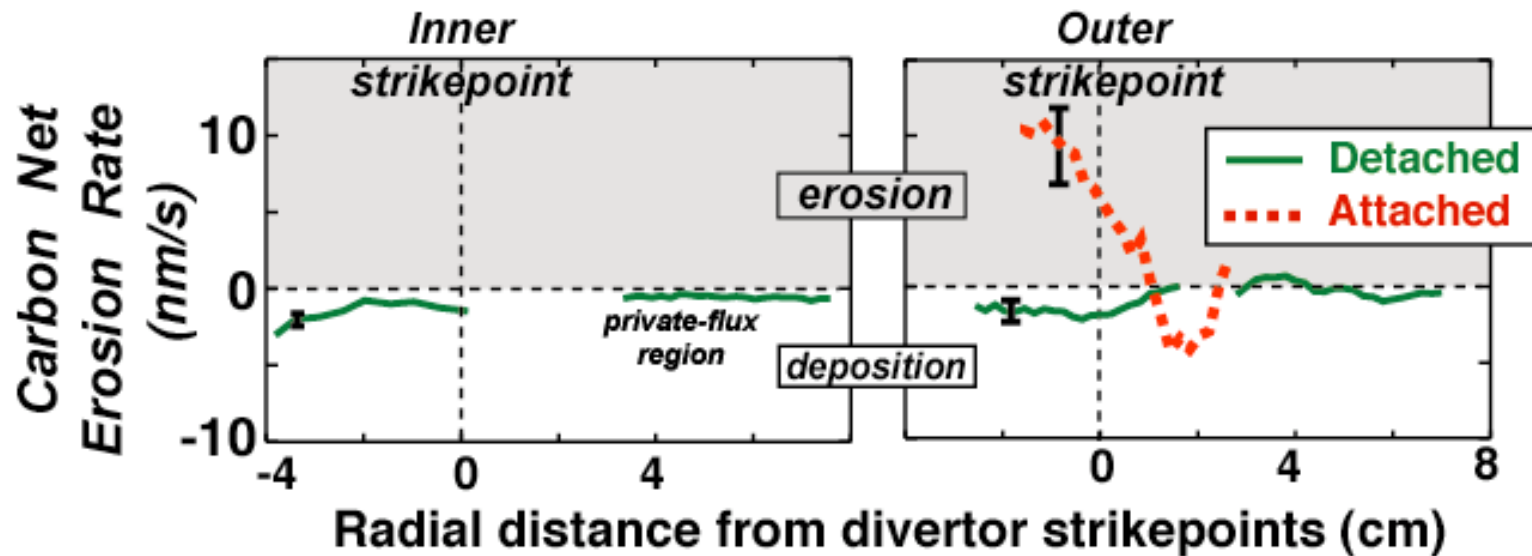
*Outer
baffle /w
cryopump*

R

- By coincidence, the optimal strikepoint location for pumping was at radial location of bolt-holes.
- Prolonged outer strikepoint exposure to high power plasmas ablated $\sim\text{cm}^3$ of graphite.
- A thick sooty carbon layer was found underneath the outer baffle with line-of-sight to bolt-holes.



DiMES mapped carbon erosion/deposition and D retention across lower divertor for detached H-mode plasma



- Lower outer divertor net erosion suppressed in detached plasma.
 - Consistent with absence of chemical erosion signatures in divertor.
- Total net deposition rate normalized to incident flux
 - **Inner divertor: ~ 4 %** **Total divertor: ~1 %** ~ $f_{C,core} = 1.5 \%$
- Source of carbon deposition seen in divertor must be main-wall for detached case.
 - However, this does NOT mean that the *entire* main-wall undergoes net erosion

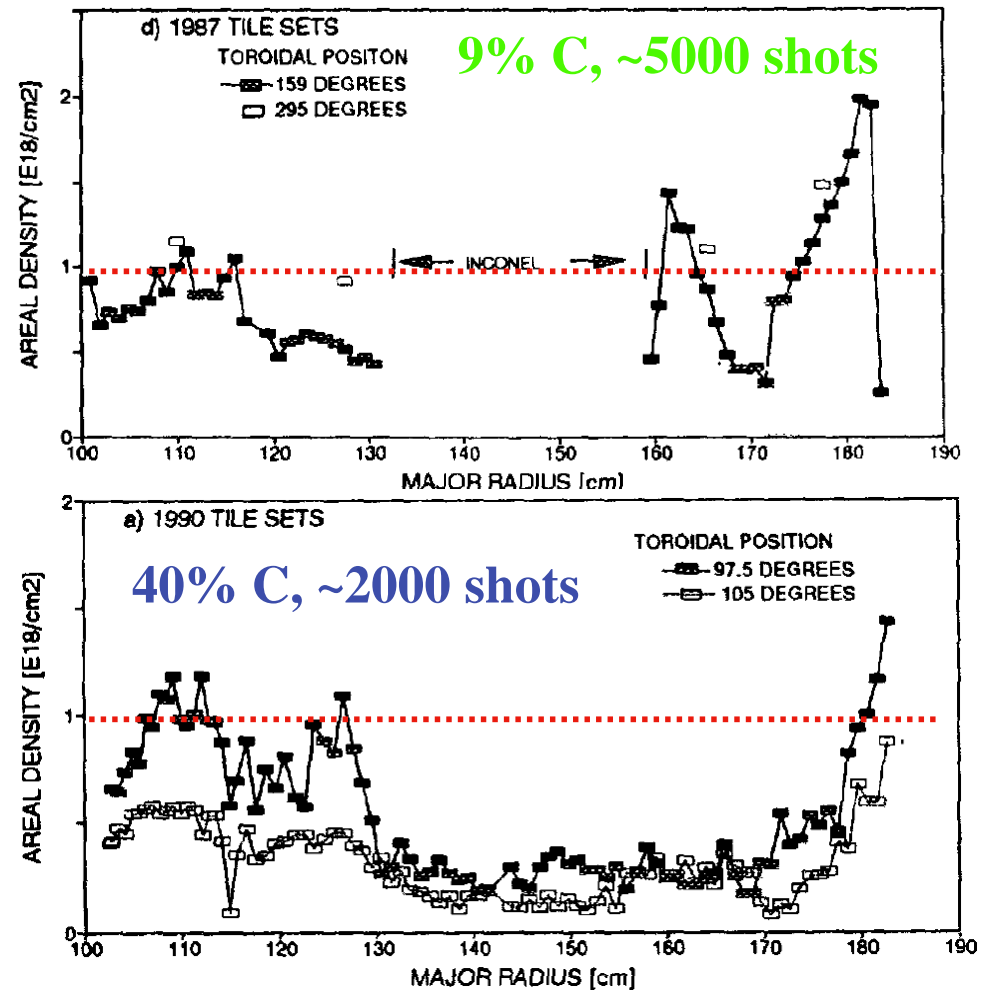


Mixed C / metal deposit layers formed on divertor graphite plates



- Metal contamination layers measured on graphite tiles after run-period.
- Metal predominately Nickel.
- Deposition patterns
 - 9% C → ~ uniform
 - 40% C → in / out asymmetry
- Estimating C deposit layer from D concentration gives ~ metal concentration at inner divertor deposits
 - 9% C → Carbon : metal ~ 2 : 1
 - 40% C → Carbon : metal ~ 20: 1
- Mixed material layer extremely stable and hard
 - Required sand-blasting to recover carbon surface.

..... ~100 nm metal equivalent layer







Why did DIII-D switch to ever increasing graphite coverage?



Observations with 40% graphite coverage

..during the quiescent phase of some higher current H-mode discharges (>1.5 MA), radiated power and high Z metal impurities accumulated in the discharge. Under some conditions, the radiated power could equal the auxiliary heating power, and a radiation collapse of the discharge could occur. The source of these metal impurities was the Inconel outer wall which comprises 60% of the plasma facing surface. Significant metal impurities were observed even though the Inconel surfaces were not directly exposed to known areas of high heat flux.

*G. L. Jackson, et al., J. Vac. Sci. Technol. A, **10** (1992) 1244.*

These results motivated low-Z film deposition (e.g. boronization) and eventually $\sim 100\%$ graphite coverage of wall.

In present day DIII-D, very quiescent H-modes (e.g. QH- mode) show central plasma nickel accumulation, with Inconel comprising $<1\%$ plasma facing surfaces!



Summary of C migration & erosion



- In DIII-D, C deposition, and therefore D co-deposition, is all at plasma-viewing surfaces. This seems a very encouraging result with regard to hydrogenic recovery.
- Greater metal coverage leads to increasingly metal-rich divertor deposit layers, and suppresses D retention.....
At the price of high-Z metal accumulation and core plasma line radiation.

Idaho National Laboratory

The Safety and Tritium Applied Research (STAR) Facility

J. P. Sharpe, R. A. Anderl, G. R. Longhurst, R. J. Pawelko, S. T. Schuetz, C. M. Stoots, R.A. Causey, D. A. Petti

7th International Workshop on Hydrogen Isotopes in Fusion Reactor Materials

Sebasco Harbor Resort, Sebasco Estates, Maine

20-21 May, 2004

Outline

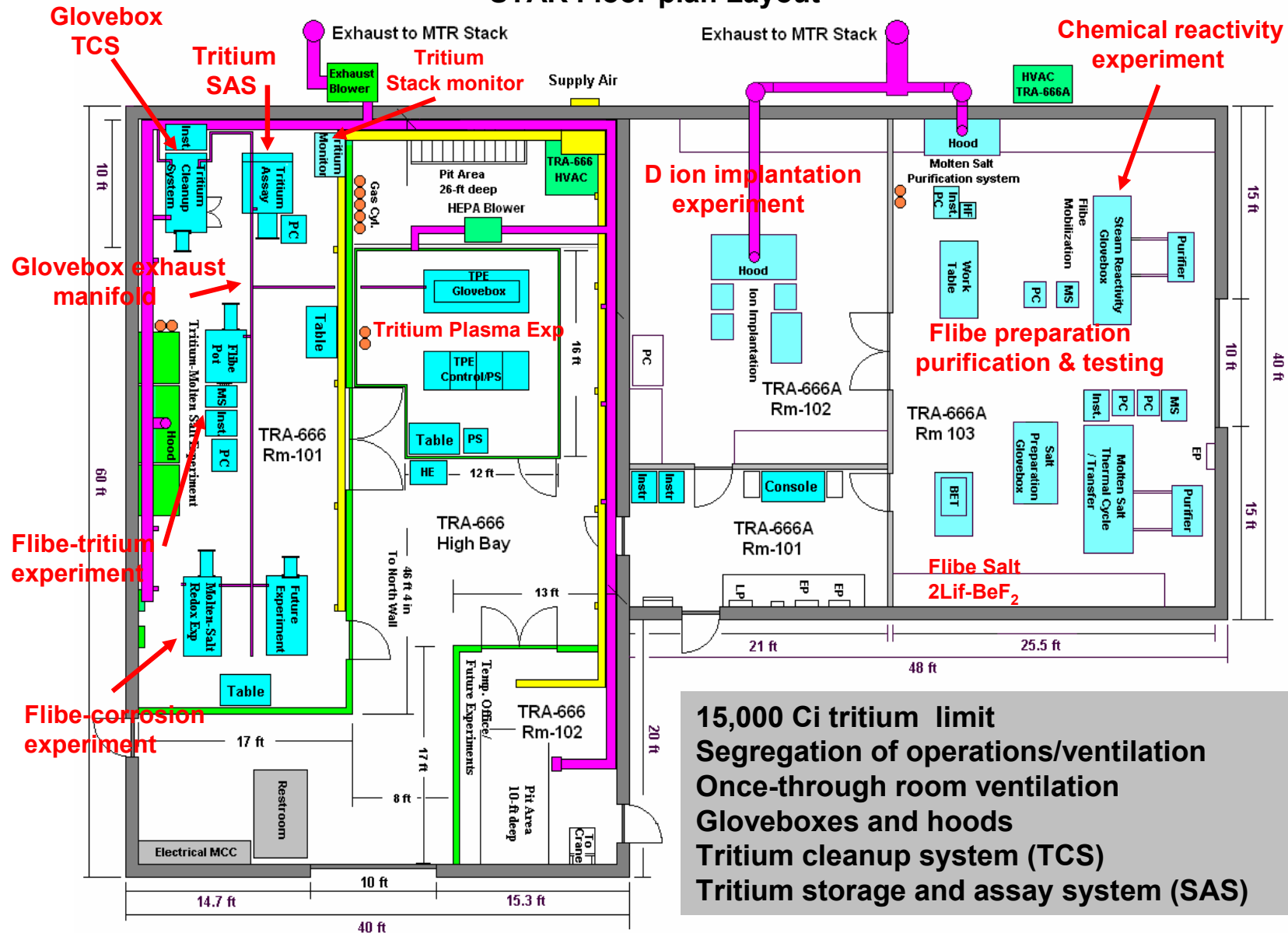
- *Facility Overview*
- *Tritium Storage and Assay System (INL designed and built)*
 - *handles reception, distribution, and accountability of tritium inventory*
 - *results from initial testing*
- *Tritium Cleanup System (M. Braun USA)*
 - *Process gases from glovebox atmospheres and experimental process systems*
 - *results of acceptance testing*
- *Experiment Systems*
 - *Tritium Plasma Experiment*
 - *Molten Salt Experiments*

STAR Mission and Research

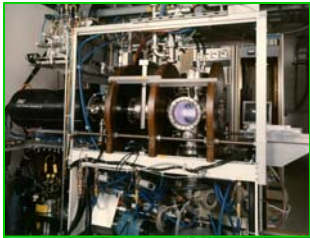
- *Provide laboratory infrastructure to study tritium science and technology issues associated with the development of safe and environmentally friendly fusion energy*
- *Designated a National User Facility*
- *Research thrust areas*
 - *Plasma-material interactions of PFC materials with energetic tritium and deuterium ions*
 - *Fusion safety: chemical reactivity, activation product mobilization and dust/debris characterization for PFC materials; tritium behavior in fusion systems*
 - *Molten salts and fusion liquids for tritium breeder and coolant applications*

Tritium and non-tritium safety research

STAR Floor-plan Layout



Key systems in STAR



Tritium Plasma Experiment and Enclosure



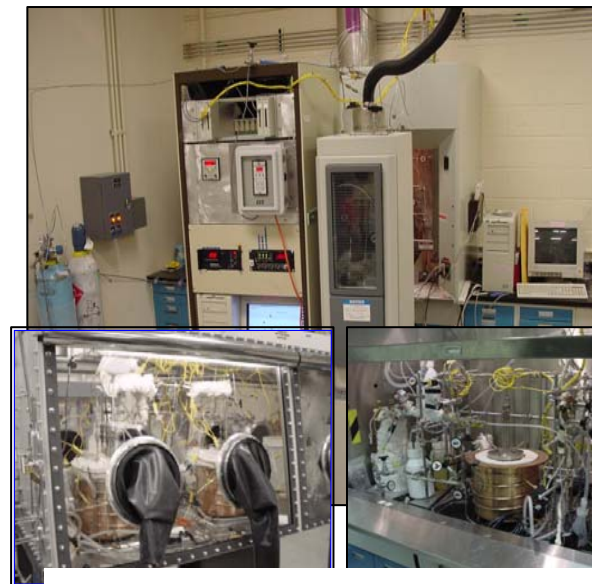
Molten Salt Tritium Behavior Experiment



Tritium Storage and Assay System



Tritium Cleanup System

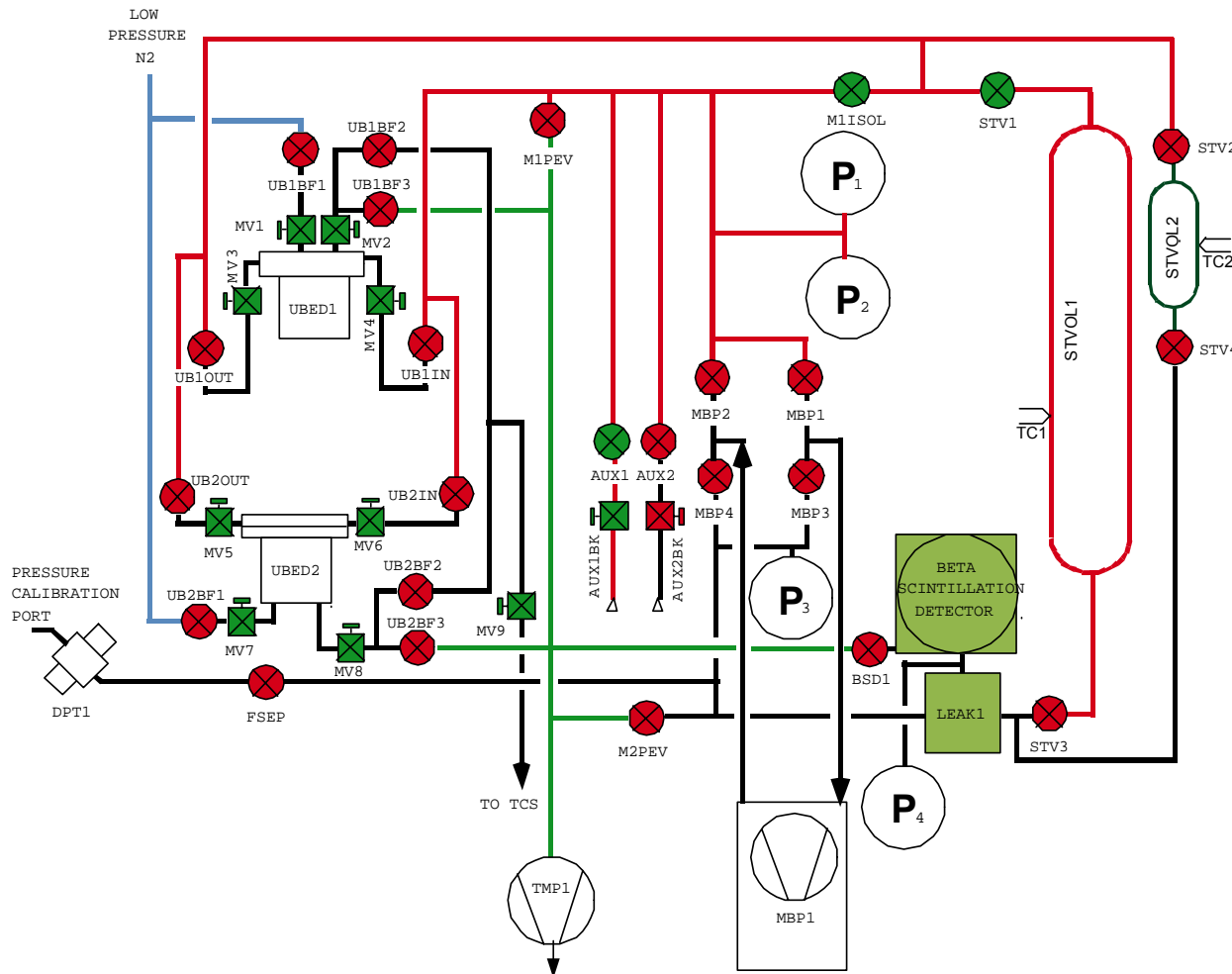


Molten Salt Preparation, Purification, and REDOX Experiments



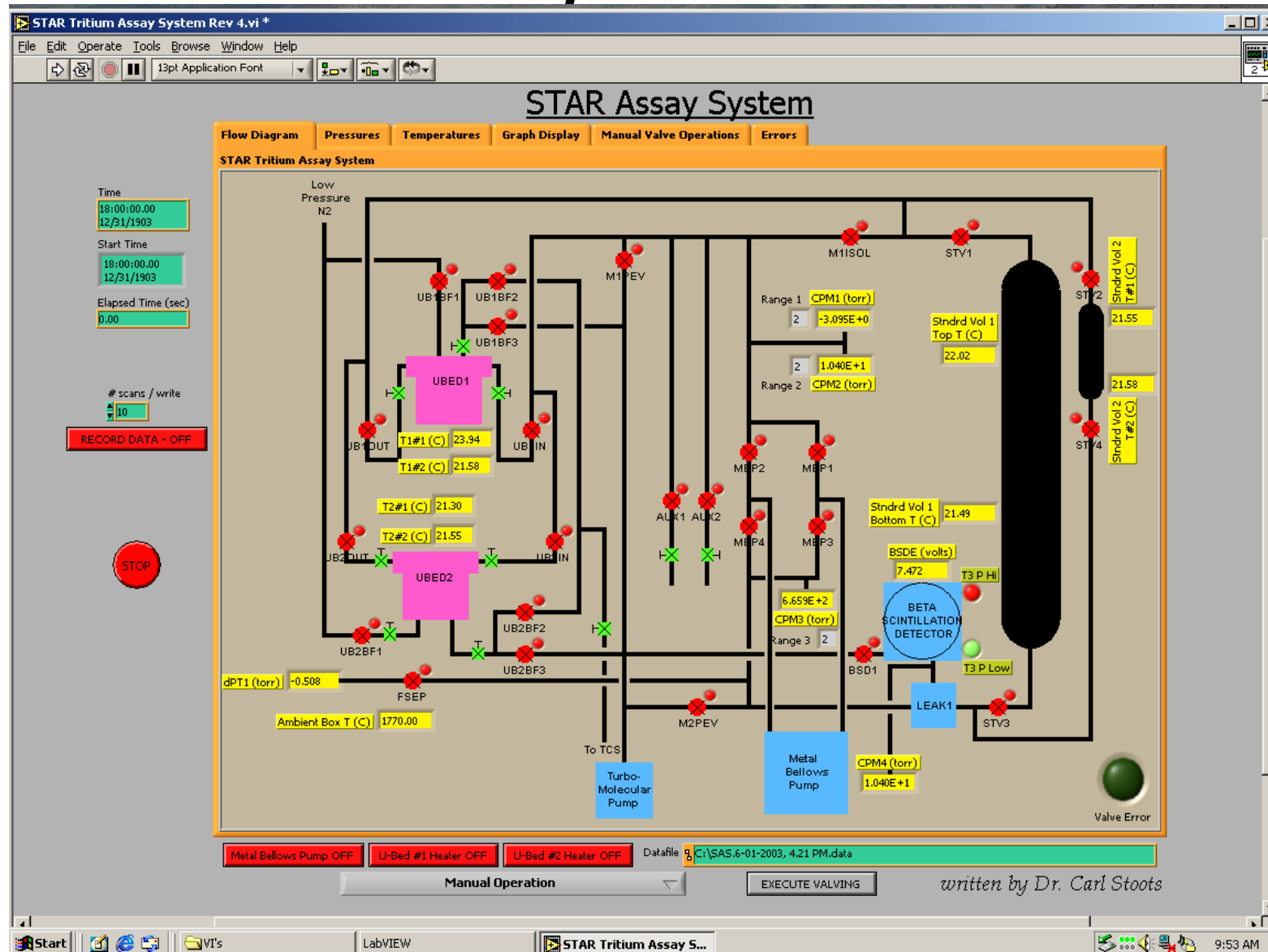
Steam and air chemical reactivity test apparatus

STAR Tritium Storage and Assay System Schematic



- Mod. of LANL LI/LO
- Two 47-g DU beds (Tyne)
- Three MKS 615A and one 590 Cap. Manometers
- Beta scintillation det. (femto-TECH)
- Quadrupole mass spec
- Std. Vol.: 4 L and 0.2 L
- MetBel 610 pump
- Pfeiffer turbo-drag pump
- Edwards scroll pump
- Type K thermocouples
- Electro-pneumatic and manual valves
- FieldPoint interface
- LabView computer control and data acquisition

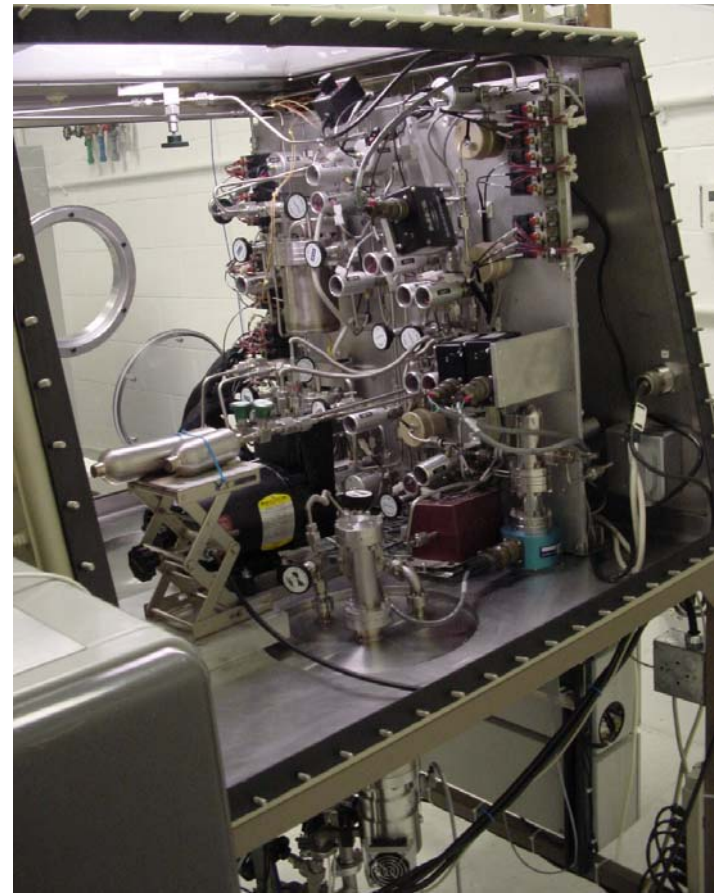
Control for Operation of SAS



Star Tritium Storage and Assay System

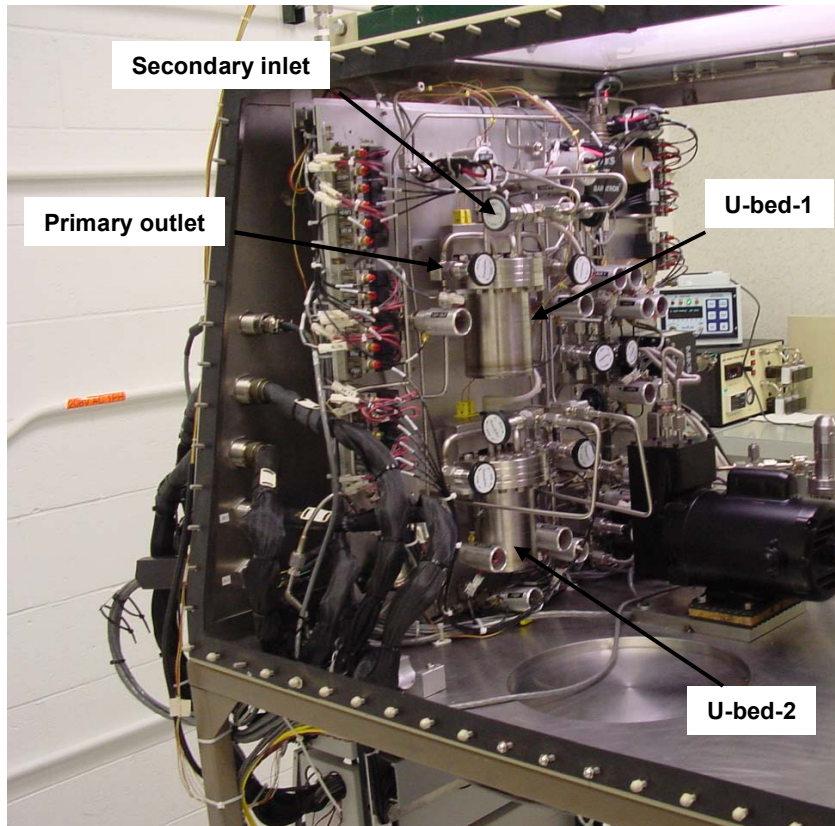


SAS glovebox Setup

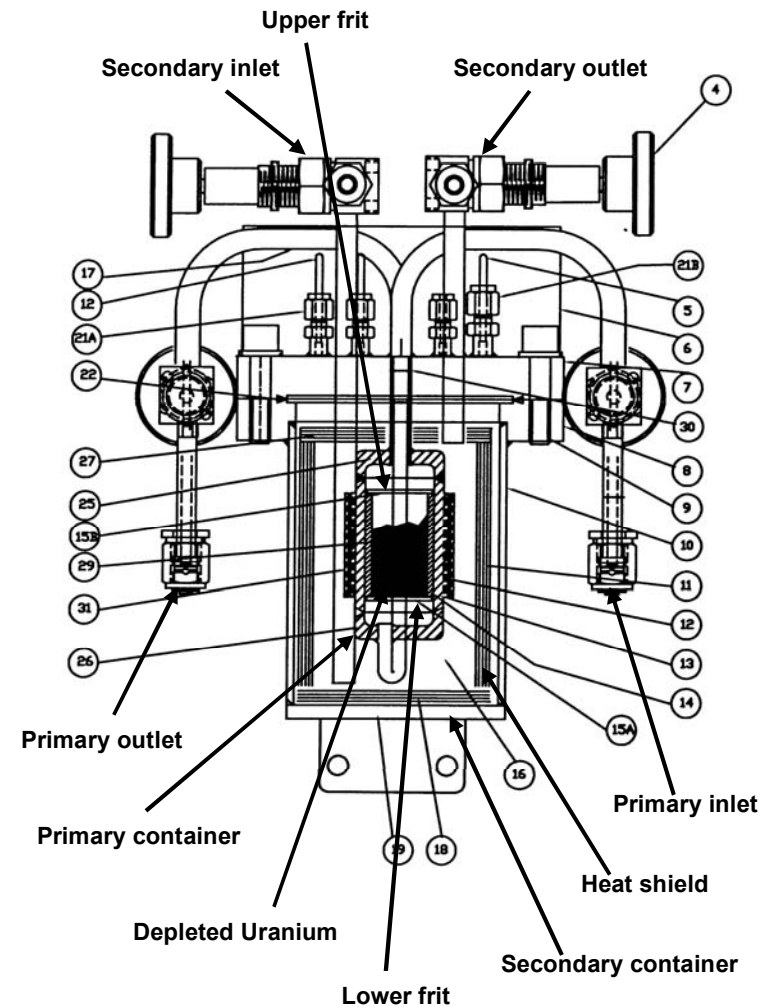


SAS manifold and vacuum pumps

Star Tritium Storage and Assay System



SAS manifold with U-beds



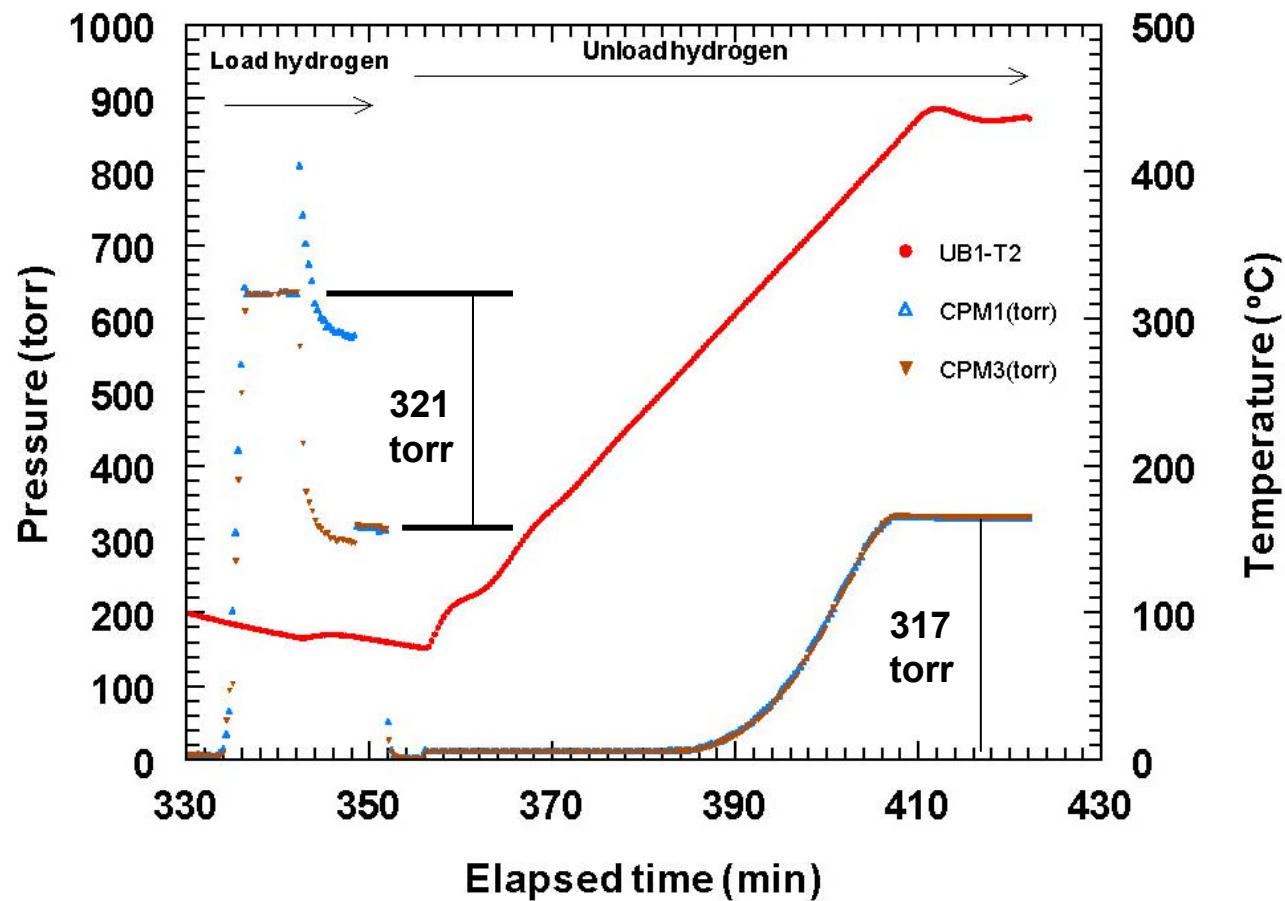
Cross section of Tyne U-bed

STAR Tritium Storage and Assay System initial testing and operation

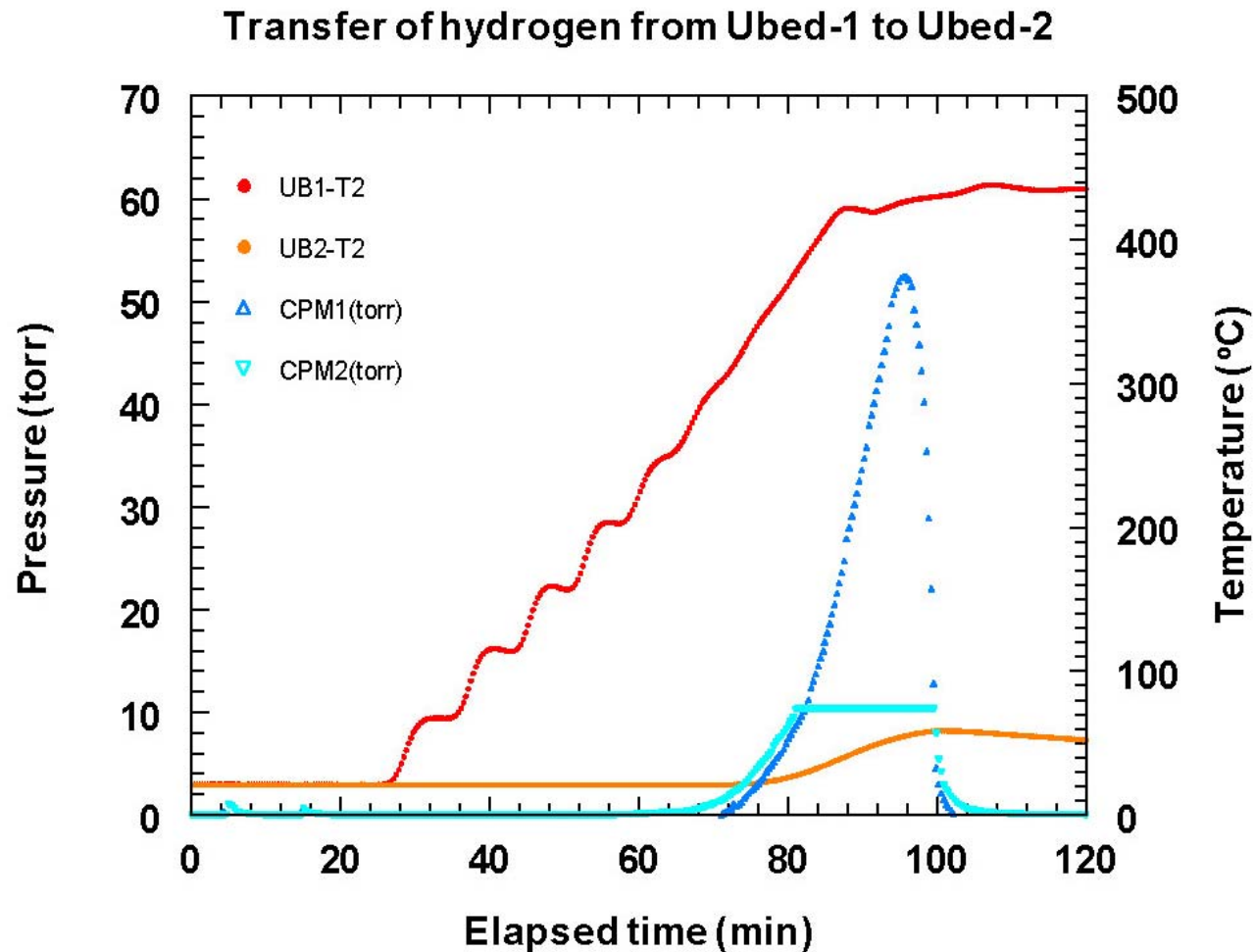
- ***Test activities completed***
 - ***Helium leak-checking of entire gas manifold and components***
 - ***Vacuum-baking of manifold***
 - ***Development and testing of LabView software for SAS operation***
 - ***Calibration of pressure sensors***
 - ***PVT measurements to derive system internal volumes***
 - ***Conditioning of U-beds by a sequential hydrogen exposure and thermal cycling to 450°C***
 - ***Functional testing of system (some results presented)***
 - ***U-bed loading and unloading***
 - ***U-bed to U-bed transfer***
- ***Planned activities***
 - ***Test of beta scintillation detector***
 - ***Functional and quantitative testing of system***
 - ***Operational procedures and safety documentation***
 - ***Integration with laboratory infrastructure***

Loading and Unloading of Ubed-1

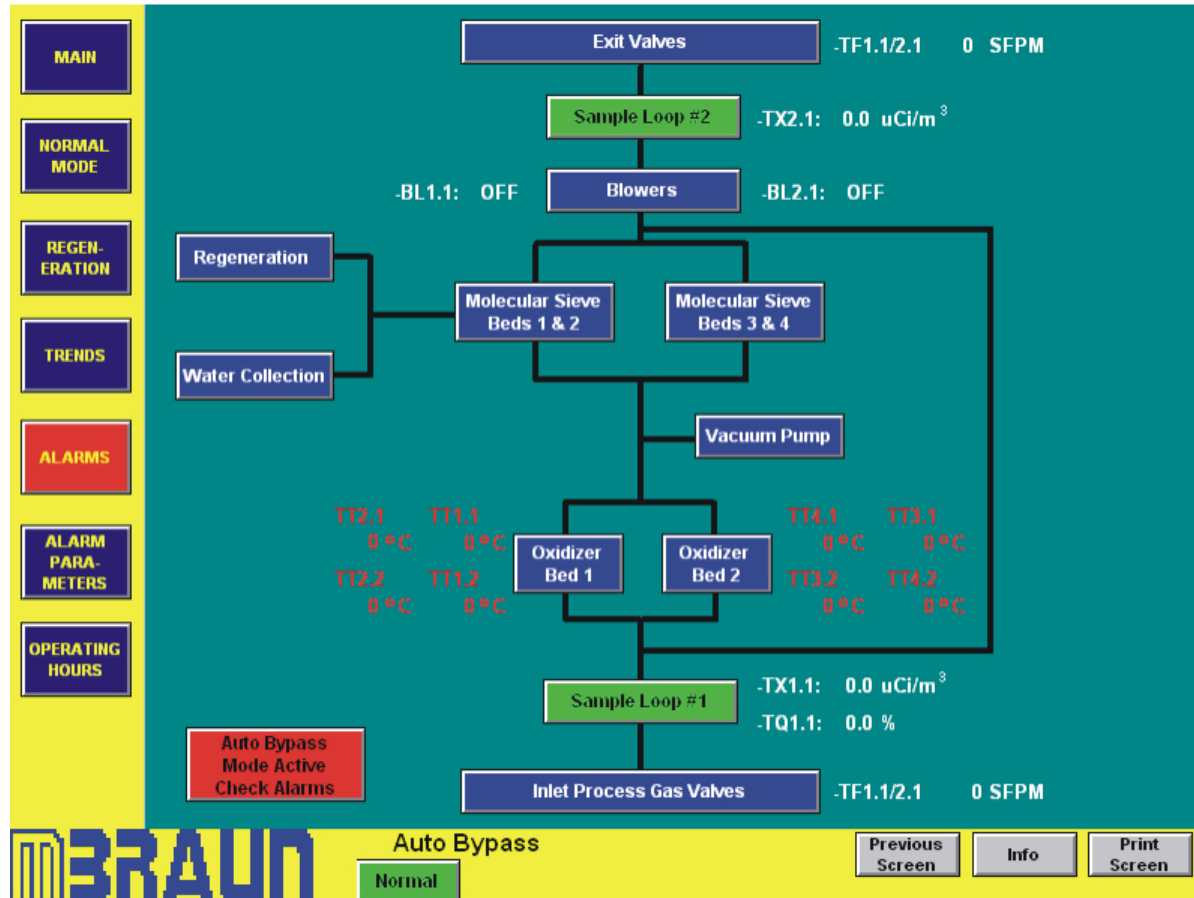
Ubed-1 pumping of hydrogen from Ar-50% H_2 gas in STV1
Unloading of hydrogen from Ubed-1 into STV1



Hydrogen transfer from Ubed-1 to Ubed-2

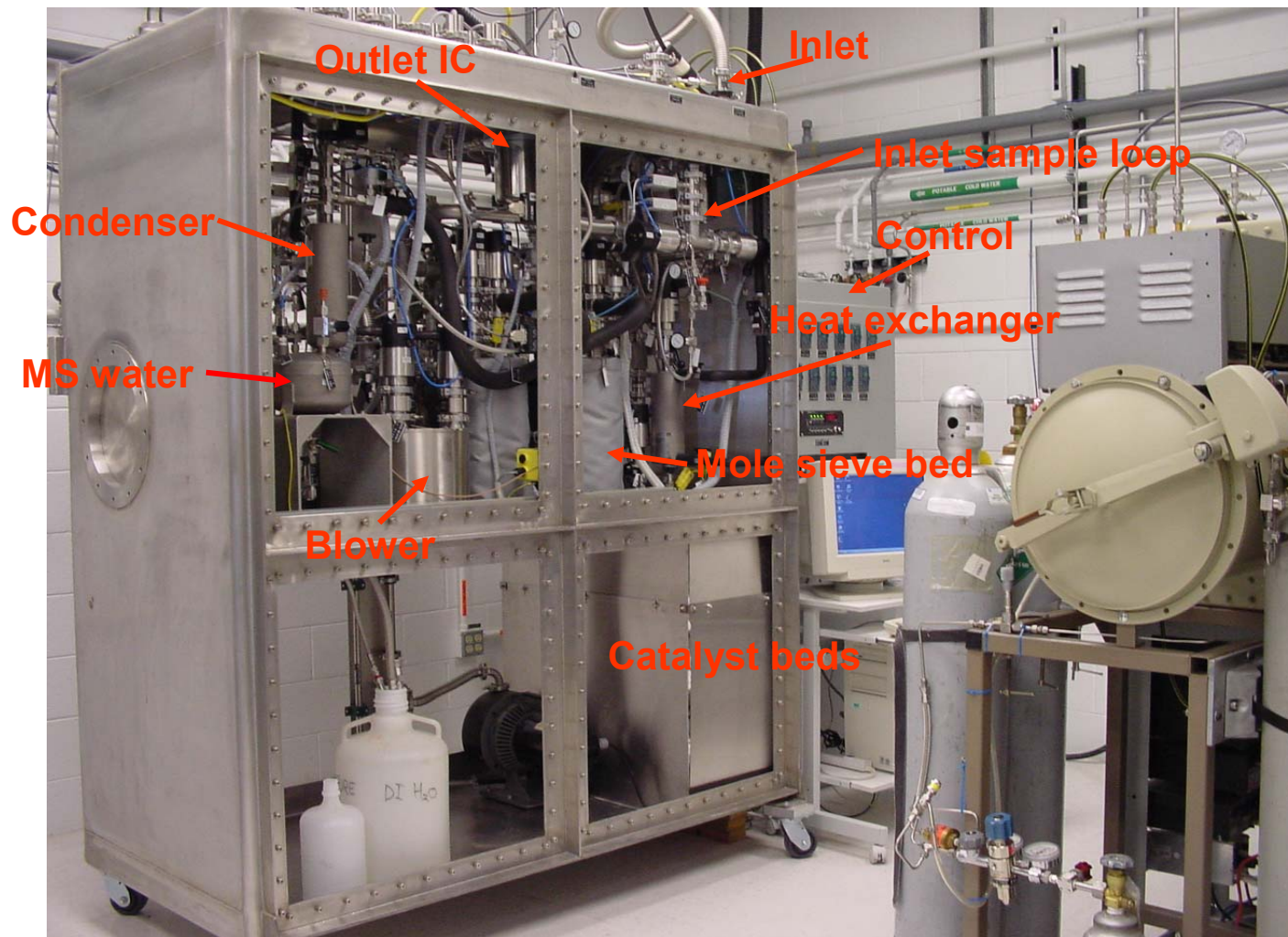


STAR Tritium Cleanup System (TCS) Schematic



- Process GB and exp. gaseous effluent
- Catalytic oxidation
BASF-RO-25/50-0.5wt% (0.5% Pd on alumina)
- Trapping on mole sieve (4A & 13X)
- Regenerate mole sieve collect and stabilize HTO in waste drum
- System fabricated by M. BraunUSA Inc. using modular components
- Siemens S7 PLC controller & Siemens WinCC GUI software

STAR Tritium Cleanup System (TCS)



Technical drawing of Section B-B of a vertical assembly. The drawing shows a cross-section of a cylindrical component with internal structures. Key features include:

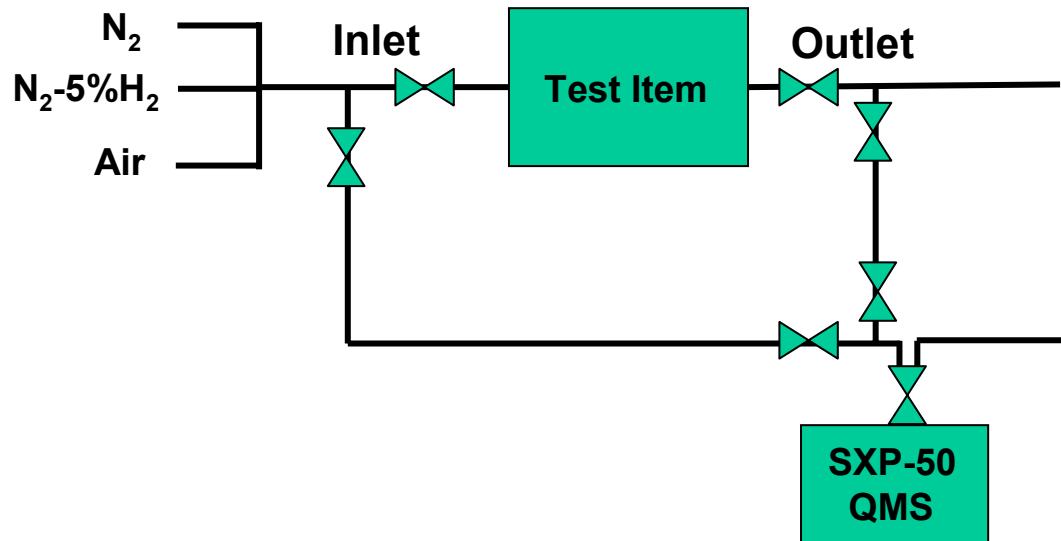
- Welds:** Indicated by 'WELD' labels and symbols at the top and bottom flanges.
- Dimensions:**
 - Top flange: .47 (12)
 - Internal spacing: 4X .98 (25), 4X .20 (5)
 - Bottom flange: .79 (20)
- Internal Components:**
 - Central vertical rods (red and blue).
 - Outer vertical rods (magenta).
 - Internal spiral or helical structures.
 - Various fasteners and bolts (circles with numbers like 18, 7, 4, 23, 24, 25, 26, 27, 28, 29, 30).
- Labels:**
 - LL (Left Limit)
 - SEE DETAIL E (pointing to a detail of the bottom flange)
 - SEE DETAIL D (pointing to a detail of the bottom flange)
 - SECTION B-B (centered at the bottom)



BASF-R0-25/50-0.5wt%

Measurement of Oxidizer Bed Performance

BASF R0-25/50 (0.5wt% Pd) Catalyst

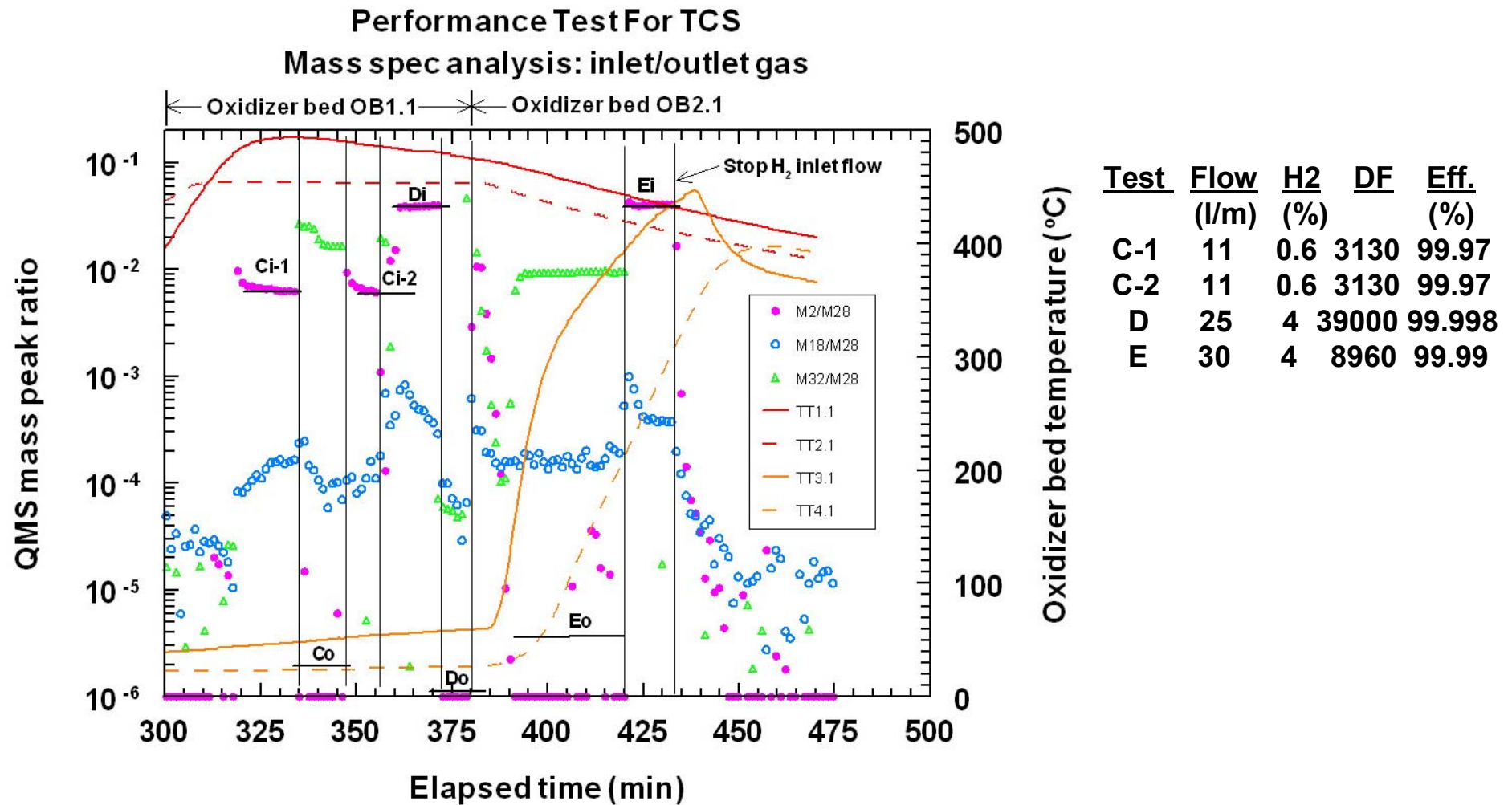


Analysis Approach

- For inlet and outlet gas streams, measure QMS peak heights for H_2 , N_2 and O_2
- $DF = (M2:M28)_{In} / (M2:M28)_{Out}$
- H_2 removal efficiency = $(1 - 1/DF) * 100\%$

1. Sample test bed (116 g catalyst in 150 cc cylinder)
(0.4-8 l/min; 0.2-4% H_2 concentration)
2. TCS Oxidizer bed (18 kg of catalyst, 22 liter volume)
(3-7 l/min; 0.8-5% H_2 concentration)
3. TCS System
(10-30 l/min; 0.6-4% H_2 concentration)

Measurements for TCS



Remarks on STAR tritium readiness

- **Planned activities**
 - **Final testing for systems**
 - **SAS Beta scintillation detector**
 - **SAS Functional and quantitative testing**
 - **TCS molecular sieve bed conditioning tests**
 - **TCS water recovery verification**
 - **Stack monitor tritium release tests**
 - **Integration of all tritium systems with infrastructure and experimental systems**
 - **Preparation of operation procedures and safety documentation**
 - **Management and operational readiness review (August 04)**

Experiments in STAR: Tritium Plasma Experiment (TPE)

System reassembly

- *moved from TSTA at LANL in December 2001*
- *significant T contamination required special enclosure*
- *facility specific connections are underway*
- *reconnection of control and diagnostics are underway*

TPE will be ready for plasma operation by the end of Summer 2004, and T operation shortly after STAR is tritium-ready

INL Fusion Safety Program



TPE Enclosure

TPE Glovebox



Experiments in STAR: Molten Salt Studies

D₂ / HT Permeation Experiment with Flibe

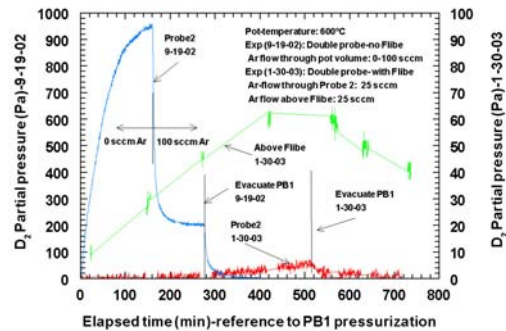
- ***explores tritium behavior to establish a reliable tritium control strategy for a Flibe breeder blanket***
- ***annular dual probe design***
- ***measure transport in stagnant and natural convection flow***
- ***mass-spectrometer gas analysis system used experiments with deuterium***
- ***tritium experiments to use on-line analysis system (ion chambers, Pd oxidizers, ethylene glycol traps)***

MS Permeation Experiment



Experiment System

Comparison MSE(1-30-03)-DBL(9-19-02)
Comparison-600-Pa-2

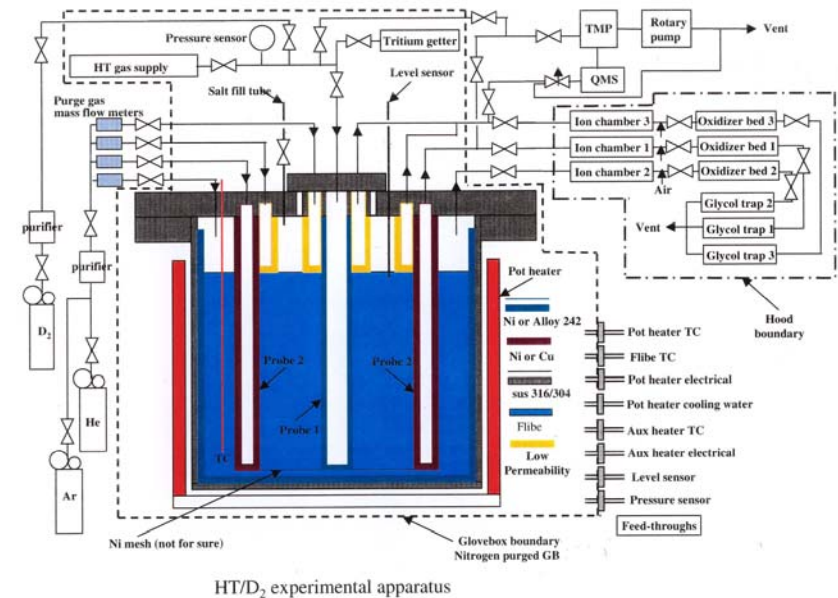


- reduction in probe-2 concentration of D_2 due to low solubility
- time delay for observation of permeation signal in probe 2 (due to slow diffusivity)

Results and Analysis



Dual Probe Assembly



HT/D₂ experimental apparatus

Configuration

Experiments in STAR: Molten Salt Studies

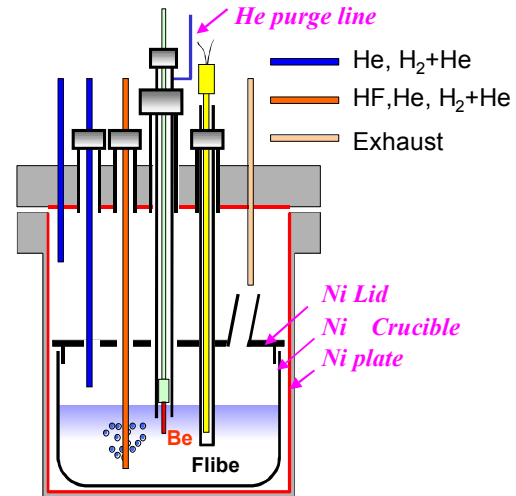
REDOX control and HF / TF recovery

- ***Breeding of LiF/BeF₂ generates TF; tritium recovery systems need T₂; hence salt must have some REDOX agent***
- ***Be is suitable: $\text{Be} + \text{TF} \rightarrow \text{BeF}_2 + \text{T}_2$***
- ***experiment to demonstrate Be redox control, and measure reaction kinetics (presently injecting HF to simulate TF generation)***
- ***measurements obtained with mass-spec and/or gas chromatograph for gas analysis, auto-titration system for HF, and acid dissolution/ICP-MS for metal fluorides in the salt***
- ***plan to use T in system, requires STAR T-readiness***

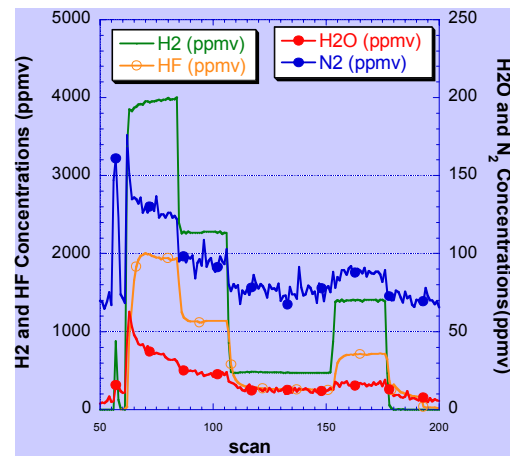
MS REDOX Control Experiment



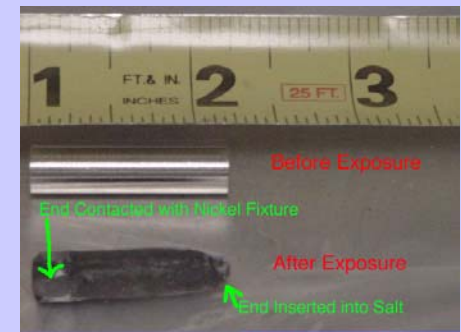
Experiment System



General Pot Configuration



Results and Analysis



Non-statistical behavior of surface-induced dissociation of HD_2^+

W. Schustereder, A. Qayyum, C. Mair, T. Tepnual, P. Scheier, T.D. Märk

Institute of Ion Physics

University of Innsbruck

Austria

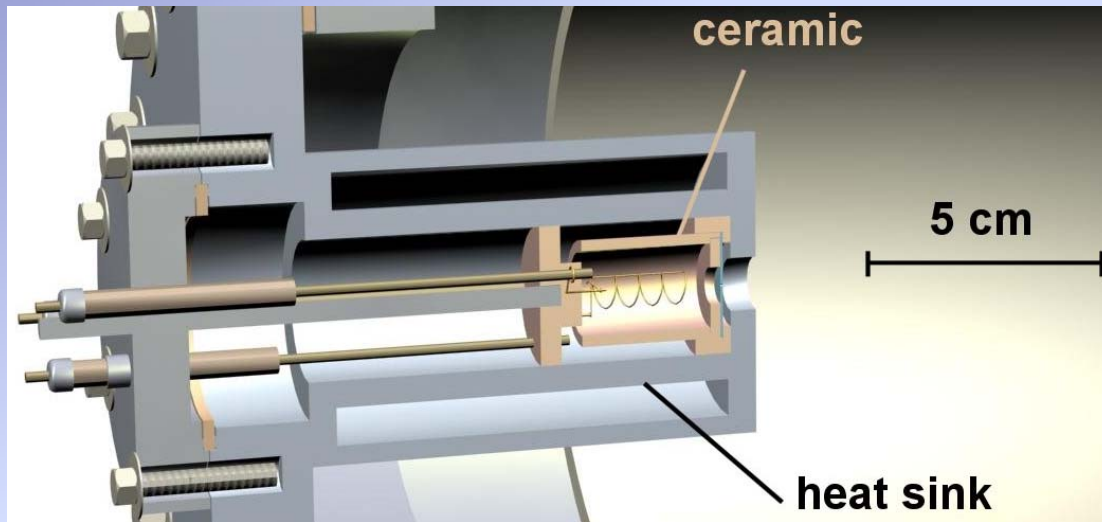


Content

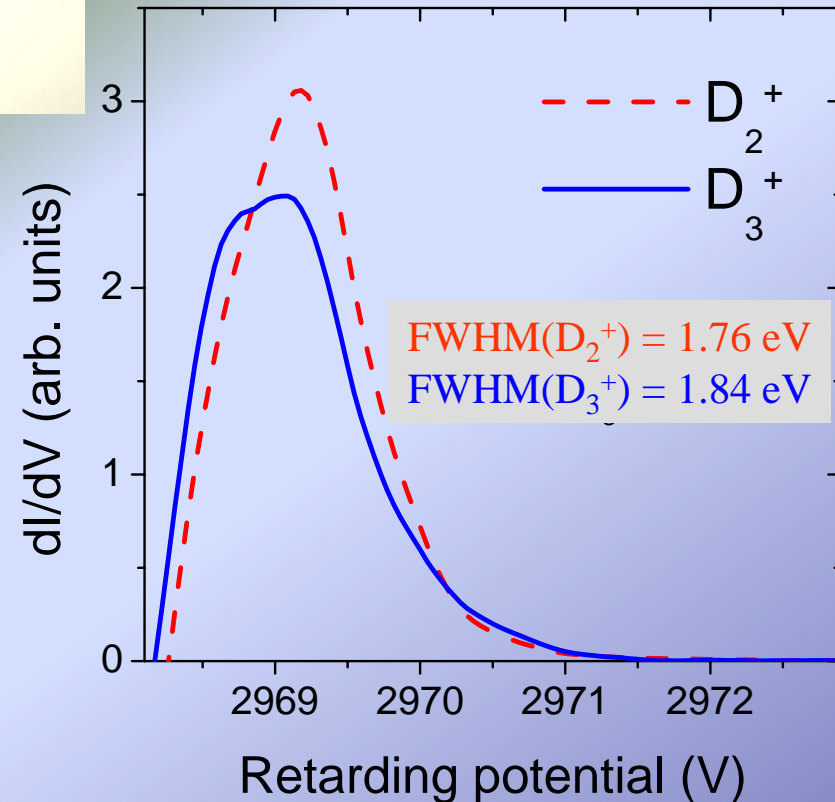


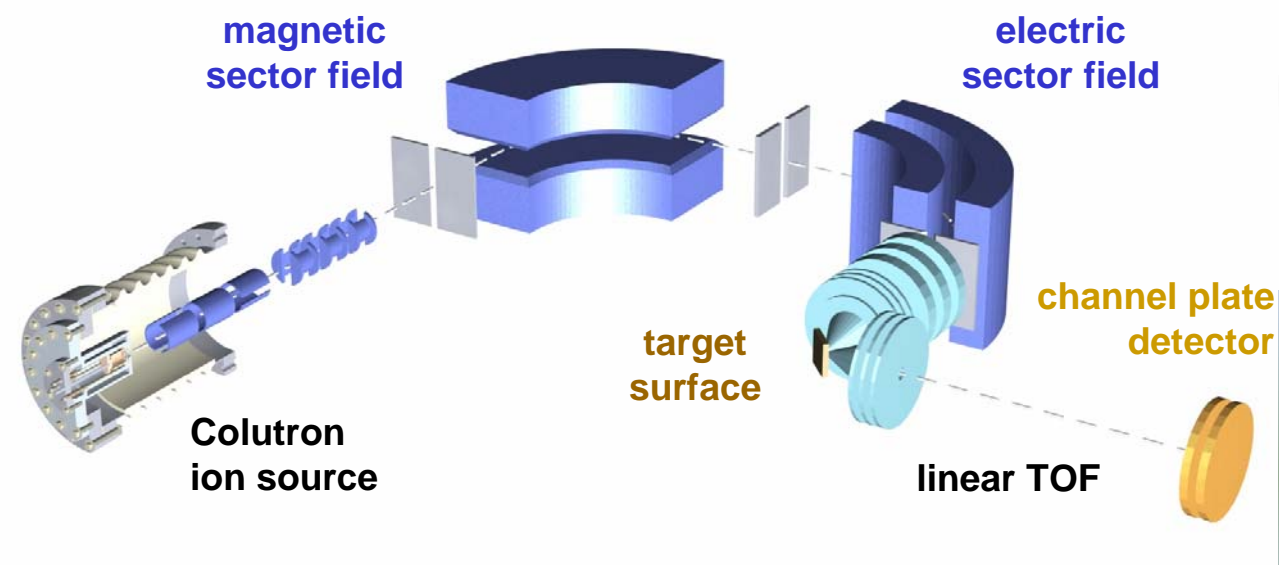
- Apparatus
- Processes
- Fusion-relevant Experiments – general trends
- HD^+ and HD_2^+

Colutron Ion Source

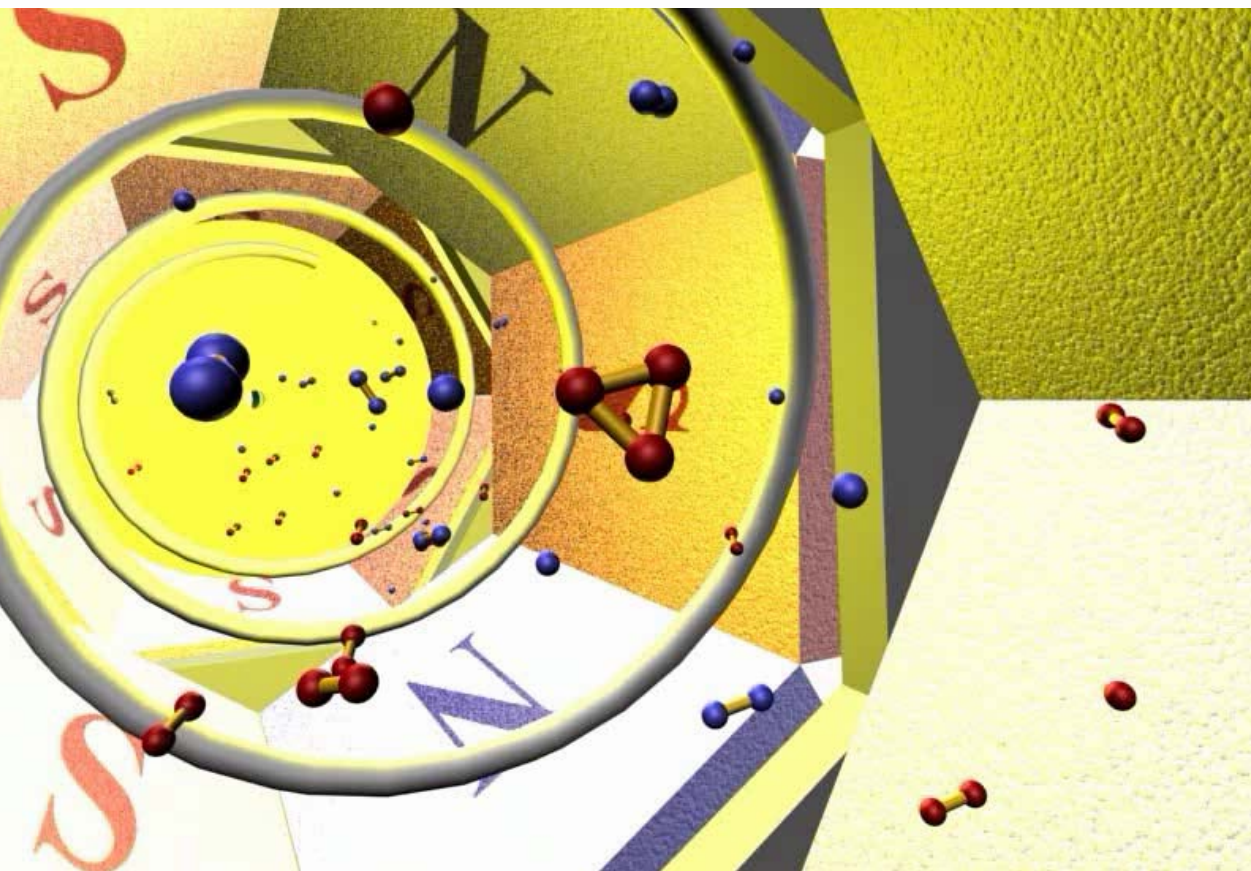


Energy spread of the D_2^+ and D_3^+ ion beam after mass and energy selection

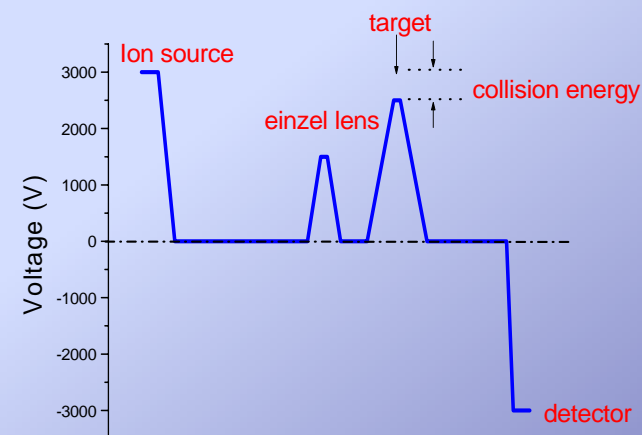




BESTOF



Potential energy curve for the ion path



Processes at Surfaces



$m_1^+ + S/AB \rightarrow m_1$	<i>Neutralization</i>
$m_1^+ + S/AB \rightarrow m_1^{+*}$	<i>Reflection</i>
$m_1^{2+} + S/AB \rightarrow m_1^+$	<i>Charge Exchange</i>
$m_1^+ + S/AB \rightarrow m_1^-$	<i>Charge Inversion</i>
$m_1^+ + S/AB \rightarrow m_2^+ + m_3$	<i>SID</i>
$m_1^+ + S/AB \rightarrow m_1AB^{+*} \text{ or } m_1A^{+*}$	<i>SIR</i>
$m_1^+ + S/AB \rightarrow m_1 + A^+$	<i>Chem. Sputtering</i>

S/AB adsorbate covered surface

Motivation



- Astrophysics – growth mechanisms of dust grains
- Thin film technology – industrial coating techniques
- Environmental research – atmospheric chemistry
- Stability of Biomolecules/DNA
- Fusion Plasma Physics
 - Elucidation of plasma/wall interaction phenomena
 - Are there isotopic effects in ion-surface reactions?
 - Does the fragmentation of hydrogen molecular ions occur at energies that are characteristic for the plasma edge?

•URGEND NEED FOR DATA ON SID OF HYDROGEN

Fusion-relevant data



- H_2^+ , D_2^+ , H_3^+ , D_3^+ , HD^+ and HD_2^+
- Hydrocarbons: CH_3^+ , CH_4^+ , CH_5^+ + deuterated species
+ larger hydrocarbons
- Other impurities like CO^+ , CO_2^+
- Also experiments with multiply charged ions
- Some general trends:
 - Exponential decrease of secondary ion signal after collision with wall
 - Pick-up reactions observed upon surface impact
 - Isotopic effects mainly seen in hydrogen experiments

HD^+ and HD_2^+

Experimental conditions

Ion source:

1:1 and 3:7 mixture of H_2 and D_2 at $p = 0.4$ torr

Beamline:

$p = 10^{-8}$ torr

$I_{\text{Ion}} = 1$ nA

Surface:

Graphite tile from Tore Supra (Cadarache)

- clean

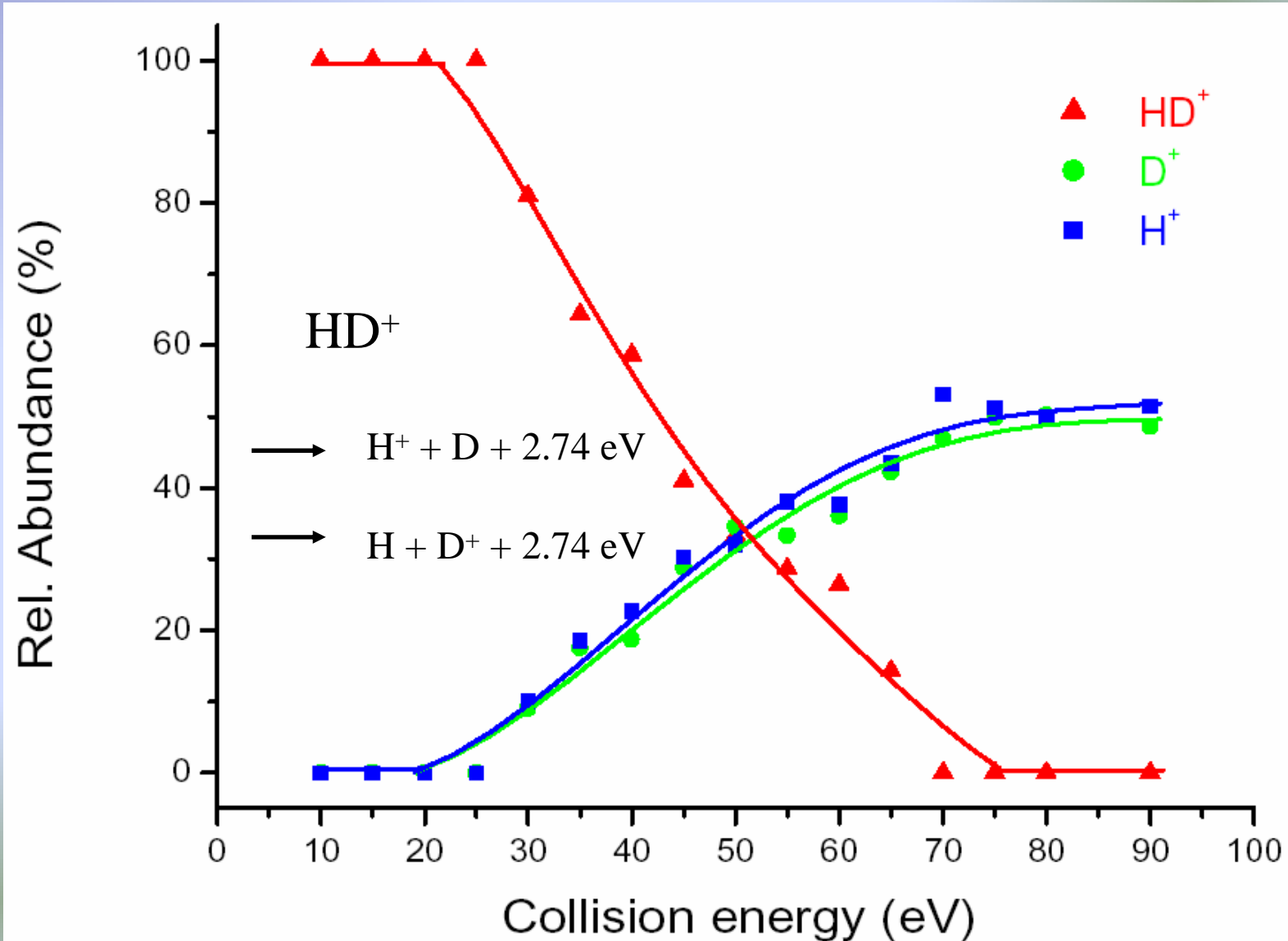
- covered with hydrocarbons

Incident angle = 45°

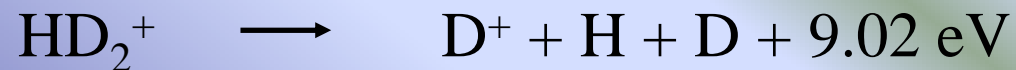
Scattering angle = 91°



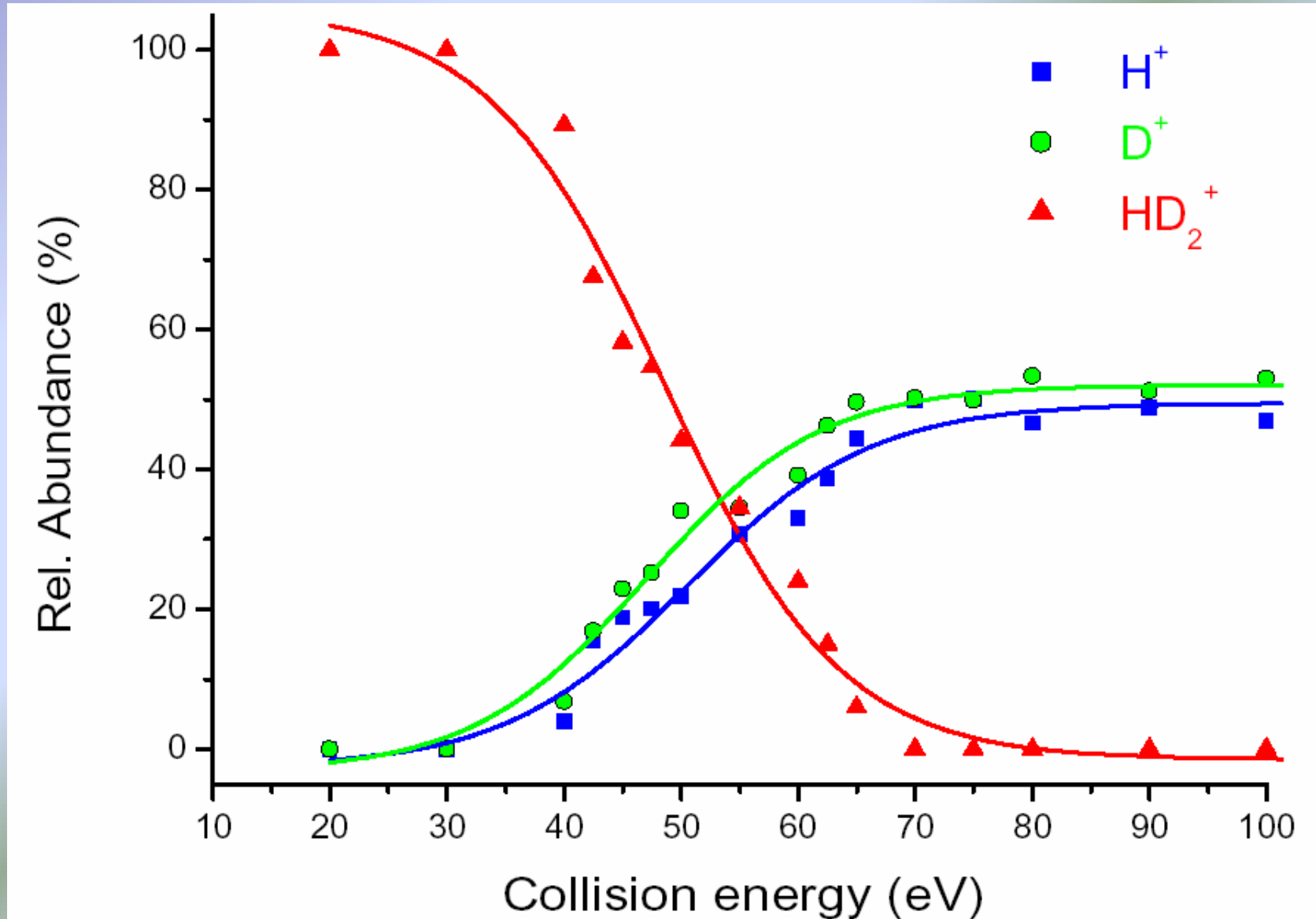
Energy Resolved SIMS of HD^+



Possible Dissociation Pathways



Energy Resolved SIMS of HD_2^+

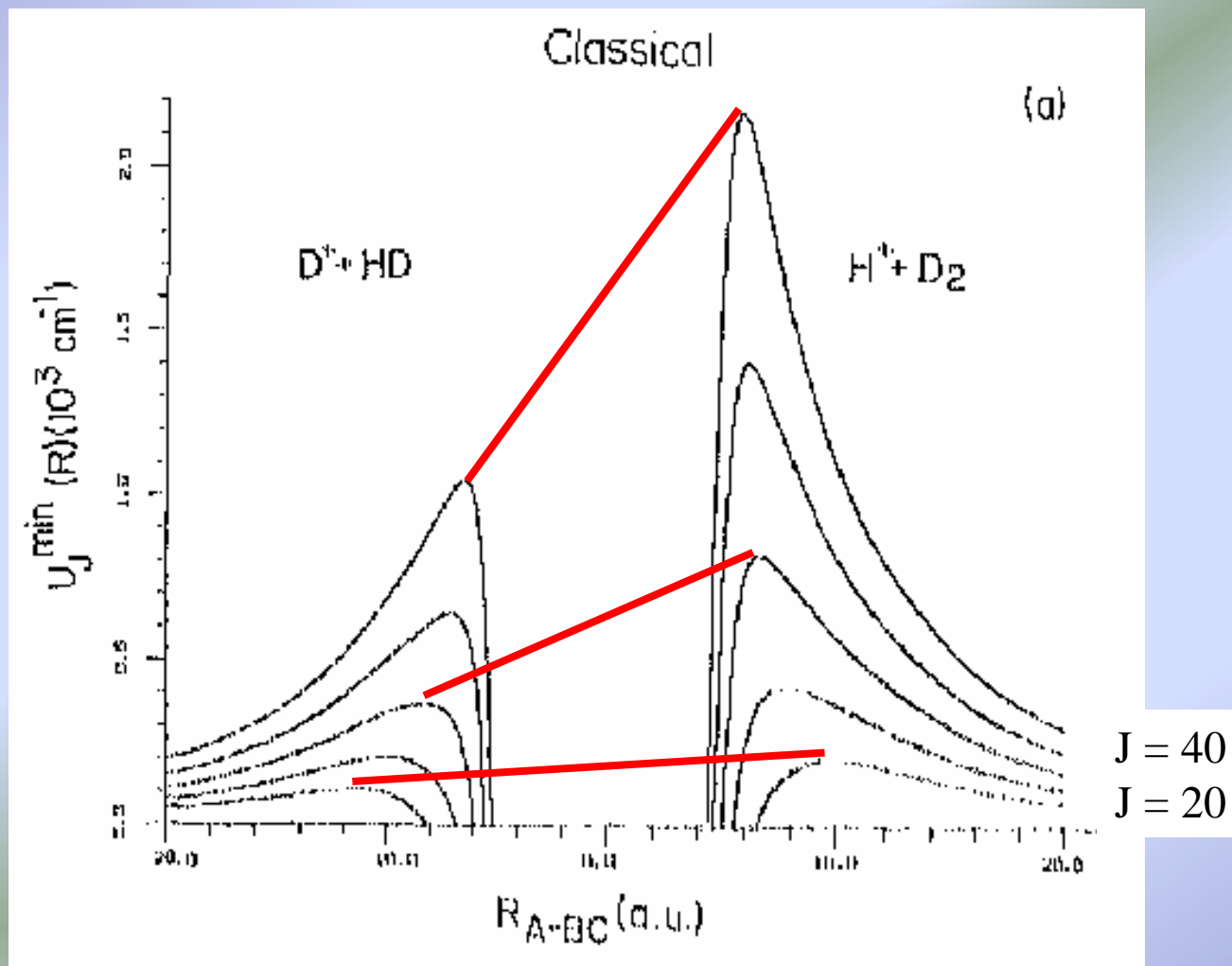


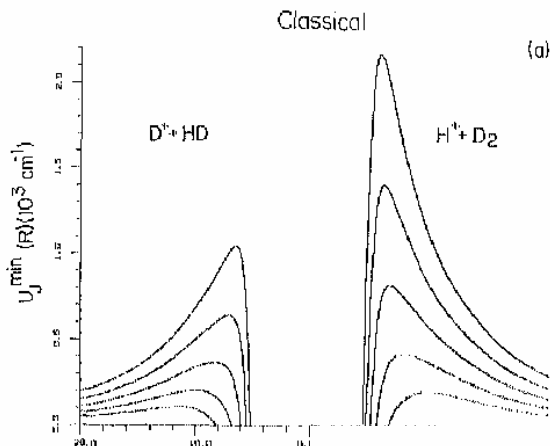
CID and Photodissociation results

CID of HD_2^+ : Occurance of all possible fragment ions
 H^+ , D^+ , HD^+ and D_2^+

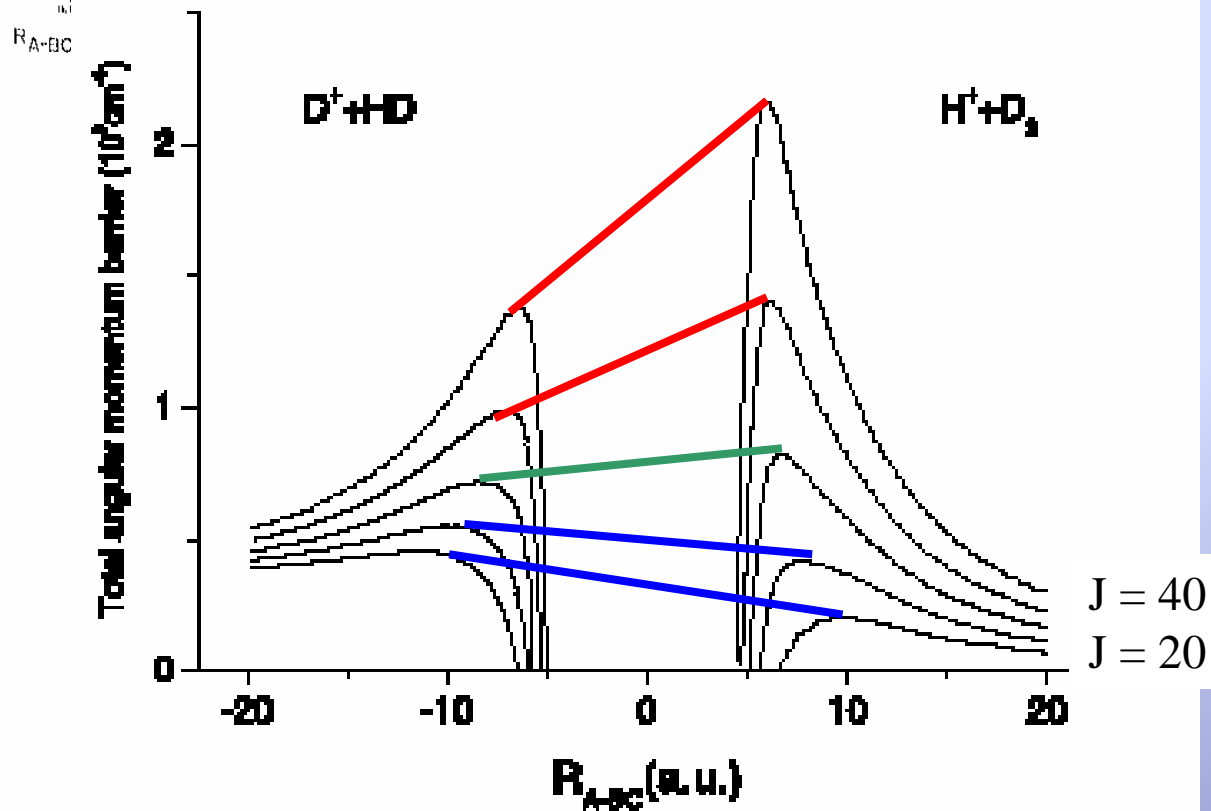
Photodissociation of HD_2^+ : Only H^+ and D^+ observed
Intensity of fragment ion D^+ was smaller
by a factor of 3 than that of H^+

Spectra from long lived resonances were
quite different





Zero point energy
also taken into account



SUMMARY



Simple systems as HD_2^+ can still surprise us

Isotopic effects can be clearly seen

Fragmentation of hydrogen molecular ions occurs at an energy regime that is similar to that in the plasma edge

Exponential decrease of the scattered primary ion signal

Non-statistical behavior of surface-induced dissociation of HD_2^+

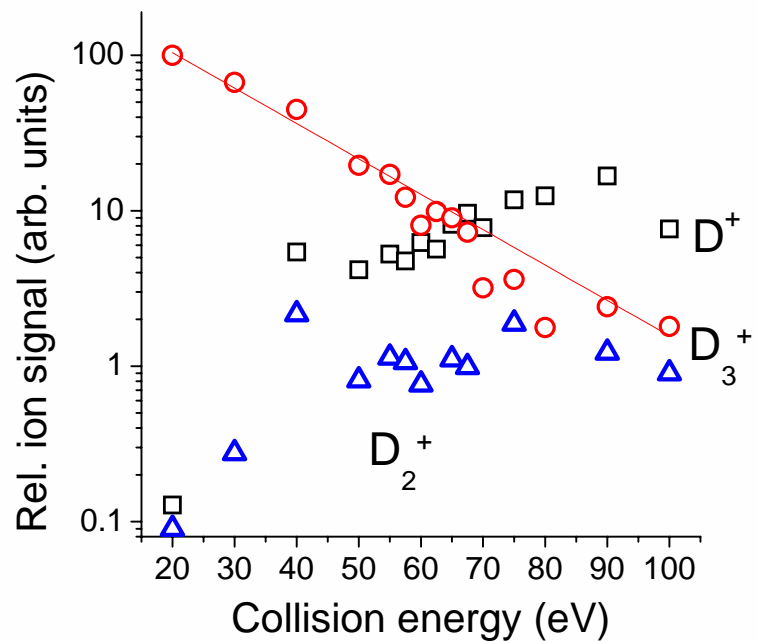
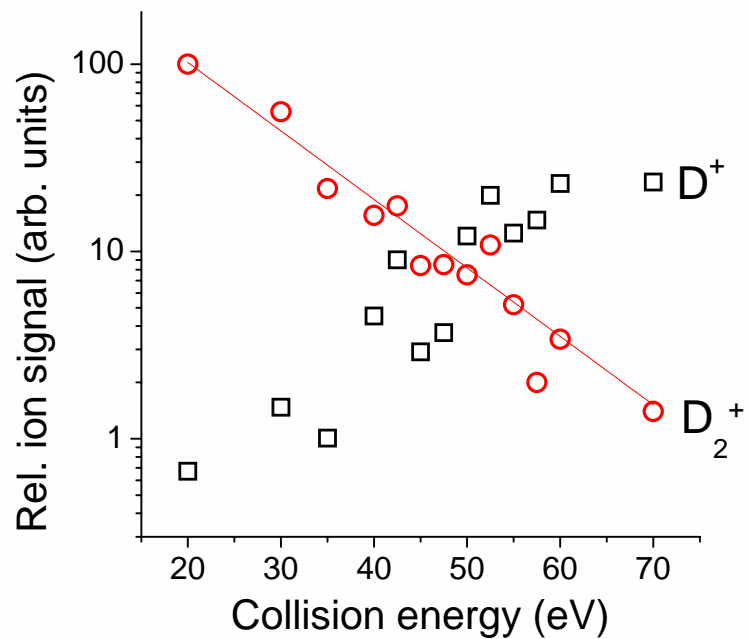
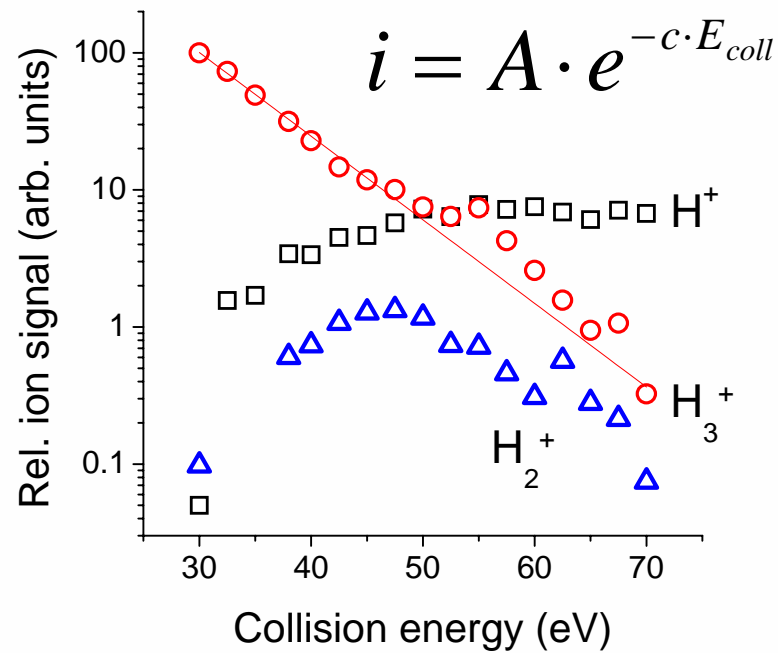
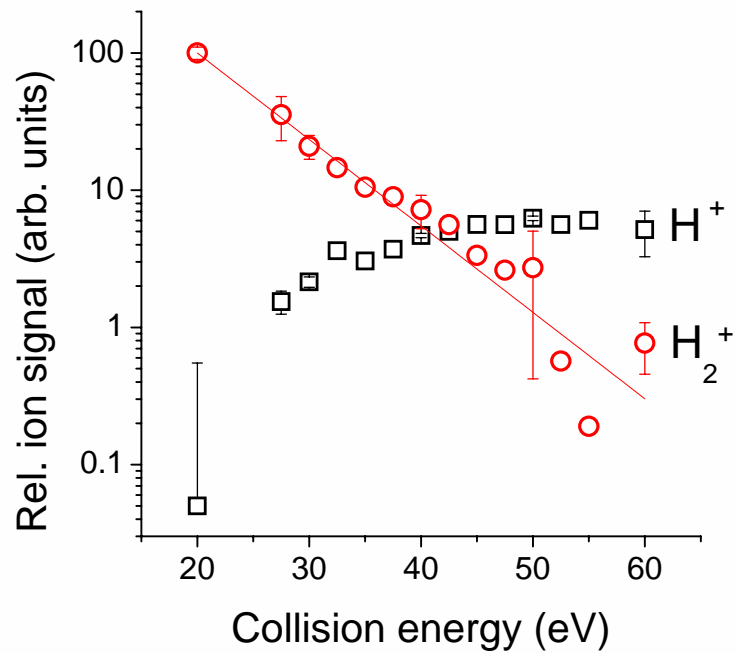


W. Schustereder, A. Qayyum, C. Mair,
T. Tepnual, P. Scheier, T.D. Märk



ÖAW/EURATOM Association and FWF, Vienna.
European Commission, Brussels.





$$i = A \cdot e^{-c \cdot E_{coll}}$$

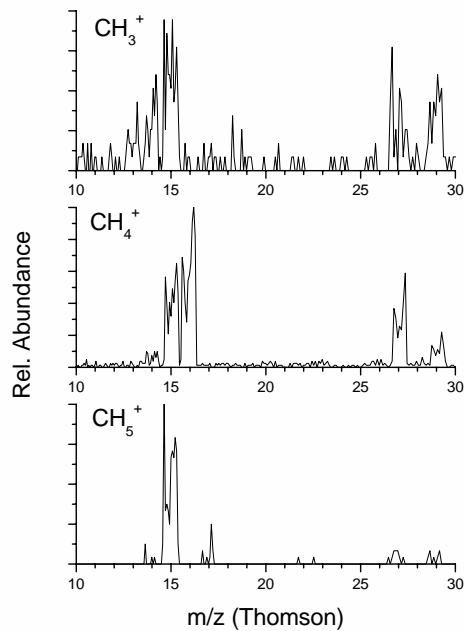
*exponential
decrease*

Projectile ion	atomic fragment H ⁺ or D ⁺				diatomic frag.
Projectile ion	E(50%)	v(50%)	i _{max}	fit parameter c	i _{max}
H ₂ ⁺	34 eV	57.1 km/s	5.6%	0.145	-
H ₃ ⁺	40 eV	50.5 km/s	7%	0.137	0.6%
D ₂ ⁺	50 eV	49.0 km/s	13%	0.085	-
D ₃ ⁺	58 eV	43.1 km/s	23%	0.052	0.8%

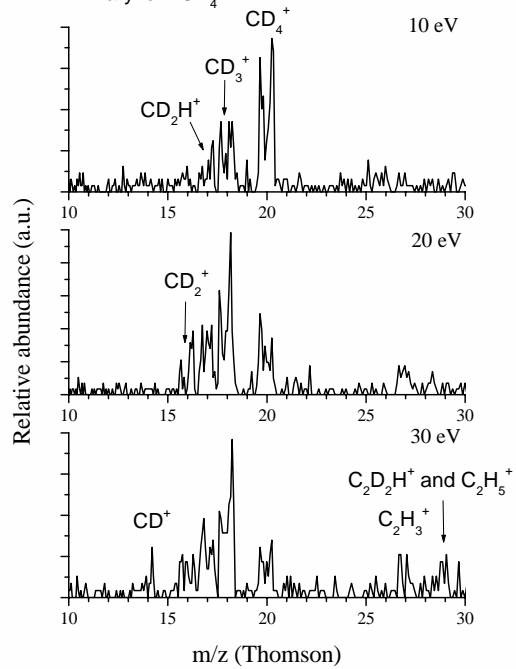
- The product ion yield decreases faster for H_2 and H_3 compared to D_2 and D_3 , respectively.
- The molecular ions containing the heavy isotope, D_2^+ and D_3^+ lead to more ionic fragments at high collision energies compared to their H containing counterparts.



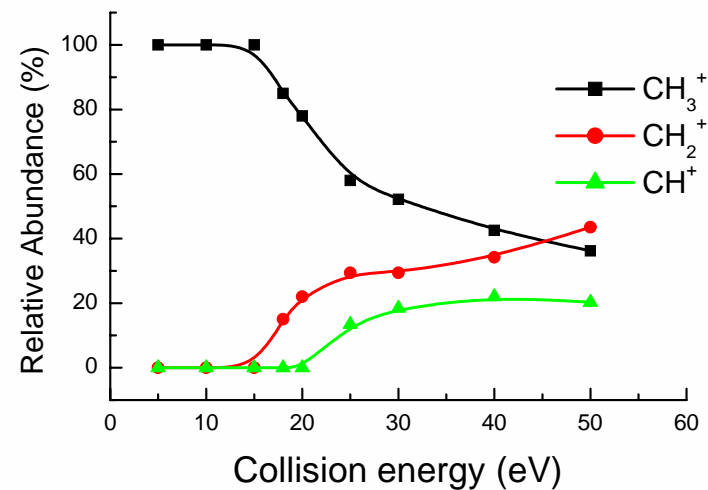
Collision energy: 25 eV



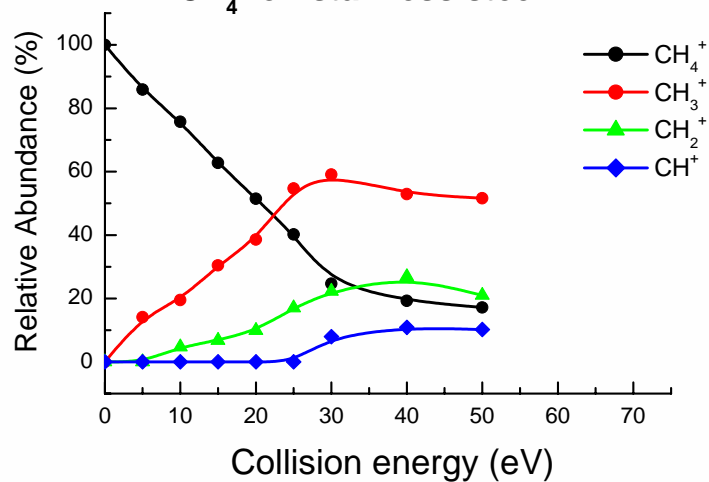
Primary ion: CD_4^+



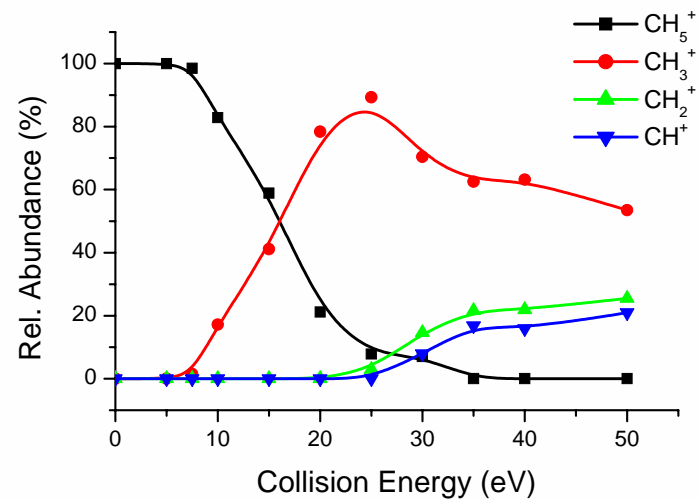
CH_3^+ on stainless steel



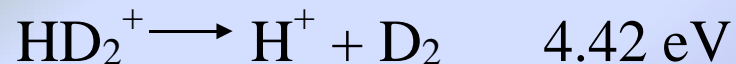
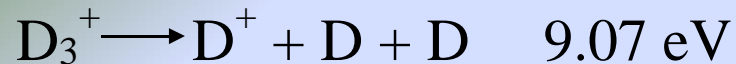
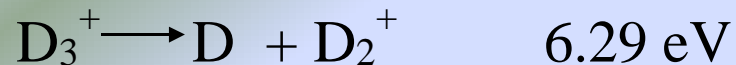
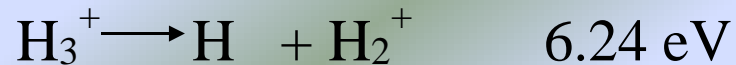
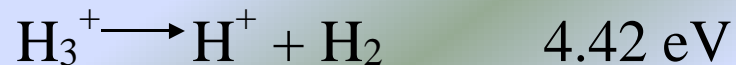
CH_4^+ on stainless steel



CH_5^+ on stainless steel



Possible Dissociation Pathways



Mechanism of hydrogen blistering on covalent bonding materials

T. Tanabe and S. Muto *Nagoya University*

Blistering mechanism

Metals (Understood rather well)

Ductile deformation; stress due to agglomerate gas bubbles
exceeds yield strength

Covalent materials (Several questions remain)

Effect of dangling bond and chemical effect

How proceed deformation (material flow) in brittle materials ?

Is deformation (blister formation) elastic or plastic?

Blistering is a key issue in understanding.....

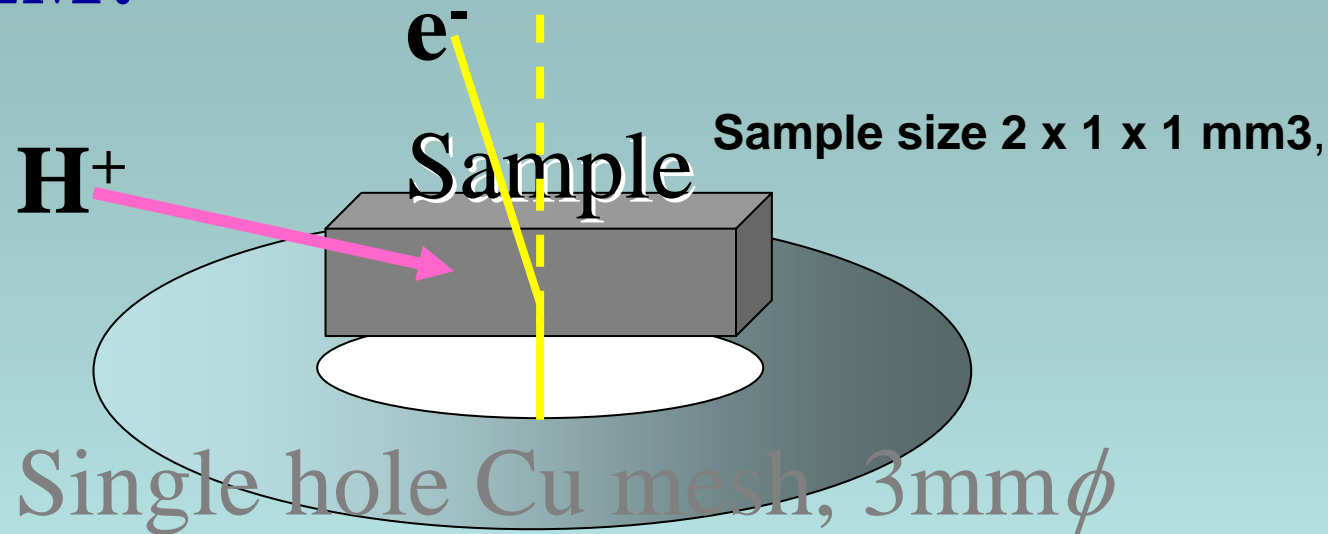
- Plasma-Surface Interaction (PSI)**
- fabrication processes of Semiconductor-On-Insulator film**
- mechanism of catalysis generated at subsurface**

Approach

In order to characterize surface protrusions such as blisters, we have used a new technique based on TEM named **grazing incidence electron microscopy (GIEM) which we have developed for non-destructive structural analysis of blistering on non-ductile materials (**Si & SiC**) heavily irradiated by H^+ , D^+ , or He^+ , together with conventional TEM for cross-sectional view.**

Various spectroscopic techniques associated with TEM, including **EELS are also applied.**

What is GIEM?



Grazing Incidence Electron Microscopy (GIEM)

Two types of imaging processes contribute to an image of GIEM:

- TEM imaging with transmitted electron, through the mesoscale protrusions such as blisters
- REM imaging with reflected electrons from the surface

GIEM enables us to.....

- observe surface protrusions **even on brittle materials**
- analyze their structure **non-destructively**

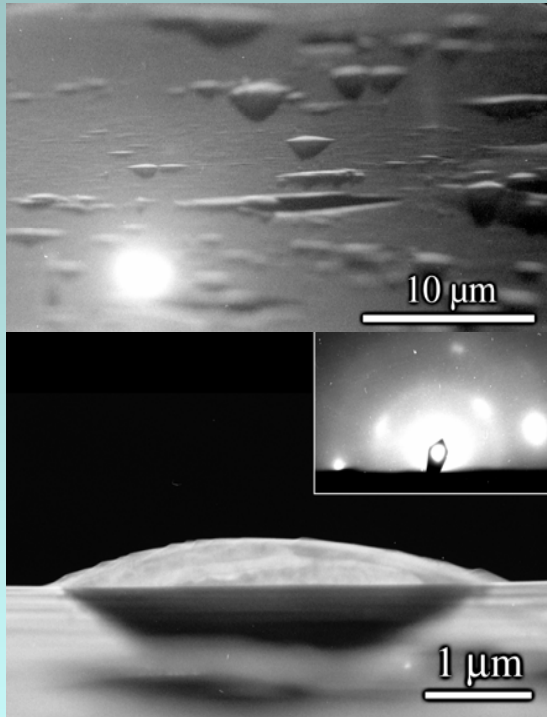
Irradiation Condition

Sample size 2 x 1 x 1 mm³,

Target	Si(100)			<0001> 6H-SiC	
Implant	H⁺	D⁺	He⁺	H⁺	He⁺
Energy [keV]	13	10	16	16	19
Projected range	~ 200 nm				
Damage distribution	~ 170 nm				
Number of Vacancies [/ion]	7	17	17	4	54

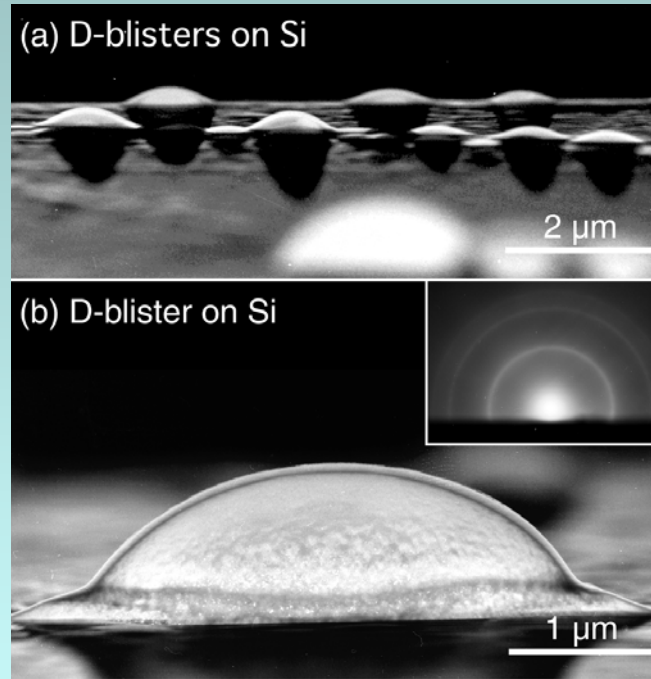
GEM Images of blisters on Si (100)

H-Blister



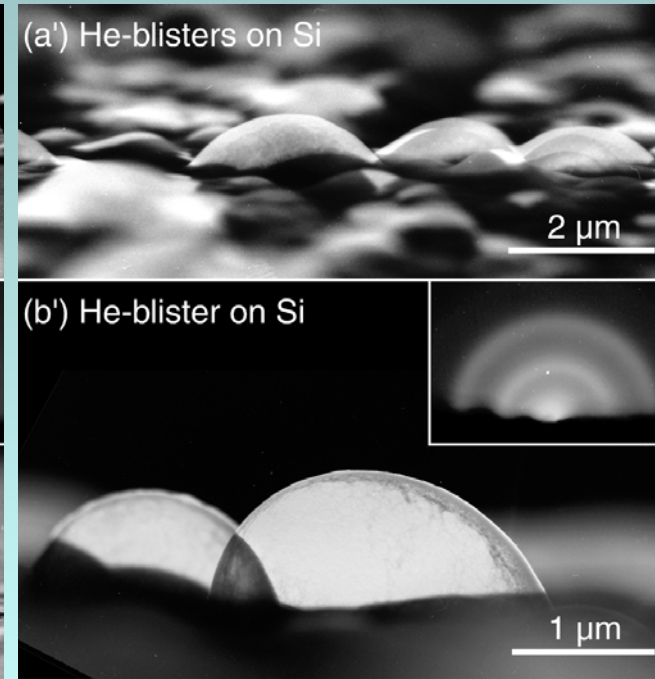
Single Crystalline
+ High density defect

D-Blister



Amorphous
+ fine crystalline

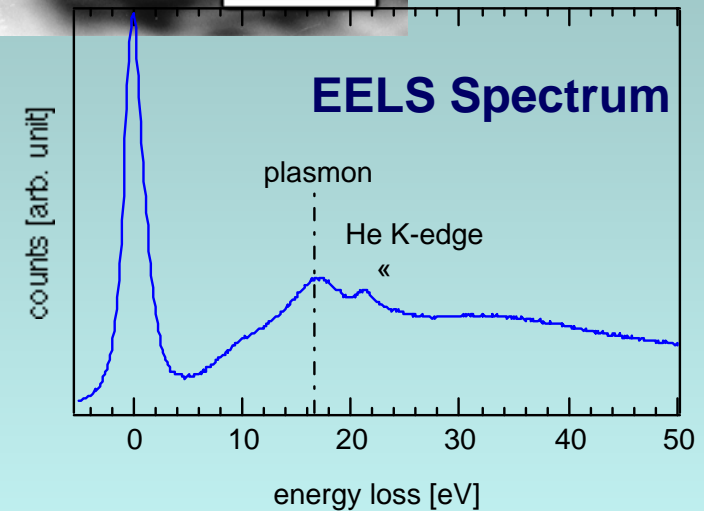
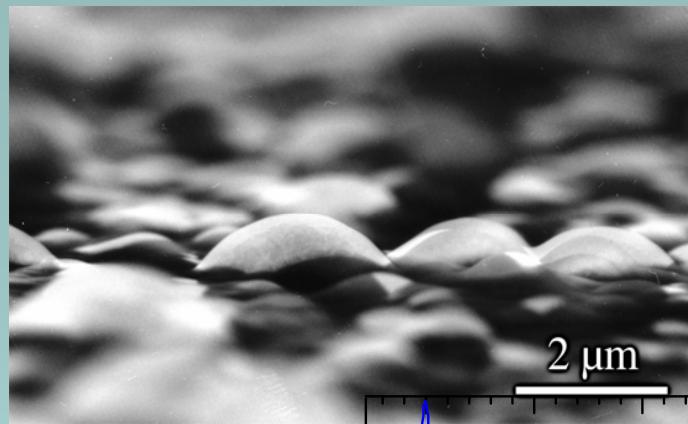
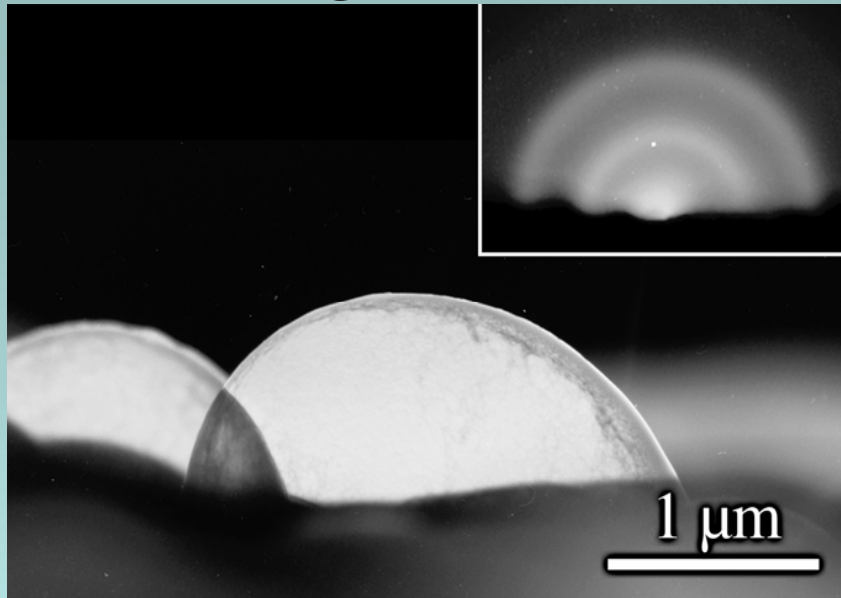
He-Blister



Amorphous

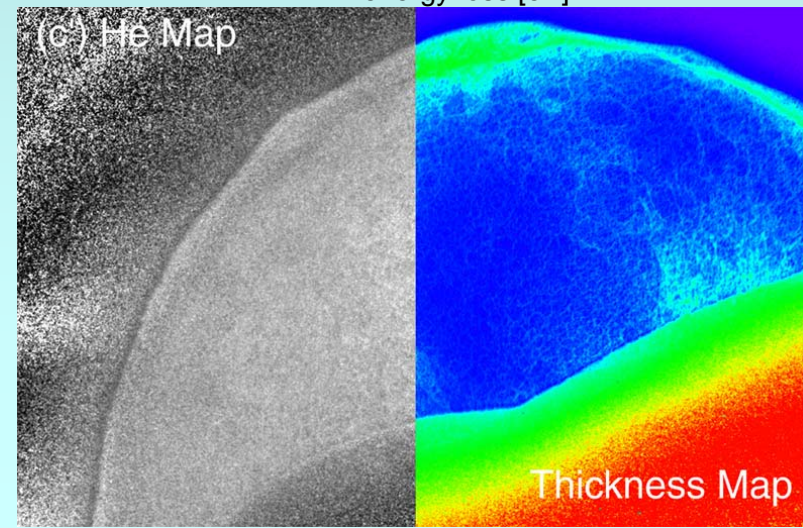
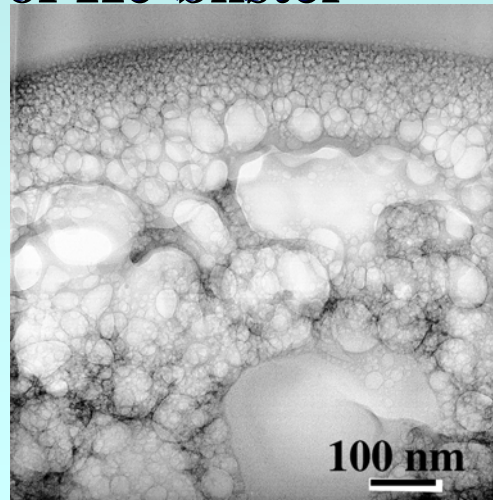
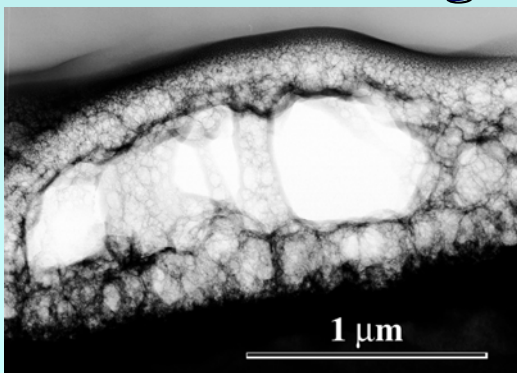
Structure of Blister Skin determined by electron diffraction

GEM images of He-blister

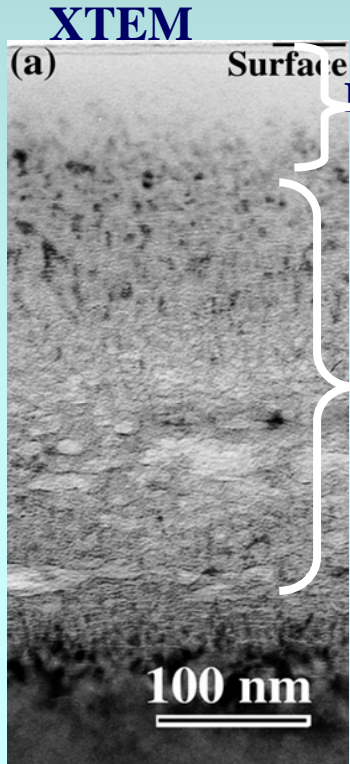
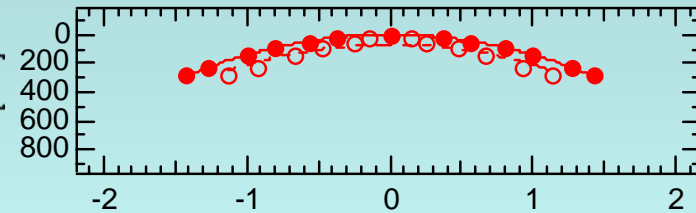
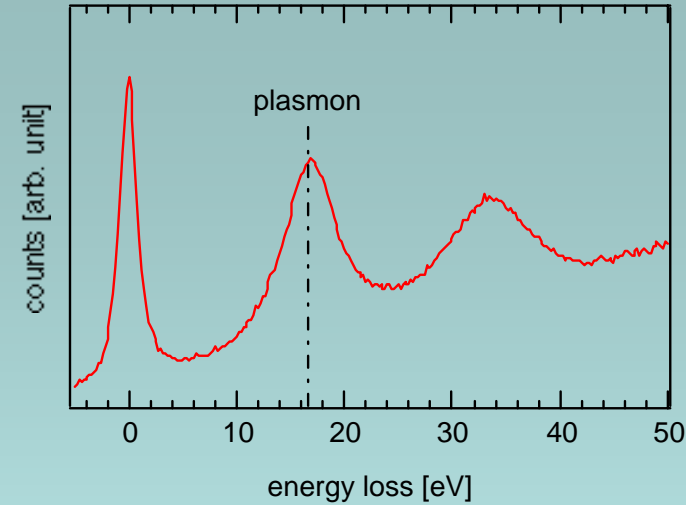
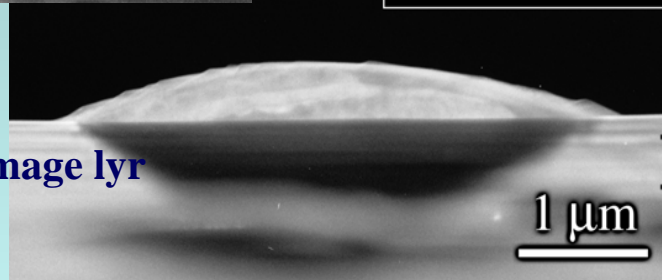
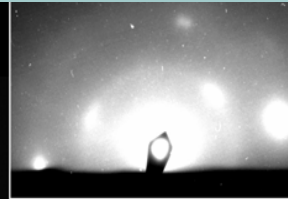
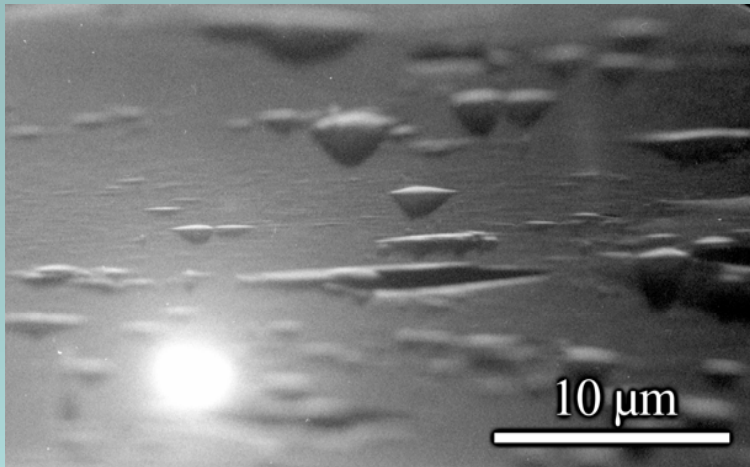


Blister skin: Amorphous structure containing a high density of He bubbles

XTEM images of He-blister



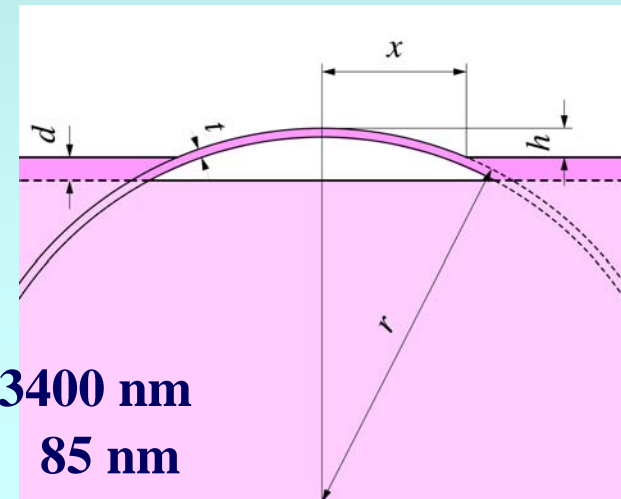
H^+ -irradiated Si with $E = 13 \text{ keV}$, $\Phi = 1.0 \times 10^{22} \text{ m}^{-2}$



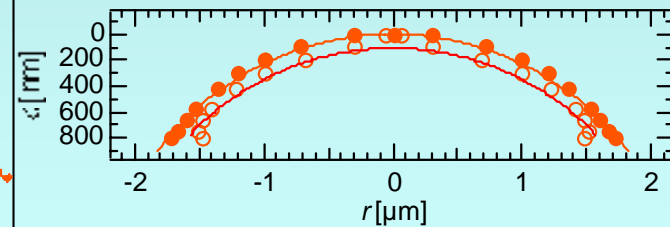
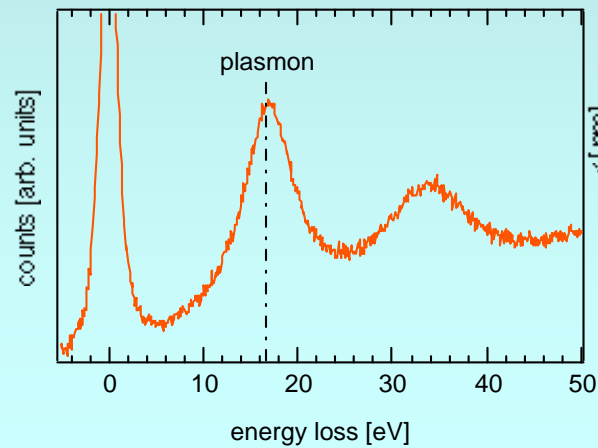
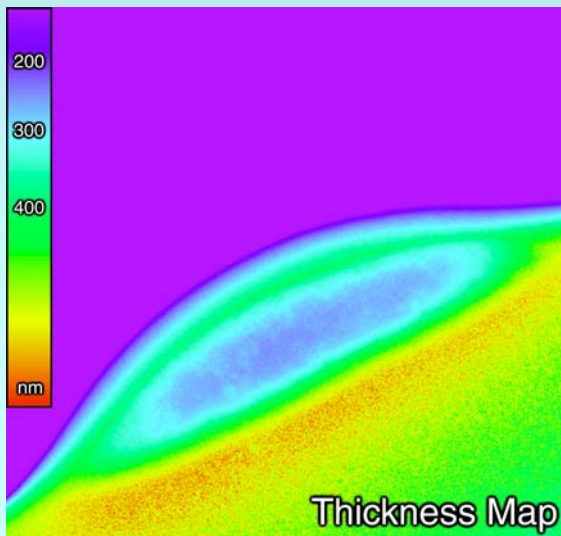
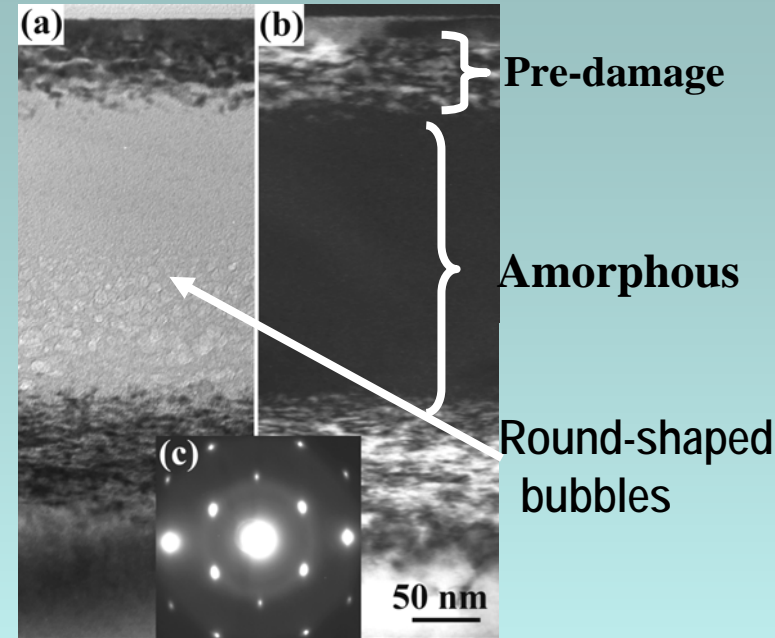
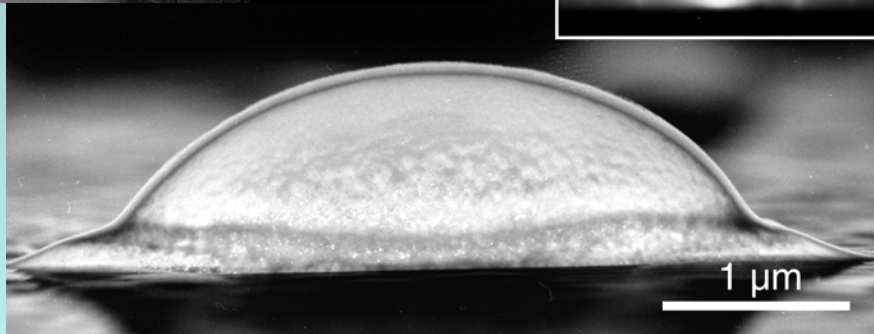
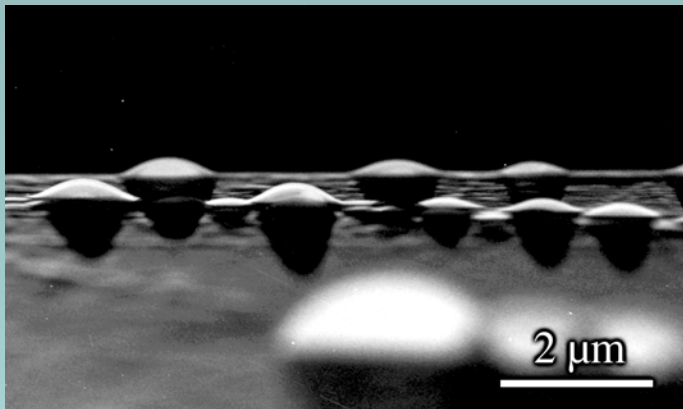
Crystalline
High dens.
defects
plate-like
bubbles on
(100)

Blister skin
— Amorphous structure
having a uniform thickness

r 3400 nm
 t 85 nm



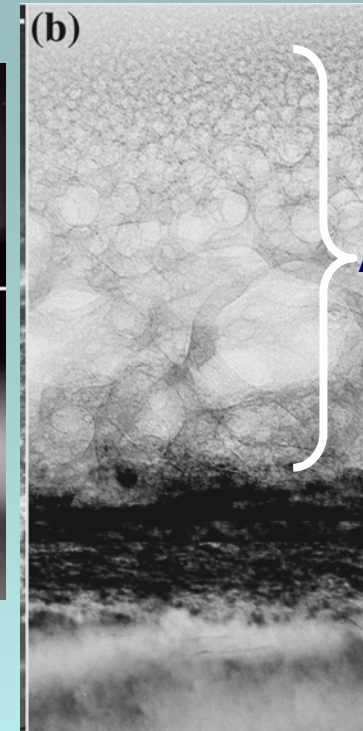
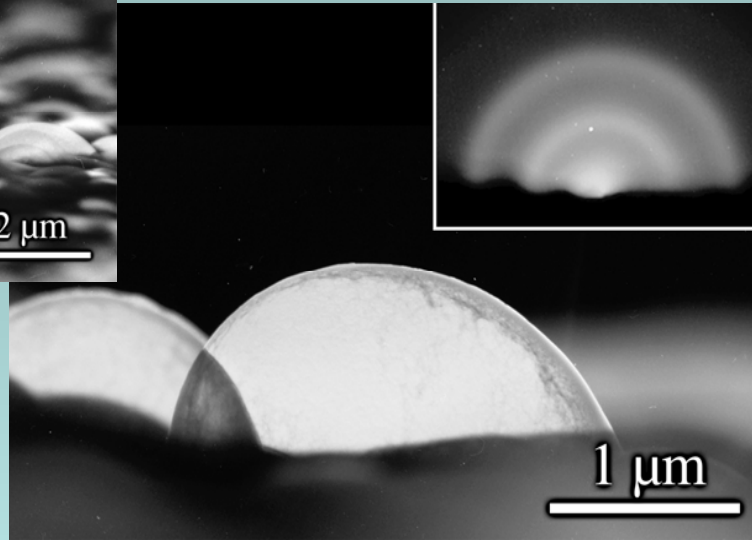
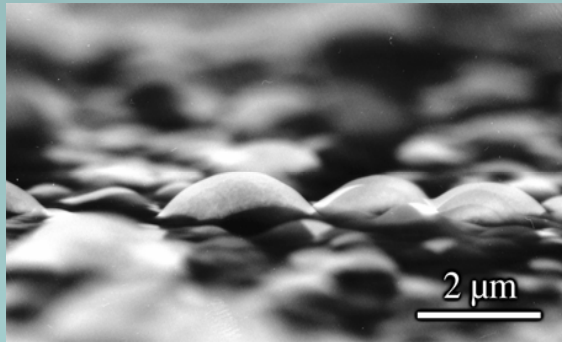
D⁺-irradiated Si with $E = 10$ keV, $\Phi = 1.0 \times 10^{22} \text{ m}^{-2}$



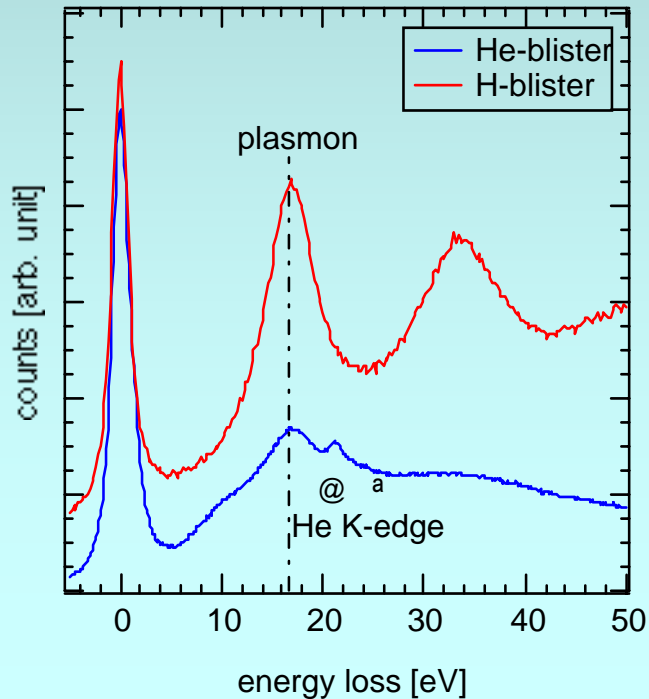
$$r = 2300 \text{ nm}$$

$$t = 82 \text{ nm}$$

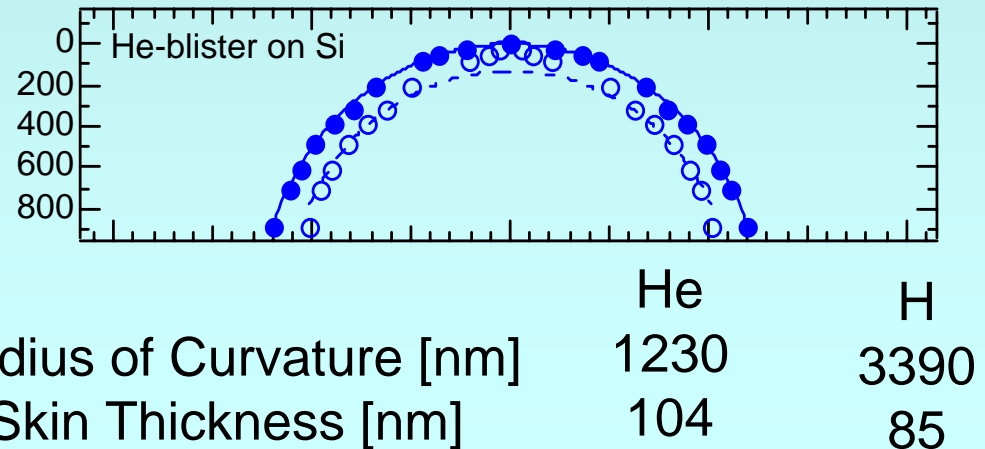
He⁺-irradiated Si with $E = 19 \text{ keV}$, $\Phi = 1.0 \times 10^{22} \text{ m}^{-2}$

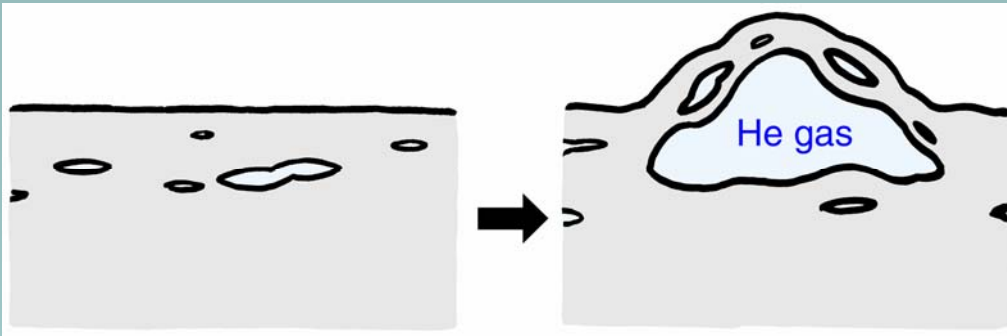


**Amorphous
High dens.
spherical
bubbles**



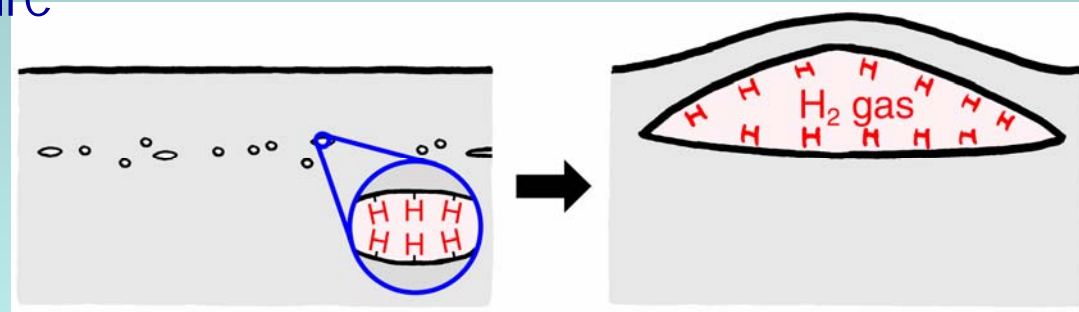
Blister skin
— **Single crystal,**
original orientation remains





Gas bubbles coalesce into larger openings. The inside gas pressure push up the surface.

- small radius of curvature
(high pressure)
- sponge-like structure
(bubble agglomerate)



Formation of Si-H(D) bonds effectively induces large crack along the projected range.

- large radius of curvature
(low pressure)
- uniform skin thickness
(crack propagation)

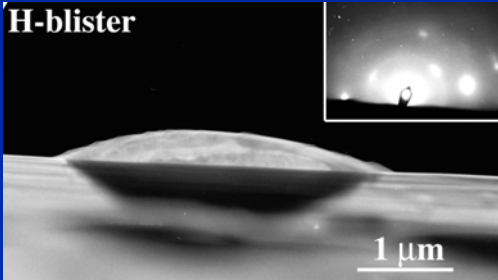

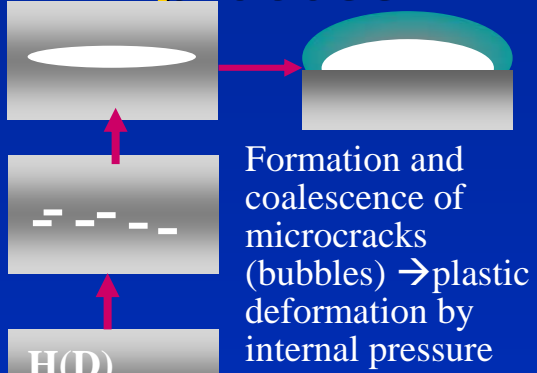
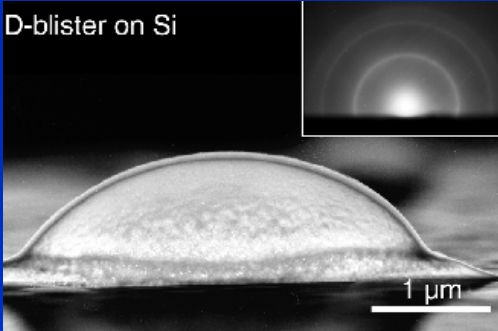
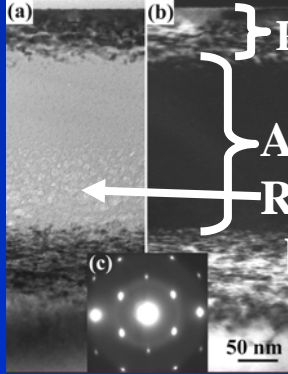
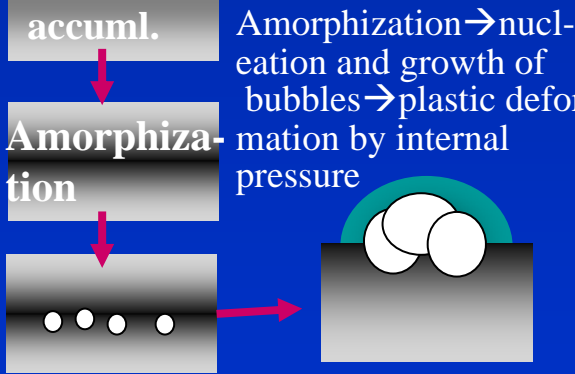
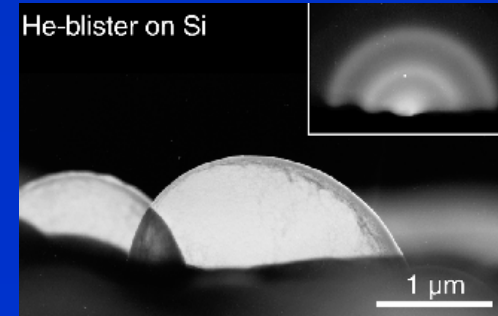
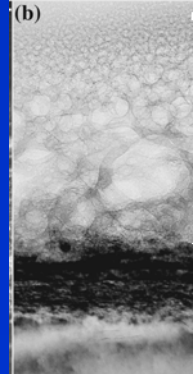
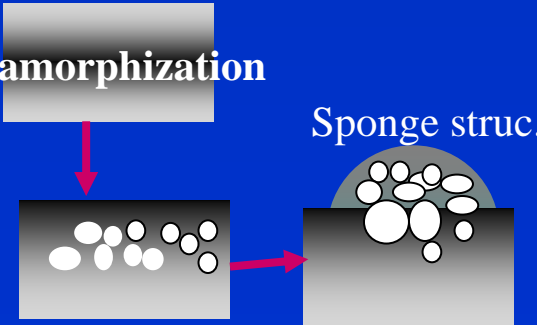
Atom fraction contributing to blistering

	Total number of gas molecules inside, A [m ⁻²]		Total fluence, B [ions/m ⁻²]		2A/B
H-blister	7.9×10^{20}		1×10^{22}		15.8%
D-blister	2.8×10^{21}		1×10^{22}		56%



Van der Waals eq.

Summary of surface blisters on Si

	GIEM	XTEM of precursors	Formation process
H		 <p>Pre-damage lyr Crystalline High dens. defects plate-like bubbles on (100)</p>	 <p>Formation and coalescence of microcracks (bubbles) → plastic deformation by internal pressure</p>
D		 <p>Pre-damage Amorphous Round-shape bubbles</p>	 <p>Amorphization → nucleation and growth of bubbles → plastic deformation by internal pressure</p>
He		 <p>Amorphous High dens. spherical bubbles</p>	 <p>Sponge struc.</p>

H^+ -irradiated Si

$E = 13 \text{ keV}$,

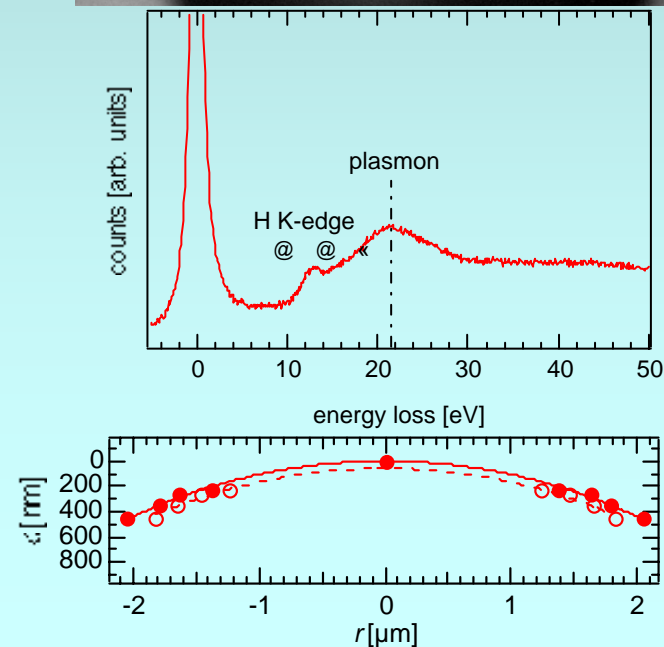
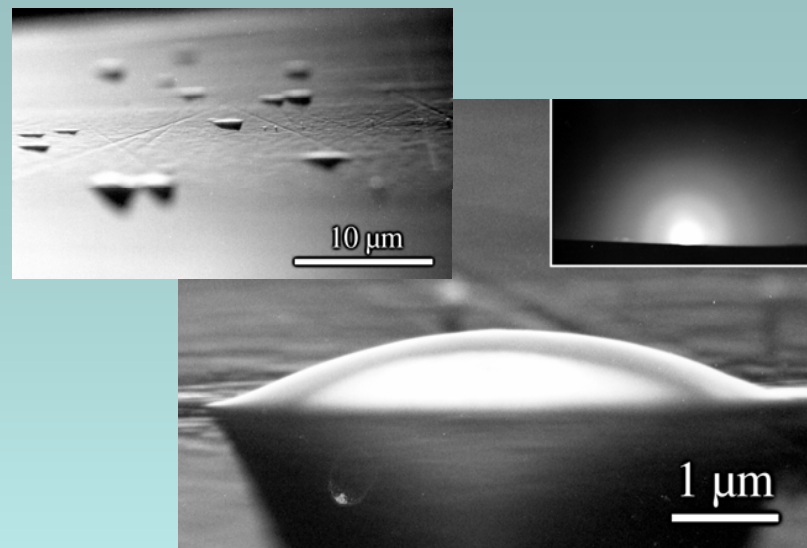
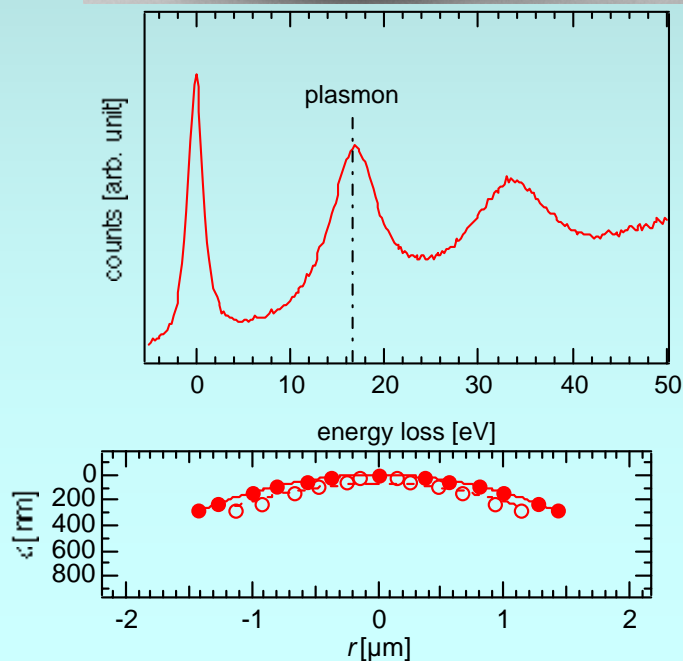
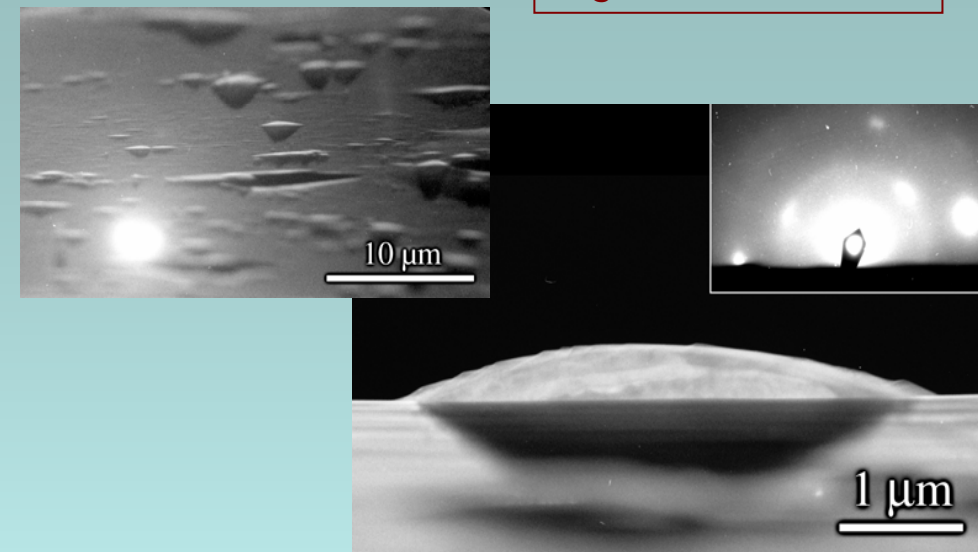
$\Phi = 1.0 \times 10^{22} \text{ m}^{-2}$

SiC needs much
higher fluence

H^+ -irradiated SiC

$E = 16 \text{ keV}$,

$\Phi = 4.0 \times 10^{22} \text{ m}^{-2}$



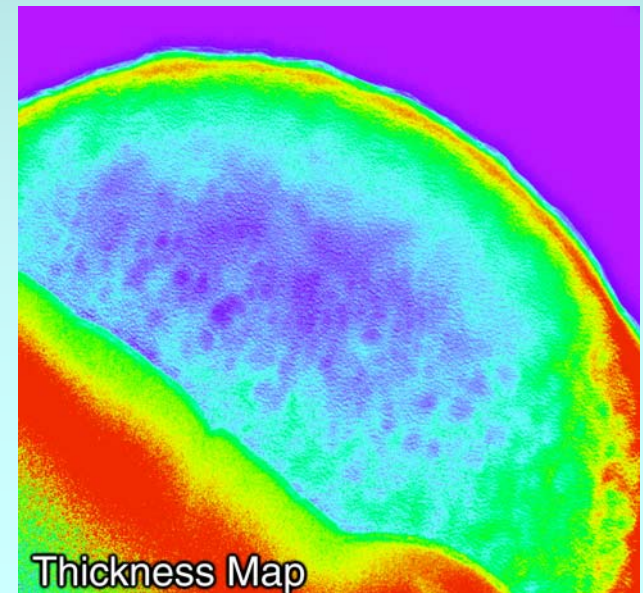
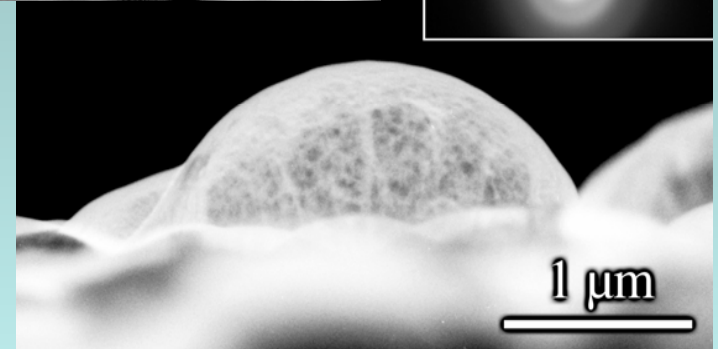
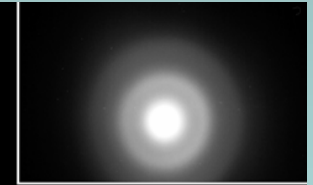
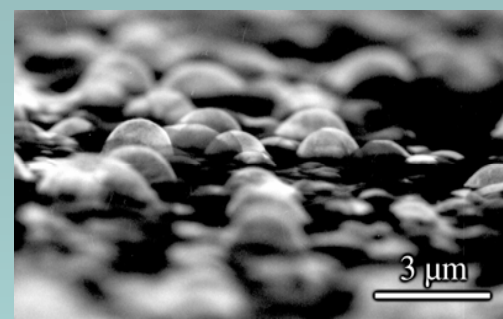
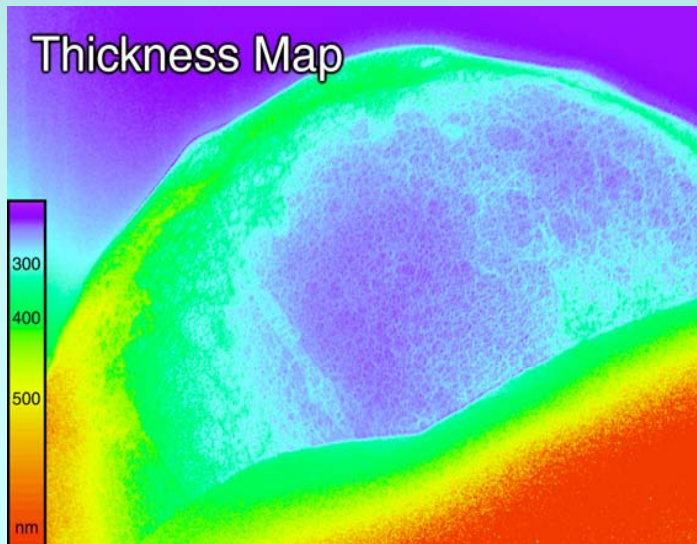
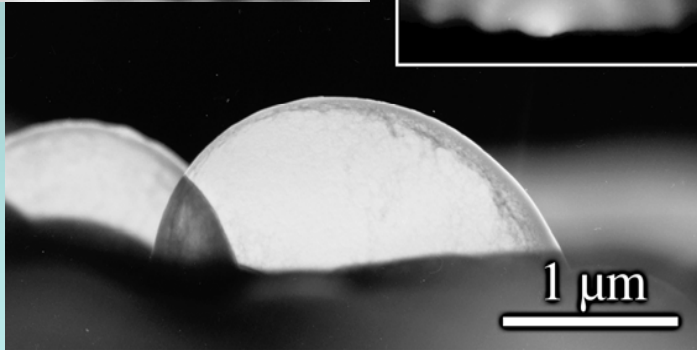
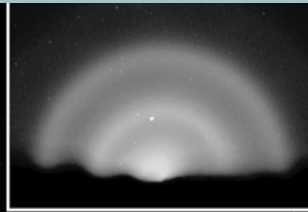
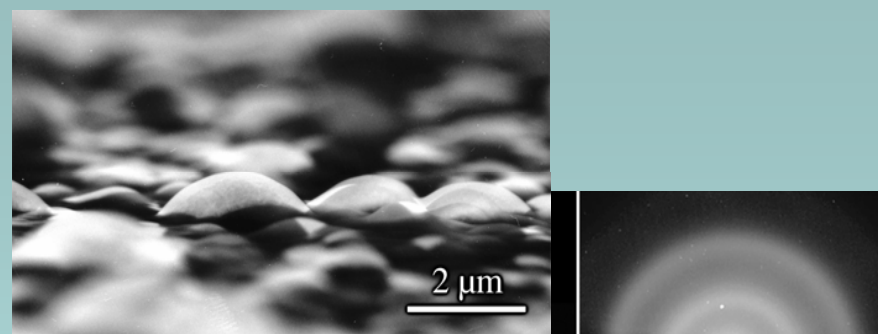
He⁺-irradiated Si

$E = 16 \text{ keV}$, $\Phi = 2.0 \times 10^{22} \text{ m}^{-2}$

Nearly same

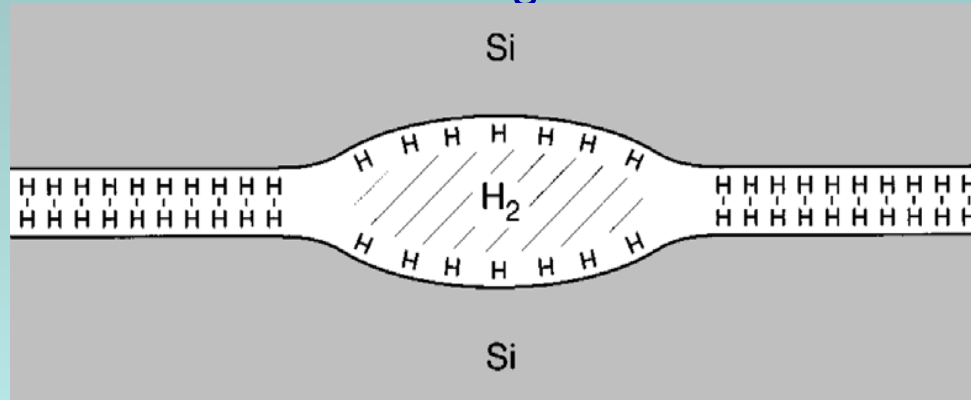
He⁺-irradiated SiC

$E = 19 \text{ keV}$, $\Phi = 2.0 \times 10^{22} \text{ m}^{-2}$



Chemical Effect of Hydrogen

The implant hydrogen atoms effectively terminate broken S-Si bonds along the projected range, which induces micro-cracks followed by coalescence into large cracks to facilitate the blistering.



Question on mechanism of H-blistering on SiC

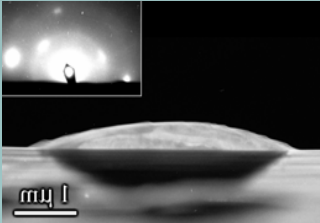
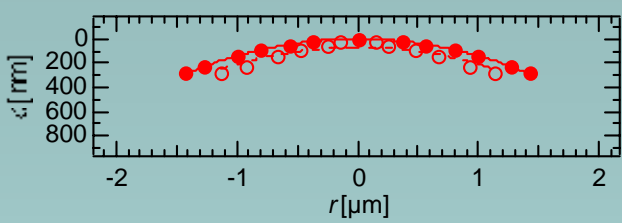
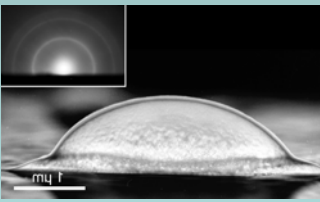
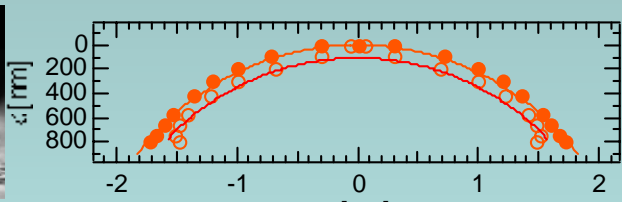
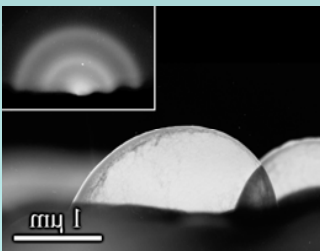
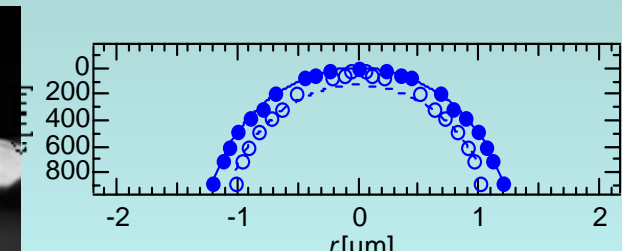
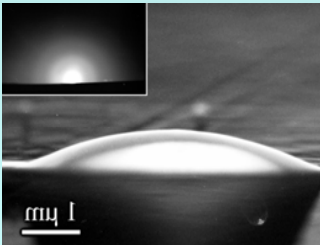
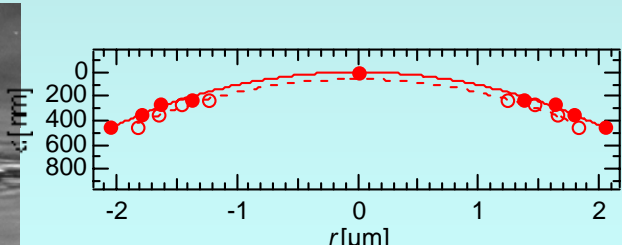
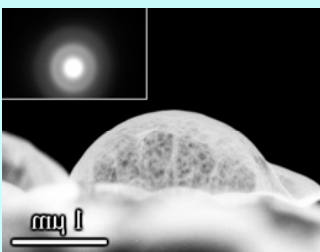
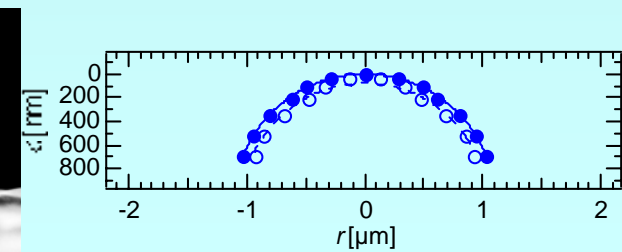
- The uniform thickness of H-blister on SiC suggests that the same mechanism works in the H-blistering as in Si.
- However the critical fluence of H-blistering on SiC is about two times as much as that required for He blistering and four times for H-blistering in Si. This seems to hinder the H-termination effect

Therefore

The difference in critical fluence of H-blistering in Si and SiC should originate from differences in the binding energies of H-Si, H-C, C-C, Si-Si.

	Si-Si	Si-C	Si-H	C-H
Binding Energy [eV/atom]	3.36	4.68	3.10	3.51

1. H atoms break the chemical bonding of Si-C.
2. The once formed Si-H and/or C-H bonds are restored to Si-C.
(Si-C bonds are more stable than the other possible combinations.)
3. Released H atoms can diffuse away out of the sample surface.
(probably escape away as the forms of H_2 , CH_4 , and/or SiH_4)
4. After the matrix is fully disordered, H can start to effectively terminate the broken bonds so as not to increase the total energy significantly.

		Radius	Thickness
H⁺-irradiated Si $E = 13 \text{ keV}$, $\Phi = 1.0 \times 10^{22} \text{ m}^{-2}$	 	3400 nm	85nm
D⁺-irradiated Si $E = 10 \text{ keV}$, $\Phi = 1.0 \times 10^{22} \text{ m}^{-2}$	 	2300 nm	82nm
He⁺-rradiated Si $E = 16 \text{ keV}$, $\Phi = 2.0 \times 10^{22} \text{ m}^{-2}$	 	1200 nm	100nm
H⁺-irradiated SiC $E = 16 \text{ keV}$, $\Phi = 4.0 \times 10^{22} \text{ m}^{-2}$	 	4800 nm	59nm
He⁺-irradiated SiC $E = 19 \text{ keV}$, $\Phi = 2.0 \times 10^{22} \text{ m}^{-2}$	 	1100 nm	78nm

Summary

- 1. Blistering occurs by the gas bubble agglomerate. In Si and SiC, H (D) atoms breaking Si-Si bonds act effectively for crack propagation.**
- 2. Formation mechanism is crack propagation along the damage peak depth. Hence H blister skin was nearly the same to the projected range and its diameter was as large as several mm**
- 3. Skin structure of H-blister: defective crystalline
D-blister: amorphous & nano-sized crystalline
He-blister: amorphous with small he bubbles**
- 4. Hydrogen termination of unsaturated Si bonds effectively acts for blistering. However H-blistering on SiC requires much more fluence, about two times as much as that required for He blistering and four times for H-blistering in Si.**

The differences between Si and SiC can be tentatively explained by the relative differences of binding energies among Si-Si, Si-C, Si-H and C-H.

A quantitative model for chemical sputtering of carbon materials in thermonuclear fusion devices

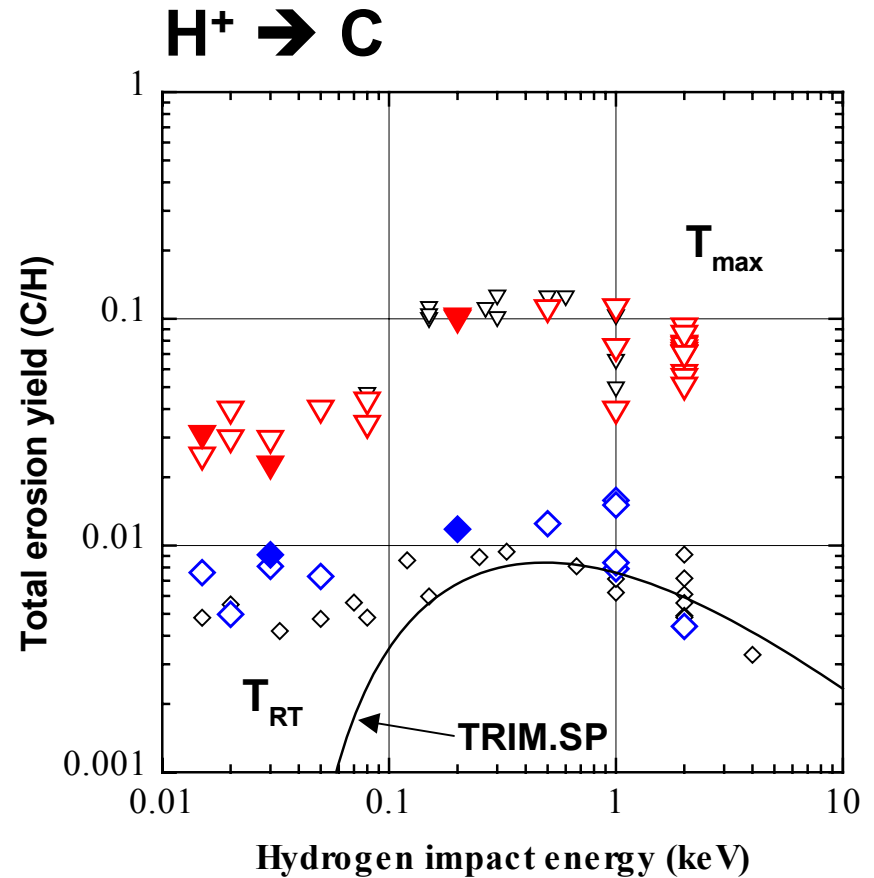
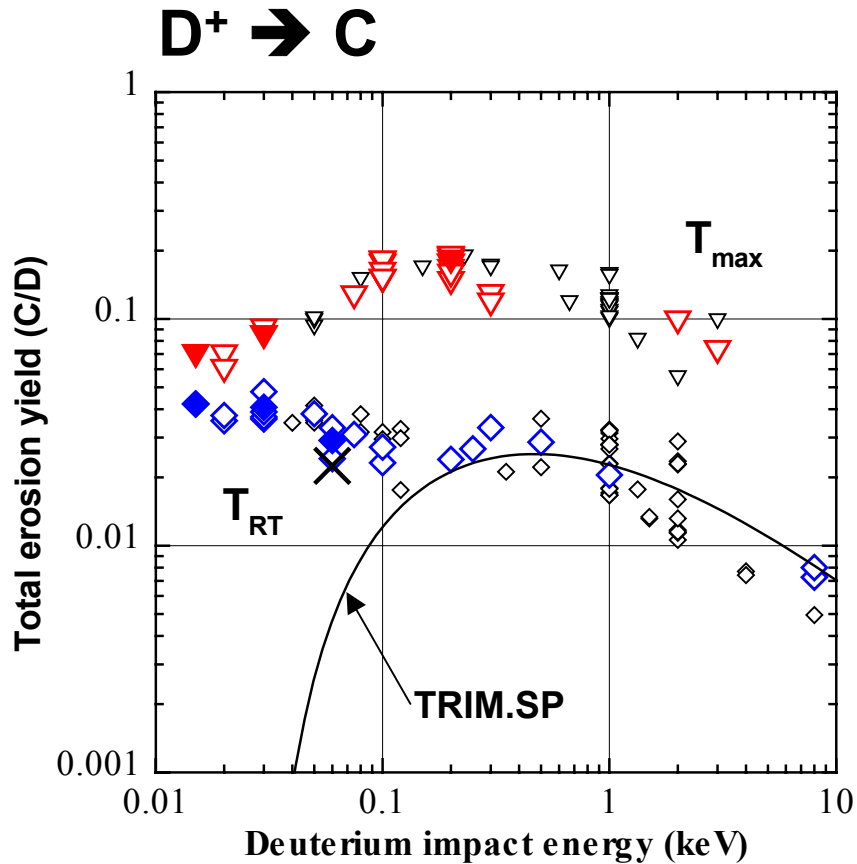
Wolfgang Jacob, Christian Hopf, and Thomas Schwarz-Selinger

Centre for Interdisciplinary Plasma Science

Max-Planck-Institut für Plasmaphysik, 85748 Garching, Germany

Content:

- Chemical erosion, physical sputtering, chemical sputtering
- Chemical Sputtering: Experimental results
- Quantitative model - energy dependence
- Summary



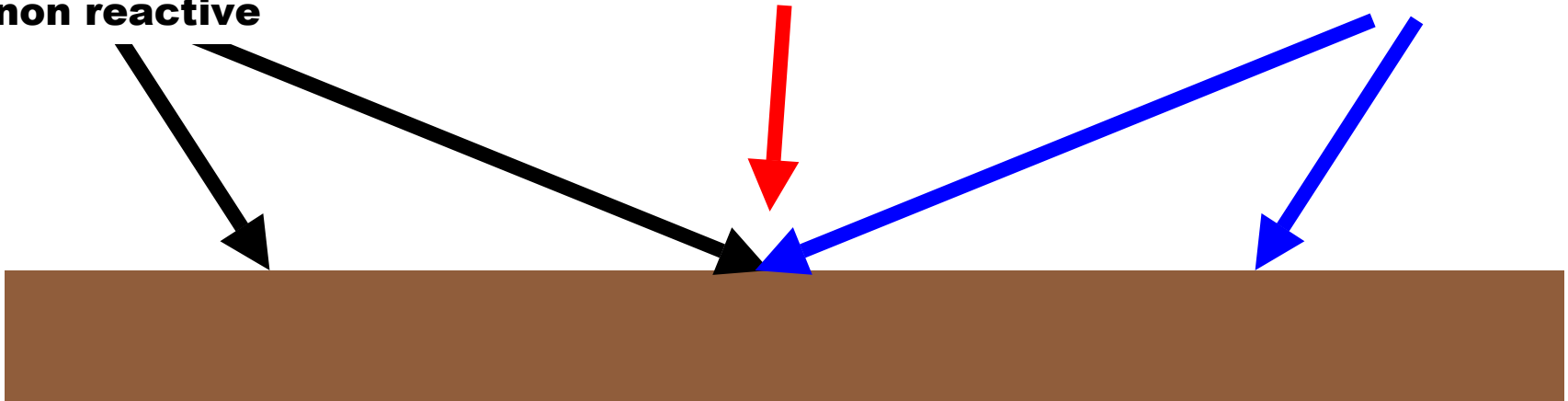
M. Balden, J. Roth, J. Nucl. Mater. **280**, 39-44 (2000)

New weight-loss measurements of the chemical erosion yields of carbon materials under hydrogen ion bombardment

**ions or energetic neutrals
non reactive**

reactive ions

H atoms



Physical sputtering

- threshold energy
- energy dependence (TRIM.SP)
- isotope effect (kinematic factor)
- no significant T dependence
- all species (incl. inert gases)

Chemical sputtering

- **ions + neutrals**
- **energy dependence**
- **T dependence**
- **very low threshold energy**
- **isotope effect**
- **ion-to-neutral ratio dep.**
- **high erosion yield**

Chemical erosion

- thermally activated (no threshold energy)
- no isotope effect
- requires chemically reactive species

Sputtering with reactive ions: physics meets chemistry

H and D bombardment of carbon

Chemical erosion, ion-induced chemical erosion, ion-enhanced chemical erosion, ion-induced etching, reactive ion etching, chemically enhanced physical sputtering, chemical sputtering, ...

A simple picture:

Chemical reactions take place at the end of range, when H isotopes are thermalized.

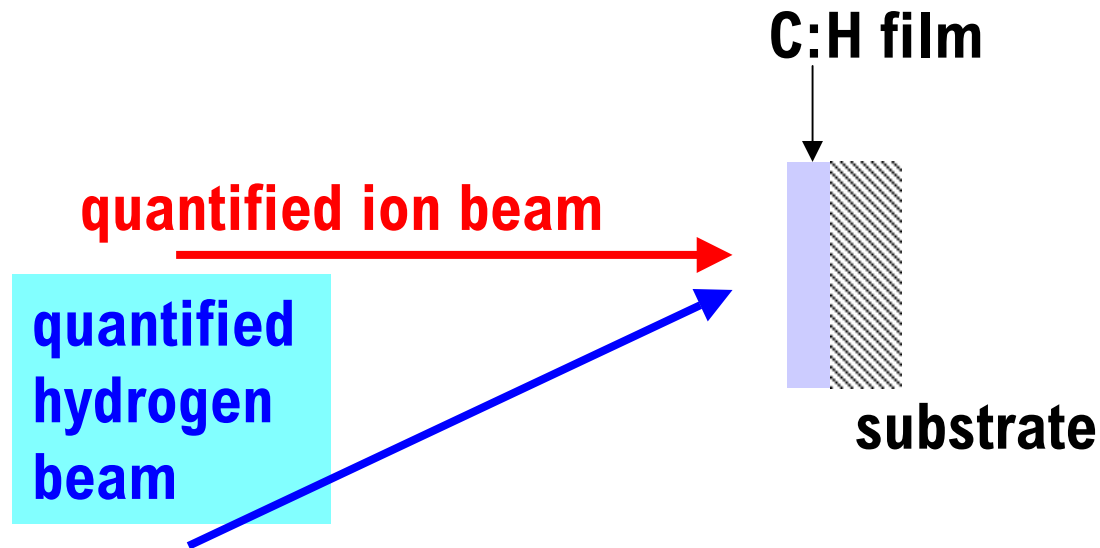
Molecules are formed locally, then they diffuse to the surface and desorb.

➔ temperature dependence of process

Temperature dependence relatively well understood,
but what about the energy dependence?

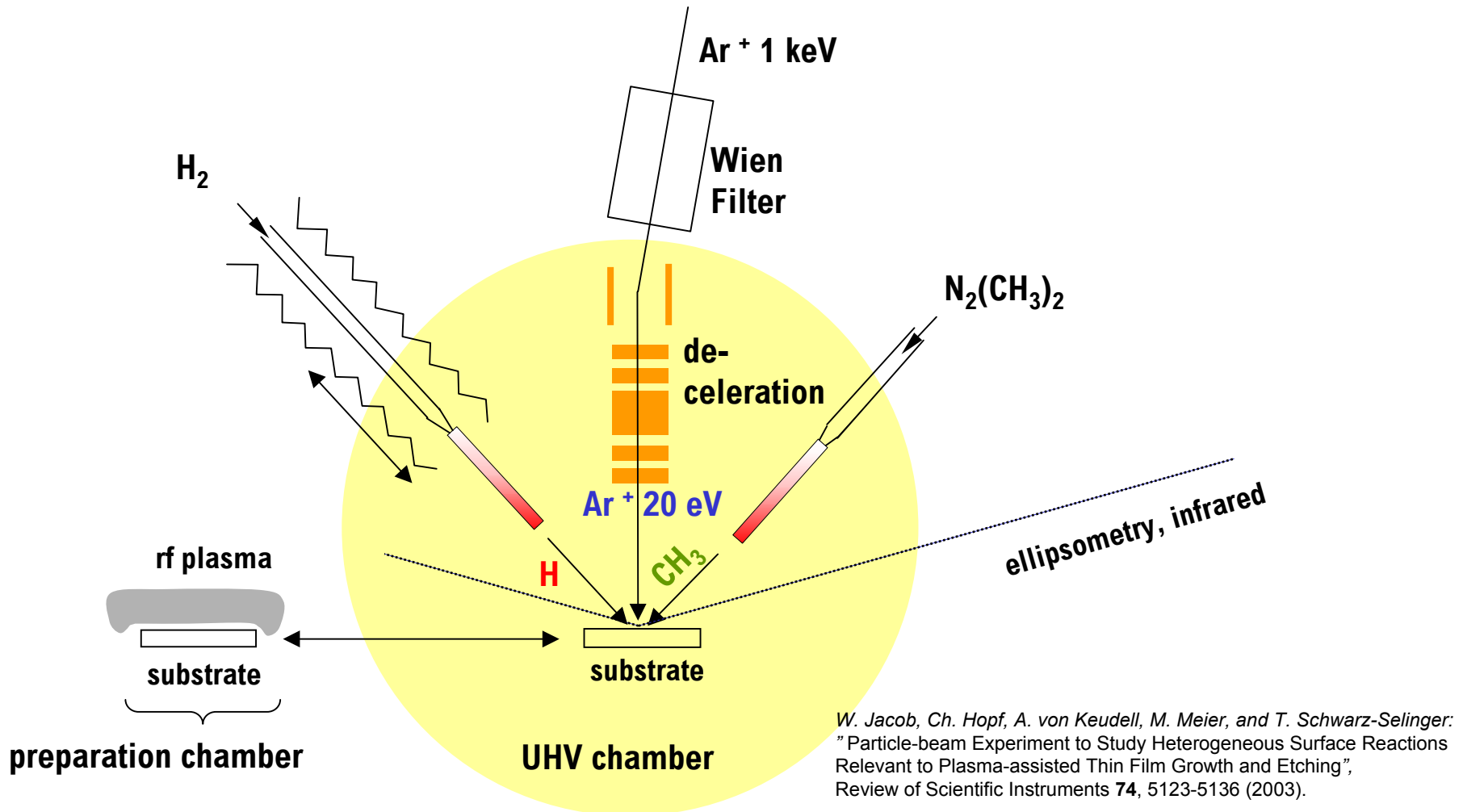
Particle-beam experiments

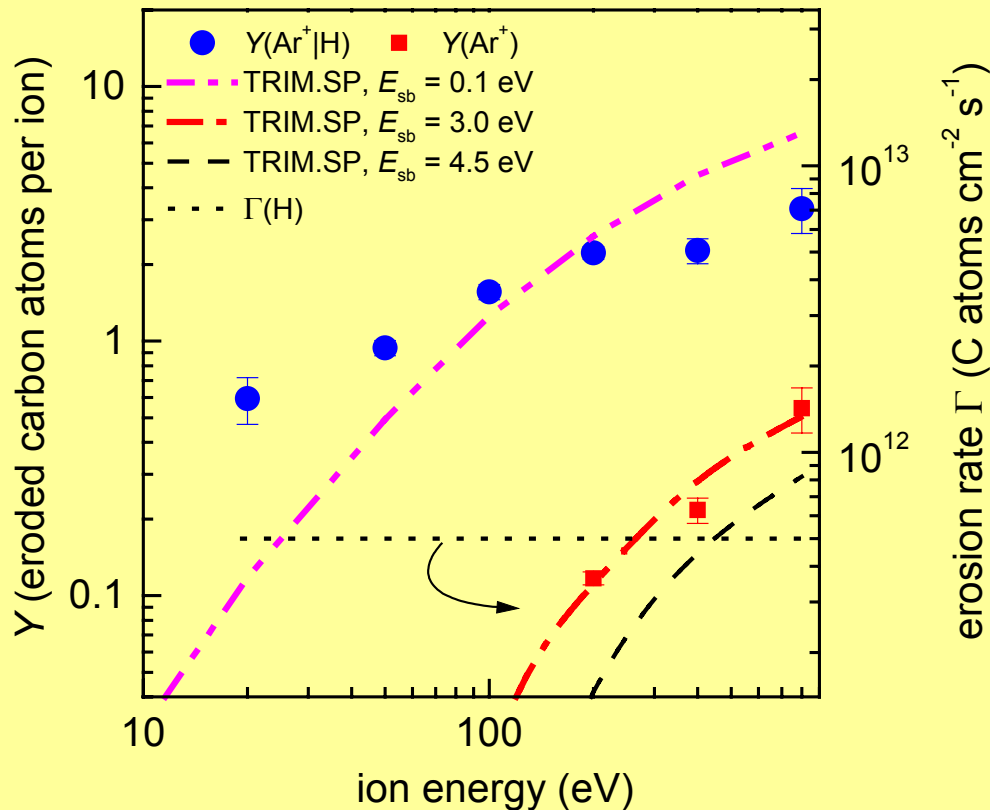
Chemical sputtering



$$\text{erosion yield} = \frac{\text{measured erosion rate in eroded carbon atoms per cm}^{-2}\text{s}^{-1}}{\text{impinging ion flux per cm}^{-2}\text{s}^{-1}}$$

UHV experiment with 2 radical beam sources and one ion beam source





Erosion of a-C:H layers

comparison of simple **physical sputtering** (red symbols) due to Ar ions with erosion due to simultaneous interaction of H and Ar^+ (blue symbols).

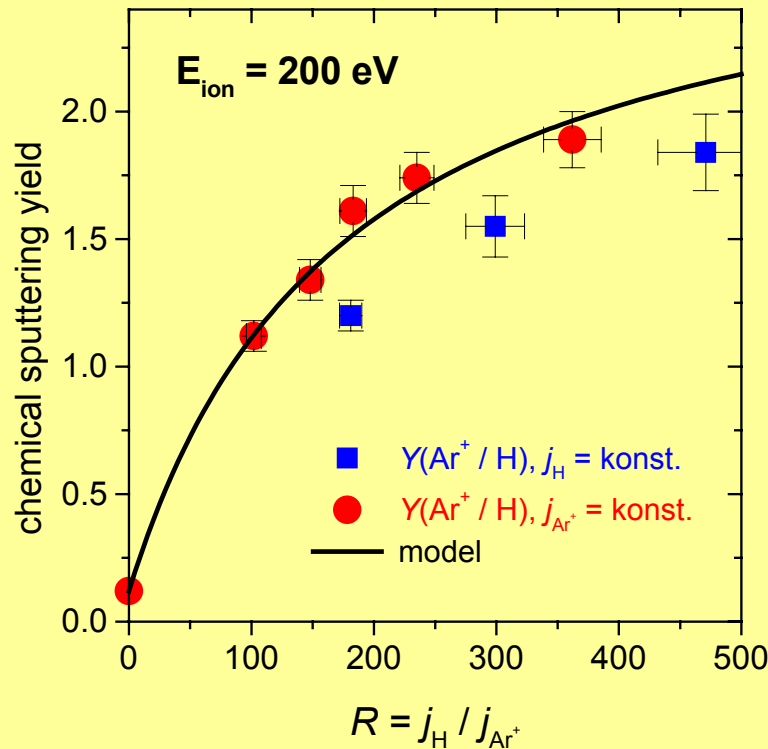
- enhanced erosion above 200 eV for simultaneous interaction
- erosion below threshold for physical sputtering (threshold energy for physical sputtering $\approx 60 \text{ eV}$)
- erosion at 20 eV \gg pure chemical erosion \Rightarrow '**chemical sputtering**'

- separation of chemical and kinematical effects due to use of Ar^+ and H
- neutral / ion ratio ≈ 400

Christian Hopf, PhD Thesis

Ch. Hopf, A. von Keudell, and W. Jacob, "Chemical Sputtering of Hydrocarbon Films by Low-energy Ar^+ Ions and H Atom Impact", *Nuclear Fusion* **42**, L27 (2002).

Ch. Hopf, A. von Keudell, and W. Jacob, "Chemical Sputtering of Hydrocarbon Films", *J. Appl. Phys.* **94**, 2373 (2003).



$$Y_{\text{Modell}} = Y_{\text{phys}}(1 - \Theta_{\text{CH}}) + Y_{\text{chem}}\Theta_{\text{CH}}$$

$$n_0 \frac{d\Theta_{\text{CH}}}{dt} = j_H(1 - \Theta_{\text{CH}})p_{\text{Einbau}}^H - j_{\text{Ion}}\Theta_{\text{CH}}p_{\text{Freisetzung}}^H$$

Mit $R = j_H / j_{\text{Ion}}$ und $S = p_{\text{Freisetzung}}^H / p_{\text{Einbau}}^H$

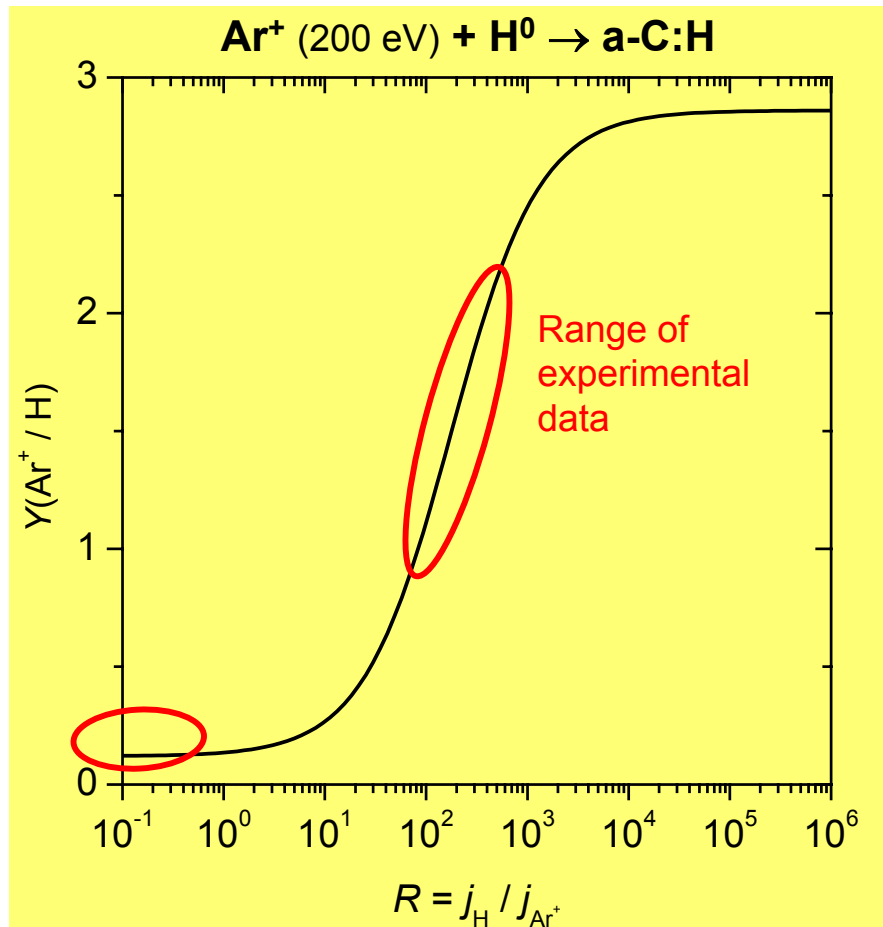
$$Y_{\text{Modell}} = Y_{\text{phys}} + \frac{R}{R + S}(Y_{\text{chem}} - Y_{\text{phys}})$$

Fit parameters:

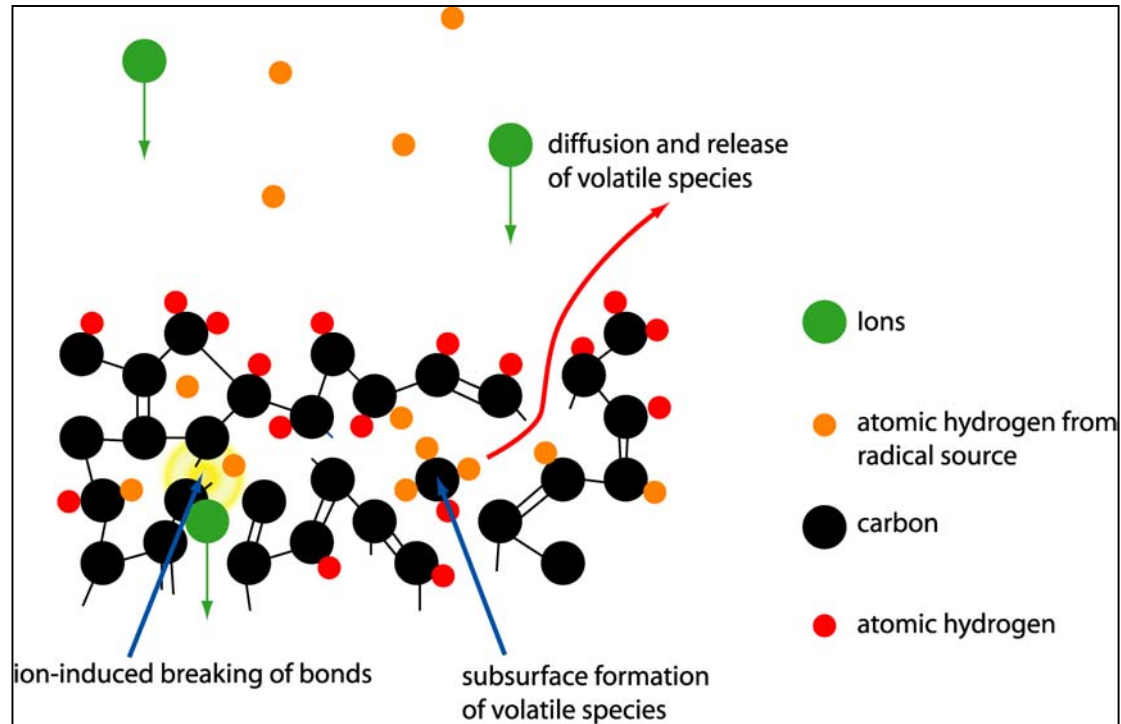
$$S = 176$$

$$Y_{\text{chem}} = 2.86$$

$$Y_{\text{phys}} = 0.12$$



Saturation requires
much more H than ions
($R > 1000$)



- ions break C—C bonds
- H passivates broken bonds
- (1) and (2) → formation of volatile hydrocarbons below the surface
- diffusion of CH compounds to the surface and desorption

$$Y(ions | H) \propto \int y_{bb}(x) \cdot p_{pass}(x) dx$$

bond breaking due to ion impact

passivation by atomic H

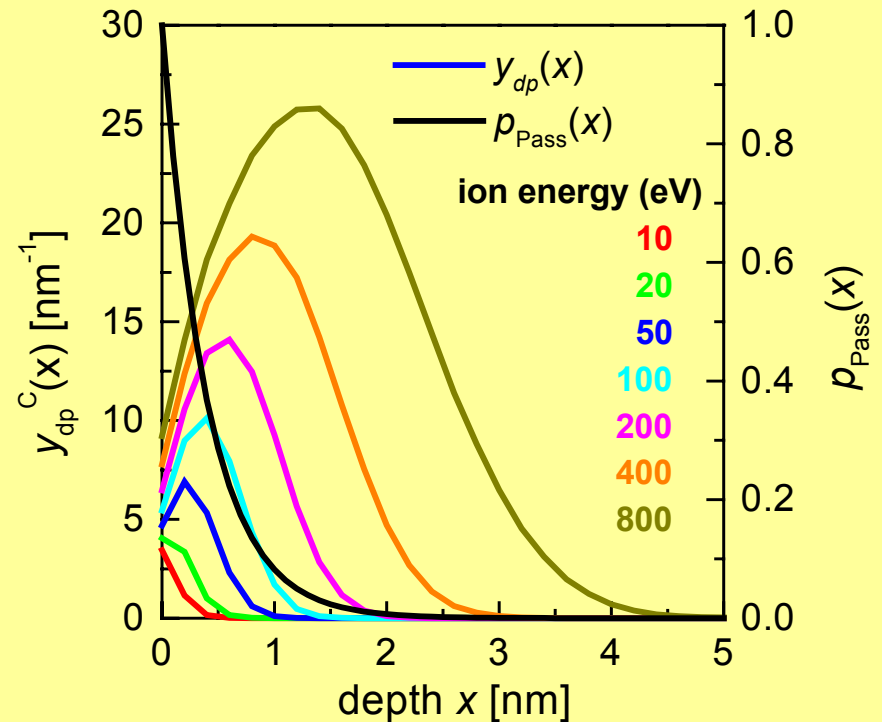
$$Y(ions | H) = a \cdot \int y_{dp}(x) \cdot e^{(-x/\lambda)} dx$$

displacement events per depth interval calculated by TRIM.SP

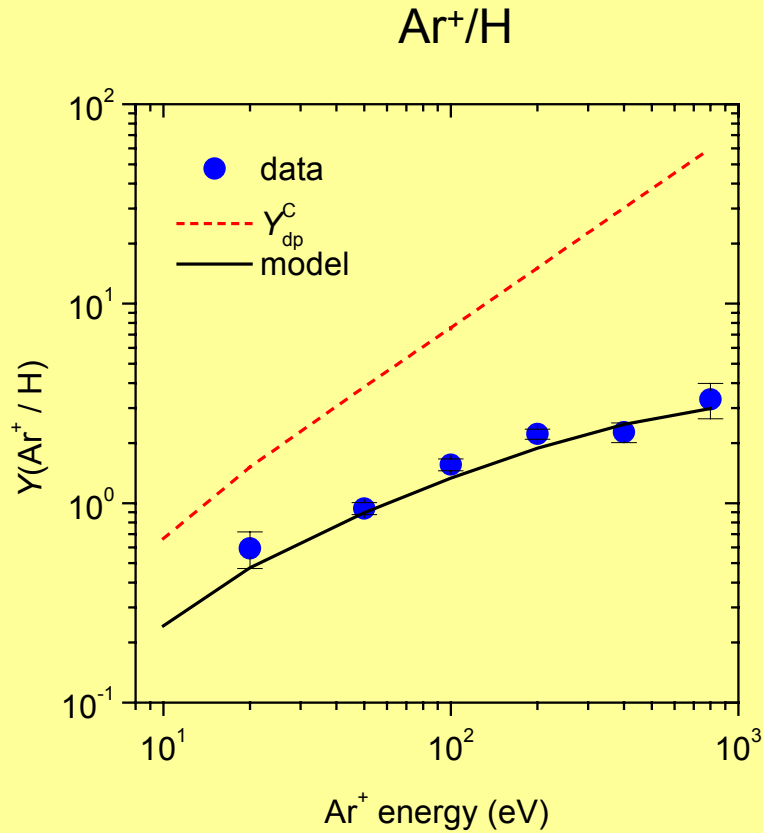
exponential decay, maximum range about 2 nm, known from plasma experiments

a is a fit parameter

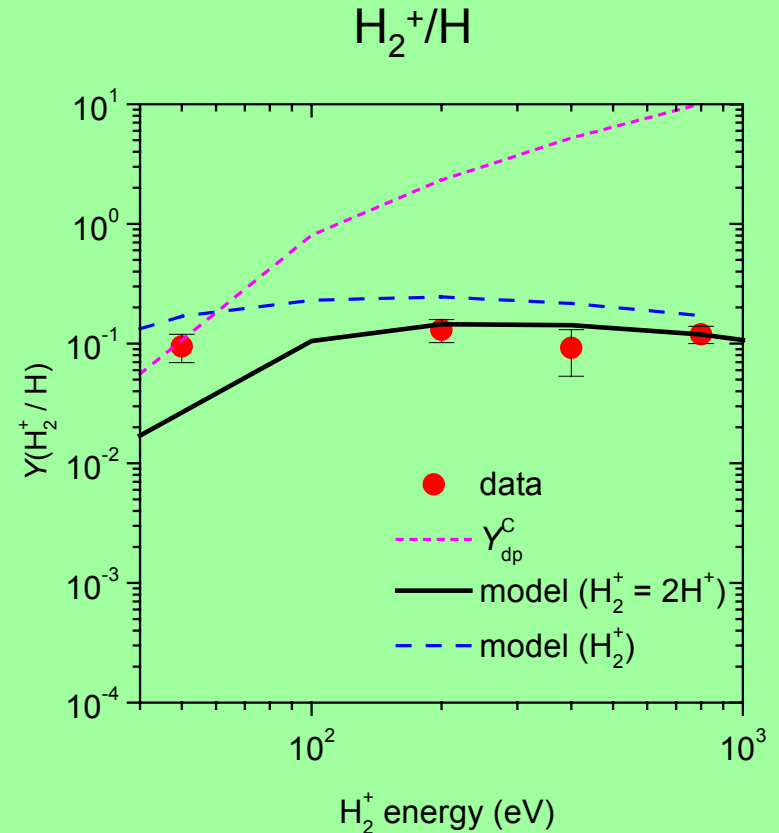
TRIM.SP simulations for Ar ions



$$E_{dp}^C = 5 \text{ eV}, \lambda = 0.4 \text{ nm}$$

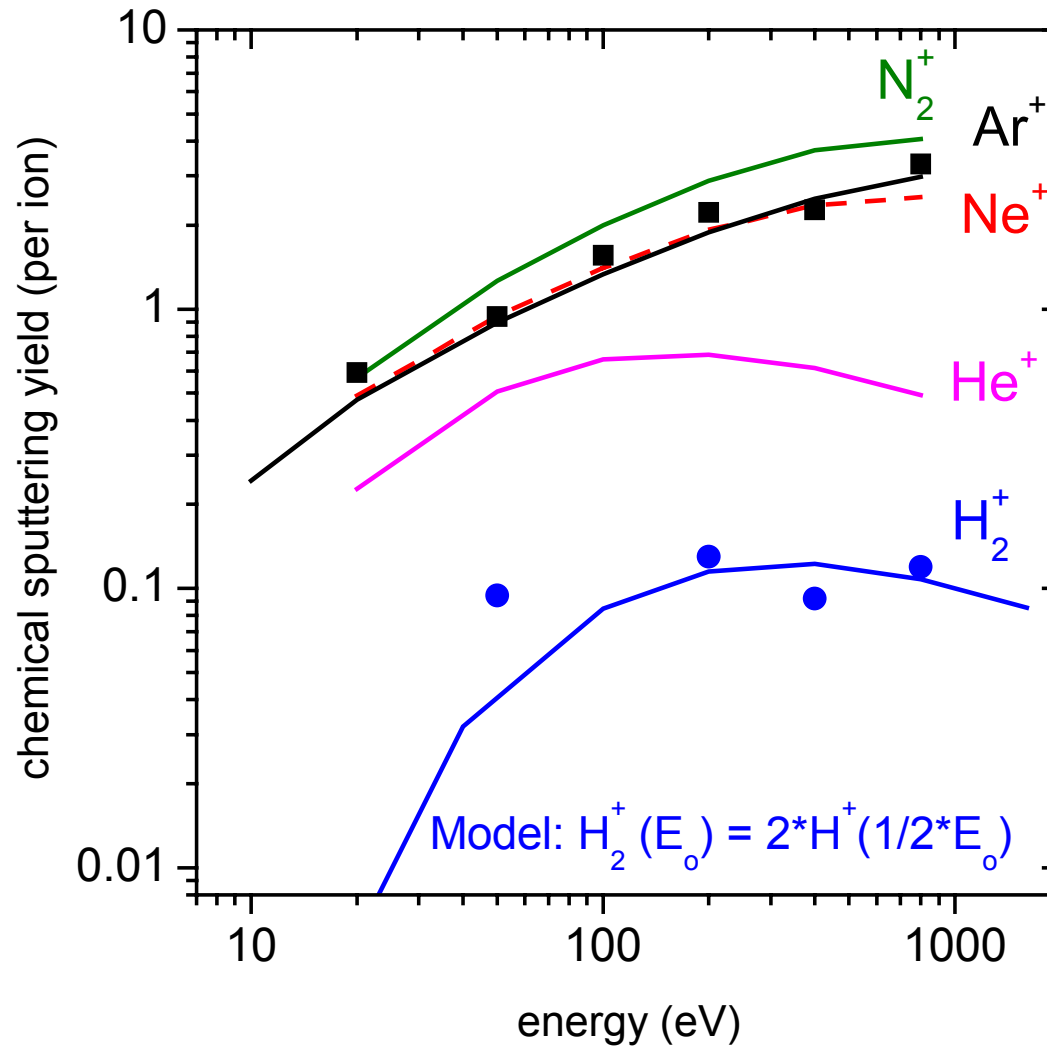


$a = 0.4$



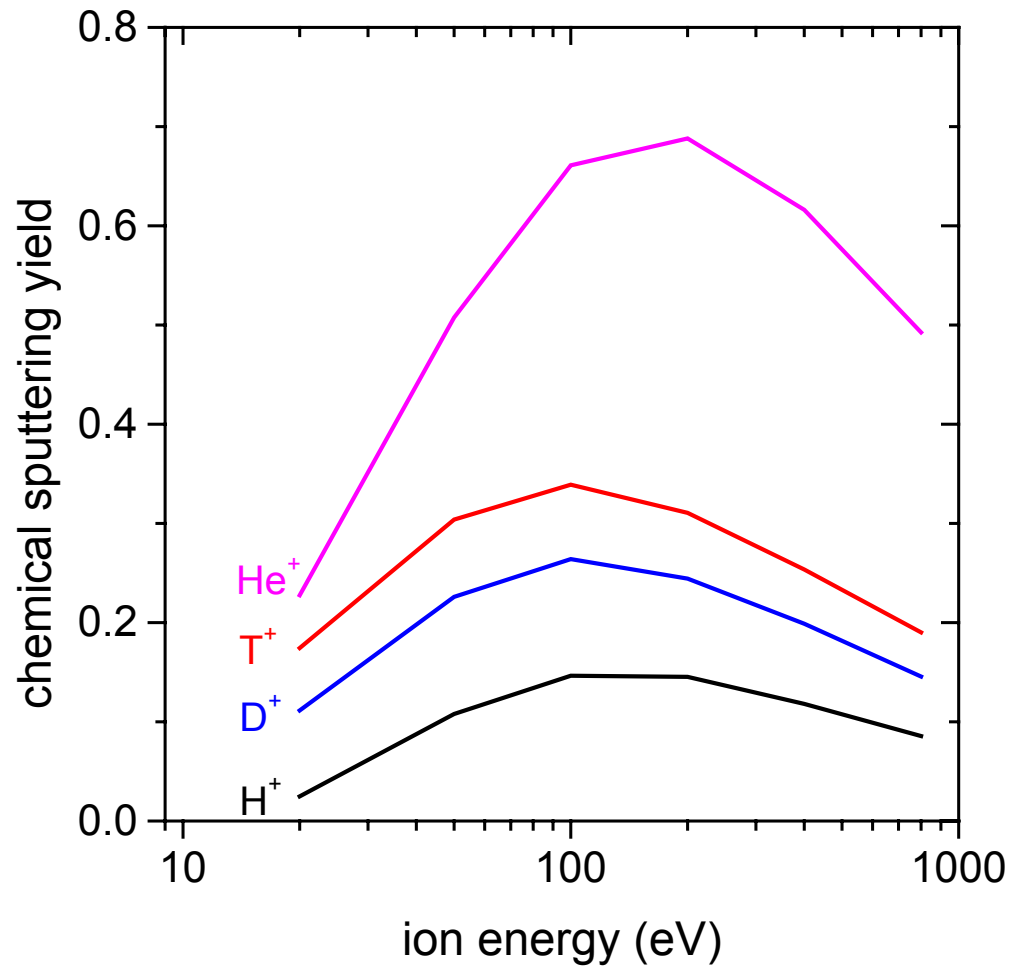
$a = 0.4$

$$j_{\text{H}} = 1.4 \times 10^{15} \text{ cm}^{-2} \text{ s}^{-1}, j_{\text{Ar}^+} = 3.6 \times 10^{12} \text{ cm}^{-2} \text{ s}^{-1}, R = j_{\text{H}}/j_{\text{Ar}^+} \approx 400$$



$a = 0.4$
 $R \approx 400$

Fusion relevant species



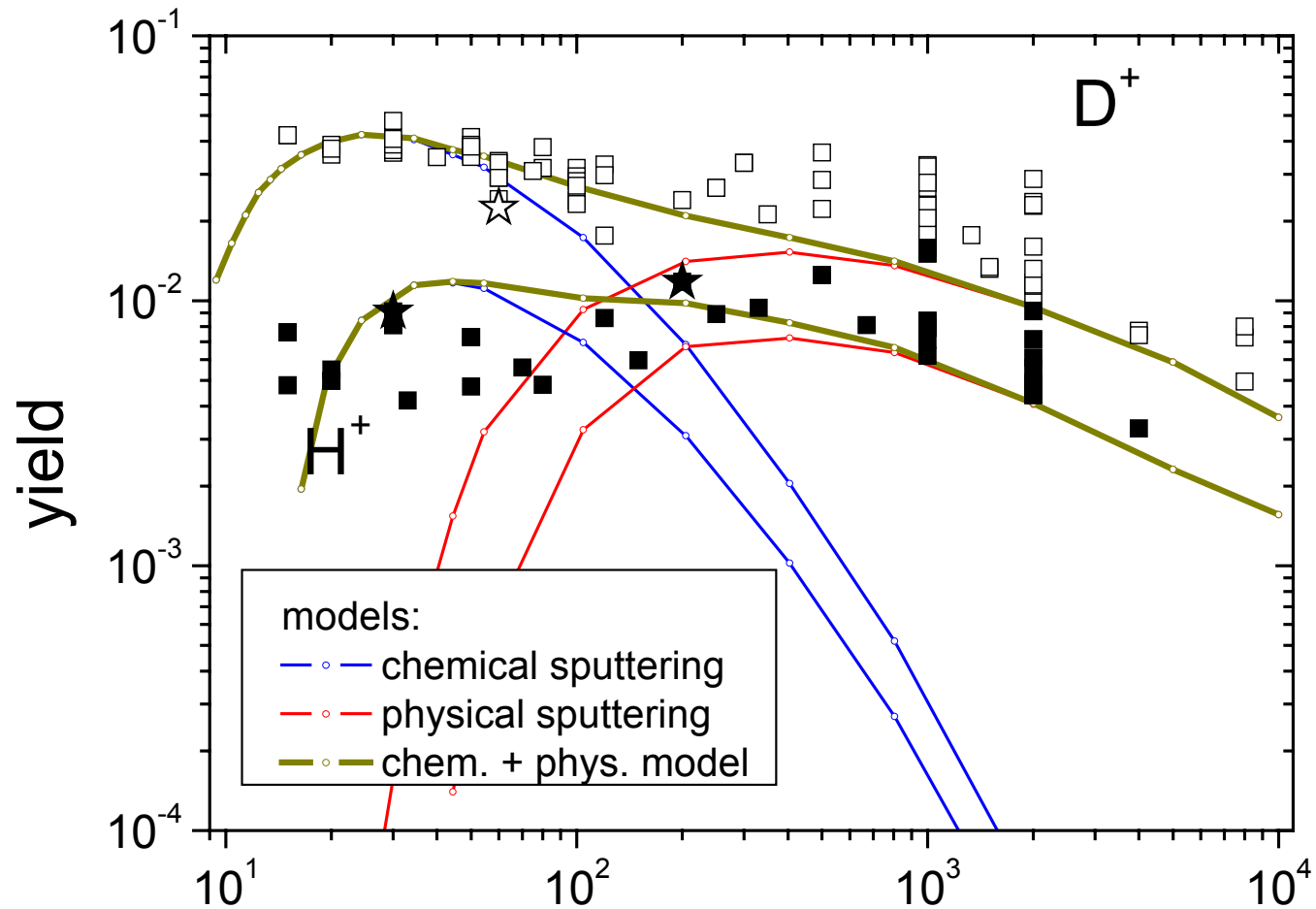
$a = 0.4$
 $R \approx 400$

- **Physical sputtering:** for the most part well understood
 - well modeled by TRIM.SP (binary collision approximation)
 - energy, projectile mass, angle, roughness
- **Chemical erosion:** for the most part well understood
 - thermally activated process
 - can be influenced by doping

- ***Chemical sputtering:*** increase of yield and lowering of threshold
- flux ratio dependence (rate equation model): high H fluxes required
- mechanistic model for *chemical sputtering*
- energy dependence: bond breaking \times passivation
- predictions for other ions, e.g. H, D, T, He, N₂, ..

Growth of a-C:H is always a competition between deposition and erosion (chemical sputtering).

H^+ , D^+ \rightarrow graphite



C. Hopf, unpublished results

total yield = chemical sputtering + physical sputtering

$$Y(E) = \int y_{\text{dp}}^{\text{C}}(x, E) n(x, E) \exp(-x / \lambda) dx + Y_{\text{phys}}(E)$$

$Y_{\text{phys}}(E)$ phys. sputtering yield

TRIM.SP

$y_{\text{dp}}^{\text{C}}(x, E)$ ion induced damage

$$E_{\text{sb}}^{\text{C}} = 7.4 \text{ eV}$$

$n(x, E)$ implanted hydrogen

$$E_{\text{dp}}^{\text{C}} = 5.0 \text{ eV}$$

$\exp(-x/\lambda)$ depth dependent probability
for outdiffusion of erosion
products

$$\lambda = 0.4 \text{ nm}$$

The end

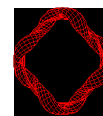
Collaborators:

Christian Hopf

Achim von Keudell

Michael Schlüter

Thomas Schwarz-Selinger



*Laboratorio Nacional de Fusión
Asociación EURATOM-CIEMAT*

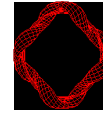
Initial results on carbon film removal by thermo-oxidation in low pressure nitrogen oxides

D. Tafalla and F.L. Tabarés

Laboratorio Nacional de Fusión por Confinamiento Magnético.

Asociación EURATOM-CIEMAT. Madrid, Spain

α -C:H codeposited layers



*Laboratorio Nacional de Fusión
Asociación EURATOM-CIEMAT*

Accumulation of tritium by codeposition with carbon (α -C:T) affects to operation and safety of ITER if CFCs are used.

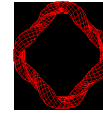
Tritium accumulated in areas with access to direct plasma could be removed by D plasma discharge or wall conditioning techniques (GDC, ICRF).

α -C:H layers can be deposited far away from the main chamber in places non accessible by plasma (JET, ASDEX-U)

Strategies:

- Prevention of codeposition: reducing the chemical erosion of CFC, inhibition of C-layers (scavengers),
- Removal of α -C:T layers "in-situ" after discharge periods (overnight)

Removal of a-C:H layers

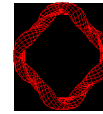


*Laboratorio Nacional de Fusión
Asociación EURATOM-CIEMAT*

Several approaches have been proposed and tested:

- Thermal desorption: high temperature required
- Physical, photochemical, laser ablation: difficult access to hidden areas.
- Thermo-oxidation: heating of C-layer in presence of a oxidizing agent.
up to now, probably most promising.

Thermo-oxidation of a-C:H layers



Laboratorio Nacional de Fusión
Asociación EURATOM-CIEMAT

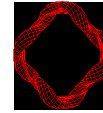
Up to now, a great diversity of samples, including graphites, tokamak codeposits and plasma-deposited films (hard and soft), have been oxidised using air, O_2 or even O_3 (*J.W. Davis and A.A. Haasz. Phys. Scr. T91, 33-35 (2001)*).

As general conclusions:

The removal rate strongly depends on the structure of the layer : Tokamak co-deposits and soft films are oxidized easier than hard films.

$T > 523$ K are necessary for an efficient removal being the efficiency a function of the temp. and the O_2 pressure

ITER restrictions



Laboratorio Nacional de Fusión
Asociación EURATOM-CIEMAT

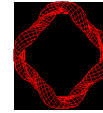
The heating in ITER is restricted to temp $< 520\text{K}$
and oxidizing gas pressure to $p < 100\text{ kPa}$ (1 atm)

under these restrictions only a few studies have been
carried out showing low removal efficiency.

TFTR sample: 10 h at 240°C and 1 kPa in O_2
removed $1/3$ of T

W.M. Shu et al. Fus. Eng. Des. 61-62, 599 (2002)

Alternatives



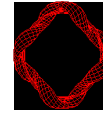
*Laboratorio Nacional de Fusión
Asociación EURATOM-CIEMAT*

In consequence, O_2 presents same problems for removal α -C:H layers under the strict conditions of ITER.

Question: Are there reliable alternatives?

- Thermo-oxidation in other oxidizing agents:
nitrogen oxides: NO , NO_2 , N_2O
hydrogen peroxide (H_2O_2)
- Isotopic exchange reactions: using H_2/D_2 or molecule rich in H/D (H-C).

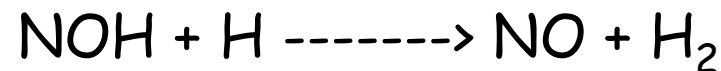
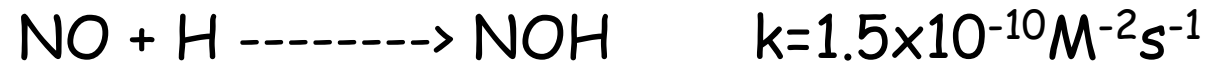
Nitrogen oxides (NO)



Laboratorio Nacional de Fusión
Asociación EURATOM-CIEMAT

Advantages:

- Strong oxidizing agent
- Gas phase reaction:



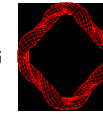
(option to remove T_2 and not T_2O)

- From catalysis studies:

Carbon is widely used in heterogeneous decomposition of NO_x (decontamination)
specific reactivity of NO_x with carbon.

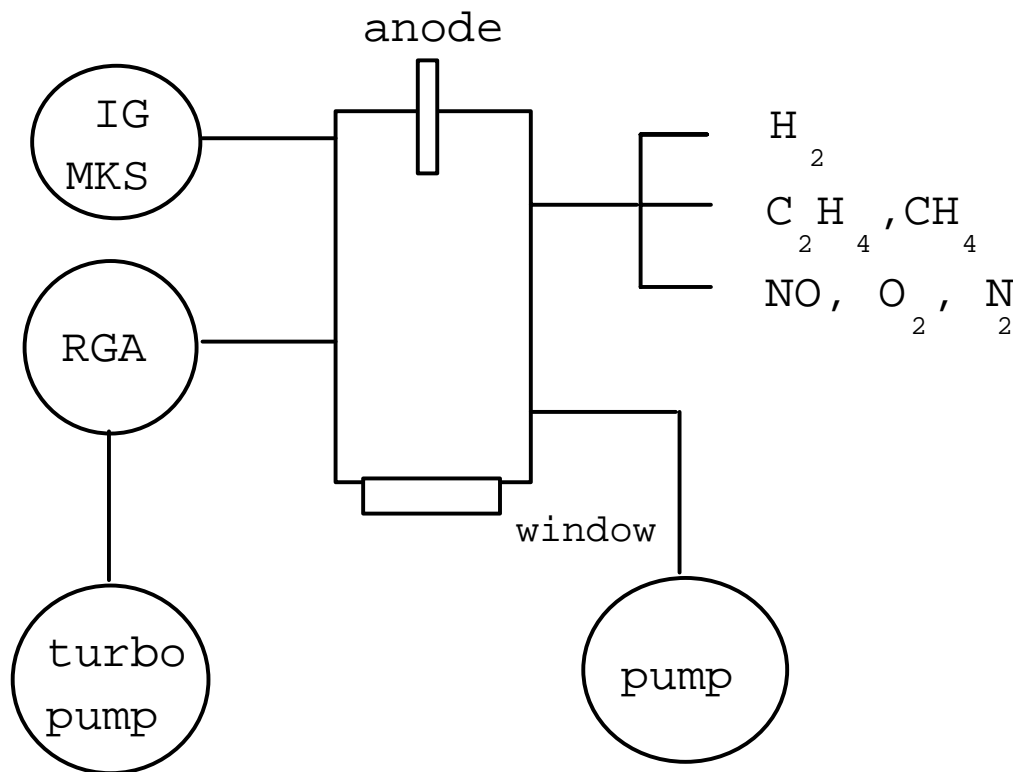
J. Zawadzki et al. Carbon 41, 235 (2003)

Experimental set-up



Laboratorio Nacional de Fusión
Asociación EURATOM-CIEMAT

vacuum chamber baked up to 573 K



α -C:H deposition:

H_2/C_2H_4 Glow discharge

$p = 0.1$ torr, $I_p = 100$ mA

$t = 1$ h

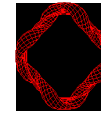
C film: soft type

Thermo-oxidation:

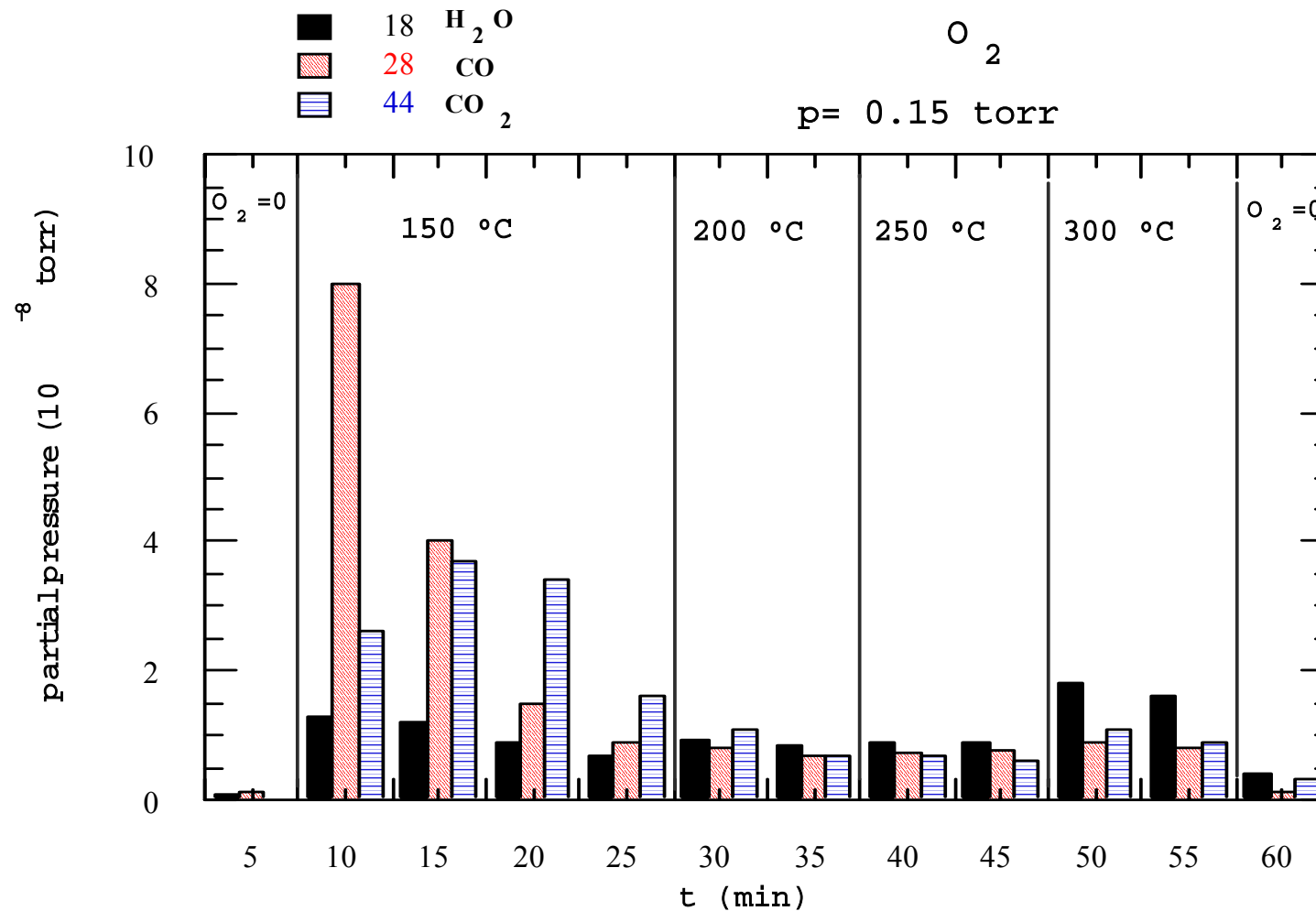
NO, O_2 (function of p , T)

All the process followed
by RGA measurements

O_2 thermo-oxidation (reference)

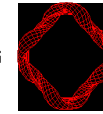


Laboratorio Nacional de Fusión
Asociación EURATOM-CIEMAT



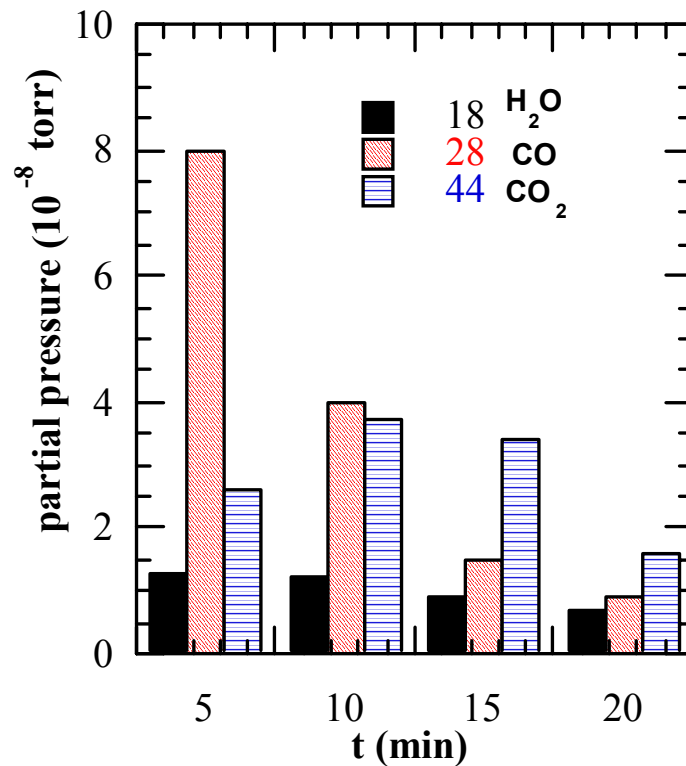
The soft C-film seems to be easily oxidized under these conditions

NO thermo-oxidation

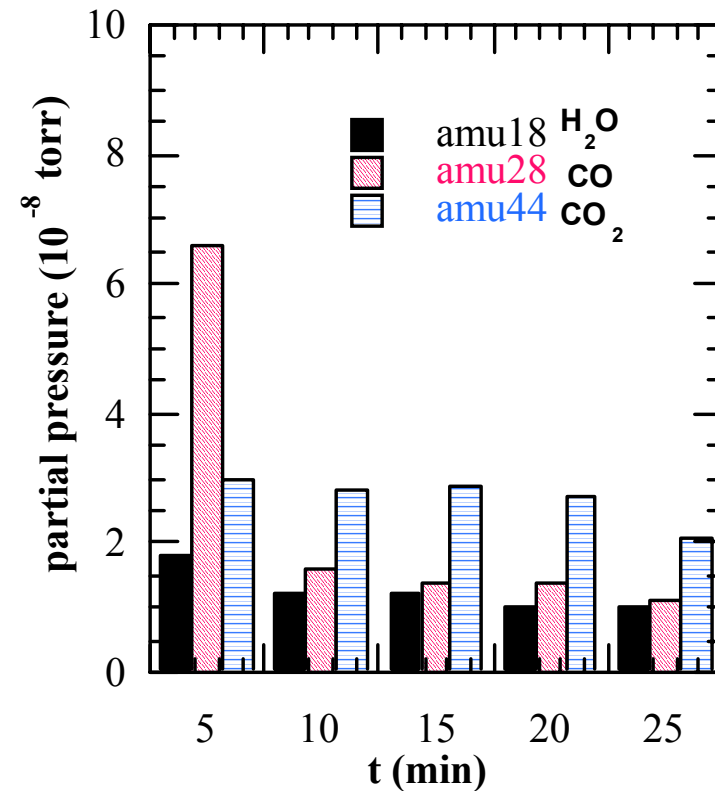


Laboratorio Nacional de Fusión
Asociación EURATOM-CIEMAT

O_2 ($p = 0.15$ torr)
 $T = 150$ °C

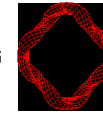


NO oxidation, $p = 0.15$ torr
 150 °C

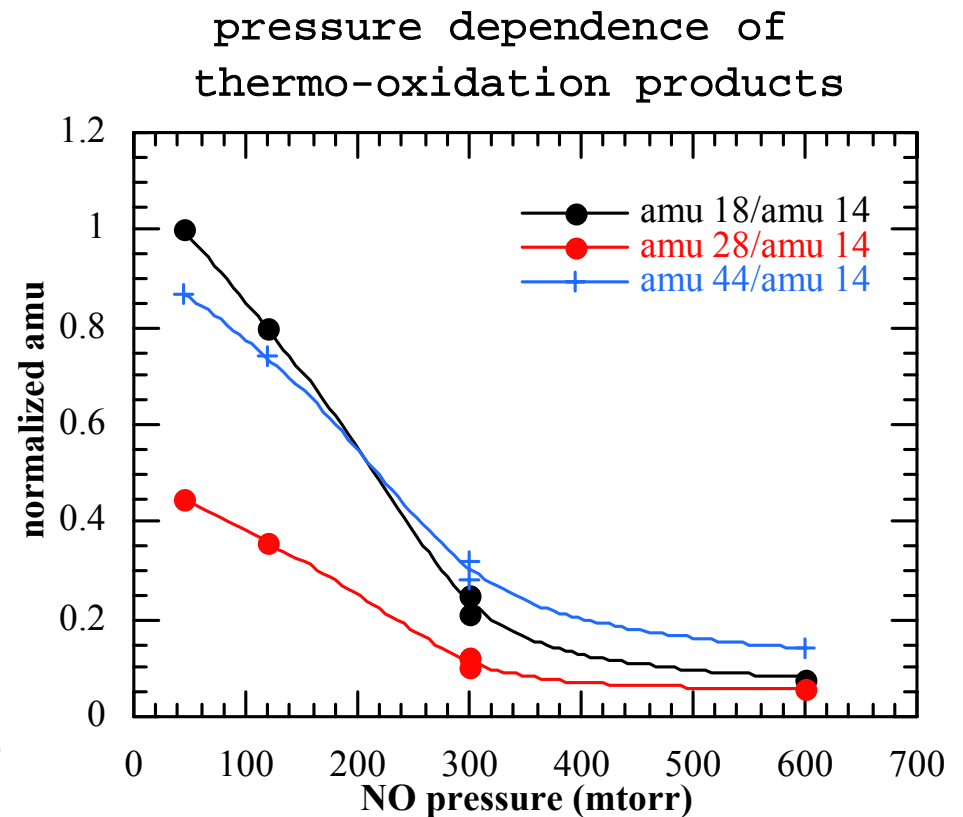
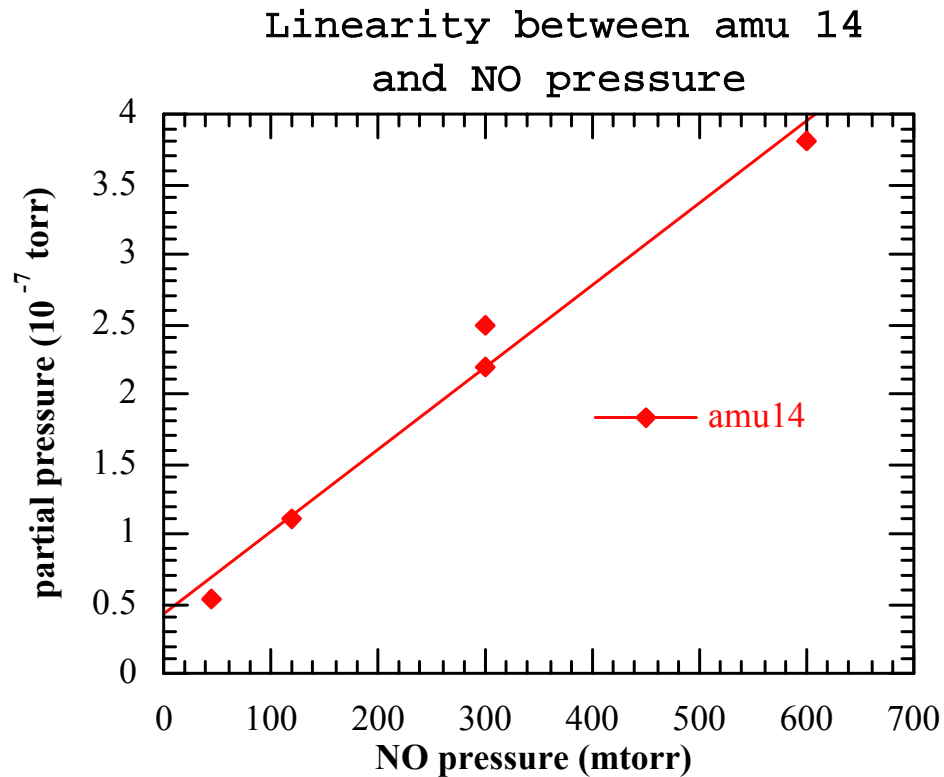


NO seems to oxidize the soft C-film as efficiently as O_2 does

NO thermo-oxidation

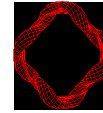


Laboratorio Nacional de Fusión
Asociación EURATOM-CIEMAT



The process seems to be more efficient at low pressure

H₂ release



Laboratorio Nacional de Fusión
Asociación EURATOM-CIEMAT

RGA measurements of H₂ during thermo-oxidation

O₂ thermo-oxidation: 6×10^{-10} torr

NO thermo-oxidation: 7×10^{-10} torr

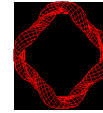
no clear dependence on the T was found (150-300 °C)

no evidence of H₂ release in NO thermo-oxidation

according to: $\text{NO} + \text{H} \longrightarrow \text{NOH}$



Conclusions



*Laboratorio Nacional de Fusión
Asociación EURATOM-CIEMAT*

NO seems to be an efficient oxidizing agent for soft a:C-H films at low temperatures

no evidence of molecular H_2 release during NO thermo-oxidation

More work must be done in order to compare NO/ O_2 thermo-oxidation

Thermal release rate data of tritium trapped in surface and bulk specimens obtained from the JET MKIIA divertor tiles

N. Bekris¹, J.P. Coad², C. Skinner³, A. Damm⁴, M. Glugla¹, W. Nägele⁴,

¹ EURATOM Association Forschungszentrum Karlsruhe, Tritium Laboratory P.O.B. 3640, 76021 Karlsruhe, Germany

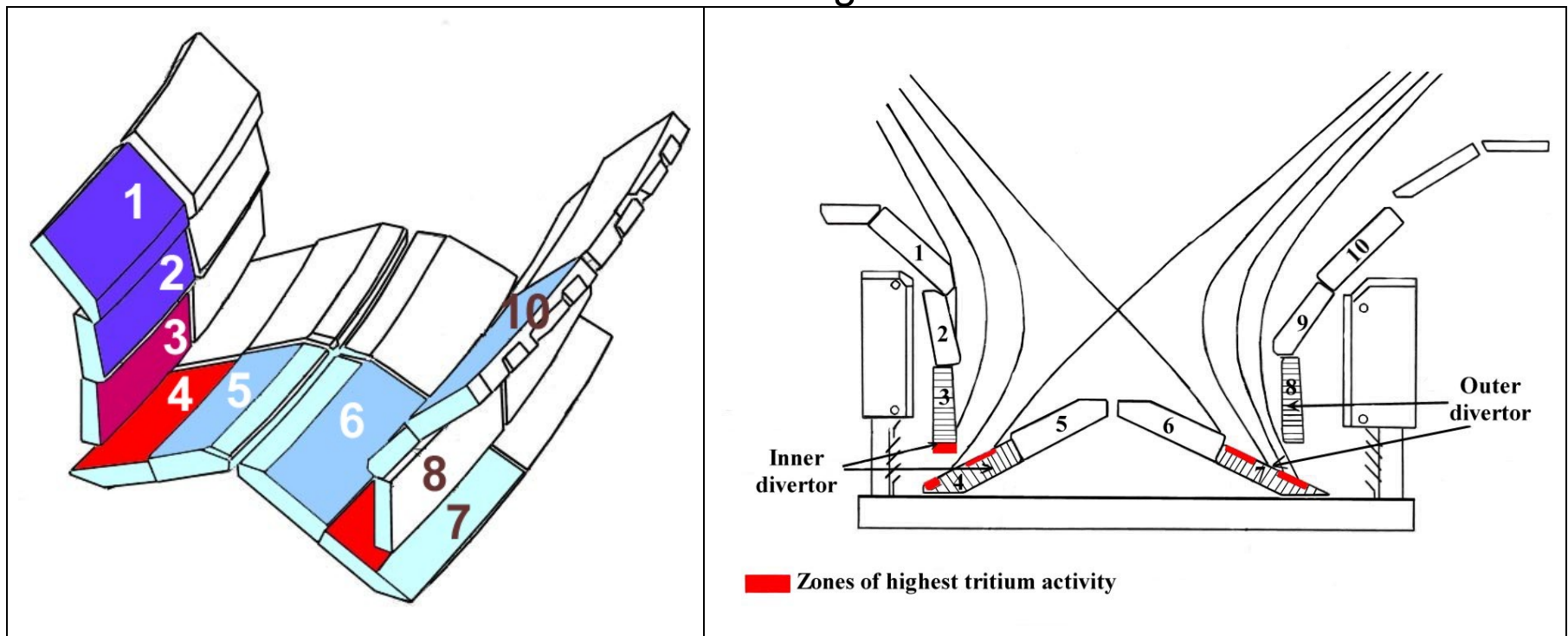
² EURATOM/UKAEA Fusion Association, Culham Science Centre, Abingdon, Oxon OX14 3DB, UK

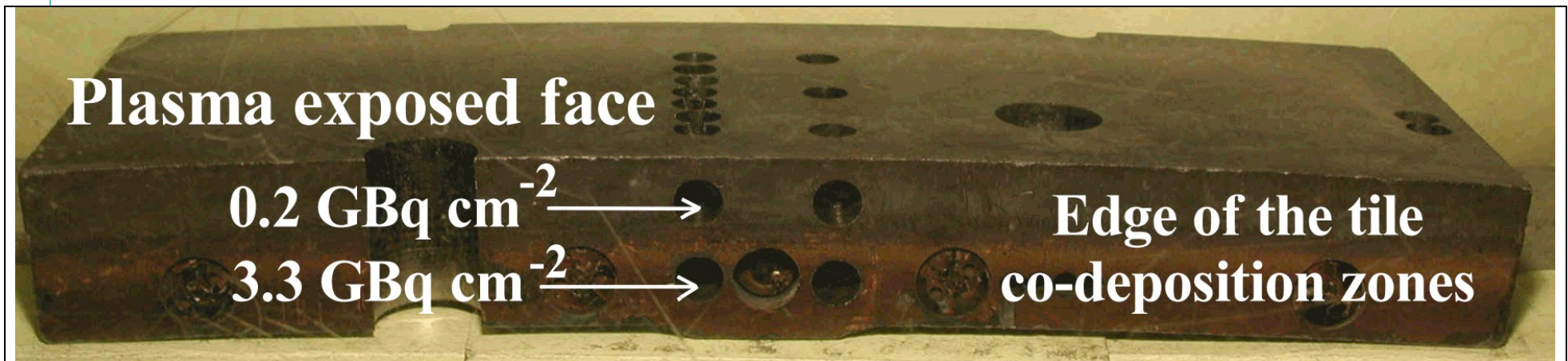
³ Princeton Plasma Physics Laboratory, Princeton, NJ 08543, USA

⁴ EURATOM Association Forschungszentrum Karlsruhe, IMF / Hot Cells, P.O.B. 3640, 76021 Karlsruhe, Germany

Introduction

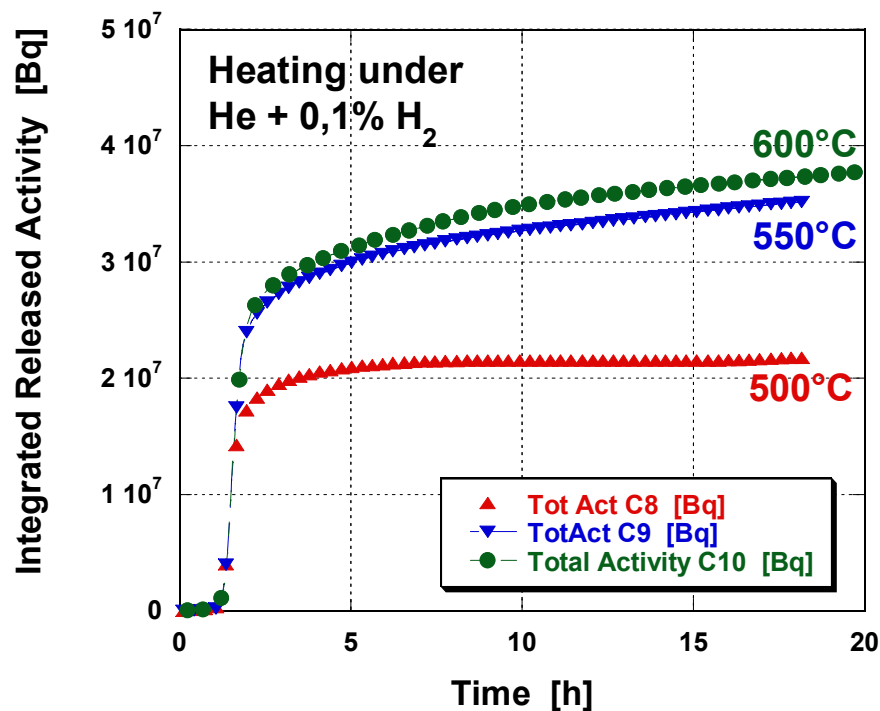
Thick carbon deposits containing high levels of hydrogen isotopes have been observed in JET in the shadowed regions of the inner divertor.





D/C ~ 0.75 and they are usually reported in the literature as a amorphous carbonaceous a-C:H layer, and sometimes, referring to their sp³ hybridisation, they are reported as “diamond-like films”

Thermodesorption experiments Isothermal heating / analysis by combustion



Cylinder/specimen	Heating range in °C (heating ramp: 7°C min ⁻¹)	Fraction released (%)	Tritium released (MBq g ⁻¹)
8A ₁	20 – 500	77.4	531
	20 – 1100	22.6	130
9A ₁	20 – 550	89.0	848
	550 – 1100	11.0	105
10A ₁	20 – 600	94.6	1000
	600 – 1100	5.4	57

Thermodesorption experiments Constant heating ramp

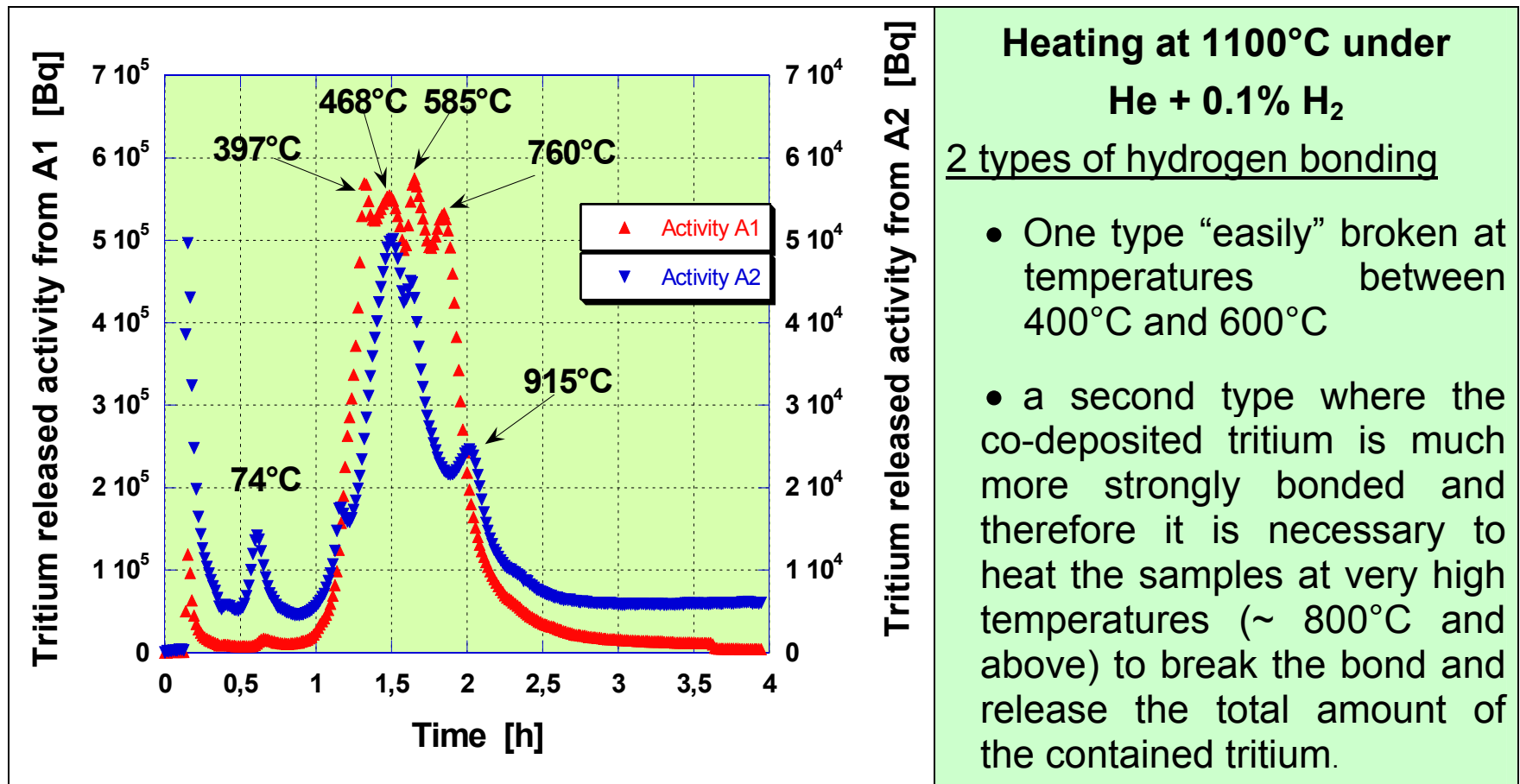


Table . Dissociation energies at room temperatures of some H-C and H-O bonds for several hydrocarbons

Bond	Hybridisation*	D ₂₉₈ [°] kJ mol ⁻¹	D ₂₉₈ [°] eV
H-COCH ₃	sp ² -sp ³	360±3	3.73±0.03
H-CHO	sp ²	364±4	3.77±0.04
CH ₃ -CH ₃	sp ³ -sp ³	368±8	3.81±0.08
H-CH ₂ CH=CH ₂	sp ³ -sp ² -sp ²	372±4	3.86±0.04
H-CH ₂ OH	sp ³	393±4	4.07±0.04
H-CH ₂ =C=CH	sp ³ -sp-sp	393±5	4.07±0.05
H-CH ₂ -CH ₃	sp ³ -sp ²	410±4	4.25±0.04
H-CH ₃	sp ³	435±4	4.51±0.04
H-O-CH ₂ -CH ₃	sp ³	436±4	4.52±0.04
H-O-CH ₃	sp ³	437±4	4.53±0.04
H-CH=CH ₂	sp ² -sp ²	452±8	4.69±0.08
H-C≡C-H	sp-sp	523±4	5.42±0.04
H-OH	-	498±4	5.16±0.04

Hybridization has an influence

The dissociation energy of the H-C bond increases as the *p* character of the carbon in the *s-p* hybridisation decreases (shorter bond).

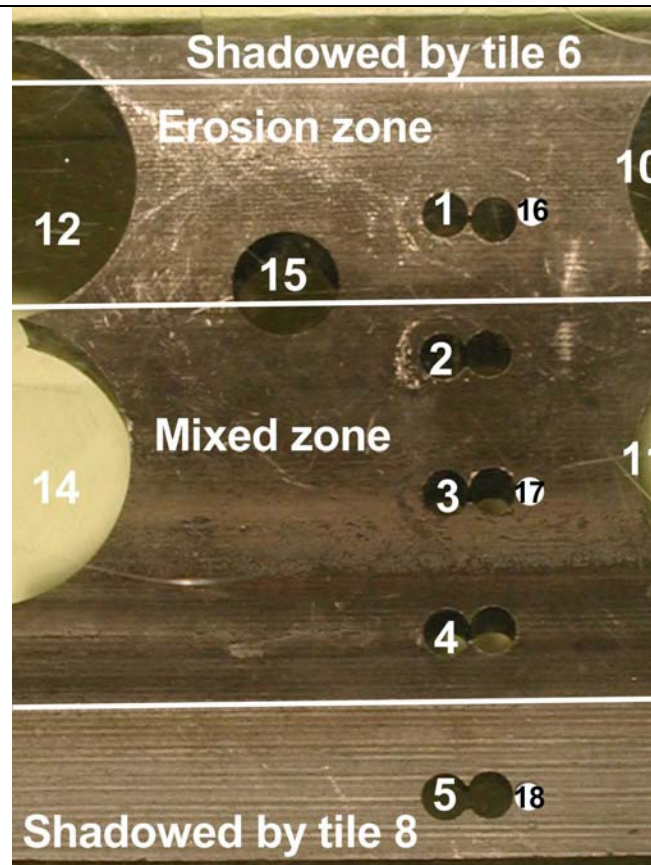
According to this we attributed the first type of the released tritium (**between 400°C and 600°C**) to the break of the **T-C** bond when the carbon has a **sp³** hybridisation and the second type (above **800°C**) when the carbon has either the **sp²** either the **sp** hybridisation. The major part of the T-C bonds are **sp³** type. The various peaks observed between 400°C and 800°C are therefore attributed to the various substitutions that the **sp³** carbon can have.

Oxygen has an influence.

If an atom of oxygen is attached on the carbon atom involved in the H-C bond then the H-C bond becomes weaker because of the very high electronegativity of oxygen compared to carbon.

Not single trap, not single bonding

Identification of the gaseous species released from surface samples exposed to D-T plasma



3 discs were retrieved from the JET divertor tile 1BN7 and treated thermally.

16 erosion zone

17 mixed zone

18 shadowed part of the tile (bare tile)

Experimental set-up

Oven able to heat up to 1100°C

He containing 0.1% Hydrogen.

Zn-Bed reducing water

Prop. Count.

MS

Thermal release / mass spectrometry

12 channels can be recorded

but only masses 2, 3, 4, 16, 17 and 18 and 20 are contributing to the total pressure

measured to be $2.1 \cdot 10^{-7}$ Torr.

Similar spectra for all three samples.

There is no water (Zn-bed) therefore, masses 16, 17, 18, and 20 have to be attributed only to **methane** and its isotopic combinations.

As mass 2 \rightarrow H₂ and mass 4 \rightarrow He (purge gas)

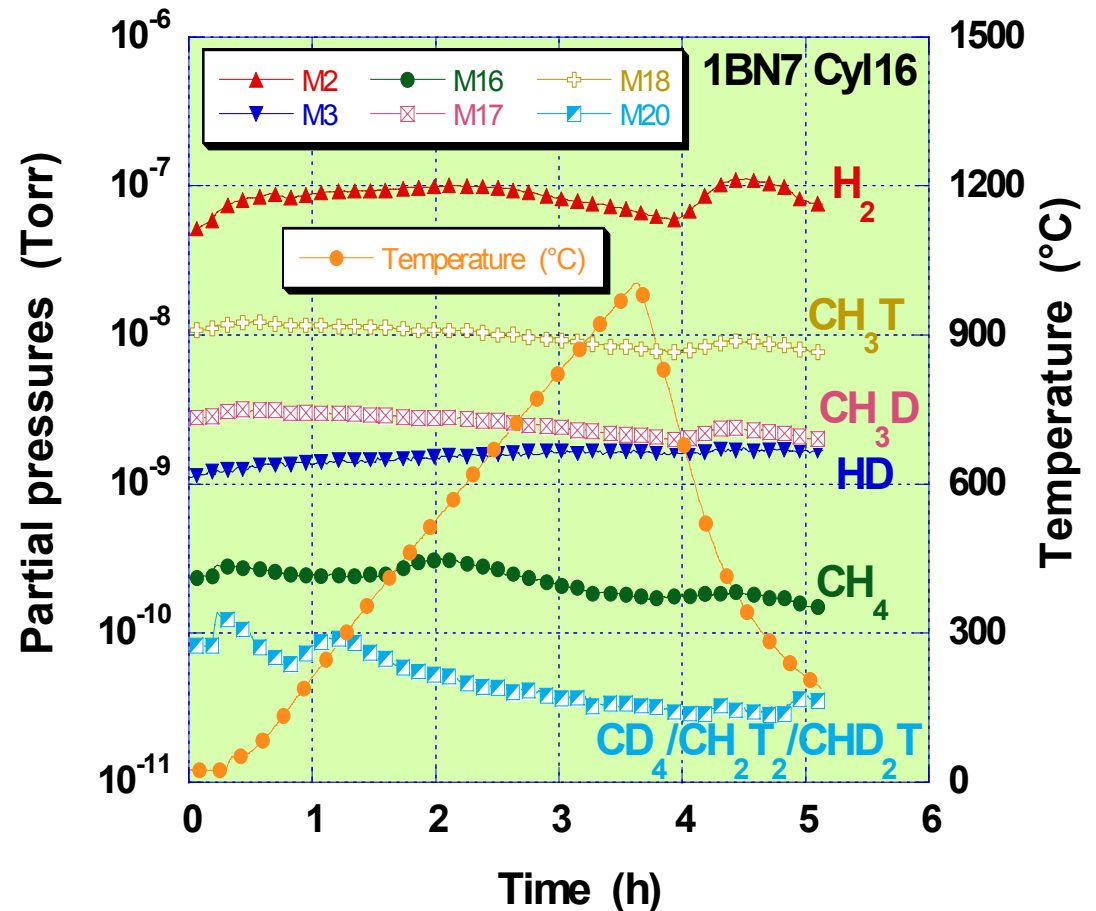
only masses 16 \rightarrow CH₄, 17 \rightarrow CH₃D and 18 \rightarrow CH₃T

are significantly above the background.

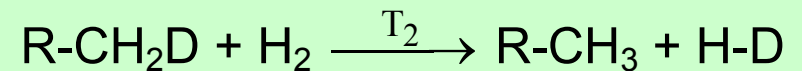
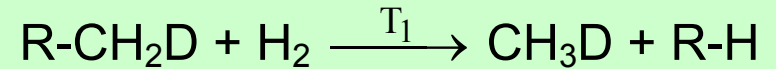
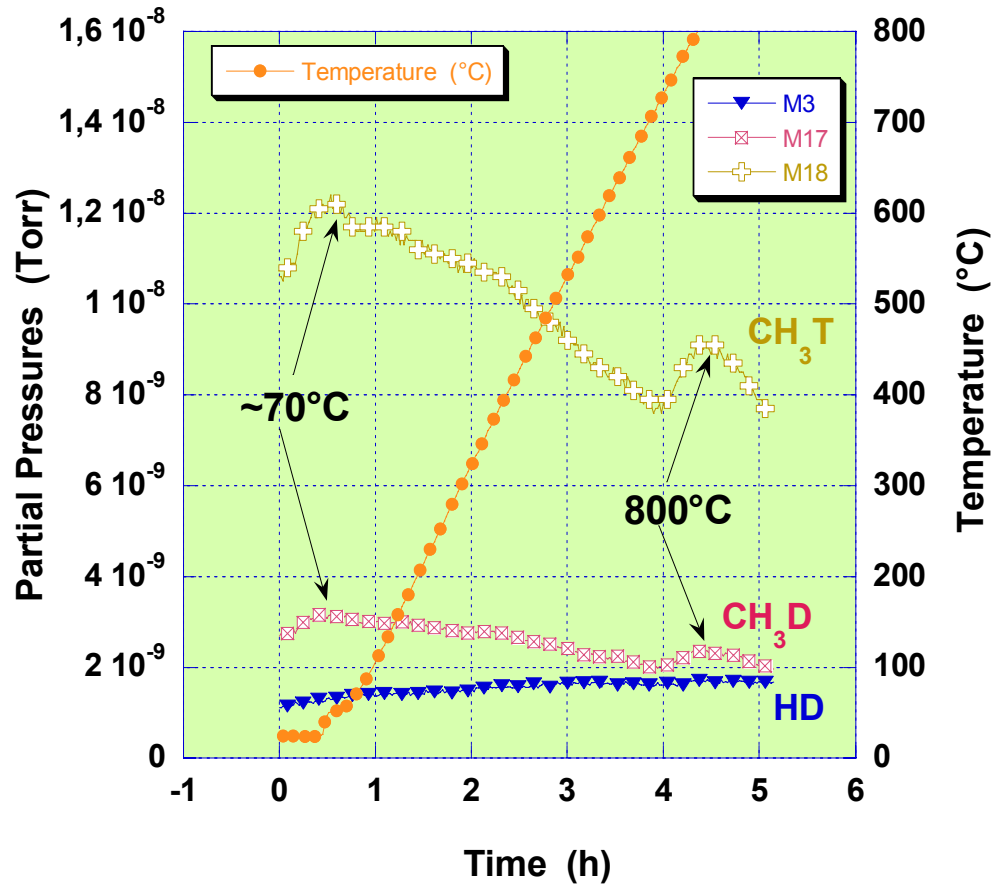
multi-substitution (mass > 18) is a less probable mechanism as it requires a multi-step reaction process on the same molecule which statistically is less favourable.

Nevertheless, very small amount of the

mass 20 \rightarrow CH₂T₂, CHD₂T, or CD₄ was detected.



Thermal release / mass spectrometry - 2



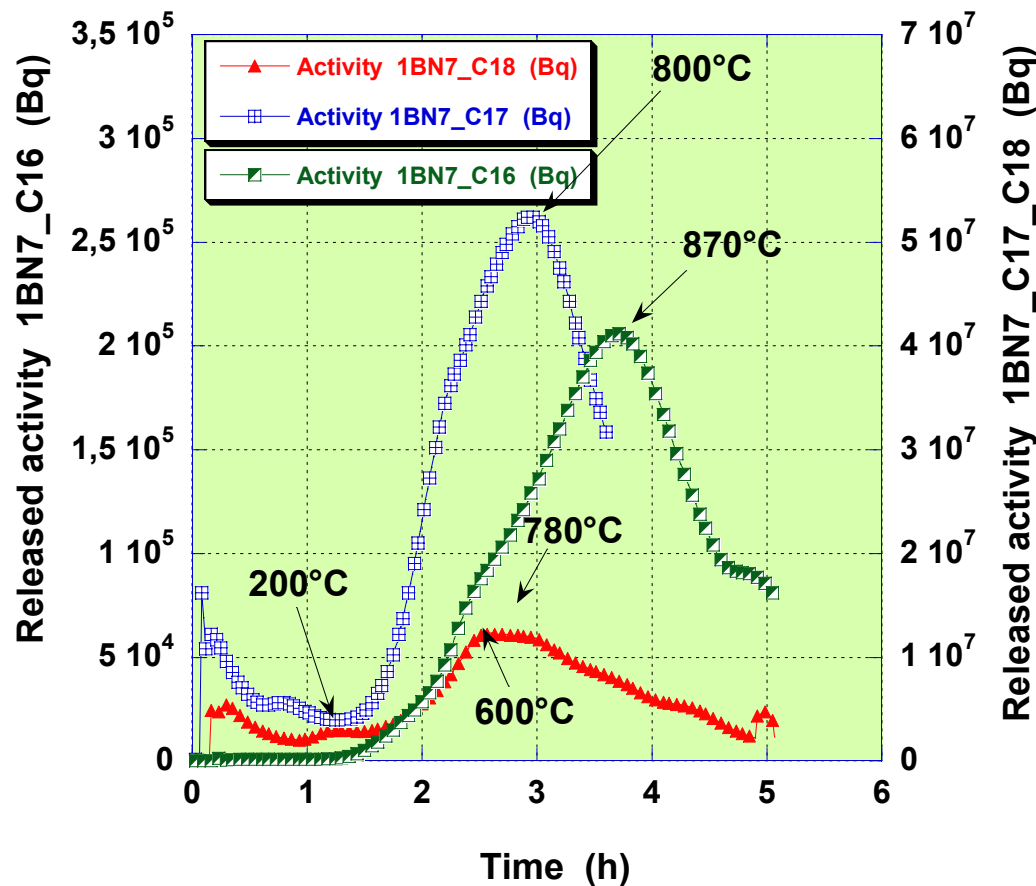
Reactions started at low temperatures and decreasing with the temperature (depleting the R-CH₂Q) species (Q=H, D, T).

However, if T ↑ (800°C) there is a recrudescence. This has to be related to type of bonding (hybridization) between R-C.

1) O-C, sp³-sp³, sp²-sp³ and sp-sp³

Same type of reactions can also been used for T instead D

Thermal release / tritium analysis



Two orders of magnitude difference between the tritium activities measured for samples C16 and the couple C17, C18. Contrary to what was expected, C18 shows a higher tritium content compared to C16. This is quite surprising as C18 is located in a shadowed area of the 1BN7 tile where co-deposition was not observed.

Secondly, the release profile of the tritium trapped by C18 is quite different to the profile exhibited by the C16 and C17 samples, located respectively in eroded and mixed areas of the tile. This can be related to a different kind of tritiated species trapped by C18 compared to C16 and C17. Indeed, we may discern a slight evolution of the peak maxima corresponding to the tritium released activity. While for 1BN7 C16 and C17 there is only a broad "single" peak at approximately 870°C and 800°C respectively, for the sample 1BN7 C18 the corresponding peak is very broadened starting at 600°C and still present at ~780°C. The interpretation of this figure could be fully understandable if there is a mislabelling between samples C16 and C18.

Summary

- Hydrogenated carbon films are deposited in shadowed regions of the inner divertor of JET.
- These films have a high hydrogen content D/C ~0.75 and they are highly tritiated $1.2 \cdot 10^{12} \text{ Bq g}^{-1}$ flakes (32,4Ci per gram of flakes).
- Thermal desorption experiments have shown the presence of at least two kinds of peaks attributed to the different hybridization of the carbon atom in the C-T bond.
- Only small chain hydrocarbons have been observed.
- In this series of experiments (due the experimental set-up) the production of methanated species was only possible but the release of tritium in form of tritiated water must also be included among the various released compounds.
- Same released species have been observed for all samples no matter their location on the tile surface.
- Sample from shadowed area exhibited high tritium concentration (probably mislabeling).

Property of tritium and carbon co-deposition on JET Mk-IIA divertor tiles

K.Sugiyama* T.Tanabe

Graduate school of Engineering, Nagoya University

Collaboration with:

N.Bekris, M.Glugla (Forschungszentrum Karlsruhe)

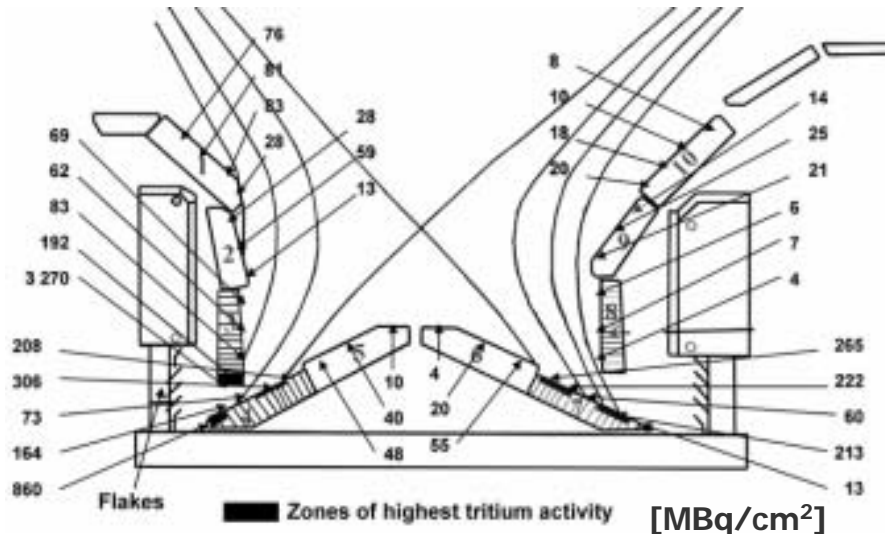
J.P.Coad (EURATOM / UKAEA)

JET Mk-IIA divertor

◆ Employed in DTE1 campaign

D-T discharges: 1400 shots (Mar ~ Nov. '97)

Total ^3T injection: 35g (Gas puff: 34.4g NBI: 0.6g)



【T distribution obtained by combustion method ⁽¹⁾】



【Mark IIA divertor】

◆ ^3T was mainly co-deposited with eroded carbon.

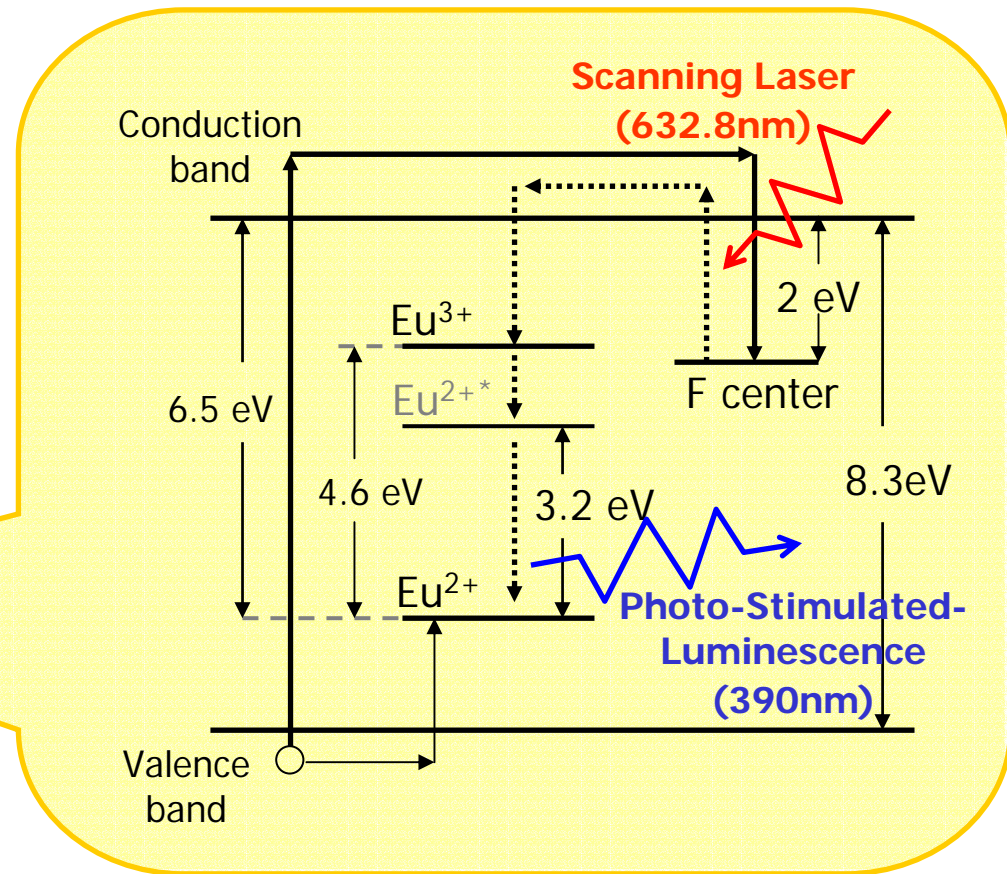
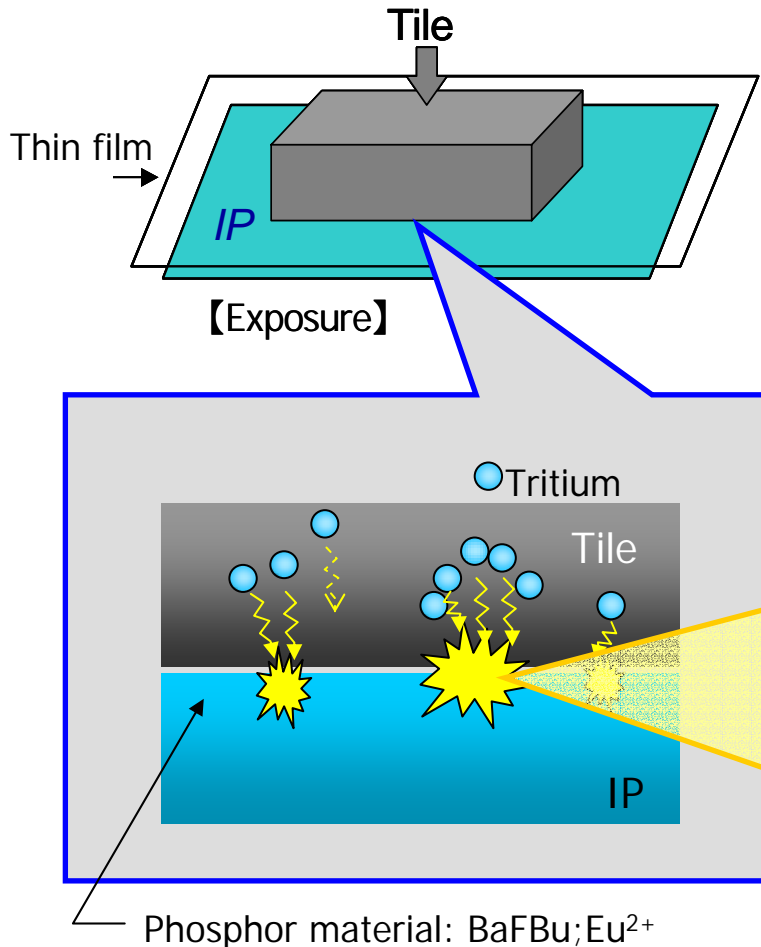
- Large amount of codeposition & flakes were observed in inner divertor region.
- Hydrocarbon radicals or neutrals could be main cause of codeposition formation.

(1) J.P.Coad et al., JMN. **290-293** (2001) 224

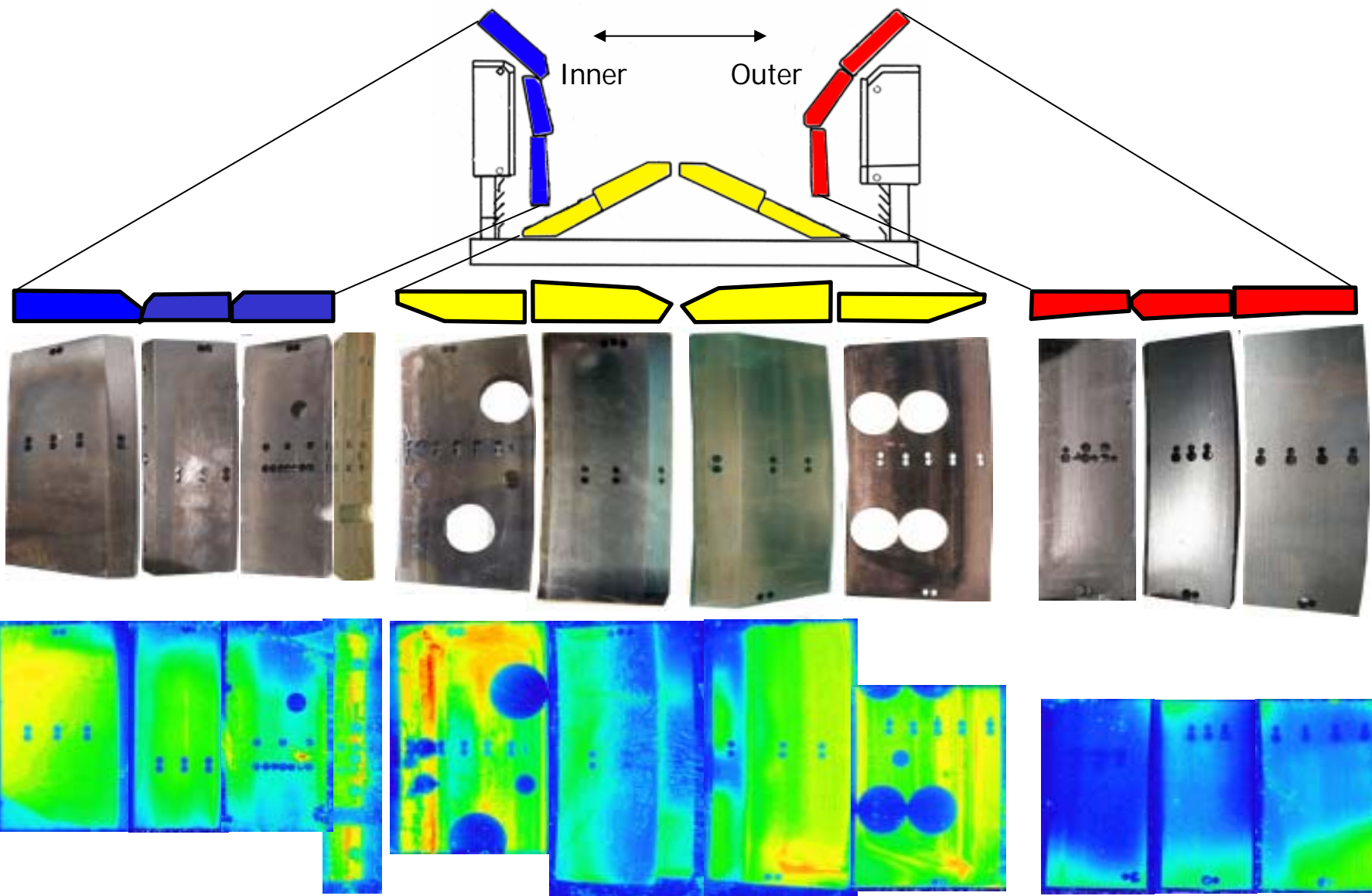
Experimental -Imaging Plate Technique -

◆ Imaging Plate (2-D Radiation detector)

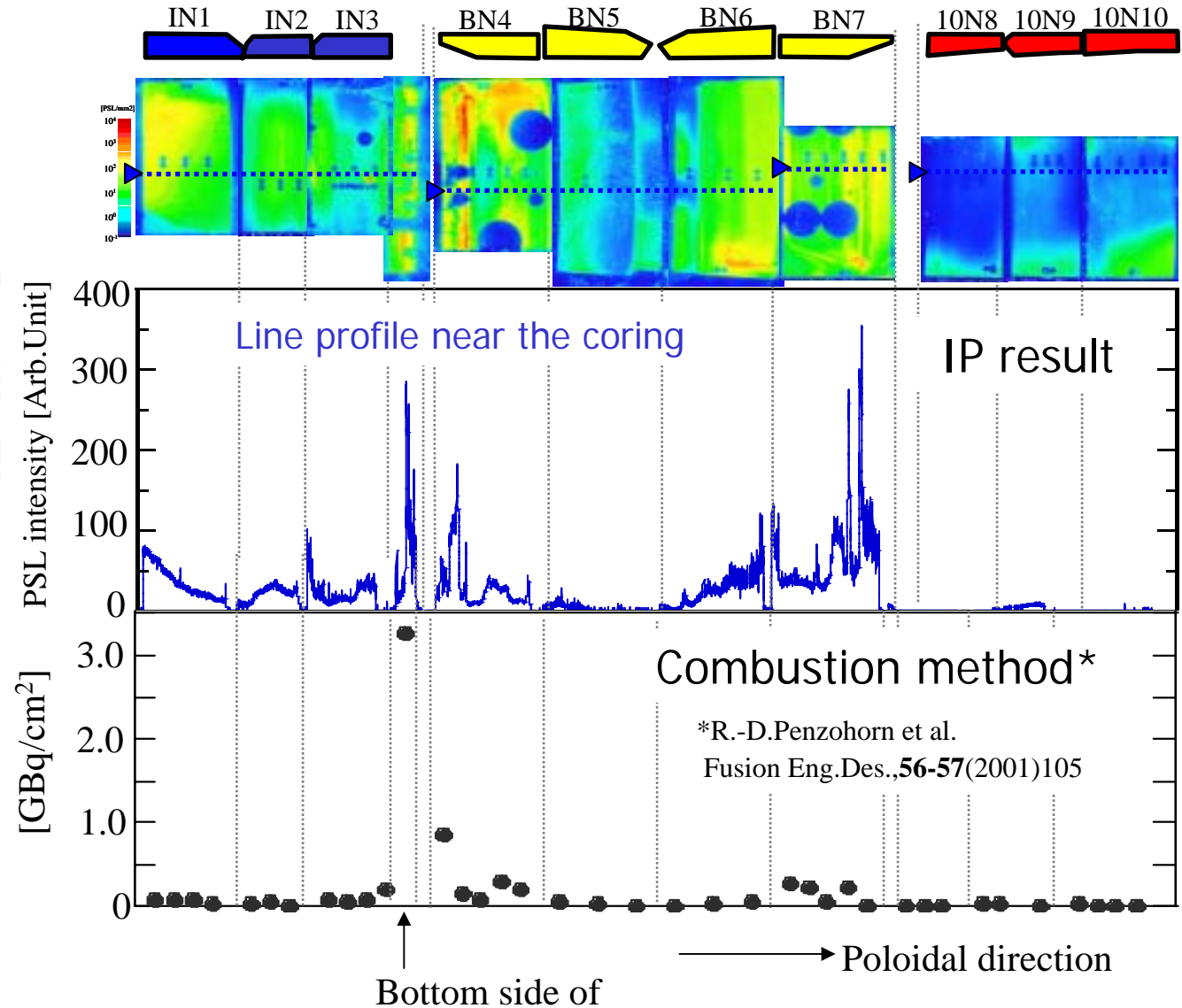
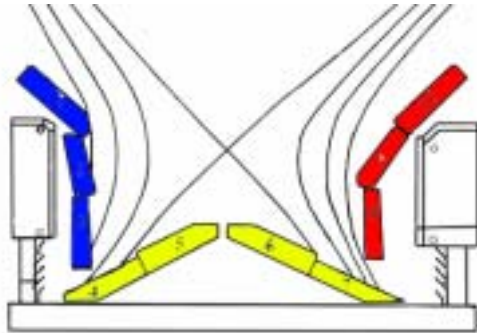
- detects ^3T β -ray with high sensitivity.
- gives ^3T intensity mapping with high resolution.



^3T distribution image



Comparison of IP and Combustion analysis

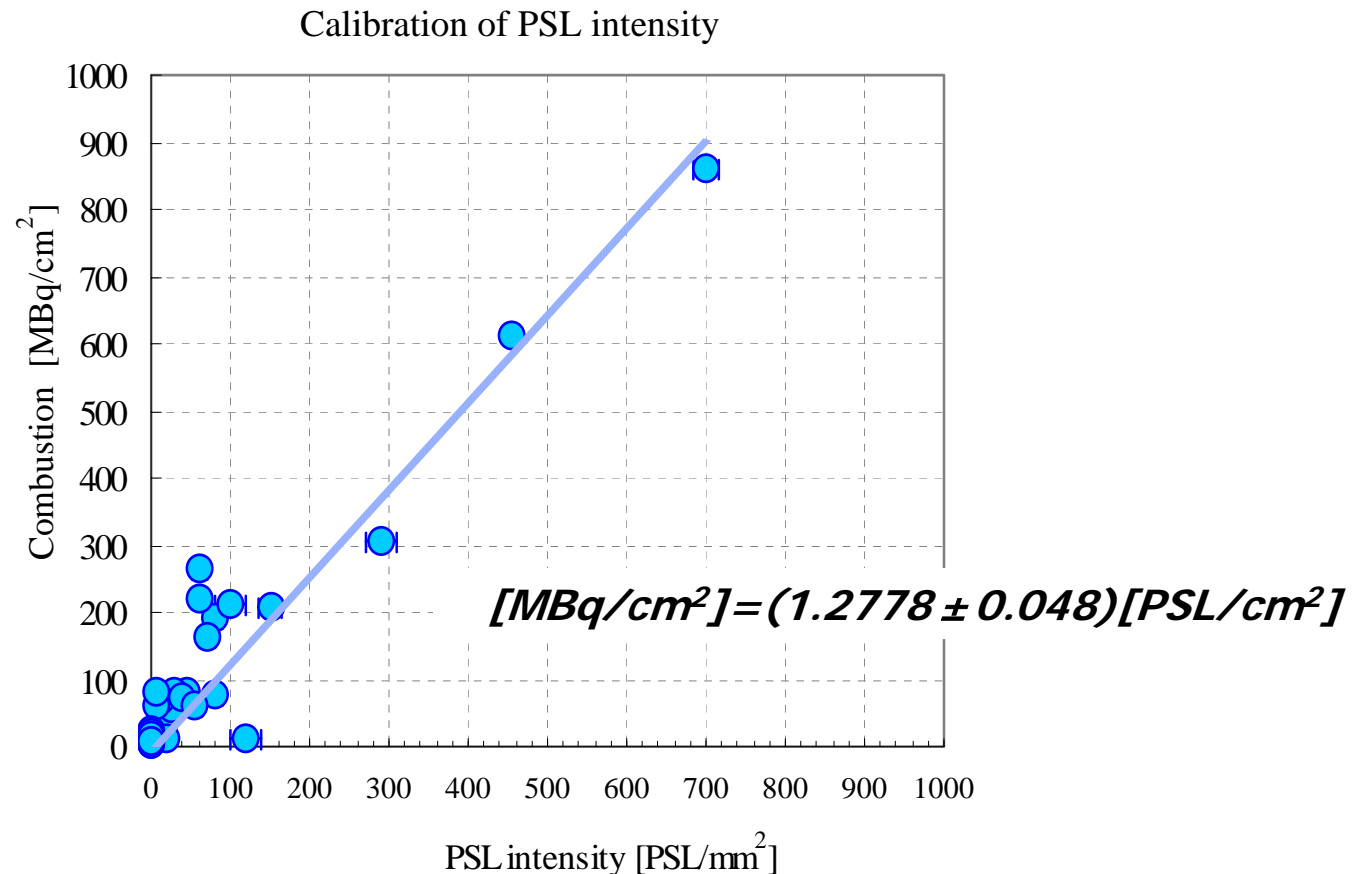


◆ IP result is good agreement with combustion method.

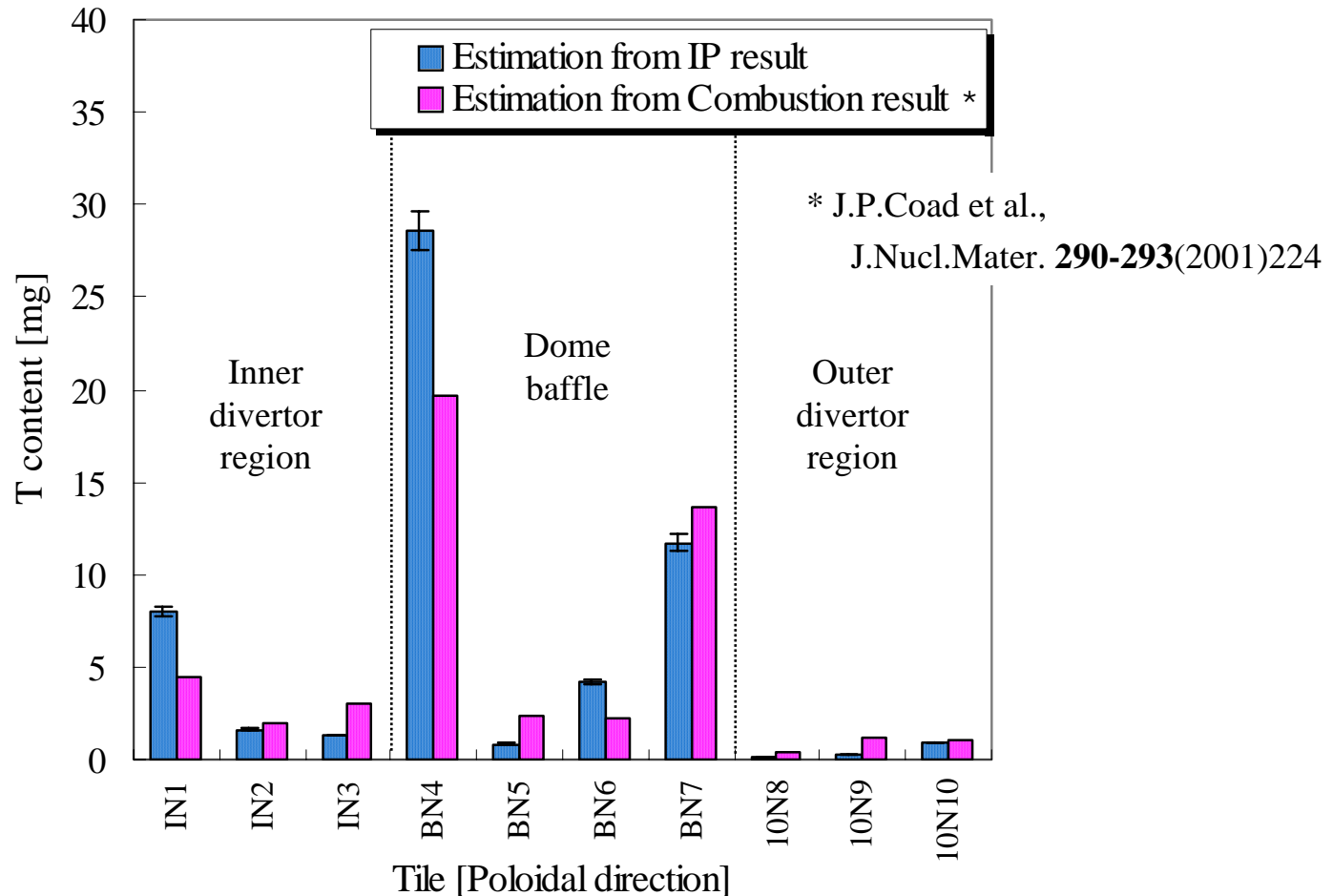
Calibration of PSL intensity

■ Procedure:

- Comparison between IP and combustion results
- PSL intensity near-by the combustion point vs combustion result



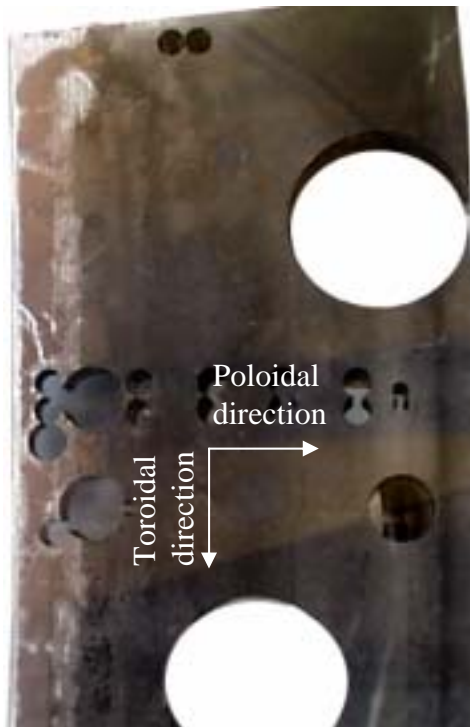
- Total PSL intensity obtained from each tile surface is converted to quantitative value.



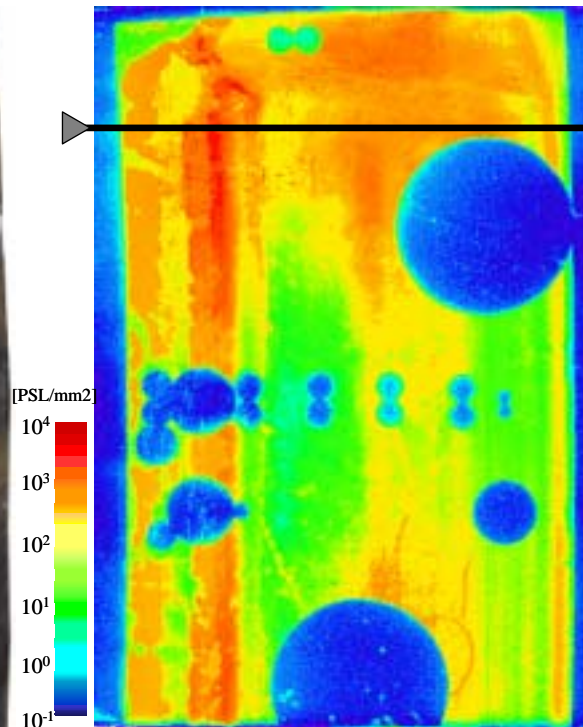
✓ Major difference is found in BN4 tile (inner horizontal target tile).

^3T concentration of codeposition

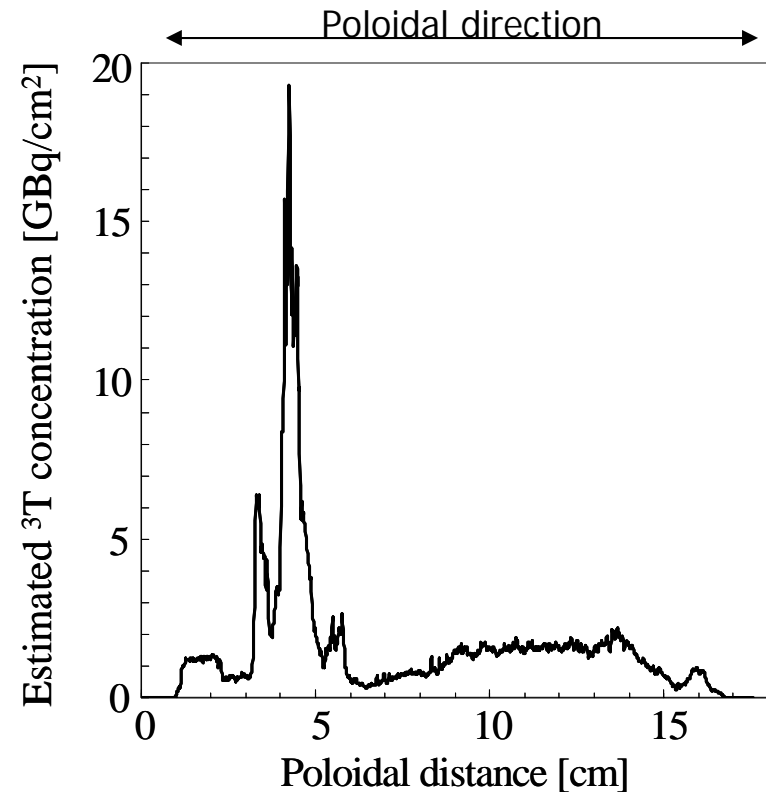
■ Heavy deposition on the inner horizontal target tile: BN4



【BN4 IP Photo.】



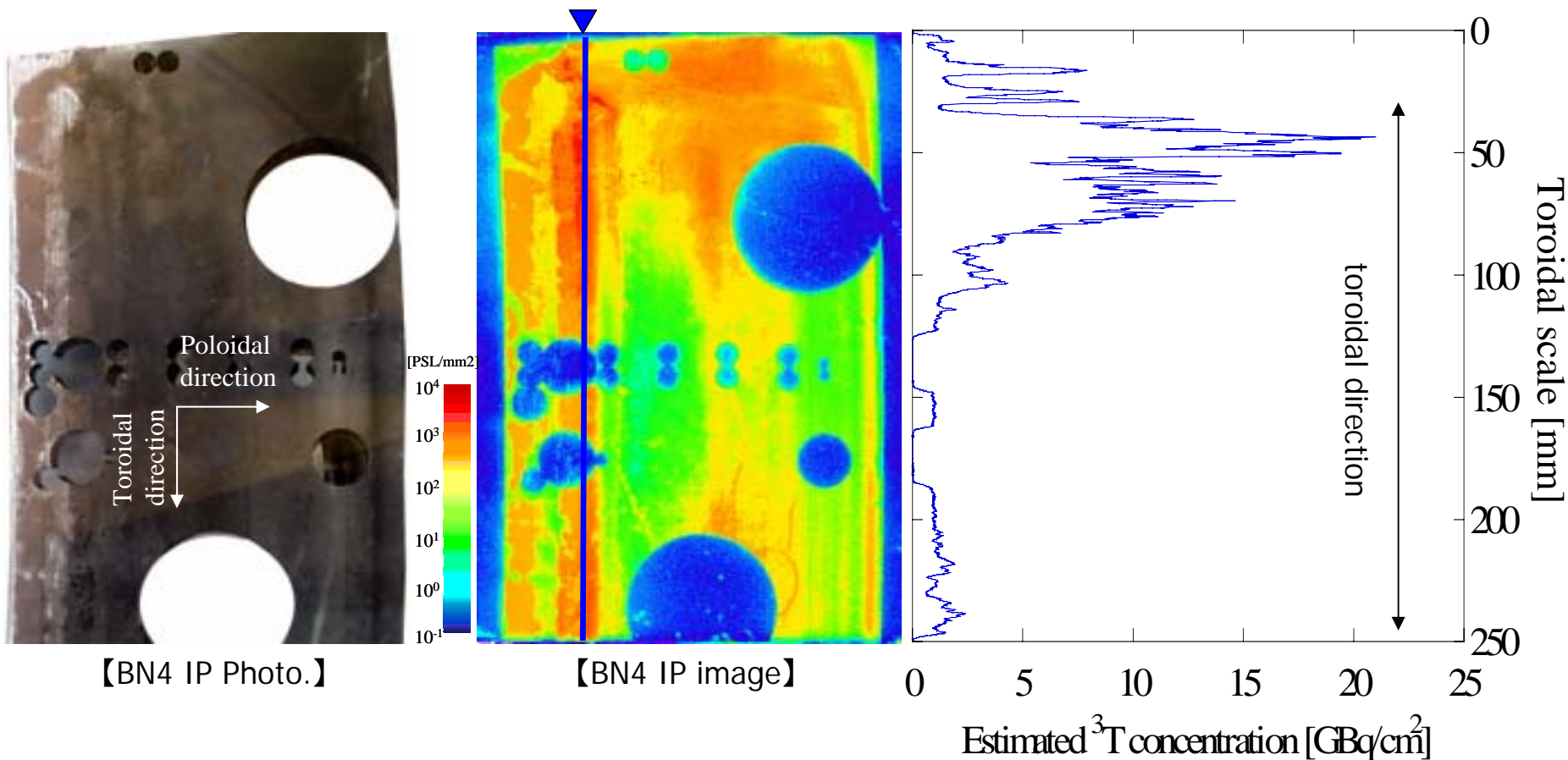
【BN4 IP image】



- ✓ ^3T distribution is rather inhomogeneous in poloidal direction.
- ✓ Codeposition stripes are observed in shadow region.

^3T concentration of codeposition

■ Heavy deposition on the inner horizontal target tile: BN4



- ✓ ^3T distribution is inhomogeneous even in toroidal direction.
→ This distribution could play an important role for ^3T retention evaluation.

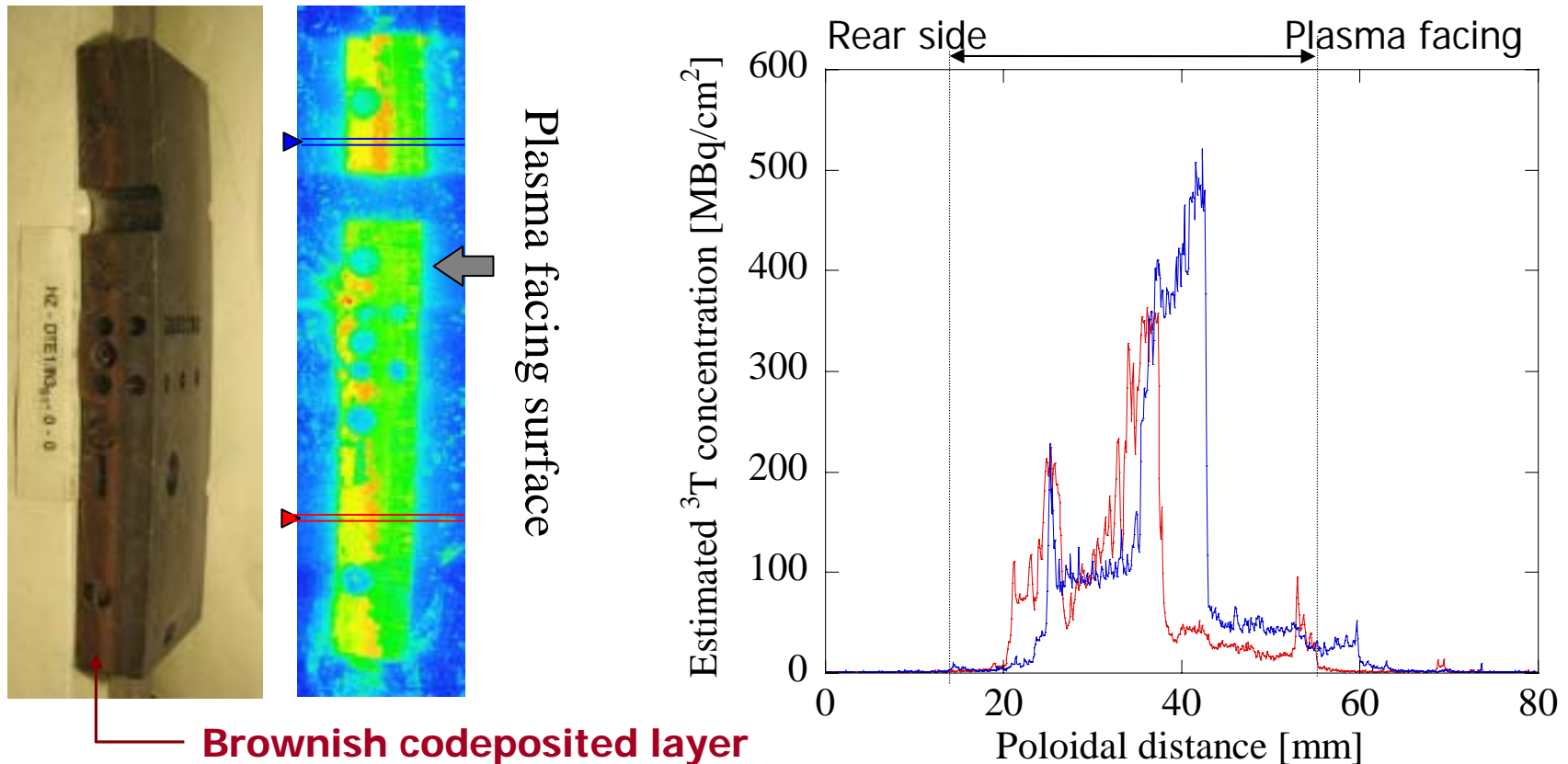
-
- BN4
- The highest T/C codeposited layer
- Poloidal direction
- Toroidal direction
- 【BN4 Photo.】
- 【BN4 IP image】
- PSL/mm²
- 10⁴
- 10³
- 10²
- 10¹
- 10⁰
- 10⁻¹
- Brownish codeposited layer

- Result of JET 5/21/2004

Codeposited layer on the IN3 tile

■ Bottom side of IN3:

The highest ^3T concentration was observed in combustion result.



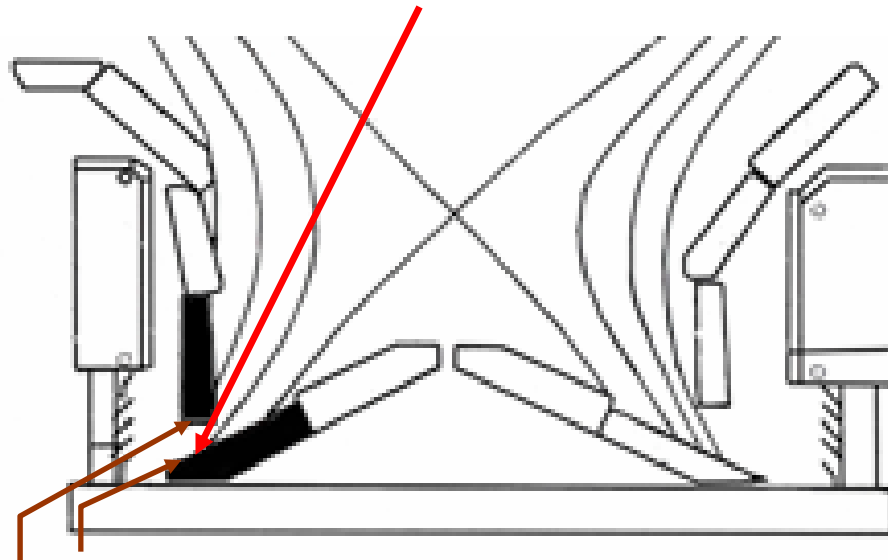
- ✓ Codeposited layer is formed in rear half side.
- ✓ The codeposited layer shows similar color and ^3T concentration to the brownish layer found on the BN4 tile.

- ^3T concentration of codeposited layer is different depending on its location.

→ Different formation mechanism??

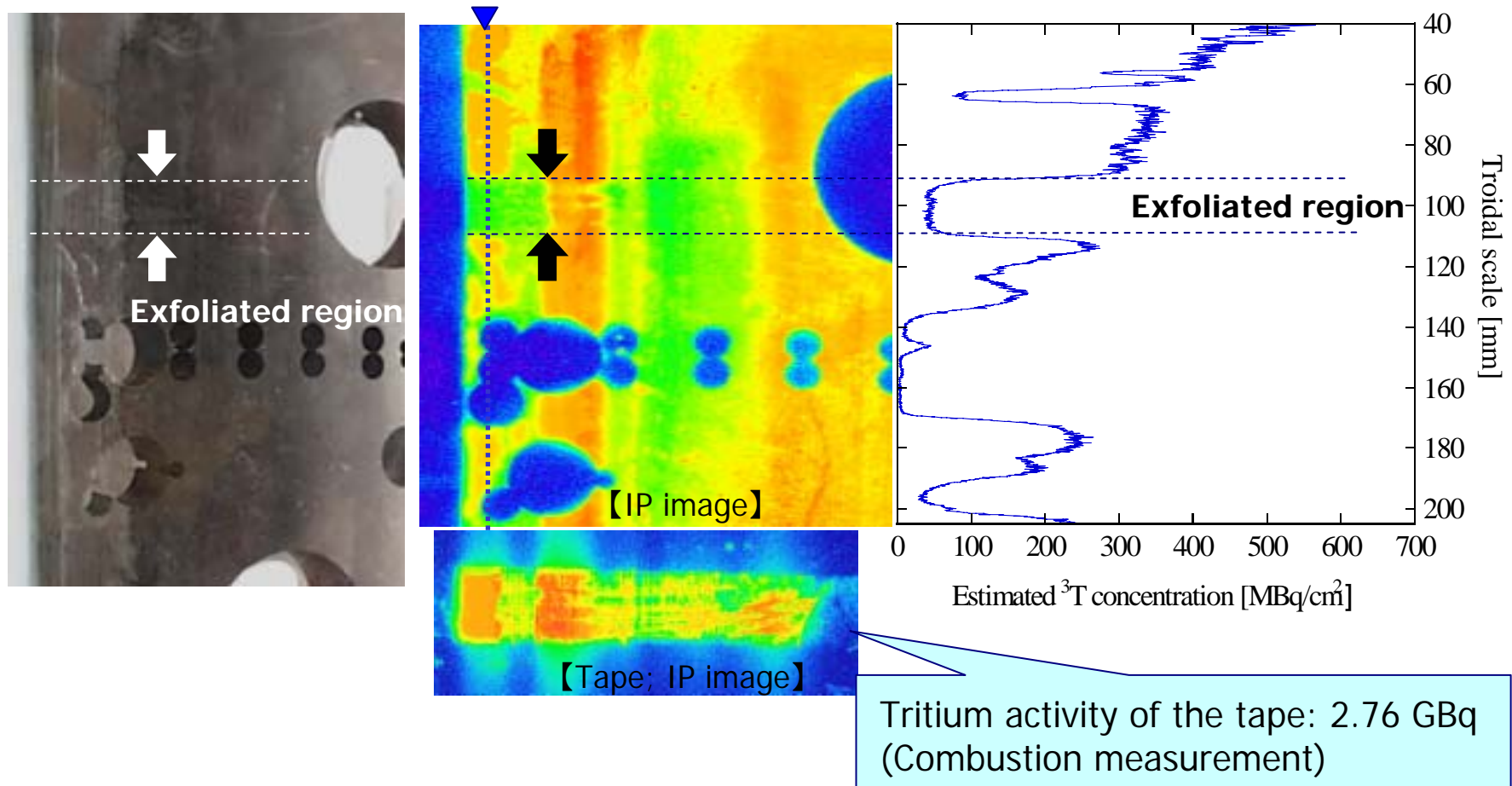
Temperature, distance from SOL or different kind of hydrocarbon sticking ...etc.

The Highest T/C co-deposited layer ($\sim 10 \text{ GBq/cm}^2$)



Brownish codeposited layer ($\sim 10^2 \text{ MBq/cm}^2$)

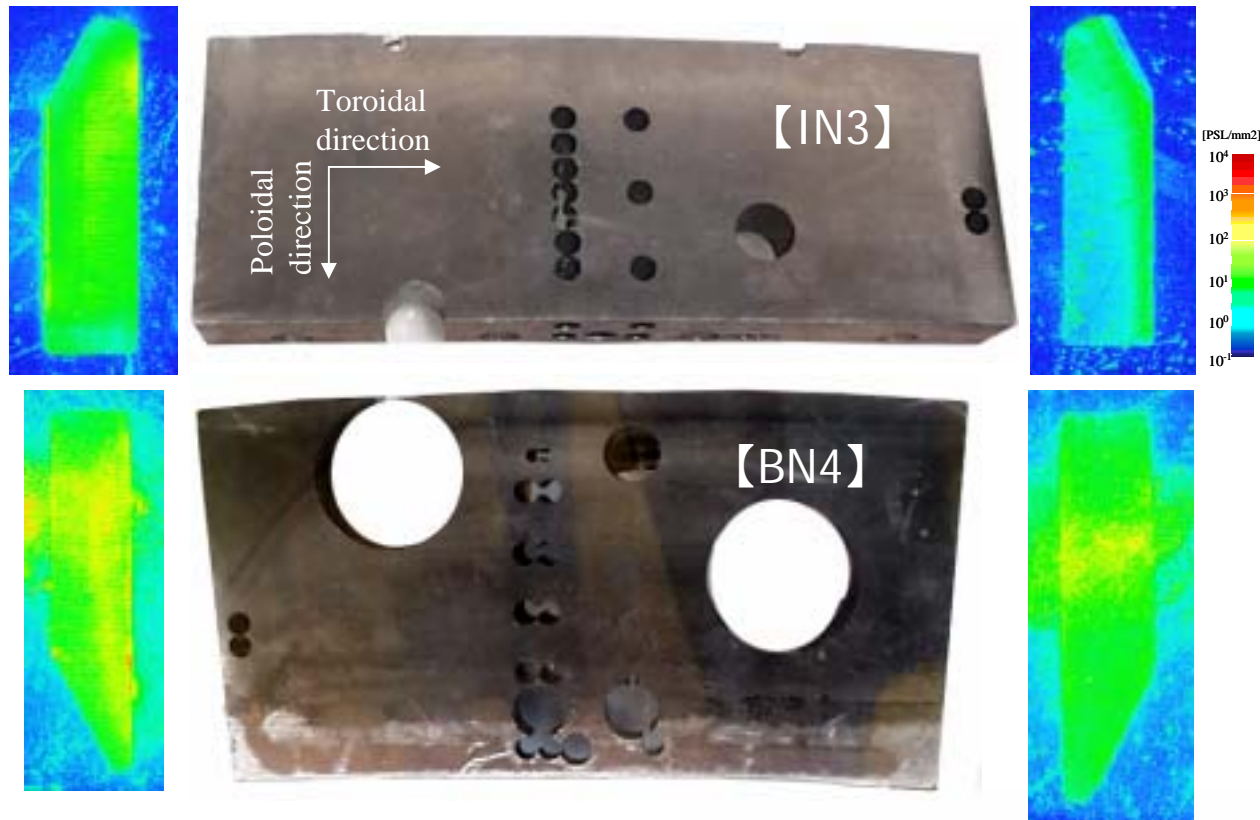
^3T profile of the codeposited layer



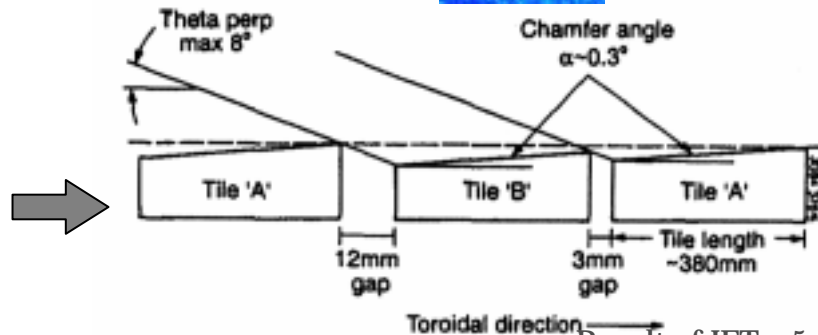
- ✓ Similar profile / intensity between front and rear side of codeposited layer.
- Tritium depth profile in the codeposition could be constant.

Codeposition on the tile gaps

■ The side surface facing to toroidal direction

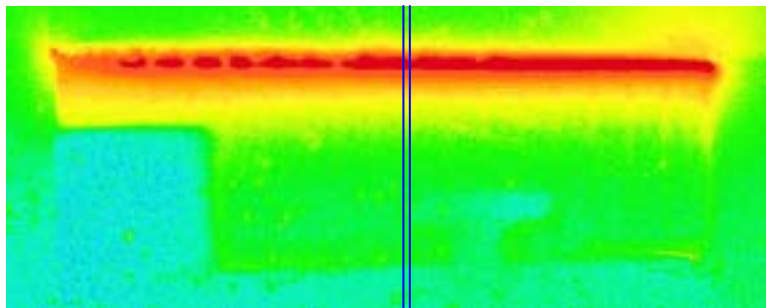


- ✓ Little codeposition on the side surface;
-- might be due to the tile design.

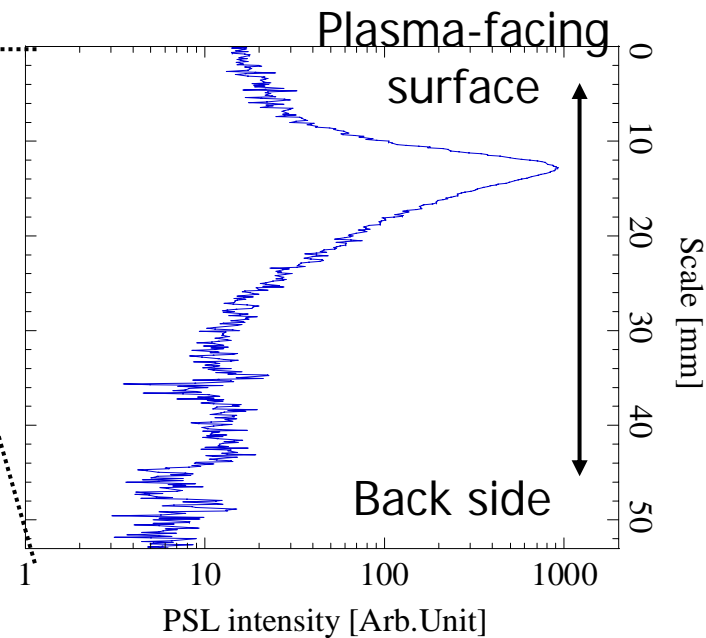


Codeposition on the tile gaps

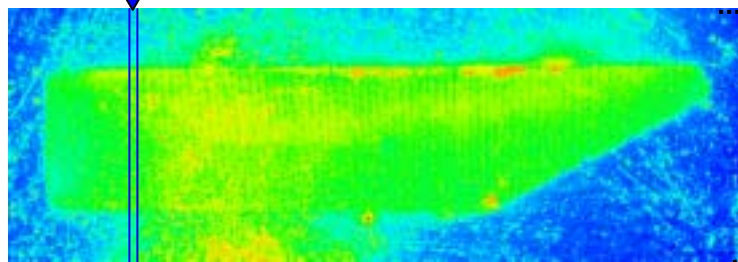
TFTR



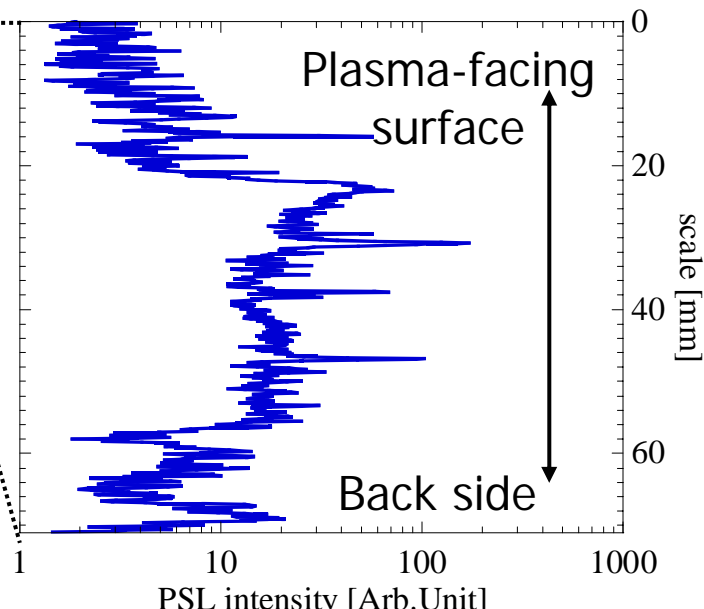
【IP image: TFTR tile KC2 side】



JET



【IP image: JET tile BN4 side】



- ◆ ^3T codeposition with eroded carbon was confirmed.

- ^3T distribution obtained by TIPT agree well with carbon deposition distribution profile. The codeposited layer with large amount of ^3T was found on the inner divertor tiles (IN3 & BN4), as pointed previous analyses

- ◆ ^3T distribution was not uniform even in toroidal direction.

- Both Hard layer (Brownish → $\text{H/C} \sim 0.4$) & soft layer ? (→ $\text{H/C} > 0.4$) were observed on the BN4.

- ◆ ^3T depth profile could be constant.

- ◆ Those property gives important information about formation process of the co-deposited layers.

- More analyses (numerical and experimental) are needed.

Comments on the estimation of tritium retention in ITER

T. Tanabe, *Nagoya Univ.*

- In ITER, carbon is excluded from most area of PFM. But why?
 - High erosion and tritium retention are main concerns.
-
- **Still low Z material is required as bumper limiters on the central column (inner first wall) for start-up.**
 - **Be can be used except its hazardous problems.**
 - **But anybody knows that Be melts above 1551 K and cannot be used in a reactor.**

Here I will revisit hydrogen retention in carbon machines

Acknowledgement to cooperation with

C. H. Skinner, C. A. Gentile; *Princeton Plasma Physics Laboratory*

N. Bekris, M. Glugla; *Tritium Laboratory, Research Center Karlsruhe*

J. P. Coad; UKAEA Fusion, *Culham, JET Joint Undertaking*

Universities ;

Y. Hirohata, *Hokkaido Univ.*

K. Okuno, Y. Morimoto, *Shizuoka Univ.*

Y. Oya, *Univ. Tokyo*

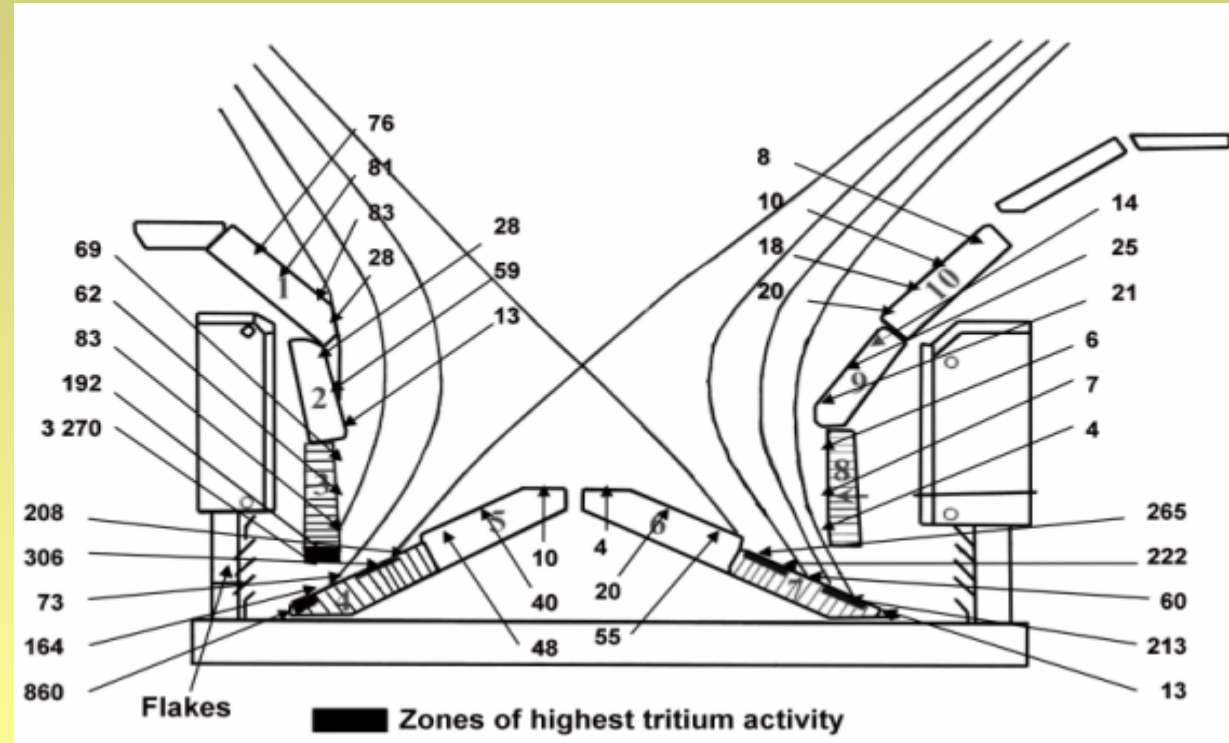
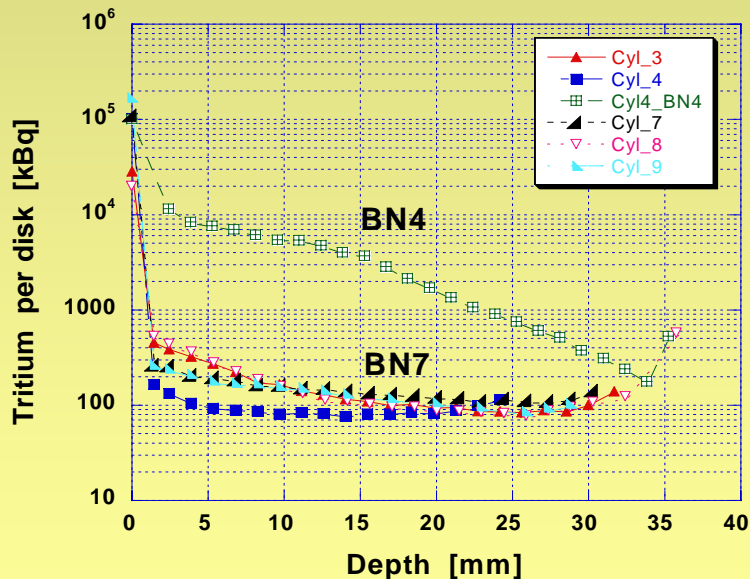
M. Nishikawa, *Kyushu Univ.*

K. Sugiyama, *Nagoya Univ.*

JAERI Naka ; Y. Gotoh, T. Arai, K. Masaki, J. Yagyu, K. Kizu, A. Kaminaga, Y. Miyo, K. Kodama, T. Hayashi, N. Miya, S. Higashijima, T. Horikawa, S. Konishi, T. Nakano, H. Kubo, M. Asakura

JAERI Tokai ; H. Nakamura, Isobe, M. Nishi,

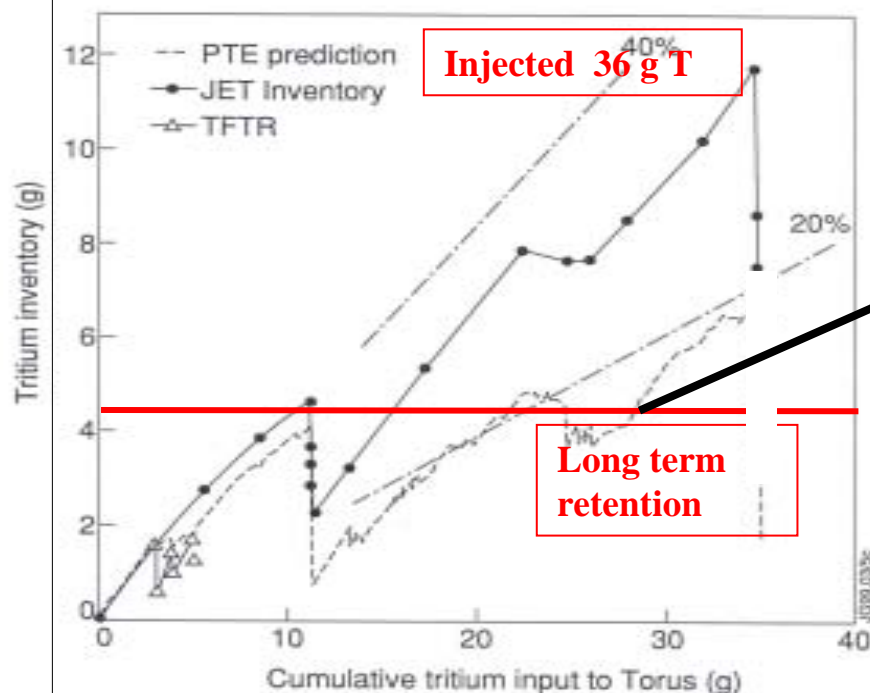
Most of tritium was codeposited with carbon at plasma shadowed area.



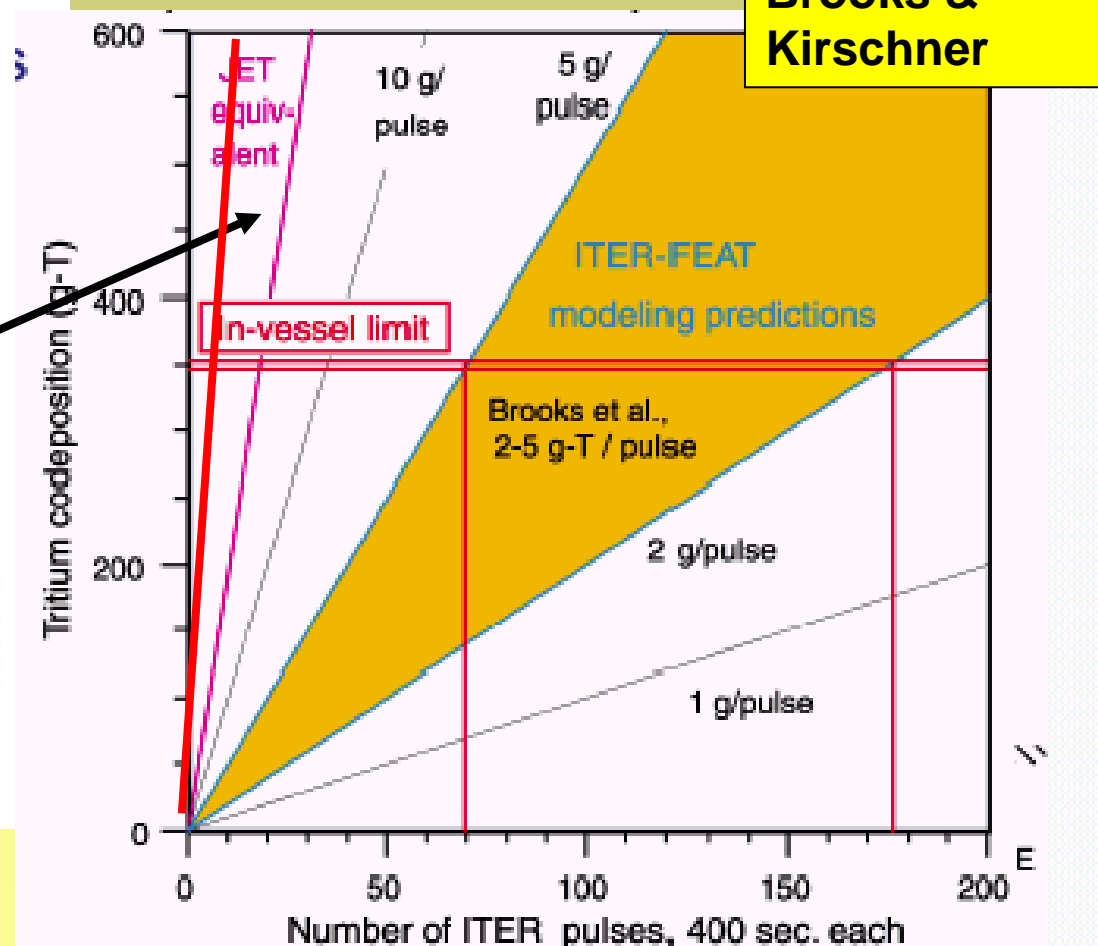
Tritium in plasma facing components



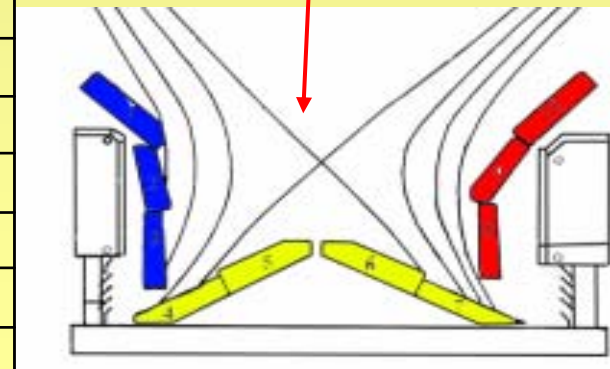
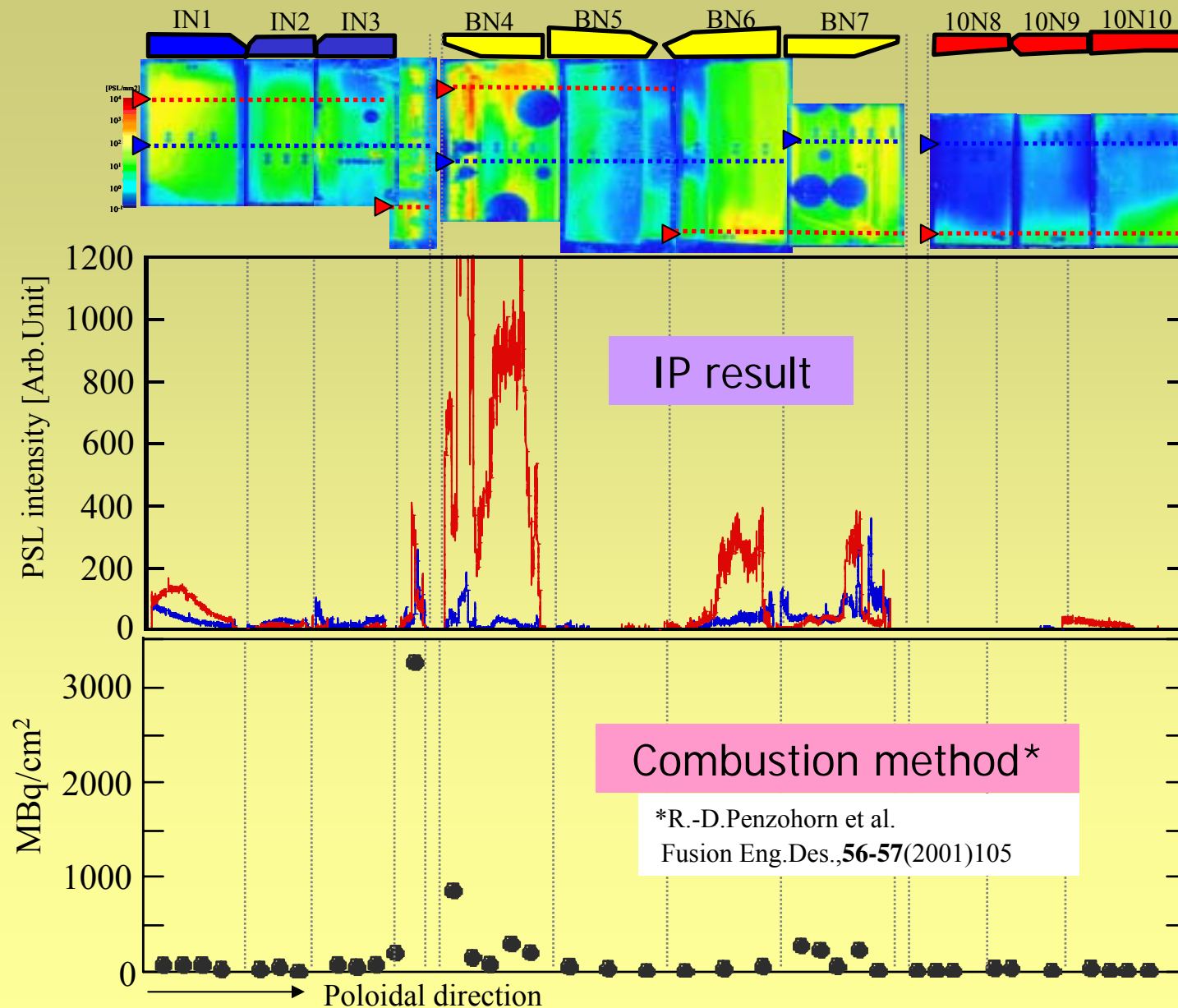
JET

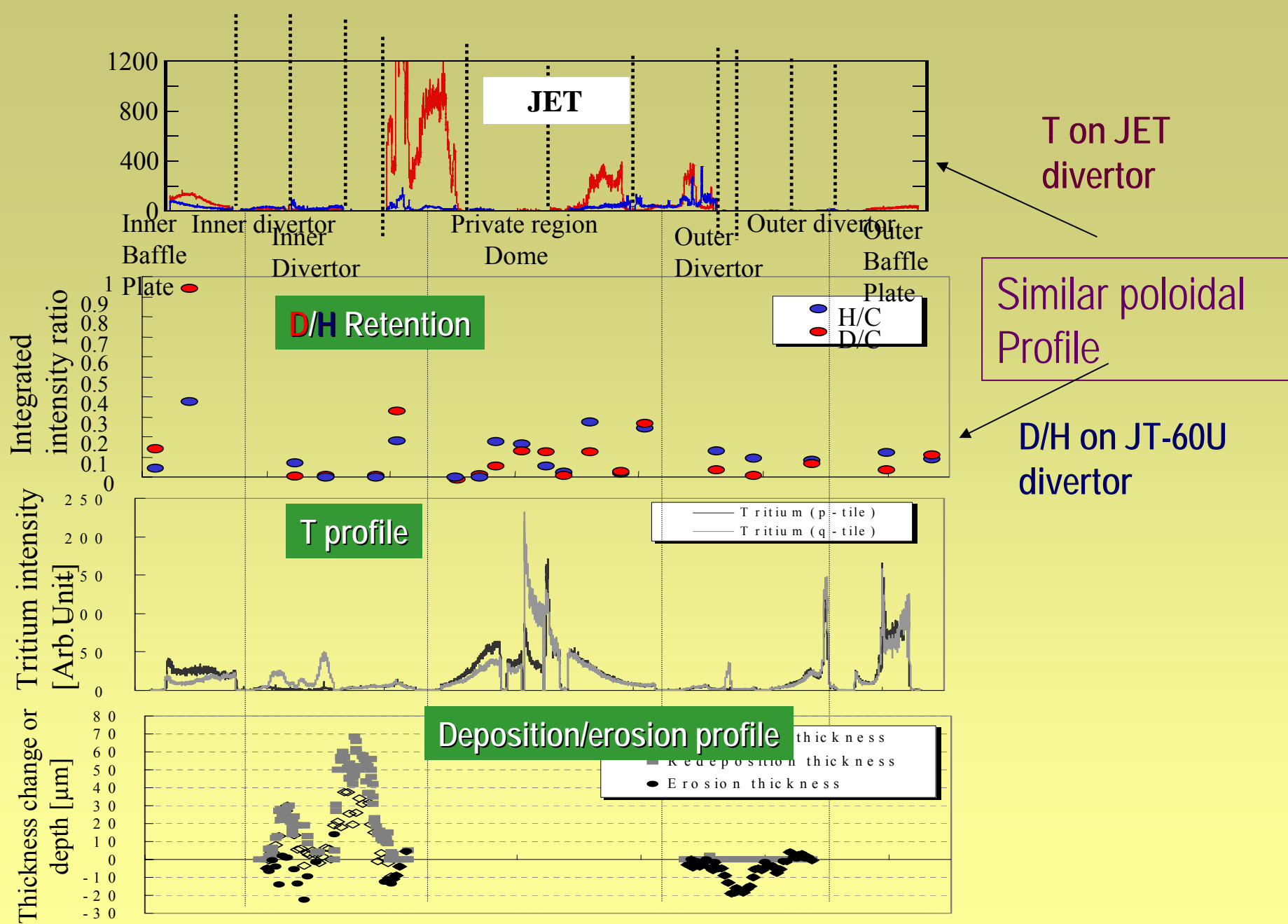


ITER



Tritium distribution on JET Mark II-2A divertor





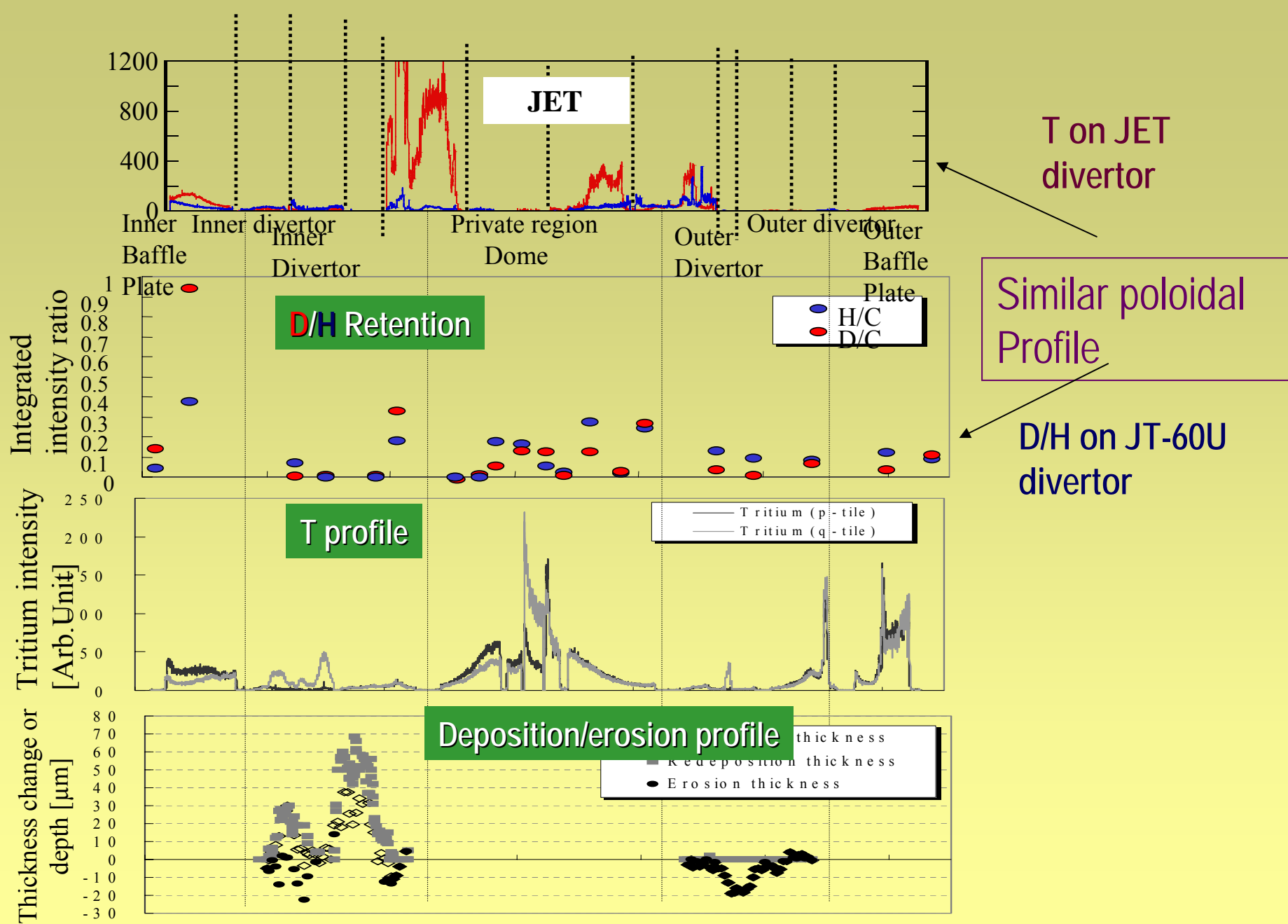
Results observed in JT-60U

- **D(H) is retained very near surface with concentration of $(H+D)/C \leq 0.05$**
 - **No correlation between D(H) and carbon deposition**
 - **$(D+H)/C$ is highest at the dome top similar to T retention**
-
- **Deposited layers of Max of 60 μ m was found on the inner divertor tiles which was strong stuck to substrate**
 - **More or less no dust nor debris was found in the vacuum vessel**
 - **No deposition in remote area even in NBI ducts and their cryo-panels**

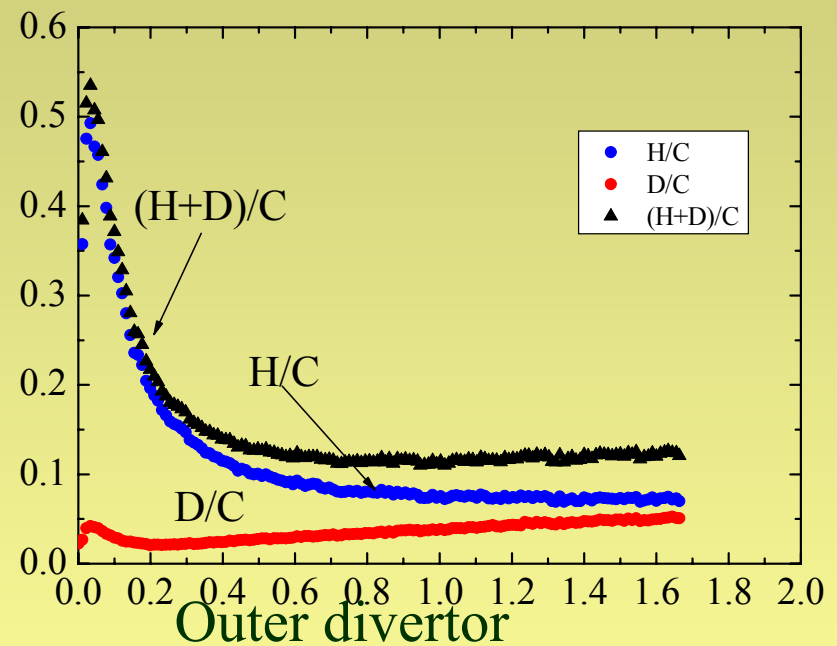
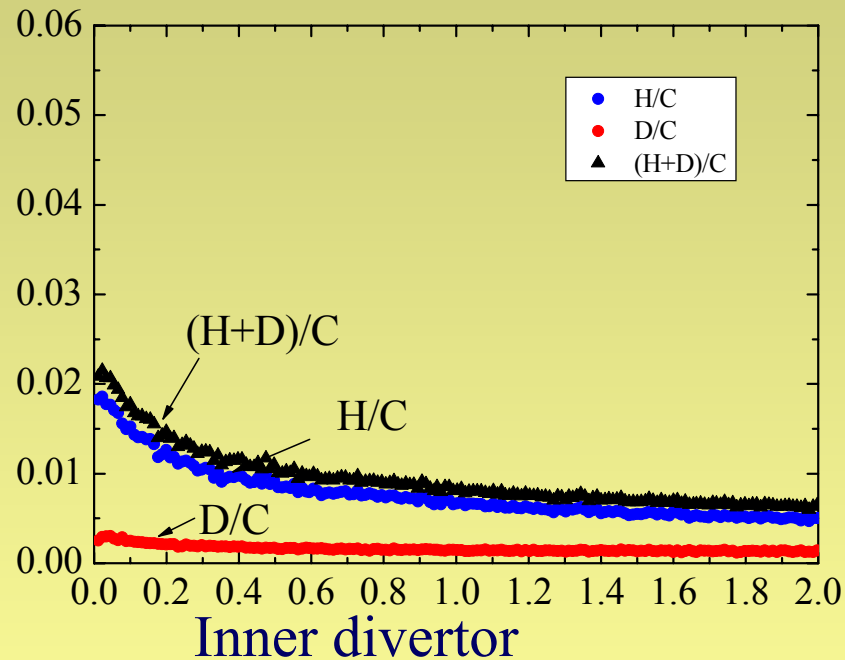
Carbon transport and tritium retention in JT-60U seem much less than those of JET

Possible reasons

- **Higher divertor surface temperature in JT-60U**
- **Better alignment of neighboring tiles (shorter tile length in toroidal direction also helps)**
- **Different geometry of divertor structure including pumping direction and pumping method**
- **Different Divertor plasma**



Depth distribution of H/ D at deposition area measured by SIMS

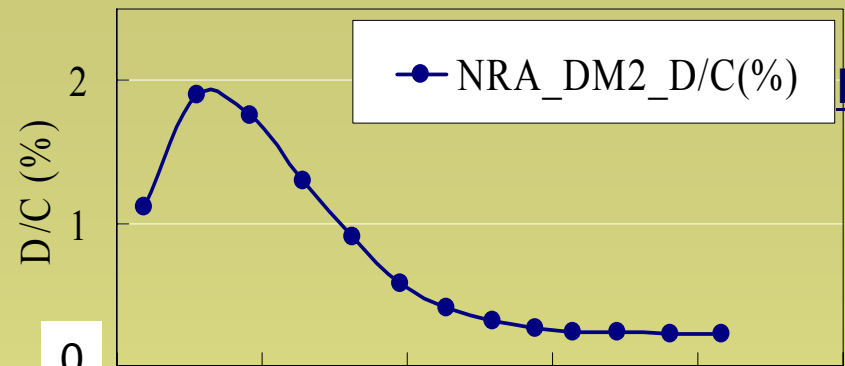
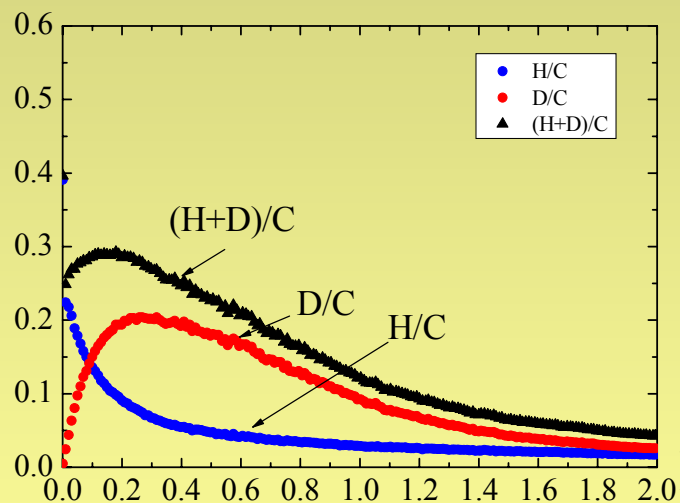


Inner divertor showed less surface H and D retention and small but constant retention in deep.

Deposition area of outer divertor which is eroded has high surface retention.

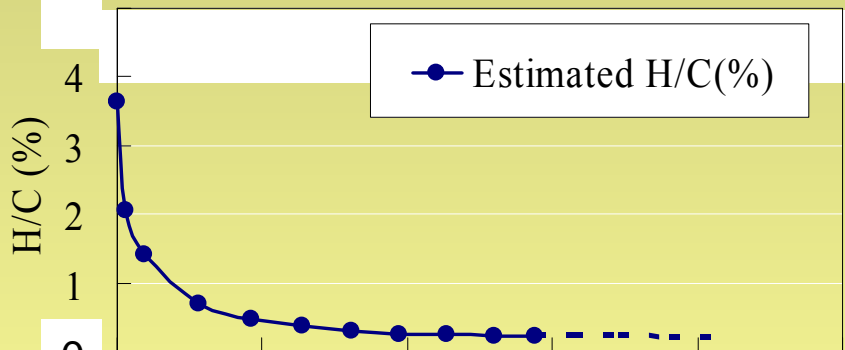
SIMS and NRA Comparison [DM2]

Dome top tile



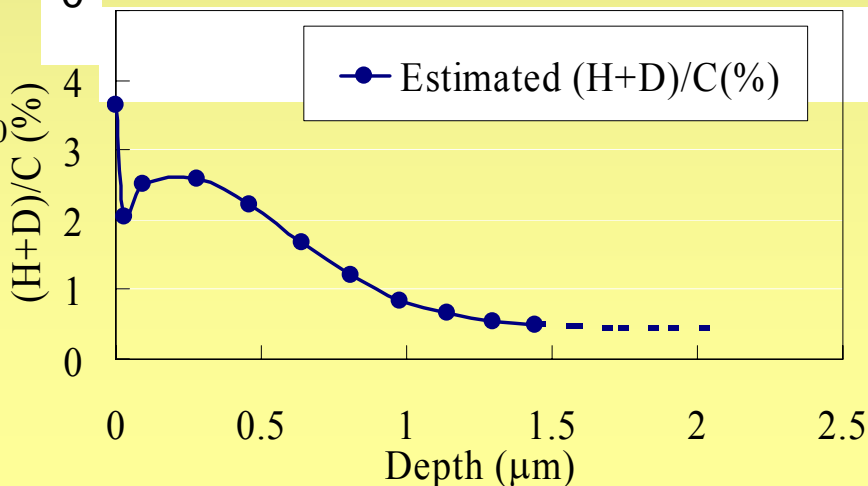
NRA:

D retention within $2.1 \mu\text{m}$
 $\sim 8.0 \times 10^{16} (/ \text{cm}^2)$
D/C $\sim 2\%$ (max)



SIMS

H retention within $<2.1 \mu\text{m}$
 $\sim 4.3 \times 10^{16} (/ \text{cm}^2)$
H/C at surface $\sim 3.5\%$



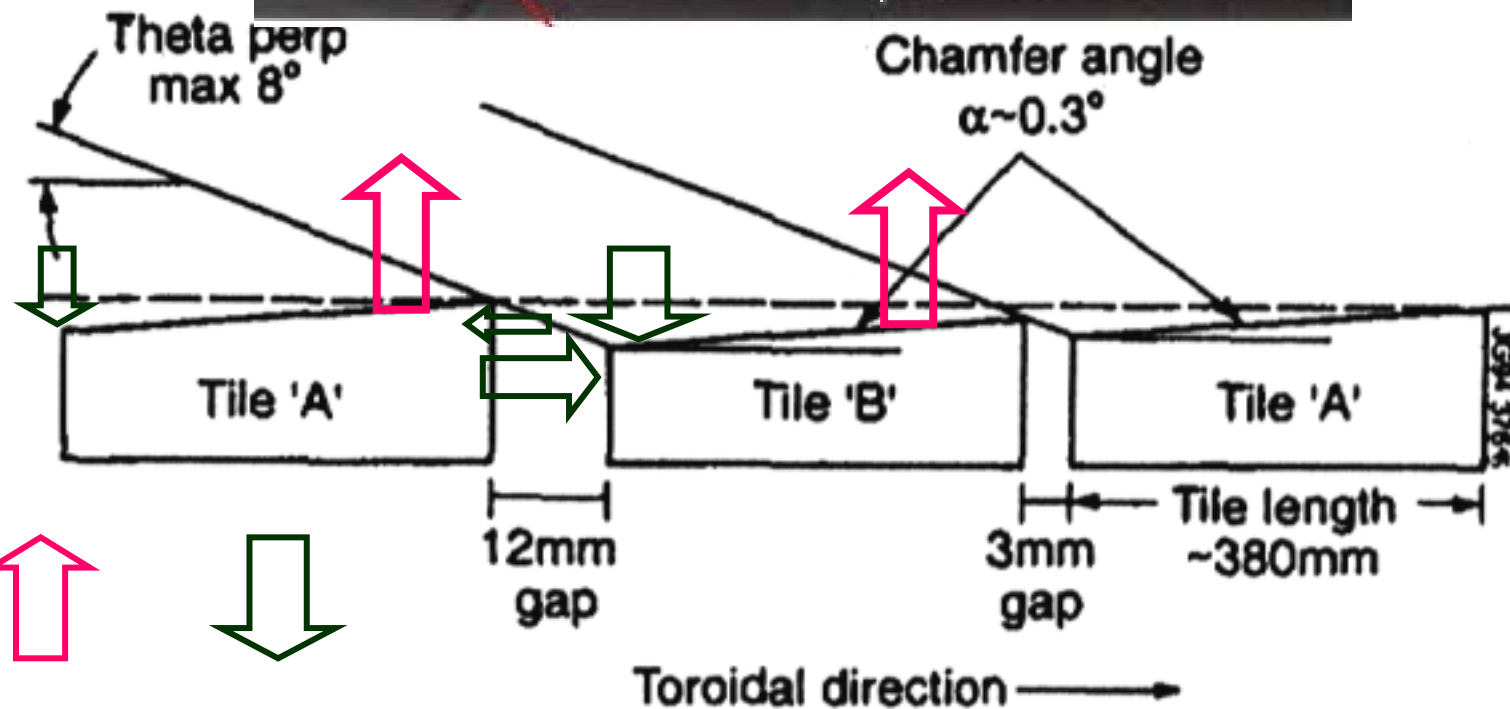
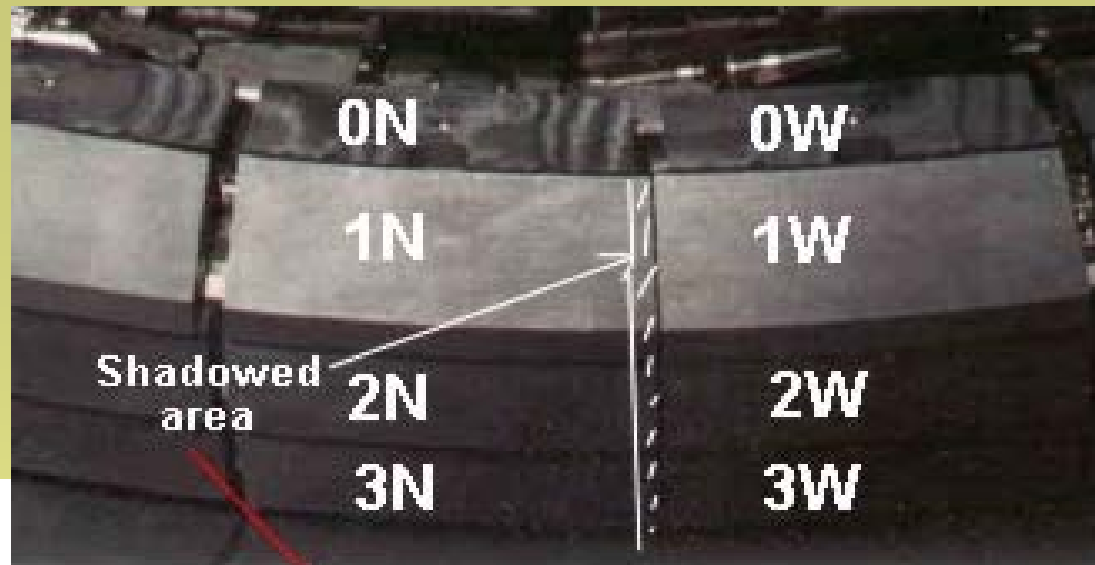
NRA + SIMS

(H+D)/C ($<2.1 \mu\text{m}$)
 $\sim 1.2 \times 10^{17} (/ \text{cm}^2)$
(H+D)/C ($<0.5 \mu\text{m}$)
(H+D)/C $\sim 2.5\%$

Where tritium would be retained in ITER, if carbon is used as PFM?

T is likely retained in carbon deposits

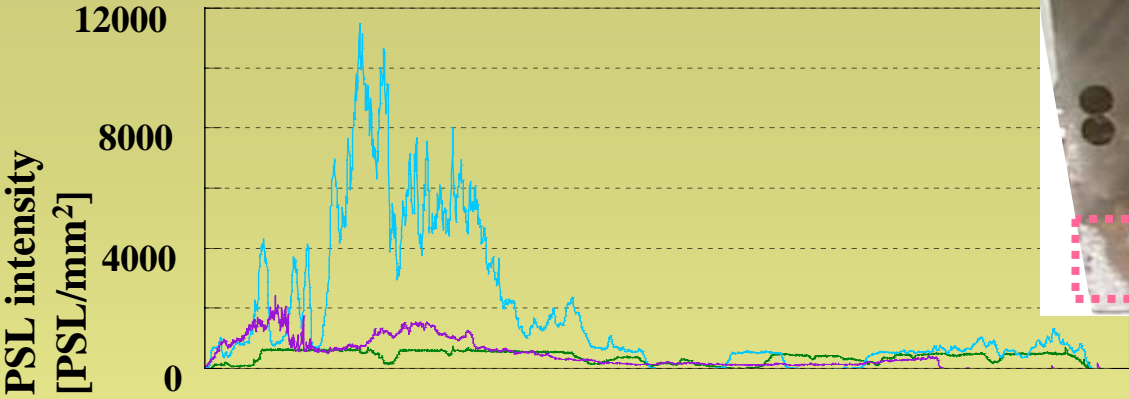
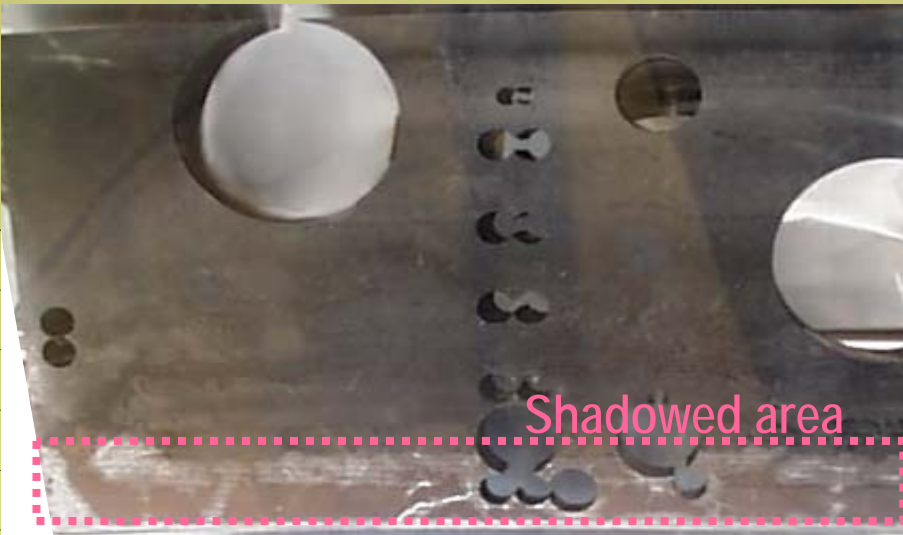
- **Where carbon codeposits?**
- **How important is geometrical structure ?**
 - Divertor structure, position and structure of pumping slot etc.**
 - Structure of armor tile, Alignment, Tile gap,**
- **How about plasma condition, energy, flux, material temperature?**
- **How important rather high energy injection near private region and baffle plate?**



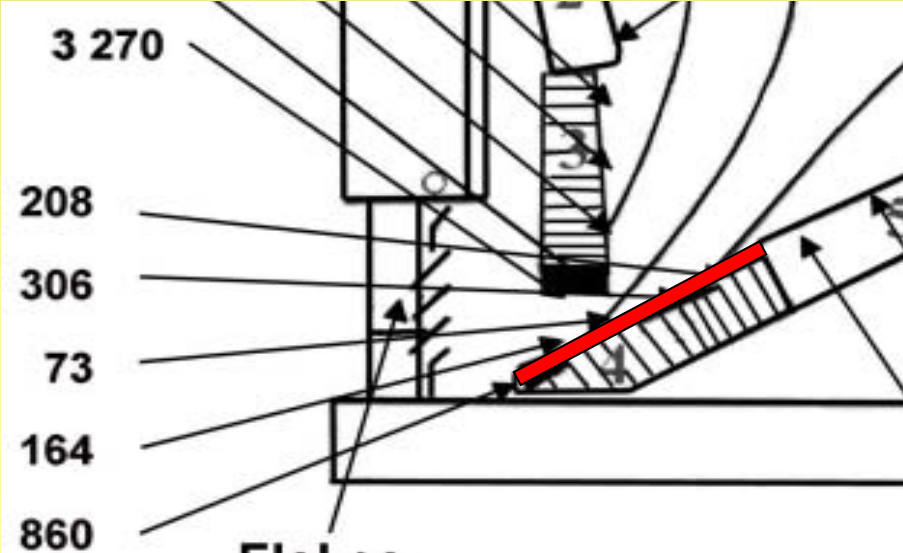
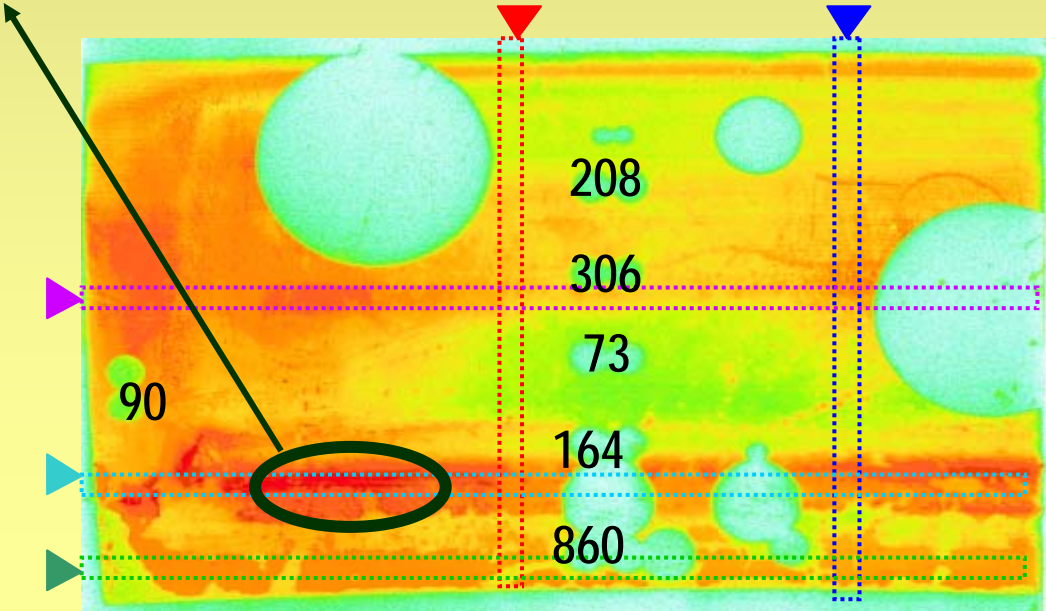
Erosion

Deposition

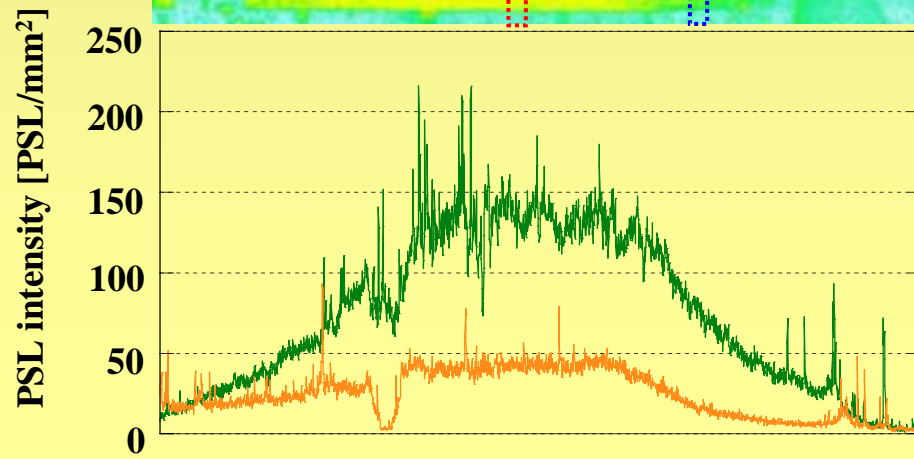
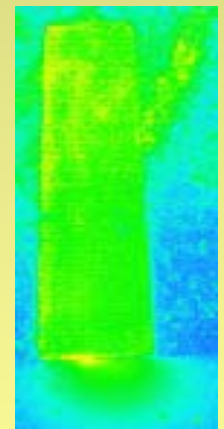
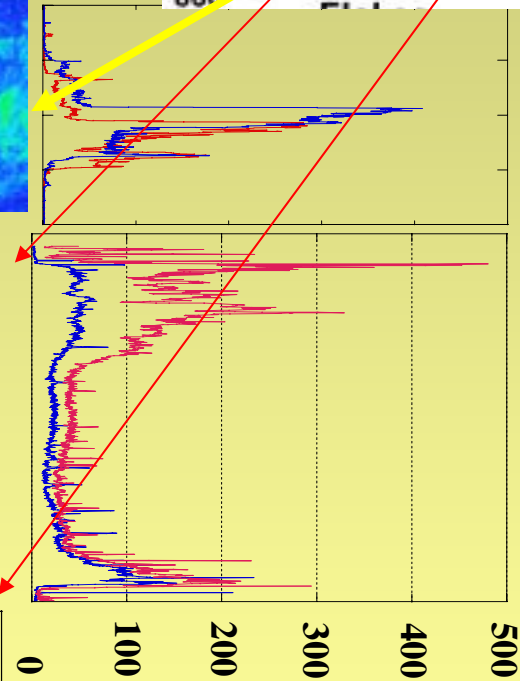
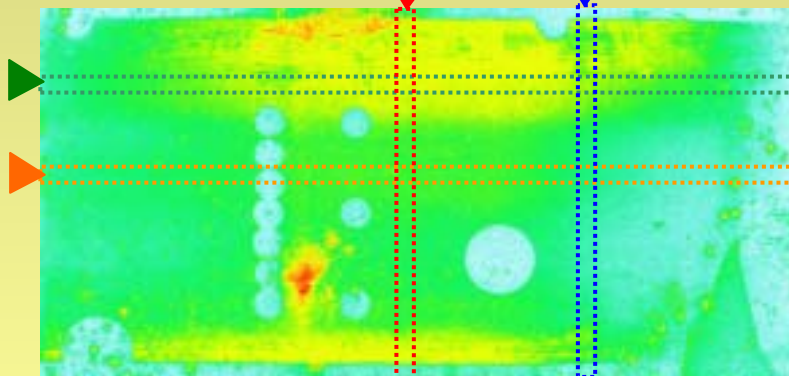
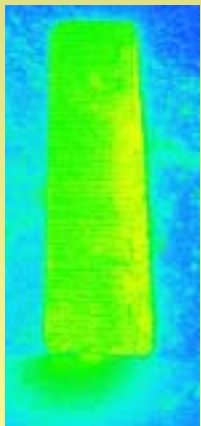
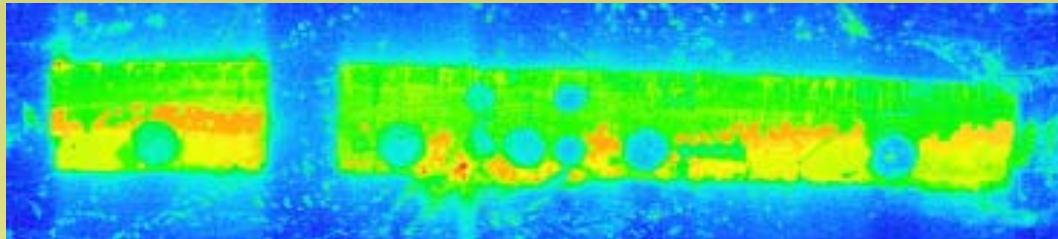
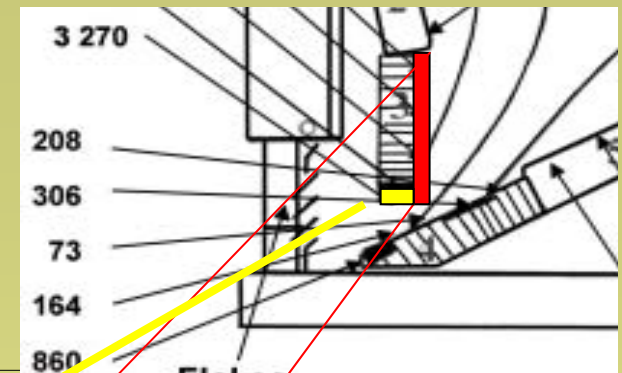
JET Divertor base tile



Highest tritium level $\hat{=}$ 3GBq/cm²



Numbers in MBq/cm²



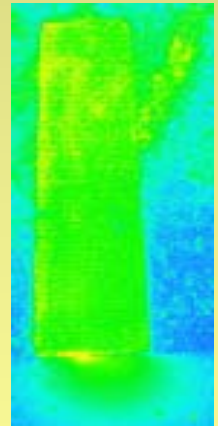
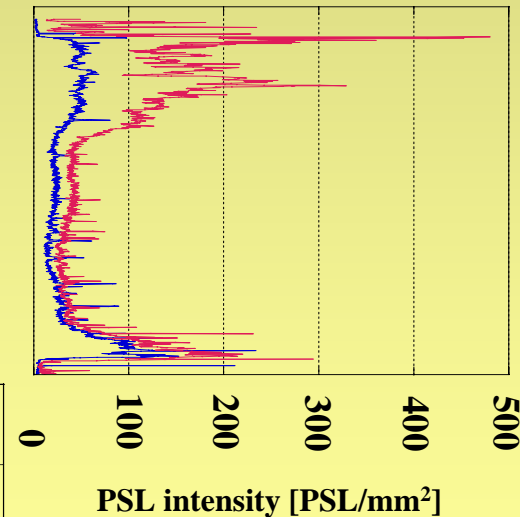
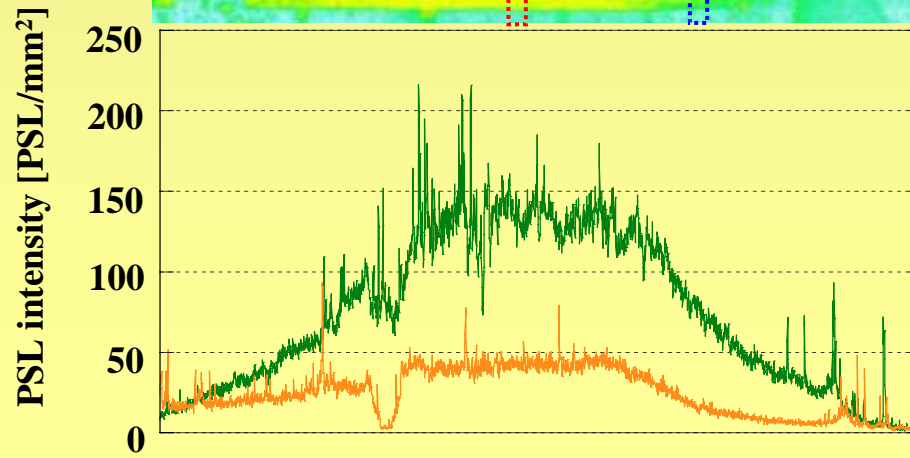
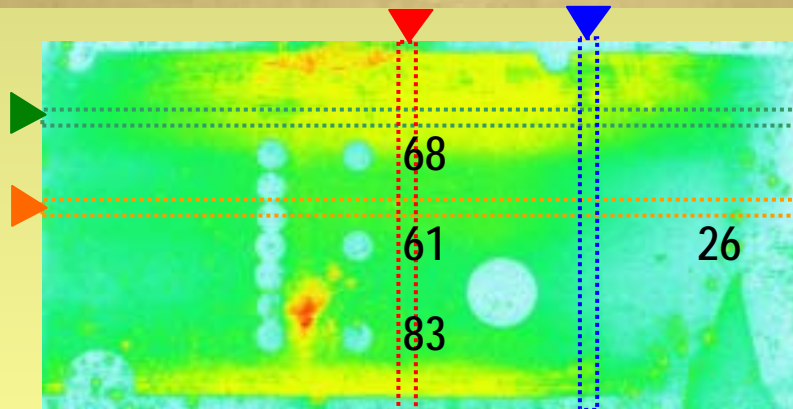
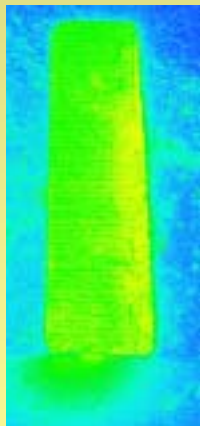
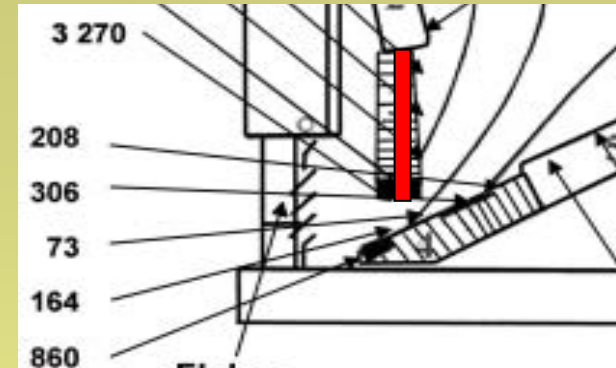
Wide gap
phasing side

Narrow gap
phasing side

Divertor tile IN3 (Inner)

Deposition at both torodial sides are very small
Difference due to gap length is not significant.
High T retention at plasma phasing central area

Inner divertor tile IN3



Wide gap
phasing side

Narrow gap
phasing side

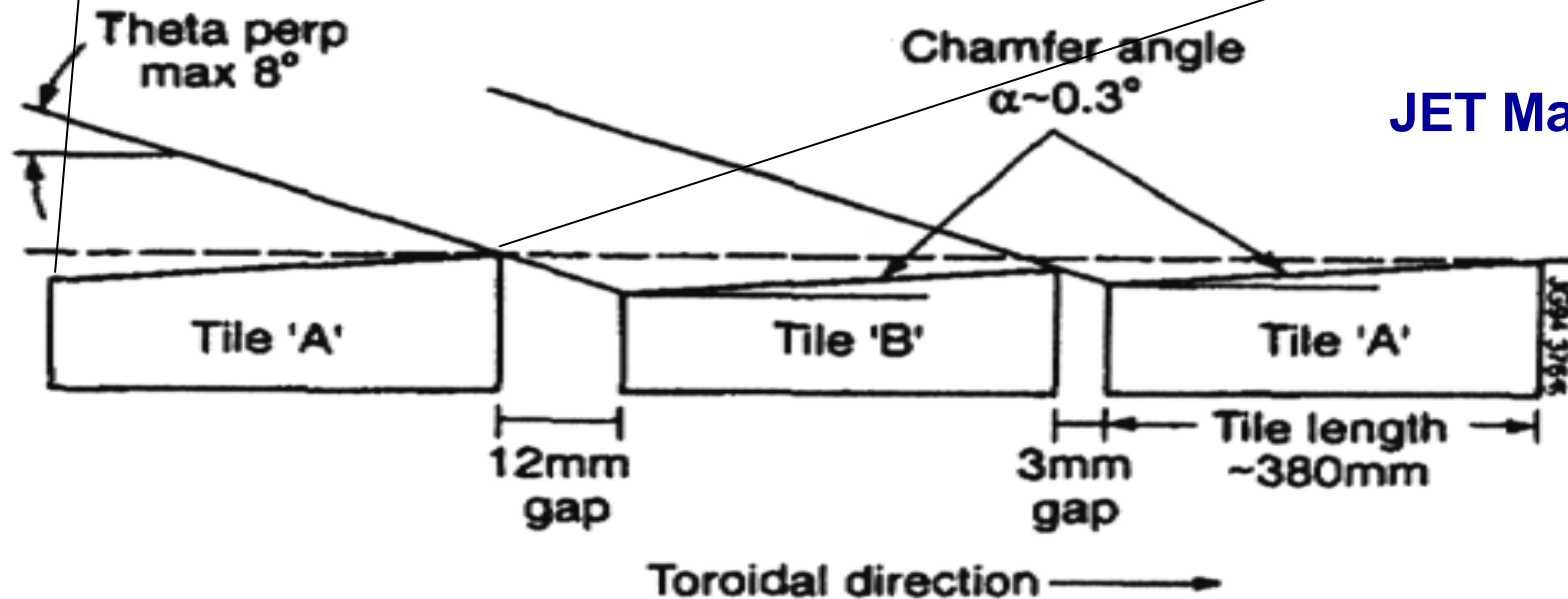
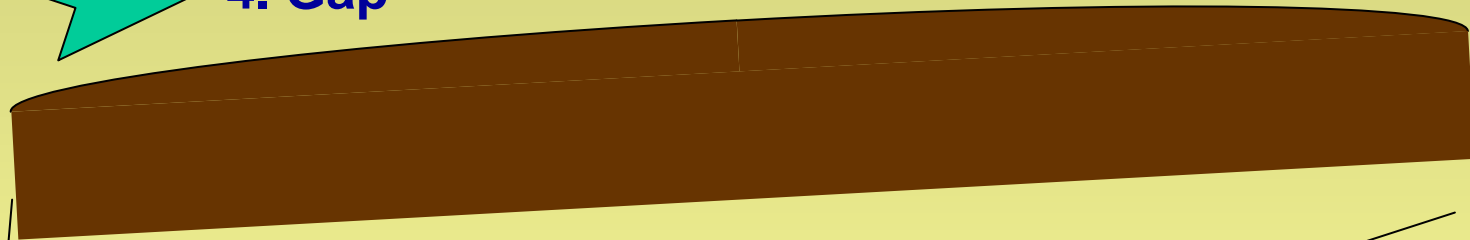
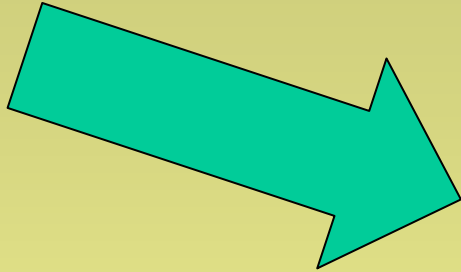
Four Important Effect

Four geometrical

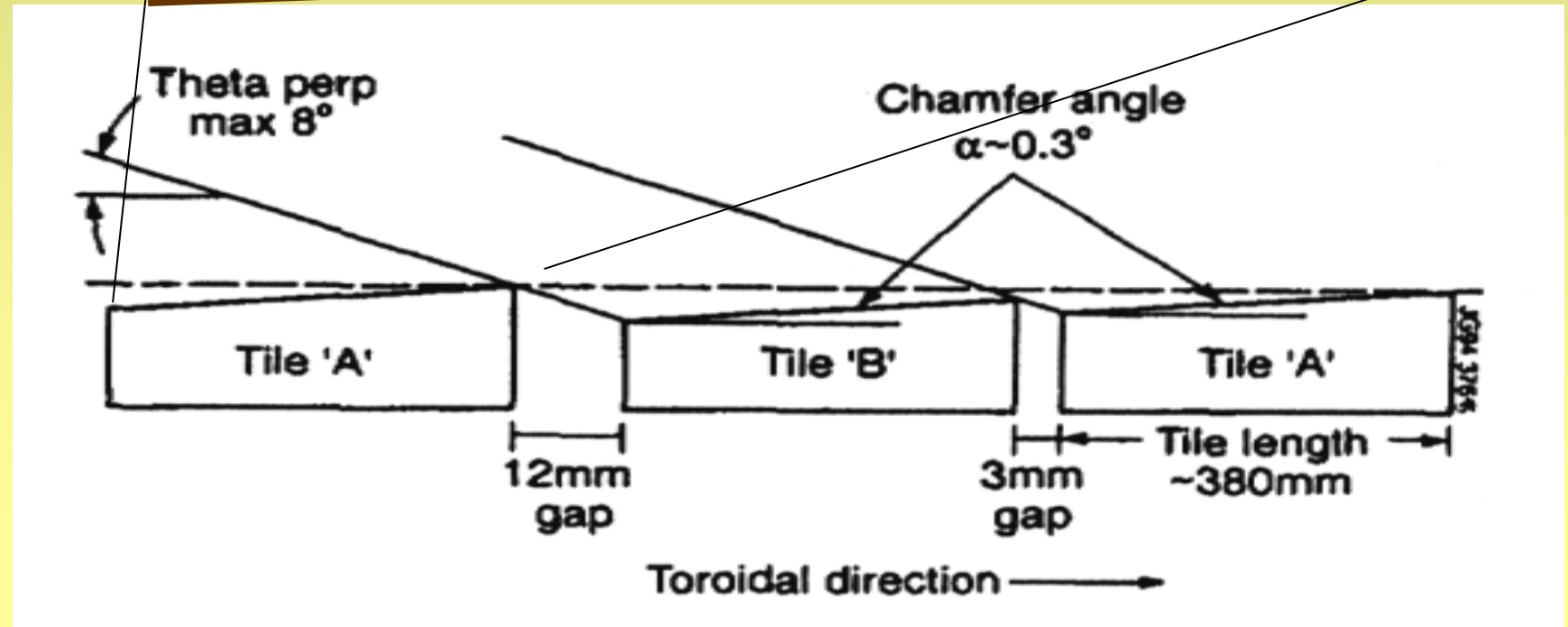
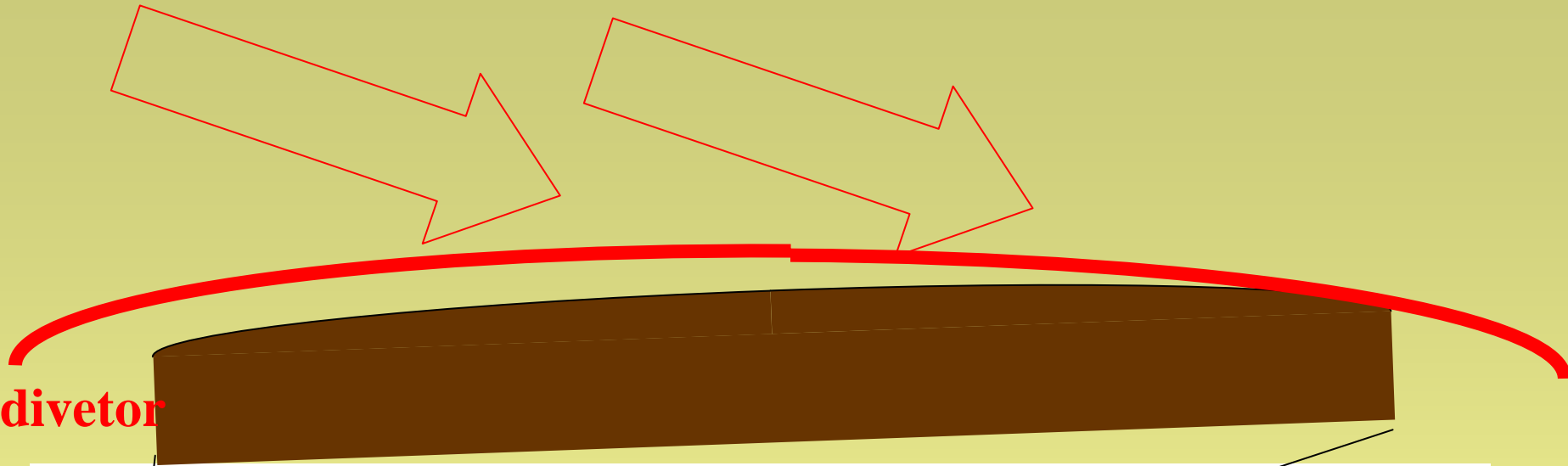
1. Divertor strucute
2. Geometry alignment
3. Tile curvature
4. Gap

Three physical

1. Plasma parameter
2. Surface temperature
3. Substrate temperature

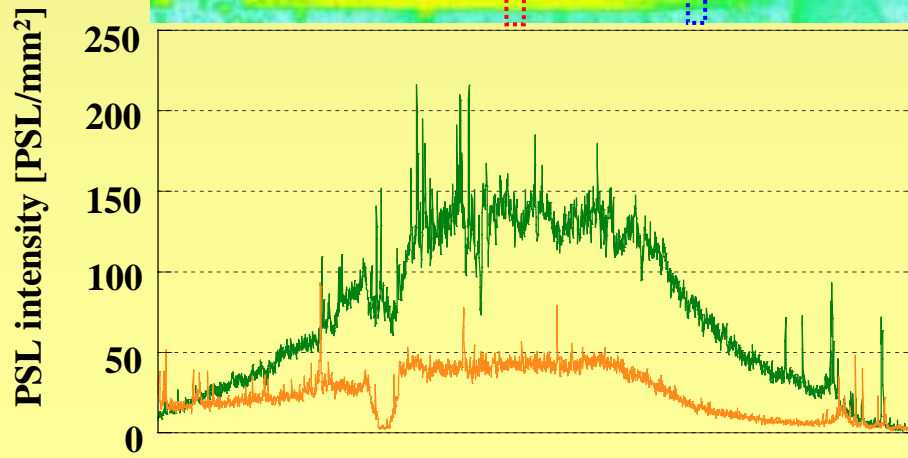
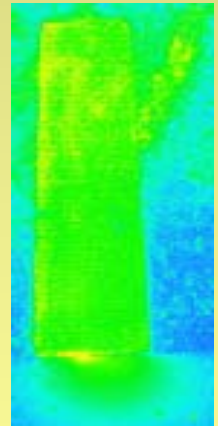
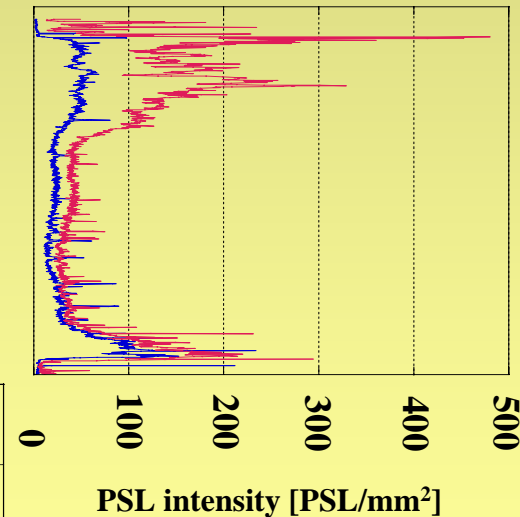
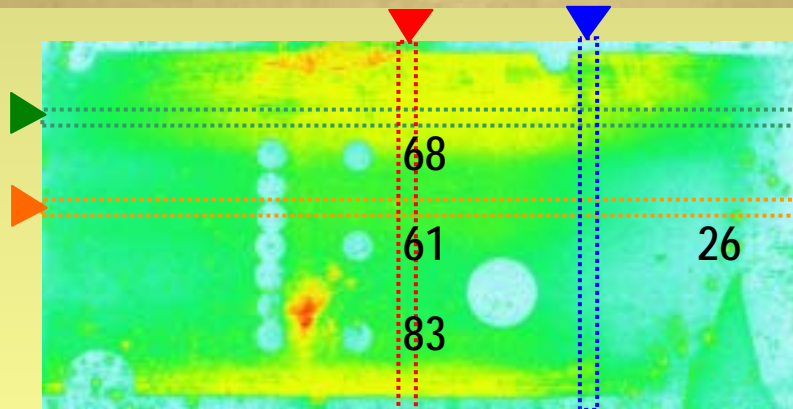
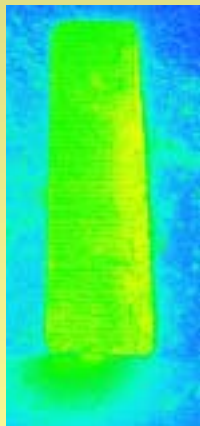
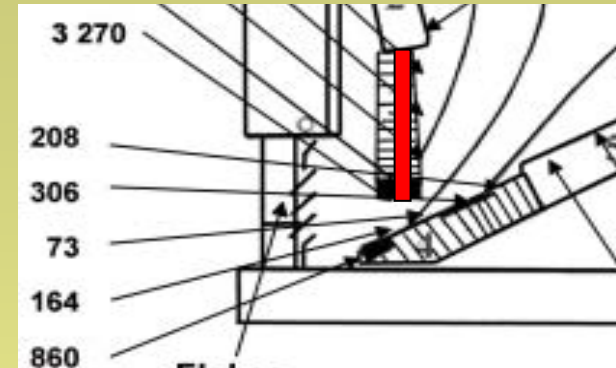


How Last closed surface hit tile surface



Deposition at both torodial sides are very small
Difference due to gap length is not significant.
High T retention at plasma phasing central area

Inner divertor tile IN3

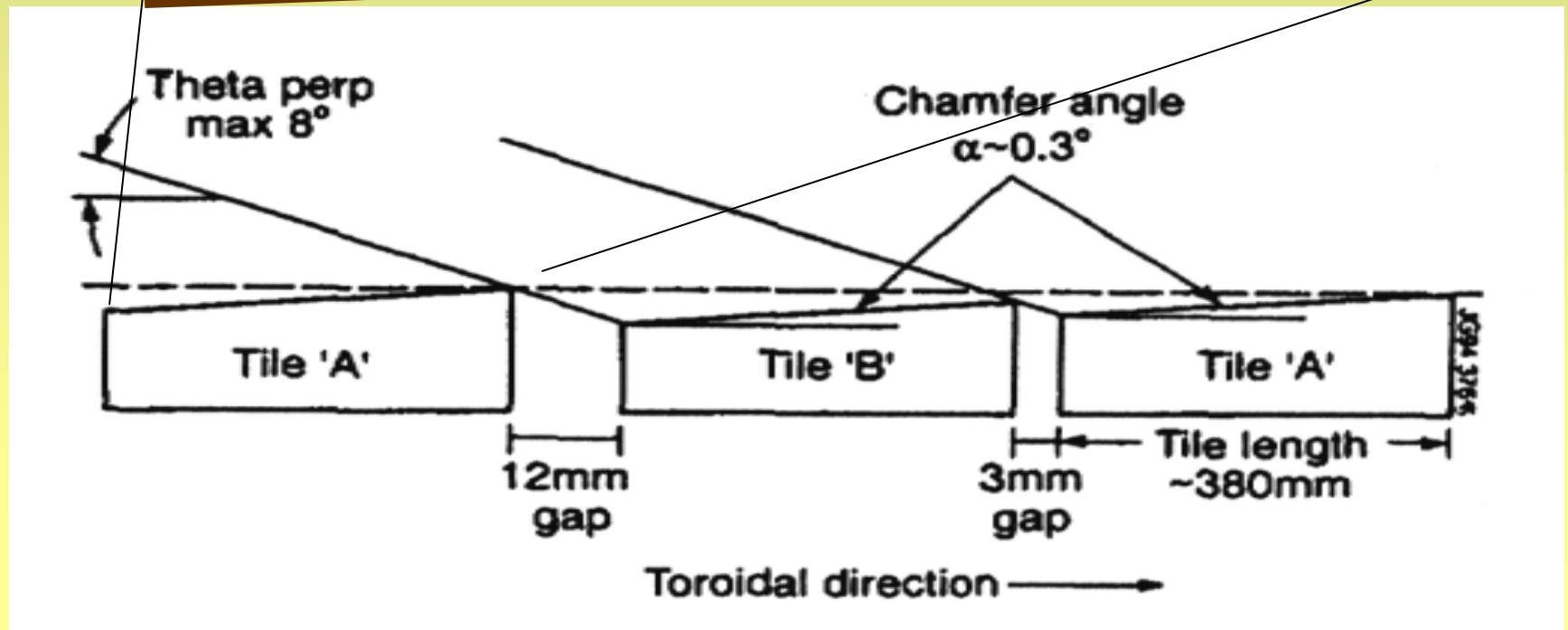


Wide gap
phasing side

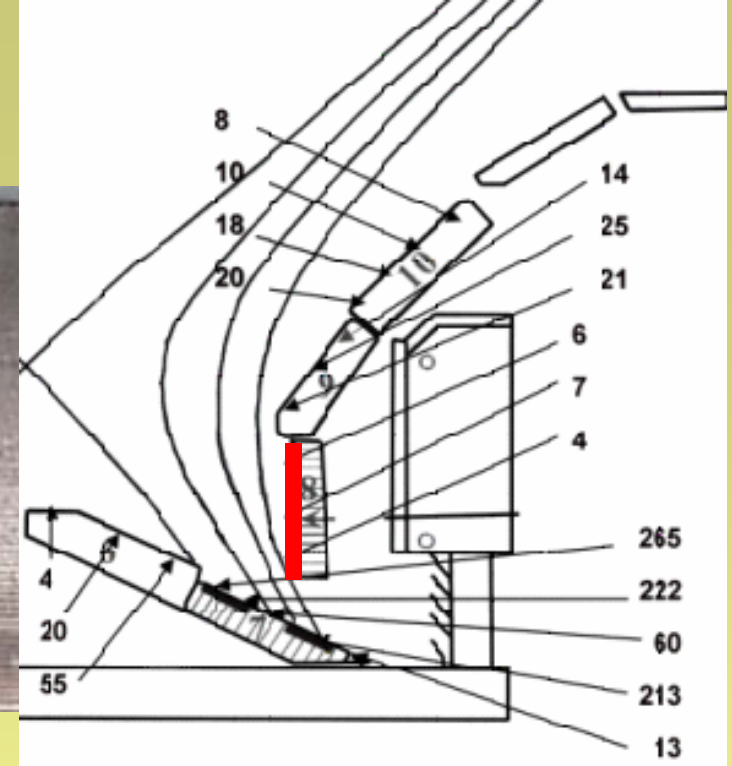
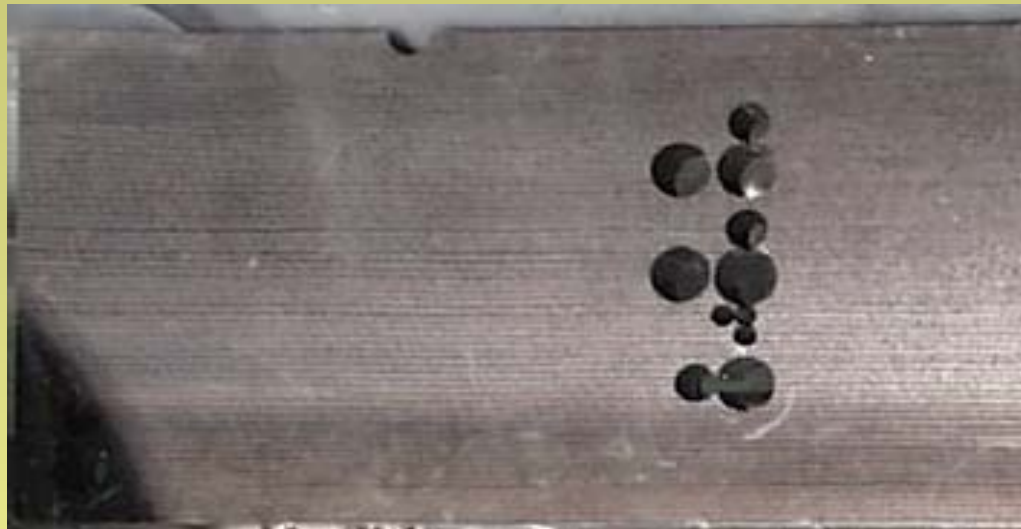
Narrow gap
phasing side

How Last closed surface hit tile surface

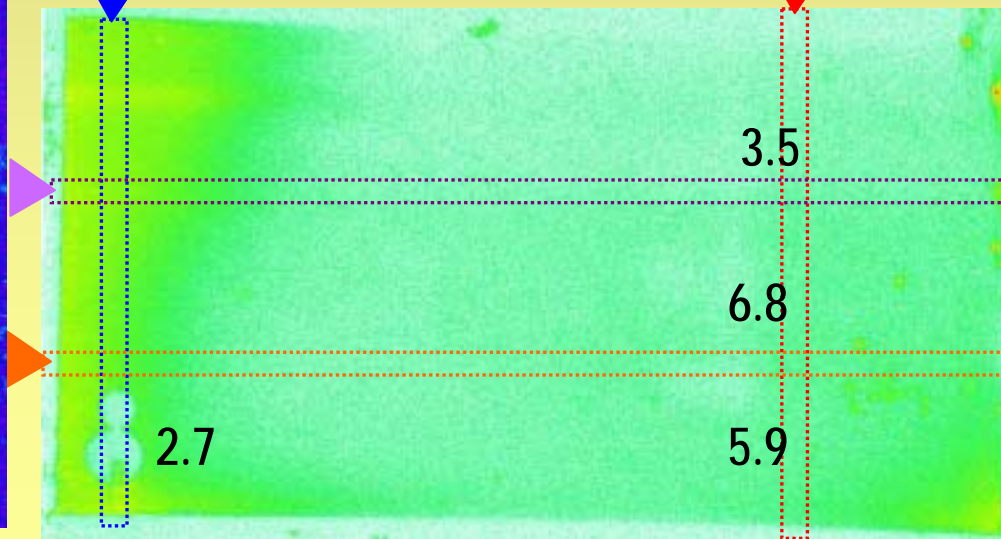
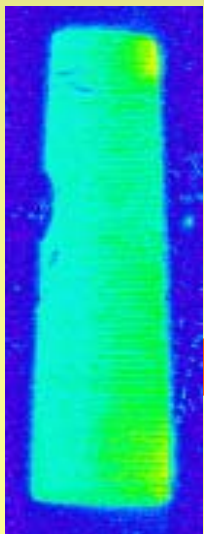
Outer divetor



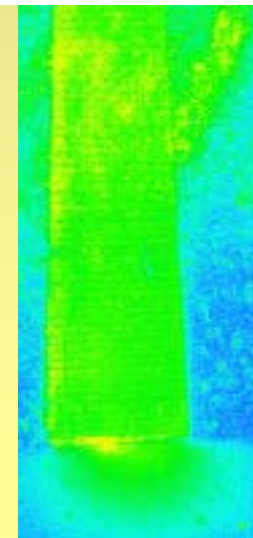
Outer Divertor tile : 10N8



0



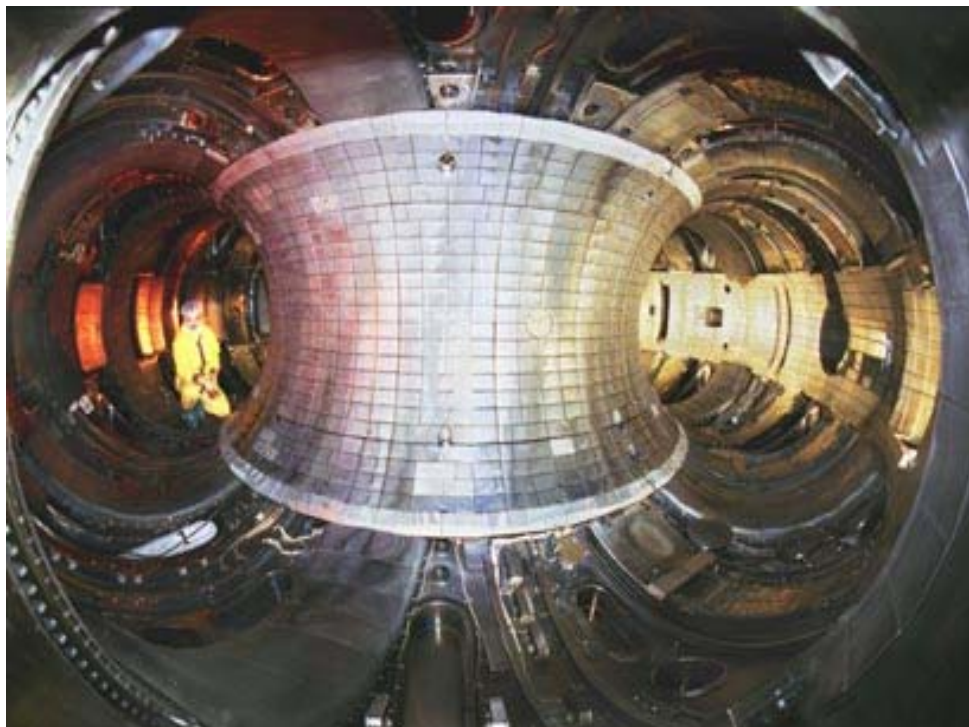
Wide gap
phasing side



Narrow gap
phasing side

3-1. D-T operation in TFTR

- . Bumper limiter machine – no divertor.
- . Walls are deposition areas (not erosion)
- . Walls heated only by plasma (limiter hotspots reached ≈ 800 C).



- 1993-1997: Tritium introduced ~ 5.2 g
- To remove tritium: GDC, Air ventilation etc.
- Long-term tritium retention
 - · 16% of totally introduced

Different edge conditions to JET

TFTR SOL

JET divertor

(TRANSP/DEGAS)

(EDGE2D)

Ne $10^{18} \sim 10^{19} \text{ m}^{-3}$

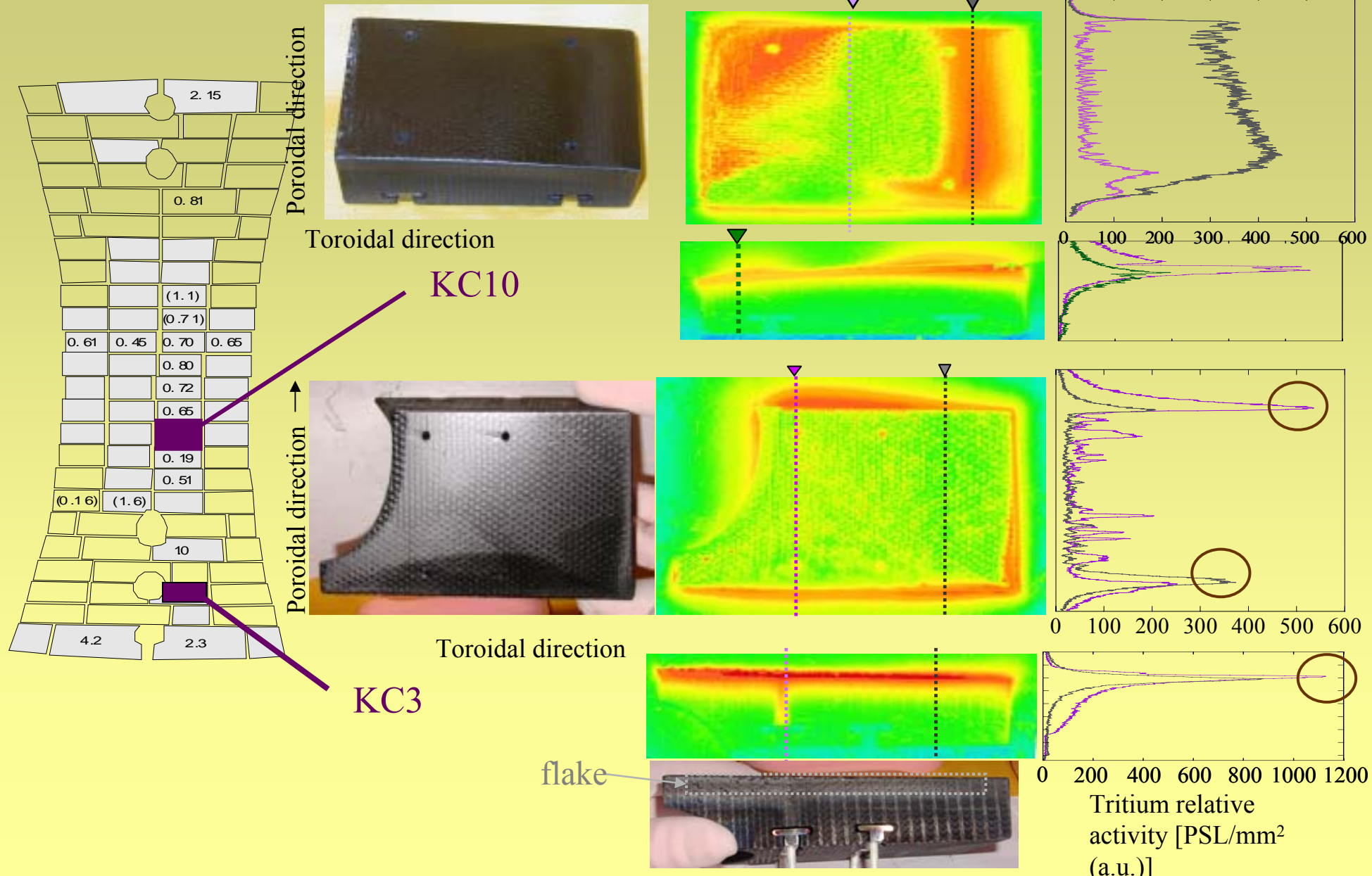
$\sim 10^{20} \text{ m}^{-3}$

Te 200 - 600eV

$< 30 \text{ eV}$

TFTR Bumper limiter tiles

Deposition at gap particularly surface eroded region is very large

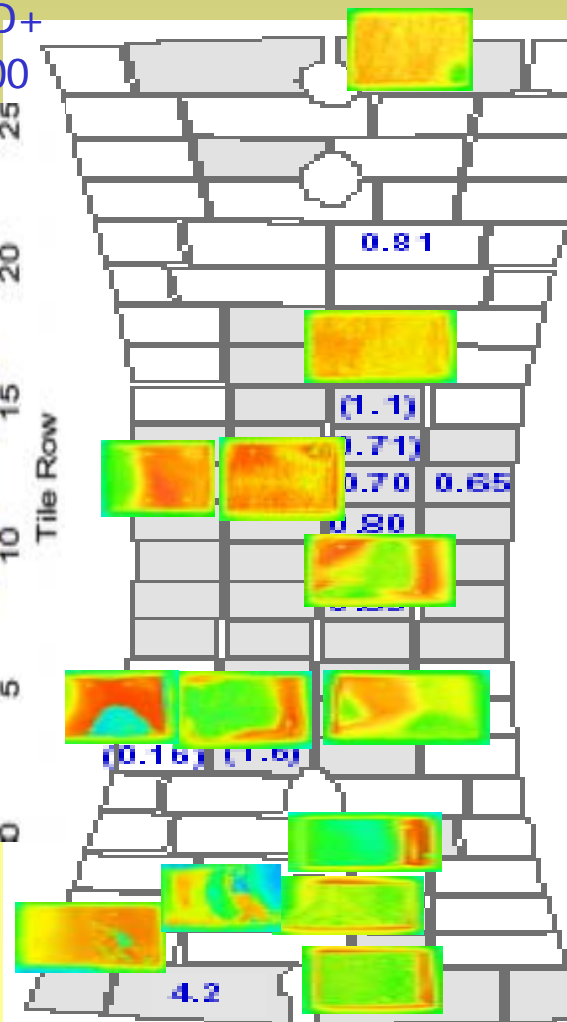
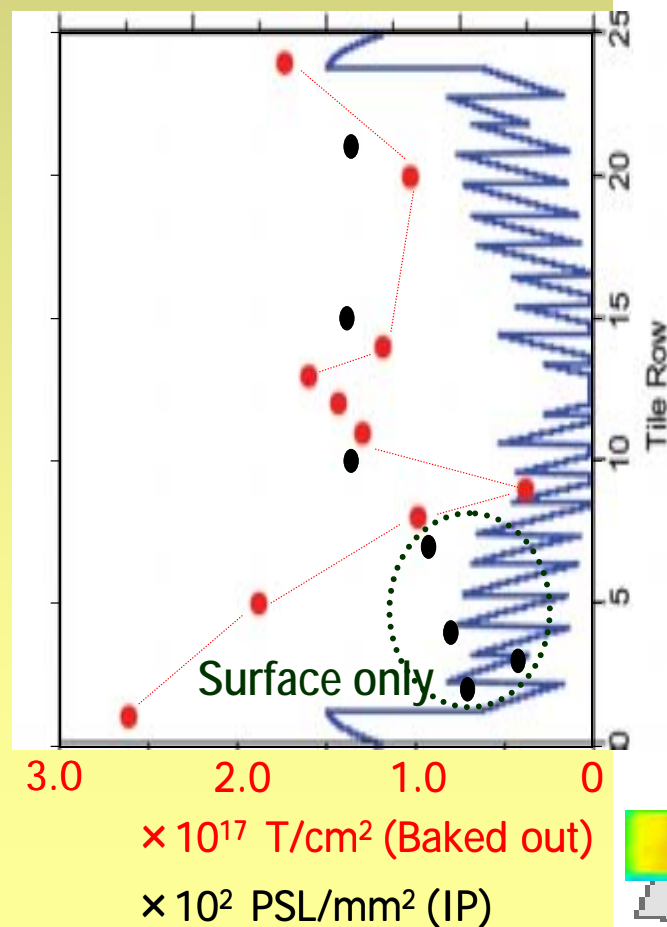


● IP : plasma facing surface only

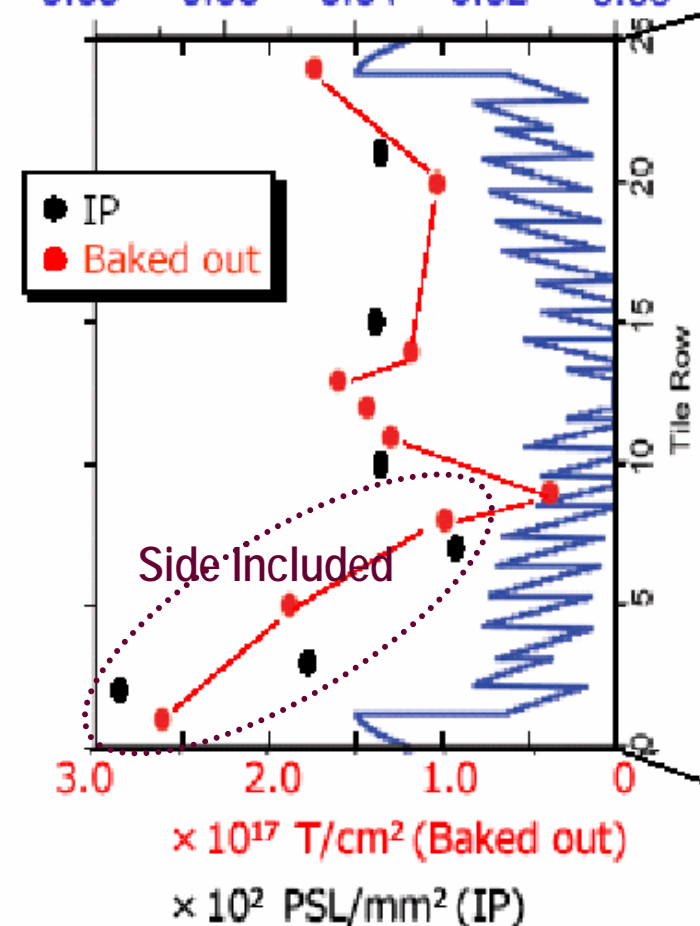
● thermally Desorbed

● IP : including tile sides

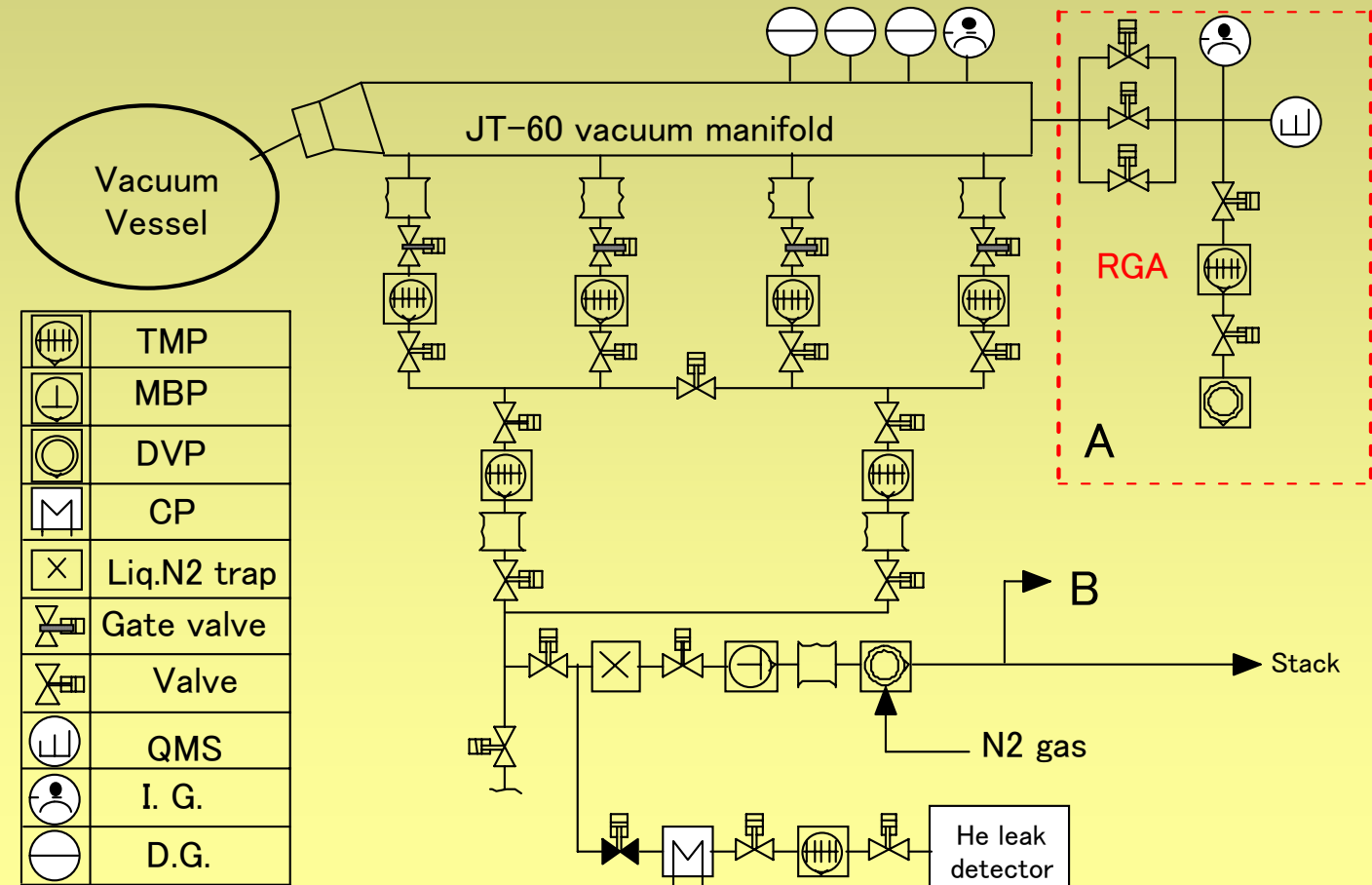
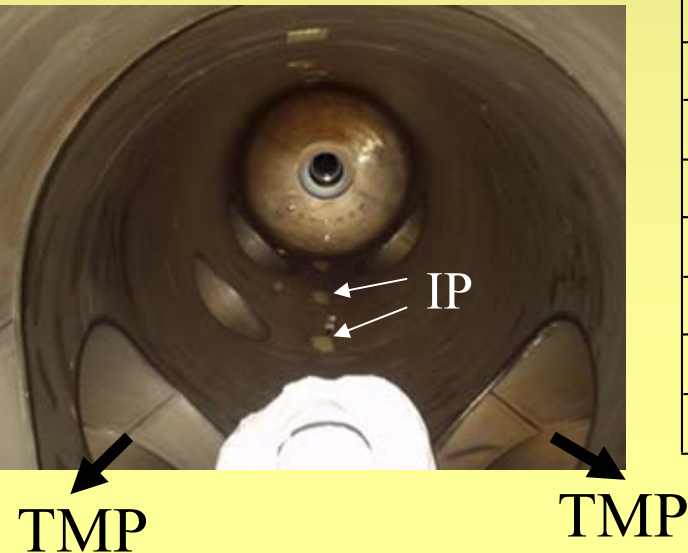
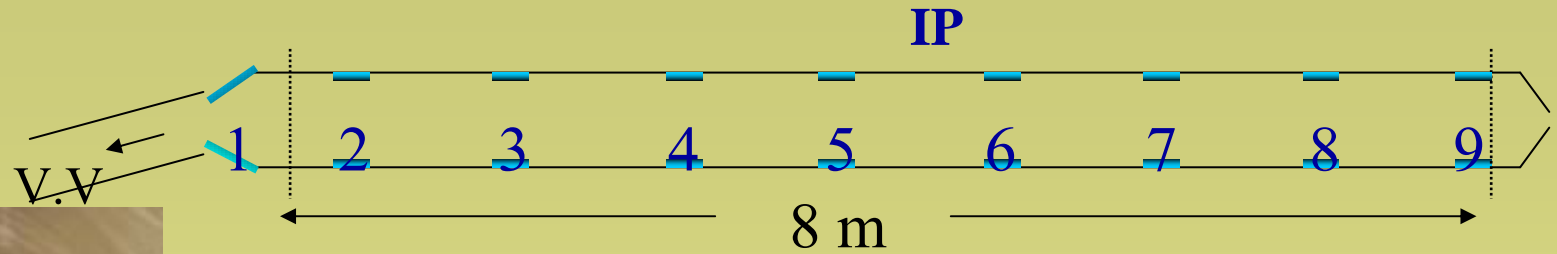
Effective sputtering yield $\Gamma C^0/\Gamma D^+$
0.08 0.06 0.04 0.02 0.00



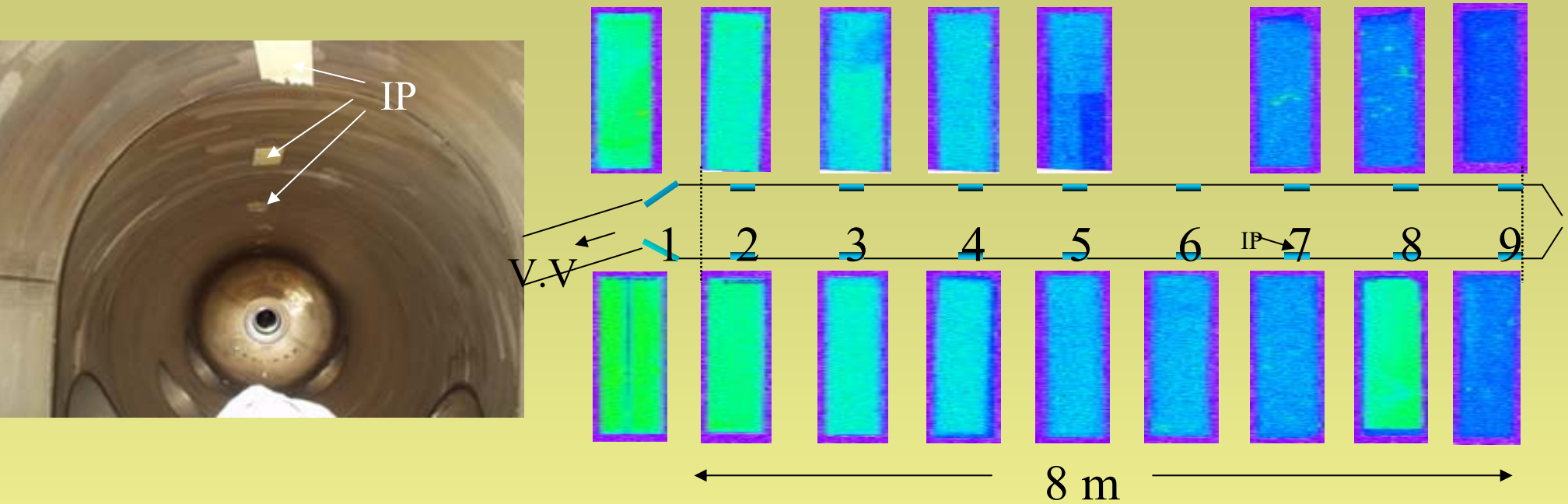
Effective sputtering yield $\Gamma C^0/\Gamma D^+$
0.08 0.06 0.04 0.02 0.00



Inspection of inside of pumping duct

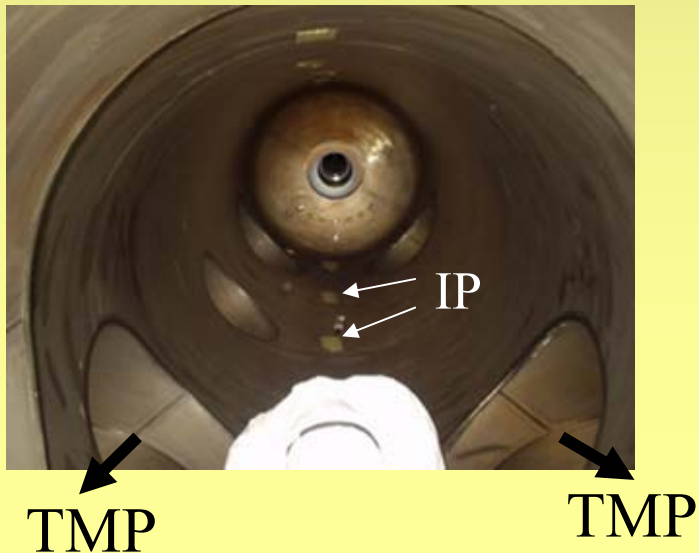


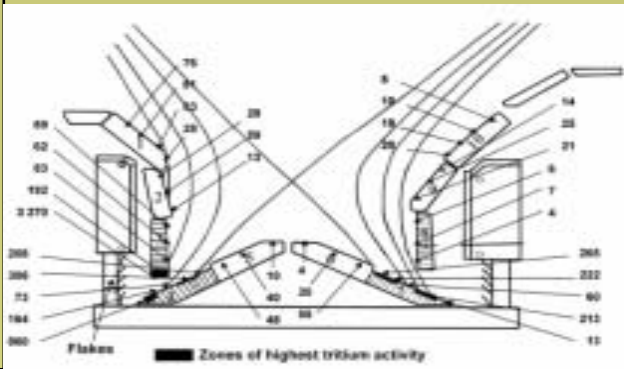

Activity measurements by IP and T monitor



Quite few deposition!!

Activity mostly comes from γ -ray



		
Deposition rate at inner divertor	55g/Ch	2.3nm/s
Erosion rate at outer divertor		0.7nm/s
D/C in deposits	0.4-0.1	< 0.07
Deposition at remote area Collected dust	Louver at inner divertor Louver 150g, Floor 800g	Beneath outer divertor 7g
Divertor Pumping	From innerside of inner divertor	From bottom of W shaped divertor
Divertor tile alignment	Large step between tiles	No step between tiles
Divertor temperature	Below 500K Water cooled	Above 600K

5. Concluding remarks on the selection of PFM materials



Be? No, I do not like

W? Yes, I did try to promote, but operational temperature window is too narrow to use. W still needs examination

Carbon based PFM kept above 800K is promising

- ☆ Main tritium source : **Implanted high energy triton**
- ☆ Tritium in deposited layer : **Very small**
- ☆ Tritium on shadowed area : **Totally temperature depend**
- ☆ Recycling : **Metal like at higher temperature**
- ☆ Erosion ? : **That is a question! (Maybe overestimated)**

Remaining issues ;

Tritium codeposition at low temperature area

Detritiation of implanted T

According the present knowledge of physics and chemistry

We can producing pyrolytic carbon containing no hydrogen by thermal decomposition of hydrocarbon above around 1000K.

As observed in JT-60U, higher temperature plasma facing surface gives less tritium (deuterium) retention.

Sputtered carbon is very likely redeposited nearby (prompt redeposition) suggesting reduced erosion by divertor swing.

Is full carbon machine not possible?

Many would say “**No! Nonsense !** because

- 1. Erosion is too high. You should replace PFM every half a year or more frequently.**
- 2. Tritium retention is too high. You need T clean-up something like every 10 shots.**
- 3. Too much hazardous dust would be produced.**

Personal questions to PFM selection (Continued)

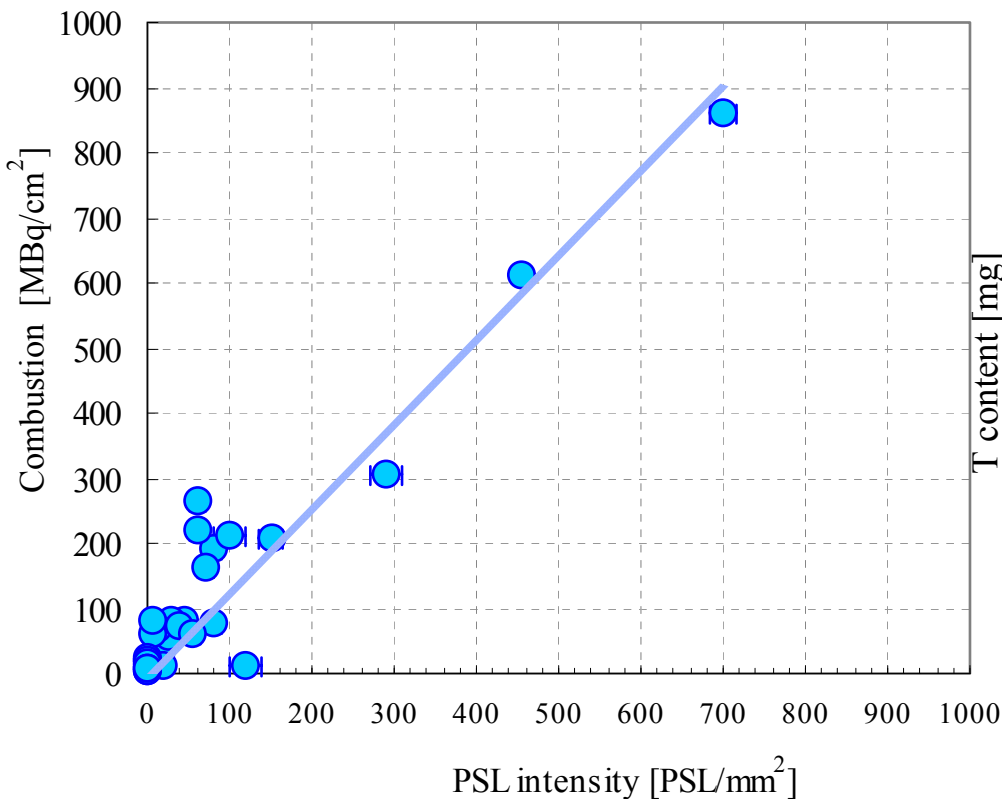
My questions to be answered in this ITPA meeting.

If both erosion and tritium retention are less than the present estimation by a factor of 10 to 100, can we start with full carbon PFM?

Is still Be needed as limiters for plasma start-up and as oxygen getter?

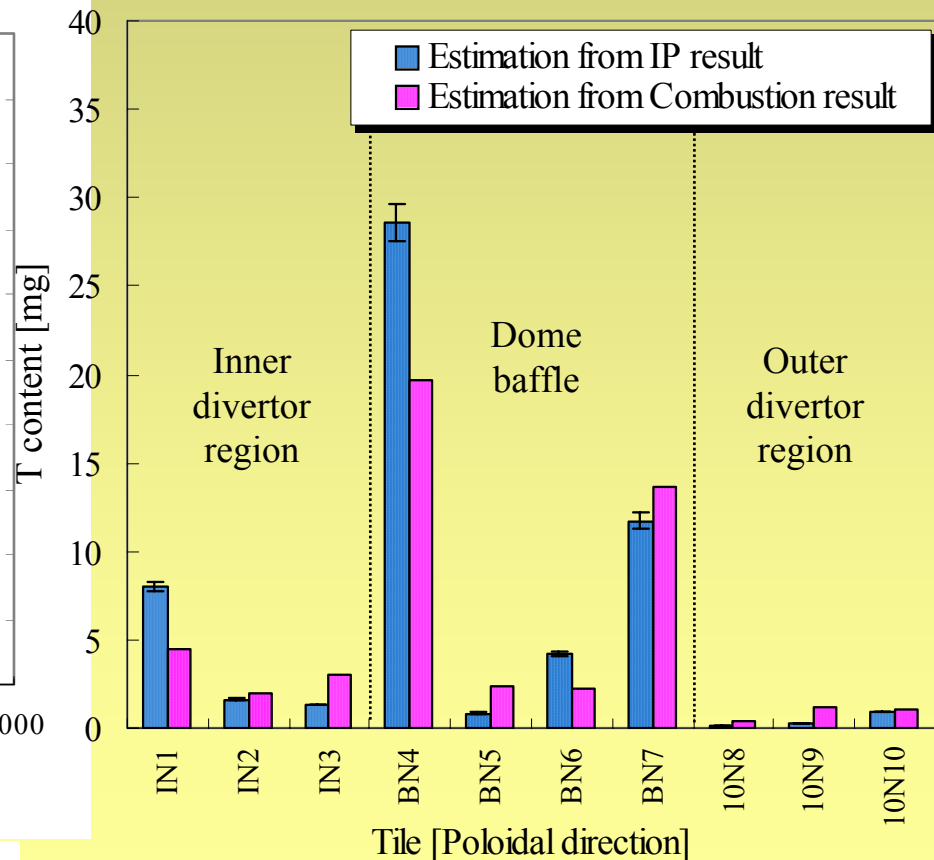
Comparison of ^3T amount for IP (near surface) and Combustion (total)

Calibration of PSL intensity



Calibration

$$[\text{MBq}/\text{cm}^2] = (1.2778 \pm 0.048)[\text{PSL}/\text{cm}^2]$$



After J.P.Coad et al., J.Nucl.Mater. **290-293**(2001)224

◆ Four different kinds of tritium sources

1. High energy triton (produced by D-D reaction with 1/300 of He by D-T reactor)

- Implanted into tiles in μm range uniformly in present tokamaks
- Toroidal and poloidal asymmetry due to magnetic field and heat load

2. Tritium fueled by gas, pellet and NBI (Similar behavior as H and D)

- Codeposits with carbon at plasma shadowed low temperature area
- Non-uniformity due to plasma flux and tile geometry
- Main contribution on low temperature machine
- Small retention at eroded area

3. Gaseous T

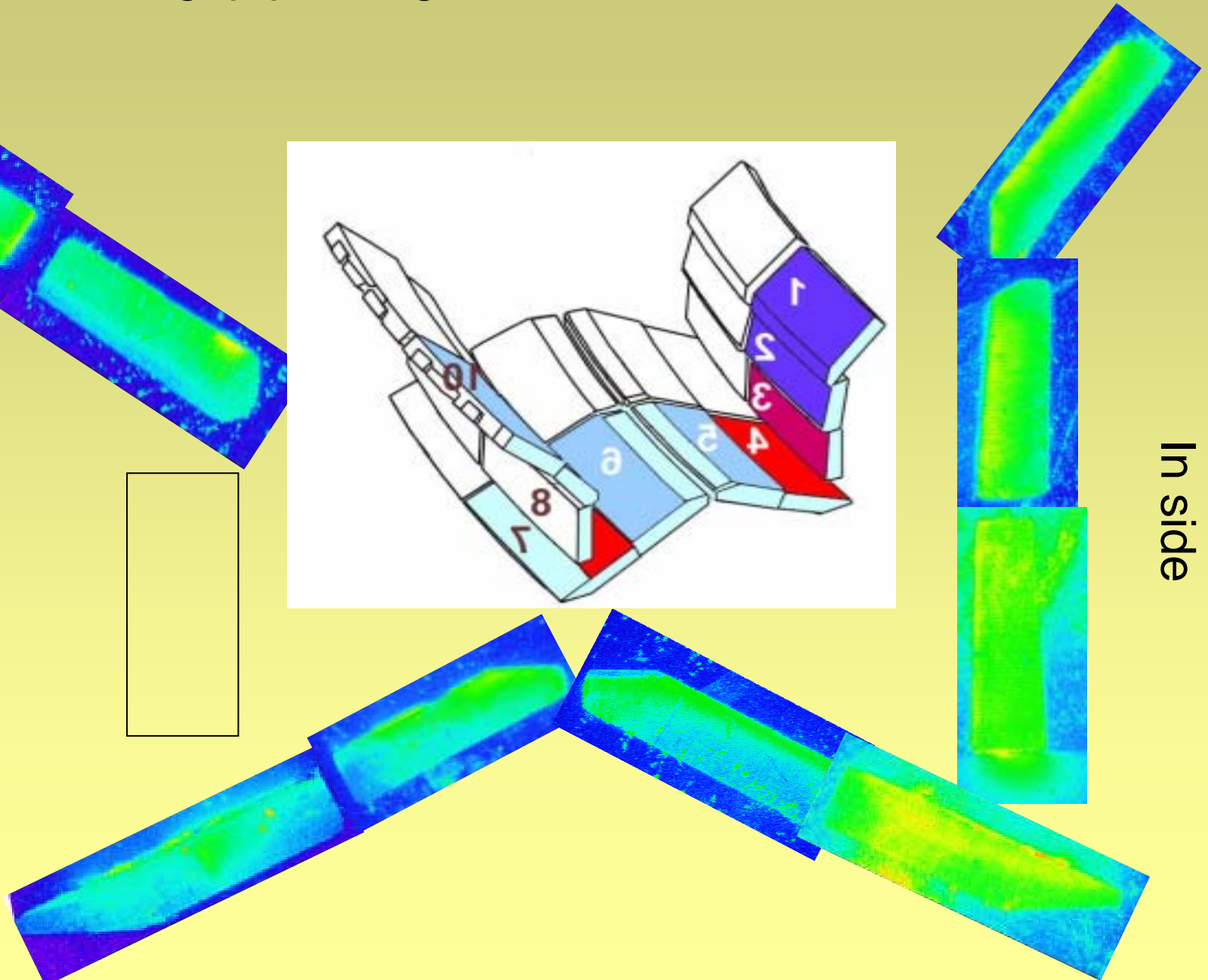
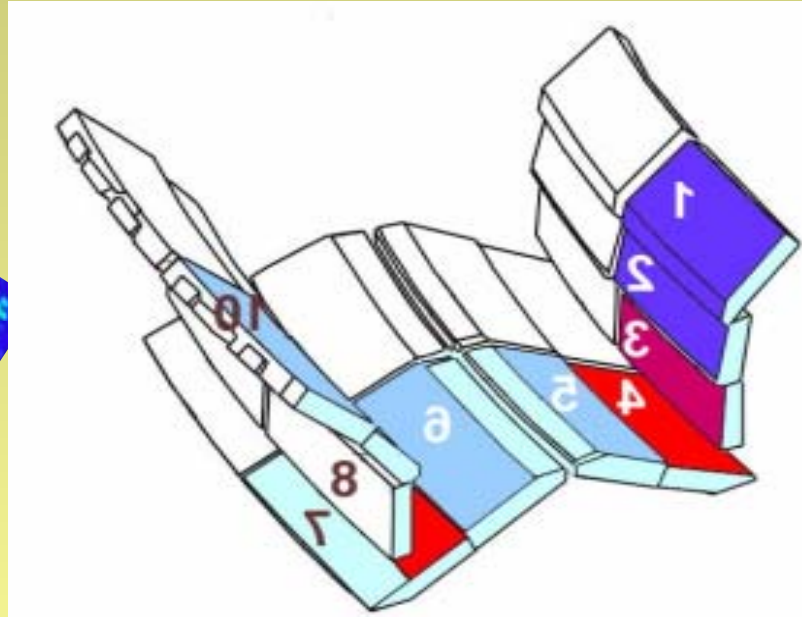
- Retention (absorption) in non-plasma exposed area
could be large tritium retention source

4. Triton produced by nuclear transmutation in materials

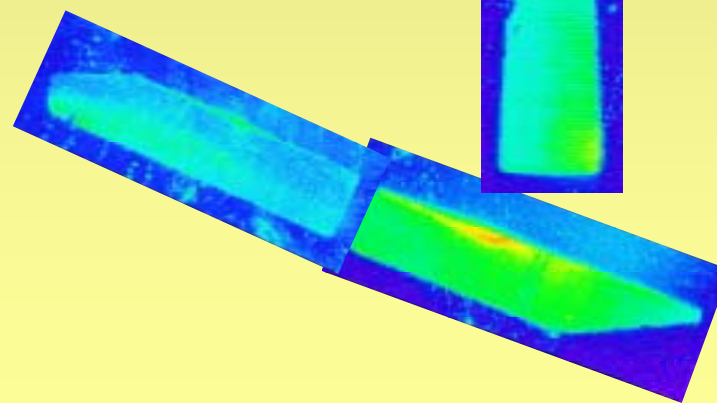
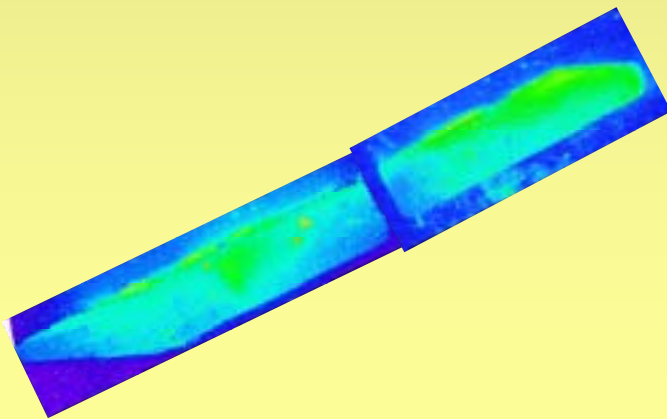
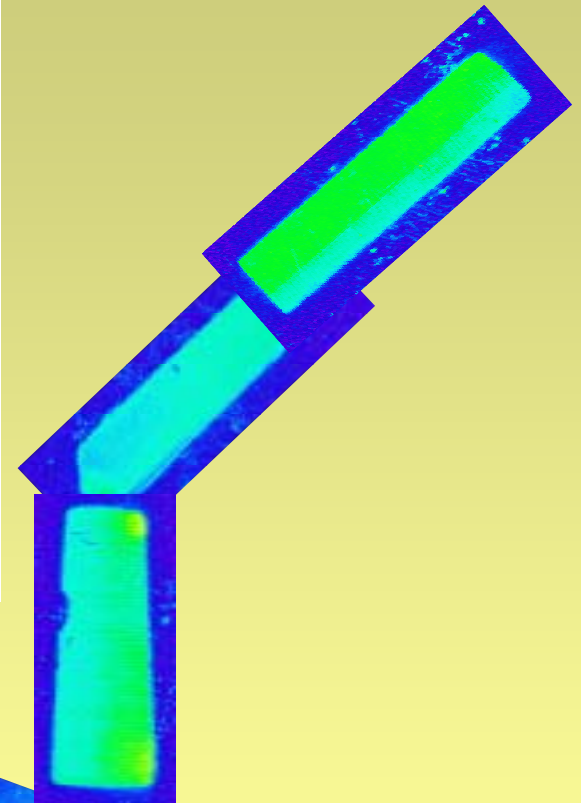
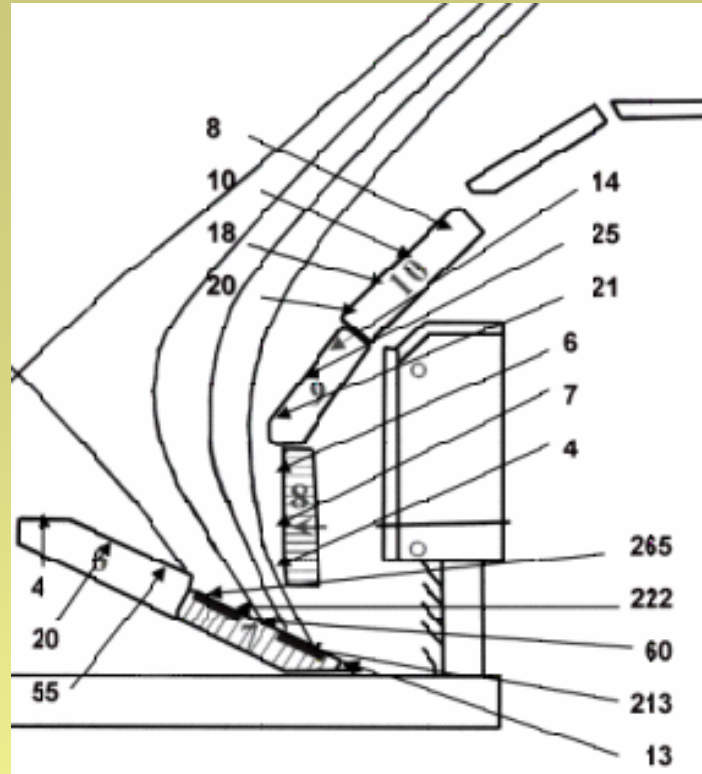
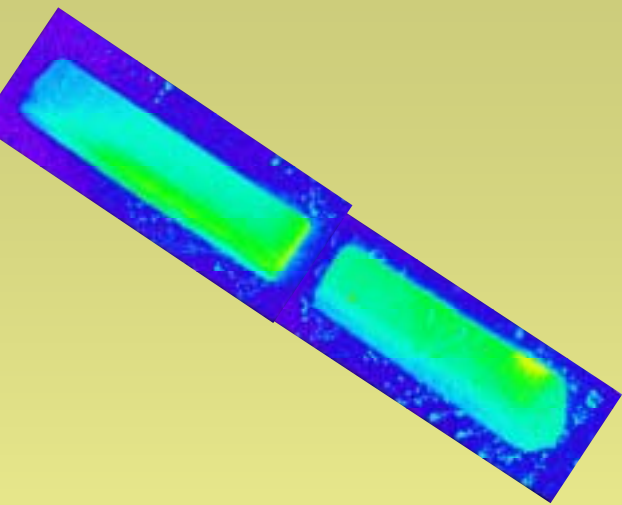
Narrow gap phasing side

Out side

In side

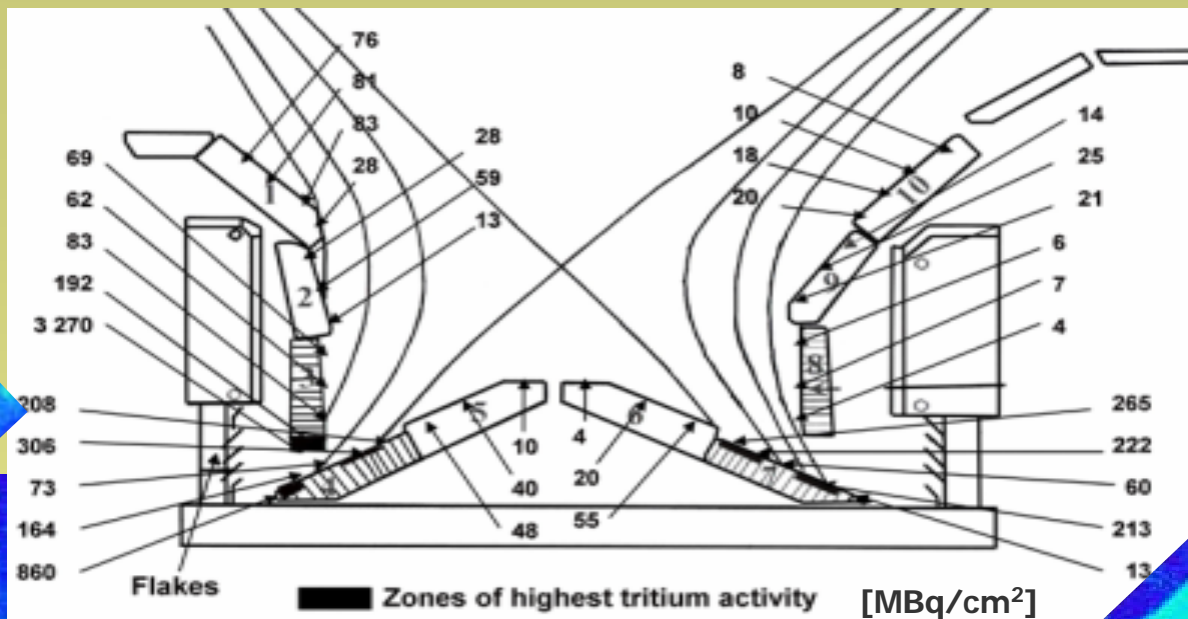


Out side



Narrow gap phasing side

Wide Gap phasing Side

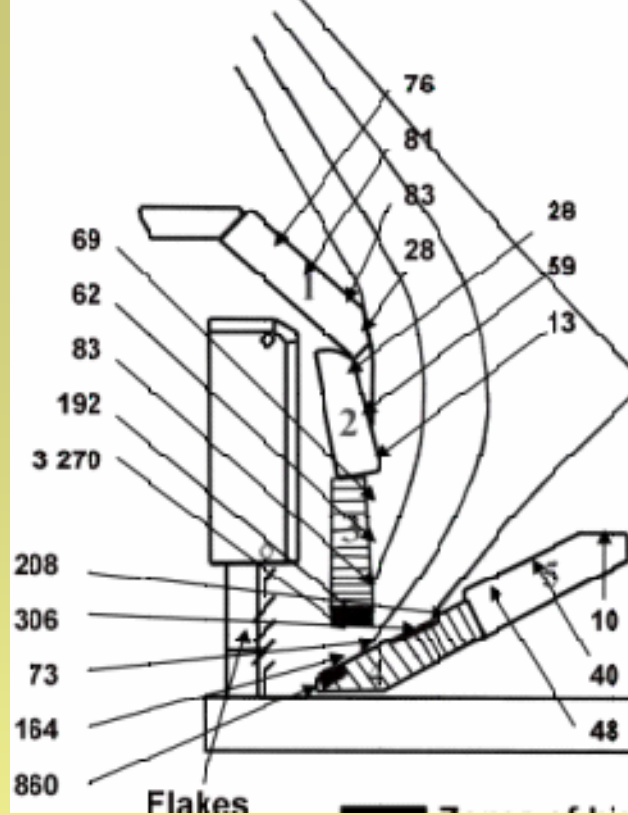


In side

Out side

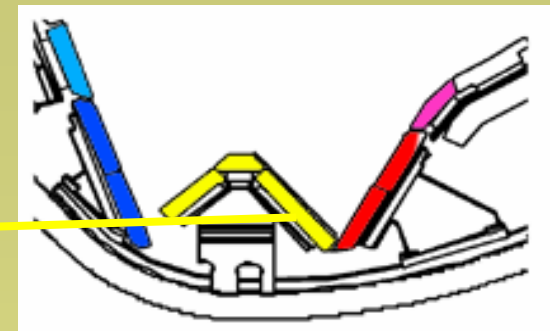
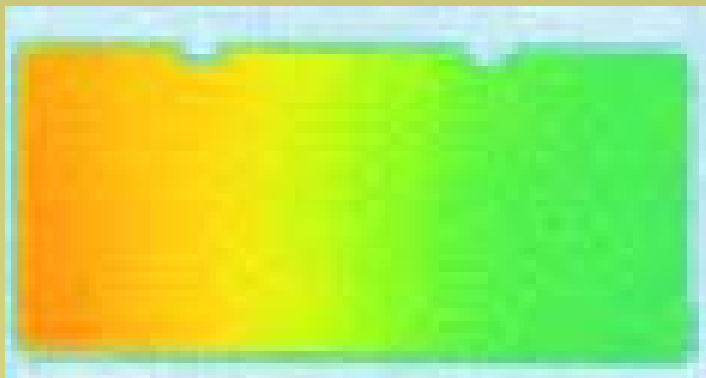
Wide Gap phasing Side

In side

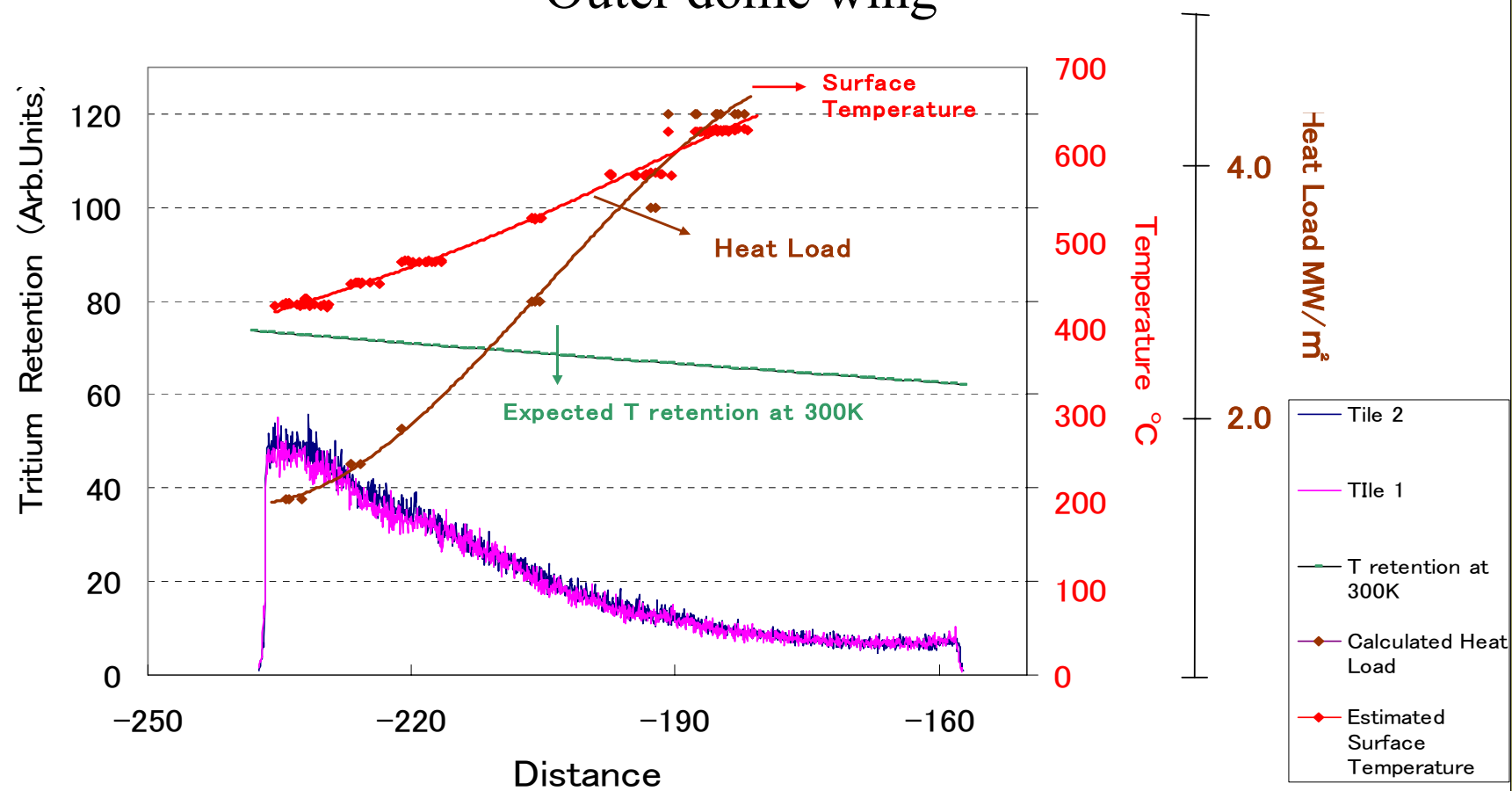


Wide Gap phasing Side

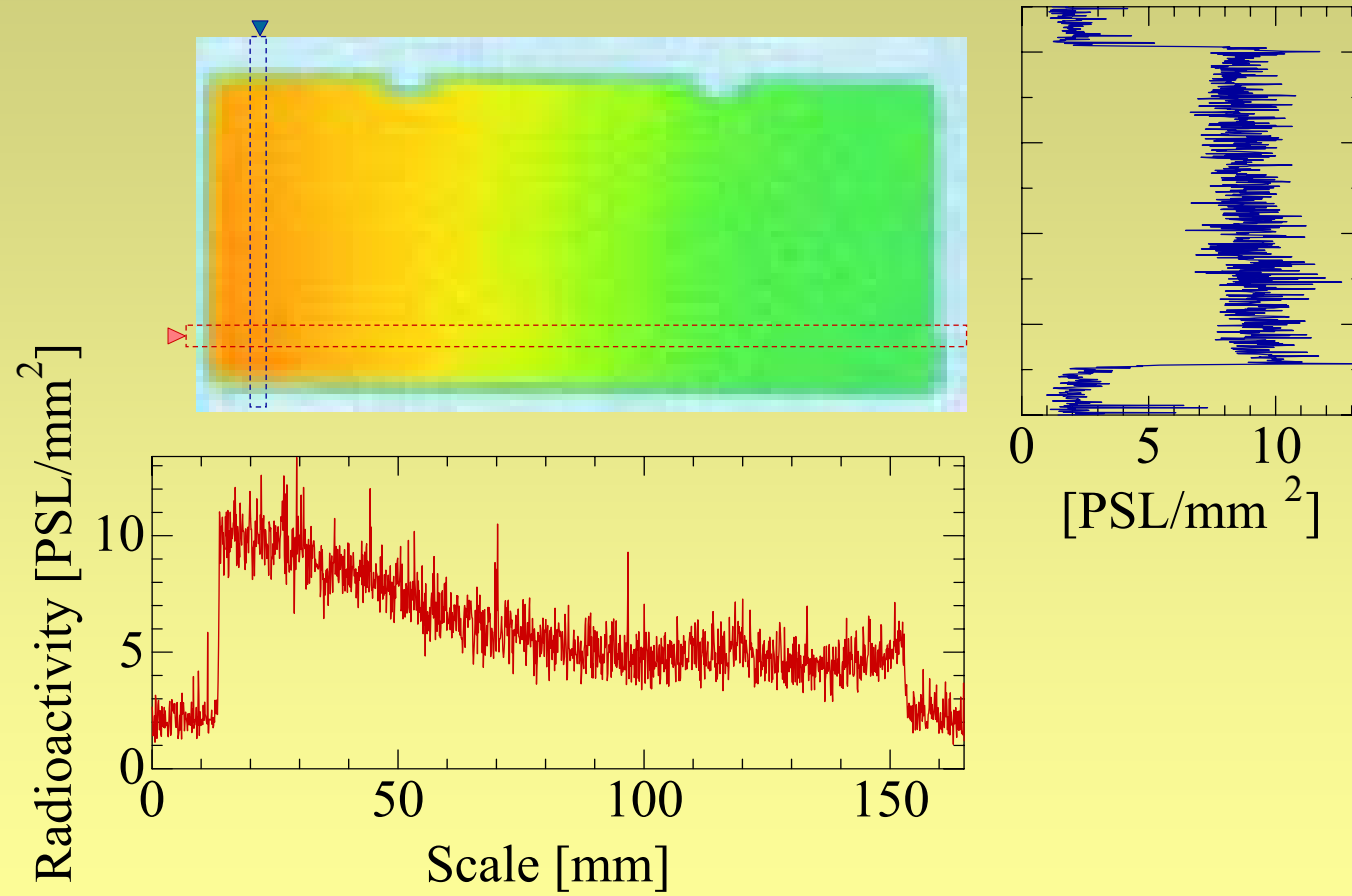
Narrow gap phasing side



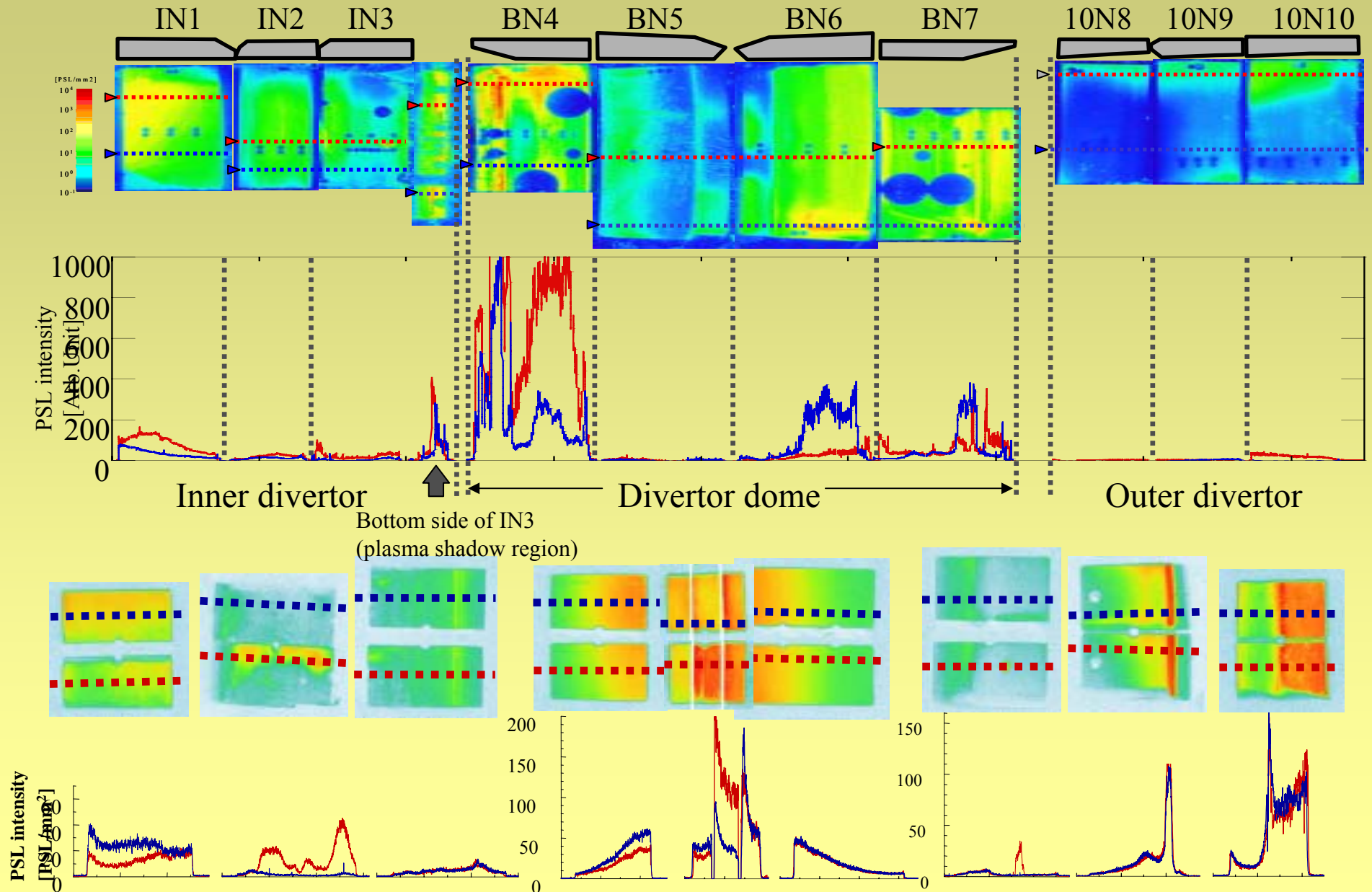
Outer dome wing



5Dm2cp (JT-60 tile)



Comparison of T profiles in JET(D-T) and JT-60U(D-D)



Defects generated by H⁺ impact onto graphite surfaces and their reactivity towards atomic H

T. Angot

E. Salançon, J.-M. Layet,
*Laboratoire PIIM, UMR 6633 CNRS-Université de Provence,
13397 Marseille, France*

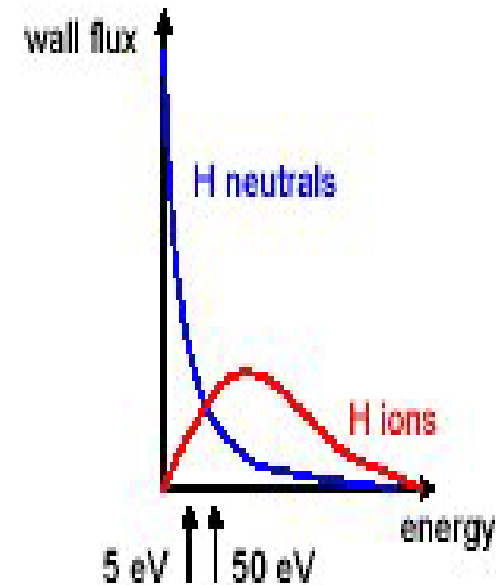
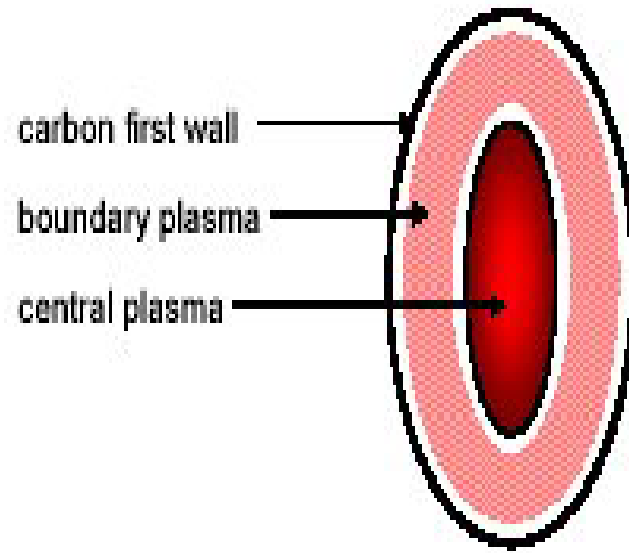
C. Brosset
*Association Euratom-CEA, CEA Cadarache, CEA/DSM/DRFC,
13108 St Paul Lez Durance, France*



PIIM



- Plasma - Surface Interaction



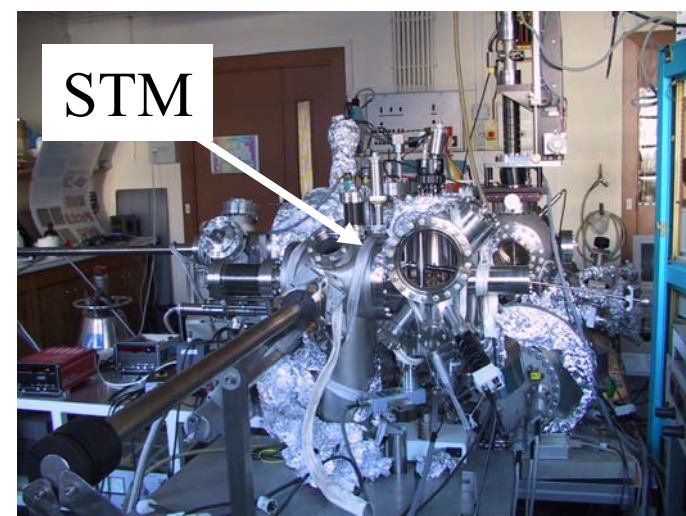
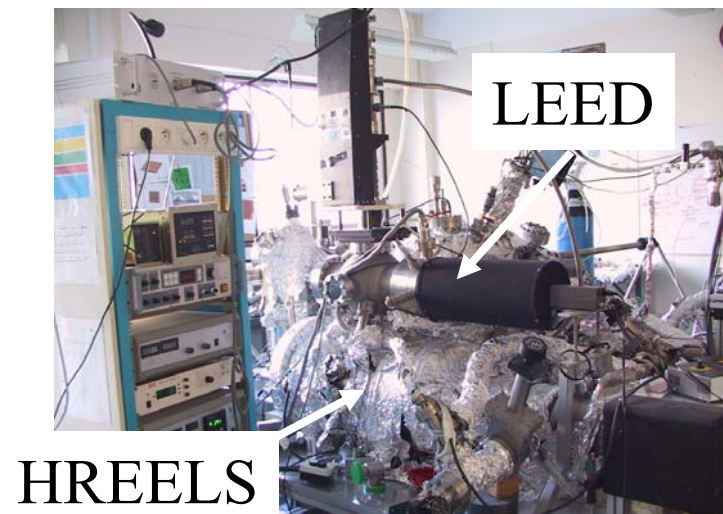
To look at the effect of each species individually

To combine them sequentially

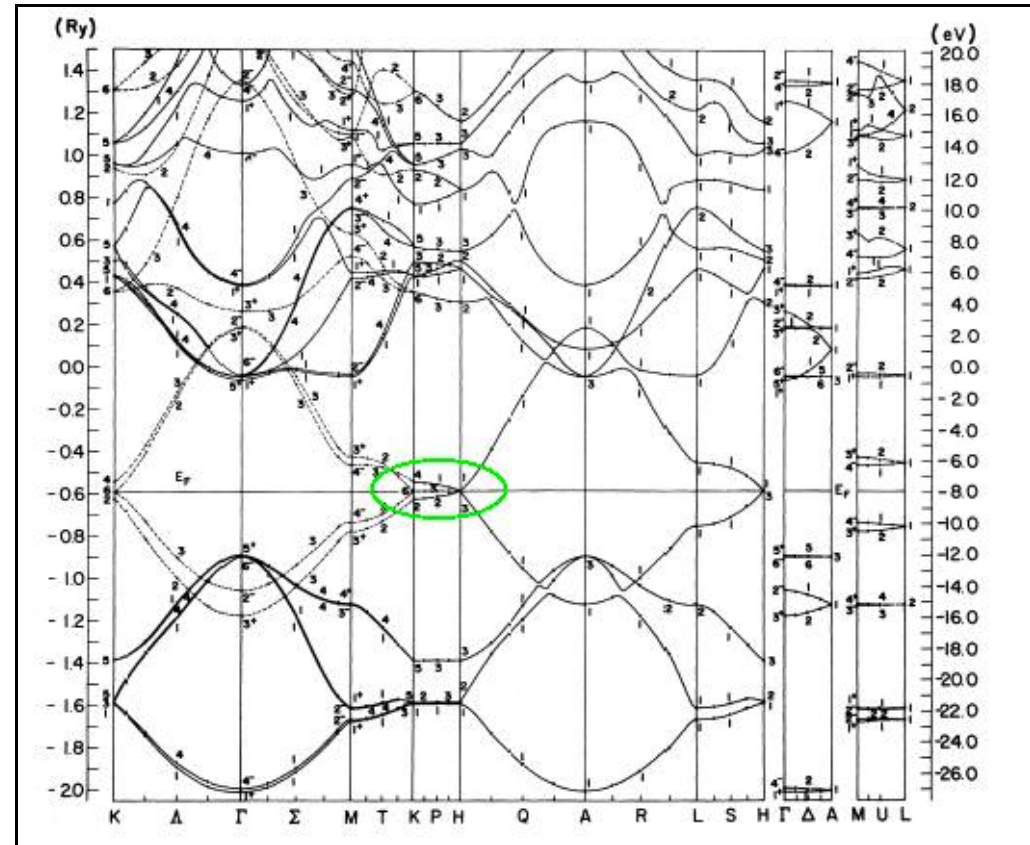
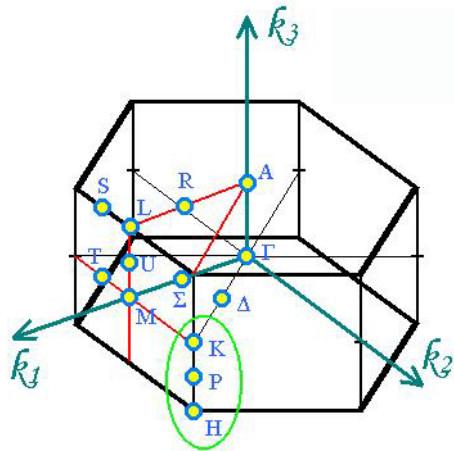
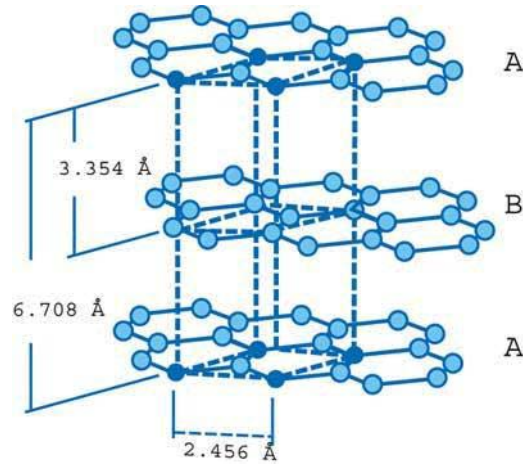
To perform a plasma exposure.

- Nanoscience -> Fullerenes
- Interstellar chemistry -> Carbon dust and heterochemistry

UHV experimental set-up Surface Analysis Techniques

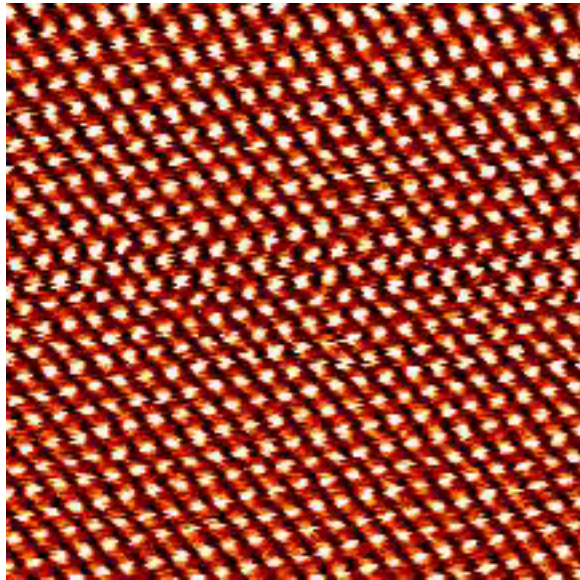


HOPG graphite



R.C. Tatar, S. Rabii, Phys. Rev. B25, 4126 (1982)

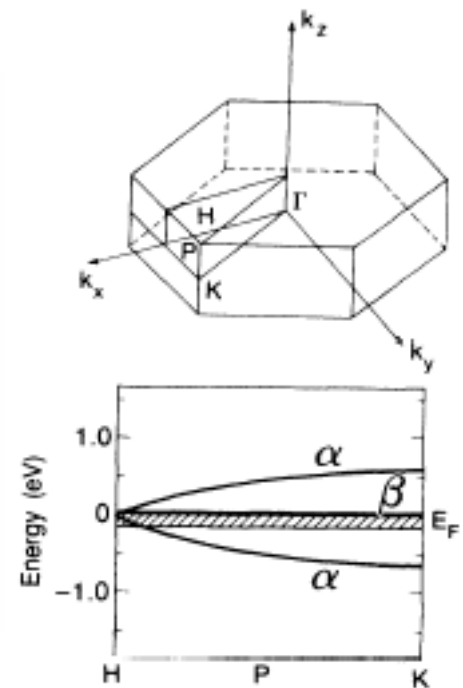
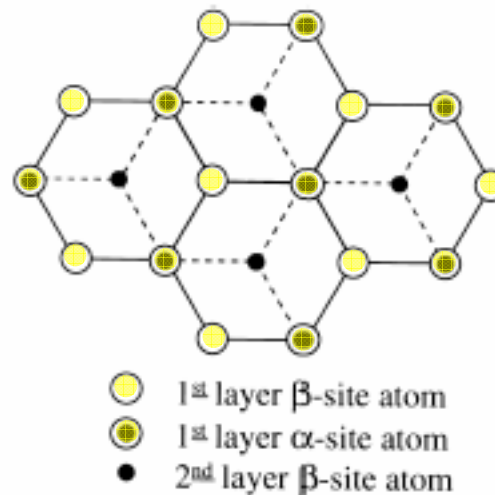
STM on HOPG surface



5.5 nm x 5.5 nm

STM probe the LDOS near
the Fermi Energy

The ABAB stacking between graphene planes in the three-dimensional crystal creates two inequivalent sites at the surface, with different properties with regard to the electronic structure



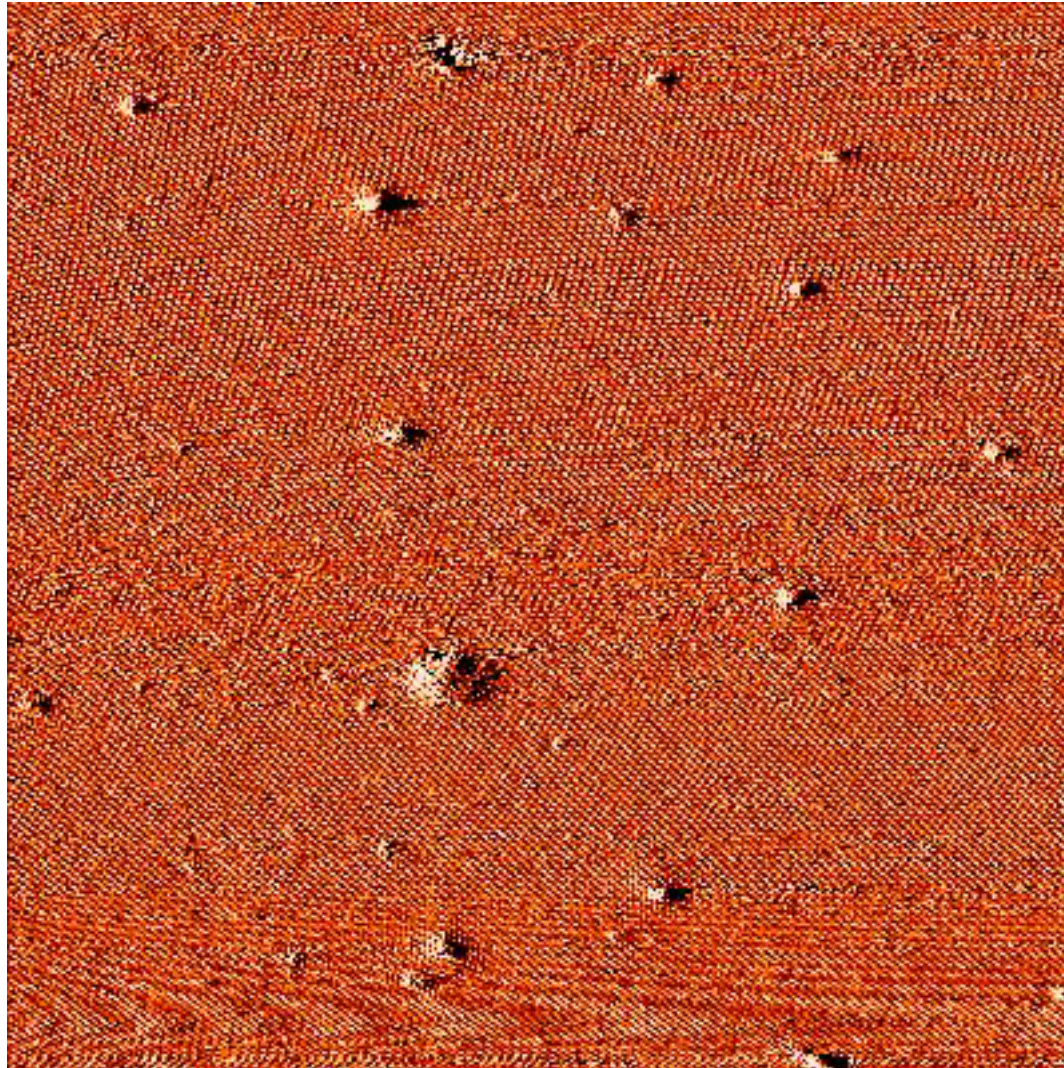
Weak vdW interaction between adjacent planes \Rightarrow
suppression of the charge density at the Fermi level
at α sites \Rightarrow imaging of the β atoms

D. Tománek & al, PRB 35, 7790 (1987)

J. Tersoff, PRL 57, 440 (1986)



$$\text{Fluence} = 5 \cdot 10^{13} \text{ H}^+/\text{cm}^2 \quad E_{\text{ions}} = 300 \text{ eV}$$



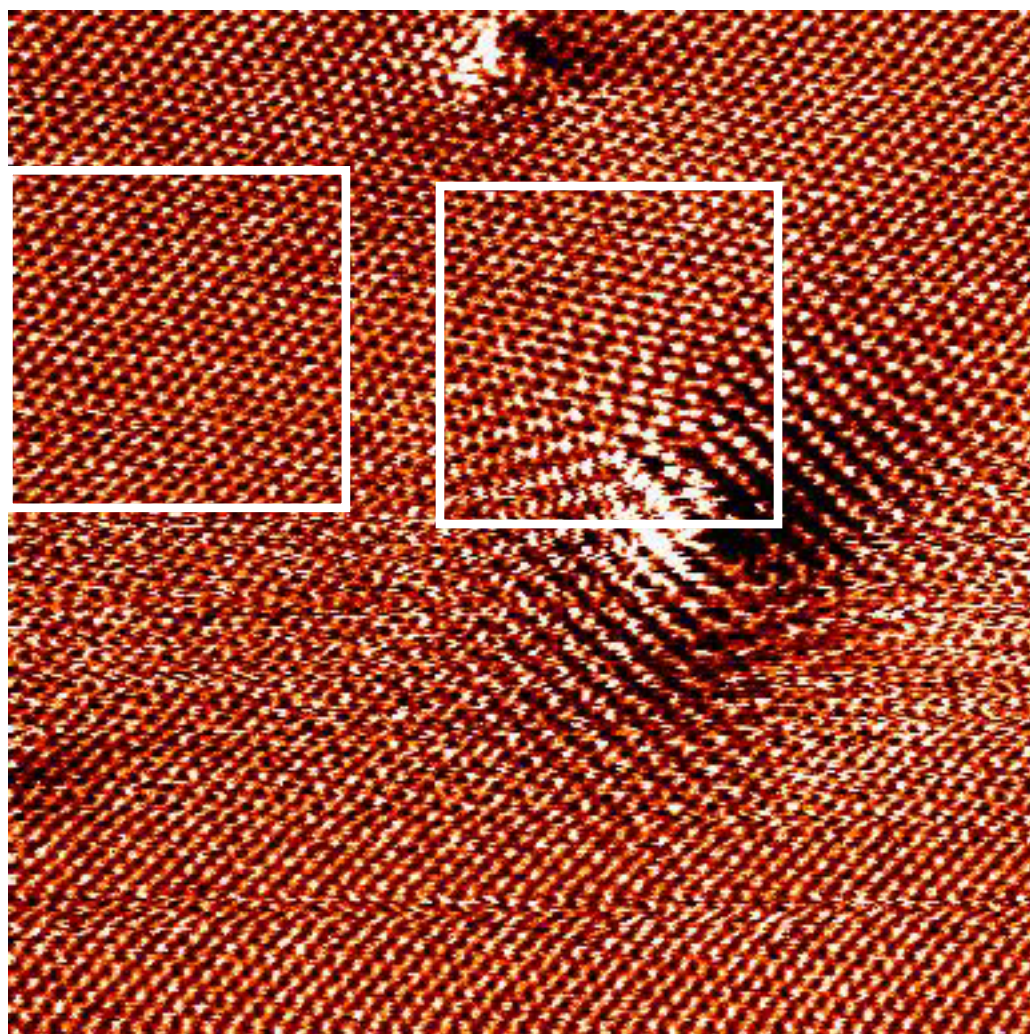
100 nm x 100 nm

... on graphite, the surface density is $3.86 \cdot 10^{15} \text{ C atoms/cm}^2$

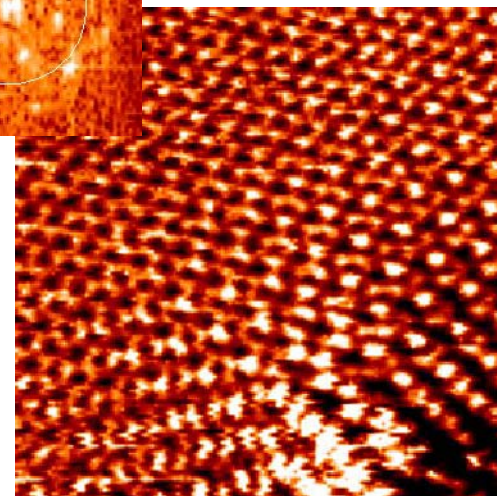
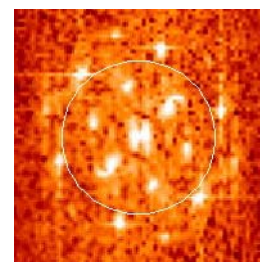
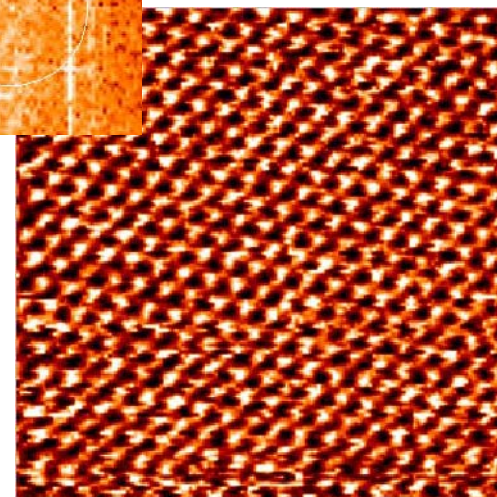
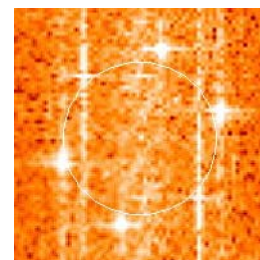


PiM

OKS



15 nm x 15 nm

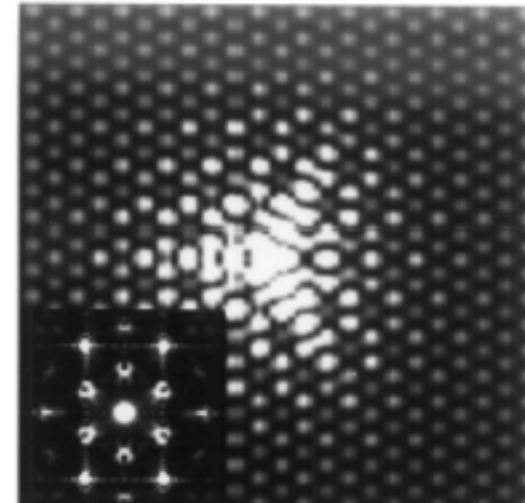
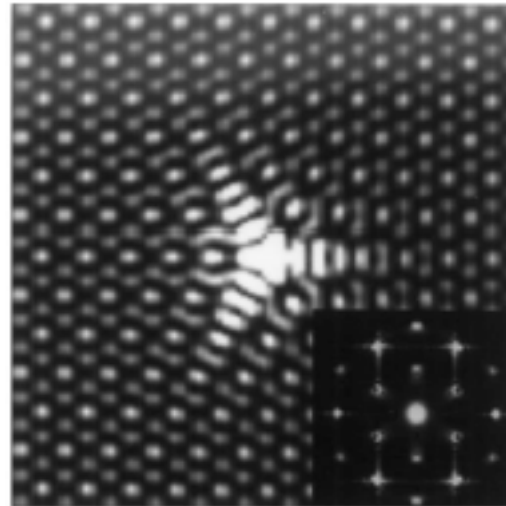


Such defects displaying $(\sqrt{3} \times \sqrt{3})R30^\circ$ superstructure have been considered as

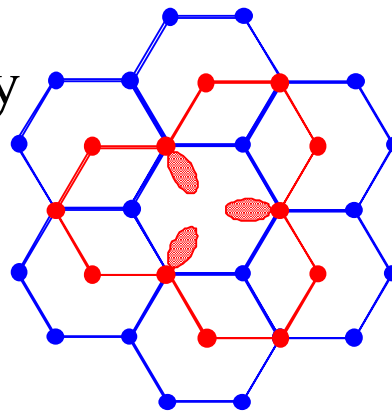
- **adatoms** H.A Mizes & J.S. Foster, Science 244, 559 (1989),
P. Ruffieux & al, PRL 84, 4910 (2000) "Hydrogen Atoms Cause Long-Range Electronic Effects on Graphite"

- **point defects**

K.F. Kelly, N.J. Halas,
Surf. Sci. 416, L1085 (1998)

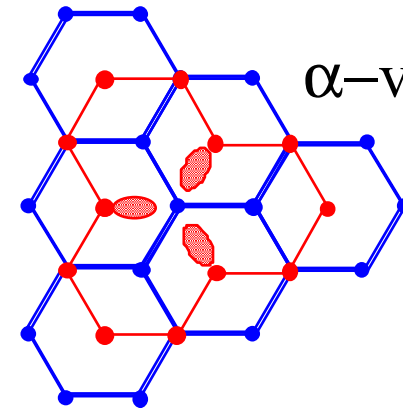


β -vacancy



- top layer
- 2nd layer

α -vacancy



PIIM

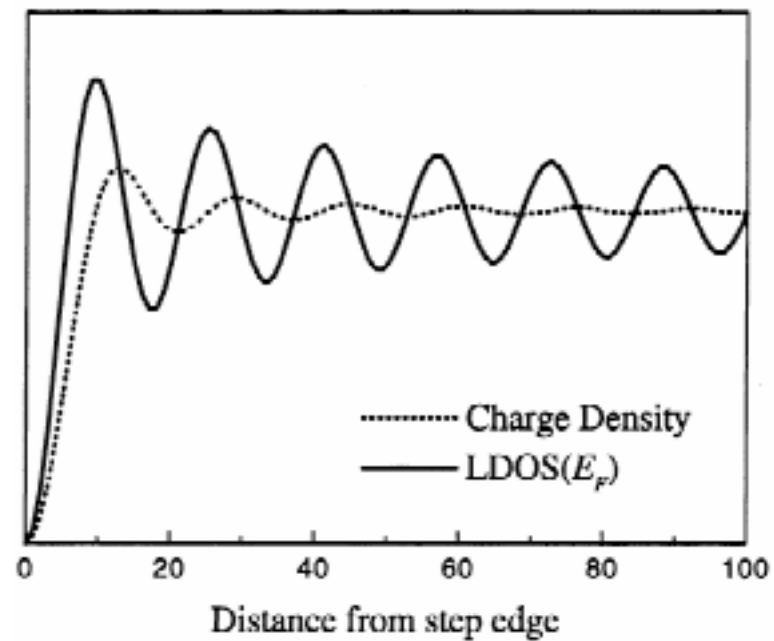
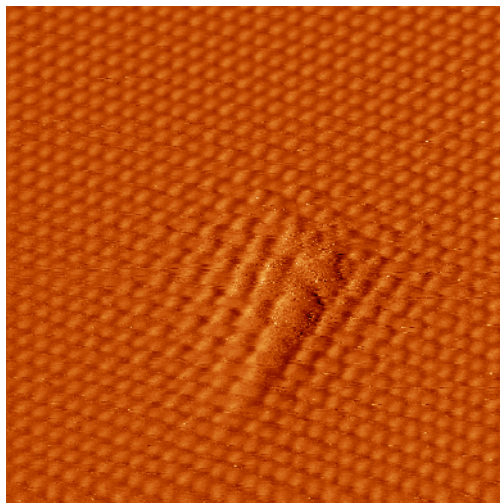
OKS

- stable displaced surface carbon atoms

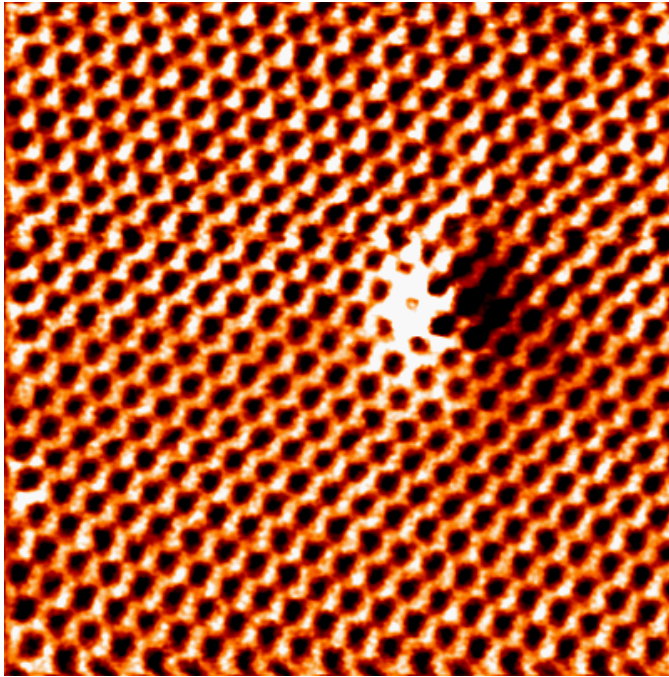
B. Rousseau, H. Estrade-Szwarckopf, A-L. Thomann & P. Brault, Applied Physics A 77, 591 (2003)

- steps, and grain boundaries

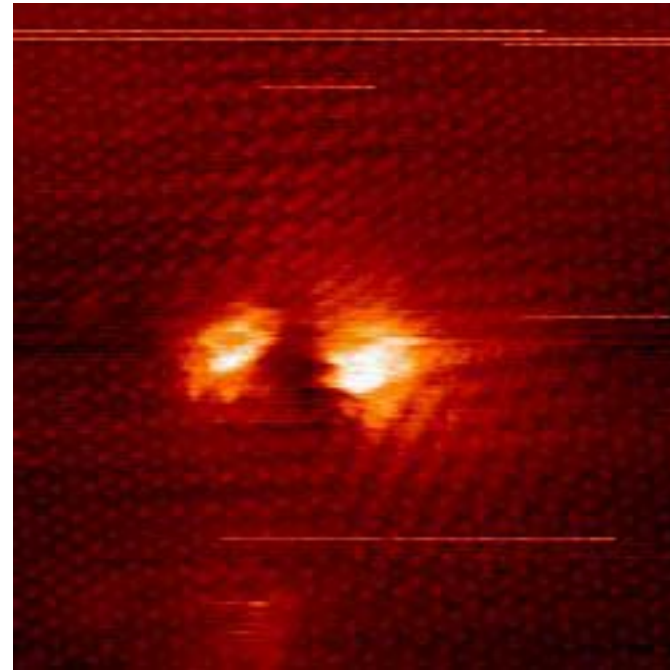
Similar to
"Friedel oscillations of charge density "



Other type of defects are encountered

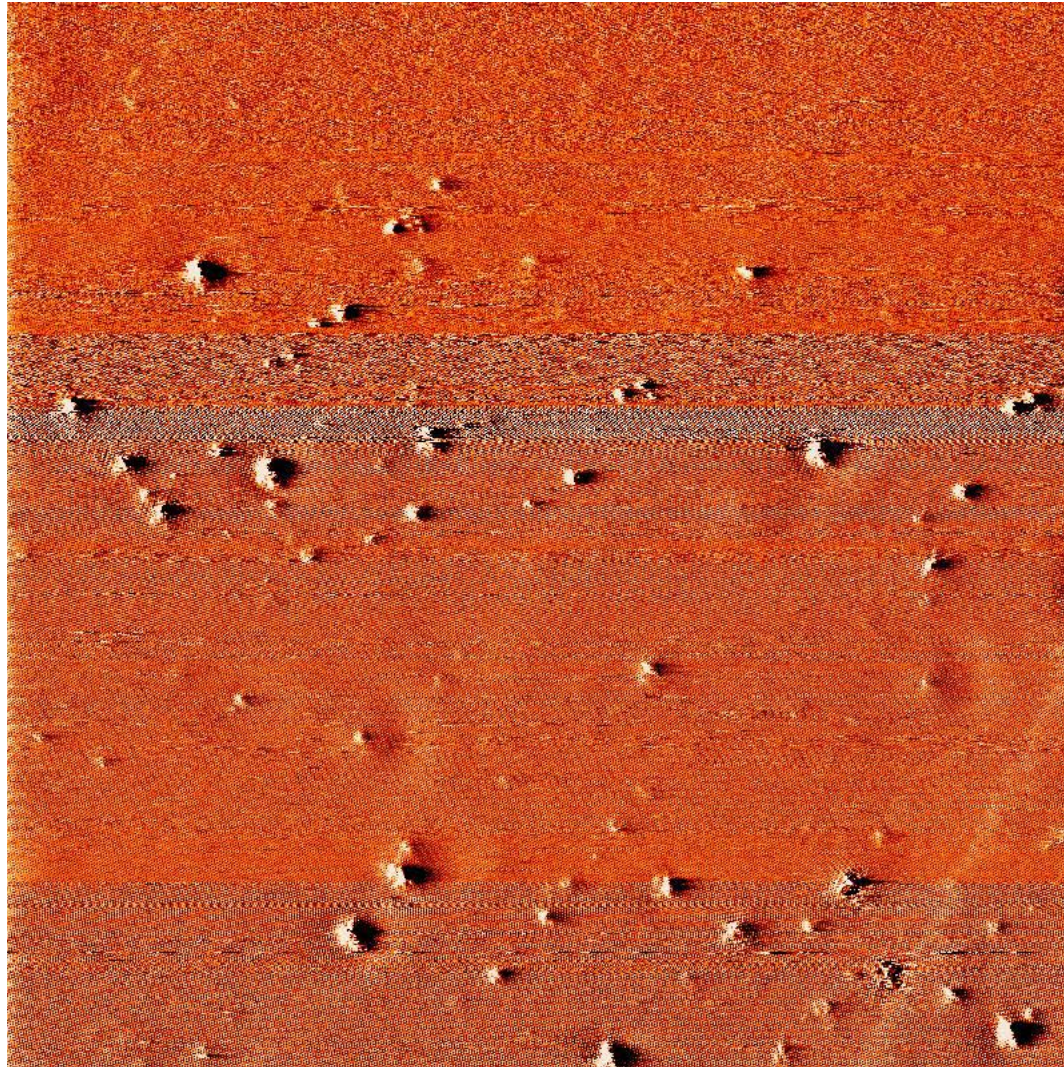


The lattice is only slightly pertubated with a C-C distance slightly larger



Pairs of defects

Fluence = $5 \cdot 10^{13} \text{ H}^+/\text{cm}^2$ $E_{\text{ions}} = 300 \text{ eV}$ + Atomic H exposure

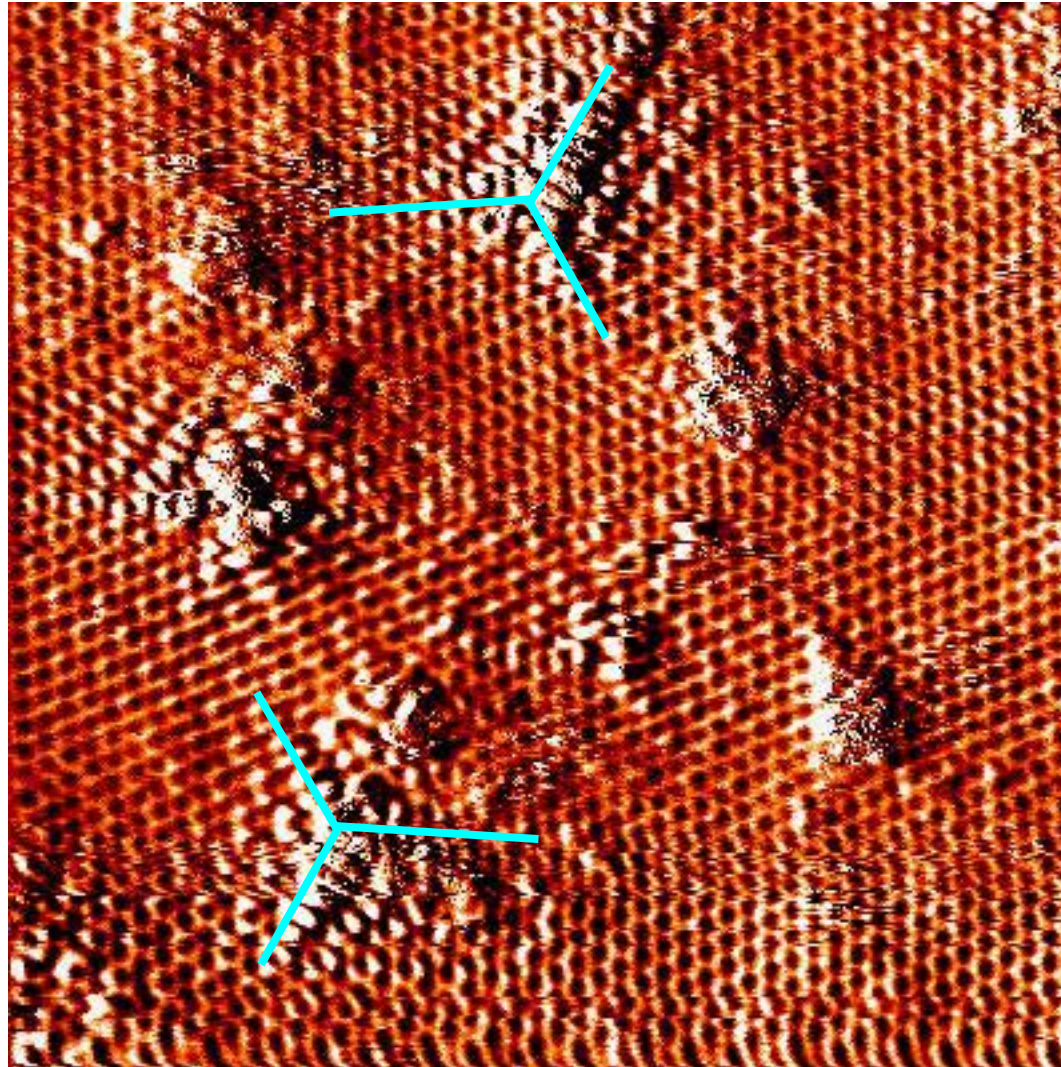


100 nm x 100 nm

No apparent modification detected by STM



Fluence = $3 \cdot 10^{14} \text{ H}^+/\text{cm}^2$ $E_{\text{ions}} = 300 \text{ eV}$



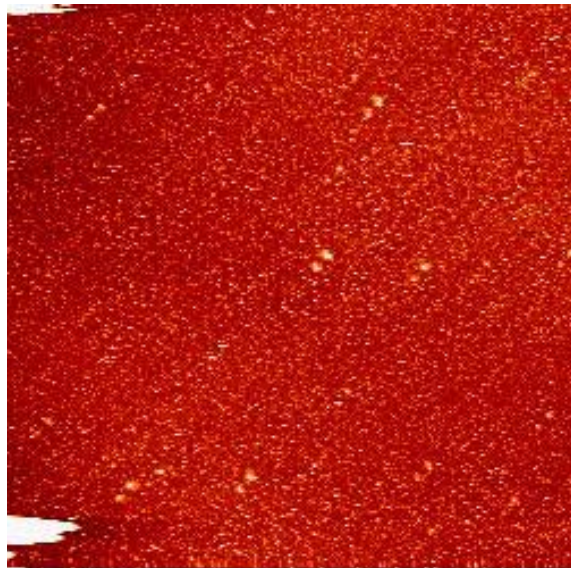
10 nm x 10 nm



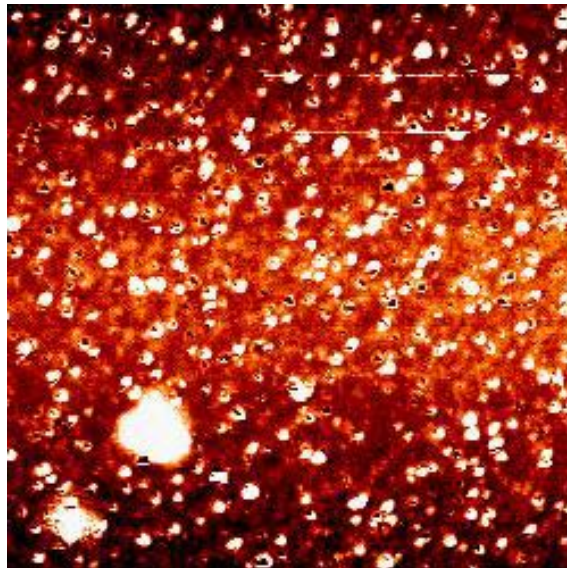
PIM

OKS

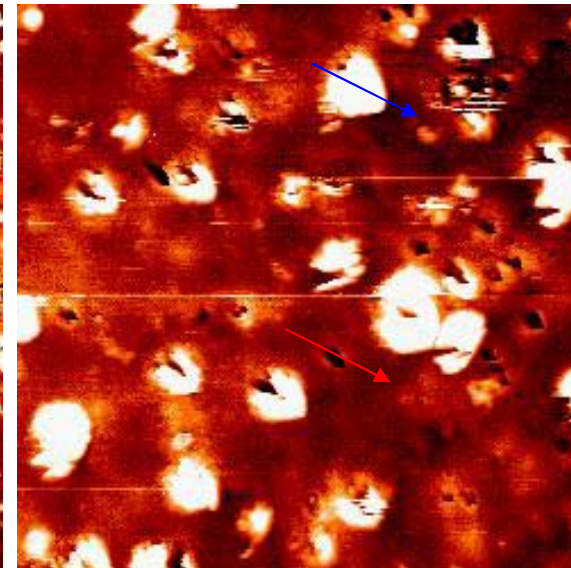
$$\text{Fluence} = 1.3 \cdot 10^{15} \text{ H}^+/\text{cm}^2 \quad E_{\text{ions}} = 300 \text{ eV}$$



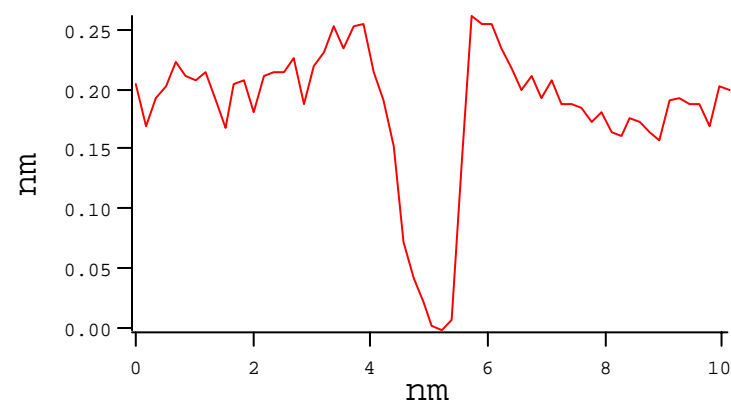
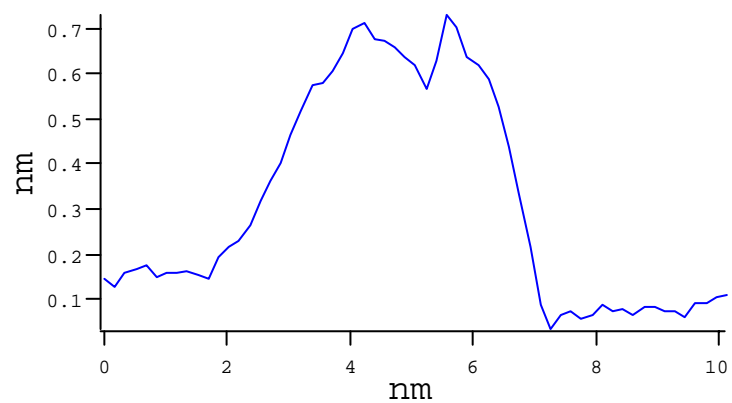
1000 nm x 1000 nm

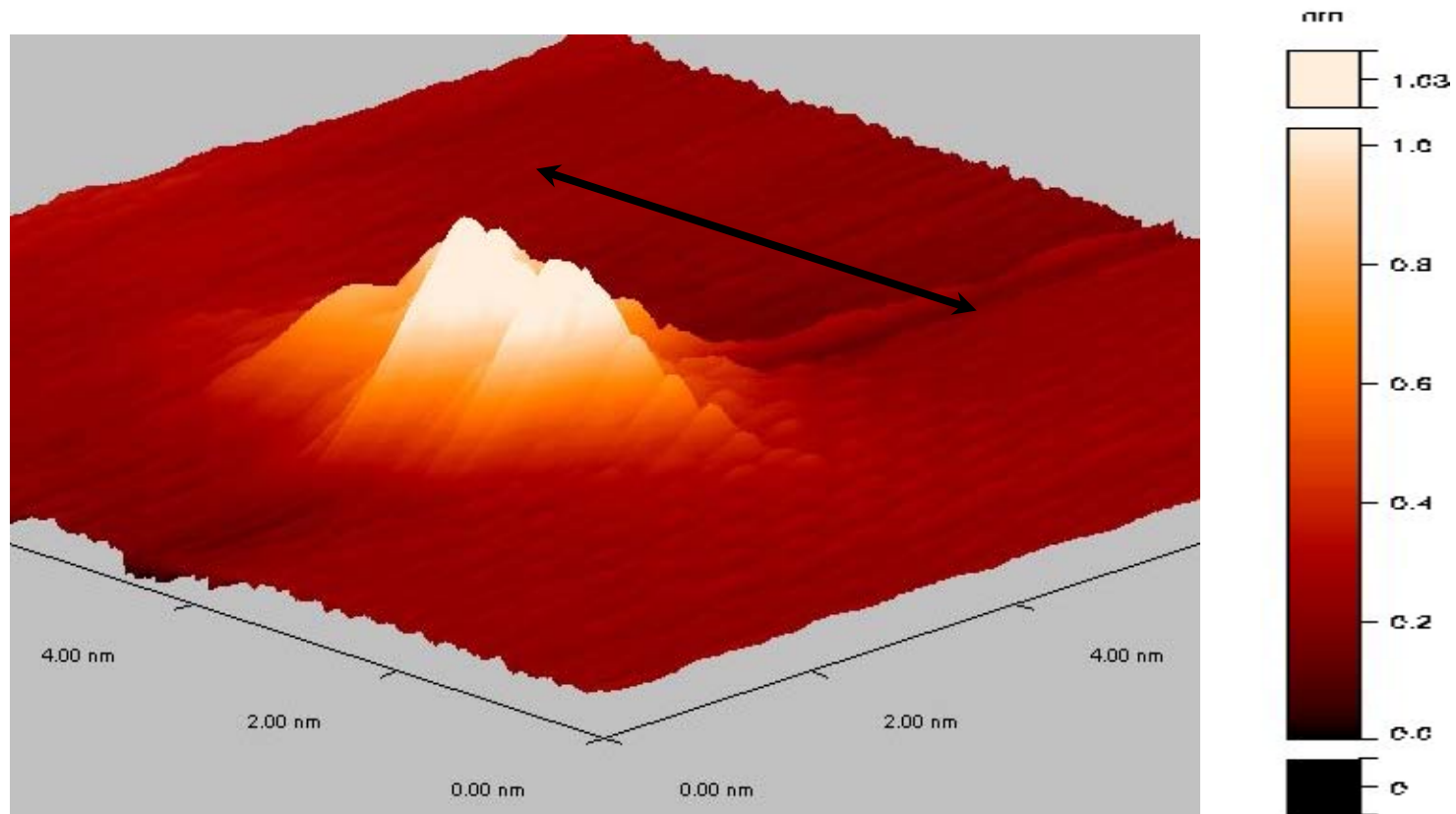


150 nm x 150 nm



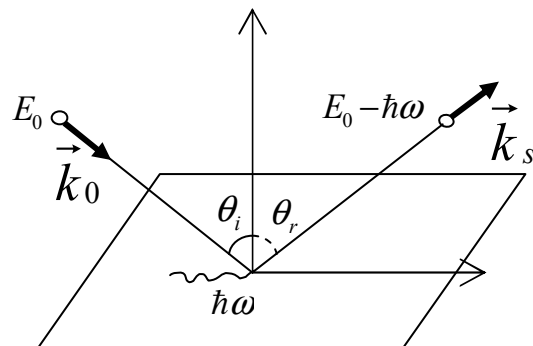
42 nm x 42 nm



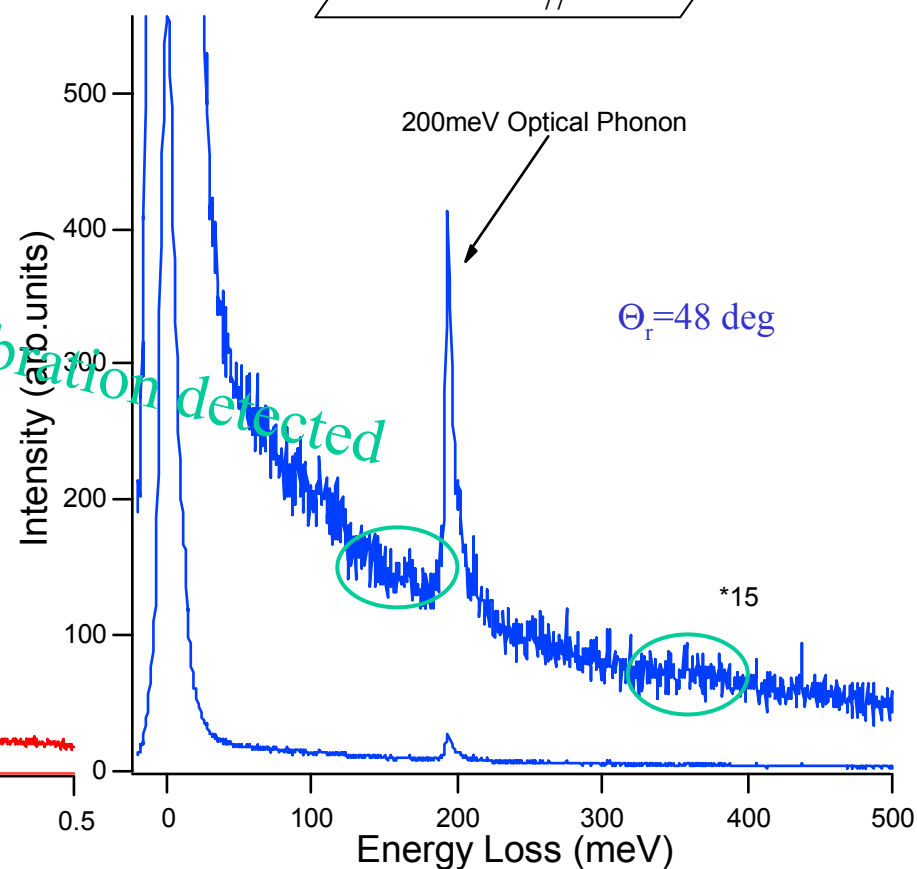
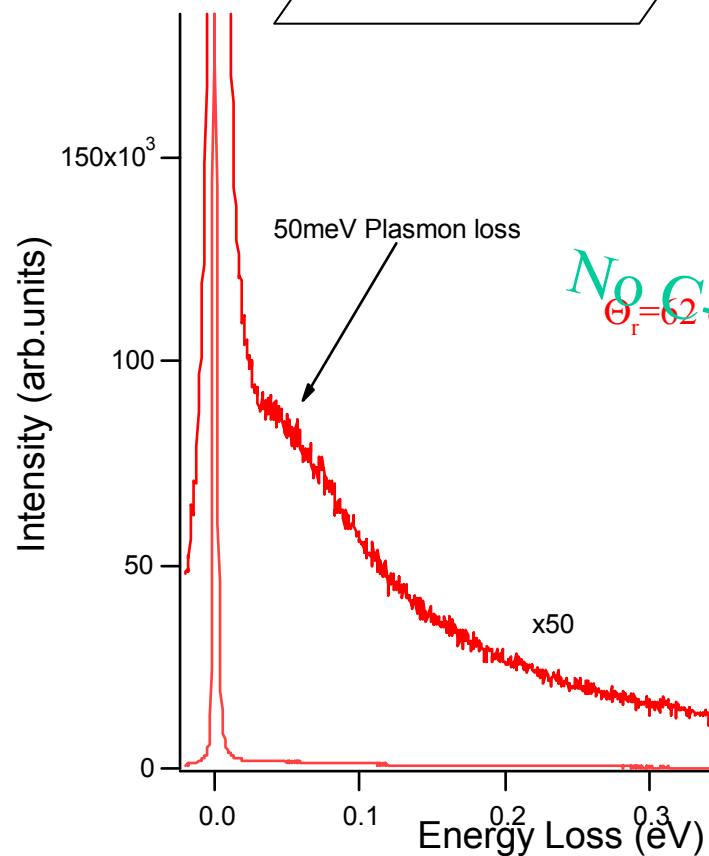
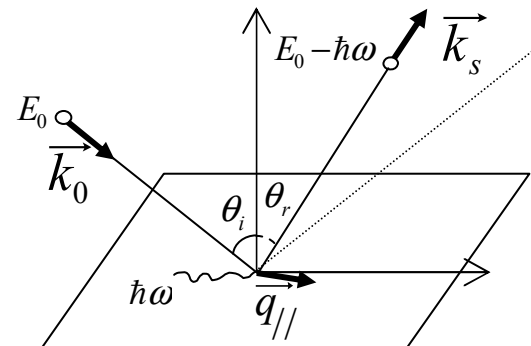


Increasing height with
fluence
ion energy (150 eV-5 keV)

HREELS on clean HOPG graphite (or exposed to atomic H)



$E_p = 7\text{ eV}$
 $\Theta_i = 62^\circ$



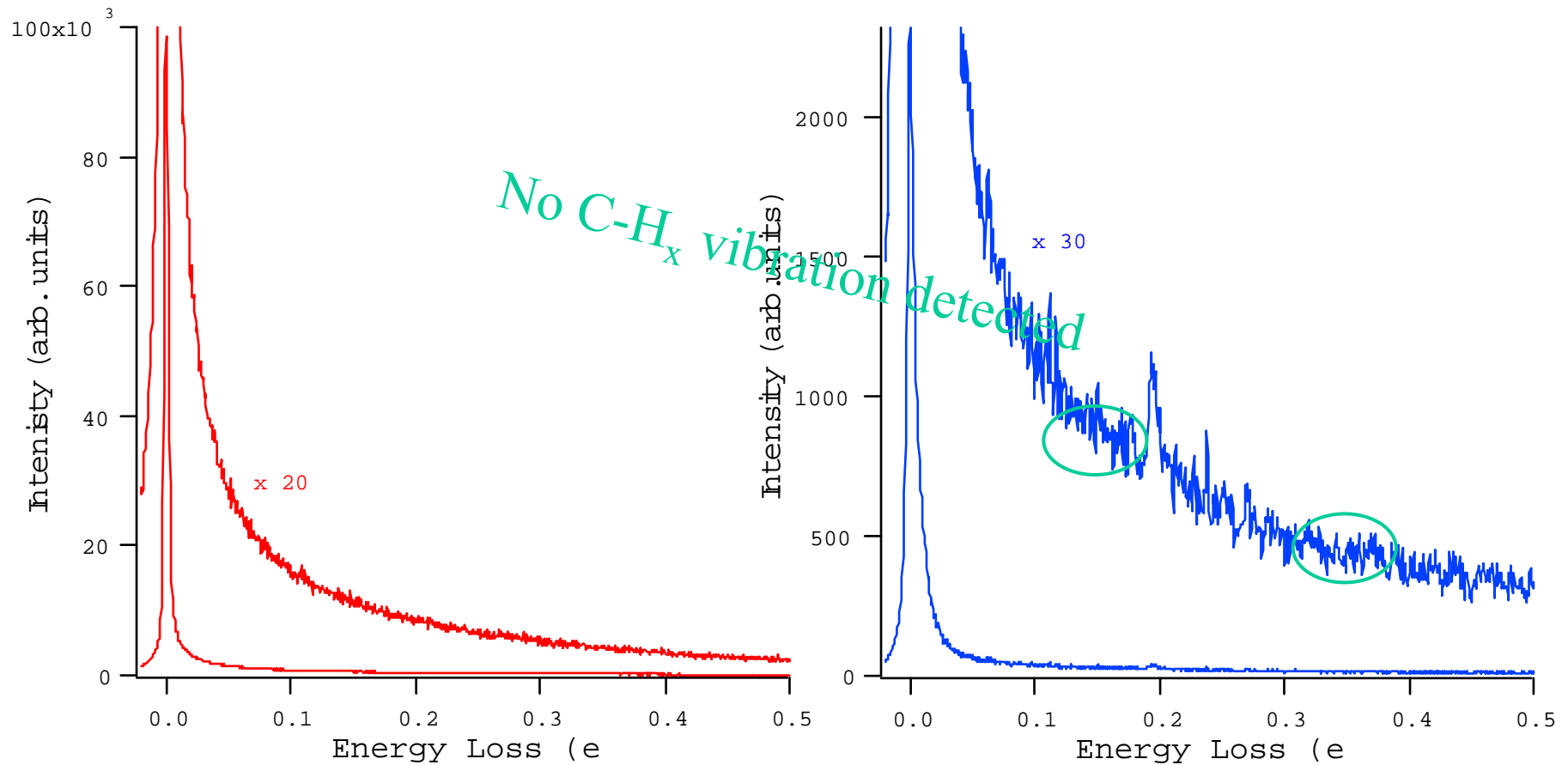
PIIM

CS

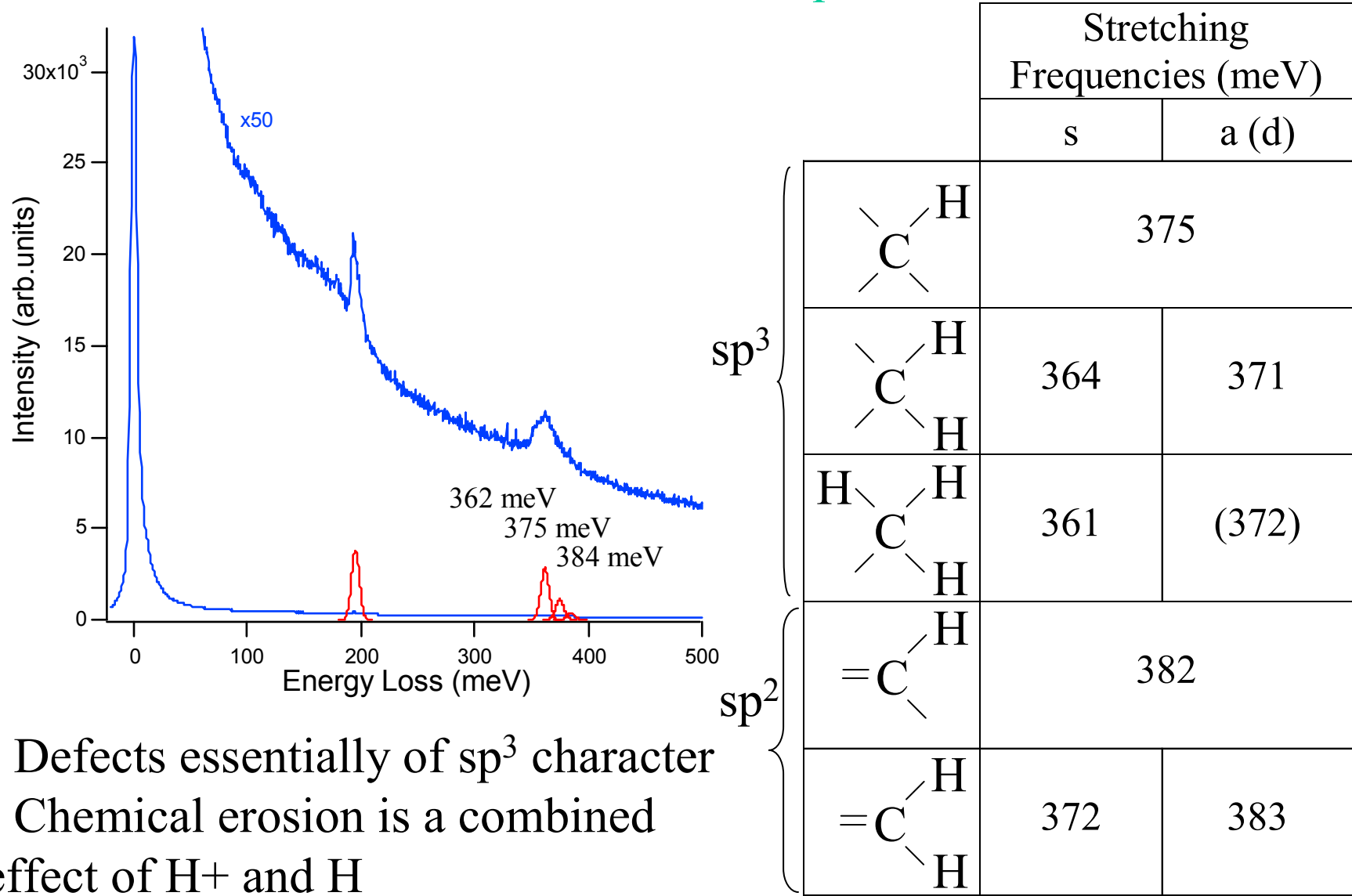
HOPG graphite, bombarded : Fluence = $3 \cdot 10^{14} \text{ H}^+/\text{cm}^2$ $E_{\text{ions}} = 300 \text{ eV}$

- Disappearance of the plasmon loss

- Apparent attenuation of the optical phonon mode - Increasing background loss



HOPG graphite, bombarded : Fluence = $3 \cdot 10^{14} \text{ H}^+/\text{cm}^2$ $E_{\text{ions}}=300 \text{ eV}$
 + atomic H exposure



- Defects essentially of sp^3 character
- Chemical erosion is a combined effect of H^+ and H



PIIM

OKS

Coming soon !

- passivation of defects

Silicon deposited on clean HOPG graphite



1000 nm x 1000 nm

... and Boron



PiM

OKS

but also !!

- Modification of surface morphology and defects with thermal treatments
- Higher fluence -> carbon clusters formation and re-deposition
- Electron bombardment
- Plasma exposure
- Your ideas are welcome !!!



Many thanks to...



PROGRAMME
COMMUNAUTAIRE
FEDER



DIII-D/TRINITI Collaboration on Carbon and Hydrogen Codeposition

W.P. West, O.I. Buzhinskij,
Dennis Whyte, Clement Wong

7th International Workshop on Hydrogen Isotopes
in Fusion Reactor Materials

May 21, 2004
Portland, Maine



DIII-D and TRINITY Labs Have Collaborated on Plasma Facing Materials Experiments in the DIII-D tokamak and on MK-200 Plasma Gun device

- DiMES Exposures of coatings B_4C and SiC on graphite and RGT samples
- Qualification of coated graphites for long term exposure in DIII-D
- Exposure of B_4C coated tiles in the DIII-D divertor for an annual campaign
- DiMES Leading Edge Experiments

Focus on Codeposition Layers formed in the Divertor region of DIII-D

The main points I want to make

- › We have observed a wide variety of morphologies in carbon/hydrogen codeposition layers.
- › These experiments constitute only a demonstration that codeposition is pervasive and complex.
- › Full characterization of the film formation processes under all these “realistic” conditions will be a difficult task.

Coatings formed on B₄C coated Divertor Graphite Tiles

Fine Grained Isotropic Graphite (ATJ) tiles were coated with B₄C using a high temperature CVD process in Russia.

One tile was tested at heat loads up to 10 MW/m² for 5 seconds and multiple cycles with very little damage using the e-beam facility at SNL, Albuquerque

Small samples of B₄C coated graphite tested at the 2MK-200 facility at TRINITI exhibited adherence.

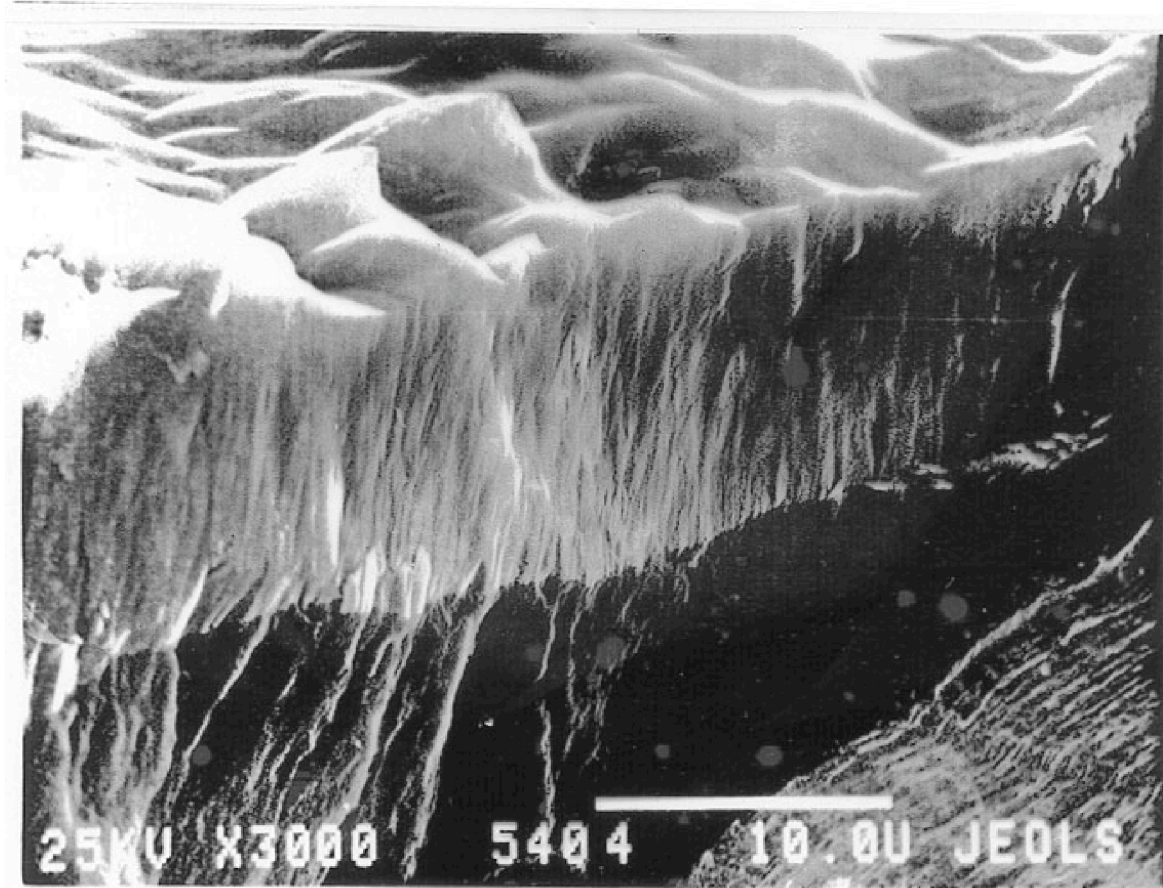
After successful transient and steady heat load testing, 5 tiles were cleaned, baked and installed in a poloidal row across the DIII-D divertor.

Tiles were removed after 6 months of plasma operation

- › About 1000 plasma discharges
- › Most of them were Lower Single Null Divertor Configuration

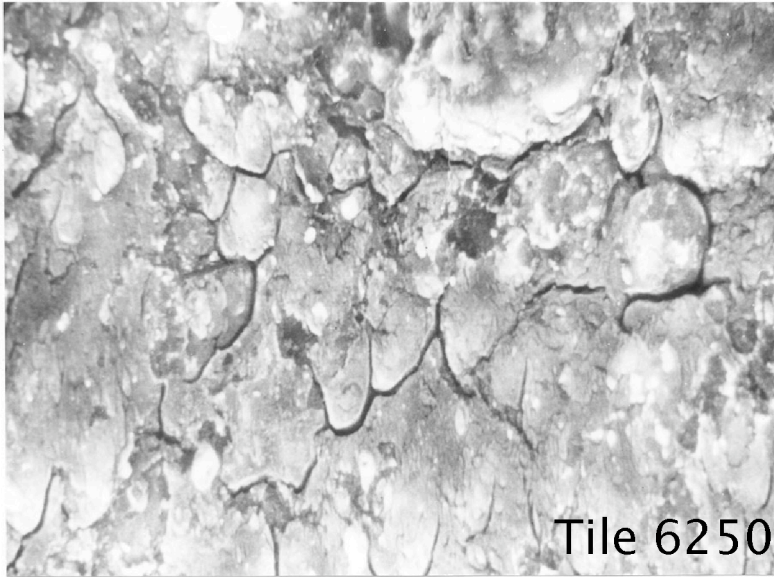


CVD B₄C Provides a Durable Coating for Graphite Tiles

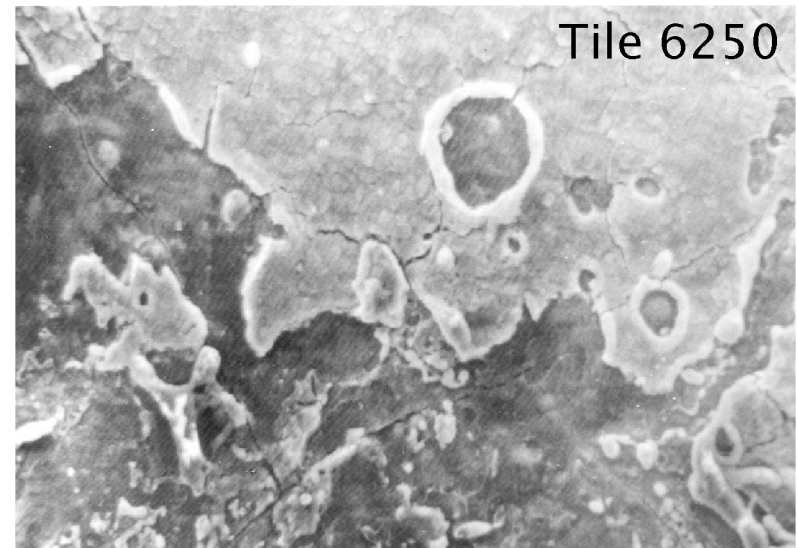


B₄C Coating after Exposure in DIII-D

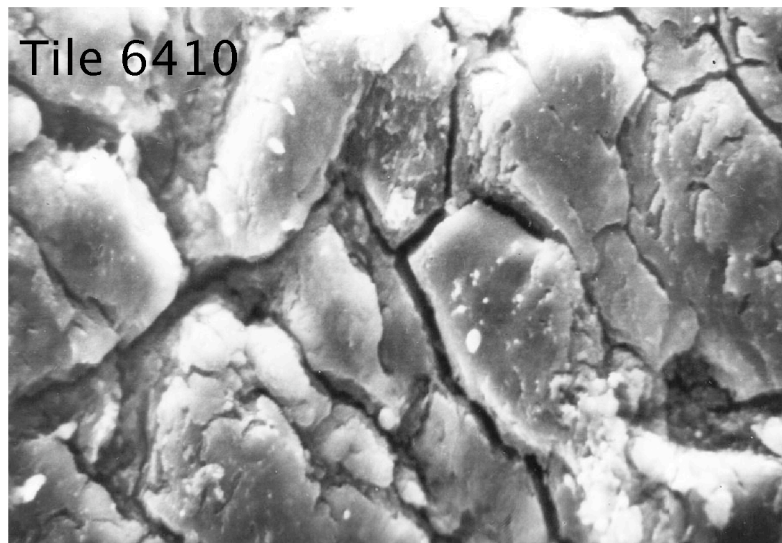
SEM Micrographs of Tile Surfaces after
Exposure show Thick Inner Divertor Redep



Inner Divertor Tile
Thick Redeposition Layer ($> 0.5 \mu\text{m}$)



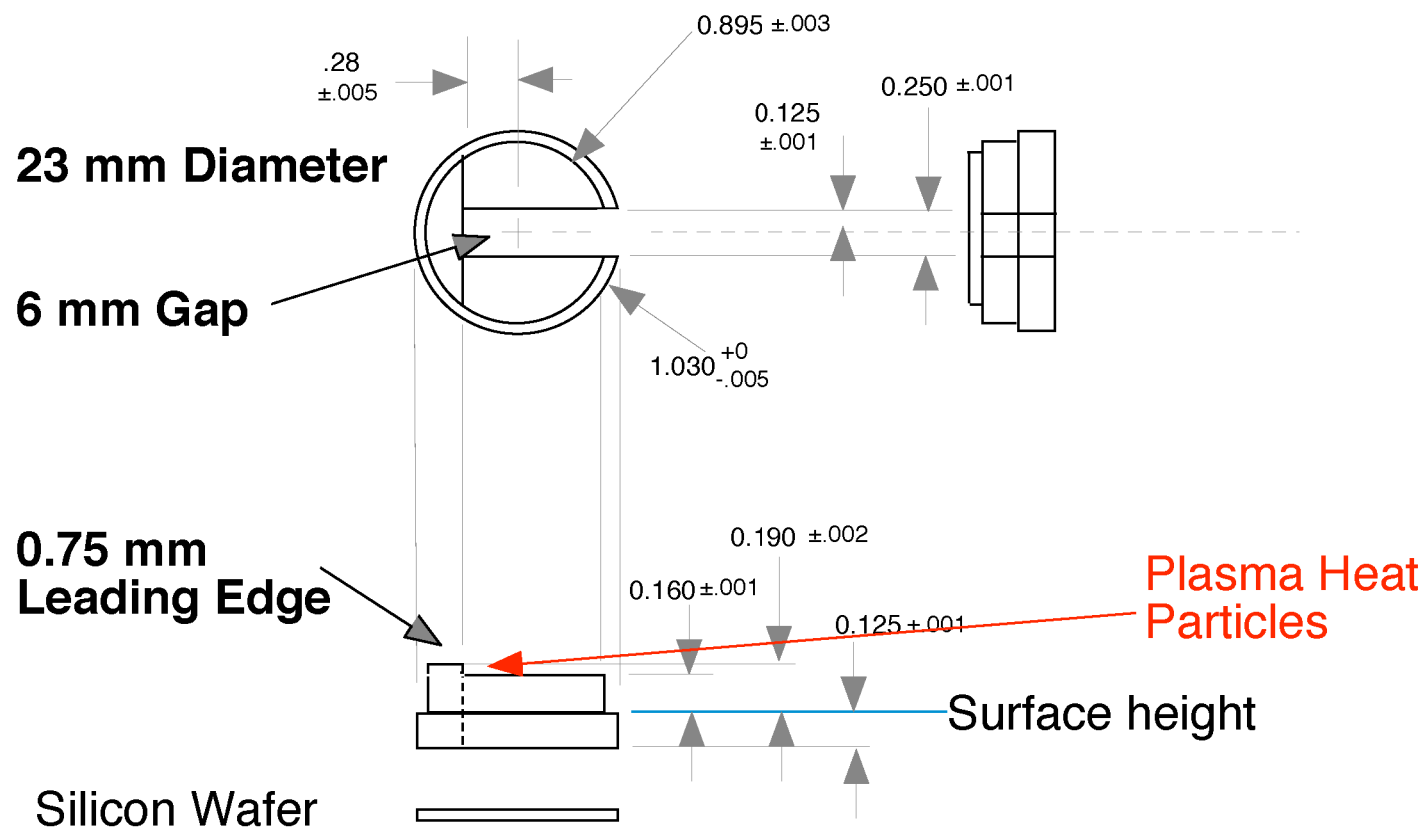
Outer Divertor Tile
Thin Redeposition and Some
(Rare) Damage to B_4C coating



B_4C coating remains in bottom
of Damaged Area



Leading Edge Sample Placed into DiMES Probe



Very Hard DLC Film formed on Shadowed Silicon Collector:

Plasma: Low Power ELMing H-mode:

Surface Heat Flux: 2 MW/m²

Parallel Heat Flux: ~75 MW/m²

Exposure Duration: Single Shot, 600 ms.

Film Formed on Shadowed Silicon Collector

Hard Diamond-Like-Carbon (Hardness 10-20 GPa (similar to sapphire)

DLC confirmed by Raman Spectroscopy and IR transmission Spectroscopy

D/C Ratio measured by IBA: 0.1 to 0.2

TDS: D₂ and HD observed, peak Release Temperature: 1250 K

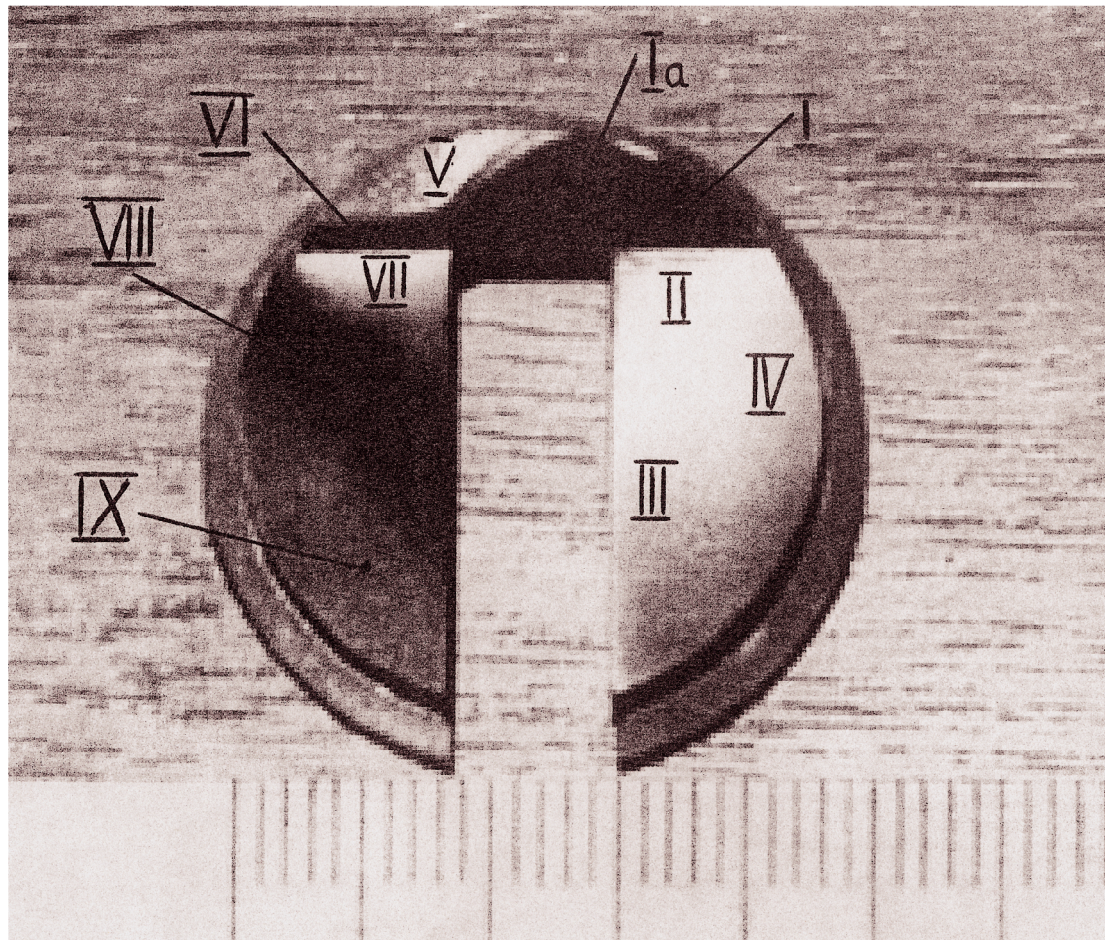
Redep Layers on Exposed Leading Edge Sample Differ by Region on Surface of Sample

Exposed to Divertor
Strike Point Plasma

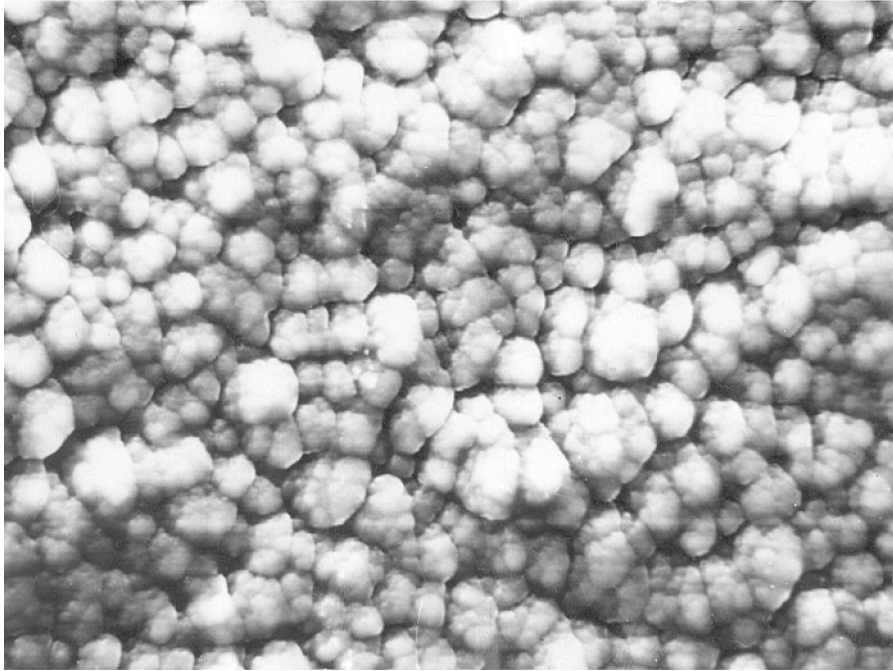
Surface Heat Flux:
 5 MW/m^2

Parallel Heat Flux:
 150 MW/m^2

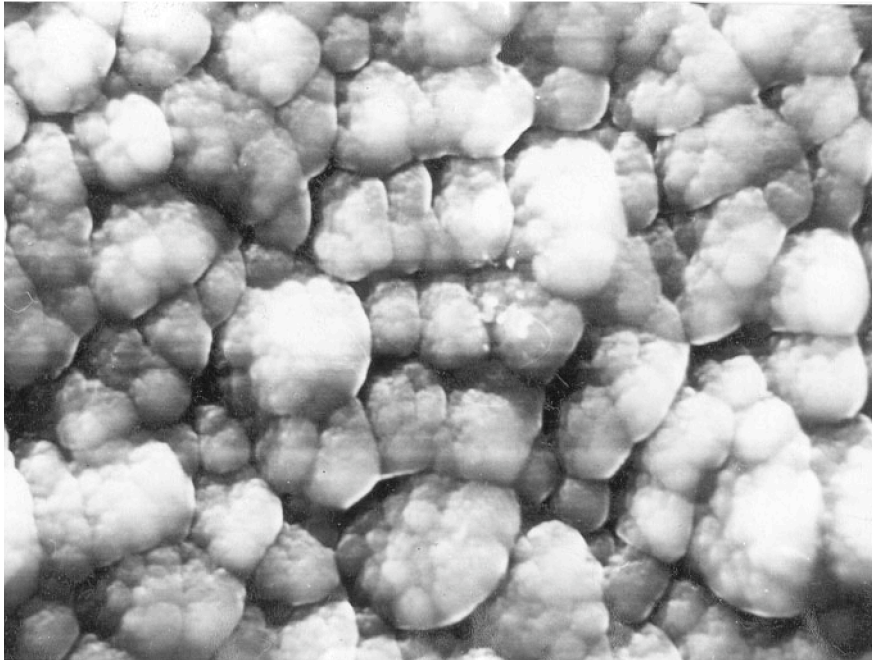
Duration 12 seconds:
4 shots
3 seconds each



Some Redep Layers Have Particulate Like Quality



Deposition Layer in Region II
Characteristic Particulate
Size 1–10 μm



Deposition Layer in Region IV
Characteristic Particulate
Size 10–20 μm

TDS Spectra:

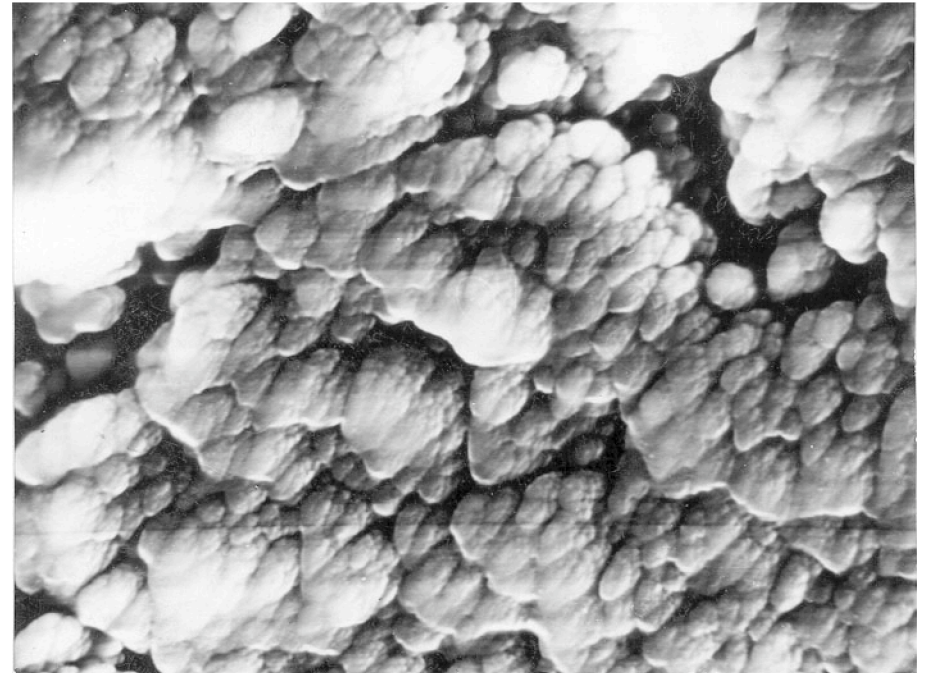
H₂ and HD observed (No D₂)

Desorption Peaks at 1000 K

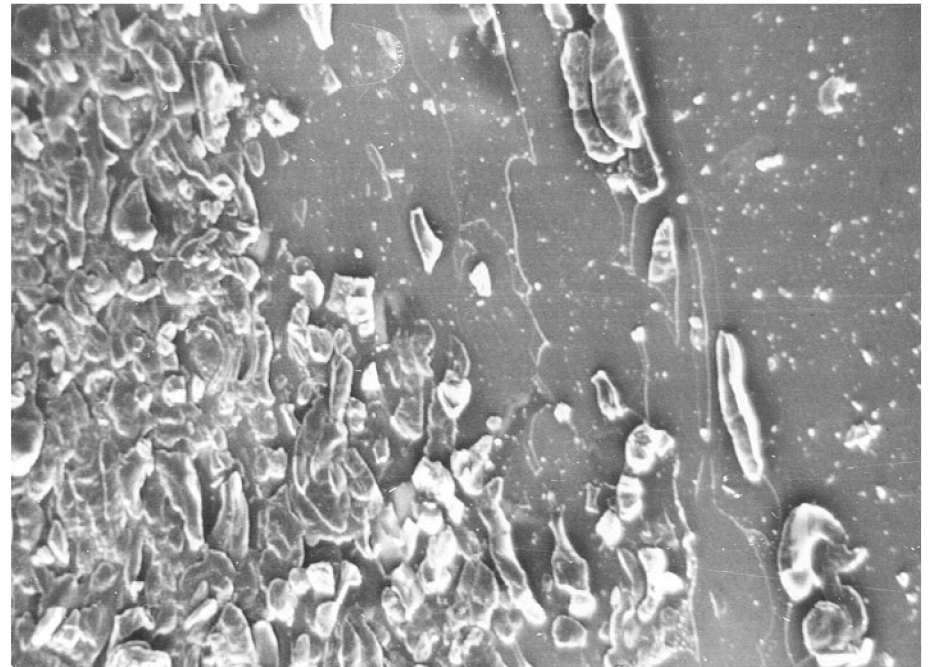
0.06 % H, 0.0004% D

Particulates of Different Character Are Observed in Other Areas

Deposition Layer in Region VIII
Aggregates of Oblong Particulates
Size $\sim 5 \times 10 \mu\text{m}$



Deposition Layer in Region III
Separated Oblong Particulates



Summary

B₄C Coated Tiles Useful for Campaign Integrated Redeposition Studies

- CVD B₄C coating is very durable

- Thick coating observed in the inner divertor region

- Typical D/C ratio 0.2

Leading Edge DiMES samples useful for High Heat Flux Studies

- Mimic Tile Gap and Misalignment Conditions

- Local Redeposition can be very high

- Very Hard DLC with D/C of 0.1 to 0.2 formed under modest loading

- Graphitic films of low H+D content formed under highly destructive loading

- Some layers exhibit a particulate like nature

7th International Workshop on Hydrogen Isotopes in Fusion Reactor Materials

May 20–21, 2004

Sabasco Harbor Resort, Sebasco Estates, Maine, USA

Participants

Thierry Angot
Matt Baldwin
Bob Bastasz
Nicolas Bekris
Jeffrey Brooks
Cristophe Brosset
Rion Causey
Jim Davis
Russell Doerner
Birger Emmoth
Tony Haasz
Wolfgang Jacob
Jean-Marc Layet
Denis Levchuk
Jari Likonen
Rick Macaulay-Newcombe

Takuji Oda
Olga Ogorodnikova
Yasuhisa Oya
Joachim Roth
Werner Schustereder
Phil Sharpe
Takahiro Shibahara
Peter Stangeby
K. Sugiyama
F. L. Tabares
David Tafalla
Tetsuo Tanabe
N. V. Volkov
Phil West
Dennis Whyte
Clement Wong

